



HAL
open science

Evaluation of the hydrogen storage system liquid organic hydrogen carrier (LOHC)

Florian d'Ambra

► **To cite this version:**

Florian d'Ambra. Evaluation of the hydrogen storage system liquid organic hydrogen carrier (LOHC). Chemical engineering. Université Grenoble Alpes [2020-..], 2023. English. NNT : 2023GRALI029 . tel-04563684

HAL Id: tel-04563684

<https://theses.hal.science/tel-04563684v1>

Submitted on 30 Apr 2024

HAL is a multi-disciplinary open access archive for the deposit and dissemination of scientific research documents, whether they are published or not. The documents may come from teaching and research institutions in France or abroad, or from public or private research centers.

L'archive ouverte pluridisciplinaire **HAL**, est destinée au dépôt et à la diffusion de documents scientifiques de niveau recherche, publiés ou non, émanant des établissements d'enseignement et de recherche français ou étrangers, des laboratoires publics ou privés.

THÈSE

Pour obtenir le grade de

DOCTEUR DE L'UNIVERSITÉ GRENOBLE ALPES

École doctorale : I-MEP2 - Ingénierie - Matériaux, Mécanique, Environnement, Energétique, Procédés, Production

Spécialité : 2MGE : Matériaux, Mécanique, Génie civil, Electrochimie

Unité de recherche : CEA Grenoble / LITEN

Evaluation du système de stockage de l'hydrogène sous forme de liquide organique transporteur d'hydrogène (LOHC)

Evaluation of the hydrogen storage system liquid organic hydrogen carrier (LOHC)

Présentée par :

Florian D'AMBRA

Direction de thèse :

Gérard GEBEL

Directeur de Recherche CEA, Université Grenoble Alpes

Directeur de thèse

Vincent FAUCHEUX

CEA Grenoble

Co-encadrant de thèse

Rapporteurs :

Valérie MEILLE

CHARGE DE RECHERCHE HDR, CNRS délégation Rhône Auvergne

Clémence NIKITINE

MAITRE DE CONFERENCES HDR, CPE Lyon

Thèse soutenue publiquement le **17 avril 2023**, devant le jury composé de :

Gérard GEBEL

DIRECTEUR DE RECHERCHE, CEA centre de Grenoble

Directeur de thèse

Valérie MEILLE

CHARGE DE RECHERCHE HDR, CNRS délégation Rhône Auvergne

Rapporteuse

Clémence NIKITINE

MAITRE DE CONFERENCES HDR, CPE Lyon

Rapporteuse

Marian CHATENET

PROFESSEUR DES UNIVERSITES, Grenoble INP

Président

Bruno AMEDURI

DIRECTEUR DE RECHERCHE, CNRS délégation Occitanie Est

Examineur

Invités :

Emmanuel NICOLAS

DOCTEUR EN SCIENCES, CEA Saclay

Thibault CANTAT

DIRECTEUR DE RECHERCHE, CEA Saclay



Remerciements

Je tiens d'abord à remercier toutes les personnes qui ont contribué de près ou de loin à cette thèse.

En particulier, merci beaucoup à mon directeur de thèse Gérard GEBEL qui, malgré de nombreuses contraintes externes, a pris le temps de m'accompagner au travers de la relecture de ce manuscrit et avec qui j'ai eu le plaisir de discuter sur de nombreux autres sujets.

Merci aussi à Vincent FAUCHEUX pour son support au quotidien et son accompagnement pragmatique de ce projet de thèse. J'ai particulièrement apprécié ta confiance en mes capacités à mener à bien cette thèse.

Un grand merci à Emmanuel NICOLAS sans lequel j'aurais eu beaucoup plus de mal à me servir de la DFT pour ces travaux. Merci pour ta patience et ta disponibilité sans faille pour répondre à mes nombreuses questions.

Merci encore à Thibault CANTAT et son équipe de recherche pour son écoute et ses nombreux encouragements au travers de cette thèse. Merci aussi pour les multiples opportunités que tu m'as ouvertes.

Je tiens aussi à remercier mon jury de thèse et en premier lieu Valérie MEILLE et Clémence NIKITINE en tant que rapporteuses de cette thèse. Egalement, merci à Bruno AMEDURI et Marian CHATENET pour leur rôle d'examineurs. Merci à tous les membres du jury pour leurs remarques constructives, questions et rigueur scientifique ; j'ai eu un grand plaisir à vous rencontrer et à échanger avec vous.

Aussi, merci à Yohann MOREAU et Jean-Pierre SIMONATO pour leur accompagnement au travers du Comité de Suivi Individuel et leur contribution à la réflexion et au déroulement de cette thèse.

Un immense merci à Parviz HAJIYEV, co-bureau de génie, toujours à l'écoute et prêt à me donner son appui scientifique et technique pour mettre en place des idées toujours plus farfelues au cours de cette thèse, je te souhaite tout le meilleur pour la suite !

Merci à l'ensemble du Laboratoire des technologies de valorisation des procédés et des matériaux pour les EnR (LVME) et en particulier aux membres permanents et temporaires de l'équipe énergie avec qui j'ai pu travailler au quotidien durant ces trois années : Olivier BLANCHOT, Christophe BROUARD, Jérôme DELMAS, Isabelle ROUGEAU, Konstantin TARASOV, Kristina BAELIEVA, Ikram BARIE, Sarah DIRENZO, Justine DORIVAL, Louis DUBRULLE, Maxime GONDREXON, Clément LESAGE, Alexie MATTEI, Huynh-Duc NGUYEN, Coralie PERRIER, Anaïs PEYRON et Héloïse DUFOUR.

Je tiens encore à remercier les doctorants et autres éphémères du C4 pour le cadre et l'ambiance à laquelle ils ont contribué au cours de cette thèse par le biais de discussions, sorties, randonnées et autres parties de papayo, tarot et 6 qui prend enragées. Merci à Romain BELLANGER, Lucie BORGET, Corentin BOURDIOL, Valentin BUREAU, Baptiste CHARPENTIER, Auriane DESPAX, Antonin DURET, Joseph FAUDOU, Ana Carolina FERNANDEZ, Antoine FONDANECHÉ, Thibault FRESNEAU, Fatine GABRIEL, Alice GONTIER, Jakob IHRENBERGER, Valentin LAFARGE, Julia LEVY, Javier MAYEN GUILLEN, Loïc PAILLARDET, Emma POCHON, Mehrsa RAFIE, Nathalie RONAYETTE, Amélie SCHULTHEISS, Lucile TERMEAU, Simon TOINET, Erwan TROUSSEL, Benoit VILLEMEJANNE et Benjamin ZANETTI; ça a été un plaisir de faire ce bout de chemin avec vous.

Merci à mes amis Aubry, Kévin, Juliette, Robin, Guillaume, Ivane, Mélanie, Manon et Benjamin avec qui j'ai pu m'évader loin de cette thèse pour y revenir avec plus d'énergie et de motivation.

Finalement, merci à ma famille, je vous aime.

Table of Contents

Remerciements	3
Glossary	6
I. Introduction.....	9
Bibliography.....	11
Table of Contents “Literature review”	13
II. Literature review	15
II.1 Current world situation	15
II.2 Hydrogen as an energy vector.....	20
II.3 H ₂ generation.....	21
II.4 State-of-the-art hydrogen storage technologies.....	24
II.5 Conclusion and research proposal	67
Bibliography.....	71
Table of Contents “Materials and Methods”	99
III. Materials and methods	101
III.1 Materials.....	101
III.2 Experimental setups.....	102
III.3 Catalysts preparation methods	104
III.4 Analysis of the LOHC	106
III.5 Analysis of the catalyst	110
III.6 Definitions	117
Bibliography.....	123
Table of Contents “Chapter 1: Evaluation of new LOHC structures”	125
IV. Chapter 1: Evaluation of new LOHC structures.....	126
IV.1 Choice of the target molecules	126
IV.2 Study of the 1-Cyclohexylethanol/Acetophenone (CHEA/APO) LOHC couple.....	135
IV.3 Conclusion	156
Bibliography.....	157
Appendix.....	164
Table of Contents “Chapter 2: Degradation study and limitation”	187
V. Chapter 2: Degradation study and limitation.....	188
V.1 Degradation mechanisms.....	188
V.2 LOHC stability assessment in the reaction conditions	191
V.3 Degradation limitation by modification of the catalyst support.....	192
V.4 Degradation limitation by additives	196
V.5 Study of the Dicyclohexylmethanol/Benzophenone (DCMA/BPO) LOHC couple.....	203

V.6	Conclusion	208
	Bibliography.....	209
	Appendix.....	211
	Table of Contents “Chapter 3: Regeneration of the intramolecular dehydration products.....	219
VI.	Chapter 3: Regeneration of the intramolecular dehydration products	220
VI.1	Regeneration process.....	220
VI.2	Regeneration of Diphenylmethane (DPM) to Benzophenone (BPO).....	222
VI.3	Study of the Dodecahydrofluoren-9-ol/Fluoren-9-one (12H-FLUA/FLUK) LOHC couple	230
VI.4	Conclusion	240
	Bibliography.....	241
	Appendix.....	244
	Table of Contents “Chapter 4: Substitution of the ketone by an ester”	253
VII.	Chapter 4: Substitution of the ketone by an ester.....	254
VII.1	Hydrogenation.....	255
VII.2	Dehydrogenation.....	258
VII.3	Stability of the ester function.....	262
VII.4	Conclusion	265
	Bibliography.....	266
	Appendix.....	267
VIII.	Conclusion and perspectives	271

Glossary

ΔH or $\Delta_r H$: Reaction enthalpy (kJ/mol or kJ/mol H₂)

$\Delta_r G$: Reaction Gibbs energy (kJ/mol or kJ/mol H₂)

$\Delta_r S$: Reaction entropy ((kJ/mol/K or kJ/K/mol H₂)

OH-Coupling: 1,3-Diphenylbutanone

OH-ROR: Bis(1-phenylethyl) ether

12H-Coupling: 1,3-Dicyclohexylbutanone

12H-FLU: Dodecahydro-fluorene

12H-FLUA: Dodecahydrofluoren-9-ol

12H-FLUK: Dodecahydro-fluoren-9-one

12H-NEC: Dodecahydro-N-Ethylcarbazole

12H-PHE: Dodecahydro-Phenazine

12H-ROR: Bis(1-cyclohexylethyl) ether

¹³C NMR: Carbon 13 NMR

18H-DBT: Perhydro-dibenzyltoluene

¹H NMR: Proton Nuclear Magnetic Resonance

4H-NEC: Tetrahydro-N-Ethylcarbazole

6H-Coupling: 1-Cyclohexyl-3-phenylbutanone and 1-Phenyl-3-cyclohexylbutanone

6H-FLU: Hexahydro-fluorene

6H-FLUK: Hexahydro-fluoren-9-one

8H-NEC: Octahydro-N-Ethylcarbazole

AB: Ammonia Borane

ACE: Acetaldehyde

ACH: Acetylcyclohexane

ACHN: Acetylcyclohex-1-ene

AcOH: Acetic acid

APCI-MS: Atmospheric Pressure Chemical Ionization

APO: Acetophenone

BA: Benzoic acid

BBE: Benzylbenzoate

BCE: Phenylcyclohexylester

BDO: 1,4-Butanediol

BET: Brunauer, Emmett and Teller method

BP: Biphenyl

BPO: Benzophenone

CA: Cyclohexancarboxylic acid

CAES: Compressed Air Energy Storage

CBE: Cyclohexylphenylester

CCS: Carbon Capture and Sequestration

CDCI₃: Deuterated Chloroform

CGH₂: compressed H₂ gas

CHEA: 1-Cyclohexylethanol

CMA: Cyclohexylmethanol

CNF: Carbon Nano Fibers

CNT: Carbon Nano Tubes

COF: Covalent-Organic Frameworks

COSMO: Conductor-like Screening Model

CPM: Cyclohexylphenylmethane

CPMK: Cyclohexylphenylketone

DBT: Dibenzyltoluene

DCM: Dicyclohexylmethan

DCMA: Dicyclohexylmethanol

DCMK: Dicyclohexylmethylketone

Dec: Decalin

DFT: Density Functional Theory

DHY: Dehydrogenation step

DoDH: Degree of dehydrogenation, similar to the DoH, but for the released H₂.

DOE: United States Department of Energy

DoH: Degree of hydrogenation, ratio between the amount of stored H₂ and the theoretical maximum H₂ amount that can be stored by the LOHC system

DPM: Diphenylmethane

DPMA: Diphenylmethanol

Ea: Activation energy (kJ/mol)

EB: Ethylbenzene

EC: Ethylcyclohexane

EDX or EDS: Energy-Dispersive X-ray spectroscopy

EHC: Exploited H₂ Capacity

EI: Electron Ionization

Enol-Cy: Enol forming on the cyclohexyl group

Enol-Me: Enol forming on the Methyl group

ESI: ElectroSpray Ionization

EtOAc: Ethyl acetate

EtOH: Ethanol

FLU: Fluorene

FLUA: Fluoren-9-ol

FLUK: Fluoren-9-one

FTIR-ATR: Fourier-Transfer InfraRed-Attenuated Total Reflectance spectroscopy

GBL: γ -Butyrolactone

GC: Gas Chromatography

GC-MS: Gas Chromatography coupled with Mass Spectrometry

GGA: Generalized Gradient Approximation

GNP: Glycine Nitrate Process

H₂: Dihydrogen, abusively called Hydrogen

H₂O₂: Hydrogen peroxide

HAADF: High Angle Annular Dark Field

HF: Hartree-Fock

HMTA: Hexamethylenetetramine

HPLC: High Performance Liquid Chromatography

HR-XPS: High Resolution X-ray Photoelectron Spectroscopy

HT: Hydrotalcite

HY: Hydrogenation step

ICP-OES: Inductive Coupled Plasma optical emission spectroscopy

IPA: Isopropanol

IR: Infrared spectroscopy

IR-AS: Infrared Reflection Absorption Spectroscopy

LH₂: cryogenic H₂ liquid

LOHC: Liquid Organic Hydrogen Carrier

m/Z: molecular weight divided by the number of charge of the structure

MALDI-TOF: Matrix Assisted Laser Desorption Ionization-Time of Flight

MCH: Methylcyclohexane

MD: Molecular Dynamics

Me-BP: Methylbiphenyl

MeOH: Methanol

MeOH-BP: Methanolbiphenyl

MOF: Metal-Organic Frameworks

MP2: Møller-Plesset second-order perturbation theory

MTH: Methylcyclohexane-Toluene-Hydrogen system

Nap: Naphtalene

NEC: N-Ethylcarbazole

NH₃: Ammonia

NHC: N-heterocyclic carbene ligands

NP: nanoparticles

P: Pressure (Pa)

P⁰: Saturated vapor pressure (Pa)

PEM: Polymer Electrolyte Membrane

PEO: 1-Phenylethanol

PGM: Platinum Group Metals or platinoids or noble metals

PHE: Phenazine

PHS: Pumped Hydro Storage

PIM: Polymers of Intrinsic Microporosity

PMA: Phenylmethanol

PMK: Benzaldehyde

PNN: Phosphorus-Nitrogen-Nitrogen tridentate ligand

PNP: Phosphorus-Nitrogen-Phosphorus tridentate ligand

Pt/Al₂O₃: Script used to describe the composition of the heterogeneous catalysts. Here the active metal Pt is supported on Alumina.

RFF: Relative Response Factors used in GC-MS analysis

rGO: reduced Graphene Oxide

SAC: Single Atom Catalyst

SAED: Selected Area Electron Diffraction

sc-CO₂: supercritical CO₂

SiCN: Silica-carbon nitride

SMD: Solvation Model based on Density

SMR: Steam Methane Reforming

SOE: Solid Oxide Electrolyte

t: reaction time (h)

T: temperature (°C)

TBHP: Tert-butylperoxide

TEM: Transmission electron microscopy

Tet: Tetralin

TGA: ThermoGravimetric Analysis

TGA-MS: TGA coupled with mass spectroscopy

THF: Tetrahydrofuran

Tol: Toluene

TPI: Toxicity Potential Indicator

UHS: Underground H₂ storage

UHV: Ultra High Vacuum

UV-VIS: Ultraviolet-Visible spectroscopy

VEB: Vinylbenzene

VEC: Vinylcyclohexane

WGSR: Water-Gas-Shift Reaction

XRD: X-Ray Diffraction

I. Introduction

The rapid reduction of greenhouse gases is a key target to limit dire consequences of global warming on the ecosystems, the biodiversity and human societies.¹ Under these circumstances, new carbon-free energy systems must be developed in order to simultaneously tackle the reduction of greenhouse gases and the access to energy for the already energy-lacking hundreds of millions in Africa, South America and South-East Asia, while anticipating a global demographics increase in the coming years.² Electricity is an energy sector where low-carbon alternatives such as nuclear power and renewable energies (namely solar power, wind power, hydro power and geothermal power) are already implemented but a rapid and substantial decrease of greenhouse emissions require to multiply their implementation by a factor 3 to 7 at equivalent energy consumption levels.^{3,4} Low-carbon energies have gained traction over the last decades, earning from their much-added benefits to safety and direct CO₂ emission reductions. However, new challenges are arising from this situation. Indeed, most of the prevalent renewable solutions (sun power, wind power, hydro power) have not a controllable production, i.e. they depend on the weather or a time cycle (day/night, seasonal, ...).

Currently, the energy variations due to the renewables are compensated by the pilotable energies (fossil fuels and nuclear). However, with their planned decrease in the energy mix, it will be progressively more and more difficult to adjust the production and consumption ratio and, increasing the risks of black out. Moreover, excess energy produced by renewable sources during fast transitional regimes is currently discarded, leading to a net loss of energy.⁵⁻⁷ Hence, developing a technology to store the excess energy of renewables for a later use is key to remove pilotable fossil fuels of the energy mix and successfully abate greenhouse gases emissions. In addition, as energy is often produced remotely, transport and storage of energy are two essential steps for energy systems.

The concept of the energy vector answers this issue: the excess energy is converted into a new form that can be easily stored and transported. Among all energy vectors, the dihydrogen (H₂), abusively named hydrogen in the rest of this thesis, can easily be produced from electricity by water electrolysis. The reverse reaction with the dioxygen (O₂) yields only water and heat as products of the reaction, making it virtually the environmental-friendliest energy technology. As the implementation of intermittent renewable energies may impose the storage of large quantities of energy (in the TWh range) over a long duration (monthly to yearly) to cover seasonal variations, the high mass energy density of H₂ (120 MJ/kg, about three times more than methane and other hydrocarbons^{8,9}) is advantageous. However, H₂ is a gas at normal temperature and pressure and presents greater barriers of implementation compared to current liquid fuels. Indeed, its density is minimal (0.09 g/L under normal conditions of temperature and pressure), causing a necessary concentration of H₂ in order to limit the size needed for storage.¹⁰ Many H₂ storage technologies aim at concentrating H₂, based either on the physical processes (compression, liquefaction) or on binding with various materials (physical adsorbents, metal hydrides, Boron-Nitrogen H₂ carriers, circular H₂ carriers and liquid organic H₂ carriers). In particular, the Liquid Organic Hydrogen Carrier (LOHC) are liquid molecules able to store and release H₂ at a desired place and time by catalytic exothermal hydrogenation and endothermal dehydrogenation reactions to respectively load and unload H₂.¹¹

Storing H₂ by covalent bonds on an organic liquid improves the handling and safety of the energy vector and retains similar volumetric densities compared to traditional physical systems, circumventing the need of heavy gas tanks and other cooling devices.^{12,13} The liquid-phase is also advantageous as the reaction can proceed without the dilution of the H₂ carrier in a solvent. In addition, most LOHCs are oil-like structures that can be easily transported by the current oil and gas infrastructures with small modifications to the system, diminishing the implementation cost of the technology.

Introduction

Different criteria have been proposed to assess the potential of a LOHC. The energy efficiency is often addressed through the dehydrogenation enthalpy value. Classic LOHC systems have comparatively high enthalpy values (between 50 and 75 kJ/molH₂) while the US Department of Energy (DOE) aims at 30-44 kJ/molH₂ so that the H₂ equilibrium pressure reaches 1 bar between -40 °C to 60 °C.¹⁴ Like the other H₂ storage systems, the gravimetric and volumetric energy densities highlight the energy storage efficiency with ultimate targets of 6.5 wt.%H₂ and 50 gH₂/L for a complete on-board system respectively. An excellent stability (>99.9%) of the LOHC is also required in order to avoid the constant replacement of the carrier during the cycling.^{15,16} Finally, the LOHC must also answer to other criteria that are heavily dependent on the targeted application (e.g. high liquid temperature range, availability, cost, H₂ gas flow and quality on release, toxicity and biodegradability).¹⁷ For example, a mobility application for individual transportation vehicles would mainly require high gravimetric and volumetric densities as well as a good cycling capacity and low dehydrogenation temperature while stationary systems would be principally driven by the cost of the LOHC and its catalysts. Lastly, massive energy storage would necessitate both a low system cost and high densities.

However, one major bottleneck of the LOHC system is the problematic toxicity of the LOHC molecules, similar to that of currently employed fossil fuels. Moreover, the classic LOHC systems are oil derivatives, so the development of structures based on renewable feedstock would be preferential. Besides, the catalysts used for the hydrogenation and dehydrogenation reactions are generally based on platinum group metals (PGM), whose rarity and prices are detrimental to the development of the technology. Finally, the stability of the LOHC structures is a major concern, especially after multiple hydrogenation/dehydrogenation cycles.

In this thesis, the viability of potential LOHC systems was assessed preliminarily by calculating their thermodynamical properties by *ab-initio* Density Functional Theory (DFT). In particular, dehydrogenation enthalpies inferior to the dehydrogenation enthalpy of the state-of-the-art N-Ethylcarbazole (50 kJ/mol H₂) were sought for. Many other aspects were also taken into account in order to choose a pertinent LOHC system such as the liquid temperature range, H₂ gravimetric and volumetric densities, synthetic accessibility and safety. These non-exhaustive secondary criteria were also discussed in the first chapter of this thesis. All criteria highlighted the interest of previously unstudied bifunctional LOHC, i.e. LOHC systems whose molecules can store/release H₂ in/from two different chemical functions like an aromatic ring/saturated ring and a ketone/alcohol. The performance and reaction mechanisms of the 1-Cyclohexylethanol/Acetophenone (CHEA/APO) couple were assessed with commercial heterogeneous catalysts in batch systems for both hydrogenation and dehydrogenation in order to develop reaction conditions suitable for its cycling.

Secondly, the degradation pathways of the LOHC were identified for both hydrogenation and dehydrogenation and the degradation products formation was linked to different components of the LOHC system. Support modification, additives and LOHC structure modification to Dicyclohexylmethanol/Benzophenone (DCMA/BPO) were tested to block the degradation pathways.

Thirdly, a methodology to regenerate the dehydrated LOHC was developed. A new couple, Dodecahydrofluoren-9-ol/Fluoren-9-one (12H-FLUA/FLUK), was suggested due to the enhanced conversion of Fluorene to Fluoren-9-one in the developed conditions. The effect of the regeneration on the cycling of the LOHC was then tested.

Lastly, the Cyclohexylmethanol/Benzylbenzoate (CMA/BBE) LOHC couple was studied to highlight the effect of the replacement of the ketone function by an ester. The modification effects on the reactivity and stability of the LOHC couple were rationalized.

Bibliography

- (1) IPCC_AR6_WGII_SummaryForPolicymakers.Pdf. https://report.ipcc.ch/ar6wg2/pdf/IPCC_AR6_WGII_SummaryForPolicymakers.pdf (accessed 2022-07-13).
- (2) *The world's energy problem*. Our World in Data. <https://ourworldindata.org/worlds-energy-problem> (accessed 2022-07-13).
- (3) Gibon, T.; Arvesen, A.; Hertwich, E. G. Life Cycle Assessment Demonstrates Environmental Co-Benefits and Trade-Offs of Low-Carbon Electricity Supply Options. *Renewable and Sustainable Energy Reviews* **2017**, *76*, 1283–1290. <https://doi.org/10.1016/j.rser.2017.03.078>.
- (4) Ritchie, H.; Roser, M.; Rosado, P. Energy. *Our World in Data* **2020**.
- (5) Revol, M. *Quand trop d'énergies renouvelables privent la Californie... d'électricité*. Le Point. https://www.lepoint.fr/economie/quand-trop-d-energies-renouvelables-privent-la-californie-d-electricite-20-08-2020-2388408_28.php (accessed 2020-08-25).
- (6) *Energy Charts*. <https://energy-charts.info/?l=fr&c=DE> (accessed 2021-01-21).
- (7) *éCO2mix - La production d'électricité par filière*. <https://www.rte-france.com/eco2mix/la-production-delectricite-par-filiere> (accessed 2022-07-27).
- (8) Le Duigou, A. La filière hydrogène Un moyen de stockage de l'énergie. <https://hal.archives-ouvertes.fr/hal-02416323/file/201500004533.pdf> (accessed 2020-08-25).
- (9) Momirlan, M.; Veziroglu, T. N. The Properties of Hydrogen as Fuel Tomorrow in Sustainable Energy System for a Cleaner Planet. *International Journal of Hydrogen Energy* **2005**, *30* (7), 795–802. <https://doi.org/10.1016/j.ijhydene.2004.10.011>.
- (10) Abbasi, T.; Abbasi, S. A. 'Renewable' Hydrogen: Prospects and Challenges. *Renewable and Sustainable Energy Reviews* **2011**, *15* (6), 3034–3040. <https://doi.org/10.1016/j.rser.2011.02.026>.
- (11) Grünenfelder, N. F.; Schucan, Th. H. Seasonal Storage of Hydrogen in Liquid Organic Hydrides: Description of the Second Prototype Vehicle. *International Journal of Hydrogen Energy* **1989**, *14* (8), 579–586. [https://doi.org/10.1016/0360-3199\(89\)90117-1](https://doi.org/10.1016/0360-3199(89)90117-1).
- (12) He, T.; Pei, Q.; Chen, P. Liquid Organic Hydrogen Carriers. *Journal of Energy Chemistry* **2015**, *24* (5), 587–594. <https://doi.org/10.1016/j.jechem.2015.08.007>.
- (13) Züttel, A. Hydrogen Storage Methods. *Naturwissenschaften* **2004**, *91* (4), 157–172. <https://doi.org/10.1007/s00114-004-0516-x>.
- (14) *Target Explanation Document: Onboard Hydrogen Storage for Light-Duty Fuel Cell Vehicles*. Energy.gov. <https://www.energy.gov/eere/fuelcells/downloads/target-explanation-document-onboard-hydrogen-storage-light-duty-fuel-cell> (accessed 2021-06-04).
- (15) Geburtig, D.; Preuster, P.; Bösmann, A.; Müller, K.; Wasserscheid, P. Chemical Utilization of Hydrogen from Fluctuating Energy Sources – Catalytic Transfer Hydrogenation from Charged Liquid Organic Hydrogen Carrier Systems. *International Journal of Hydrogen Energy* **2016**, *41* (2), 1010–1017. <https://doi.org/10.1016/j.ijhydene.2015.10.013>.
- (16) Teichmann, D.; Arlt, W.; Wasserscheid, P. Liquid Organic Hydrogen Carriers as an Efficient Vector for the Transport and Storage of Renewable Energy. *International Journal of Hydrogen Energy* **2012**, *37* (23), 18118–18132. <https://doi.org/10.1016/j.ijhydene.2012.08.066>.
- (17) Aakko-Saksa, P. T.; Cook, C.; Kiviaho, J.; Repo, T. Liquid Organic Hydrogen Carriers for Transportation and Storing of Renewable Energy – Review and Discussion. *Journal of Power Sources* **2018**, *396*, 803–823. <https://doi.org/10.1016/j.jpowsour.2018.04.011>.

Table of Contents “Literature review”

II. Literature review.....	15
II.1 Current world situation	15
II.2 Hydrogen as an energy vector.....	20
II.3 H ₂ generation.....	21
II.3.1 Non-renewable H ₂ production (grey/brown hydrogen).....	21
II.3.2 Water electrolysis (blue hydrogen).....	22
II.3.3 Renewable H ₂ generation (green H ₂)	22
II.3.4 Cost comparison of H ₂	23
II.4 State-of-the-art hydrogen storage technologies.....	24
II.4.1 Physical-based hydrogen storage.....	24
II.4.1.1 Compressed gas H ₂ (CGH ₂)	24
II.4.1.2 Liquid H ₂ (LH ₂).....	25
II.4.1.3 Underground H ₂ storage	25
II.4.2 Chemical-based hydrogen storage.....	25
II.4.2.1 Physical sorbents.....	25
II.4.2.1.1 Carbon nanomaterials.....	26
II.4.2.1.2 Polymers of intrinsic microporosity	26
II.4.2.1.3 Covalent-organic frameworks and Metal-organic frameworks	26
II.4.2.1.4 Zeolites	27
II.4.2.1.5 Clathrates	27
II.4.2.2 Metal hydrides/Interstitial hydrides.....	27
II.4.2.2.1 Low-temperature hydrides	28
II.4.2.2.2 High temperature hydrides.....	28
II.4.2.2.3 Complex hydrides.....	28
II.4.2.3 B-N H ₂ carriers	29
II.4.2.4 Circular hydrogen carriers	30
II.4.2.4.1 Ammonia (NH ₃)	30
II.4.2.4.2 Methanol (MeOH)	31
II.4.2.5 Liquid organic hydrogen carrier (LOHC)	32
II.4.2.5.1 Cycloalkanes.....	33
II.4.2.5.1.1 Methylcyclohexane/Toluene (MCH/Tol).....	34
II.4.2.5.1.2 Decalin/Naphtalene (Dec/Nap).....	37
II.4.2.5.1.3 Perhydro-dibenzyltoluene/Dibenzyltoluene (18H-DBT/DBT)	39
II.4.2.5.2 N-heterocycles.....	43

Literature review

II.4.2.5.2.1	Perhydro-N-Ethylcarbazole /N-Ethylcarbazole (12H-NEC/NEC)	44
II.4.2.5.2.2	Perhydro-Phenazine/Phenazine (12H-PHE/PHE)	49
II.4.2.5.3	O-heterocycles	49
II.4.2.5.4	Primary alcohol/Aldehydes-esters-carboxylic acids.....	50
II.4.2.5.4.1	Hydrogenation of carbonyl compounds.....	51
II.4.2.5.4.2	Primary alcohols/aldehydes	51
II.4.2.5.4.3	Primary alcohols/Carboxylic acids.....	52
II.4.2.5.4.4	Primary alcohols/Esters.....	54
II.4.2.5.4.4.1	Intermolecular homo-esters	54
II.4.2.5.4.4.2	Intermolecular hetero-esters	56
II.4.2.5.4.4.3	Intramolecular esters/Lactones	56
II.4.2.5.4.5	Secondary alcohols/Ketones	58
II.4.2.5.5	Alcohol and amine couplings	59
II.4.2.5.5.1	Amides.....	59
II.4.2.5.5.2	Carbamides.....	60
II.4.2.5.5.3	Imides	61
II.4.2.5.6	Amines/Nitriles.....	62
II.4.2.5.7	S-containing LOHC.....	63
II.4.2.5.8	B,N-containing LOHC.....	64
II.4.2.5.9	Si-containing LOHC.....	65
II.4.2.5.10	Others.....	66
II.5	Conclusion and research proposal	67
	Bibliography.....	71

II. Literature review

II.1 Current world situation

Access and use of external energy have always been a preoccupation of human societies to facilitate the satisfaction of basic needs such as food cultivation/preparation, warmth production or crafting of everyday materials. Our ancestors had simple energy forms at their disposal such as human muscle, animal muscle, burning of biomass and wind, hydro and sun power.¹ While used for tens of millennia, the development of stationary steam-powered engines supplied by fossil fuels in the late 18th century revolutionized the means of production. The development of new and more efficient processes like the replacement of wood for coal in the iron industry, deeper mining or chemicals (especially sulphuric acid and sodium carbonate) durably modified the western societies, leading to the Industrial Revolution.²⁻⁶ Since then, a strong increase of the global atmospheric concentrations of greenhouse gases such as carbon dioxide (CO₂), methane (CH₄) and nitrous oxide (N₂O) was observed and their heat trapping property started to abnormally modify the global climate, being later dubbed as climate change.⁷ Over the past decades, this increase has been linked to anthropogenic emissions related to the combustion of fossil fuels (coal, oil, gas) for CO₂ and agricultural malpractices for CH₄ (manure and biomass burning) and N₂O (synthetic inorganic fertilizers).⁸⁻¹⁰ As the effects of climate change are already visible and partially irreversible, the rapid reduction of greenhouse gases is a key target to limit dire consequences on the ecosystems, the biodiversity and human societies.¹¹ Under these circumstances, new carbon-free energy systems must be developed in order to simultaneously tackle the reduction of greenhouse gases and the access to energy for the already energy-lacking hundreds of millions in Africa, South America and South-East Asia, while anticipating a global demographics increase.¹²

Electricity is an energy sector where low-carbon alternatives such as nuclear power and renewable energies (namely solar power, wind power, hydro power and geothermal power) are already implemented.¹³ Low-carbon energies have gained traction over the last decades, earning from their much-added benefits to safety and direct CO₂ emission reductions. The CO₂ emission factor obtained by Life-Cycle Analysis for each power generation source without carbon capture is presented in Figure II-1.^{14,15}

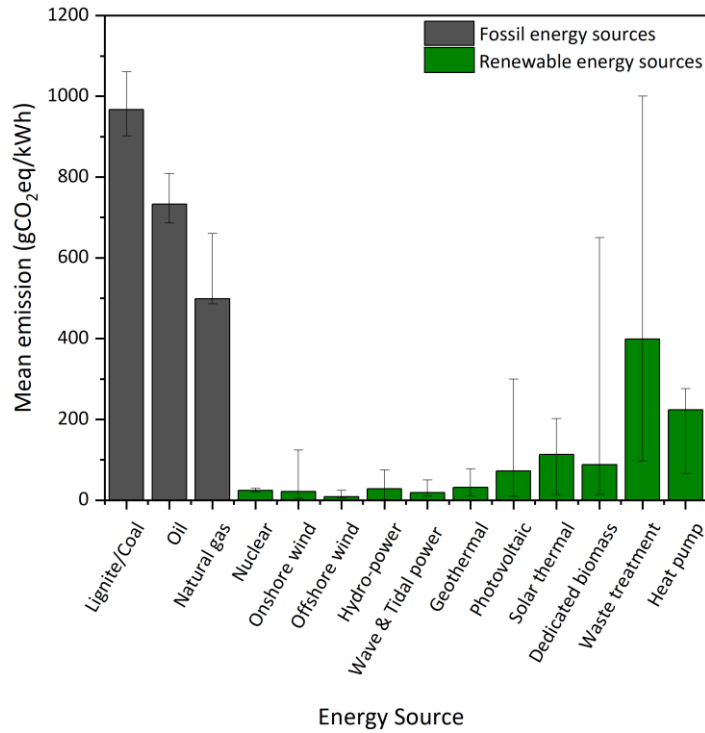


Figure II-1 – Direct and indirect life cycle CO₂ emission factors for different types of power generation systems, adapted from ^{14,15}.

While the production electricity can be attained by low-carbon technologies, it is important to note that 84% of the global primary energy production still came from fossil fuels in 2019.¹ Hence a strong electrification of our societies is proposed to further the use of low-carbon technologies. As a consequence, the part of renewable energy sources has been steadily increasing from 14% to 22% in the French energy mix between 1990 and 2021, aiming for 32% in 2030 (Figure II-2).¹⁶⁻¹⁸

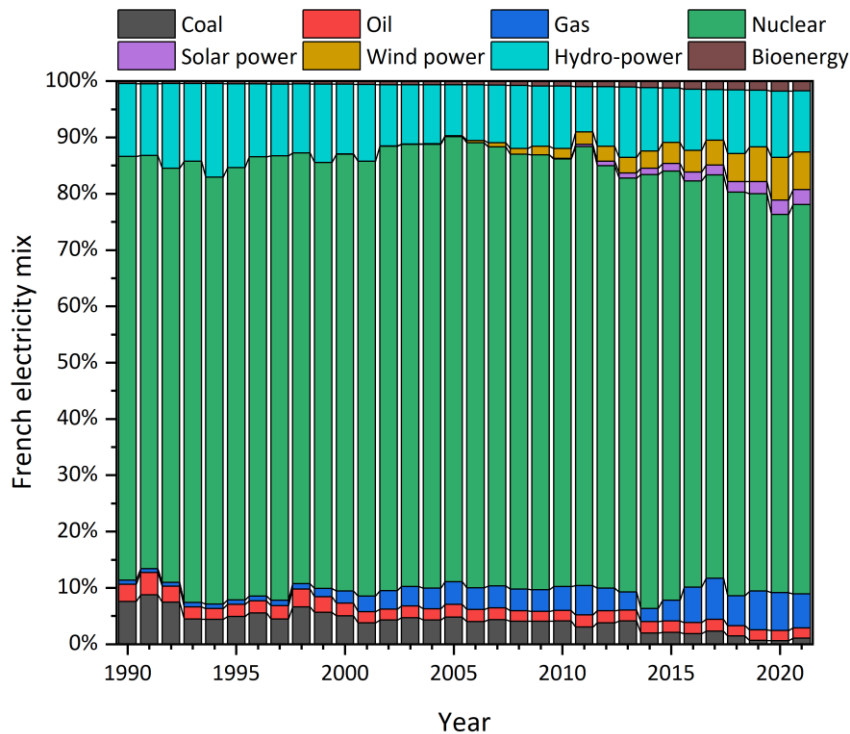


Figure II-2 - French electricity mix from 1990 to 2021, adapted from ¹⁷.

Literature review

Although this energy transition has mainly consisted in reducing the part of nuclear power to the energy mix, new challenges are arising from this situation. Indeed, most of the prevalent renewable solutions (sun power, wind power, hydro power) have not a controllable production, i.e. they depend on the weather or a time cycle (day/night, seasonal, ...) (Figure II-3).¹⁹

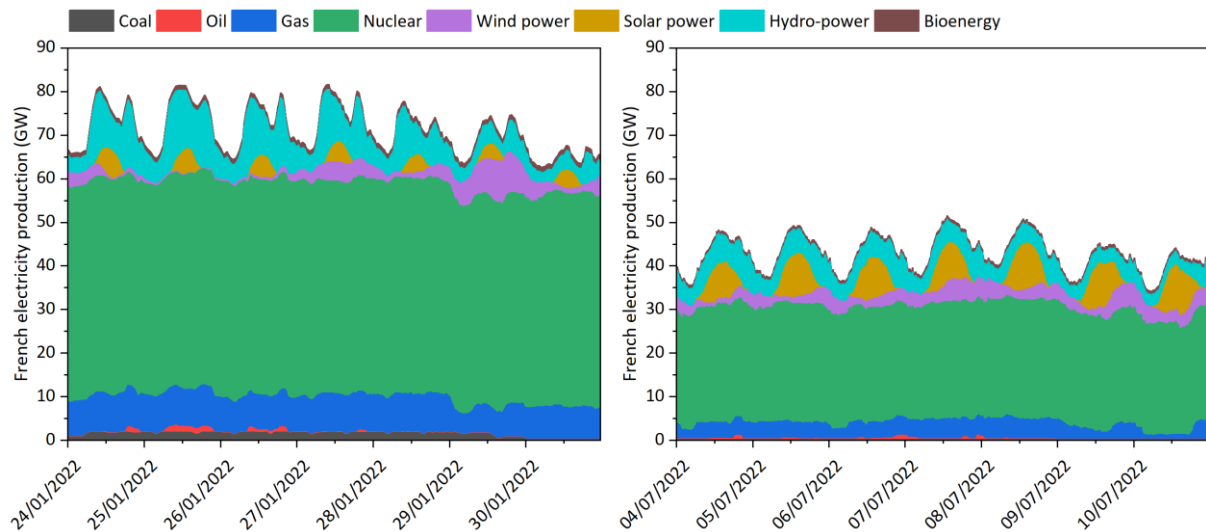


Figure II-3 – Energy production in France in January 2022 (left) and July 2022 (right), adapted from ²⁰.

The energy variations due to the renewables are currently compensated by the pilotable energies (fossil fuels and nuclear). However, with their planned decrease in the energy mix, it will be progressively more and more difficult to adjust the production/consumption ratio and, in a hypothetical 100% renewables scenario, such compensation mechanism would be strictly impossible. Moreover, excess energy produced by renewable sources during fast transitional regimes is currently discarded, leading to a net loss of energy.^{20–22} Hence, developing a technology to store the excess energy of renewables for a later use is key to remove pilotable fossil fuels of the energy mix and successfully abate greenhouse gases emissions. In addition, energy uncertainty management methods demand the integration of the energy storage systems in the electric power distribution networks and that the probable oversizing of the renewable power capacity.^{23,24}

Thus, design smarter energy systems is sorely needed. An energy system is characterized by a succession of operations such as storage, transportation, conversion and transformation on a set of energy resources to produce in fine usable energy for a desired purpose (e.g. heat up our house). Following this example of our everyday life in a cradle-to-gate approach, an energy resource (for example coal) is extracted from the ground, then refined (conversion), stored, transported to a coal power plant, transformed to electricity which is then transported to our house and finally transformation of this electricity to heat in a resistance in a heater (Figure II-4). It is important to note that each step can produce waste and interact with the environment so limiting the number of steps usually is an efficient method to minimize adverse effects.

Literature review

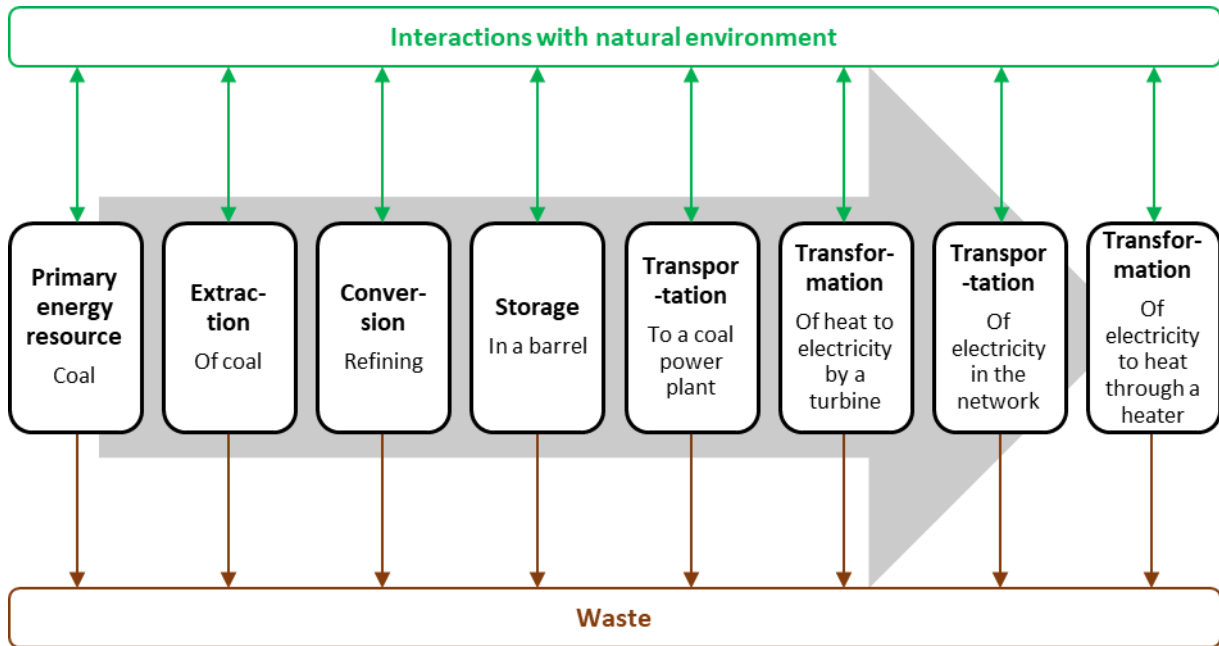


Figure II-4 - Example of an energy system to produce heat through a heater from coal.

Transport and storage of energy are two steps that are essential for energy systems as energy is often produced remotely. Moreover, the need for instantaneous and continuous energy output requires additional energy to be stored in order to back up the energy systems in case of supply disruption. In our previous example, coal is a solid that can easily be stored and transported before use. However, swapping coal for renewable energy like solar power drastically changes our energy system as storing vast amounts of electricity becomes much more complex than a solid (Figure II-5).

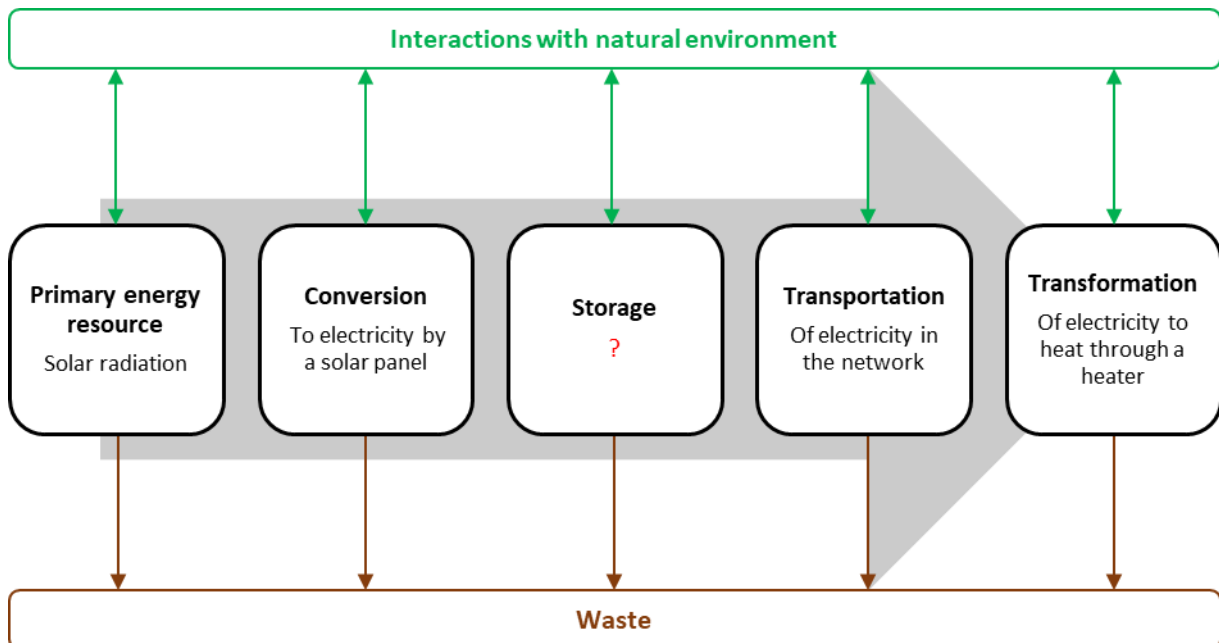


Figure II-5 - Example of an energy system to produce heat from a heater from solar radiation.

The concept of the energy vector answers this issue: the energy is converted into a new form that can be easily stored and transported. It is crucial to make a clear distinction between primary energy source and energy vector. In the energy system chain, a primary energy source such as fossil fuels, nuclear power and the renewable energies directly produces energy: this energy is readily available and will

Literature review

be lost if not used or stored otherwise. Primary energy resources can be separated into either renewable energy resources (solar radiation, water, biomass, wind, earth, sea, biological and bacterial) that can be reformed in the environment by natural processes or non-renewable resources (coal, oil, gas and nuclear fuels) that cannot be regenerated by the environment in a period of time comparable to their use. Alternatively, a potential definition of an energy vector is human-made energy that is intended to replace a primary energy source at a required place and time.²⁵ In recent history, coal, oil and natural gas have been the go-to energy vectors backing up for most of our energy systems. Other energy vectors include electricity, hydrogen (H₂), synthetic fuels (methanol, ethanol, biodiesel, biogas, syngas), heat transfer fluids (low viscosity mineral oils), mechanical vectors (mechanical, oil-dynamic and pressure-dynamic transmissions) and radiation. Each energy vector transports energy under a different form, either chemical, electric, thermal, mechanical or radiative. In addition, energy vectors are not strictly replaceable with one another as each possesses its intrinsic limitations on its transportation and storage potential. A brief overview that does not take into account the storage efficiencies of the mentioned energy vectors transportation and storage capabilities is found in Figure II-6.

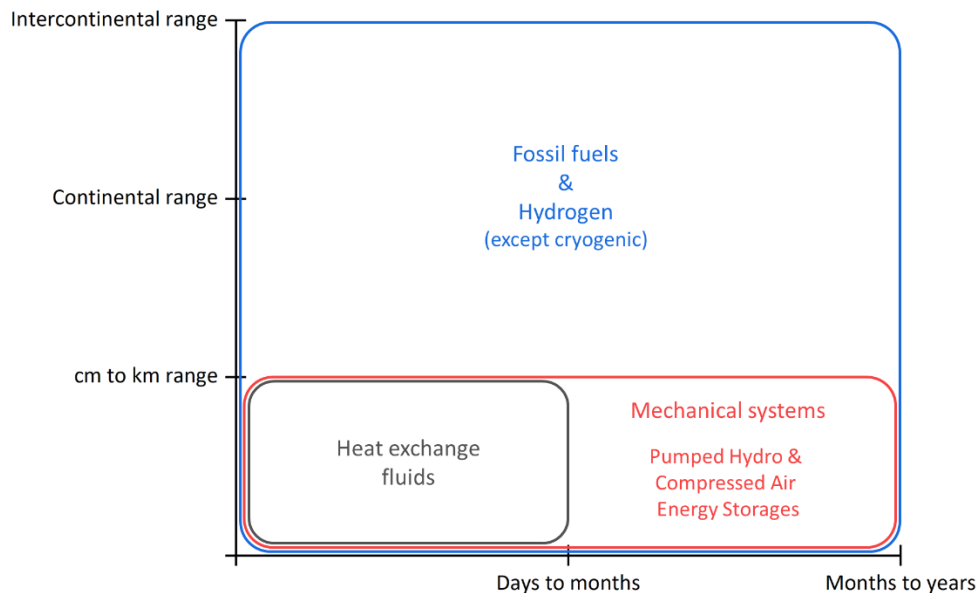
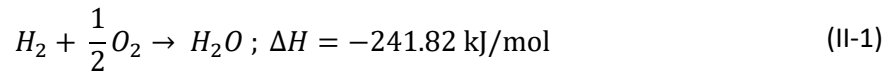


Figure II-6 - Transport range and storage time of energy vectors. Electricity and radiation cannot be directly stored and thus are not included in the diagram.

Among the energy vectors, H₂ possesses a transport range and a storage time comparable to the currently employed fossil fuels depending on the employed storage technology. Mechanical systems based on physical phenomena such as compression used in Compressed Air Energy Storage (CAES)²⁶ or potential energy for Pumped Hydro Storage (PHS)²⁷ and heat exchange fluids can efficiently store energy, but their transportation properties of the stored energy are limited. Conversely, electricity under the form of electrons can only be stored in limited amounts by supercapacitors with high self-discharging rates.²⁸ Hence conversion of electricity is usually needed to indirectly store it in electrochemical devices such as batteries (Li-ion, Pb acid, NaS, ...).²⁹ Finally, radiation such as light cannot be stored; it has however the theoretical highest transport range in vacuum, making it the best energy vector for interplanetary energy transfer.³⁰

II.2 Hydrogen as an energy vector

As presented in the Figure II-6, H₂ presents transportation and storage properties similar to that of fossil fuels such as namely natural gas. Another interesting characteristic of hydrogen is its simple reactivity with O₂ to yield only water and heat as products of the reaction, making it virtually the environmental-friendliest technology (II-1).



Moreover, as seen previously, the implementation of intermittent renewable energies imposes the storage of large quantities of energy (in the TWh range) over a long duration (monthly to yearly) to cover seasonal variations. Fortunately, H₂ possesses a high mass energy density of 120 MJ/kg, about three times more than methane and other hydrocarbons.^{31,32} However, as H₂ is a gas at normal temperature and pressure, it presents greater barriers of implementation compared to current liquid fuels: its density is minimal (0.09 g/L under normal conditions of temperature and pressure), causing a necessary concentration of H₂ in order to limit the size needed for storage.³³ Other characteristic disadvantages of H₂ are its small size which allows it to permeate out of containers, its reactivity with metals that commonly constitute pipelines such as steel, leading to embrittlement and potential ozone depletion if released in significant quantities.³⁴⁻³⁷ Thus, the energy density of hydrogen must be increased and these preliminary considerations must be taken into account.

Despite these limitations, H₂ is globally considered as fitting to store energy for the long term or to use as a secondary energy source for out-of-network applications and to make it new contender for large-scale energy storage systems. Pushed forward by carbon regulations, H₂ is becoming an opportunity to achieve a clean and secure energy future and its deployment is supported by different policies in various countries (Figure II-7).²⁸

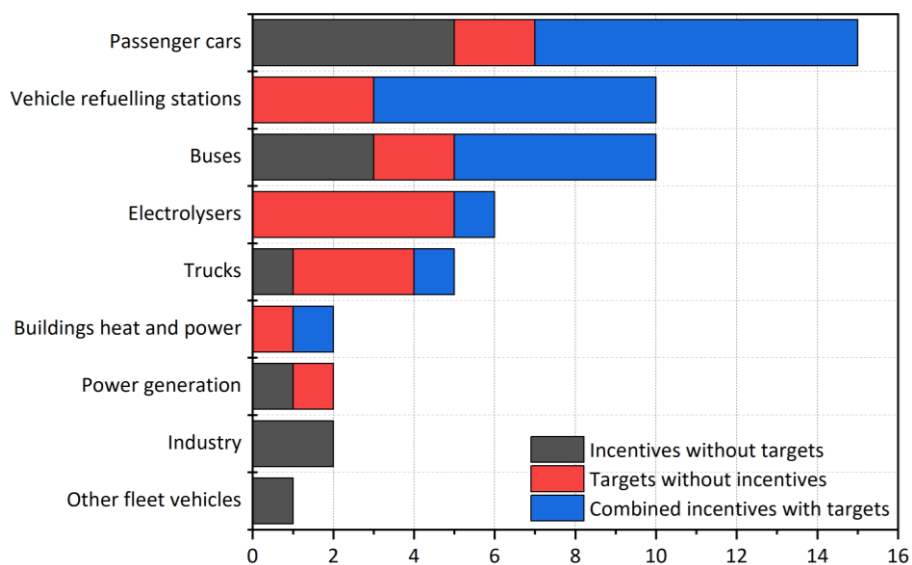


Figure II-7 – Number of policies around the world supporting hydrogen deployment, International Energy Agency, 2018.²⁸

From this assessment, it is clear that building a hydrogen economy faces mainly financial and technological barriers. Hence, understanding of the key steps of the H₂ economy chain value is primordial, especially the production of H₂ and its storage, in order to boost its competitiveness. The production of H₂ will be covered to give a brief overview of the currently available technologies before focusing on the H₂ storage technologies.

II.3 H₂ generation

Except in some rare occurrences, pure H₂ is unavailable in nature due to its low density allowing it to leave the atmosphere.^{39–41} Therefore, H₂ needs to be produced from resources in the environment. Current H₂ production principally relies on converting non-renewable feedstock such as coal, natural gas (NG) and oil while only 5% is produced by renewable sources like water electrolysis and biomass as presented in Figure II-8.^{42,43}

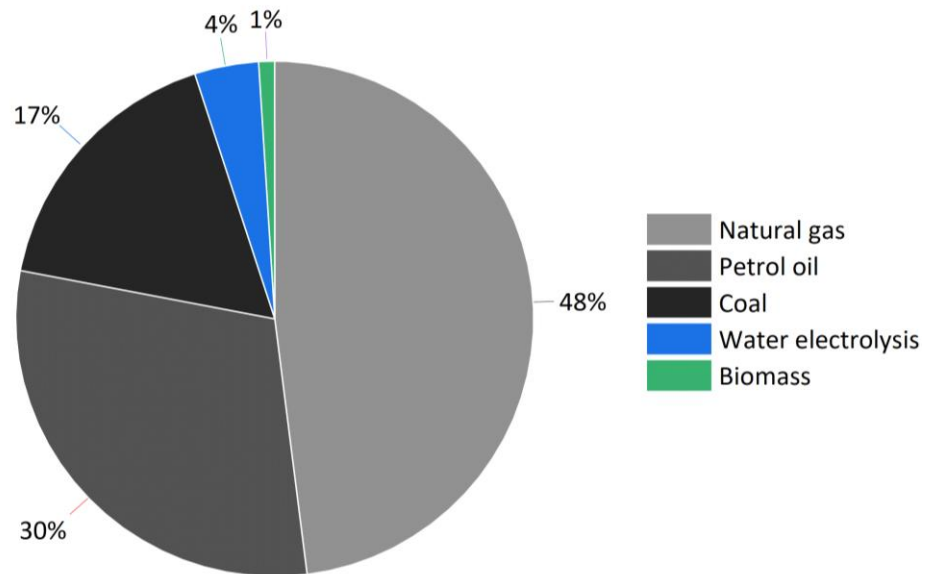


Figure II-8 – Feedstock repartition for the production of H₂, adapted from ^{42,43}.

This section will review the different technologies available to produce hydrogen and their potential with regard to the energy transition.

II.3.1 Non-renewable H₂ production (grey/brown hydrogen)

On the non-renewable side, three main reforming processes are currently employed to produce H₂ and carbon monoxide (CO) from fossil carbonaceous substrates in presence of a catalyst: steam (methane) reforming (SMR), partial oxidation of hydrocarbons and autothermal reforming.^{44–47} Further refinement of CO can be performed by the water-gas-shift reaction (WGSR) in order to produce a supplementary equivalent of H₂ and CO₂. Here, the main issues with these processes come from the concomitant production of CO₂ as well as their high energetic cost due to the high pressure (up to 100 bar) and temperature (500-1500 °C) required for the reactions to occur. Although carbon capture and sequestration (CCS) at the exhaust is getting more prominent, it does not intrinsically solve the thermodynamics issue and the efficient valorization of the CO₂ is yet to be addressed.⁴⁸ More recently, the pyrolysis of hydrocarbons is being rapidly developed as it is theoretically able to cleanly produce solid carbon and H₂ at a reduced energy cost (38 kJ/molH₂) compared to water electrolysis (285 kJ/molH₂) (see II.3.2).^{49,50} As no CO₂ is formed during the process and solid carbon can be valorized in different fields (e.g. soil enhancer), this technology is promising and companies like BASF are planning for industrialization in 2025.⁵¹ However, critics are also rising due to the use of methane (CH₄) as the hydrocarbon feedstock. Indeed, as CH₄ emissions play a huge role in global warming, the hydrocarbons pyrolysis would be yielding beneficial effects only if the global CH₄ emissions diminish faster than the decarbonization of the electricity.⁵² Finally, all hydrocarbon-based processes are dependent on the quality of the feedstock. In particular, sulphur can poison the catalytic surfaces and react with H₂ to form H₂S, decreasing the purity of the gas and the overall efficiency of the reaction.

II.3.2 Water electrolysis (blue hydrogen)

Water electrolysis was discovered in 1789 by Jan Rudolph Deiman and Adriaan Paets van Troostwijk by producing electrostatic discharge between electrodes immersed in water.⁵³ While industrial interest sparked in the 1920s and 1930s, only recently has it been rediscovered as a convenient way to convert the intermittent electricity produced by renewable energies.⁵⁴ Water electrolysis is considered as eco-friendly due to the lack of direct CO₂ emissions in the process. However, the electric sources used to power the cell and the significant amount of power needed play a huge role in the environmental impact of the process (hydro, wind, sun, nuclear versus gas, oil, coal).^{42,55} As the price of renewable electricity is plummeting, decarbonization plans in Europe are promoting water electrolysis as the leading technology to produce renewable H₂. In the wake of this trend, huge electrolysis facilities are being built around the world.⁵⁶

Nowadays, water electrolysis is an umbrella term for different electrolysis technologies, namely alkaline⁵⁷, polymer electrolyte membrane (PEM) technologies based on the transfer of protons⁵⁸ or anions⁵⁹ and solid oxide electrolyte (SOE)⁶⁰. On a general basis, these technologies are based on the application of an electric current to dissociate the atoms of H₂O and then recombine them to form high purity H₂ and O₂ (II-2).



From a thermodynamic standpoint, this reaction is endothermic and nonspontaneous (see (II-1)). In standard conditions, a thermodynamic potential of 1.23 V is sufficient to produce H₂. However, the irreversible energy costs to the operation of the electrolysis cell must be taken into account like the slow formation of oxygen compared to hydrogen and ohmic losses due to resistances in each component of the circuit, in particular the resistance of the electrolyte. Therefore, the power-to-H₂ efficiency depends on the employed technology: 60-70% for alkaline electrolysis, 60-80% for PEM electrolysis and 40-60% for SOE electrolysis.⁶¹ However, with a supplied external heat of 150-180 °C to generate steam, up to 95% power-to-hydrogen efficiencies could be obtained for SOE electrolysis.^{62,63} Finally, the alkaline electrolysis is currently the only commercially available technology while the PEM electrolysis should be available in the near future and SOE electrolysis is yet to be fully developed.

II.3.3 Renewable H₂ generation (green H₂)

Renewable sources of H₂ can be separated into distinct classes as the production of H₂ can be obtained either by transformation of a renewable resource or conversion of renewable energy into H₂. It is important to notice that most of these renewable H₂ sources can act as energy storage systems, but of low capacity and/or only on a short-term basis.

Biomass usage possesses numerous beneficial environmental, social and economical aspects such as restoration of degraded lands, poverty reduction and CO₂ entrapment in carbon wells. Its conversion through various processes holds great promises for sustainable H₂. Biological processes are based on anaerobic digestion⁶⁴ and fermentation followed by alcohol reforming^{65,66}. These technologies are promising, but work only in optimal conditions and/or with little outputs. Other renewable H₂ technologies revolve around biomass thermochemical processes such as pyrolysis⁶⁷, gasification⁶⁸ and supercritical water gasification⁶⁹. As thermochemical processes are closer to the current industrial processes, they gather great interest. However, as numerous intermediate species can be produced, liquid and gas purification costs might be a major hurdle for these technologies.

II.3.4 Cost comparison of H₂

The cost comparison of the different technologies used to produce H₂ is presented in Figure II-9.⁷⁰⁻⁷⁹

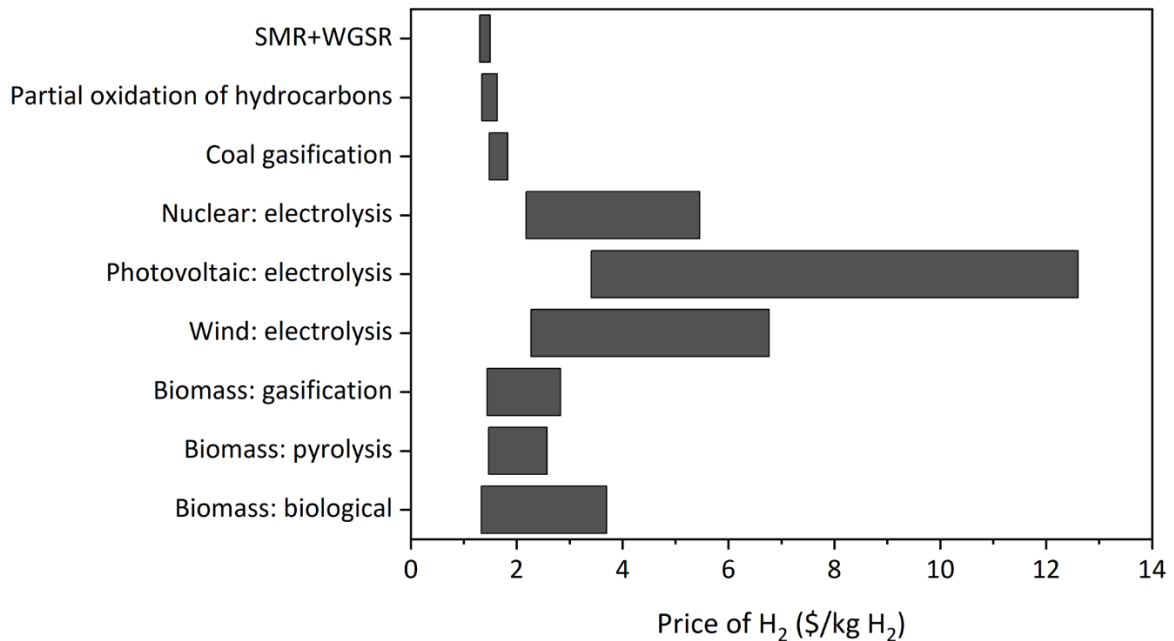


Figure II-9 – Process-dependent price of H₂, adapted from ⁷⁰⁻⁷⁹.

As numerous apparatus exist for each process, some variations in the hydrogen cost can be found for the same technology. Currently, the combined technologies SMR+WGSR without CCS is the cheapest energy source to industrially produce H₂. Here, it is worth noting that H₂ is nowadays proposed to store the excess of intermittent renewable energies; therefore, the price of H₂ issued by this process would need to be drastically increased to be competitive with non-renewable H₂ production costs. Moreover, recent market price variations have also to be taken into account due to the addition of new legislations, environmental and global tensions.

Nevertheless, most articles in the literature limit their framework to the economic aspects of the technologies. To overcome this bias, a recent contribution from Al-Qahtani et al. suggests to take into account external factors into the price of H₂ such as the costs on human health, ecosystem quality and resource depletion by using life cycle monetisation. The cheapest energy source for H₂ production was still SMR+WGSR with direct carbon capture for 5 \$/kgH₂. Nevertheless, the most efficient energy sources with regard to the external factors were nuclear power, wind power and solar power where 86%, 77% and 86% respectively of the H₂ cost was due to the selected technology.⁸⁰ The cost diminution of renewables should then play a key role in increasing their competitiveness for H₂ production.

II.4 State-of-the-art hydrogen storage technologies

Once produced, H₂ needs to be stored if not readily used. However, economic H₂ storage is not straightforward due to its abysmal density: 11 m³ (size of a trunk of a big utility vehicle) would be required to store 1 kg of H₂, whose energy is equivalent to driving in a car for 100 km. Many H₂ storage technologies aim at concentrating H₂, based either on the physical properties of H₂ (compressed gas (CGH₂), cryogenic liquid (LH₂) and underground storage systems (UHS)) or on chemical properties of materials (physical adsorbents, metal hydrides, B-N H₂ carriers, circular H₂ carriers and liquid organic H₂ carriers) as presented in the Figure II-10.

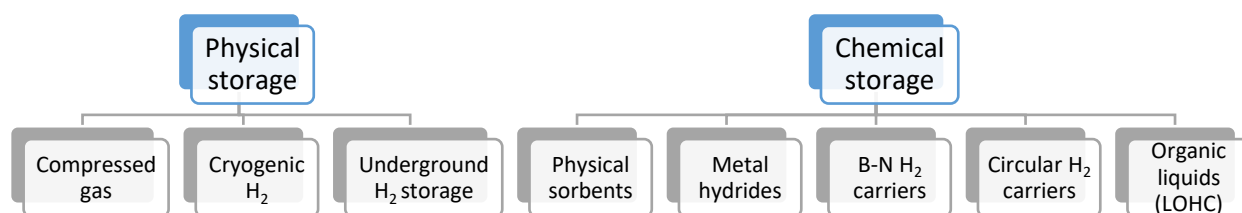


Figure II-10 - Reviewed H₂ storage technologies.

Each technology will be briefly reviewed and a focus will be made on liquid organic hydrogen carriers (LOHC). Technologies can always be compared by the H₂ weight storage density (wt.%H₂) and the H₂ volumetric storage density (gH₂/L), but, depending on the encompassed element of the storage system, the said densities can be drastically modified. Here we will only focus on the theoretical maxima of the hydrogenated species for chemical systems.

II.4.1 Physical-based hydrogen storage

Physical H₂ storage technologies are based on controlling external parameters such as the pressure and temperature to concentrate H₂, leaving the H₂ molecule unmodified.

II.4.1.1 Compressed gas H₂ (CGH₂)

Compressed gas H₂ (CGH₂) in steel cylinders is the most frequent H₂ storage technology, storing a pressure of 200 bar (16.8 gH₂/L, without the weight of the system). In theory, a continuous increase of the H₂ pressure is the simplest way to improve the storage efficiency, providing that pressure-resistant materials are available. However, the H₂ volumetric density is not linearly correlated with its pressure and technical as well as economic restrictions limit the compression well below pressures equivalent to cryogenic H₂ storage (2000 bar, 70 gH₂/L, see II.4.1.2).⁸¹ As a compromise between energy need and costs, the industry targets a pressure of 700 bar H₂ with a total H₂ and container system mass of 125 kg (including H₂) using light-weight polymer fiber-reinforced vessels. Such systems could reach a weight density of 5 wt.%H₂ and a volumetric density of 30 gH₂/L, appropriate for personal vehicle transportation.⁸² While this solution is practical and applied in various fields like heavy-duty transportation, it poses safety issues in case of violent breach of containment or uncontrolled accumulation of H₂ in an enclosed space like an underground parking.⁸³ Finally, reaching a pressure of 700 bar of H₂ has a non-negligible energy cost. In ideal isothermal conditions, 2.21 kWh/kgH₂ are needed to compress H₂ from atmospheric pressure to 700 bar. As the compression is not isothermal in real conditions due to self-heating upon applying pressure, the compression cost is significantly higher (up to 4 kWh/kgH₂, more than 10% of the energy stored).^{84,85}

II.4.1.2 Liquid H₂ (LH₂)

Hydrogen is a gas that reaches its liquefaction point at -252 °C, with volumetric density of 70.8 gH₂/L and a system weight density up to 90 wt.%H₂ depending on the container.⁸⁶ However, liquefaction of H₂ is not trivial due to its specific properties (inverse Joule-Thomson effect).⁸⁷ Moreover, gas phase H₂ is present under two forms depending on the nuclear spin alignment of its individual atoms (75% ortho) or not (25% para) while liquid phase H₂ is stable at 99.8% in the para form, leading to the necessary conversion from ortho to para.⁸⁷ Unfortunately, this conversion is slow and exothermal ($\Delta H = 525$ kJ/kg), which leads to the unavoidable evaporation of H₂ (latent heat of vaporization = 476 kJ/kg), also called boil-off.⁸⁸ To facilitate this slow conversion during the cooling process, a catalyst is often integrated in the heat exchanger.⁸⁹ If this phenomenon is not accounted for, the pressure could drastically increase in a closed system, hence LH₂ storage must be kept open to avoid disastrous events.⁹⁰ Open systems pose the question of efficient thermal insulation, with current systems losing roughly 1.5 wt.%H₂/day. Finally, current industrial liquefaction plants consume between 13 and 15 kWh to produce 1 kg of LH₂ (40 to 45% of the stored energy) and are not expected to drop below 5 kWh/kg LH₂ (15% of the stored energy).⁸⁷ Thus, the energetic cost of liquefaction is prohibitive for large-scale deployment and, while early projects targeted car mobility, LH₂ will probably be used only for specific energy-intensive applications like rockets.^{91–93}

II.4.1.3 Underground H₂ storage

Underground H₂ storages (UHS) is a potential large-scale mid to long-term stationary storage technology. Underground geological structures like empty gas or oil reservoirs, aquifers and salt caverns can act as a gas vessel to store pressurized pure H₂ or a mixture of gases that contain H₂. An appropriate UHS possesses a solid rock formation and an inert impermeable layer to prevent H₂ leaks as H₂ can slowly react with the minerals composing the UHS to form carbonates.⁹⁴ UHS also have to withstand an internal pressure of 30 to 80% of the lithostatic pressure in order to limit H₂ leaks.⁹⁵ For the time being, only 4 artificial salt caverns are exploited worldwide.⁹⁶ For example, the most massive salt cavern (Spindletop, USA) occupies a volume of 906 000 m³ for a pressure reaching up to 200 bar (16.8 gH₂/L) and could in theory store up to 500 GWh of H₂, roughly 0.02% of the yearly French primary energy consumption in 2020.⁹⁷ Salt caverns are the most efficient UHS, but represents only 8% of the worldwide capacity. Finally, while highly promising, UHS are especially sensitive to geological events like earthquakes, challenging to conceive/monitor, limited to specific geological conditions and are in competition with other underground gas storage systems like CAES or CO₂ storage.

II.4.2 Chemical-based hydrogen storage

The modification of the physical properties of H₂ such as its temperature or pressure increases its energy density, but requires a high energetic cost in order to reach efficient storage. A decrease of this energetic cost (equivalent to more than 10% of the energy stored for 700 bar CGH₂ and between 40 to 45% for LH₂) is necessary if H₂ is to become a competitive energy vector. Hence finding new materials able to store H₂ by forming bonds ranging from weak Van der Waals interactions to covalent bonding has been an ongoing topic of research over the past decades. The main technologies of chemical-based storage will be reviewed hereinafter.

II.4.2.1 Physical sorbents

Physical sorbents can be compared to sponges for gaseous H₂ where molecular H₂ is adsorbed by physisorption on the surface of microporous materials by Van der Waals interactions. H₂ adsorption is usually carried out at cryogenic temperature and high pressure (20-200 bar) for better performances. However, the main issue resides in the fact that these materials must be kept at cryogenic

temperatures and high pressures to be able to store high quantities of H₂, increasing over time the energy cost of the storage. Moreover, the H₂ intake is not linear with the increased pressure as a strong adsorption is usually observed at low pressures (up to a few bars) where capillarity or monolayer phenomena take place in the structure micropores. The intake increases slowly at higher pressures as all micropores are filled or multiple gas layers start to stack on top of each other, creating a non-adsorbed gas phase.⁹⁸ By heating up the material to room temperature or above, pure H₂ can easily be collected with only small amounts of H₂ trapped in the structure. Finally, serious doubt has been casted on the validity of early results of physical sorbents for H₂ storage. Indeed, the lack of reproducibility and high gravimetric H₂ storage were linked to gas leaks and to adsorption of molecules of higher molecular weight like water.⁹⁹ Current materials used for the physisorption of H₂ are carbon nanomaterials (nanotubes, activated carbon, nanofibers, fullerenes and so on), polymers of intrinsic microporosity (PIM), covalent-organic frameworks (COF), metal-organic frameworks (MOF), zeolites and water clathrates. The characteristics of each family of materials will be briefly described.

II.4.2.1.1 Carbon nanomaterials

Carbon nanotubes (CNT), activated carbon, nanofibers, fullerenes and graphenes are able to store H₂, but this property is heavily dependent on their structure, geometry, operating temperature, pressure and other parameters of the material. These materials possess multiple complex H₂ adsorption sites that lead to extremely variable H₂ capacity with a theoretic maximum of 10.8 wt.%H₂ at 77 K and 60 bar.¹⁰⁰ However, it has been shown that the same material can produce inconsistent results. For example, a K-doped CNT was reported to store 1.8 wt.%H₂ and 14 wt.%H₂ in the same operating conditions.^{101,102} In addition, work by General Motors reveal that all H₂ capacities above 1 wt.%H₂ are probably due to experimental errors attributed to leaks.¹⁰³ Thus, the usual storage capacity at room temperature and high pressure is usually below 2 wt.%H₂.¹⁰⁴ Higher storage capacities can be reached when adsorption is conducted at cryogenic temperatures, with capacities of 6.5 wt.%H₂ reported for activated carbon.¹⁰⁵ Chemisorption as π -bonding on aromatic cycles is possible when treated at extreme pressures (>500 bar) and high temperatures (500-600 K), adding one more H₂ molecule per aromatic cycle.¹⁰⁶ Desorption happens around 400 K, but the extreme conditions for H₂ chemisorption prevent it from being a viable H₂ storage method.¹⁰⁷

II.4.2.1.2 Polymers of intrinsic microporosity

Microporous polymers (PIM) are able to store H₂ due to their rigid structure that forms interconnected cavities in the nanometer range, facilitating the H₂ adsorption.¹⁰⁸ Their intrinsic advantages are their easy customization by varying the monomer structure, their lightness, low-cost and simplicity to process. Nonetheless, they suffer from disadvantages similar to that of carbon nanomaterials as they require cryogenic temperatures and higher pressures to store relevant H₂ amounts. Indeed, PIM can absorb up to 1.4 wt.%H₂ at 1 bar and 77 K, increased to 1.7 wt.%H₂ at 10 bar.¹⁰⁹ PIM showed improved properties when mixed with another physical sorbent, exhibiting up to 2.5 times more H₂ adsorption and is the current research focus for this technology.¹¹⁰

II.4.2.1.3 Covalent-organic frameworks and Metal-organic frameworks

Covalent-organic frameworks (COF) are rigid porous structures composed of organic molecules that are linked together by covalent bonds and are used for gas adsorption, separation and catalysis like pesticide degradation.^{111,112} Due to their organic nature, COF are extremely light, low cost, highly stable and show great structure versatility in both 2D and 3D networks with different cavity sizes able to accept various molecules.¹¹³ H₂ adsorption in the structure can be achieved, usually at cryogenic temperatures (77 K) and at high pressures (20-100 bar). Temperature is the main factor contributing to their performance, as increasing the temperature above cryogenic levels drastically reduce their H₂ adsorption capacity. To this date, a variation of the COF-102 show impressive gravimetric and

volumetric densities of 25 wt.%H₂ and 43 gH₂/L at 77 K and 100 bar. However, room temperature H₂ adsorption measurements on the same material show decreased densities of 6 wt.%H₂ and 10 gH₂/L.¹¹⁴ Doping the structure with metal ions was proposed in computational studies to improve the H₂ capacity at room-temperature, but no practical study has been reported so far.¹¹⁵

Similar to COF, Metal-organic frameworks (MOF) are composed of metallic single atoms or clusters linked together by organic molecules, forming a porous crystalline structure able to adsorb H₂ at cryogenic temperatures (77 K) and at high pressures (20-100 bar) depending on the cavity sizes and affinity with the metal and/or the organic linkers.¹¹⁶ The current best H₂ adsorption MOF is DUT-32 with a gravimetric density of 14.21wt.%H₂ at 77 K and 82 bar.¹¹⁷ Addition of a metal catalyst in the structure and a porous support like activated carbon could favor hydrogen spillover, where H₂ is split into atoms and is incorporated to the support, allowing for room temperature H₂ storage. While numerous publications reported a significant improvement of the hydrogen storage properties, spillover was heavily dependent on a number of inconsistent parameters, creating irreproducibility and even questions about improvement of MOF by spillover.¹¹⁸⁻¹²⁰

II.4.2.1.4 Zeolites

Zeolites are crystalline materials defined by their network of pores and have been used for decades as sorbent materials and molecular sieves.¹²¹ H₂ absorbing zeolites are composed of aluminosilicate porous structures with dimensions comparable to that of carbon nanotubes. Moreover, the charge of the framework is counterbalanced by metal cations that are readily exchangeable, which enable the tuning of the properties of the zeolite. H₂ absorption is believed to follow two mechanisms depending on the temperature. At high temperature, encapsulation is the preferred mechanism: the openings of the zeolites are thermally activated which forces the absorption of H₂ in the structure and the following cooling traps H₂.^{122,123} However, this mechanism does not substantially increase the amount of H₂ stored in the structure as only a maximum of 0.8 wt.%H₂ absorption was reported.¹²² At room temperature, the zeolite entrances were not activated, requiring high pressures to force H₂ in the structure, leading to poor performances (<0.1wt.%H₂).^{123,124} Better results were obtained when cooling the zeolite to cryogenic temperatures, with a maximum of 2.19 wt.%H₂ for a CaX zeolite at 77 K and 15 bar.¹²⁵ Nevertheless, the theoretical maximum storage capacity was calculated to be less than 3 wt.%H₂ which limits the efficiency of this storage technology.¹²⁶

II.4.2.1.5 Clathrates

Clathrates are supramolecular materials able to trap H₂ in cavities formed by water molecules, without being covalently linked to them.¹²⁷ Pure H₂-water clathrates can be formed and stabilized at cryogenic temperature (77 K) or extreme pressures (150 bar to 23 kbar reaching densities of 5.5wt.%H₂ and 45 gH₂/L.^{128,129} The addition of small amount of promoters like tetrahydrofuran (THF) stabilized the clathrates while limiting the temperature and pressure conditions for storage at the cost of a H₂ storage capacity reduced to 1-2wt.%H₂ or less depending on the pressure.¹³⁰ Except for pure H₂-water clathrates that are formed and stored in extreme conditions, the performance of hydrates clathrates do not deviate from other physical sorbents.

II.4.2.2 Metal hydrides/Interstitial hydrides

Metal hydrides are solid-state materials that attracted very early attention for individual transportation due to the reversible H₂ absorption properties of metals M at high temperature (II-3) in less than an hour.¹³¹ The dehydrogenation reaction produces in the same time-scale the original metallic phase and H₂ with its kinetics being controlled by the temperature, the pressure and presence of a catalyst.¹³² In addition, some Mg-based metal composite hydrides can be cycled up to 2000 cycles with good reversibility without major decrepitation due to the scaffolding effect of the composite.¹³³



In general, hydrides are heavy materials with low gravimetric and volumetric densities. Moreover, they are air- and water-sensitive (pyrophoricity) as oxygen tends to slowly evolve hydrogen to produce oxides, hydroxides and carbon-oxygen compounds in the form of a surface passivation layer. Removal of this layer with H_2 at high temperatures is necessary in order to increase the hydrogenation kinetics.^{134–136} Sulphur compounds are also a common poison.¹³⁷ Finally, these materials consume a non-negligible amount of metals and their solid-state complicates its handling from an industrial standpoint.

Metal hydrides can be grouped in low-temperature hydrides, high-temperature hydrides and complex hydrides depending on their desorption temperature and composition. A brief overview of the properties of each class of materials will be presented.

II.4.2.2.1 Low-temperature hydrides

Low temperature metal hydrides, also known as intermetallic hydrides, can release H_2 close to room temperature and atmospheric pressure, which is advantageous as almost no energy is required to harness H_2 but also a drawback due to safety issues in case of undesired heating.¹³⁸ Intermetallic hydrides are synthesized from a mixture of high hydrogen affinity elements “A” like Ca, Sc, Y, Ti, Zr and other lanthanides and low affinity elements “B” like Cr, Mn, Fe, Co or Ni that act as dissociation promoters to create ternary $A_xB_yH_n$ materials.¹³⁹ During the absorption, H_2 is dissociated in H atoms on the surface and form covalent bonds before migration in the bulk of the material by atomic diffusion to the interstitial sites of the lattice.¹³⁴ Therefore, the defined crystalline structures (AB_5 , AB_2 , A_2B , ...) play a primordial role in the H_2 adsorbing properties as the size of their interstitial sites is phase-dependent.¹⁴⁰ However, due to their weight, the maximum energy density of intermetallic hydrides stays usually below 2 wt.% H_2 , far from the necessary 6 wt.% H_2 for mobility applications according to the United States Department of Energy (DOE).^{141,142}

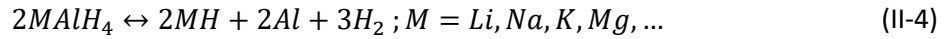
II.4.2.2.2 High temperature hydrides

High temperature metal hydrides require desorption temperatures above 200 °C to break the ionically bound hydrogen atoms. Most high temperature hydrides are based on magnesium and its alloys due to its lightness, abundance, low cost and good reversibility. The most studied one is MgH_2 , which possesses a high weight density of 7 wt.% H_2 . Unfortunately, this material requires a temperature of at least 300 °C to harness H_2 due to its high stability, slow kinetics and sensitivity to decrepitation.^{143,144} Alloys of high temperature metal hydrides with transition metals like Ti, V, Mn, Ni and Fe have shown improved thermodynamics, H_2 uptake/release kinetics and stability by promoting the dissociation/recombination of H_2 .¹⁴⁵ Nanostructuring the metal hydride is also a conventional technique to decrease the size of the metal clusters to the nanometer range in order to improve the thermal and mechanical stability, thermodynamics and kinetics.^{146–148} Finally, akin to nanostructuring, nanoconfinement relies on the nano-scale properties of hollow light-weight nano-porous chemically inactive materials like carbon-based materials, mesoporous silica, zeolites and MOFs to promote H_2 physisorption, H_2 dissociation, desorption thermodynamics and kinetics and stability by limiting the agglomeration of the metal hydride nanoparticles.^{149–151}

II.4.2.2.3 Complex hydrides

Over the past two decades, complex hydrides containing only low molecular weight atoms have been heavily studied.¹⁵² Compared to the desorption temperature of low-temperature metal hydrides (room temperature to 100 °C) and high-temperature metal hydrides (200-300 °C), their intermediate desorption temperature (100-200 °C) presents a good compromise between safety and energy efficiency. Such desorption temperatures are achieved by exploiting the versatile nature of the

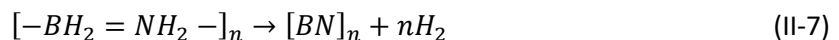
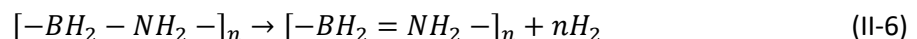
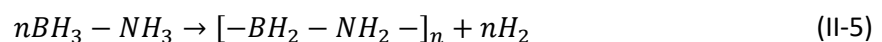
hydrogen atom that can act as both a cation H^+ and an anion H^- . Indeed, H_2 is stored in complex hydrides by a mix of ionic and covalent bonds, usually forming tetrahedrons with boron or aluminium at the center and hydrogen atoms at the corners while the charge is balanced by one or more spectator cations like Li or Na. The dehydrogenation process is heavily dependent on the metallic center, however it typically consists in the formation of a pure metallic phase and a cation-hydride phase, e.g. in the case of alanates (II-4):



In general, complex hydrides are synthesized by mechano-chemistry like ball milling which limits their industrialization. In addition, they present a high chemical risk as they are highly reactive in the presence of water and then must be used only in anhydrous conditions.¹⁵³ Moreover, reversibility can be limited due to the lack of hydrogen-deficient intermetallic compounds and the formation of multiple phases during the dehydrogenation.¹⁵⁴ Thus, efficient regeneration procedures are still in development to further develop this technology. Complex hydrides can be grouped depending on their metallic anion. Alanates like $NaAlH_4$ ^{155,156} (7.4 wt% H_2 and 67 g H_2 /L) and borohydrides like $LiBH_4$ ¹⁵⁷ (18.5 wt.% H_2 and 122 g H_2 /L) are the most studied complex hydrides, but new amide-hydride composites like $Li(NH_2)\text{-}2LiH$ ¹⁵⁸ (10 wt.% H_2 and 104 g H_2 /L) are presenting promising properties.

II.4.2.3 B-N H_2 carriers

B-N hydrogen carriers are composed of two key atoms: boron that acts as a metallic center for hydrides and nitrogen for protons. Ammonia-borane (AB) was initially proposed as an alternative to borohydrides due to its high gravimetric and volumetric densities (19.4 wt.% H_2 and 144 g H_2 /L resp.).¹⁵⁹ As AB is a solid, liquid phase dehydrogenation of AB is carried out in a protic solvent like water or methanol. However, this hydrolysis or alcoholysis induces the formation of oxidized dehydrogenated boron species that require a harsh regeneration with the extensive use of strong hydrides or other complex processes.^{160,161} The dehydrogenation of solid AB can be achieved by thermolysis. Heating up to 100 °C is sufficient to dehydrogenate AB to linear, branched or cyclic polyaminoborane species depending on the reaction environment (II-5).¹⁶² Two other H_2 equivalents can be produced when increasing the temperature to 120-130 °C and 500 °C in order to form polymeric borazine (II-6) and boron nitride (II-7) respectively.^{163,164}



As boron nitride is a very stable chemical, the dehydrogenation is usually limited to the first two steps to ensure the regeneration of the material, diminishing the effective densities to 12.9 wt.% H_2 and 96 g H_2 /L. In addition, side-products like ammonia and other boron and nitrogen containing gaseous products have been reported in large quantities (>20 wt.% of the AB weight) due to AB decomposition.¹⁶⁵ However, as the mechanism of degradation is heavily dependent on the conditions of reaction (solvent, solid-state, ...), it is not yet fully elucidated. AB solubilization in an aprotic solvent like ionic liquids improved the dehydrogenation as the solvent disrupted the proton-hydride intramolecular bonding and limited the carrier oxidation.¹⁶⁶ Similarly, dopant addition diminished the induction period and increased the kinetics and selectivity of dehydrogenation.¹⁶⁷ Nanoconfinement of AB in a nanostructure acted in the same fashion than metal hydrides (see II.4.2.2.2).¹⁶⁸ Lastly, the incorporation of alkali, alkaline-earth or metals (Al) to the AB structure created heavier amidoboranes, where the partial replacement of the protons by a more electropositive element increased the selectivity and dehydrogenation kinetics at the cost of a portion of the H_2 capacity.¹⁶⁹⁻¹⁷¹

II.4.2.4 Circular hydrogen carriers

Circular hydrogen carriers store H₂ through chemical bonds on small gaseous molecules like N₂ or CO₂ to form respectively Ammonia or Methanol. Other products like Hydrazine, Formic acid, Formaldehyde, Methane, Dimethylethers, Carbonates or Carbamates are also circular hydrogen carriers but they will not be discussed due to their comparatively low technological development.

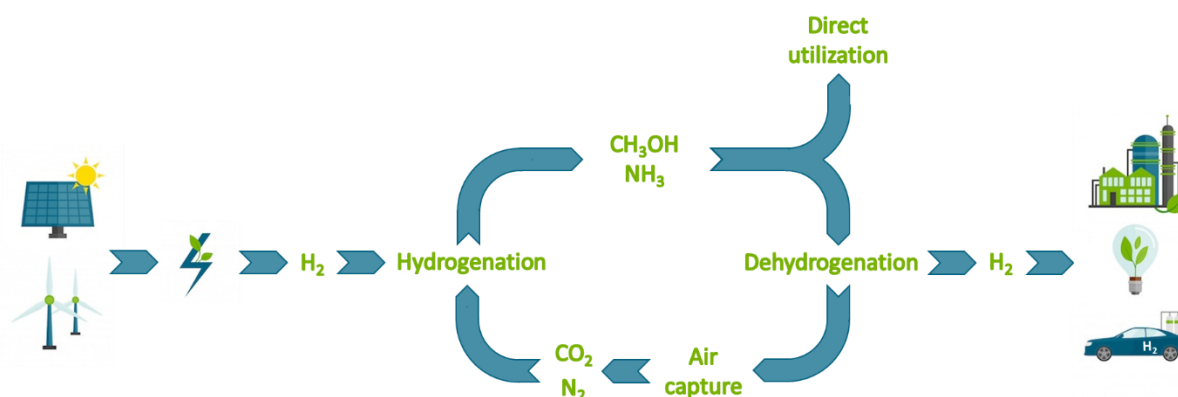


Figure II-11 - Key steps of the circular hydrogen carriers value chain.¹⁷²

The main advantage of circular H₂ carriers is their convenient transportation properties that allow for the production of H₂ at a place of convenience where the lean-carrier that can be captured before recycling. In addition, the hydrogenated carriers are also high value chemicals that can also directly be used in chemical processes but H₂ will not be retrieved in that case. The main issue revolves around the necessary gas separation and purification of the lean-carriers from H₂ during the dehydrogenation as well as large-scale gas handling.

II.4.2.4.1 Ammonia (NH₃)

Ammonia (NH₃) is a valued chemical for the synthesis of fertilizers that can act as an energy vector able to store H₂ in liquid form with good gravimetric (17.8 wt.%H₂) and volumetric (107 gH₂/L) densities when pressurized at 8.6 bar at room temperature. Current production is guaranteed by the Haber-Bosch process that produces roughly 185 millions of tons of NH₃ per year in 2020.^{173,174}

- Hydrogenation

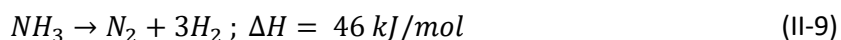
NH₃ is produced in extreme conditions of temperature and pressure from N₂ and H₂ with a low conversion of 15% per pass, thus requiring numerous cycling of the reactants to achieve complete conversion (II-8).



In addition, as presented previously (see II.3), most of the currently produced H₂ originates from fossil fuels. As a consequence, this industrial process consumes between 1 and 2% of the annual global energy production and generates 3 equivalents of CO₂ per 8 equivalents of NH₃.^{175,176} Nevertheless, as this process is almost completely optimized, CO₂ mitigation can only happen by developing low-carbon H₂ sources (water electrolysis instead of SMR) and by implementing CCS. New ammonia production processes are also studied in order to create an improved disrupting process. Current alternatives require high electrical input and/or temperatures to produce ammonia via electrochemistry, either directly from N₂ with water, in a two-step process where N₂ reacts with H₂ produced by electrolysis or a Li-mediated three-step cycle where the hydrolysis of Li₃N facilitates the production of NH₃.^{177,178} However, these new processes are still energy-intensive and their scalability is yet to be demonstrated.

- Dehydrogenation

Ammonia decomposition was historically achieved at high temperatures (>400 °C) on Fe or Ru transition metal catalysts supported on alumina due to the endothermicity of the process.^{179,180}



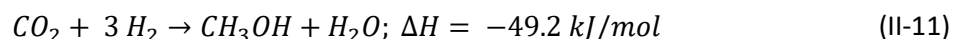
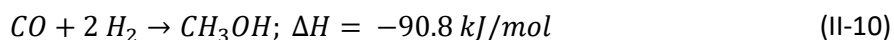
The decomposition rate is determined by the desorption of N₂ that is dependent on the active metal (Ru>Ni>Rh>Co>Ir>Fe≈Pt>Cr>Pd>Cu≈Te, Se, Pb on Al₂O₃), the support (basic and conductor like Al₂O₃, MgO, CNT, ...) and promoters (electron donors on Ru like K>Na>Li>Ce>Ba>La>Ca>pristine).^{181–183} NH₃ shows promises as a H₂ carrier, but its implementation for on-board applications is limited by the NH₃-PEM incompatibilities (high decomposition temperature, membrane poisoning, catalyst cost, NH₃ toxicity and corrosivity).¹⁸⁴ However, these NH₃-PEM incompatibilities can be partially lifted with a SOE fuel cell.¹⁸⁵ Finally, NH₃ most practical application could be massive energy transportation.

II.4.2.4.2 Methanol (MeOH)

Methanol is one of the most produced chemicals worldwide with up to 164 millions of tons per year as a number of key industrial processes rely on it to produce high value chemicals such as formic acid, formaldehyde, esters, ethers, olefins and others.^{186–189} Moreover, MeOH has also been proposed as a fuel similar to Bioethanol in the so-called “Methanol Economy”.¹⁹⁰ From a H₂ storage perspective, MeOH has excellent gravimetric and volumetric densities of 12.5 wt.%H₂ and 99 gH₂/L. In addition, due to its only carbon, β-elimination cannot take place, limiting the number of potential side-reactions.

- Hydrogenation

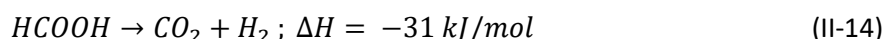
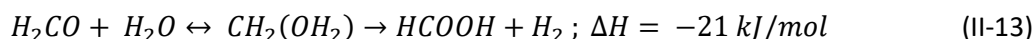
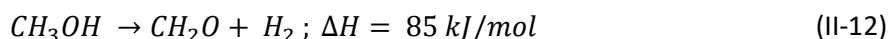
Methanol formation from either CO (II-10) or CO₂ (II-11) with Cu-based catalysts at high temperatures (300-450 °C) was reported and patented many times since the 1960s.^{191–195}



However, the harsh temperature conditions used in these processes furthered the research of process with milder conditions. Nowadays, new production processes of MeOH from CO₂ are emerging, like biogenic synthesis¹⁹⁶, amine/alkaline¹⁹⁷ or acid-assisted¹⁹⁸ CO₂ reaction, formic acid disproportionation¹⁹⁹ and gas-solid phase²⁰⁰, but the scalability has yet to be demonstrated.

- Dehydrogenation

MeOH non-oxidative dehydrogenation is a multi-step process that requires the presence of water. A first H₂ equivalent can be retrieved by its dehydrogenation to formaldehyde (II-12), then, after addition of water, 2 other H₂ equivalents can be recovered to produce CO₂ by the equations (II-13) and (II-14).



The dehydrogenation is heterogeneously catalyzed by Co, Ni, Cu, Pd, Ru, or Ir at temperatures superior to 200 °C.²⁰¹ However, CO by-production during the dehydrogenation could prove fatal to PEM fuel cells.²⁰² Direct Methanol Fuel Cells present lower energy output due to slow kinetics and fuel permeation through the membrane.¹⁹⁰ Despite its good compatibility with the current infrastructures and good biodegradability, MeOH has still a few barriers to overcome as its point of ebullition is low (64.7 °C) and its flammability and toxicity could prove too dangerous for public usage.²⁰³

II.4.2.5 Liquid organic hydrogen carrier (LOHC)

The Liquid Organic Hydrogen Carrier (LOHC) technology was developed back into the 1970s in order to store the excess of nuclear electricity via water electrolysis under the form of an automotive fuel.^{204,205} Recent developments and environmental considerations promoted this technology as a mean to store vast quantities of energy (GWh to TWh ranges) for long time duration (seasonal). Much like the circular hydrogen carriers, the LOHC are liquid molecules able to store and release H₂ at a desired place and time by catalytic hydrogenation and dehydrogenation reactions to respectively load and unload H₂.²⁰⁶

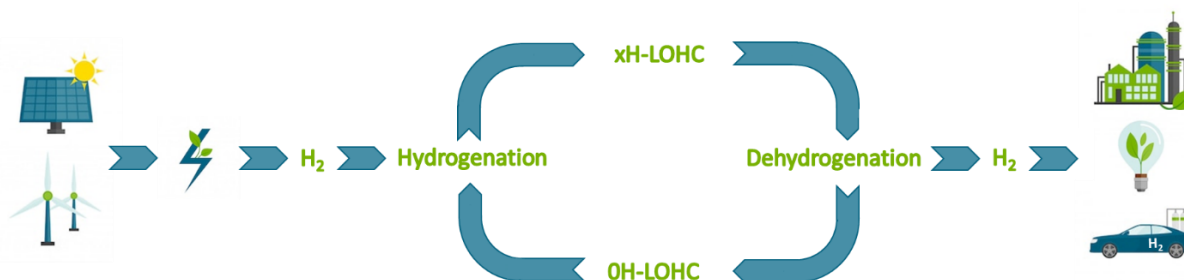


Figure II-12- Key steps of the liquid organic hydrogen carrier value chain.¹⁷²

Storing H₂ by covalent bonds on an organic liquid improves the handling and safety of the energy vector and retains similar volumetric densities compared to traditional physical systems, circumventing the need of heavy gas tanks and other cooling devices.^{207,208} The liquid-phase is also advantageous as the reaction can proceed without the dilution of the H₂ carrier in a solvent. In addition, most LOHCs are oil-like structures that can be easily transported by the current oil and gas infrastructures with small modifications to the system, eventually diminishing the implementation cost of the technology. Finally, social acceptance of the LOHC as a mobility option is favorable as the carrier system is similar to currently employed fuels.²⁰⁹

Different criteria have been proposed to assess the potential of a LOHC. The energy efficiency is often addressed through the dehydrogenation enthalpy value. Classic LOHC systems have comparatively high enthalpy values (between 50 and 75 kJ/molH₂) while the US Department of Energy (DOE) aims for 30-44 kJ/molH₂ so that the H₂ equilibrium pressure reaches 1 bar between -40 °C to 60 °C.²¹⁰ Like the other H₂ storage systems, the gravimetric and volumetric energy densities highlight the energy storage efficiency with ultimate targets of 6.5 wt.%H₂ and 50 gH₂/L for a complete on-board system respectively. An excellent stability (>99.9%) of the LOHC is also required in order to avoid the constant replacement of the carrier during the cycling.^{211,212} Finally, the LOHC must also answer to other criteria such as a high liquid temperature range, its availability or ease to mass-produce from preferentially renewable feedstock, its cost, the H₂ gas flow and quality on release (especially for fuel cells), the carrier toxicity and biodegradability.²¹³ It is important to note that the properties of the LOHC can be heavily modified depending on the application and the time-scale of storage. For example, a mobility application for individual transportation vehicles would mainly require high gravimetric and volumetric densities as well as a good cycling capacity and low dehydrogenation temperature while stationary systems (off-grid system) would be principally driven by the cost of the LOHC and its catalysts. Lastly, massive energy storage (seasonal storage) would necessitate both a low system cost and high densities.

The LOHC system possesses numerous advantages, but also drawbacks compared to other technologies. One major bottleneck is the problematic toxicity of the LOHC molecules, similar to that of currently employed fossil fuels. Moreover, the classic LOHC systems are oil derivatives, so the development of bio-based structures would be preferential. Besides, the catalysts used for the

hydrogenation and dehydrogenation reactions are generally based on platinum group metals (PGM) that are rare and expensive. Finally, the stability of the LOHC structures is a major concern, especially after multiple hydrogenation/dehydrogenation cycles.

The next part of this literature review will focus on key molecules for the LOHC technology and the development of the associated heterogeneous catalytic systems and conditions for both the hydrogenation and dehydrogenation reactions. In addition, chemical functions able to store and release H₂ will also be reviewed in order to broaden the perspective of LOHC structures.

Moreover, no normalized procedure has been developed yet to compare reactions performed in different conditions like the temperature, pressure, reaction atmosphere, catalytic loading and composition, reactor type and so on. In consequence, as the performance of the reaction is highly dependent on these parameters, it is often difficult to draw an easily generalizable conclusion. Whenever possible, key-points were summarized in the introduction and conclusion of each part.

Finally, we would like to report some recently published good reviews on the topic.²¹³⁻²¹⁷

II.4.2.5.1 Cycloalkanes

Cycloalkanes have been the first structures studied for the LOHC technology, as homocyclic structures are cheap and readily available due to their presence in the oil refining processes. Moreover, the dehydrogenation of homocyclic structures is facilitated by the aromatization and the specificity of the C-H bond-breaking over C-C bond-breaking, allowing for the development of selective catalytic systems since the 1910s with seminal work from Zelinsky and coworkers.^{218,219} From a thermodynamic standpoint, most aromatic structures have dehydrogenation enthalpies in the 50-80 kJ/molH₂ range. In addition, conjugation in polyaromatic systems diminishes the energy needed during the dehydrogenation, with the exception of anthracene-based systems that see their dehydrogenation enthalpy increase after 3 conjugated cycles (Figure II-13).

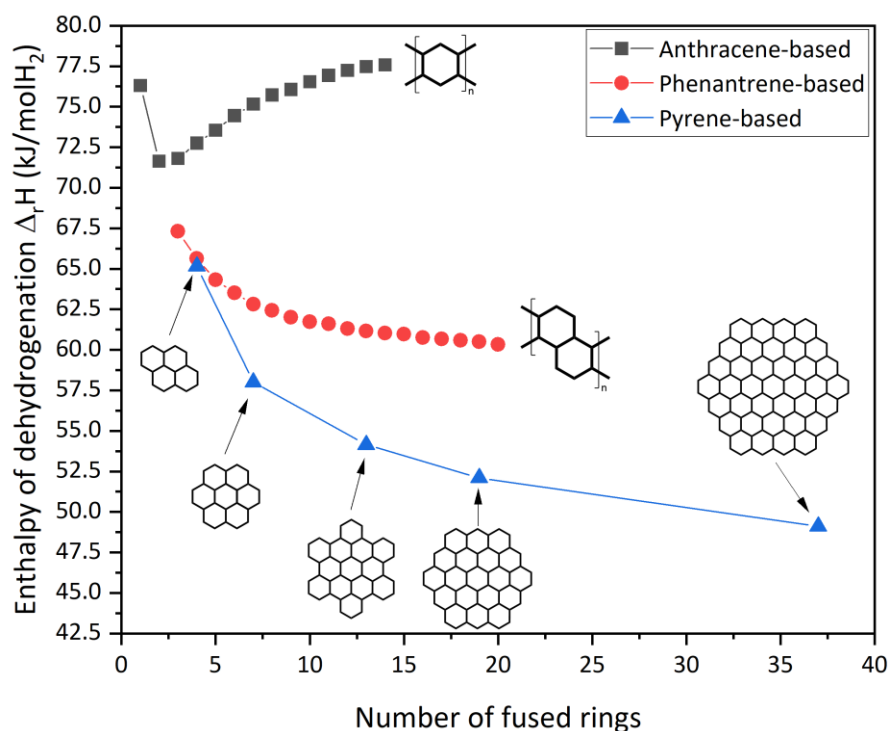


Figure II-13 - Dehydrogenation enthalpies calculated by the PM3 semi-empirical method as a function of the number of fused rings. Adapted from reference.²²⁰

This effect described by Clar's rule that links stability in fused polybenzoic structures to the number of its stable sextets.^{221,222} Thus the stability increases from anthracene-type to phenanthrene-type to pyrene-type structures. Moreover, anthracene-type structures produces Clar structures with a unique sextet but an increasing number of benzene rings, provoking the destabilization of larger structures.

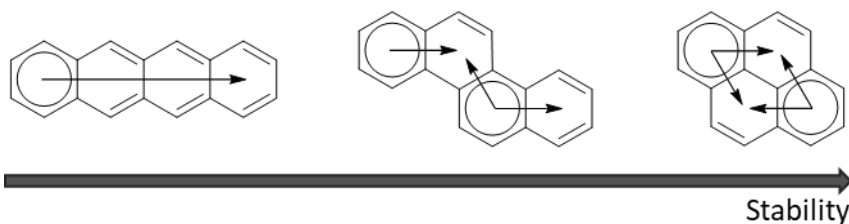


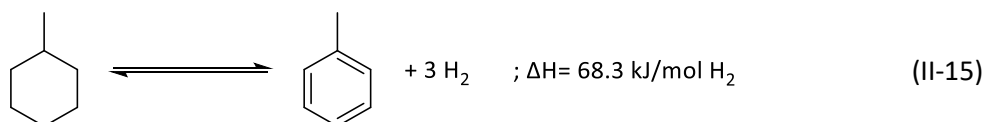
Figure II-14 – Clar structures for 4 fused rings: anthracene-type (left), phenanthrene-type (middle) and pyrene-type (type).

Interestingly, graphene materials should then have the best thermodynamic properties of polybenzoic structures, reaching theoretical dehydrogenation enthalpies in the 34 to 46 kJ/molH₂ range.²²⁰ However, due to their solid state, high fusion point and low solubility, efficient hydrogenation and dehydrogenation of such materials are yet to be achieved.^{223,224} In addition, steric hindrance in fused rings systems is detrimental to the hydrogenation and dehydrogenation as reactivity limitations arise at the nodes on the rings due to poor accessibility and the formation of less reactive isomers. In comparison, linearly linked hydrocarbons were shown to be more kinetically active.²²⁵

Whilst numerous aromatic molecules have been tested for the LOHC technology, this work will focus on the most studied ones, i.e. the couples Methylcyclohexane/Toluene, Decalin/Naphtalene and Perhydrodibenzyltoluene/Dibenzyltoluene. Benzene, Benzyltoluene, Fluorene, Biphenyl and their respective hydrogenated counterparts will not be discussed due to the lack of significant system variations with the Methylcyclohexane/Toluene, Perhydro-dibenzyltoluene/Dibenzyltoluene or Decahydronaphtalene/Decalin couples and the scarcity of development compared to the latter.

II.4.2.5.1.1 Methylcyclohexane/Toluene (MCH/Tol)

Due to its good gravimetric and volumetric densities (resp. 6.2 wt.%H₂ and 48 gH₂/L), abundance, low cost (0.3 €/kg), reactive simplicity, lower toxicity compared to the cyclohexane/benzene LOHC couple and lower computational cost compared to bigger LOHC like Dibenzyltoluene, MCH/Tol is often used as a model carrier for the LOHC technology.²¹⁴ In addition, industrial development by the Chiyoda corporation have recently renewed interest in its research.²²⁶ Recently, a conglomerate composed of Chiyoda, Mitsubishi, Mitsui and the Japanese government demonstrated the feasibility of massive H₂ transportation by ocean tanker with the MCH/Tol LOHC couple from Brunei to Japan.



Historically, extensive research was conducted on the Methylcyclohexane-Toluene-Hydrogen (MTH) system for both mobile and stationary applications from the late 1970s to the late 1990s.^{206,227} Indeed, it was first proposed as a H₂ fuel for automotive mobility in 1975 by Sultan and Shaw but was deemed inefficient compared to gasoline.²⁰⁴ Taube et al proposed the MTH system again in the early 1980s as a solution to store excess nuclear power for automotive transportation.²⁰⁵ Concomitantly, multiple pilot trucks were conceived to support the development of this technology.^{206,228} While the dehydrogenation reaction was not perfectly selective, this issue was circumvented by burning a fraction of the toluene or the impurities to kick-start and maintain the endothermal dehydrogenation.

As the dehydrogenation is supposed to happen during times of low energy availability, lowering the energy consumption during the dehydrogenation is key to design energetic and cost efficient systems.

Further developments highlighted that the total catalytic oxidation of less than 10% of the produced toluene covered the complete calorie consumption of the dehydrogenation and a minimum of 6% could be theoretically achieved by further optimization.²²⁹ Similarly, extracting a portion of the heat produced by a H₂ thermal engine could compensate the dehydrogenation enthalpy, at the cost of a diminished H₂ production.²³⁰ Moreover, this approach would be ineffective in the case of a PEM-fuel cell engine due to their lower operating temperature. Finally, due to the low boiling point of MCH and Tol (resp. 100.9 °C and 110.6 °C), the dehydrogenation is a gas-phase reaction that is hence thermodynamically limited by H₂ accumulation in closed systems.²³¹ Therefore, catalytic Pd-Ag membrane reactors were proposed as an answer to separate H₂ from Tol during the reaction and push the thermodynamics forward.²³² Nevertheless, more development is required on these systems to reduce the amount of precious materials and to enhance their long-term stability in operating conditions.²³³

- Hydrogenation

Hydrogenation of cycloalkanes to aromatics was first achieved in 1911 and 1912 by Zelinskii and coworkers with Pt and Pd catalysts supported on Al₂O₃ at 300 °C and 1 bar H₂.^{218,219} Since then, Ru/Al₂O₃ was shown to be the best monometallic catalyst for the hydrogenation of Tol to MCH, with extensive research on Pt, Ir and Rh based catalysts over the last three decades.^{234–236} In addition, Ru presented a synergistic effect when doped with Pt.²³⁷ Synergies were also studied for Pt, Pd, and Pd–Pt catalysts supported on Al₂O₃ to no avail.²³⁸ However, alloying Pt and Pd increased the sulphur resistance of the catalyst at temperature above 200 °C, while a rise of the support acidity increased the sulphur resistance at low temperatures (120 °C).²³⁹

Atmospheric pressure hydrogenation of Tol was also achieved by non-noble catalysts such as Ni/Al₂O₃ at 170 °C with perfect selectivity. Temperatures above 170 °C favored the desorption of H₂, directly hindering the kinetics of the system.²⁴⁰ Multimetal NiCoMo supported on zeolites allowed for the conversion of Tol to MCH at 200 °C and 20 bar H₂. Side reactions such as ring contraction was observed in trace amounts.²⁴¹ Moreover, the hydrogen spillover effect, i.e. the migration of protons between the active metal nanoparticle and the support, also potentially played a role in the efficiency of the conversion. Indeed, hydrogenation with Pt/Al₂O₃ mixed/diluted with WO₃/Al₂O₃ and solid acids showed improved conversion compared to the pristine catalyst due to the LOHC adsorption on acidic sites of the surface.²⁴² This effect was also observed on a Ru/NiCo/Ni(OH)₂–Co(OH)₂-nanoislands supported on carbon catalyst where the combination of the different sites achieved 100% conversion in liquid phase at 60 °C in 1 h for an activity ten times more superior to that of the equivalent Ru/C catalyst.²⁴³

- Dehydrogenation

Dehydrogenation of cycloalkanes to aromatics was also first achieved in 1911 and 1912 by Zelinskii and coworkers with Pt and Pd catalysts supported on Al₂O₃ at 300 °C.^{218,219} However, these catalysts tended to deactivate due to preferential adsorption of the dehydrogenated products. Besides, side-reactions like coke formation and dealkylation were observed at high temperatures (> 350 °C).²⁴⁴ A series of noble metal catalysts supported on nitrogen-doped carbon showed that Pt was the most active catalyst, with the activity order Pt>Pd>Rh>Ir.²⁴⁵ Extensive study of Pt supported on metal oxides and perovskites showed that 1 wt.% catalysts were more efficient than 3 wt.% catalysts, potentially due to the smaller size of the Pt nanoparticles.²⁴⁶ Substrate modification with addition of boron to a Pt/Al₂O₃ catalyst allowed for the tuning of strong acid sites into weak acidic sites, limiting the coke formation

while retaining the stability of the metal nanoparticles on the substrate. This approach answered the lack of efficiency of alkaline addition that indistinctively covered all of the acidic sites and limits the dehydrogenation activity.²⁴⁷ A Pt/Na-Y zeolite showed that hydrogenation or hydrogen transfer reactions happen during the dehydrogenation of methylcyclohexene, yielding both MCH and Tol.²⁴⁸ As shown by previous contributions, the dehydrogenation rate-determining step is the toluene desorption.²⁴⁹

The synthesis of bimetallic catalysts is known to yield potential synergistic effects between the metals. Here, Pt-Re/Al₂O₃ showed a negligible influence of the H₂ partial pressure on the dehydrogenation rate compared to Pt/Al₂O₃, indicating an alleviation of the thermodynamic equilibrium.²⁵⁰

As the diminution of the active metal nanoparticle usually increased the activity of a catalyst, single atom catalyst (SAC) have a great potential to reach high kinetics. Recently, a Pt SAC supported on CeO₂ nanorods was reported to catalyze both hydrogenation and dehydrogenation in continuous flow with activities 30 times superior compared to 2.5 nm Pt NP on CeO₂ nanorods.²⁵¹ Similarly to Pt SAC, liquid metal solutions like Ga₅₂Pt/SiO₂ could atomically disperse Pt and maximize the gas-liquid interface, reaching up to 84.5% selectivity to Tol. While CO₂ was observed, no coking formation was visible which was in agreement with the stable activity observed over 75 h.²⁵² Surface protonics are also a promising technique to lower the temperature of a reaction by applying an electric current.²⁵³ Using a conductive Pt/TiO₂ anatase catalyst submitted to a 5 mA electric current, the proton hopping specific properties of the support were increased, lowering the activation energy from 47.9 kJ/mol to 22.8 kJ/mol. Moreover, the dehydrogenation temperature could be decreased to 175 °C and the reaction equilibrium was displaced from 25% to 37% conversion.²⁵⁴ As numerous effects occur simultaneously due to the specific nature of the TiO₂ anatase support and electricity (Joule heating, ...), more work is required to rationalize the effective influence of an electric field on the dehydrogenation.

Non-noble metals are being heavily scrutinized as they may present an opportunity to replace critical and expensive platinum group metals at usually the cost of higher catalytic loadings. Thus, dehydrogenation of MCH to Tol was catalyzed by 20 wt.% Ni/Al₂O₃ catalyst, reaching a stable 92% conversion during 175 h on stream.²⁵⁵ Further work on bimetallic Ni-M catalysts were pursued with Zn, Ag, Sn and In. The Ni-Zn bimetallic catalyst showed a reduced activity (32.2% instead of 36.2% for pure Ni/Al₂O₃) with an increased selectivity to Tol (96.6% and 66.9% resp.). Nevertheless, the performance was still mediocre compared to a Pt/Al₂O₃ catalyst that reached full conversion and almost perfect selectivity (99.9%) in the same conditions.²⁵⁶ Interestingly, flow kinetics with the NiZn catalyst in atmospheric pressure Ar demonstrated the insensitivity of the system to the MCH partial pressure above 0.1 bar and even a positive effect of H₂ for partial pressure up to 0.4 bar, indicating that the hydrogenation of a species on the catalyst was necessary for the dehydrogenation. The increased selectivity by Zn doping was linked to the inhibition of low-coordination sites that were responsible for C-C cleavage.²⁵⁷

- DFT

Computing techniques like Density Functional Theory (DFT) have been extensively used to rationalize and predict the mechanism of reaction as well as propose catalyst modifications. A thesis on the dehydrogenation mechanisms of MCH on sub-nanometric Pt/Al₂O₃ proposed a DFT modelling coupled with kinetic experiments to rationalize the elementary steps during the dehydrogenation. DFT modelling showed that the cleavage of all C-H bonds were preferred compared to the migration and recombination of the protons. In addition, it exhibited the interactions between the LOHC and the support. Finally, the rate-determining step was difficult to assess due to the similar energies of either the third C-H bond cleavage or the desorption of toluene as often postulated in the literature.^{258,259}

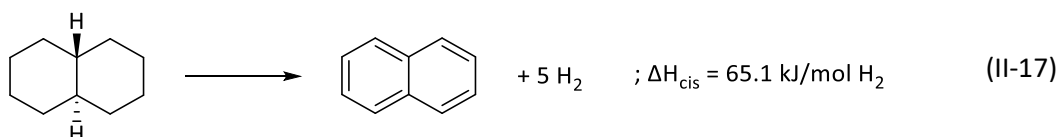
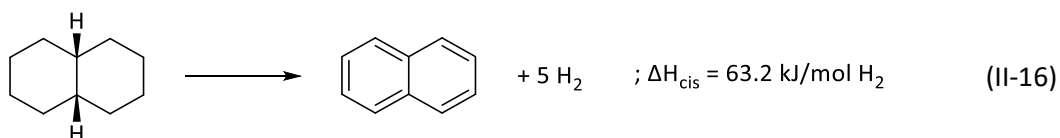
Predictive DFT was also used to estimate the influence of Sn-doping on a Pt/Al₂O₃ catalyst. The synthesis of a Sn₄Pt phase could enhance the reaction kinetics due to lower activation energies compared to pristine Pt.²⁶⁰ Lastly, DFT modelling showed that low-concentration of promoters (<1%) like Si, P or Se could theoretically boost the dehydrogenation similarly to the already demonstrated S additives. Higher concentration of doping elements showed no lowering of the reaction energy.^{261,262}

- Conclusion

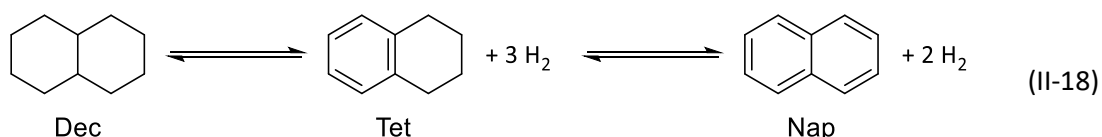
From a techno-economic standpoint, the dehydrogenation is the bottleneck of the MTH system as high performance and low cost PGM-free catalysts need to be developed while continuous H₂ purification of the outlet feed and lower temperature of reaction are also to be addressed. In particular, the hydrogen performance, i.e. the stability of the LOHC, over the cycling is the principal concern due to isomerization and C-C cleavage side-reactions. Nevertheless, the high-energy consumption during the dehydrogenation could be circumvented if using industrial heat waste or SOE-fuel cell systems. The rest of the economic chain is already ready as all dedicated infrastructures are in place and may just need a slight retrofit to adapt to the physical characteristics of the LOHC (higher viscosity).²⁶³

II.4.2.5.1.2 Decalin/Naphtalene (Dec/Nap)

Decalin is an inexpensive (0.6 €/kg) polycyclic fused-rings molecule that possesses high gravimetric and volumetric densities (7.4 wt.%H₂ and 66 gH₂/L resp.).²¹⁴ However, Naphtalene is a solid up to 80 °C, which implies either incomplete conversion or dilution of the LOHC in a solvent in order to keep the system liquid. As calculated by Pez et al., multiple fused rings diminish the enthalpy of dehydrogenation (Figure II-13) compared to free-standing or unfused rings.^{220,264} In addition, stereocenters are created by the fusion of the cycles, allowing for the formation of cis- and trans-hydrogenated isomers. Interestingly, the cis-isomer can undergo a ring flip reaction (II-16), while the trans-isomer has its conformation blocked and is the most stable isomer (II-17).



Similarly to the MCH/Tol couple, the ebullition temperatures of Decalin (185 °C) and Naphtalene (218 °C) are lower than the reaction temperatures for both hydrogenation and dehydrogenation, implying either gas-separation and/or purification or thermodynamical limitations on the conversion in batch systems. In addition, a stable intermediate, Tetralin (Tet), can form during the reaction (II-18).



- Hydrogenation

As Nap is a homocyclic LOHC, its hydrogenation to Dec can usually be achieved by noble metal catalysts such as Ru, Pt or Pd at high temperatures (> 200 °C).^{265,266} However, control over which isomer forms preferentially is dependent on the catalyst used, the reaction temperature and the pressure.²⁶⁷ The effect of the support was shown by a series of Pt-Pd supported on (Al₂O₃)_(1-x)/(CeO₂)_(x) (x from 0 to 0.5)

catalysts used for the hydrogenation at 290 °C and 55 bar in a batch reactor. The presence of CeO₂ improved the conversion up to 99.5% in 3 h and this effect was attributed to the adsorption of Nap on acidic sites (Ce⁴⁺) as well as modification of the redox properties of the acidic sites and additional spillover reaction.²⁶⁸

Non-noble catalysts such as NiMo supported on Zr, Al or Ti-hexagonal mesoporous silica (HMS) showed a selectivity to Dec due to the modification of the Mo=O or Ni oxide active sites by the Zr, Al or Ti dopants while the less active NiMo/Al₂O₃ converted Nap to the intermediate Tet.²⁶⁹

- Dehydrogenation

Similarly to MCH dehydrogenation, the dehydrogenation of Nap happens in gas phase due to the necessary high dehydrogenation temperature. To circumvent that issue, liquid film state reactors were proposed as they favor reactive distillation that is known to facilitate the dehydrogenation compared to “suspended-state” conditions due to the constant removal of the dehydrogenated products.²⁷⁰ These conditions could be achieved either by batch reaction in a large volume²⁷¹ or by spray pulse.²⁷² Unsurprisingly, Pt was also shown to be the best metal to catalyze the complete dehydrogenation to Nap compared to Pd.²⁷³ Experimental dehydrogenation on Pt/C and Pd/C showed that Pt was more active for Dec formation while it was the contrary for Tet formation in the same conditions. These results were rationalized by DFT, showing that molecular alignment on the metallic surface was more important than the intrinsic activity of the metals.²⁷⁴ For the time being, only Pt with additives such as W and Re achieved a conversion superior to 90% in 1 h at 280 °C and fulfilled the required H₂ rate of fuel cells for mobility applications.^{203,275} The relationship between the synthesis of highly dispersed Pt nanoparticles was linked to a high specific surface of the support²⁷⁶, the preparation method of the catalyst with ion-exchange, polyol method and chemical reduction more efficient than precipitation and impregnation²⁷⁷ and the additives such as Ti or Ca during the synthesis.²⁷⁸ The acid-neutralizing additives also limited the formation of coke promoted by strong acidic sites of the support.^{271,278}

Pt supported on carbon materials were shown to yield excellent results (85% conversion and 95% selectivity to Nap, 5% to Tet) in contrast to catalysts supported on Al₂O₃, potentially due to the spillover of hydrogen on the activated carbon support.²⁷⁹ The microstructure of the carbon support had a significant impact on the dehydrogenation properties of Pt as shown in carbon nanofibers (CNF): a positive effect was observed in the order platelet > fishbone > tube where platelet corresponds to the edges of stacked graphene and tube corresponds to basal graphene.²⁸⁰ These results were confirmed by DFT calculations that showed stronger interactions between Pt and the edge planes of the CNF compared to the basal plane of CNT.²⁸¹ In addition, the wettability, i.e. the affinity of the LOHC with the support, modified the catalytic activity of the system. Pt supported on CNT synthesized with O modifications induced a better Pt dispersion but a worst performance due to the lower affinity between the apolar LOHC and the polar surface.²⁸⁰ On the contrary, N modifications doubled the catalytic activity compared to pristine CNT as N-modified CNT retained a good surface apolarity and favored electron transfers from the metal to the support, facilitating the Nap desorption.²⁸² Electron transfers were also observed for a Pt/MgAl₂O₄ catalyst, linking the positively charged Pt particles to the weakened adsorption of Nap. In addition, the edges of the Pt nanoparticles were identified as the active sites of the catalyst by DFT and size analysis experiments.^{283,284}

The dehydrogenation of Dec was rarely complete due to the faster dehydrogenation rate of the cis-Dec compared to the trans-isomer.²⁷⁹ Indeed, the preferential conversion of the cis-isomer was linked to its flexible nature that can better accommodate the active site.²⁸⁵ In addition, the cis-to-trans isomerization on the support acidic sites was favored compared to the trans-to-cis isomerization.^{275,286} As the cis-to-trans isomerization and the dehydrogenation were also kinetically controlled by the

temperature, with isomerization being favored at low temperature and dehydrogenation at high temperature, all elements supposed the slower dehydrogenation kinetics of the trans-isomer.²⁸⁷

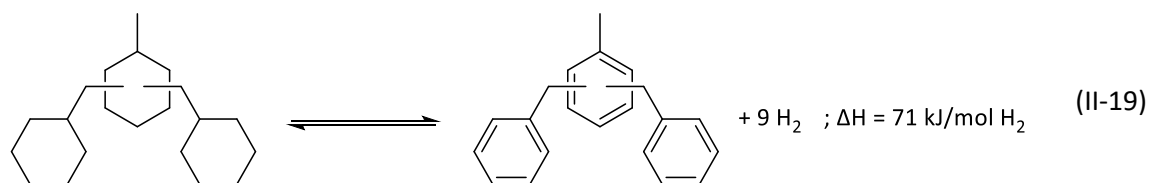
The partial or total replacement of noble metals by transition metals was sought since the end of the 1970s, when a Ni-Mo oxides/Al₂O₃ (80-100%)-SiO₂ (0-20%) yielded low conversion (up to 25%) at high temperature (370 °C). An adverse effect was observed when increasing the SiO₂ content, potentially due to the stronger acidity of the support.²⁸⁸ Since then, Pt-Ni/C catalysts were proposed due to the metals synergistic effect. In fact, the hydrogen energy binding (HBE) values were higher for the Ni-Pt surface with Ni on top of Pt compared to the Pt-Ni surface with Pt on top of Ni, rationalizing why the former had a higher dehydrogenation activity.²⁸⁹ Purely non-noble catalysts like 8%Ni-2%Cu/C catalysts were used in a spray pulsed system at 350 °C for an activity 10 times superior to other catalytic systems in spray pulsed mode. However, the activity is still 4.5 to 6 times lower than noble systems in batch or flow reactors. The Cu addition supposedly suppressed the hydrogenolysis reaction (cleavage of the C-C bond by H₂) and promoted the C-H bond breaking.²⁹⁰ Finally, Ni-WC/C replaced Pt without side reactions and coking in a flow system. 93% conversion and 100% selectivity to Nap were achieved at 300 °C with a high catalytic stability over 22 h. The good catalytic activity of Ni-WC was corroborated by DFT: Ni-Pt and Ni-WC had close HBE values, implying that they should have similar catalytic activities.²⁹¹

- Conclusion

Despite better dehydrogenation enthalpy and gravimetric and volumetric densities compared to the MCH/Tol LOHC couple, Dec/Nap presents an intrinsic limitation due to the formation of a highly stable intermediate and 2 hydrogenated isomers that hinders the system during both hydrogenation and dehydrogenation. While the boiling point of both Dec and Nap is slightly higher than the MCH/Tol couple, the dehydrogenation still happens in gas-phase, which further limits the system. Finally, Nap is a solid at room-temperature, inducing either incomplete conversion, temperature control of the reaction/storage vessel or dilution in a solvent. Therefore, the Dec/Nap LOHC couple probably exhibit too many barriers to be efficiently implemented.

II.4.2.5.1.3 Perhydro-dibenzyltoluene/Dibenzyltoluene (18H-DBT/DBT)

Dibenzyltoluene (DBT) and its hydrogenated counterpart (18H-DBT) were proposed as a LOHC couple in the 2010s and tremendous work by the Wasserscheid group and their collaborators was achieved since then.²⁹² A start-up named Hydrogenious was created by former members of the Wasserscheid group to develop, with the help of a German consortium, the LOHC technology centered on the 18H-DBT/DBT couple.²⁰⁹ 18H-DBT possesses good gravimetric and volumetric densities (6.2 wt.%H₂ and 57 gH₂/L resp.).²⁹³ In addition, both forms are liquid on a wide range of temperature (-39 to 390 °C), albeit viscosity would increase drastically at temperatures below 20 °C.^{292,294} From a chemical risk standpoint, 18H-DBT and DBT have a much lower toxicity and ecotoxicity than the MCH/Tol couple and a lower vapor pressure than Dec/Nap, making it a safe couple to handle. In contrast, the 18H-DBT/DBT couple have a higher enthalpy of dehydrogenation (II-19).²⁹²



Finally, DBT is cheap (4 €/kg) and commercially available as a heat-transfer oil under the name Marlotherm® SH, owing to its excellent thermal stability.^{214,295} Scale-up projects for the DBT technology

have started in both hydrogenation and dehydrogenation in 2017-2018.²⁹⁶ As extensive work on DBT-related systems was published in the literature, a portion of this review will be dedicated to them.

- Hydrogenation

Complete hydrogenation of DBT was first achieved by a Ru/Al₂O₃ catalyst in 4 h at 150 °C and 50 bar.²⁹² Recent advances proposed a K-doped Ru supported on MgO catalyst as K was shown by DFT to favor the heterolytic H₂ adsorption at low concentrations by charge transfer from Ru and the substrate. At higher concentrations, K interacted directly with H₂, decreasing the catalyst activity.²⁹⁷ However, it also became clear that the hydrogenation occurred first on the side-rings before the center ring, as shown by follow-up of the reaction with 1H NMR and High Performance Liquid Chromatography (HPLC).²⁹⁸ The hydrogenation of the center ring was the rate-limiting step of the hydrogenation that forced the development of more active catalysts. The complete hydrogenation of DBT by a Pt on Al₂O₃ eggshell was observed for temperatures above 220 °C and 30 bar.²⁹⁹ Further work carried out the hydrogenation with Pt supported on Al₂O₃ at 140 °C and 30-40 bar in 35 min. The Al₂O₃ support was found more reactive than the SBA-15 (60 min), Hydroxyapatite (100 min) and activated carbon (280 min) supports.³⁰⁰ Hydrogenation with non-noble metals was also achieved by a Ni Raney catalyst in 30 h at 170 °C and 50 to 70 bar.³⁰¹ Later, a Ni catalyst, NISAT 310, accomplished the complete hydrogenation at 150 °C and lower pressures (4-16 bar) in flow conditions.³⁰² Finally, a recent advance proposed the hydrogenation of DBT with a Mg₂NiH₄ metal hydride able to transfer H₂ from the gas phase to the LOHC at 280 °C and 60 bar, reaching an adsorption of 5.70 wt% (92% DoH) in 20 h.³⁰³

- Dehydrogenation

The dehydrogenation of 18H-DBT was first achieved with Pt based catalysts and Pd based catalysts, with Pd catalysts being less active than their Pt counterparts. Support modification proved primordial, with activated carbon yielding the best results compared to Al₂O₃ and SiO₂. In addition, the diminution of the Pt loading increased the dispersion of Pt on the surface and further improved the catalytic activity. Finally, temperature modification from 230 °C to 290 °C increased the conversion from 16% to 92% in 3.5 h, achieving a H₂ dehydrogenation rate comparable to other state-of-the art LOHC N-Ethylcarbazole (see II.4.2.5.2.1).²⁹² Other studies confirmed the effectiveness of activated carbon as a support and hinted at other metal oxides like TiO₂ anatase-rutile nanopowder capable to compete with activated carbon, although further rationalization was still required.³⁰⁴ While activated carbon was proven a good support for Pt, the high reaction temperature (>300 °C) could prove detrimental to the LOHC stability. Thus, extensive work was pursued on more stable metal oxides like Al₂O₃ as a support that achieved high H₂ production rate of roughly 1 gH₂/gPt/min.³⁰⁵

The catalyst preparation method was also significant to improve the activity, as a supercritical CO₂ (sc-CO₂) assisted Pt/Al₂O₃ catalyst was more active than its analogue prepared by wet-impregnation. However, this increased activity was not selective as more by-products and carbon impurities at the catalyst surface were observed for the sc-CO₂ catalyst, potentially due to the catalyst higher surface acidity.³⁰⁶ S-doped Pt/Al₂O₃ catalysts were prepared by solvent-deficient preparation in order to effectively block the defect-sites that formed by-products on the Al₂O₃ surface. A better contact between Pt and S was also achieved compared to wet-impregnation, increasing the creation of electronically deficient species Pt that weakened DBT adsorption and favored 18H-DBT adsorption. Moreover, the catalyst performed with an excellent stability over 5 cycles without sulphur losses even during the regeneration of the catalyst under H₂.³⁰⁷ Finally, the glycine nitrate process (GNP) was also used to simultaneously synthesize by combustion the active metal and support, producing highly dispersed Pt/Al₂O₃ and Pt/CeO₂ catalysts. Pt/CeO₂ was more active than Pt/Al₂O₃, probably due to the smaller pore size of the Al₂O₃ support that limited the mass transport of the LOHC. Nonetheless,

Pt/CeO₂ was still 4 times more active than a benchmark Pt/Al₂O₃ catalyst (81% and 18% conversion in 2.5 h resp.).³⁰⁸ Recent advances revealed that the H₂ bubble nucleation was a rate-limiting step under defavorable conditions. Indeed, H₂ supersaturation limited the liquid-gas oscillation in the pores of the catalyst, effectively decreasing the Pt/Al₂O₃ catalyst activity to less than 1.8% of its original activity. Bubble nucleation inhibition was linked to the excellent wettability of DBT on the catalyst support and hydrophilisation of the support lifted the nucleation inhibition. However, a poor wettability could also lead to reduced performances.²⁸⁰ Catalyst drying to reintroduce gas-liquid interfaces and overheating of the catalyst pellet were also sufficient to lift the nucleation barrier.³⁰⁹ Extra work was pursued to increase the selectivity by activating the Al₂O₃ surface with H₂ and O₂ plasma. The modification of hydroxyl surface groups (with O₂) and oxygen vacancies (with H₂) improved the Pt dispersion. However, an improved stability of the catalyst with better long-term performance was observed only when the number of hydroxyl groups was increased. Hydroxyl surface groups were linked to spillover promotion and the increase of Pt(0) proportion reduced the number of side-reactions.³¹⁰

Alloying Pt with other noble metals was pursued to reduce the coking of the catalysts. However, Pt-Pd alloying was reported less active than Pt and Pd and these activities were linked to the H abstraction energies by DFT. In theory, specific atomic layering Pt-Pd-Pt could yield similar results than pristine Pt.³⁰⁵ However, another DFT study proposed the Pt-Pd-Pd combination.³¹¹ Finally, the adsorption of DBT on Pt, Pd and PtPd was also dependent on the catalytic surface in the order (110)>(100)>(111).³¹² In conclusion, it is important to keep in mind that conclusions based on DFT articles are not universally applicable as DFT is heavily dependent on the calculation conditions (functional, basis set, convergence criteria, ...).

Alloying with transition metal was accomplished with a Pt-WO_x/Al₂O₃ catalyst. When 22% of Pt was replaced by W, the catalyst presented better yields (+6 to 9%) which were attributed to a spillover effect of H to W confirmed by DFT calculations.³¹³ DFT studies also pointed at other transition metals like Cu, Ni or Fe to tune the electronic properties of Pt. The rate-determining step was the first C-H bond breaking on the middle ring and the reaction energy was linked to the H adsorption energy.³¹⁴

- System

The 18H-DBT/DBT couple has been an excellent candidate to model and design LOHC systems whose physical, chemical and thermodynamical properties are scarce. Thermophysical and chemical parameters of the DBT system were measured and calculated to favor the process design, modeling and engineering of the LOHC couple.²⁹⁴ While GC-FID and ¹³C NMR ex-situ follow-up techniques were classically used to assess the hydrogenation and dehydrogenation reaction progress as a function of the pressure and temperature of reaction³¹⁵, machine learning was recently proposed to predict the influence of the temperature, pressure, stirring speed and relative quantities of catalyst and DBT on the H₂ storage. Up to 98.7% accuracy were achieved using data from the literature.³¹⁶ Moreover, online measurements of the physico-chemical properties of the reaction mixture such as the density, refractive index, UV-Vis, Raman spectroscopy and viscosity were proposed to replace the classic lab-scale GC, NMR or elemental analysis for industrial application. Density or refractive index were highly promising due to the intrinsic measurement accuracy and the low temperature dependence of the measurement as well as the small deviation in measure even for different mixtures of same the DoDH (Degree of Dehydrogenation, i.e. the amount of evolved H₂ with regard to the stored amount of H₂ in the LOHC). Ultraviolet-Visible spectroscopy (UV-VIS) was limited by the high absorbance of aromatic compounds that complicated the measurement process at higher concentrations of DBT. Raman was deemed challenging and costly for a low accuracy to follow the evolution of the LOHC. However, its low temperature dependence and usefulness to probe other parameters of the system such as the

catalyst could prove interesting. Finally, the viscosity measurements were inefficient as different mixtures with the same DoDH have different viscosities in the case of the 18H-DBT/DBT couple.³¹⁷

Reactor development is key to fully optimize the LOHC system. Dehydrogenation with Pt/Al₂O₃ in 12 h at 290 °C in a microchannel reactor allowed for better conversions than its stirred reactor counterpart (58% vs 19% resp.), which permitted to use less catalyst for equivalent performances.³¹⁸ The development of swing reactors and reversible catalysts like Pt/Al₂O₃ allowed for the hydrogenation and dehydrogenation to occur in the same reactor. Thus, compact systems demanding less handling (no operation between the hydrogenation and dehydrogenation) with decreased cost (only one reactor) could be conceived. Moreover, such systems had a higher reactive availability as they could be kept heated up due to the hydrogenation and dehydrogenation being controlled only by the equilibrium pressure (around 3 bar for 18H-DBT/DBT) and the stirring speed. The catalyst was also regenerated at high pressure of H₂ during the hydrogenation, keeping its activity over 4 cycles.²⁹⁹ Another study confirmed the feasibility of a reversible reactor with Pt/Al₂O₃ but a rapid loss of cycling capacity (-25% after 1 cycle, hydrogen capacity decreased from 60% to 20% after 5 cycles) was observed and attributed to the deactivation of the catalyst due to coking, surface modification and side-reactions of DBT such as ring opening and cracking.³⁰⁰ Thereby, reversible systems present an interesting option for stationary H₂ generation and storage, providing their optimization for both reactions and connection to industrial waste heat to facilitate the heat integration.

The LOHC stability is key to ensure the reuse of the structure over numerous cycles. Early work quantified only traces (<0.01%) of by-products during the dehydrogenation at 270 °C in 72 h.²⁹² The system resilience was later estimated to 14000 h under hydrogenation conditions (150 °C and 50 bar H₂) while 8000 h were estimated under dehydrogenation conditions (310 °C and 1 bar).³¹⁹ Dehydrogenation stress tests at 355 °C showed the formation of by-products such as Benzyltoluene, Toluene, Xylene, Methylfluorene and their isomers in the liquid phase while CH₄ was observed in the gas phase. The impurities disappearance after the hydrogenation implied that cracking reactions also happened on the hydrogenation catalyst. If the limitation for toxic byproducts is low (<0.5mol%), DBT use would be limited to less than a year as a model built on accelerated stress tests predicted the formation of 7.4 mol% impurities after 89 h reaction in the normal operating conditions (300 °C).³⁰²

The quality of H₂ obtained from the DBT dehydrogenation must be stringent (>99.99%) as fuel cells cannot tolerate high contaminants levels, especially CO. The impurities in the produced H₂ came from the impurities found initially in the DBT like water that produced CO and CO₂ as shown by Infrared spectroscopy (IR) and isotopic replacement with O¹⁸. The addition of Dicyclohexylmethanol to represent oxidized organic species also favored the production of oxygenated impurities as a correlation was found between the organic alcohol and the CO and CH₄ levels. By using a recycled LOHC whose impurities were already phased out or by purifying/drying the LOHC beforehand, the H₂ stream quality improved. Both methods increased the H₂ purity to >99.999% levels, with CO being found at traces levels (<0.2 ppmv).³²⁰ Another technique usually reserved for gas phase dehydrogenation was the use of a PdAg membrane reactor. Its use diminished the impurities in the gas phase from 200 ppmv in the reactor to 3 to 7 ppmv after the membrane. Nevertheless, contaminants traces could disturb the H₂ flux in the membrane, making routine cleaning membrane procedures mandatory to ensure a continuous H₂ flux quality.³²¹ Carbon filters also proved efficient to purify contaminants in the H₂ gas feed with a constant 20 ppm CH₄ contamination and an aromatic contamination increasing from 2 to 6 ppm over 9 h. The H₂ output was controlled by using a simple pressure algorithm and a buffer volume, practically regulating the pressure variations of due to the reactor temperature variations and allowing for a PEM fuel cell to produce 6.6 kW over 4.5 h in a dynamic system.³²²

The modification of the LOHC properties was performed by mixing DBT with Benzyltoluene (BT) to lower its viscosity for applications in colder regions. The dehydrogenation was improved by 12 to 16% at 260 °C when compared to pure DBT due to the presence of BT in the gas phase that diluted the H₂ in gas-phase, thus displacing the reaction equilibrium similarly to reactive distillation.³²³

Finally, 18H-DBT and the other hydrogenated LOHC are a source of hydrogen for transfer hydrogen reactions. The reaction of 18H-DBT with Tol allowed for an almost thermoneutral reaction to produce MCH with a conversion superior to 99% in 5 h on a Pt/Al₂O₃ catalyst.²¹¹ DBT was also used for the transfer hydrogenation of Acetone to Isopropanol in order to produce electricity with direct Isopropanol/Acetone fuel cells. Pt/SiO₂ was a great candidate as SiO₂ limited the formation of acetone condensation by-products.³²⁴ Direct isopropanol fuel cells have reached 254 mW/cm², comparable to methanol/air fuel cells, which showcase the interest for this technology.³²⁵

- Conclusion

18H-DBT/DBT has been well developed from a catalytic standpoint and its system integration was also rigorously described in the literature. Most importantly, considerations such as online measurements, reactor design, LOHC stability, H₂ quality and purification as well as physicochemical properties modification and alternative fuel cell development were covered. From a commercial perspective, DBT was extensively marketed by Hydrogenious and social acceptance of such LOHC carrier would be high due to its non-flammable nature. However, its high dehydrogenation enthalpy and temperature intrinsically limit the applicability of this LOHC if no free heat is provided.

II.4.2.5.2 N-heterocycles

In the 2000s, Pez *et al.* proposed N-heterocyclic from the carbazole family as LOHC due to their reduced enthalpies compared to homocyclic analogues, revealing that conjugated 5-membered rings fused with 6-membered rings had a high potential for hydrogenation and dehydrogenation.²²⁰ DFT modelling by Clot *et al.* linked the integration of N atoms to the diminution of the enthalpy of dehydrogenation depending on their number, position and size of the ring (5 or 6).³²⁶

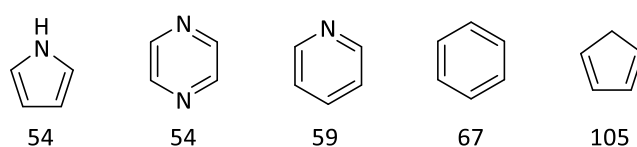


Figure II-15 – Influence of the size of the ring, the presence of N atoms and their number on the enthalpy of dehydrogenation (kJ/molH₂). Adapted from reference.³²⁶

The addition of a N atom in a 5 membered ring creates an aromaticity that strongly decreases the enthalpy of dehydrogenation. Further modelling showed that including electrodonating substituents stabilized the aromatic cycle, decreasing the enthalpy as a function of the Hammett parameter σ (para).³²⁷ Moreover, faster dehydrogenation kinetics were observed for heterocycles compared to the analogous homocycles due to the destabilization of the α C-H bond induced by the N atom.³²⁸

Whilst numerous heterocyclic molecules have been tested for the LOHC technology, this work will focus on the most studied couple Dodecahydro-N-Ethylcarbazole /N-Ethylcarbazole (12H-NEC/NEC) as an example of a 5-membered N-heterocycle and the promising couple Dodecahydro-Phenazine/Phenazine (12H-PHE/PHE) as an example of 6-membered N-heterocycle. Pyrrole, Indoline, Pyridine, Triazolidine, Quinoline, Naphtyridine, Carbazole, their alkylated or arylated derivatives and their hydrogenated counterparts will not be discussed due to the lack of significant system variations

with the 12H-NEC/NEC or 12H-PHE/PHE couples, their poor stability, selectivity or low gravimetric density due to incomplete dehydrogenation.

II.4.2.5.2.1 Perhydro-N-Ethylcarbazole /N-Ethylcarbazole (12H-NEC/NEC)

Inductive and mesomeric donations as well as conjugation and aromaticity favor lower enthalpies, hence carbazoles, indoles or their derivatives are attractive for the LOHC technology. Seminal work by Pez et al. showcased the capacity of this class of compounds to selectively store and unload H₂ as well as their lower dehydrogenation enthalpy with regard to classic systems.^{220,329} Carbazole and their derivatives showed the best results out of the structures presented in the Figure II-16:

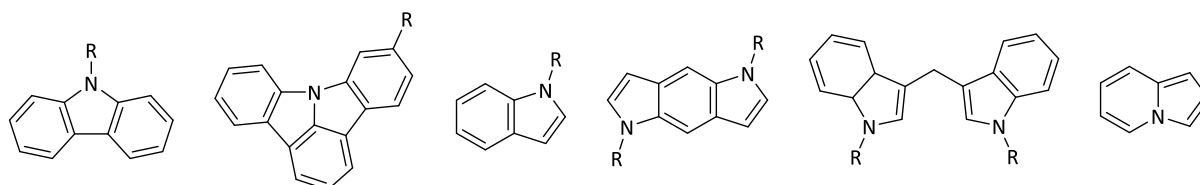
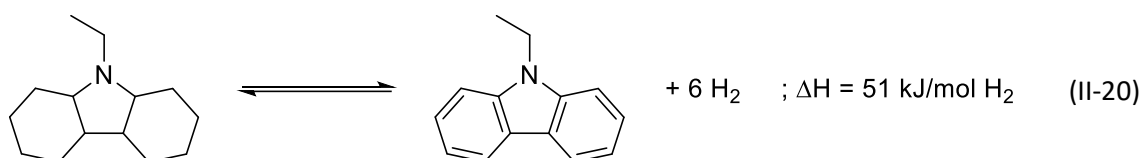


Figure II-16 - Examples of structures studied by Pez et al. From left to right: carbazole, indolo[3,2,1-jk]carbazole, indole, pyrroloindole, bis-indolylmethane and pyrrocoline.²²⁰

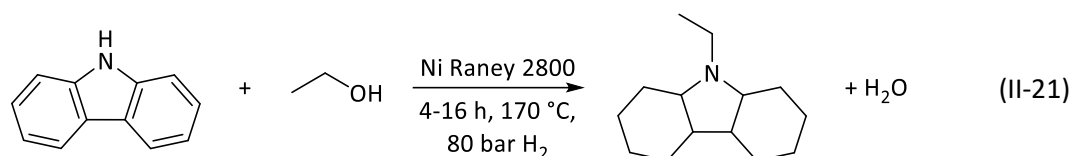
Carbazole presents high gravimetric densities (6.7 wt.%H₂), however its high fusion point (250 °C) is detrimental as it cannot exist as a liquid at near ambient temperatures or must be diluted in a solvent. Alkylated analogues such as N-Ethylcarbazole has a much lower melting point (70 °C) which facilitates their use while still possessing good gravimetric and volumetric densities (5.7 wt.%H₂ and 63 gH₂/L resp.).^{214,220} In addition, N-alkylation prevents catalyst poisoning and the subsequent slower catalytic activity due to the strong N adsorption on the metal nanoparticles.³²⁸ The advantage of the alkylation compared to the simple Carbazole was demonstrated by DFT in particular for the dehydrogenation. Indeed, the interaction strength between the NEC, Carbazole, Fluorene and a Pd surface was probed, revealing that Carbazole interacted strongly with Pd by its N moiety comparatively to NEC, while Dodecahydrofluorene had an even stronger interaction.³³⁰ Experimentally, the presence of the ethyl group facilitated the desorption of NEC, thus freeing the active site.³³¹



NEC has been extensively studied as a LOHC material since its discovery by Air Products and new LOHC players in Asia are rising since 2014. Hynertech was founded by a former Air Products partner, Prof. Hansong Cheng, that was chosen by the Chinese government to develop energy storage technologies at destination of the Chinese market in order to cover logistics mobility applications.³³² The first 10000 tons production plant of Hynertech LOHC was operational in 2020 and, in November 2022, a H₂ storage and supply system releasing 400 kg H₂ per day was commissioned at a price of 40 €/kg.^{214,333}

- Hydrogenation

NEC hydrogenation was first performed in diluted Tetrahydrofuran (THF) solution or simply melted with Ru, Rh and Ni Raney catalysts. Ni Raney 2800 was particularly efficient as it allowed for the in-situ hydrogenation and synthesis of NEC from Carbazole and the desired anhydrous alcohol (II-21).²²⁰



Another study with Raney-Ni showed the effect of temperature and pressure on the direct hydrogenation of NEC to 12H-NEC, with an optimum at 200 °C and 50 bar H₂ respectively, completely carrying out the hydrogenation in 1 h.³³⁴ NEC hydrogenation was also performed with Ru/Al₂O₃ in 1 h at 150 °C and 70 bar H₂, yielding 98% conversion and a selectivity superior than 95% for 12H-NEC.³³¹ Similarly, Ru/Al₂O₃ yielded 100% conversion and 98% selectivity to 12H-NEC in 1 h at 140 °C and 60 bar, with a stringent effect of the H₂ pressure, stirring speed and catalyst dosage.³³⁵

Both commercial and synthesized by chemical reduction catalysts were screened, showing that the active metal reactivity order was Ru>Pd>Pt>Ni and the support order was Al₂O₃>TiO₂>SiO₂-Al₂O₃>zeolite>graphite>activated carbon. The synthesized catalysts yielded better results due to a better atom efficiency and an inverse relationship between the catalytic activity and the particle size was observed.³³⁶ Subsequent hydrogenation studies at 130 °C and 70 bar confirmed the active metal reactivity order with Ru>Rh>Pd and linked the catalyst activity to the d-band center position. Indeed, a low d-band center indicated a strong interaction between the metal and the NEC, implying that the rate-determining step was the adsorption of NEC on the surface.³³⁷ However, a DFT study proposed the 10H-NEC to 12H-NEC conversion as the rate-determining step which was confirmed by a later study.^{338,339} However, as the DFT study was applied only to the LOHC structure and not to the LOHC-metal system, energy levels might vary considering the various stable intermediates forming depending on the metal: 8H-NEC on Ru, 4H-NEC on Pd and no stable intermediate on Pt. The hexagonal compact packing structure of Ru, compared to the face-centered cubic structure of other metals surfaces was also linked to the stability of 8H-NEC.³⁴⁰

Moreover, the isomerization of 12H-NEC was observed. As 12H-NEC possesses 4 stereocenters due to the presence of fused rings, 16 potential isomers exist, while only 6 isomers are possible due to symmetries. The trans, trans isomer (A) is the most stable and the cis-syn-cis the least stable (B) (Figure II-17).

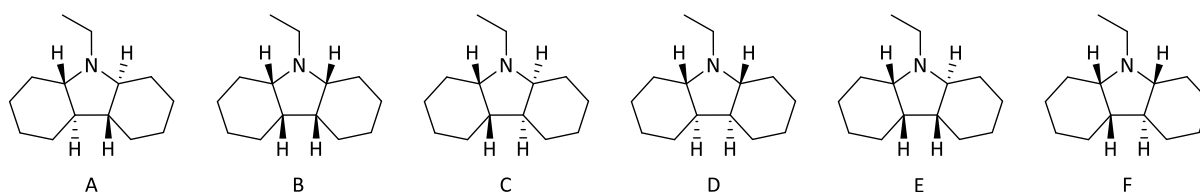


Figure II-17 - Isomer structures of the 12H-NEC. The most stable is the isomer A, while the least stable is the isomer B. The structures A to D are symmetric while the structures E and F are asymmetric.

The production of unstable isomers could theoretically simplify the dehydrogenation as less energy would be required.²²⁰ Both symmetric and asymmetric products were observed by 1D and 2D NMR techniques by using the number of carbon resonances to determine the symmetry (8 for symmetric compounds and 14 for asymmetric compounds in ¹³C NMR).³⁴¹ As the H₂ addition was supposedly concerted, asymmetric products implied isomerisation either on weakly bonding metal particles or on the support. These findings were confirmed as the isomer formation was dependent on the hydrogenation catalyst by a desorption/readsorption mechanism due to either a weak NEC-metal interaction or the hydrophilicity of the support surface as well as low temperatures yielding more kinetically favored isomers.^{337,340} DFT on flat Ru (001) and low-coordination sites (109) confirmed that

isomers formed from the desorption of the 8H-NEC from flat (001) due to steric constraints and readsorption to edge sites (109), limiting the activity of the Ru catalyst as a side-effect.³³⁶ Finally, DFT, Conductor-like Screening Model (COSMO) and Molecular Dynamics (MD) simulations corroborated that unstable isomers were favorable at low temperatures due to higher energy efficiencies.³⁴²

Bimetallic catalysts like Pd₂Ru/SiCN also yielded better results than the sum of their part or Ir and the corresponding commercial Al₂O₃ or C supports.³⁴³ Further development aimed at the reduction of precious metal in the catalyst composition. Therefore, Ru-Ni catalysts were synthesized on TiO₂ whose structure was primordial. Rutile was more active than anatase, but less selective while a commercial Anatase/Rutile in a 1:4 mix yielded improved results compared to both pristine phases. The Ni addition to Ru slightly increased the activity compared to Ru due to a potential hydrogen spillover effect.³⁴⁴ A spillover effect was also found on a Ru_{4.5}Ni_{0.5} supported on biochar prepared by carbothermic reduction. Better catalytic activities and stability were obtained compared to chemically reduced catalysts due to partial graphitization of the surface that favored electronic transfers and the embedding of the active nanoparticles (NP) in the support cavities, maintaining similar performances over 10 cycles.³⁴⁵ Lately, a Ru_{0.7}Ni_{0.3}/SBA-15 (a mesoporous silica) catalyst yielded better hydrogenation performances at 60 °C than a commercial Ru/Al₂O₃ catalyst at 90 °C due to improved electronic transfers from Ni to Ru. The good stability between the NP and the support was attributed to the ionic interactions with the hydroxyl surface groups.³⁴⁶ Similar results were also observed on a Ru/layered MgAl double hydroxide (LDH)/CNT prepared by ultrasonication that rapidly evolved 98.4% H₂ in 24 min at 120 °C and 60 bar and was stable for 8 cycles. The improved catalyst was also more active at 80 °C than a classic Ru/Al₂O₃ due to highly dispersed Ru NP and fast electron transfers between the LDH and the CNT.³⁴⁷

Hydride additions to the catalyst as a support material for Ru yielded better performances than a classic Ru/Al₂O₃ catalyst. YH₃ was comparatively more efficient than LaH₃ and GdH₃ due to hydride transfers from the support to the adsorbed Ru-NEC materials and the regeneration of hydrogen-deficient YH_{2-x} to YH₃ by H₂ in solution, allowing for complete hydrogenation at 90 °C and 10 bar.³⁴⁸ These results were confirmed on a Ni-YH₃/Al₂O₃ catalyst that achieved complete conversion when both YH₃ and Ni/Al₂O₃ showed no activity. The mechanism was unchanged with H transfer from YH₃ to the Ni-NEC interfaces and YH₃ as a H₂ splitting site. The contact between Ni and YH₃ was primordial as 500 nm Ni particles were more reactive than 10 nm Ni nanoparticles.³⁴⁹ A composite Co-B-YH₃/Al₂O₃ catalyst also showed a remarkable activity comparable to the best Ru catalysts. However, gradual reduction of activity was observed over 5 cycles due to the phase detachment from the support.³⁵⁰ Finally, LaNi_{5.5} nanoparticles, or LaNi₅ core with a Ni-rich shell, catalysed the complete H₂ absorption in 8 h at 180 °C, and 70 bar H₂. The LaNi₅ phase could form a partial hydride phase depending on the pressure that enabled H transfers to the Ni shell. While no H₂ capacity modification was noted, a diminution of kinetics due to the partial decomposition to LaH₃ was observed after 9 cycles.³⁵¹

- Dehydrogenation

Seminal work by Pez et al. described the dehydrogenation reactivity of the active metal in the order Pd>Pt>Ni over alumina and lithium aluminate, with Pd/Al₂O₃ reaching the best conversion. Re-doped Pt catalysed the dehydrogenation comparatively to Pd/Al₂O₃, while Pt-Pd or Pt-Sn catalysts were less active. The addition of 3 mol% additives had a neutral effect for Brønsted acids and bases and a negative effect for Lewis acids or bases. Finally, hydrogen purity measurements revealed that low methane formation (<200 ppm) was observed for both Pt-Re/Al₂O₃ and Pd/Al₂O₃ while ethane formation due to the decomposition or dealkylation of NEC was detected in concentrations superior than 6000 ppm for Pt-Re/Al₂O₃ and below 50 ppm for Pd/Al₂O₃.²²⁰

From an activity standpoint, the H₂ production-rate was extremely dependent on the temperature. At 270 °C, up to 9 gH₂/gPt/min were observed for a Pt/Al₂O₃ catalyst for a DoDH of 100%. However, thermal stability tests revealed roughly 2% degradation due to dealkylation after 72 h.²⁹² By diminishing the temperature at 180 °C, the activity went down to 0.67 gH₂/gPt/min with the same catalyst at DoDH=100%. Finally, Pd/Al₂O₃ was more active and selective than Pt/Al₂O₃, reaching 0.8 gH₂/gPd/min at DoDH=100%, equivalent to the best DBT performances.³⁵²

The dehydrogenation mechanism with Pd/Al₂O₃ followed a 3-stepped process, starting from the center ring and with the formation of the 8H-NEC and 4H-NEC intermediates. Interestingly, each dehydrogenation step started at a different temperature (128 °C, 145 °C and 178 °C for the conversion of the 12H-NEC, 8H-NEC and 4H-NEC species respectively), indicating that the temperature dehydrogenation could not be reduced below 178 °C to achieve completion. Moreover, the LOHC could be cycled 10 times with less than 0.1 wt.% capacity loss and a high H₂ purity of >99.99% with the only gaseous by-product being ethane.³⁵³ Advanced analytic studies on Pd/Al₂O₃ model catalysts in ultra high vacuum (UHV) with Infrared Reflection Absorption Spectroscopy (IR-AS), DFT and High Resolution X-ray Photoelectron Spectroscopy (HR-XPS) showed the adsorption of 12H-NEC on both the metal NP and the support with preferential migration to Pd.³⁵⁴ The adsorption of 12H-NEC started first from -100 °C, forming only a mono layer by desorption of non-chemisorbed species from -63 °C. The C-H activation of the 5 membered ring started from -50 °C and the 6-membered ring from 0 °C. C-N scission was observed above 77 °C.³⁵⁵ Similar work was carried out on Pt(111) with in-situ synchrotron radiation-based HR-XPS. The dehydrogenation in UHV presented similar patterns: adsorption of multi layers of 12H-NEC from -133 °C, desorption of the physisorbed 12H-NEC to let only a mono layered chemisorbed 12H-NEC up to -33 °C, dehydrogenation to 8H-NEC (57 °C), then to NEC at 107 °C before fragmentation of the carrier above 117 °C to form Carbazole or carbon residues on the catalyst. The dehydrogenation started with the formation of the pyrrole ring as the benzene formation required higher temperatures.³⁵⁶ The same results were observed in UHV with IR-AS, DFT and classic HR-XPS.³⁵⁷ Further studies indicated that the Pt edge and corner sites favored C-N bond scission at low temperatures and that well-ordered Pt facets favored the dehydrogenation, which would require bigger particles and consequently diminish the reactivity.³⁵⁸

Numerous kinetics studies on various supports such as Al₂O₃³⁵², SiCN³⁴³, TiO₂^{359,360}, reduced graphene oxide (rGO)³⁶¹ and SiO₂^{331,362} revealed that the metal reactivity order was usually Pd>Pt>Rh≈Ru>Au. For most Pd catalysts, the rate-determining step is the 4H-NEC to NEC dehydrogenation, with the kinetics constants diminishing in the order 12H-NEC to 8H-NEC>8H-NEC to 4H-NEC>4H-NEC to NEC.^{352,360–365} These results were confirmed by DFT.³⁶⁶ Only one study reported the 12H-NEC to 8H-NEC dehydrogenation as the rate-determining step for Pd supported on Al₂O₃, TiO₂, and SiO₂, except for the activated carbon support where the 8H-NEC to 4H-NEC dehydrogenation was.³⁶⁷ The effect of the support on Pd catalysts was probed by different studies, with the classic reactivity order being SiCN>C>Al₂O₃>TiO₂>SiO₂.^{343,367} However, the dehydrogenation process on Pd/Al₂O₃ was superior to Pd/C due to overall better kinetics that limited the accumulation of intermediates. Moreover, a volcano plot was observed when comparing the Pd NP size with regard to the catalytic activity, in agreement with previous studies.^{358,367} A high Pd reduction also yielded better results.³⁶⁷ Finally, the facet-dependent activity of the dehydrogenation was proved by a series of Pd/rGO catalysts with (100), (110) and (111) facets. At 180 °C, the complete dehydrogenation was achieved in 30 min on the (100) facet, 2 h on (110) and 7 h on (111). This activity change was linked to a better NEC adsorption on low index facets. In particular, the Pd (100) facet facilitated the rate-determining step 4H-NEC to NEC and DFT characterized the rate-determining step as the conversion of 3H-NEC* to 2H-NEC*.³⁶⁶

Highly ordered mesoporous supports have been the focus of recent advances. Pd supported on a MIL-101 MOF presented a better activity than commercial Pd/Al₂O₃, evolving 100% H₂ in 4 h at 170 °C. 89% catalytic activity was retained after 5 cycles.³⁶⁴ Moreover, a Pd/SBA-15 catalyst showed a remarkable 98.7% DoDH in 1 h at 180°C with a high stability between Pd and hydroxyl group due to the ionic adsorption of the Pd on the surface.³⁶⁸ Finally, Pd/MgAl-LDH synthesized by ultrasonic reduction achieved 100% conversion and 99.3% DoH at 180 °C in 6 h. 98% stability was observed after 6 cycles, down to 86% stability after 3 cycles for an analogous chemically reduced catalyst due to sintering.³⁶⁹

While less active and selective than Pd, a few Pt catalysts were proposed to carry out the dehydrogenation of 12H-NEC. Interestingly, Pt/TiO₂ was found more active than its Al₂O₃ counterpart due to a strong metal-support interaction that favored electronic transfers from Pt to the support. The rate determining step was facilitated due to the strengthening of the 4H-NEC-Pt interaction or the weakening of the NEC-Pt adsorption, but no more work was pursued in that direction probably due to the C-N cleavage properties of Pt.³⁶⁵

Among the Pd-based bimetallic catalysts, Pd₂Ru/SiCN was an early example with an improved reactivity compared to the monometallic catalysts.³⁴³ Further developments with a series of Pd-M/TiO₂ catalysts (M=Pt, Ru, Ni, Cr, W, Ge) revealed that Pt and Ru were the best co-catalysts. Microwave irradiation was also more efficient than conventional heating at the same temperature due to Pd absorbing the radiation and presenting overheated surfaces.³⁵⁹ Another series of bimetallic Pd-M (M=Au, Ag, Ru, Rh) supported on rGO revealed the high effectiveness of Au as a co-catalyst (Au>Ru>Rh>Ag). The modification of the Au/Pd ratio presented an optimum at Au₁Pd_{1.3}, achieving complete conversion and selectivity to NEC in 4 h and reducing by 43% the reaction time comparatively to Pd/rGO. A good catalyst stability was also observed over 5 cycles.³⁷⁰ Another study on PdAu NP alloys supported on SiO₂ showed that Pd₃Au was 2.26 times more active than pure Pd and these results were correlated by DFT on (111) surfaces.³⁶²

Pd alloys with non-noble metals were also studied with bimetallic Pd_xCu_y/rGO catalysts. Pd_{1.2}Cu showed 100% selectivity for NEC in 7 h, being as efficient as Pd/rGO while reducing the Pd amount. The catalytic activity was linked to the particle size and the amount of Cu: from 0 to 50% Cu replacement, no variation of the Pd binding energy was measured, indicating similar catalytic activities to pure Pd, while above 50% Cu addition saw a decrease in catalytic activity due to electronic transfers to Cu.³⁷¹ A recent PdNi/KIT-6 catalyst produced by sonochemistry was able to anchor ultrafine NP on the Si-OH surface. Pd₄Ni₁/KIT-6 catalyst was 1.7 times more active than Pd/KIT-6 at 180 °C due to electron transfers between Pd and Ni and retained more than 90% stability over 5 cycles.³⁷²

Hydrides were also used as supports and dopants for noble metal-free dehydrogenation catalysts. A Co-B-YH₃/Al₂O₃ catalytic system enabled activities comparable Pd catalysts, but a gradual loss of performance was observed over 5 cycles due to phase detachment from the support.³⁵⁰ Lastly, a LaNi_{5.5} catalyst composed of a LaNi₅ core and a Ni-rich shell was active for dehydrogenation at 200 °C in 4 h. Due to the low pressure and high temperature, the LaNi₅ bonding sites were empty during the dehydrogenation, which promoted the migration and desorption of H₂.³⁵¹

- Conclusion

NEC has been the go-to academic LOHC with most recent work originating from research groups in Asia, exhibiting great promises as a LOHC with comparative performances to DBT and a reduced enthalpy cost. Nonetheless, selectivity is still an issue due to C-N bond cleavage during the reaction at higher temperatures. In addition, the solid phase hydrogenated compound might complicate the application of this LOHC, although the presence of different isomers can form a liquid eutectic mixture at room temperature. Finally, its high toxicity might impede its further development.

II.4.2.5.2.2 Perhydro-Phenanzine/Phenazine (12H-PHE/PHE)

Polycyclic aromatic molecules containing 2 N atoms or more included in 6-membered rings have been studied by Pez et al up to 2012.²²⁰ Numerous structures were proposed, in particular phenantrolines, dipyridils, bipyrimidines, quinazoline, terpyridines and naphthyridines (Figure II-18).

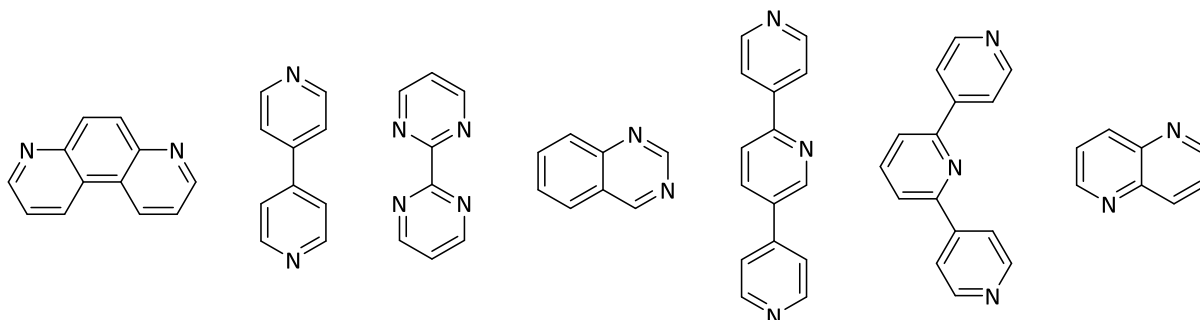
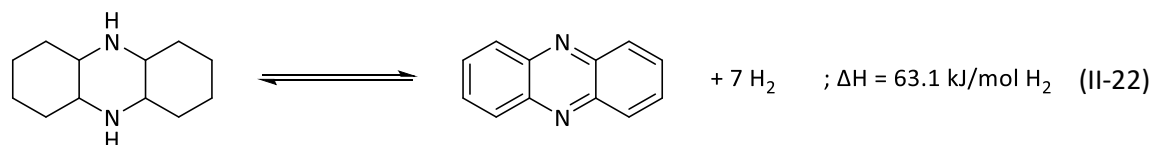


Figure II-18 - Examples of structures studied by Pez et al. From left to right: 4,7-phenantroline, 4,4-dipyridil, 2,2'-bipyrimidine, quinazoline, 4,2':5',4''-terpyridine, 4,2':6',4''-terpyridine and 1,5-naphthyridine.²²⁰

Most studied systems were unreactive or unselective due to incomplete reaction, side-reactions like ring-opening except the 4,7-phenantroline for which Pd/C evolved more than 90% of the H₂ capacity in 8 h at 250 °C. No follow-up work was found in the literature.

12H-PHE/PHE is a recent LOHC couple that possesses high gravimetric and volumetric densities (7.2 wt.%H₂ and 69 gH₂/L) ((II-22)). It is expensive (26 €/kg) but its synthesis from lignin was demonstrated.³⁴³ Nonetheless, PHE is solid up to 172 °C and dilution in solvents is then required.



Pd₂Ru/SiCN completely catalyzed both hydrogenation in solvent conditions (dioxane/water) in 24 h at 115 °C and 50 bar H₂ and dehydrogenation in solvent conditions (diglyme) in 24 h at 190 °C, hence solvent separation is needed after reaction. Further development of the 12H-PHE/PHE system would require solvent-free conditions, but no advances were reported to this date.

II.4.2.5.3 O-heterocycles

O-heterocycles are less advantageous than N-heterocycles as the inclusion of a O atom in a cycle does not store hydrogen during the hydrogenation. However, the addition of O atoms modifies the thermodynamics of the aromatic rings in a similar fashion than N atom addition as shown by the comparison of the dehydrogenation enthalpies performed by Pez et al. using DFT modelling (Figure II-19).^{220,329}

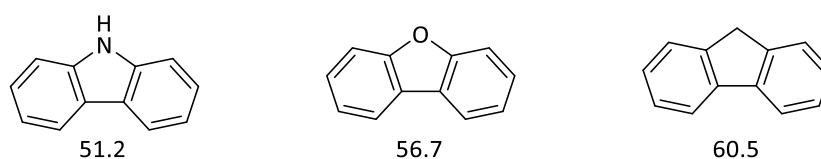


Figure II-19 – Comparison of the inclusion of heteroatoms on the dehydrogenation enthalpy (kJ/molH₂).²²⁰

While the thermodynamics gain is smaller for O-heterocycles than N-heterocycles, O-heterocycles still have lower dehydrogenation enthalpies than homocyclic LOHC and could prove useful to tune the physico-chemical properties of the LOHC and access bio-based structures.

Dibenzofuran, the analogous structure of NEC, possesses high gravimetric and volumetric densities (6.7 wt.%H₂ and 67 gH₂/L). Early results presented its hydrogenation with a Ru/LiAl₅O₈ catalyst, yielding 90% of the hydrogenated carrier at 100 °C and 60 bar H₂ and 10% of hydrogenolysed products.²²⁰ Here, the cleavage of the C-O bond by H₂ for O-heterocycles required the hydrogenation of the rings prior to the hydrogenolysis (Figure II-20).³⁷³

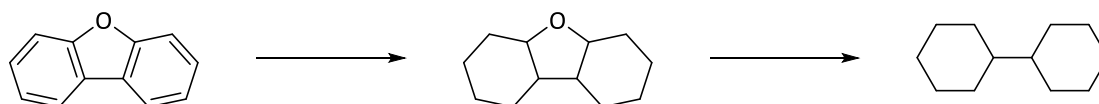


Figure II-20 – Simplified mechanism of the hydrogenation followed by the hydrodeoxygenation of dibenzofuran.

In addition, numerous articles reported the hydrodeoxygenation of Dibenzofuran with non-noble NiMo/Al₂O₃³⁷⁴ or noble Pd/COK-12³⁷⁵ metal catalysts. In particular, Pt, Pd or Ru/SiO₂ catalysts were used to probe the metal activity for hydrogenation and hydrogenolysis. Ru was the most active metal with a high hydrogenolysis capacity while Pt showed a higher selectivity to O-heterocycles in the same conditions but slower hydrogenation activity.³⁷⁶

The dehydrogenation was performed with a Pd/C catalyst at 225 °C and evolved 60% H₂ in 24 h without hydrogenolysis, confirming that Ru or high H₂ pressure were responsible for the hydrogenolysis.²²⁰ Thus, except if the hydrogenation is carried out at low temperature and pressure with selective catalytic systems, O-heterocycles would show poor cycling performances as LOHCs. Recent developments with the selective hydrogenation (>99%) of eutectic mixtures containing Diphenylether with a Pd/Al₂O₃ catalyst at 50 bar and 120 °C in 189 h and especially a Rh/C catalyst at 20 bar H₂ and 60 °C in 18 h could spark new interest in O-heterocycles, but no development have been published to date.³⁷⁷

Here, no other molecule was unanimously reported in the literature as a LOHC. Therefore, we suggest to present acceptorless dehydrogenation reactions that could prove useful to build new LOHC structures. When possible, a focus on heterogeneous catalytic systems was performed as they often are a good indicator to probe the progress of such reactions on the industrialization state.

II.4.2.5.4 Primary alcohol/Aldehydes-esters-carboxylic acids

The irreversible decomposition of alcohols by reforming produces H₂, but the reversible hydrogenation/dehydrogenation of primary and secondary alcohols would be more appropriate for the LOHC technology and pave the way for easily bio-sourced LOHC structures.³⁷⁸ Here, the different heterogeneous catalysts used for hydrogenation of carbonyl compounds will be reviewed and then specific catalysts for the dehydrogenation of Ethanol (EtOH) will be discussed. EtOH was chosen due to its chemical simplicity that allows studying its dehydrogenation into Acetaldehyde (ACE), Acetic acid (AcOH) and Ethyl acetate (EtOAc) (II-23).

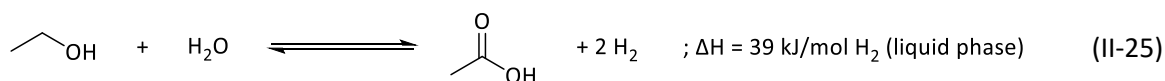
to ACE, 9.6% to Ethyl acetate and Acetic acid was also observed. In addition, the catalyst deactivated over time, losing 14% activity after 28 h, but its regeneration was possible by using H₂.³⁹⁹ Since then, multiple supports were tested in order to tune the acidic/basic sites and stabilize the active Cu NP. A Cu supported on N-rich carbon achieved 98% selectivity to ACE due to its affinity for well-dispersed Cu NP and its enhanced adsorption properties promoted by the nitrogen atoms.⁴⁰⁰ SiO₂/SiC and C/SiC supports were then developed as the Si-OH groups promoted the dispersion of the NP.⁴⁰¹ The C/SiC support was advantageous due to its improved desorption properties that blocked side-reactions. At 280 °C, the comparison of Cu/SiO₂/SiC and Cu/C/SiC showed that the former achieved the best conversion (81% vs 66% resp.) while the latter was the most selective (94% vs 99% resp.).⁴⁰² Metal oxides and HT structures were also tested as supports for Cu and revealed that the O-H EtOH bond breaking on support acidic sites was the rate-determining step. However, the rate-determining step was also the C_α-H cleavage depending on the reaction conditions (EtOH pressure, strongly acidic catalysts).⁴⁰³ In addition, chemically inert supports like ZnAl₂O₄ showed high conversion and selectivity (90% and 95% resp.) at 300 °C, but higher temperatures promoted dehydration and coke deposition.⁴⁰⁴ Finally, Cu supported on KIT-6 mesoporous silica was modified to obtain moderate acid sites on the surface and an optimum distribution Cu species that enabled superior EtOH conversion and ACE selectivity (96.8% and >99% resp.) at 250 °C with C_α-H cleavage as the rate-determining step.⁴⁰⁵

Other active metals such as Ru and other platinum group metals^{406,407}, Ag⁴⁰⁸, Au⁴⁰⁹ and Co⁴¹⁰ were tested with less success. Selectivity was usually an issue for platinum group metals due to their higher tendency to promote condensation and dehydration reactions.^{406,407} While the conversion were originally low for Ag/HT (17% in 72 h)⁴⁰⁸, recent developments on Ag catalysts supported on SiO₂ and CeO₂-SiO₂ allowed for a better dispersion of the Ag NP, increasing at 300 °C the conversion of EtOH to 50% with 95-100% selectivity to ACE in a fixed-bed reactor.⁴¹¹ Further work revealed the necessary concerted mechanism between Si-OH and Ag sites to activate the O-H bond.⁴¹² Conversely, Au/TiO₂ followed a different mechanism with the adsorption preference of ethoxy species on Ti⁴⁺, the promotion of the C_α-H cleavage by the support and Au NP activation by spillover.⁴⁰⁹ Later, Au supported on ZnZrO_x catalysed the selective conversion of EtOH to ACE at 300 °C with a yield of 60%. Nevertheless, higher temperatures showed a decrease in ACE due to Acetone formation.⁴¹³ Finally, while early attempts with Co catalysts mainly induced the reforming of the carrier⁴¹⁴, recent advances proposed Co supported on N-doped carbon catalysts, with an EtOH conversion of 66% and a selectivity of 84% to ACE at 400 °C. Nonetheless, the dehydration to Ethylene was also observed as a competing reaction attributed to the presence of oxidized Co species formed during the reaction.⁴¹⁰

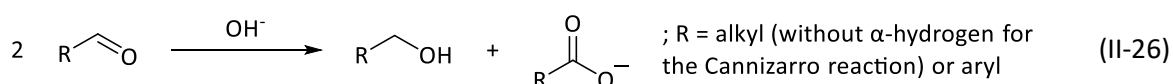
The dehydrogenation of primary alcohols to aldehyde seems rather challenging as dimerization (ester and ether formation), dehydration and overoxidation are side-reactions that are difficult to overcome. From a practical standpoint, dimerisation is usually limited by diluting EtOH by a carrier vector and overoxidation could theoretically be prevented by ensuring that the reaction medium is air- and water-free. Nonetheless, dehydration would still occur due to the high reaction temperature and promotion by acid sites on the support.

II.4.2.5.4.3 Primary alcohols/Carboxylic acids

Acetic acid (AcOH) is a potential LOHC that can be obtained by the dehydrogenation of equimolar ethanol-water solutions, reaching densities of 6.3 wt.%H₂ and 54 gH₂/L (II-25) with lower dehydrogenation enthalpies than homocyclic and heterocyclic systems.^{398,415}



Originally, the conversion of a primary alcohol to a carboxylic acid required the oxidation of the carrier, using either air or harsher chemicals as oxidant and Au-based heterogeneous catalysts in liquid phase.⁴¹⁶ However, the presence of O₂ can shift the reaction equilibrium by unfavorably converting H₂ to H₂O by combustion reaction (II-1). The first acceptorless dehydrogenation was carried out by Milstein et al. with a homogeneous Ru catalyst in presence of a NaOH aqueous solution where water acted as the oxygen donor, producing carboxylate salts with the concomitant release of H₂.⁴¹⁷ This reactivity was based on Cannizzaro or Tishchenko reactions that allowed for the disproportionation of aldehydes in alkaline conditions by direct hydride transfer or ester formation and hydrolysis respectively to form the primary alcohols and carboxylate salts (II-26).^{418,419} Hence, any catalyst converting the selective dehydrogenation of primary alcohols to aldehydes could theoretically be relevant for this reaction.

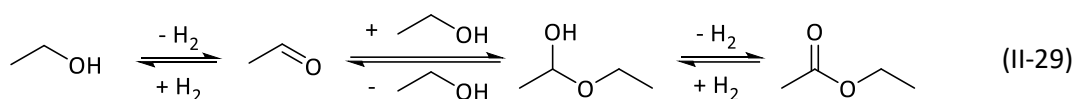


The first example of heterogeneous acceptorless dehydrogenation used Rh/C in a closed vessel with 2.2 equivalents of base in H₂O at 100 °C under Ar, obtaining 100% conversion but limited selectivity (<55%) to the carboxylic acid with NaOH in 24 h.⁴²⁰ Subsequent work by the same group assessed the noble metal efficiency for the reaction, with the activity order Pd>Rh>Pt>Ru/C. The effect of the base was also investigated with the reactivity order NaOH>KOH>LiOH>Na₂CO₃>NaHCO₃>no base. In addition, the reaction was performed under reduced pressure (0.8 bar) and 80 °C to facilitate the removal of H₂. Reactions on both aliphatics and benzylic alcohols achieved quantitative yields in 6 h.⁴²¹ Further catalytic development on noble metals were scarce. Recent advances reported Pd/NiO NP able to dehydrogenate benzylic alcohols up to 97% yields in the presence of 1.1 equivalents of KOH in 6 h at 110 °C. 50-70% yields could also be achieved for aliphatic alcohols with longer reaction times. Moreover, the catalyst showed only little activity loss (<10%) over 6 cycles.⁴²² Finally, supported Ru homogeneous catalysts also catalyzed the reaction with 1.1 equivalents of KOH at 110 °C, achieving up to 99% conversion and selectivity for both benzyl alcohols and aliphatic alcohols. The catalyst was stable for 20 cycles, retaining 99% of its original activity.⁴²³

Noble metal-free catalysts were also developed. ZnO with 2 equivalents of KOH catalyzed the conversion at 164 °C in 36 h in 65-85% yields for aliphatic product and similar yields were obtained for benzylic alcohols in 18 h. The reaction pathway occurred through a zinc alkoxide species that further dehydrogenated to aldehydes and esters through a Tishchenko mechanism.⁴²⁴ Co catalysts were also used for the clean conversion of benzylic alcohol to the corresponding carboxylic acids. Co/N-doped CNT fully converted benzyl alcohol with 99% selectivity for the carboxylic acid in 24 h at 100 °C. The conversion of aliphatic alcohols was generally slower but good yields (>80%) were obtained if the base amount and time were increased.⁴²⁵ Similarly, Co/N-doped carbon achieved 100% conversion of benzyl alcohol and 88% selectivity to benzoic acid when reacted with 1.2 equivalents of KOH in 24 h at 164 °C. The aliphatic alcohols reactivity was lower, but 80% yields were achieved in 36 h. In addition, the catalyst showed an excellent stability with 15 cycles without a significant loss of activity and was easily retrieved from the reaction mixture by magnetic separation.⁴²⁶ Recently, a bimetallic ZnCoO_x rod-like catalyst with 1.2 eq NaOH achieved up to 96% yield for benzylic alcohols in 18 h at 135 °C. Aliphatic alcohols were only slightly less reactive, with 85-88% yields in 20 h. Gram-scale (5 g) reactions were performed for both benzyl and aliphatic substrates in similar yields. Finally, the catalyst showed an excellent stability over 10 cycles. Interestingly, the reaction pathway was here more akin to a Cannizzaro-type reaction as no ester formation and disproportionation of the aldehyde to the alcohol and the acid were observed.⁴²⁷

220 °C.⁴³⁴ Key steps of the mechanism were also elucidated on this catalyst, rationalizing the multi-step mechanism and the by-products formation pathways. Finally, dehydrogenation under different pressures revealed a positive effect on the selectivity, indicating that by-products formation was dependent on the accumulation of ACE. Indeed, when increasing the pressure to 8 bar at 200 °C, up to 93% selectivity was achieved, but the conversion was reduced by 9%.⁴³⁵

Cu-Cr catalysts that also showed high conversion and selectivity and at 200 °C, Cu/Cr₂O₃ catalyzed the formation of EtOAc with 95% selectivity, highlighting the role of Brønsted acid sites on the selectivity.⁴³⁶ Further catalytic development introduced the doping of alumina with BaCrO₄ to form a CuCrO₄/CuO/Cu/BaCrO₄/Al₂O₃ catalyst that increased the EtOH conversion to 65-70% and the selectivity above 98% at 220 °C and 20 bar in flow conditions. Here, the rate-determining step for each released H₂ molecule was assessed, revealing that the first rate-determining step was the dissociative adsorption of EtOH to produce an adsorbed ethoxy group and the second rate-determining step was the condensation of ACE with EtOH in a hemiacetal that acted as an intermediate before further dehydrogenation to EtOAc (II-29).⁴³⁷



The rate-determining step was catalyst-dependent as a DFT study on Cu (111) reported that the rate-determining step was the dissociation of EtOH⁴³⁸, while the condensation of an alcohol and an aldehyde was reported for Cu/ZrO₂.⁴³³ In addition, each component of the catalytic system has a dedicated role that could be summarized as follow: reduced Cu⁰ for the dehydrogenation activity of EtOH, Cu⁺-metal oxide interface as the preferential site for EtOH adsorption and the support for the catalysis of the O-H bond cleavage to form Cu-alkoxides and side-reactions like dehydration.^{433,439} In particular, tuning the Cu⁰/Cu⁺ ratio by the modification of the NP size was paramount for the selectivity as ACE would form at low ratios while EtOAc would form at higher ratios.⁴⁴⁰ In fact, the effect of size modification (i.e. Cu⁰/Cu⁺ ratio modification) was also promoted by support replacement⁴⁴¹, support phase modification⁴⁴² or Cu content adjustment⁴³⁰.

As other metals such as Au, Pd, Pt, Co or Ag and their alloys were active for the dehydrogenation of EtOH to ACE (see II.4.2.5.4.2), these catalysts could be theoretically active for the dehydrogenation of EtOH to EtOAc, but only limited examples have been reported. The comparison of active metals supported on ZrO₂ for the dehydrogenation of EtOH to AcOEt was first performed with a reactivity order Cu>Ni>Ag>Pt>Ru>Ir>Pd≈without metal.⁴³³ Interestingly, this order was dependent on the support as a series of catalysts supported on SnO₂ had a reversed order of reactivity with a surprisingly inactive Cu catalyst: Pt>Rh>Ir>Pd>Re>Ru>Ag=Ni=Co=Cu=0. Here, the synergistic effect of basic supports with Pt was attributed to the activation of the aldehyde species by the acidic Sn⁴⁺ metal center and O²⁻ basic sites. Other supports were tested with their activity ranked in the order SnO₂>ZrO₂>CeO₂>Nb₂O₅>TiO₂>C=Al₂O₃=SiO₂=HBEA zeolite=MgO=0.⁴⁴³ Finally, Pd/ZnO was also able to achieve the dehydrogenation to EtOAc, but the reaction was not selective as ACE was the main by-product, potentially due to the Pd structure that increased the stability of ACE on the surface.⁴⁴⁴

Homo-esterification presents numerous advantages like low-cost Cu-based catalysts and a high tenability of the selectivity by modification of the support, the addition of promoters and distribution of the Cu species. However, due to the multistep nature of the mechanism, different stable intermediates can form such as aldehydes, which can limit the control of the system. Finally, dehydration at high temperatures in presence of acidic species is still a major side-reaction.

II.4.2.5.4.4.2 Intermolecular hetero-esters

Dehydrogenative cross-esterification is challenging and still in its infancy. Indeed, while process techniques such as drop-wise addition facilitate the cross-coupling of a primary alcohol with a secondary or tertiary alcohol, homocoupling was difficult to overcome when mixing two different primary alcohols. Attempts for direct cross-esterification were also performed with heterogeneous transition metal sulfides MoS₂ and WS₂ at 230 °C, achieving 52% conversion in 24 h under 5 bar He pressure but a mixture of symmetrical and asymmetrical esters was obtained.⁴⁴⁵ Most successful heterocoupling were performed with homogeneous catalysts, using P and N bidentate or tridentate pincer ligands as well as monodentate N-heterocyclic carbene (NHC) ligands to control the coordination sphere of the molecules on the catalyst. Examples of such ligands are presented in the Figure II-21

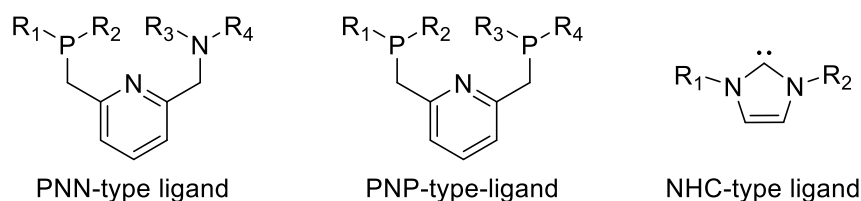
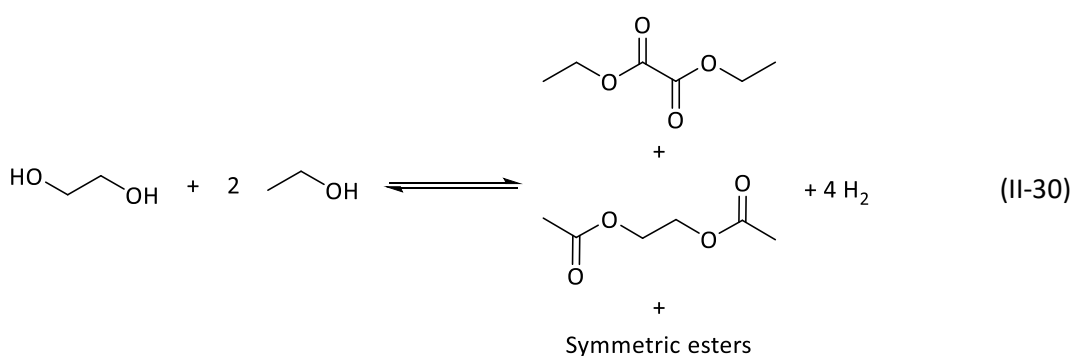


Figure II-21 - Classic ligands used in homogeneous catalytic systems for the acceptorless dehydrogenation reaction. $R_1, R_2, R_3, R_4 = H, \text{ alkyls, aromatics.}$

A first example to yield asymmetrical esters relied on the trans-esterification of symmetric esters using a secondary alcohol with Ru PNN-pincer catalyst in 17-36 h at 135 °C with up to 95% selectivity.⁴⁴⁶ Direct cross-coupling of primary alcohols was originally performed with a dimeric Rh homogeneous catalyst in the presence of 0.5 equivalent of NaHCO₃, achieving 67-97% yields on a variety of aromatic substrates.⁴⁴⁷ Recent advances proposed a Mn PNN-pincer catalyst in presence of a base to yield the cross-coupling of primary alcohols in 71-95% yields and trans-esterification with high selectivity (70%).⁴⁴⁸ To date, the best example was published by Milstein et al. with the Ethylene glycol+Ethanol/Diethyloxalate couple using a Ru PNP-pincer complex under solvent-free and base-free conditions to yield a reversible mixture of different esters including symmetrical esters like EtOAc (13%) and other asymmetrical esters like Ethane-1,2-diyl diacetate (18.5%) (II-30).⁴⁴⁹



While such structures present a great interest to tune the hydrogen capacity of the LOHC systems, progress on that account have been limited due to a lack of selective heterogeneous dehydrogenation catalysts for the asymmetrical esterification.

II.4.2.5.4.4.3 Intramolecular esters/Lactones

Intramolecular esterification has been mainly studied through the 1,4-butanediol/ γ -butyrolactone (BDO/GBL) couple as succinic acid showed great promises as a platform chemical derived from biomass.⁴⁵⁰ In addition, BDO can store up to 4.4 wt.%H₂ and 45 gH₂/L and presents an attractive

- Liquid-phase

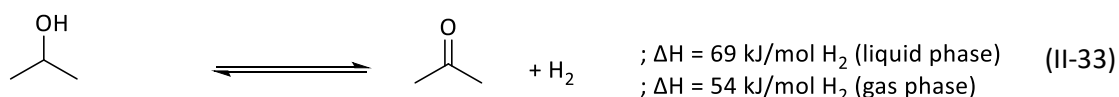
Liquid-phase dehydrogenation was much less studied than the gas-phase dehydrogenation of BDO to GBL, often due to its lower kinetics: for the (6:1:2:2) CuO:ZnO:ZrO₂:Al₂O₃, the dehydrogenation at 200 °C had a similar selectivity but the full conversion was achieved for a residence time 6 to 7 times longer.⁴⁵⁸ Interestingly, the Cu activity in liquid-phase was much lower than that of noble metals and an early study showed that GBL was obtained in 94% yield with Ru/AlO(OH) at 110 °C in 32 h and in dilute conditions.⁴⁶⁷ A comparative study of metal activity on SnO₂ at 180 °C showed that the order of was Pt>Ir>Ni>Pd>Co>Rh>Cu>Re>Ag while it was Pt>Rh>Pd when supported on rutile TiO₂ in photocatalytic conditions.^{468,469} Interestingly, Pt required different supports than Cu: ZrO₂ or MgO were inactive while SnO₂ or Al₂O₃ catalyzed the reaction. In solvent-free conditions, Pt/SnO₂ achieved 100% conversion and 80% selectivity in 36 h at 180 °C. The exceptional activity of this catalyst was linked to Sn⁴⁺ acid sites that activated the aldehyde intermediate.⁴⁶⁸ Photocatalysis at room temperature in 1 h with different TiO₂ phases showed the lactone instability on the anatase phase while the rutile phase cleanly catalyzed the dehydrogenation. By adding Al₂O₃ with weak acid sites, the photocatalytic mechanism was promoted while strong acid sites protonated titanate nanotubes addition was linked to dehydration and coupling products formation. Unfortunately, the dehydrogenation was much more active for the aromatic phthalides than BDO that achieved 90% and 20% conversion respectively.⁴⁶⁹

- Conclusion

Lactonization has been quite developed using heterogeneous catalytic systems based on Cu and noble metals. Gas-phase dehydrogenation (> 200 °C) presents higher kinetics than liquid-phase dehydrogenation due to the higher reaction temperature, but some limiting diffusion phenomenon might also take place in the liquid-phase, hindering the reaction. Moreover, as thermodynamics favor the formation of 5-membered rings, the BDO/GBL couple might enable the research of low dehydrogenation enthalpy LOHC.

II.4.2.5.4.5 Secondary alcohols/Ketones

Ketones and secondary alcohols are abundant in nature and are hence of great interest in order to produce LOHC from renewable feedstock.⁴⁷⁰ In addition, Isopropanol (IPA) and Acetone industrial production total more than 8 millions of tons showcasing their availability.⁴⁷¹ Nevertheless, IPA has moderate gravimetric and volumetric densities (3.3 wt.%H₂ and 26 gH₂/L) as well as a dehydrogenation enthalpy equivalent to homocyclic systems (II-33).^{398,472} Moreover, contrary to primary alcohols, secondary alcohols are less sensitive to overoxidation, facilitating their storage and recyclability. However, they can be extremely reactive with peroxides and are prone to aldolisation in alkaline conditions.



The earliest example of IPA dehydrogenation to Acetone was reported by Sabatier and Sanderens with a Cu heterogeneous catalyst that achieved up to 75% Acetone yield at 420 °C.³⁸¹ During the 20th century, the dehydrogenation of IPA to Acetone was often performed in a reactive distillation setup with Ni Raney at 82.5 °C, using the boiling point difference of Acetone (56 °C) and IPA (82.4 °C) to remove Acetone from the reaction mixture in order to displace the reaction equilibrium and increase the reaction rate.^{473–475} This setup allowed for the design of a chemical heat pump able to store waste heat by using H₂ as an energy vector. Nevertheless, the conversion was quite slow with less than 5% yield after 6 h at 80 °C.⁴⁷⁵ A comparison at 90 and 100 °C revealed that the reaction proceeded 5 to 10 times faster in gas phase and that the reaction rate was less dependent on the Acetone

concentration.⁴⁷⁶ Ru and Ru-Pt supported on activated carbon were also tested and showed an improved conversion from 5 to more than 85% in 2 h at 100 °C due to a better thermodynamic equilibrium displacement when performing the reaction in the liquid film state.⁴⁷⁷ A later study reported an improved setup able to evolve up to 5 L_{H₂}/h with a Ni Raney catalyst.⁴⁷⁸

Gas-phase dehydrogenation was pursued when it became clear that reactive distillation would not yield sufficient activities. Pt, Cu and their alloy supported on activated carbon were found to be reactive in the order Pt>Pt-Cu>Cu at 175 °C. As expected, kinetics experiments showed that the reaction rate was favored by IPA concentration and slightly disfavored by H₂ and Acetone concentrations. Moreover, the rate-determining step was attributed to be the cleavage of the hydroxyl bond.^{479,480} Cu-based catalyst were principally studied due to their activity above 200 °C. The microstructure of the carbon had no influence on the dehydrogenation rate but modified the selectivity, with platelets achieving 100% selectivity to Acetone at 200 °C. Ce addition increased the activity by 6, but favored the dehydration reaction to propene.⁴⁸¹ Later, Cu⁺ was described as the active species and the addition of NiO increased the charge transfers between Cu⁺ and Ni³⁺, further improving the basicity of the catalyst which allowed for a better Acetone desorption.⁴⁸² Recent catalyst composition included CuO/TiO₂-ZrO₂ with PtO as a promoter to increase the basicity and reactivity of the support⁴⁸³ while a CuO supported on a carbonized MOF achieved 100% conversion and selectivity in a fixed bed reactor at 275 °C by tuning the flux rate.⁴⁸⁴

- Conclusion

Secondary alcohols are intrinsically limited by their low H₂ densities if no H₂ can be exploited on the β-carbons. However, the case of IPA/Acetone is highly interesting as it shows that the dehydrogenation of secondary alcohols can happen with noble metal-free heterogeneous catalysts at the operating temperature of PEM-fuel cells, which would allow for an excellent system integration. Unfortunately, the kinetics are still quite low and most achieved work has been related to system development. Therefore, catalytic development of such reactivity would be of great interest.

II.4.2.5.5 Alcohol and amine couplings

Alcohol and amine couplings can produce various chemical motive such as amides, ureas, imides or carbamides which enable the innovative design of alternative structures for the LOHC technology. In addition, amino acids could be platform chemicals for the production of renewable bio-based O, N-LOHC.

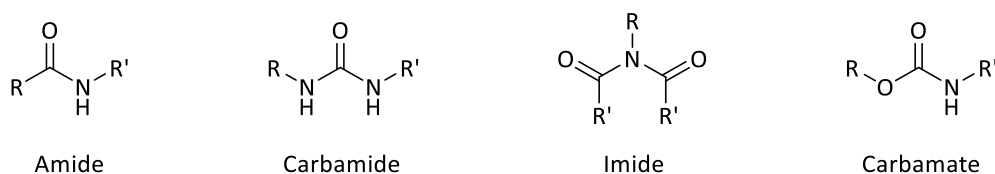


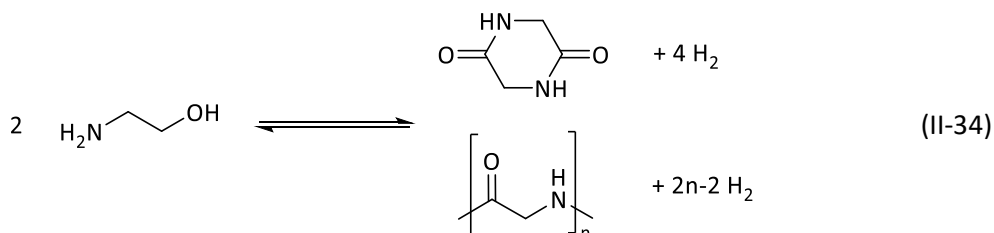
Figure II-22 - O and N mixed motives obtained by the coupling of alcohols and amines

While no heterogeneous catalyst was reported to date, amides, carbamides and imides have already been successfully reversibly produced by the dehydrogenation/hydrogenation of alcohols and amines in homogeneous conditions thanks to the tremendous efforts from the Milstein group.

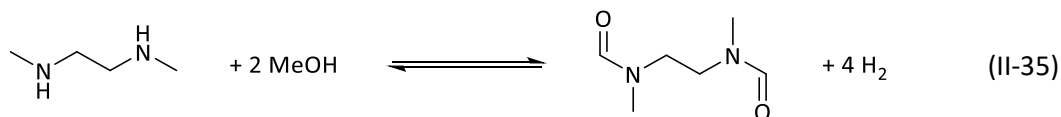
II.4.2.5.5.1 Amides

Amide synthesis applications range from polymer synthesis⁴⁸⁵ to bio-engineering of polypeptides⁴⁸⁶. The first catalyst to achieve the dehydrogenative coupling of a primary amine and a primary alcohol to an amide was a Ru PNN-pincer (Figure II-21) with up to 99% yield in 8 h at 110 °C in toluene for both aromatic and aliphatic compounds. No conversion was observed for the reaction of esters to amides

by amine addition.⁴⁸⁷ Further articles developed Ru-NHC^{485,488,489}, Ru-PNN^{486,490,491} and Ru-PNP⁴⁹² pincer-type catalysts to achieve better conversions and selectivity on a wide variety of substrates. Most Ru-pincer systems necessitated a basic additive, often KOtBu or NaH, and the amides were obtained in yields ranging from 70 to 98% in 24 h at 110 °C in dilute conditions.^{485,489} Later results reported a Ru PNP-pincer catalyst able to hydrogenate and dehydrogenate in solvent-free conditions with 76% and 60% yields respectively⁴⁹² and further development reduced the temperature of dehydrogenation to 35-55 °C⁴⁹⁰. An experimental study coupled with DFT modelling revealed that the amide formation required the stabilization of the catalyst-aldehyde adduct formed during the dehydrogenation of the alcohol so that the nucleophilic attack of the aldehyde by the amine resulted in an intermediate hemiaminal species analogous to the hemiacetal formed during the dehydrogenation of alcohols to esters. Different effects were also probed such as the catalyst loading, the nature and loading of the base, the limitations due to the steric hindrance of the substrate and the ring size dependence for intramolecular amide formation.⁴⁹³ Amide intramolecular formation was often studied as an analogue of the BDO/GBL couple, but only moderate yields (45-68%) were obtained.^{485,489} To date, the most efficient LOHC system were based on β -amino alcohols that formed either linear peptides or cyclic dipeptides depending on the bulkiness of the substituents linked to the β -carbon. High bulkiness promoted cyclic dipeptide formation up to 99% yields in 19 h at 135 °C in dioxane.⁴⁸⁶ Neat dehydrogenation produced the polyamide in limited yields (48%) while diluted conditions favored the production of the cyclic dimer with selectivity up to 70%. Ethanolamine (6.5 wt.%H₂ and 67 gH₂/L) was formed back by the hydrogenation of the dehydrogenated reaction mixture in quantitative yields and the presence of polyamides was responsible for an increased reaction time. The stability of the system was limited as a decrease of 25% of conversion for both steps was observed over 3 cycles (II-34).⁴⁹¹



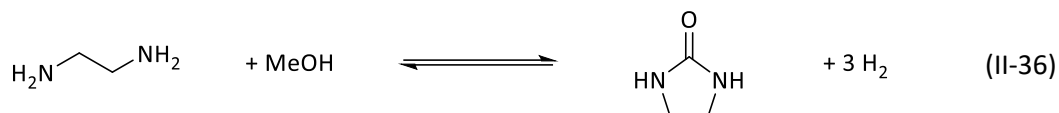
Recent development promoted the use of Mn PNN⁴⁹⁴ and PNP⁴⁹⁵ pincer catalysts that catalyzed the reaction of symmetric esters with amines to amides in a similar fashion to transesterification.⁴⁹⁴ In addition, Dimethylethylenediamine and Methanol were used as a hydrogenated feedstock to produce the corresponding diamide (II-35).



The catalytic system was efficient for both hydrogenation and dehydrogenation with complete conversion of the starting material and 86% selectivity.⁴⁹⁵

II.4.2.5.5.2 Carbamides

Carbamides are found in numerous natural chemicals such as urea. Their synthesis was achieved by the acceptorless dehydrogenation of Ethylenediamine and Methanol with Ru PNP⁴⁹² and PNN⁴⁹⁶ pincer catalysts to form 2-Imidazolidinone (6.5 wt.%H₂ and 58 gH₂/L using the density of Ethylenediamine) (II-36).

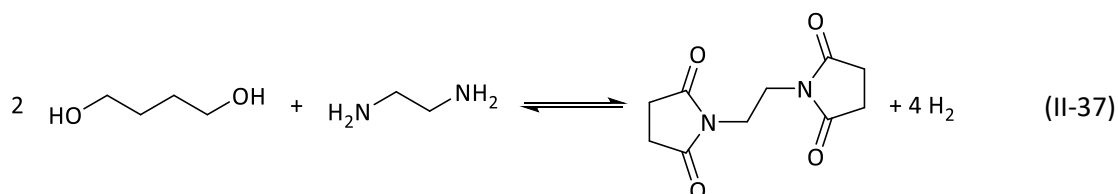


The dehydrogenation was performed in 24-48 h with a Ru PNN-pincer catalyst to produce the carbamide, acyclic monoamide and acyclic diamide species. All obtained products were regenerated in 1.5 days at 170 °C and 60 bar H₂ to their hydrogenated constituents with up to 83% yield for Ethylenediamine while Methanol was always obtained in lower yields.⁴⁹⁶

II.4.2.5.5.3 Imides

Imides and especially aromatic imides are important synthesis intermediates for the fabrication of pigments and are highly valued in high-added value niche applications such as electronics parts.⁴⁹⁷ While early attempt at the hydrogenation of cyclic imides by Pez et al. was proven unsuccessful using a heterogeneous Ru/LiAl₅O₈ catalyst at 170 °C²²⁰, recent advances reported the production of cyclic imides through the dehydrogenation of BDO with amines by Mn⁴⁹⁸ and Ru⁴⁹⁹ PNN pincer catalysts. Early results with a Mn PNN-pincer catalyst and KH as an additive performed the dehydrogenation of BDO with a variety of amines in 60-99% yields in 40 h at 110 °C. In particular, diamines were particularly reactive and produced dicyclic imide structures. Moreover, the high reactivity of GBL with amines was revealed and the mechanism for the coupling could follow simultaneously two reactive pathways, either a direct nucleophilic attack akin to an amide formation from an alcohol and an amine or a ring opening mechanism due to a nucleophilic attack on GBL. The imide formation then proceeded through a hemiaminal intermediate.⁴⁹⁸

Further development with a Ru PNN-pincer catalyst and KO^tBu achieved in 40 h at 135 °C and 40 bar H₂ the hydrogenation of cyclic imides to BDO and the corresponding aromatics or aliphatic amines in 99% conversion with 99% yields for both BDO and the amines. BDO and Ethylenediamine were especially studied due to their high combined gravimetric and volumetric density of 6.7 wt.%H₂ and 68 gH₂/L (with regard to the density of BDO) (II-37).



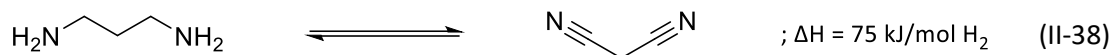
The dehydrogenation with the same catalyst in presence of KO^tBu in Dioxane achieved 99% conversion and 70% selectivity to the imide, 12% to the lactone and oligoamides in 24 h at 120 °C. No complete cycling was performed, but the the cyclic imide yield was 64% after the second dehydrogenation.⁴⁹⁹

- Conclusion

Alcohol and amine couplings were recently discovered and developed by the Milstein group, opening a key segment of bio-based molecules to the LOHC technology. The main limitations of such systems originate from the homogeneous catalysts that require strong bases as additives, the presence of solvents and the formation of polymeric by-products. Moreover, it should be noted that the extremely low temperature achieved in these studies could be achieved due to the dilution of H₂ in an unreactive gas vector, effectively performing the dehydrogenation against a vacuum due to the almost null H₂ partial pressure. Therefore, evaluation of these reactivities under 1 bar H₂ might strongly modify the required reaction temperature. In addition, H₂ dilution in a gas might also require gas separation in order to achieve high energy in integrated systems.

II.4.2.5.6 Amines/Nitriles

H₂ storage in the primary amine/nitrile function was proposed by Pez et al.²²⁰ and later theorized⁵⁰⁰ as a hydrogen storage system able to store up to 13.3 wt.%H₂, effectively doubling the best gravimetric densities of classic homocyclic LOHC. In particular, LOHC couples like 1,3-Propanediamine/Malononitrile could reach exceptionally high gravimetric and volumetric densities (10.8 wt.%H₂ and 95 gH₂/L resp.) at the cost of an increased reaction enthalpy and toxicity (II-38).²⁶⁴



Patents related to the dehydrogenation of amines to imines and nitriles were published in 2010⁵⁰¹ and 2014⁵⁰² respectively and a start-up named ASEMBLON Inc. was created by the main inventor, E. Naeemi, based on this IP. The start-up developed stationary energy storage systems able to release 99.99% pure H₂ in a dual-bladder fuel tank.⁵⁰³

- Hydrogenation

The first example of nitrile hydrogenation was published by Sabatier in 1905 with a reduced Ni catalyst that performed the unselective reduction of nitriles with H₂ to primary, secondary and tertiary amines.⁵⁰⁴ While numerous catalytic systems have been developed such as colloidal Pd⁵⁰⁵, Ni Raney⁵⁰⁶, Pt oxide⁵⁰⁷, Raney Co⁵⁰⁸, Cu₂Cr₂O₅⁵⁰⁹, supported platinum group metals⁵¹⁰, metal borides⁵¹¹, metal alloys⁵¹², the less active Raney nickel and copper chromite are still used industrially due to their lower price. However, their problematic toxicity promoted the development of non-noble transition metals Ni⁵¹³, Co⁵¹⁴, Cu⁵¹⁵, and Fe⁵¹⁶ heterogeneous catalysts. Interestingly, most recent systems carried out the hydrogenation in presence of ammonia in order to thermodynamically disfavor the transamination reaction that produced the dialkyl and trialkylamines compounds. In particular, Ni/SiO₂ achieved the complete conversion and 84% selectivity to the monoalkylamine in 5 h at 100 °C and 13 bar H₂ in ethanol.⁵¹⁷ Further development highlighted the efficiency of K-NiCo/Al₂O₃ to selectively (>99.9%) convert Isophthalonitrile to m-Xylylenediamine at 80 °C and 60 bar H₂ in presence of NaOH and in a mixture of Toluene and Methanol.⁵¹⁸ More heterogeneous and homogeneous catalytic systems used to perform the hydrogenation of nitriles to primary amines can be found in excellent reviews.^{519,520}

- Dehydrogenation

An early example of amine dehydrogenation was performed with a Mo catalyst that showed amine dehydrogenation with disproportionation, achieving nitrile selectivity inferior to 5% due to imine couplings.⁵²¹ Since then, no selective heterogeneous catalyst have been reported for this reaction in solvent-free conditions. Further work relied on Ru⁵²² and Ir⁵²³ pincer catalysts in order to control the active center., Ir homogeneous catalysts showed great promises to catalyze the reaction when in presence of a base as co-catalyst. Depending on the base amount, 97% conversion and 98% selectivity to nitrile at 160 °C in 24 h were obtained, diminishing to 2% nitrile without base.⁵²³ However, due to its high price, Ru was often proposed as an alternative catalyst. The first selective Ru catalyst yielded nitriles in 20-80% rates without oxidant or H₂-acceptor in toluene at 110 °C in 24 h.⁵²² The mechanistic analysis of the Ru NNN-pincer catalyst revealed a fast dehydrogenation of the imine intermediate was required in order to avoid a nucleophilic addition on the aldimine center resulting in transamination, thus dilution in a solvent facilitated the selectivity to the nitrile compounds.⁵²⁴ These results were confirmed by DFT analysis and showed the impact of steric hindrance of the ligand and the primordial role of the non-covalent interactions such as H-bonding on thermodynamic stability of the intermediate species.⁵²⁵ The role of the ligand as a hydride transfer reaction center was exemplified with a Ru-hexamethylenetetramine (HMTA) catalyst that achieved 90% conversion of aromatic

primary amines to the nitriles species in 24 h at 110 °C in toluene.⁵²⁶ Recent developments achieved similar performances on comparable systems, showcasing the ligand diversity able to promote this reaction: Pyrazole NNN⁵²⁴, HMTA^{527,528} and NHC-N-P⁵²⁹. Lastly, a Ru heterogeneous catalyst supported on the UiO66(Ce) MOF structure achieved 25-90% yields to nitriles in H₂O in 16 h at 130 °C. Although the structure seemed stable for 4 cycles, the yield dropped by 50% after 6 cycles due to structural collapse.⁵³⁰

Electrooxidation have also been employed to electro-oxidize amines to nitriles at the anode and produce H₂ at the cathode. In 1982, an early example reported a Ni(OH)₂ anode in KOH/H₂O that converted Benzylamine in Benzonitrile with 90% yield in 4 h at 40 °C.⁵³¹ Recent examples used NiSe⁵³² and Ni₂Si⁵³³ anodes in KOH/H₂O solution at room-temperature that achieved the conversion in 3 h with a faradic efficiency over 95% and 40 min with a faradic efficiency over 99% respectively.

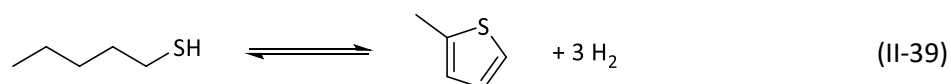
- Conclusion

Primary amines have the highest theoretical gravimetric and volumetric densities of any LOHC, therefore their study seems rather compelling. Nonetheless, these systems are usually limited by their low selectivity due to the transamination reaction. As this side-reaction is particularly prevalent in neat conditions, the development of efficient amine/nitrile based LOHC is limited if no selective catalyst is designed. Moreover, their high toxicity and corrosivity is another barrier to their implementation.

II.4.2.5.7 S-containing LOHC

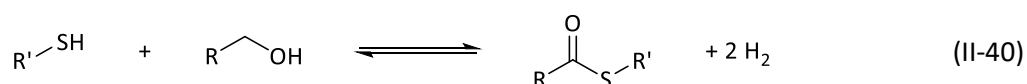
S-containing LOHC have been often dismissed due to their high tendency to undergo hydrodesulphurization in presence of H₂ and to strongly inhibit the noble metal catalyst activity by irreversible binding.⁵³⁴ Early hydrogenation attempts of Toluene and Naphtalene in presence of Dibenzothiophene with Pt-Pd/SiO₂-Al₂O₃ revealed the conversion of Dibenzothiophene, but no analysis was performed on the obtained products.⁵³⁵ Later, hydrogenation with Ru/C yielded no conversion of Dibenzothiophene and no study have reported it ever since.³⁷³

A patent was filled in 2007 by Naeemi reporting for the dehydrogenation to 2-Methylthiophene by the cyclization of 1-Pentanethiol (5.8 wt.%H₂ and 48 gH₂/L), with an Au catalyst (II-39).⁵³⁶



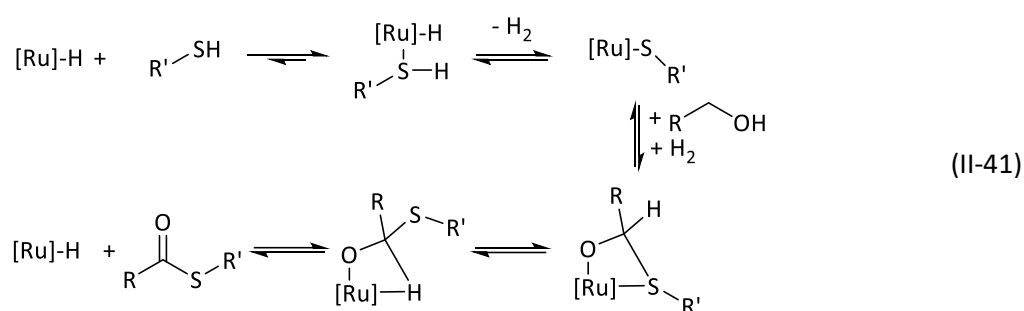
2-Methylthiophene hydrogenation to Tetrahydromethylthiophene was later reported with noble metal catalysts exhibiting a better selectivity to the desired product than bimetallic, phosphide and sulfide catalysts. The selectivity was inversely dependent on the number of basic active sites that favored hydrodesulfurisation, however no catalyst could efficiently carry out the reaction.⁵³⁷

Recently, the hydrogenation of thioesters was achieved with a Ru-acridine homogeneous catalyst with conversion >99% and yields >90% for both the alcohol and the thiol on a wide variety of examples in 36 h at 135 °C and 20 bar H₂ in dioxane. Equivalent performances were obtained at 40 bar H₂ for the conversion of thiocarbamates and thioamides to the corresponding thiols and the respective amides and amines (II-40).⁵³⁸ However, the comparison of the densities of the thioester analogue of ethyl acetate shows a diminution of both densities due to the atomic weight of the S atom (S-Ethyl thioacetate: 3.7 wt.%H₂ and 29-48 gH₂/L depending on Ethanol and Thioethyl densities respectively)



The dehydrogenation of alcohols and thiols to thioesters with a similar Ru homogeneous catalyst was reported soon after.^{539,540} Alcohols were converted to esters, while a mixture of alcohol or aldehyde with a thiol yielded mainly the thioester. A strong pressure dependence was observed as the yields dropped from 93% to less than 1% when the H₂ pressure was increased from 0 to 1.9 bar.

Interestingly, DFT modelling showed that the kinetic competition between the ester and thiol formation was controlled by the stronger and quasi-irreversible Ru-thiolate bonding due to the stronger acidity of the thiol compared to the alcohol. Although the ester was the most stable product, the thermodynamic control of the intermediate led to the less thermodynamically favored thioester product. Further mechanistic studies revealed that the thioester formation followed a pathway where the thiol bonded and was subsequently dehydrogenated on a vacant site of the Ru catalyst. The insertion and subsequent dehydrogenation of the alcohol to the aldehyde was achieved in an outer sphere mechanism before the formation of the C-S bond and β-H elimination to form the thioester and regenerate the catalyst (II-41).

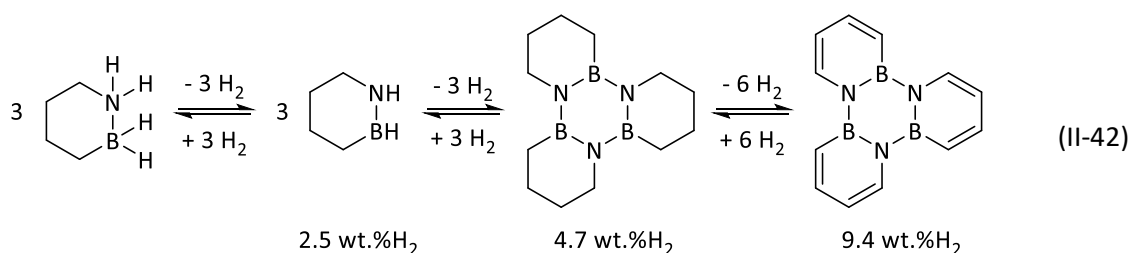


- Conclusion

S-based LOHC exploration have been scarce due to the negative influence of sulphur on the catalysts and the rapid (de)hydrosulfuration of the structures producing toxic H₂S. In addition, the atomic weight of the sulphur atom is detrimental to the gravimetric density of the LOHC system, hence o-containing LOHC were principally studied instead. Therefore, S-containing LOHC are of little interest if no catalytic system is able to efficiently answer these issues.

II.4.2.5.8 B,N-containing LOHC

The 1,2-Dihydro-1,2-azaborine/1,2-BN-Cylcohexane couple represents the frontier between ammonia-borane and the LOHC technologies which in theory can store up to 9.4 wt.%H₂ if the system is completely dehydrogenated (II-42). From the ammonia-borane point of view, 1,2-BN-cylcohexane can undergo an intramolecular dehydrogenation on the B-N moiety and a trimerisation process. On the LOHC side, the carbon atoms of the trimer can be dehydrogenated to form the analogous aromatic compound.



While these systems are air and moisture stable⁵⁴¹, 1,2-BN-Cylcohexane is a solid that melts at 62-63 °C and is usually diluted in solvent like in a 35 wt.% THF solution, diminishing the gravimetric density to 3.3 wt.%H₂ and volumetric density to for the complete dehydrogenation.⁵⁴²

- Hydrogenation

The hydrogenation of the monocyclic aromatized structure was performed in two steps. Direct hydrogenation of the carbon atoms was achieved in 4 h at 80 °C and 3 bar H₂, yielding the hydrogenated cycle in 99% yield by GCMS and 89% by NMR. Hydrogenation of the B and N atoms was more complicated and required hydride (KH) and acid (HCl) treatments respectively to afford their hydrogenated form in quantitative yields.⁵⁴³ Trimer regeneration was performed by MeOH solvolysis treatment in 12 h at room temperature followed by the use of strong hydrides like LiAlH₄ or BH₃-THF to regenerate the boron atom in 47% and 71% yields from the trimer respectively.⁵⁴⁴ The thermodynamic equilibrium of hydrogenation at 80 °C and 10 bar H₂ was calculated to 95% conversion of the starting material.⁵⁴²

- Dehydrogenation

The quantitative trimerization was originally observed at 150 °C in toluene in 2 h without any catalyst, for a 4.7 wt.%H₂ density. No further dehydrogenation to the aromatized structure was obtained.⁵⁴¹ Thermodynamic computational calculations showed an enthalpy of 32 kJ/mol H₂ for the dehydrogenation of the monocyclic structure to its aromatized form, revealing the beneficial effect of the B-N bond on the thermodynamics of the system.⁵⁴³ In addition, further thermodynamic calculations that the equilibrium conversion would be 99% for the dehydrogenated form under 1 bar H₂.⁵⁴² Further catalytic development revealed that CoCl₂ was an excellent catalyst of the reaction that achieved the quantitative trimerization in 15 min at 80 °C in toluene. The neat dehydrogenation was also performed in the same conditions, but required in 4 h instead. The dehydrogenation of the cycles of the trimer was achieved with an Ir pincer catalyst in presence of an H₂ acceptor in Mesithylene, reaching >99% conversion and 90% selectivity to the fully dehydrogenated product in 18 h at 160 °C. No attempts of the aromatic dehydrogenation of the trimer was reported without any H₂ acceptor.⁵⁴⁴

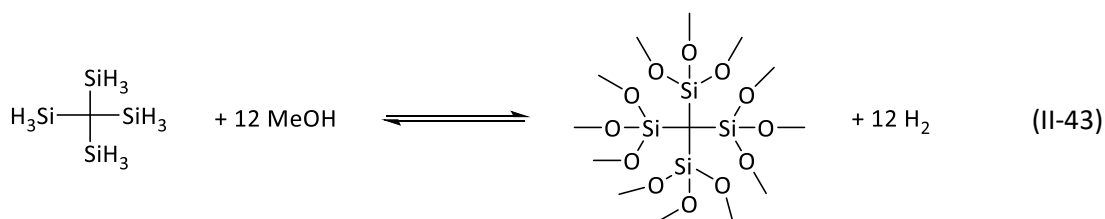
Finally, new generation 1,6;2,3-bis-BN cyclohexane was proposed as a novel carrier system able to thermally release up to 9 wt.%H₂ at 180 °C with only a slight decomposition of the carrier and while the catalytic dehydrogenation with Pd/C released only 1.47 wt.%H₂ at 50 °C.⁵⁴⁵

- Conclusion

B,N-containing LOHC interest is high due to their theoretically lower dehydrogenation enthalpy and high gravimetric density. Nevertheless, their stability and regeneration are key issues that still need to be addressed before B,N-LOHC can be industrially used.

II.4.2.5.9 Si-containing LOHC

Silanes in presence of an alcohol evolve H₂, producing an alkoxy silane as a by-product. The potential best monosilane system is SiH₄ with MeOH (5.0 wt.%H₂) but SiH₄ is a gas. To date, most studies were based on the PhMe₂SiH-Methanol couple that possesses an abysmal gravimetric density of only 0.7 wt.%H₂. Polysilanes have then been rapidly suggested as more efficient storage systems and Tetrasilylmetane-Methanol couple could potentially reach a gravimetric density of 8.82 wt.%H₂ and 70 gH₂/L (using the density of Methanol) (II-43).



- Hydrogenation

Much like alkoxy-boron (see II.4.2.3), alkoxy-silane are highly stable, which poses a problem for their regeneration. While the direct hydrogenation with heterogeneous catalysts is yet to be achieved, advances have been reported. Classic reducing agents like LiAlH_4 ⁵⁴⁶ or borane species with sacrificial reagent like NaBH_4 and Ethylbromide⁵⁴⁷ were originally used. New procedures are starting to emerge as shown by the regeneration of silyl triflates with 4 bar H_2 and an Ir catalyst in presence of a base, achieving 95% conversion at 60 °C in 48 h.⁵⁴⁸

- Dehydrogenation

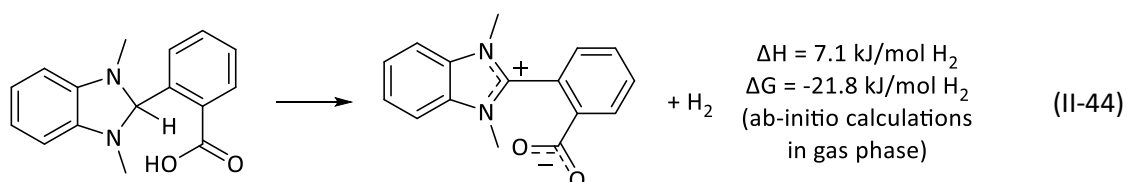
Contrarily to LOHC couples, the dehydrogenation is exothermic. The first dehydrogenation examples of silanes dehydrogenation used water as a source of proton with a heterogeneous Ag/Hydroxyapatite catalyst that achieved complete conversion in 15 min.⁵⁴⁹ However, the obtained Si-OH species were difficult to regenerate by classic methods and Si-O-Si species were also created. H_2 was also released in catalyst free-conditions using Silane and Sodium methoxide at room temperature in 15 s.⁵⁵⁰ Polysilanes and Methanol coupling under Bu_4NF activation achieved an impressive 100% conversion at 25 °C in 10 s.⁵⁵¹ The reaction activity was linked to the steric hindrance of the alcohol and diols could also be used on dihydrides silanes with yields superior to 90% at 60-90 °C.⁵⁵² Recent catalytic systems consisted on Ru⁵⁵³ and Ir⁵⁵⁴ complexes supported on rGO that could achieve superior conversion and stability on stream for 1 h.⁵⁵⁵ Finally, an heterogeneous Cu-doped on ZIF-8 zeolite was proposed to achieve the complete dehydrogenation of PhMe_2SiH and in 9 h at 110 °C.⁵⁵⁶

- Conclusion

Silanes present theoretically high gravimetric properties, with an energy profile better suited for an intermittent energy scenario due to an exothermic dehydrogenation that can be performed at room-temperature. However, their clean regeneration is not yet achieved, although recent progress with silyl triflates might pave the way for direct hydrogenation with H_2 .

II.4.2.5.10 Others

LOHC can be turned into ionic liquids when linked to an imidazolium group by a 1 to 3 carbon chain. The addition of Si atoms in the chain allowed for the liquid state of the structure at room temperature. Hydrogenation and dehydrogenation experiments were performed with Pd/C and quantitative conversions and stability were observed up to 220 °C. However, the gravimetric densities were lowered to 2.05 wt.% H_2 for the carbon linker, 1.58 wt.% H_2 for the C-Si linker.⁵⁵⁷ Finally, H_2 can also be stored in frustrated-Lewis-pair-like benzimidazoline structures able to release H_2 at temperatures as low as 80 °C using $\text{Pd}(\text{OH})_2/\text{C}$.



While this example showcased the possibility of creating organic hydride with exergonic properties, the system gravimetric density is abysmal (0.7 wt.% H_2) and its reversibility has yet to be proven.⁵⁵⁸

II.5 Conclusion and research proposal

Numerous H₂ storage methods exist, but each of them have drawbacks (energy, stability, synthetic accessibility, economic, ...). However, a simple comparison of both gravimetric and volumetric densities of each chemical-based H₂ storage system is pertinent to know at first glance which system could be theoretically efficient to store the highest H₂ amounts (Figure II-23).

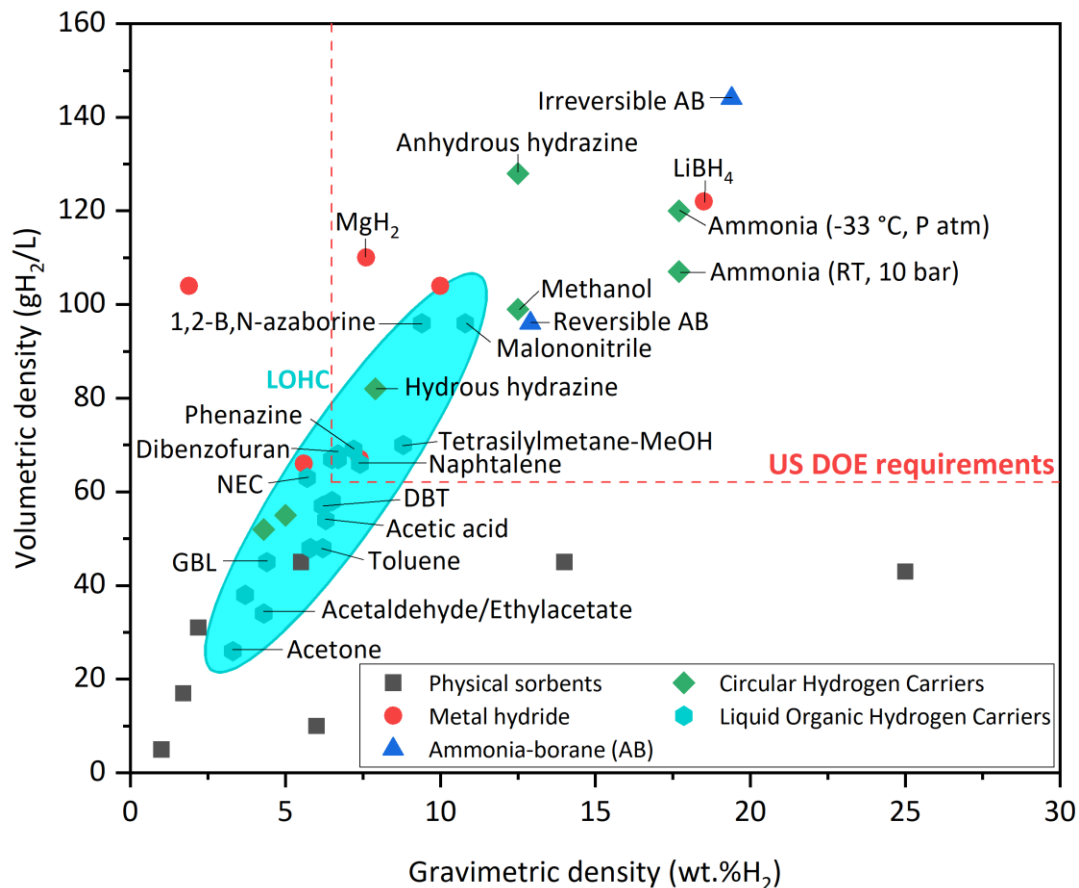


Figure II-23 - Comparison of each chemical-based H₂ storage systems based on their gravimetric and volumetric H₂ densities. The dotted lines represent the gravimetric and volumetric densities required by the US DOE for H₂ storage⁵⁵⁹.

From a quick look, high gravimetric and volumetric densities materials are composed of metal hydrides, ammonia-borane and circular hydrogen carriers while physical sorbents present reduced H₂ storage properties. Comparatively, the LOHC (grey area) present intermediate gravimetric (3-11 wt.%H₂) and volumetric (38-96 gH₂/L) densities which are sufficient to answer the US DOE criteria of 6.5 wt.%H₂ and 62 gH₂/L for vehicular transportation as long as the complete system is not much heavier than the LOHC capacity.⁵⁵⁹

In addition, many other aspects must be taken into account in order to choose an appropriate H₂ storage technology such as its cycling capacity, energy cost like the dehydrogenation enthalpy, reaction phase, catalysts, presence of solvents or additives, synthetic accessibility, cost, safety, transportability, environmental impact, produced H₂ quality and flux and so on. These non-exhaustive secondary criteria are actually primordial and highly dependent on the targeted application. A comparison of different LOHC presented over various secondary criteria this literature review are presented in Table II-1. Here, no state-of-the art LOHC complies with all selected secondary criteria, indicating that the development of new LOHC couples is still necessary to overcome the presented barriers.

Literature review

Dehydrogenated LOHC	Cycling capacity	Dehydrogenation enthalpy (<50 kJ/mol H ₂)	Liquid-phase reaction (no gas separation)	Non-PGM or homogeneous catalyst	Solvent- and additives-free reaction
Toluene					
Naphtalene					
DBT					
N-Ethylcarbazole					
Phenazine					
Dibenzofuran					
Acetaldehyde/Ethylacetate					
Acetic acid					
γ-Butyrolactone			Slow reaction in liquid phase		
Acetone			Distillative reaction		
Glycine anhydride (imide)					
2-imidazolidinone (carbamide)					
BDO+ethylenediamine (imide)					
Malononitrile					
S-Ethyl thioacetate					
1,2-B,N-azaborine					
Tetrasylymetane-MeOH					

Table II-1 - Comparison of different LOHC over various secondary criteria. Green signifies that the LOHC complies with the criterion, red that it does not.

Finally, the complexity of the industrial system must also be taken into account for further development, in particular the size and weight of the system, the network for the H₂ recharging (containers, distribution, competition with already-in-use systems...), economic costs and lastly the overall efficiency of the system.

Comparatively to solid hydrogen storage systems like metal hydrides and ammonia-borane, the LOHC technology fares better on the transportability and economic aspects due to the possibility of using the current oil and gas infrastructures with only small modifications to the current system. In addition, due to their oil-like nature, LOHC also present a better social acceptance for mobility option due to its similarity with the currently employed fuels.²⁰⁹ Circular hydrogen carriers are serious contenders for the LOHC technology but are less attractive due to the gaseous nature of their hydrogen-lean molecules that induce gas separation and recovery. Therefore, recent developments and

environmental considerations promoted the LOHC technology as a mean to store vast quantities of energy (GWh to TWh ranges) for seasonal energy storage.

However, through this literature review, barriers for the current state-of-the art LOHC systems were highlighted, in particular, their high dehydrogenation enthalpy, intrinsic toxicity, rarity and cost of the platinum group metals (PGM) used for the current hydrogenation and dehydrogenation catalysts and finally the LOHC stability after multiple hydrogenation/dehydrogenation cycles. The current perspectives on each point are presented hereafter.

1) Dehydrogenation enthalpy

The development of organic structures with novel reactivities following the reviewed literature such as C-O bonds might provide low dehydrogenation enthalpy LOHC structures. Nevertheless, the development of a high throughput methodology to test new couples catalysts/support is still required.

2) PGM-free heterogeneous metal catalysts

Overall, the development of high kinetics non-PGM selective heterogeneous hydrogenation and dehydrogenation catalysts is required for the LOHC technology to be further implemented. The design and comprehension of the LOHC-metal-support interfaces in heterogeneous catalytic systems is also key as the objective of complete reaction selectivity might be unachievable if these interfaces cannot be rationally constituted and analyzed. As the metal catalyst activity is dependent on the LOHC structure, refinement of the LOHC molecular design could also be beneficial. Indeed, the development of C-O-based structures is particularly interesting as non-noble metal catalysts such as Cu catalyze both hydrogenation and dehydrogenation reactions. As numerous C-O bonds-containing exist in nature, it is only a matter of time before their pivotal role as LOHC is recognized.

3) LOHC stability

As complex structures tend to induce more side-reactions, the simplification of the molecular systems, might be efficient to lower the formation of side-products. However, structure simplification is often synonymous with low-molecular weight structures and accordingly lower boiling points, thus this method is rather limited if the dehydrogenation reaction is to occur in liquid phase. Finally, a more realistic approach might be to observe which degradation structures with H₂ storage capacity are formed during the cycling of the current state-of-the art LOHC as they probably are the most stable LOHC structures with the currently available catalytic systems.

4) H₂-to-power setups and heat integration

Down the H₂ value chain, the presence of degradation products in the H₂ output could be detrimental for the H₂-to-Power setups such as PEM fuel cells where membrane contamination will drastically shorten their life expectancy. SOE fuel cells are less sensitive to contaminants than PEM fuel cells, but their presence requires monitoring to ensure that no excessive degradation occurs. Conversely, thermal engines are however unaffected by traces of contaminants, but while release greenhouse gases such as CO₂ and NO_x accordingly. Heat integration from these conversion devices could theoretically compensate the dehydrogenation enthalpy providing the dehydrogenation temperature is lower than their operating temperature. Therefore, PEM fuel cells do not permit heat integration for the time being as the state-of-the art LOHC dehydrogenation temperatures are 100 to 200 °C above their operating temperature. Conversely, SOE fuel cells are suitable for dehydrogenation heat integration. Nevertheless, their extreme operating temperature limits the application possibilities, especially for on-board systems. Finally, much like SOE-fuel cells, thermal engines can circumvent the dehydrogenation enthalpy cost but their extreme operating temperature produce NO_x from air.

In conclusion, massive energy storage is a major concern due to the implementation of intermittent renewable energies in order to phase out fossil fuels out of our energy mix. Both must concentrate research efforts to achieve a successful energy transition. While early studies targeted individual mobility as a LOHC application, the dehydrogenation temperature, limited H₂ gravimetric and volumetric densities as well as a low cycling capacity of most current LOHC systems make this application unsuitable. Conversely, stationary systems for off-grid energy generation might be interesting if the system cost is low (LOHC molecules, catalysts, H₂ production, hydrogenation, dehydrogenation and H₂-to-power setups) and the system volume might be less of an issue. Here, the degradation products could be used as either H₂ storage materials of reduced capacity or fuel to compensate the high dehydrogenation energy. Thus, an efficient answer to the previously highlighted barriers would be to develop organic structures with novel reactivities following the reviewed literature. Nonetheless, before that, it is important to take into account that a LOHC system is described by its molecules (gravimetric and volumetric H₂ densities, dehydrogenation enthalpy) but also its catalysts (active metals, catalytic supports, additives, preparation method, performance and stability) and dedicated reaction systems. Then, it is worth noting that numerous LOHC systems can be considered and that all of the previously mentioned technical aspects cannot be completely covered over this thesis. In addition, as there is to date no better assessment for LOHC systems than catalytic screening, we suggest to use commercial heterogeneous catalysts in batch systems to simplify the design and evaluation of the new LOHC systems. Although homocyclic LOHC can present similarities in their reactivity, generalization to other LOHC classes is often impossible. Thus, each LOHC system must be studied separately from the ground up.

Firstly, the physico-chemical properties (gravimetric density, elemental composition, melting point and boiling point, toxicity, reactivity, ...) of potential LOHC structures will be gathered to ensure that only pertinent molecules are chosen. Combined DFT studies of LOHC and their catalysts were presented in the literature review, however, it will not be done in this thesis due to its more system-focused approach. Here, an *ab-initio* DFT methodology will be developed to estimate the dehydrogenation enthalpy of these structures, aiming for dehydrogenation enthalpies inferior to 50 kJ/mol H₂ if possible. By using these criteria as segregation tools, previously unreported LOHC structures will then be suggested. An experimental catalytic study on the most promising structure, 1-Cyclohexylethanol/Acetophenone, will be conducted afterwards for both hydrogenation and dehydrogenation reactions before a complete cycling of the LOHC. A special attention will be brought to the understanding the reaction pathway as well as the formation of the side-products.

Secondly, the degradation pathways of the chosen structure identified during both hydrogenation and dehydrogenation will be rationalized. Their formation will be linked to the components of the LOHC system such as the molecule choice, catalyst, reaction conditions and so on. Then, strategies to limit their prevalence will then be presented with the 1-Cyclohexylethanol/Acetophenone (CHEA/APO) and Dicyclohexylmethanol/Benzophenone (DCMA/BPO) couples.

Thirdly, as some degradation pathways could not be efficiently neutralized, a methodology to partially regenerate the LOHC will be proposed and its effect on the Dicyclohexylmethanol/Benzophenone (DCMA/BPO) and Dodecahydrofluoren-9-ol/Fluoren-9-one (12H-FLUA/FLUK) will be estimated as an opportunity for improvement.

Lastly, a variation based on different hydrogenation/dehydrogenation reactivities than these studied with the previously presented LOHC couples will be presented. Here, the modification effects on the reactivity and stability of the Cyclohexylmethanol/Benzyl benzoate (CMA/BBE) couple will then be rationalized.

Bibliography

- (1) Ritchie, H.; Roser, M.; Rosado, P. Energy. *Our World in Data* **2020**.
- (2) Bruland, K.; Smith, K. Assessing the Role of Steam Power in the First Industrial Revolution: The Early Work of Nick von Tunzelmann. *Research Policy* **2013**, *42* (10), 1716–1723. <https://doi.org/10.1016/j.respol.2012.12.008>.
- (3) Clark, G.; Jacks, D. Coal and the Industrial Revolution, 1700–1869. *European Review of Economic History* **2007**, *11* (1), 39–72. <https://doi.org/10.1017/S1361491606001870>.
- (4) Clow, A.; Nan, L. C. Vitriol in the Industrial Revolution. In *Science, Technology and Economic Growth in the Eighteenth Century*; Routledge, 1972.
- (5) Nicolas Leblanc (1742-1806).Pdf. <https://pubs.acs.org/doi/pdf/10.1021/ed019p567> (accessed 2022-07-27).
- (6) Kanefsky, J.; Robey, J. Steam Engines in 18th-Century Britain: A Quantitative Assessment. *Technology and Culture* **1980**, *21* (2), 161–186. <https://doi.org/10.2307/3103337>.
- (7) Alley, R. B.; Berntsen, T.; Bindoff, N. L.; Chen, Z.; Chidthaisong, A.; Friedlingstein, P.; Hegerl, G. C.; Heimann, M.; Hewitson, B.; Hoskins, B. J.; Joos, F.; Jouzel, J.; Kattsov, V.; Lohmann, U.; Manning, M.; Matsuno, T.; Molina, M.; Nicholls, N.; Overpeck, J.; Qin, D.; Raga, G.; Ramaswamy, V.; Ren, J.; Rusticucci, M.; Solomon, S.; Somerville, R.; Stocker, T. F.; Stott, A.; Stouffer, R. J.; Whetton, P.; Wood, R. A.; Wratt, D.; Arblaster, J.; Brasseur, G.; Christensen, J. H.; Denman, K. L.; Fahey, D. W.; Forster, P.; Jansen, E.; Jones, P. D.; Knutti, R.; Treut, H. L.; Lemke, P.; Meehl, G.; Mote, P.; Randall, D. A.; Stone, D. A.; Trenberth, K. E.; Willebrand, J.; Zwiers, F. IPCC Sixth Assessment, summary for Policymakers. 18.
- (8) *2006 IPCC Guidelines for National Greenhouse Gas Inventories, Volume I, General Guidance and Reporting*. <https://www.ipcc-nggip.iges.or.jp/public/2006gl/vol1.html> (accessed 2021-01-20).
- (9) Karl, T. R.; Trenberth, K. E. Modern Global Climate Change. *Science* **2003**, *302* (5651), 1719–1723. <https://doi.org/10.1126/science.1090228>.
- (10) Montzka, S. A.; Dlugokencky, E. J.; Butler, J. H. Non-CO₂ Greenhouse Gases and Climate Change. *Nature* **2011**, *476* (7358), 43–50. <https://doi.org/10.1038/nature10322>.
- (11) IPCC_AR6_WGII_SummaryForPolicymakers.Pdf. https://report.ipcc.ch/ar6wg2/pdf/IPCC_AR6_WGII_SummaryForPolicymakers.pdf (accessed 2022-07-13).
- (12) *The world's energy problem*. Our World in Data. <https://ourworldindata.org/worlds-energy-problem> (accessed 2022-07-13).
- (13) Gibon, T.; Arvesen, A.; Hertwich, E. G. Life Cycle Assessment Demonstrates Environmental Co-Benefits and Trade-Offs of Low-Carbon Electricity Supply Options. *Renewable and Sustainable Energy Reviews* **2017**, *76*, 1283–1290. <https://doi.org/10.1016/j.rser.2017.03.078>.
- (14) Hondo, H. Life Cycle GHG Emission Analysis of Power Generation Systems: Japanese Case. *Energy* **2005**, *30* (11), 2042–2056. <https://doi.org/10.1016/j.energy.2004.07.020>.
- (15) Amponsah, N. Y.; Troldborg, M.; Kington, B.; Aalders, I.; Hough, R. L. Greenhouse Gas Emissions from Renewable Energy Sources: A Review of Lifecycle Considerations. *Renewable and Sustainable Energy Reviews* **2014**, *39*, 461–475. <https://doi.org/10.1016/j.rser.2014.07.087>.
- (16) Chiffres clés de l'énergie - Édition 2019. 80.
- (17) *Global Electricity Review 2022*. Ember. <https://ember-climate.org/insights/research/global-electricity-review-2022/> (accessed 2022-07-27).
- (18) *LOIN° 2015-992 Du 17 Août 2015 Relative à La Transition Énergétique Pour La Croissance Verte*; 2015.
- (19) Bremen, L. V. Large-Scale Variability of Weather Dependent Renewable Energy Sources. In *Management of Weather and Climate Risk in the Energy Industry*; Troccoli, A., Ed.; NATO Science for Peace and Security Series C: Environmental Security; Springer Netherlands: Dordrecht, 2010; pp 189–206. https://doi.org/10.1007/978-90-481-3692-6_13.
- (20) *éCO2mix - La production d'électricité par filière*. <https://www.rte-france.com/eco2mix/la-production-delectricite-par-filiere> (accessed 2022-07-27).
- (21) Revol, M. *Quand trop d'énergies renouvelables privent la Californie... d'électricité*. Le Point. https://www.lepoint.fr/economie/quand-trop-d-energies-renouvelables-privent-la-californie-d-electricite-20-08-2020-2388408_28.php (accessed 2020-08-25).
- (22) *Energy Charts*. <https://energy-charts.info/?l=fr&c=DE> (accessed 2021-01-21).
- (23) Saboori, H.; Hemmati, R.; Ghiasi, S. M. S.; Dehghan, S. Energy Storage Planning in Electric Power Distribution Networks – A State-of-the-Art Review. *Renewable and Sustainable Energy Reviews* **2017**, *79*, 1108–1121. <https://doi.org/10.1016/j.rser.2017.05.171>.

Literature review

- (24) Akinyele, D. O.; Rayudu, R. K. Review of Energy Storage Technologies for Sustainable Power Networks. *Sustainable Energy Technologies and Assessments* **2014**, *8*, 74–91. <https://doi.org/10.1016/j.seta.2014.07.004>.
- (25) Orecchini, F. The Era of Energy Vectors. *International Journal of Hydrogen Energy* **2006**, *31* (14), 1951–1954. <https://doi.org/10.1016/j.ijhydene.2006.01.015>.
- (26) Chen, L.; Zheng, T.; Mei, S.; Xue, X.; Liu, B.; Lu, Q. Review and Prospect of Compressed Air Energy Storage System. *Journal of Modern Power Systems and Clean Energy* **2016**, *4* (4), 529–541. <https://doi.org/10.1007/s40565-016-0240-5>.
- (27) Geth, F.; Brijs, T.; Kathan, J.; Driesen, J.; Belmans, R. An Overview of Large-Scale Stationary Electricity Storage Plants in Europe: Current Status and New Developments. *Renewable and Sustainable Energy Reviews* **2015**, *52*, 1212–1227. <https://doi.org/10.1016/j.rser.2015.07.145>.
- (28) Capacitor-with-Cover-Page-v2.Pdf. https://d1wqtxts1xzle7.cloudfront.net/37529848/capacitor-with-cover-page-v2.pdf?Expires=1659090864&Signature=eapHQ26cLxI5EYHnjAcJCdb2J58PiZFmqWg0DBjpJPDtI0lYKMswtAUxxAk1gRDbga9MHzF9PB0BR8dglRiGMBfRUBI78yps36c8sqJBCvhwOmdwssOK9ZF82iNayTVmuTOHjm22Do1TE5tG2LfhzvL6iEOG6115sLdmD1iyd5GYCVc87x0c2eI9VIBB4GZbD4f7Ti3sJPUdF1FF4ma6qcJJN~YOummS7D118UDSgg11-rSi5xDcY~HQdgt3fciKibPwMIImQkmoyvWRYLz72NHPqXsUfNPrX60az1lsLh51RB8zIR-6MFXG4USspZtxuy~0CyDGPXKIZ11surGRfA__&Key-Pair-Id=APKAJLOHF5GGSLRBV4ZA (accessed 2022-07-29).
- (29) Kebede, A. A.; Kalogiannis, T.; Van Mierlo, J.; Berecibar, M. A Comprehensive Review of Stationary Energy Storage Devices for Large Scale Renewable Energy Sources Grid Integration. *Renewable and Sustainable Energy Reviews* **2022**, *159*, 112213. <https://doi.org/10.1016/j.rser.2022.112213>.
- (30) Park, K.; Zhang, Z. FUNDAMENTALS AND APPLICATIONS OF NEAR-FIELD RADIATIVE ENERGY TRANSFER. *Frontiers in Heat and Mass Transfer (FHMT)* **2013**, *4* (1).
- (31) Le Duigou, A. La filière hydrogène Un moyen de stockage de l'énergie. <https://hal.archives-ouvertes.fr/hal-02416323/file/201500004533.pdf> (accessed 2020-08-25).
- (32) Momirlan, M.; Veziroglu, T. N. The Properties of Hydrogen as Fuel Tomorrow in Sustainable Energy System for a Cleaner Planet. *International Journal of Hydrogen Energy* **2005**, *30* (7), 795–802. <https://doi.org/10.1016/j.ijhydene.2004.10.011>.
- (33) Abbasi, T.; Abbasi, S. A. 'Renewable' Hydrogen: Prospects and Challenges. *Renewable and Sustainable Energy Reviews* **2011**, *15* (6), 3034–3040. <https://doi.org/10.1016/j.rser.2011.02.026>.
- (34) Holbrook, J. H.; Cialone, H. J.; Collings, E. W.; Drauglis, E. J.; Scott, P. M.; Mayfield, M. E. 5 - Control of Hydrogen Embrittlement of Metals by Chemical Inhibitors and Coatings. In *Gaseous Hydrogen Embrittlement of Materials in Energy Technologies*; Gangloff, R. P., Somerday, B. P., Eds.; Woodhead Publishing Series in Metals and Surface Engineering; Woodhead Publishing, 2012; Vol. 1, pp 129–153. <https://doi.org/10.1533/9780857095374.1.129>.
- (35) Holbrook, J. H.; Cialone, H. J.; Scott, P. M. *Hydrogen Degradation of Pipeline Steels. Summary Report*; BNL-51855; Battelle Columbus Labs., OH (USA), 1984. <https://www.osti.gov/biblio/5985541> (accessed 2020-03-04).
- (36) Veziroglu, T. N. *Metal-Hydrogen Systems: Proceedings of the Miami International Symposium on Metal-Hydrogen Systems, 13-15 April 1981, Miami Beach, Florida, U.S.A.*; Elsevier, 2016.
- (37) Gupta, R. B. *Hydrogen Fuel: Production, Transport, and Storage*; CRC Press, 2008.
- (38) *The Future of Hydrogen – Analysis*. IEA. <https://www.iea.org/reports/the-future-of-hydrogen> (accessed 2021-01-22).
- (39) Christensen, H.; Bjergbakke, E. *Radiolysis of Ground Water from Spent Fuel*; SKBF-KBS-TR--82-18; Svensk Kaernbraenslefoerserjning AB, 1982. http://inis.iaea.org/Search/search.aspx?orig_q=RN:14788675 (accessed 2020-06-30).
- (40) Prinzhofer, A.; Tahara Cissé, C. S.; Diallo, A. B. Discovery of a Large Accumulation of Natural Hydrogen in Bourakebougou (Mali). *International Journal of Hydrogen Energy* **2018**, *43* (42), 19315–19326. <https://doi.org/10.1016/j.ijhydene.2018.08.193>.
- (41) Stevens, T. O.; McKinley, J. P. Abiotic Controls on H₂ Production from Basalt–Water Reactions and Implications for Aquifer Biogeochemistry. *Environ. Sci. Technol.* **2000**, *34* (5), 826–831. <https://doi.org/10.1021/es990583g>.
- (42) Hosseini, S. E.; Wahid, M. A. Hydrogen Production from Renewable and Sustainable Energy Resources: Promising Green Energy Carrier for Clean Development. *Renewable and Sustainable Energy Reviews* **2016**, *57*, 850–866. <https://doi.org/10.1016/j.rser.2015.12.112>.
- (43) Cao, L.; Yu, I. K. M.; Xiong, X.; Tsang, D. C. W.; Zhang, S.; Clark, J. H.; Hu, C.; Ng, Y. H.; Shang, J.; Ok, Y. S. Biorenewable Hydrogen Production through Biomass Gasification: A Review and Future Prospects. *Environmental Research* **2020**, *186*, 109547. <https://doi.org/10.1016/j.envres.2020.109547>.

- (44) Sengodan, S.; Lan, R.; Humphreys, J.; Du, D.; Xu, W.; Wang, H.; Tao, S. Advances in Reforming and Partial Oxidation of Hydrocarbons for Hydrogen Production and Fuel Cell Applications. *Renewable and Sustainable Energy Reviews* **2018**, *82*, 761–780. <https://doi.org/10.1016/j.rser.2017.09.071>.
- (45) Kothari, R.; Buddhi, D.; Sawhney, R. L. Comparison of Environmental and Economic Aspects of Various Hydrogen Production Methods. *Renewable and Sustainable Energy Reviews* **2008**, *12* (2), 553–563. <https://doi.org/10.1016/j.rser.2006.07.012>.
- (46) Baruah, R.; Dixit, M.; Basarkar, P.; Parikh, D.; Bhargav, A. Advances in Ethanol Autothermal Reforming. *Renewable and Sustainable Energy Reviews* **2015**, *51*, 1345–1353. <https://doi.org/10.1016/j.rser.2015.07.060>.
- (47) da Silva Veras, T.; Mozer, T. S.; da Costa Rubim Messeder dos Santos, D.; da Silva César, A. Hydrogen: Trends, Production and Characterization of the Main Process Worldwide. *International Journal of Hydrogen Energy* **2017**, *42* (4), 2018–2033. <https://doi.org/10.1016/j.ijhydene.2016.08.219>.
- (48) Muradov, N. Z. How to Produce Hydrogen from Fossil Fuels without CO₂ Emission. *International Journal of Hydrogen Energy* **1993**, *18* (3), 211–215. [https://doi.org/10.1016/0360-3199\(93\)90021-2](https://doi.org/10.1016/0360-3199(93)90021-2).
- (49) *Methane splitting and turquoise ammonia – Ammonia Energy Association*. <https://www.ammoniaenergy.org/articles/methane-splitting-and-turquoise-ammonia/> (accessed 2022-08-03).
- (50) Machhammer, O.; Bode, A.; Hormuth, W. Financial and Ecological Evaluation of Hydrogen Production Processes on Large Scale. *Chemical Engineering & Technology* **2016**, *39* (6), 1185–1193. <https://doi.org/10.1002/ceat.201600023>.
- (51) 1 Scale up BASF.Pdf. <https://arpa-e.energy.gov/sites/default/files/1%20Scale%20up%20BASF.pdf> (accessed 2022-08-03).
- (52) Keller, M. Comment on “Methane Pyrolysis for Zero-Emission Hydrogen Production: A Potential Bridge Technology from Fossil Fuels to a Renewable and Sustainable Hydrogen Economy.” *Ind. Eng. Chem. Res.* **2021**, *60* (48), 17792–17794. <https://doi.org/10.1021/acs.iecr.1c03926>.
- (53) Chisholm, G.; Cronin, L. Chapter 16 - Hydrogen From Water Electrolysis. In *Storing Energy*; Letcher, T. M., Ed.; Elsevier: Oxford, 2016; pp 315–343. <https://doi.org/10.1016/B978-0-12-803440-8.00016-6>.
- (54) Smolinka, T.; Bergmann, H.; Garche, J.; Kusnezoff, M. Chapter 4 - The History of Water Electrolysis from Its Beginnings to the Present. In *Electrochemical Power Sources: Fundamentals, Systems, and Applications*; Smolinka, T., Garche, J., Eds.; Elsevier, 2022; pp 83–164. <https://doi.org/10.1016/B978-0-12-819424-9.00010-0>.
- (55) Ursua, A.; Gandia, L. M.; Sanchis, P. Hydrogen Production From Water Electrolysis: Current Status and Future Trends. *Proceedings of the IEEE* **2012**, *100* (2), 410–426. <https://doi.org/10.1109/JPROC.2011.2156750>.
- (56) *Electrolysers – Analysis*. IEA. <https://www.iea.org/reports/electrolysers> (accessed 2023-01-11).
- (57) Zeng, K.; Zhang, D. Recent Progress in Alkaline Water Electrolysis for Hydrogen Production and Applications. *Progress in Energy and Combustion Science* **2010**, *36* (3), 307–326. <https://doi.org/10.1016/j.peccs.2009.11.002>.
- (58) Sahu, A. K.; Pitchumani, S.; Sridhar, P.; Shukla, A. K. Nafion and Modified-Nafion Membranes for Polymer Electrolyte Fuel Cells: An Overview. *Bull Mater Sci* **2009**, *32* (3), 285–294. <https://doi.org/10.1007/s12034-009-0042-8>.
- (59) Vincent, I.; Bessarabov, D. Low Cost Hydrogen Production by Anion Exchange Membrane Electrolysis: A Review. *Renewable and Sustainable Energy Reviews* **2018**, *81*, 1690–1704. <https://doi.org/10.1016/j.rser.2017.05.258>.
- (60) Vielstich, W. J. O’M. Bockris, B. E. Conway, E. Yeager, R. E. White (Eds.): *Electrochemical Processing*, Vol. 2 Aus: Comprehensive Treatise of Electrochemistry, Plenum Press, New York, London 1981. 616 Seiten, Preis: \$ 57.50. *Berichte der Bunsengesellschaft für physikalische Chemie* **1982**, *86* (6), 575–576. <https://doi.org/10.1002/bbpc.19820860631>.
- (61) Holladay, J. D.; Hu, J.; King, D. L.; Wang, Y. An Overview of Hydrogen Production Technologies. *Catalysis Today* **2009**, *139* (4), 244–260. <https://doi.org/10.1016/j.cattod.2008.08.039>.
- (62) Nechache, A.; Hody, S. Alternative and Innovative Solid Oxide Electrolysis Cell Materials: A Short Review. *Renewable and Sustainable Energy Reviews* **2021**, *149*, 111322. <https://doi.org/10.1016/j.rser.2021.111322>.
- (63) Seitz, M.; von Storch, H.; Nechache, A.; Bauer, D. Techno Economic Design of a Solid Oxide Electrolysis System with Solar Thermal Steam Supply and Thermal Energy Storage for the Generation of Renewable Hydrogen. *International Journal of Hydrogen Energy* **2017**, *42* (42), 26192–26202. <https://doi.org/10.1016/j.ijhydene.2017.08.192>.
- (64) Zheng, H.; O’Sullivan, C.; Mereddy, R.; Zeng, R.; Duke, M.; Clarke, W. Production of Bio-Hydrogen Using a Membrane Anaerobic Reactor: Limitations Due to Diffusion. **2021**.

- (65) Lee, H.-S.; Salerno, M. B.; Rittmann, B. E. Thermodynamic Evaluation on H₂ Production in Glucose Fermentation. *Environ. Sci. Technol.* **2008**, *42* (7), 2401–2407. <https://doi.org/10.1021/es702610v>.
- (66) Bshish, A.; Yaakob, Z.; Narayanan, B.; Ramakrishnan, R.; Ebshish, A. Steam-Reforming of Ethanol for Hydrogen Production. *Chemical Papers* **2011**, *65* (3), 251–266. <https://doi.org/10.2478/s11696-010-0100-0>.
- (67) Fahmy, T. Y. A.; Fahmy, Y.; Mobarak, F.; El-Sakhawy, M.; Abou-Zeid, R. E. Biomass Pyrolysis: Past, Present, and Future. *Environ Dev Sustain* **2020**, *22* (1), 17–32. <https://doi.org/10.1007/s10668-018-0200-5>.
- (68) Demirbas, A. Hydrogen Production from Carbonaceous Solid Wastes by Steam Reforming. *Energy Sources, Part A: Recovery, Utilization, and Environmental Effects* **2008**, *30* (10), 924–931. <https://doi.org/10.1080/10826070601082658>.
- (69) Calzavara, Y.; Jousot-Dubien, C.; Boissonnet, G.; Sarrade, S. Evaluation of Biomass Gasification in Supercritical Water Process for Hydrogen Production. *Energy Conversion and Management* **2005**, *46* (4), 615–631. <https://doi.org/10.1016/j.enconman.2004.04.003>.
- (70) Oni, A. O.; Anaya, K.; Giwa, T.; Di Lullo, G.; Kumar, A. Comparative Assessment of Blue Hydrogen from Steam Methane Reforming, Autothermal Reforming, and Natural Gas Decomposition Technologies for Natural Gas-Producing Regions. *Energy Conversion and Management* **2022**, *254*, 115245. <https://doi.org/10.1016/j.enconman.2022.115245>.
- (71) Bartels, J. R.; Pate, M. B.; Olson, N. K. An Economic Survey of Hydrogen Production from Conventional and Alternative Energy Sources. *International Journal of Hydrogen Energy* **2010**, *35* (16), 8371–8384. <https://doi.org/10.1016/j.ijhydene.2010.04.035>.
- (72) Kreutz, T.; Williams, R.; Consonni, S.; Chiesa, P. Co-Production of Hydrogen, Electricity and CO₂ from Coal with Commercially Ready Technology. Part B: Economic Analysis. *International Journal of Hydrogen Energy* **2005**, *30* (7), 769–784. <https://doi.org/10.1016/j.ijhydene.2004.08.001>.
- (73) Simbeck, Mr. D. R. - Hydrogen Costs with CO₂ Capture. In *Greenhouse Gas Control Technologies 7*; Rubin, E. S., Keith, D. W., Gilboy, C. F., Wilson, M., Morris, T., Gale, J., Thambimuthu, K., Eds.; Elsevier Science Ltd: Oxford, 2005; pp 1059–1066. <https://doi.org/10.1016/B978-008044704-9/50108-7>.
- (74) Damen, K.; Troost, M. van; Faaij, A.; Turkenburg, W. A Comparison of Electricity and Hydrogen Production Systems with CO₂ Capture and Storage. Part A: Review and Selection of Promising Conversion and Capture Technologies. *Progress in Energy and Combustion Science* **2006**, *32* (2), 215–246. <https://doi.org/10.1016/j.pecs.2005.11.005>.
- (75) Levene, J.; Kroposki, B.; Sverdrup, G. Wind Energy and Production of Hydrogen and Electricity -- Opportunities for Renewable Hydrogen: Preprint. *2006 POWER-GEN Renewable Energy and Fuels Technical Conference, Las Vegas, Nevada* **2006**, 18.
- (76) Olateju, B.; Kumar, A. A Techno-Economic Assessment of Hydrogen Production from Hydropower in Western Canada for the Upgrading of Bitumen from Oil Sands. *Energy* **2016**, *115*, 604–614. <https://doi.org/10.1016/j.energy.2016.08.101>.
- (77) El-Emam, R. S.; Özcan, H. Comprehensive Review on the Techno-Economics of Sustainable Large-Scale Clean Hydrogen Production. *Journal of Cleaner Production* **2019**, *220*, 593–609. <https://doi.org/10.1016/j.jclepro.2019.01.309>.
- (78) Padro, C. E. G.; Putsche, V. *Survey of the Economics of Hydrogen Technologies*; NREL/TP-570-27079, 12212; 1999; p NREL/TP-570-27079, 12212. <https://doi.org/10.2172/12212>.
- (79) BITS Pilani-Dubai Campus, Dubai; Sathyaprakasan, P.; Kannan, G.; BITS Pilani-Dubai Campus, Dubai. Economics of Bio-Hydrogen Production. *IJESD* **2015**, *6* (4), 352–356. <https://doi.org/10.7763/IJESD.2015.V6.617>.
- (80) Al-Qahtani, A.; Parkinson, B.; Hellgardt, K.; Shah, N.; Guillen-Gosalbez, G. Uncovering the True Cost of Hydrogen Production Routes Using Life Cycle Monetisation. *Applied Energy* **2021**, *281*, 115958. <https://doi.org/10.1016/j.apenergy.2020.115958>.
- (81) Liquide, A. *Encyclopédie des gaz Air Liquide*. Encyclopédie des gaz Air Liquide. <https://encyclopedia.airliquide.com/fr> (accessed 2022-08-05).
- (82) von Helmolt, R.; Eberle, U. Fuel Cell Vehicles: Status 2007. *Journal of Power Sources* **2007**, *165* (2), 833–843. <https://doi.org/10.1016/j.jpowsour.2006.12.073>.
- (83) Pasman, H. J.; Rogers, W. J. Risk Assessment by Means of Bayesian Networks: A Comparative Study of Compressed and Liquefied H₂ Transportation and Tank Station Risks. *International Journal of Hydrogen Energy* **2012**, *37* (22), 17415–17425. <https://doi.org/10.1016/j.ijhydene.2012.04.051>.
- (84) Hua, T. Q.; Ahluwalia, R. K.; Peng, J.-K.; Kromer, M.; Lasher, S.; McKenney, K.; Law, K.; Sinha, J. Technical Assessment of Compressed Hydrogen Storage Tank Systems for Automotive Applications. *International Journal of Hydrogen Energy* **2011**, *36* (4), 3037–3049. <https://doi.org/10.1016/j.ijhydene.2010.11.090>.

- (85) Parks, G.; Boyd, R.; Cornish, J.; Remick, R. *Hydrogen Station Compression, Storage, and Dispensing Technical Status and Costs: Systems Integration*; NREL/BK-6A10-58564, 1130621; 2014; p NREL/BK-6A10-58564, 1130621. <https://doi.org/10.2172/1130621>.
- (86) *Comment stocker l'hydrogène ?* Air Liquide Energies. <https://energies.airliquide.com/fr/mediatheque-planete-hydrogene/comment-stocker-lhydrogene> (accessed 2022-08-05).
- (87) Aasadnia, M.; Mehrpooya, M. Large-Scale Liquid Hydrogen Production Methods and Approaches: A Review. *Applied Energy* **2018**, *212*, 57–83. <https://doi.org/10.1016/j.apenergy.2017.12.033>.
- (88) Bliesner, R. M. PARAHYDROGEN-ORTHOHYDROGEN CONVERSION FOR BOIL-OFF REDUCTION FROM SPACE STAGE FUEL SYSTEMS. 49.
- (89) TZIMAS, E.; FILIOU, C.; Peteves, S.; VEYRET, J.-B. HYDROGEN STORAGE: STATE-OF-THE-ART AND FUTURE PERSPECTIVE. **2003**.
- (90) Makridis, S. Hydrogen Storage and Compression; 2016; pp 1–28. https://doi.org/10.1049/PBPO101E_ch1.
- (91) Peschka, W. Liquid Hydrogen as a Vehicular Fuel—a Challenge for Cryogenic Engineering. *International Journal of Hydrogen Energy* **1984**, *9* (6), 515–523. [https://doi.org/10.1016/0360-3199\(84\)90104-6](https://doi.org/10.1016/0360-3199(84)90104-6).
- (92) Stewart, W. F. Operating Experience with a Liquid-Hydrogen Fueled Buick and Refueling System. *International Journal of Hydrogen Energy* **1984**, *9* (6), 525–538. [https://doi.org/10.1016/0360-3199\(84\)90105-8](https://doi.org/10.1016/0360-3199(84)90105-8).
- (93) Furuhashi, S.; Kobayashi, Y. Development of a Hot-Surface-Ignition Hydrogen Injection Two-Stroke Engine. *International Journal of Hydrogen Energy* **1984**, *9* (3), 205–213. [https://doi.org/10.1016/0360-3199\(84\)90120-4](https://doi.org/10.1016/0360-3199(84)90120-4).
- (94) Hassannayebi, N.; Azizmohammadi, S.; De Lucia, M.; Ott, H. Underground Hydrogen Storage: Application of Geochemical Modelling in a Case Study in the Molasse Basin, Upper Austria. *Environ Earth Sci* **2019**, *78* (5), 177. <https://doi.org/10.1007/s12665-019-8184-5>.
- (95) Zivar, D.; Kumar, S.; Foroozesh, J. Underground Hydrogen Storage: A Comprehensive Review. *International Journal of Hydrogen Energy* **2021**, *46* (45), 23436–23462. <https://doi.org/10.1016/j.ijhydene.2020.08.138>.
- (96) Michalski, J.; Bünger, U.; Crotogino, F.; Donadei, S.; Schneider, G.-S.; Pregger, T.; Cao, K.-K.; Heide, D. Hydrogen Generation by Electrolysis and Storage in Salt Caverns: Potentials, Economics and Systems Aspects with Regard to the German Energy Transition. *International Journal of Hydrogen Energy* **2017**, *42* (19), 13427–13443. <https://doi.org/10.1016/j.ijhydene.2017.02.102>.
- (97) durable, C. général au développement. *Bilan énergétique de la France*. Chiffres clés de l'énergie - Édition 2021. <https://www.statistiques.developpement-durable.gouv.fr/edition-numerique/chiffres-cles-energie-2021/6-bilan-energetique-de-la-france.php> (accessed 2022-08-10).
- (98) Zhou, L. Progress and Problems in Hydrogen Storage Methods. *Renewable and Sustainable Energy Reviews* **2005**, *9* (4), 395–408. <https://doi.org/10.1016/j.rser.2004.05.005>.
- (99) Ansón, A.; Benham, M.; Jagiello, J.; Callejas, M. A.; Benito, A. M.; Maser, W. K.; Züttel, A.; Sudan, P.; Martínez, M. T. Hydrogen Adsorption on a Single-Walled Carbon Nanotube Material: A Comparative Study of Three Different Adsorption Techniques. *Nanotechnology* **2004**, *15* (11), 1503–1508. <https://doi.org/10.1088/0957-4484/15/11/023>.
- (100) Zhou, L.; Zhou, Y.; Sun, Y. Enhanced Storage of Hydrogen at the Temperature of Liquid Nitrogen. *International Journal of Hydrogen Energy* **2004**, *29* (3), 319–322. [https://doi.org/10.1016/S0360-3199\(03\)00155-1](https://doi.org/10.1016/S0360-3199(03)00155-1).
- (101) Chen, P.; Wu, X.; Lin, J.; Tan, K. L. High H₂ Uptake by Alkali-Doped Carbon Nanotubes Under Ambient Pressure and Moderate Temperatures. *Science* **1999**, *285* (5424), 91–93. <https://doi.org/10.1126/science.285.5424.91>.
- (102) Yang, R. T. Hydrogen Storage by Alkali-Doped Carbon Nanotubes—Revisited. *Carbon* **2000**, *38* (4), 623–626. [https://doi.org/10.1016/S0008-6223\(99\)00273-0](https://doi.org/10.1016/S0008-6223(99)00273-0).
- (103) Tibbetts, G. G.; Meisner, G. P.; Olk, C. H. Hydrogen Storage Capacity of Carbon Nanotubes, Filaments, and Vapor-Grown Fibers. *Carbon* **2001**, *39* (15), 2291–2301. [https://doi.org/10.1016/S0008-6223\(01\)00051-3](https://doi.org/10.1016/S0008-6223(01)00051-3).
- (104) Liu, C.; Chen, Y.; Wu, C.-Z.; Xu, S.-T.; Cheng, H.-M. Hydrogen Storage in Carbon Nanotubes Revisited. *Carbon* **2010**, *48* (2), 452–455. <https://doi.org/10.1016/j.carbon.2009.09.060>.
- (105) Zhao, W.; Fierro, V.; Fernández-Huerta, N.; Izquierdo, M. T.; Celzard, A. Impact of Synthesis Conditions of KOH Activated Carbons on Their Hydrogen Storage Capacities. *International Journal of Hydrogen Energy* **2012**, *37* (19), 14278–14284. <https://doi.org/10.1016/j.ijhydene.2012.06.110>.
- (106) Kolesnikov, A. I.; Antonov, V. E.; Bashkin, I. O.; Li, J. C.; Moravsky, A. P.; Ponyatovsky, E. G.; Tomkinson, J. Neutron Spectroscopy of Fullerite Hydrogenated under High Pressures. *Physica B: Condensed Matter* **1999**, *263–264*, 436–438. [https://doi.org/10.1016/S0921-4526\(98\)01403-3](https://doi.org/10.1016/S0921-4526(98)01403-3).

- (107) Liu, C.; Fan, Y. Y.; Liu, M.; Cong, H. T.; Cheng, H. M.; Dresselhaus, M. S. Hydrogen Storage in Single-Walled Carbon Nanotubes at Room Temperature. *Science* **1999**, *286* (5442), 1127–1129. <https://doi.org/10.1126/science.286.5442.1127>.
- (108) Ramimoghadam, D.; Gray, E. M.; Webb, C. J. Review of Polymers of Intrinsic Microporosity for Hydrogen Storage Applications. *International Journal of Hydrogen Energy* **2016**, *41* (38), 16944–16965. <https://doi.org/10.1016/j.ijhydene.2016.07.134>.
- (109) McKeown, N. B.; Gahnem, B.; Msayib, K. J.; Budd, P. M.; Tattershall, C. E.; Mahmood, K.; Tan, S.; Book, D.; Langmi, H. W.; Walton, A. Towards Polymer-Based Hydrogen Storage Materials: Engineering Ultramicroporous Cavities within Polymers of Intrinsic Microporosity. *Angewandte Chemie* **2006**, *118* (11), 1836–1839. <https://doi.org/10.1002/ange.200504241>.
- (110) Tian, M.; Rochat, S.; Polak-Krašna, K.; Holyfield, L. T.; Burrows, A. D.; Bowen, C. R.; Mays, T. J. Nanoporous Polymer-Based Composites for Enhanced Hydrogen Storage. *Adsorption* **2019**, *25* (4), 889–901. <https://doi.org/10.1007/s10450-019-00065-x>.
- (111) Côté, A. P.; Benin, A. I.; Ockwig, N. W.; O’Keeffe, M.; Matzger, A. J.; Yaghi, O. M. Porous, Crystalline, Covalent Organic Frameworks. *Science* **2005**, *310* (5751), 1166–1170. <https://doi.org/10.1126/science.1120411>.
- (112) Freund, R.; Zaremba, O.; Arnauts, G.; Ameloot, R.; Skorupskii, G.; Dincă, M.; Bavykina, A.; Gascon, J.; Ejsmont, A.; Goscianska, J.; Kalmutzki, M.; Lächelt, U.; Ploetz, E.; Diercks, C. S.; Wuttke, S. The Current Status of MOF and COF Applications. *Angewandte Chemie International Edition* **2021**, *60* (45), 23975–24001. <https://doi.org/10.1002/anie.202106259>.
- (113) Han, S. S.; Furukawa, H.; Yaghi, O. M.; Goddard, W. A. Covalent Organic Frameworks as Exceptional Hydrogen Storage Materials. *J. Am. Chem. Soc.* **2008**, *130* (35), 11580–11581. <https://doi.org/10.1021/ja803247y>.
- (114) Klontzas, E.; Tylianakis, E.; Froudakis, G. E. Designing 3D COFs with Enhanced Hydrogen Storage Capacity. *Nano Lett.* **2010**, *10* (2), 452–454. <https://doi.org/10.1021/nl903068a>.
- (115) Pramudya, Y.; Mendoza-Cortes, J. L. Design Principles for High H₂ Storage Using Chelation of Abundant Transition Metals in Covalent Organic Frameworks for 0–700 Bar at 298 K. *J. Am. Chem. Soc.* **2016**, *138* (46), 15204–15213. <https://doi.org/10.1021/jacs.6b08803>.
- (116) Shet, S. P.; Shanmuga Priya, S.; Sudhakar, K.; Tahir, M. A Review on Current Trends in Potential Use of Metal-Organic Framework for Hydrogen Storage. *International Journal of Hydrogen Energy* **2021**, *46* (21), 11782–11803. <https://doi.org/10.1016/j.ijhydene.2021.01.020>.
- (117) Grünker, R.; Bon, V.; Müller, P.; Stoeck, U.; Krause, S.; Mueller, U.; Senkovska, I.; Kaskel, S. A New Metal–Organic Framework with Ultra-High Surface Area. *Chemical Communications* **2014**, *50* (26), 3450–3452. <https://doi.org/10.1039/C4CC00113C>.
- (118) Campesi, R.; Cuevas, F.; Latroche, M.; Hirscher, M. Hydrogen Spillover Measurements of Unbridged and Bridged Metal–Organic Frameworks—Revisited. *Phys. Chem. Chem. Phys.* **2010**, *12* (35), 10457–10459. <https://doi.org/10.1039/C0CP00037J>.
- (119) Luzan, S. M.; Talyzin, A. V. Hydrogen Adsorption in Pt Catalyst/MOF-5 Materials. *Microporous and Mesoporous Materials* **2010**, *135* (1), 201–205. <https://doi.org/10.1016/j.micromeso.2010.07.018>.
- (120) Prins, R. Hydrogen Spillover. Facts and Fiction. *Chem. Rev.* **2012**, *112* (5), 2714–2738. <https://doi.org/10.1021/cr200346z>.
- (121) Barrer, R. M. *Zeolites and Clay Minerals as Sorbents and Molecular Sieves*; Academic Press, 1978. https://scholar.google.com/scholar_lookup?title=Zeolites+and+clay+minerals+as+sorbents+and+molecular+sieves&author=Barrer%2C+R.+M.+%28Richard+Maling%29&publication_year=1978 (accessed 2022-08-23).
- (122) Fraenkel, D.; Shabtai, J. Encapsulation of Hydrogen in Molecular Sieve Zeolites. *J. Am. Chem. Soc.* **1977**, *99* (21), 7074–7076. <https://doi.org/10.1021/ja00463a058>.
- (123) Weitkamp, J.; Fritz, M.; Ernst, S. Zeolites as Media for Hydrogen Storage. *International Journal of Hydrogen Energy* **1995**, *20* (12), 967–970. [https://doi.org/10.1016/0360-3199\(95\)00058-L](https://doi.org/10.1016/0360-3199(95)00058-L).
- (124) Nishimiya, N.; Kishi, T.; Mizushima, T.; Matsumoto, A.; Tsutsumi, K. Hyperstoichiometric Hydrogen Occlusion by Palladium Nanoparticles Included in NaY Zeolite. *Journal of Alloys and Compounds* **2001**, *319* (1), 312–321. [https://doi.org/10.1016/S0925-8388\(01\)00921-5](https://doi.org/10.1016/S0925-8388(01)00921-5).
- (125) Langmi, H. W.; Book, D.; Walton, A.; Johnson, S. R.; Al-Mamouri, M. M.; Speight, J. D.; Edwards, P. P.; Harris, I. R.; Anderson, P. A. Hydrogen Storage in Ion-Exchanged Zeolites. *Journal of Alloys and Compounds* **2005**, *404–406*, 637–642. <https://doi.org/10.1016/j.jallcom.2004.12.193>.
- (126) Vitillo, J. G.; Ricchiardi, G.; Spoto, G.; Zecchina, A. Theoretical Maximal Storage of Hydrogen in Zeolitic Frameworks. *Phys. Chem. Chem. Phys.* **2005**, *7* (23), 3948–3954. <https://doi.org/10.1039/B510989B>.
- (127) Veluswamy, H. P.; Kumar, R.; Linga, P. Hydrogen Storage in Clathrate Hydrates: Current State of the Art and Future Directions. *Applied Energy* **2014**, *122*, 112–132. <https://doi.org/10.1016/j.apenergy.2014.01.063>.

Literature review

- (128) Mao, W. L.; Mao, H. Hydrogen Storage in Molecular Compounds. *Proceedings of the National Academy of Sciences* **2004**, *101* (3), 708–710. <https://doi.org/10.1073/pnas.0307449100>.
- (129) Vos, W. L.; Finger, L. W.; Hemley, R. J.; Mao, H. Novel H_2 - H_2 Clathrates at High Pressures. *Phys. Rev. Lett.* **1993**, *71* (19), 3150–3153. <https://doi.org/10.1103/PhysRevLett.71.3150>.
- (130) Lee, H.; Lee, J.; Kim, D. Y.; Park, J.; Seo, Y.-T.; Zeng, H.; Moudrakovski, I. L.; Ratcliffe, C. I.; Ripmeester, J. A. Tuning Clathrate Hydrates for Hydrogen Storage. *Nature* **2005**, *434* (7034), 743–746. <https://doi.org/10.1038/nature03457>.
- (131) Feucht, K.; Hurich, W.; Komoschinski, N.; Povei, R. Hydrogen Drive for Road Vehicles-Results from the Fleet Test Run in Berlin. *International Journal of Hydrogen Energy* **1988**, *13* (4), 243–250. [https://doi.org/10.1016/0360-3199\(88\)90092-4](https://doi.org/10.1016/0360-3199(88)90092-4).
- (132) Zaluska, A.; Zaluski, L.; Ström-Olsen, J. O. Structure, Catalysis and Atomic Reactions on the Nano-Scale: A Systematic Approach to Metal Hydrides for Hydrogen Storage. *Appl Phys A* **2001**, *72* (2), 157–165. <https://doi.org/10.1007/s003390100783>.
- (133) Dehouche, Z.; Djaozandry, R.; Huot, J.; Boily, S.; Goyette, J.; Bose, T. K.; Schulz, R. Influence of Cycling on the Thermodynamic and Structure Properties of Nanocrystalline Magnesium Based Hydride. *Journal of Alloys and Compounds* **2000**, *305* (1), 264–271. [https://doi.org/10.1016/S0925-8388\(00\)00718-0](https://doi.org/10.1016/S0925-8388(00)00718-0).
- (134) Bloch, J.; Mintz, M. H. Kinetics and Mechanisms of Metal Hydrides Formation—a Review. *Journal of Alloys and Compounds* **1997**, *253–254*, 529–541. [https://doi.org/10.1016/S0925-8388\(96\)03070-8](https://doi.org/10.1016/S0925-8388(96)03070-8).
- (135) Reilly, J. J.; Wiswall, R. H. Formation and Properties of Iron Titanium Hydride. *Inorg. Chem.* **1974**, *13* (1), 218–222. <https://doi.org/10.1021/ic50131a042>.
- (136) Sakaguchi, H.; Tsujimoto, T.; Adachi, G. The Confinement of Hydrogen in LaNi₅ by Poisoning of the Hydride Surface. *Journal of Alloys and Compounds* **1995**, *223* (1), 122–126. [https://doi.org/10.1016/0925-8388\(94\)01489-2](https://doi.org/10.1016/0925-8388(94)01489-2).
- (137) Myhra, S.; Kisi, E. H.; Gray, E. M. A Surface Analytical Study of SO₂ Stabilisation of LaNi₅H_x Surfaces. *Journal of Alloys and Compounds* **1995**, *224* (2), 305–315. [https://doi.org/10.1016/0925-8388\(95\)01535-3](https://doi.org/10.1016/0925-8388(95)01535-3).
- (138) Tarasov, B. P.; Fursikov, P. V.; Volodin, A. A.; Bocharnikov, M. S.; Shimkus, Y. Y.; Kashin, A. M.; Yartys, V. A.; Chidziva, S.; Pasupathi, S.; Lototskyy, M. V. Metal Hydride Hydrogen Storage and Compression Systems for Energy Storage Technologies. *International Journal of Hydrogen Energy* **2021**, *46* (25), 13647–13657. <https://doi.org/10.1016/j.ijhydene.2020.07.085>.
- (139) Rusman, N. A. A.; Dahari, M. A Review on the Current Progress of Metal Hydrides Material for Solid-State Hydrogen Storage Applications. *International Journal of Hydrogen Energy* **2016**, *41* (28), 12108–12126. <https://doi.org/10.1016/j.ijhydene.2016.05.244>.
- (140) Okada, M.; Kuriiwa, T.; Kamegawa, A.; Takamura, H. Role of Intermetallics in Hydrogen Storage Materials. *Materials Science and Engineering: A* **2002**, *329–331*, 305–312. [https://doi.org/10.1016/S0921-5093\(01\)01580-5](https://doi.org/10.1016/S0921-5093(01)01580-5).
- (141) Principi, G.; Agresti, F.; Maddalena, A.; Lo Russo, S. The Problem of Solid State Hydrogen Storage. *Energy* **2009**, *34* (12), 2087–2091. <https://doi.org/10.1016/j.energy.2008.08.027>.
- (142) Gasiorowski, A.; Iwasieczko, W.; Skoryna, D.; Drulis, H.; Jurczyk, M. Hydriding Properties of Nanocrystalline Mg₂-xMxNi Alloys Synthesized by Mechanical Alloying (M=Mn, Al). *Journal of Alloys and Compounds* **2004**, *364* (1), 283–288. [https://doi.org/10.1016/S0925-8388\(03\)00544-9](https://doi.org/10.1016/S0925-8388(03)00544-9).
- (143) Jain, I. P.; Lal, C.; Jain, A. Hydrogen Storage in Mg: A Most Promising Material. *International Journal of Hydrogen Energy* **2010**, *35* (10), 5133–5144. <https://doi.org/10.1016/j.ijhydene.2009.08.088>.
- (144) Mushnikov, N. V.; Ermakov, A. E.; Uimin, M. A.; Gaviko, V. S.; Terent'ev, P. B.; Skripov, A. V.; Tankeev, A. P.; Soloninin, A. V.; Buzlukov, A. L. Kinetics of Interaction of Mg-Based Mechanically Activated Alloys with Hydrogen. *Phys. Metals Metallogr.* **2006**, *102* (4), 421–431. <https://doi.org/10.1134/S0031918X06100097>.
- (145) Liang, G.; Huot, J.; Boily, S.; Van Neste, A.; Schulz, R. Catalytic Effect of Transition Metals on Hydrogen Sorption in Nanocrystalline Ball Milled MgH₂-Tm (Tm=Ti, V, Mn, Fe and Ni) Systems. *Journal of Alloys and Compounds* **1999**, *292* (1), 247–252. [https://doi.org/10.1016/S0925-8388\(99\)00442-9](https://doi.org/10.1016/S0925-8388(99)00442-9).
- (146) Sadhasivam, T.; Kim, H.-T.; Jung, S.; Roh, S.-H.; Park, J.-H.; Jung, H.-Y. Dimensional Effects of Nanostructured Mg/MgH₂ for Hydrogen Storage Applications: A Review. *Renewable and Sustainable Energy Reviews* **2017**, *72*, 523–534. <https://doi.org/10.1016/j.rser.2017.01.107>.
- (147) Shao, H.; Xin, G.; Zheng, J.; Li, X.; Akiba, E. Nanotechnology in Mg-Based Materials for Hydrogen Storage. *Nano Energy* **2012**, *1* (4), 590–601. <https://doi.org/10.1016/j.nanoen.2012.05.005>.
- (148) Fichtner, M. Properties of Nanoscale Metal Hydrides. *Nanotechnology* **2009**, *20* (20), 204009. <https://doi.org/10.1088/0957-4484/20/20/204009>.

- (149) Vajo, J. J. Influence of Nano-Confinement on the Thermodynamics and Dehydrogenation Kinetics of Metal Hydrides. *Current Opinion in Solid State and Materials Science* **2011**, *15* (2), 52–61. <https://doi.org/10.1016/j.cossms.2010.11.001>.
- (150) Lai, Q.; Wang, T.; Sun, Y.; Aguey-Zinsou, K.-F. Rational Design of Nanosized Light Elements for Hydrogen Storage: Classes, Synthesis, Characterization, and Properties. *Advanced Materials Technologies* **2018**, *3* (9), 1700298. <https://doi.org/10.1002/admt.201700298>.
- (151) Zhao-Karger, Z.; Hu, J.; Roth, A.; Wang, D.; Kübel, C.; Lohstroh, W.; Fichtner, M. Altered Thermodynamic and Kinetic Properties of MgH₂ Infiltrated in Microporous Scaffold. *Chem. Commun.* **2010**, *46* (44), 8353–8355. <https://doi.org/10.1039/C0CC03072D>.
- (152) He, T.; Cao, H.; Chen, P. Complex Hydrides for Energy Storage, Conversion, and Utilization. *Advanced Materials* **2019**, *31* (50), 1902757. <https://doi.org/10.1002/adma.201902757>.
- (153) Tanaka, H.; Tokoyoda, K.; Matsumoto, M.; Suzuki, Y.; Kiyobayashi, T.; Kuriyama, N. Hazard Assessment of Complex Hydrides as Hydrogen Storage Materials. *International Journal of Hydrogen Energy* **2009**, *34* (7), 3210–3218. <https://doi.org/10.1016/j.ijhydene.2009.01.064>.
- (154) Urganli, J.; Torres, F. J.; Palumbo, M.; Baricco, M. Hydrogen Release from Solid State NaBH₄. *International Journal of Hydrogen Energy* **2008**, *33* (12), 3111–3115. <https://doi.org/10.1016/j.ijhydene.2008.03.031>.
- (155) Bogdanović, B.; Schwickardi, M. Ti-Doped Alkali Metal Aluminium Hydrides as Potential Novel Reversible Hydrogen Storage Materials. Invited Paper Presented at the International Symposium on Metal-Hydrogen Systems, Les Diablerets, August 25–30, 1996, Switzerland. *Journal of Alloys and Compounds* **1997**, *253–254*, 1–9. [https://doi.org/10.1016/S0925-8388\(96\)03049-6](https://doi.org/10.1016/S0925-8388(96)03049-6).
- (156) Pohlmann, C.; Röntzsch, L.; Hu, J.; Weißgärber, T.; Kieback, B.; Fichtner, M. Tailored Heat Transfer Characteristics of Pelletized LiNH₂-MgH₂ and NaAlH₄ Hydrogen Storage Materials. *Journal of Power Sources* **2012**, *205*, 173–179. <https://doi.org/10.1016/j.jpowsour.2012.01.064>.
- (157) Züttel, A.; Wenger, P.; Rentsch, S.; Sudan, P.; Mauron, Ph.; Emmenegger, Ch. LiBH₄ a New Hydrogen Storage Material. *Journal of Power Sources* **2003**, *118*, 1–7. [https://doi.org/10.1016/S0378-7753\(03\)00054-5](https://doi.org/10.1016/S0378-7753(03)00054-5).
- (158) Chen, P.; Xiong, Z.; Luo, J.; Lin, J.; Tan, K. L. Interaction of Hydrogen with Metal Nitrides and Imides. *Nature* **2002**, *420* (6913), 302–304. <https://doi.org/10.1038/nature01210>.
- (159) Chandra, M.; Xu, Q. A High-Performance Hydrogen Generation System: Transition Metal-Catalyzed Dissociation and Hydrolysis of Ammonia-Borane. *Journal of Power Sources* **2006**, *156* (2), 190–194. <https://doi.org/10.1016/j.jpowsour.2005.05.043>.
- (160) Hua, T. Q.; Ahluwalia, R. K. Off-Board Regeneration of Ammonia Borane for Use as a Hydrogen Carrier for Automotive Fuel Cells. *International Journal of Hydrogen Energy* **2012**, *37* (19), 14382–14392. <https://doi.org/10.1016/j.ijhydene.2012.07.013>.
- (161) Ramachandran, P. V.; Gagare, P. D. Preparation of Ammonia Borane in High Yield and Purity, Methanolysis, and Regeneration. *Inorg. Chem.* **2007**, *46* (19), 7810–7817. <https://doi.org/10.1021/ic700772a>.
- (162) Al-Kukhun, A.; Hwang, H. T.; Varma, A. Mechanistic Studies of Ammonia Borane Dehydrogenation. *International Journal of Hydrogen Energy* **2013**, *38* (1), 169–179. <https://doi.org/10.1016/j.ijhydene.2012.09.161>.
- (163) Baitalow, F.; Baumann, J.; Wolf, G.; Jaenicke-Röbler, K.; Leitner, G. Thermal Decomposition of B-N-H Compounds Investigated by Using Combined Thermoanalytical Methods. *Thermochimica Acta* **2002**, *391* (1), 159–168. [https://doi.org/10.1016/S0040-6031\(02\)00173-9](https://doi.org/10.1016/S0040-6031(02)00173-9).
- (164) Frueh, S.; Kellett, R.; Mallery, C.; Molter, T.; Willis, W. S.; King'ondo, C.; Suib, S. L. Pyrolytic Decomposition of Ammonia Borane to Boron Nitride. *Inorg. Chem.* **2011**, *50* (3), 783–792. <https://doi.org/10.1021/ic101020k>.
- (165) Zhang, L.; Xia, G.; Ge, Y.; Wang, C.; Guo, Z.; Li, X.; Yu, X. Ammonia Borane Confined by Nitrogen-Containing Carbon Nanotubes: Enhanced Dehydrogenation Properties Originating from Synergetic Catalysis and Nanoconfinement. *Journal of Materials Chemistry A* **2015**, *3* (41), 20494–20499. <https://doi.org/10.1039/C5TA05540G>.
- (166) Bluhm, M. E.; Bradley, M. G.; Butterick, R.; Kusari, U.; Sneddon, L. G. Amineborane-Based Chemical Hydrogen Storage: Enhanced Ammonia Borane Dehydrogenation in Ionic Liquids. *J. Am. Chem. Soc.* **2006**, *128* (24), 7748–7749. <https://doi.org/10.1021/ja062085v>.
- (167) Heldebrant, D. J.; Karkamkar, A.; Hess, N. J.; Bowden, M.; Rassat, S.; Zheng, F.; Rappe, K.; Autrey, T. The Effects of Chemical Additives on the Induction Phase in Solid-State Thermal Decomposition of Ammonia Borane. *Chem. Mater.* **2008**, *20* (16), 5332–5336. <https://doi.org/10.1021/cm801253u>.
- (168) Wahab, M. A.; Zhao, H.; Yao, X. D. Nano-Confined Ammonia Borane for Chemical Hydrogen Storage. *Front. Chem. Sci. Eng.* **2012**, *6* (1), 27–33. <https://doi.org/10.1007/s11705-011-1171-3>.

Literature review

- (169) Owarzany, R.; Jaroń, T.; Leszczyński, P. J.; Fijalkowski, K. J.; Grochala, W. Amidoboranes of Rubidium and Caesium: The Last Missing Members of the Alkali Metal Amidoborane Family. *Dalton Trans.* **2017**, 46 (46), 16315–16320. <https://doi.org/10.1039/C7DT03590J>.
- (170) Ramzan, M.; Silvearv, F.; Blomqvist, A.; Scheicher, R. H.; Lebègue, S.; Ahuja, R. Structural and Energetic Analysis of the Hydrogen Storage Materials LiNH_2BH_3 and NaNH_2BH_3 from Ab Initio Calculations. *Phys. Rev. B* **2009**, 79 (13), 132102. <https://doi.org/10.1103/PhysRevB.79.132102>.
- (171) Wu, H.; Zhou, W.; Yildirim, T. Alkali and Alkaline-Earth Metal Amidoboranes: Structure, Crystal Chemistry, and Hydrogen Storage Properties. *J. Am. Chem. Soc.* **2008**, 130 (44), 14834–14839. <https://doi.org/10.1021/ja806243f>.
- (172) *Macrovector*. Freepik. <https://fr.freepik.com/auteur/macrovector> (accessed 2022-11-30).
- (173) *Catalyst: NH₃ as an Energy Carrier | Elsevier Enhanced Reader*. <https://doi.org/10.1016/j.chempr.2017.10.004>.
- (174) *Ammoniac*. Techniques de l'Ingénieur. <https://www.techniques-ingenieur.fr/base-documentaire/procedes-chimie-bio-agro-th2/fabrication-des-grands-produits-industriels-en-chimie-et-petrochimie-42319210/ammoniac-j6135/> (accessed 2022-10-10).
- (175) 2014_ifa_ff_ammonia_emissions_july.Pdf. https://www.fertilizer.org/images/Library_Downloads/2014_ifa_ff_ammonia_emissions_july.pdf (accessed 2022-10-10).
- (176) Rafiqul, I.; Weber, C.; Lehmann, B.; Voss, A. Energy Efficiency Improvements in Ammonia Production—Perspectives and Uncertainties. *Energy* **2005**, 30 (13), 2487–2504. <https://doi.org/10.1016/j.energy.2004.12.004>.
- (177) Wang, M.; A. Khan, M.; Mohsin, I.; Wicks, J.; H. Ip, A.; Z. Sumon, K.; Dinh, C.-T.; H. Sargent, E.; D. Gates, I.; Golam Kibria, M. Can Sustainable Ammonia Synthesis Pathways Compete with Fossil-Fuel Based Haber–Bosch Processes? *Energy & Environmental Science* **2021**, 14 (5), 2535–2548. <https://doi.org/10.1039/D0EE03808C>.
- (178) McEnaney, J. M.; Singh, A. R.; Schwalbe, J. A.; Kibsgaard, J.; Lin, J. C.; Cargnello, M.; Jaramillo, T. F.; Nørskov, J. K. Ammonia Synthesis from N₂ and H₂O Using a Lithium Cycling Electrification Strategy at Atmospheric Pressure. *Energy Environ. Sci.* **2017**, 10 (7), 1621–1630. <https://doi.org/10.1039/C7EE01126A>.
- (179) Kunsman, C. H. The Decomposition of Ammonia on Iron Catalysts. *Science* **1927**, 65 (1691), 527–528. <https://doi.org/10.1126/science.65.1691.527-a>.
- (180) Kunsman, C. H. THE THERMAL DECOMPOSITION OF AMMONIA ON IRON CATALYSTS. II. *J. Am. Chem. Soc.* **1929**, 51 (3), 688–695. <https://doi.org/10.1021/ja01378a005>.
- (181) Lamb, K. E.; Dolan, M. D.; Kennedy, D. F. Ammonia for Hydrogen Storage; A Review of Catalytic Ammonia Decomposition and Hydrogen Separation and Purification. *International Journal of Hydrogen Energy* **2019**, 44 (7), 3580–3593. <https://doi.org/10.1016/j.ijhydene.2018.12.024>.
- (182) Makepeace, J. W.; He, T.; Weidenthaler, C.; Jensen, T. R.; Chang, F.; Vegge, T.; Ngene, P.; Kojima, Y.; de Jongh, P. E.; Chen, P.; David, W. I. F. Reversible Ammonia-Based and Liquid Organic Hydrogen Carriers for High-Density Hydrogen Storage: Recent Progress. *International Journal of Hydrogen Energy* **2019**, 44 (15), 7746–7767. <https://doi.org/10.1016/j.ijhydene.2019.01.144>.
- (183) Marakatti, V. S.; Gaigneaux, E. M. Recent Advances in Heterogeneous Catalysis for Ammonia Synthesis. *ChemCatChem* **2020**, 12 (23), 5838–5857. <https://doi.org/10.1002/cctc.202001141>.
- (184) Chatterjee, S.; Parsapur, R. K.; Huang, K.-W. Limitations of Ammonia as a Hydrogen Energy Carrier for the Transportation Sector. *ACS Energy Lett.* **2021**, 6 (12), 4390–4394. <https://doi.org/10.1021/acseenergylett.1c02189>.
- (185) Wang, W.; Su, C.; Wu, Y.; Ran, R.; Shao, Z. Progress in Solid Oxide Fuel Cells with Nickel-Based Anodes Operating on Methane and Related Fuels. *Chem. Rev.* **2013**, 113 (10), 8104–8151. <https://doi.org/10.1021/cr300491e>.
- (186) *Methanol Industry Installed Capacity and Capital Expenditure (CapEx) Forecast by Region and Countries including details of All Active Plants, Planned and Announced Projects, 2021-2026*. Market Research Reports & Consulting | GlobalData UK Ltd. <https://www.globaldata.com/store/report/methanol-market-analysis/> (accessed 2022-10-18).
- (187) Tian, P.; Wei, Y.; Ye, M.; Liu, Z. Methanol to Olefins (MTO): From Fundamentals to Commercialization. *ACS Catal.* **2015**, 5 (3), 1922–1938. <https://doi.org/10.1021/acscatal.5b00007>.
- (188) Boocock, D. G. B. Process for Production of Fatty Acid Methyl Esters from Fatty Acid Triglycerides. US6712867B1, March 30, 2004. <https://patents.google.com/patent/US6712867B1/en> (accessed 2022-11-30).

Literature review

- (189) Park, H.; Woo, Y.; Jung, H. S.; Kim, G.; Bae, J. W.; Park, M.-J. Development of Dimethyl Ether Synthesis Processes Using By-Product Gas from a Steel-Making Plant: Single-vs. Two-Step Processes. *Journal of Cleaner Production* **2021**, *326*, 129367. <https://doi.org/10.1016/j.jclepro.2021.129367>.
- (190) Olah, G. A.; Goepfert, A.; Prakash, G. K. S. *Beyond Oil and Gas: The Methanol Economy*; John Wiley & Sons, 2018.
- (191) Courty, P.; Travers, C.; Durand, D.; Forestière, A.; Chaumette, P. Process for the Preparation of Catalysts Comprising Copper, Zinc and Aluminium, Useful in the Production of Methanol from Synthesis Gas. EP0152314B1, August 12, 1987. <https://patents.google.com/patent/EP0152314B1/en> (accessed 2022-11-30).
- (192) Magoon, E. Production of Methanol. US3709919A, January 9, 1973. [https://patents.google.com/patent/US3709919A/en?q=+Shell%2c+US+3709919%2c+1973+\(E.F.+Magoon\)](https://patents.google.com/patent/US3709919A/en?q=+Shell%2c+US+3709919%2c+1973+(E.F.+Magoon)) (accessed 2022-11-30).
- (193) Gallagher, J. T.; Kidd, J. M. Methanol Synthesis. GB1159035A, July 23, 1969. <https://patents.google.com/patent/GB1159035A/en?q=GB+1159035> (accessed 2022-11-30).
- (194) Schneider, M. D. D.-C.; Kochloefl, K. D. D.-C.; Ladebeck, J. D. D.-C. Katalysator Für Die Methanolsynthese. EP0125689B1, June 16, 1987. <https://patents.google.com/patent/EP0125689B1/en?q=EP+0125689> (accessed 2022-11-30).
- (195) Höppener, R. H.; Doesburg, E. B. M.; Scholten, J. J. F. Preparation and Characterization of Stable Copper/Zinc Oxide/Alumina Catalysts for Methanol Synthesis. *Applied Catalysis* **1986**, *25* (1), 109–119. [https://doi.org/10.1016/S0166-9834\(00\)81227-0](https://doi.org/10.1016/S0166-9834(00)81227-0).
- (196) Shamsul, N. S.; Kamarudin, S. K.; Rahman, N. A.; Kofli, N. T. An Overview on the Production of Bio-Methanol as Potential Renewable Energy. *Renewable and Sustainable Energy Reviews* **2014**, *33*, 578–588. <https://doi.org/10.1016/j.rser.2014.02.024>.
- (197) Xie, S.; Zhang, W.; Lan, X.; Lin, H. CO₂ Reduction to Methanol in the Liquid Phase: A Review. *ChemSusChem* **2020**, *13* (23), 6141–6159. <https://doi.org/10.1002/cssc.202002087>.
- (198) Huff, C. A.; Sanford, M. S. Cascade Catalysis for the Homogeneous Hydrogenation of CO₂ to Methanol. *J. Am. Chem. Soc.* **2011**, *133* (45), 18122–18125. <https://doi.org/10.1021/ja208760j>.
- (199) Miller, A. J. M.; Heinekey, D. M.; Mayer, J. M.; Goldberg, K. I. Catalytic Disproportionation of Formic Acid to Generate Methanol. *Angewandte Chemie International Edition* **2013**, *52* (14), 3981–3984. <https://doi.org/10.1002/anie.201208470>.
- (200) Kanega, R.; Onishi, N.; Tanaka, S.; Kishimoto, H.; Himeda, Y. Catalytic Hydrogenation of CO₂ to Methanol Using Multinuclear Iridium Complexes in a Gas–Solid Phase Reaction. *J. Am. Chem. Soc.* **2021**, *143* (3), 1570–1576. <https://doi.org/10.1021/jacs.0c11927>.
- (201) Sá, S.; Silva, H.; Brandão, L.; Sousa, J. M.; Mendes, A. Catalysts for Methanol Steam Reforming—A Review. *Applied Catalysis B: Environmental* **2010**, *99* (1), 43–57. <https://doi.org/10.1016/j.apcatb.2010.06.015>.
- (202) Eberle, U.; Felderhoff, M.; Schüth, F. Chemical and Physical Solutions for Hydrogen Storage. *Angewandte Chemie International Edition* **2009**, *48* (36), 6608–6630. <https://doi.org/10.1002/anie.200806293>.
- (203) Hodoshima, S.; Arai, H.; Takaiwa, S.; Saito, Y. Catalytic Decalin Dehydrogenation/Naphthalene Hydrogenation Pair as a Hydrogen Source for Fuel-Cell Vehicle. *International Journal of Hydrogen Energy* **2003**, *28* (11), 1255–1262. [https://doi.org/10.1016/S0360-3199\(02\)00250-1](https://doi.org/10.1016/S0360-3199(02)00250-1).
- (204) Sultan, O.; Shaw, H. *Study of Automotive Storage of Hydrogen Using Recyclable Liquid Chemical Carriers. [Catalytic Dehydrogenation of Naphthalenes]*; TEC-75/003; Exxon Research and Engineering Co., Linden, N.J. (USA). Government Research Lab., 1975. <https://www.osti.gov/biblio/5000657> (accessed 2020-03-03).
- (205) Taube, M.; Taube, P. *A Liquid Organic Carrier of Hydrogen as a Fuel for Automobiles*; EIR--379; Eidgenössisches Inst. fuer Reaktorforschung, 1979. http://inis.iaea.org/Search/search.aspx?orig_q=RN:13652276 (accessed 2020-03-03).
- (206) Grünenfelder, N. F.; Schucan, Th. H. Seasonal Storage of Hydrogen in Liquid Organic Hydrides: Description of the Second Prototype Vehicle. *International Journal of Hydrogen Energy* **1989**, *14* (8), 579–586. [https://doi.org/10.1016/0360-3199\(89\)90117-1](https://doi.org/10.1016/0360-3199(89)90117-1).
- (207) He, T.; Pei, Q.; Chen, P. Liquid Organic Hydrogen Carriers. *Journal of Energy Chemistry* **2015**, *24* (5), 587–594. <https://doi.org/10.1016/j.jechem.2015.08.007>.
- (208) Züttel, A. Hydrogen Storage Methods. *Naturwissenschaften* **2004**, *91* (4), 157–172. <https://doi.org/10.1007/s00114-004-0516-x>.
- (209) Riha, M. *Hydrogenious LOHC Technologies GmbH*. FUTURIUM - European Commission. <https://ec.europa.eu/futurium/en/tech-society-2020/hydrogenious-lohc-technologies-gmbh> (accessed 2022-11-02).

- (210) *Target Explanation Document: Onboard Hydrogen Storage for Light-Duty Fuel Cell Vehicles*. Energy.gov. <https://www.energy.gov/eere/fuelcells/downloads/target-explanation-document-onboard-hydrogen-storage-light-duty-fuel-cell> (accessed 2021-06-04).
- (211) Geburtig, D.; Preuster, P.; Bösmann, A.; Müller, K.; Wasserscheid, P. Chemical Utilization of Hydrogen from Fluctuating Energy Sources – Catalytic Transfer Hydrogenation from Charged Liquid Organic Hydrogen Carrier Systems. *International Journal of Hydrogen Energy* **2016**, *41* (2), 1010–1017. <https://doi.org/10.1016/j.ijhydene.2015.10.013>.
- (212) Teichmann, D.; Arlt, W.; Wasserscheid, P. Liquid Organic Hydrogen Carriers as an Efficient Vector for the Transport and Storage of Renewable Energy. *International Journal of Hydrogen Energy* **2012**, *37* (23), 18118–18132. <https://doi.org/10.1016/j.ijhydene.2012.08.066>.
- (213) Aakko-Saksa, P. T.; Cook, C.; Kiviahio, J.; Repo, T. Liquid Organic Hydrogen Carriers for Transportation and Storing of Renewable Energy – Review and Discussion. *Journal of Power Sources* **2018**, *396*, 803–823. <https://doi.org/10.1016/j.jpowsour.2018.04.011>.
- (214) Niermann, M.; Beckendorff, A.; Kaltschmitt, M.; Bonhoff, K. Liquid Organic Hydrogen Carrier (LOHC) – Assessment Based on Chemical and Economic Properties. *International Journal of Hydrogen Energy* **2019**, *44* (13), 6631–6654. <https://doi.org/10.1016/j.ijhydene.2019.01.199>.
- (215) Modisha, P. M.; Ouma, C. N. M.; Garidzirai, R.; Wasserscheid, P.; Bessarabov, D. The Prospect of Hydrogen Storage Using Liquid Organic Hydrogen Carriers. *Energy Fuels* **2019**, *33* (4), 2778–2796. <https://doi.org/10.1021/acs.energyfuels.9b00296>.
- (216) Rao, P. C.; Yoon, M. Potential Liquid-Organic Hydrogen Carrier (LOHC) Systems: A Review on Recent Progress. *Energies* **2020**, *13* (22), 6040. <https://doi.org/10.3390/en13226040>.
- (217) Cho, J.-Y.; Kim, H.; Oh, J.-E.; Park, B. Y. Recent Advances in Homogeneous/Heterogeneous Catalytic Hydrogenation and Dehydrogenation for Potential Liquid Organic Hydrogen Carrier (LOHC) Systems. *Catalysts* **2021**, *11* (12), 1497. <https://doi.org/10.3390/catal11121497>.
- (218) Zelinsky, N. Über Dehydrogenisation Durch Katalyse. *Berichte der deutschen chemischen Gesellschaft* **1911**, *44* (3), 3121–3125. <https://doi.org/10.1002/cber.191104403168>.
- (219) Zelinsky, N. Über Die Selektive Dehydrogenisations-Katalyse. *Berichte der deutschen chemischen Gesellschaft* **1912**, *45* (3), 3678–3682. <https://doi.org/10.1002/cber.191204503126>.
- (220) Alan C. Cooper. *Design and Development of New Carbon-Based Sorbent Systems for an Effective Containment of Hydrogen*; 86-377-P, 1039432; 2012; pp 86-377-P, 1039432. <https://doi.org/10.2172/1039432>.
- (221) Clar, E. The Aromatic Sextet. In *Mobile Source Emissions Including Polycyclic Organic Species*; Rondia, D., Cooke, M., Haroz, R. K., Eds.; NATO ASI Series; Springer Netherlands: Dordrecht, 1983; pp 49–58. https://doi.org/10.1007/978-94-009-7197-4_4.
- (222) Solà, M. Forty Years of Clar’s Aromatic π -Sextet Rule. *Frontiers in Chemistry* **2013**, *1*.
- (223) Pumera, M.; An Wong, C. H. Graphane and Hydrogenated Graphene. *Chemical Society Reviews* **2013**, *42* (14), 5987–5995. <https://doi.org/10.1039/C3CS60132C>.
- (224) Luo, Z.; Yu, T.; Kim, K.; Ni, Z.; You, Y.; Lim, S.; Shen, Z.; Wang, S.; Lin, J. Thickness-Dependent Reversible Hydrogenation of Graphene Layers. *ACS Nano* **2009**, *3* (7), 1781–1788. <https://doi.org/10.1021/nn900371t>.
- (225) Kalenchuk, A.; Bogdan, V.; Dunaev, S.; Kustov, L. Influence of Steric Factors on Reversible Reactions of Hydrogenation-Dehydrogenation of Polycyclic Aromatic Hydrocarbons on a Pt/C Catalyst in Hydrogen Storage Systems. *Fuel* **2020**, *280*, 118625. <https://doi.org/10.1016/j.fuel.2020.118625>.
- (226) Hydrogen, C. S. MITSUBISHI HITACHI POWER SYSTEMS LTD. Development Bank of Japan Inc. 3.
- (227) Vanhanen, J. P.; Lund, P. D. Computational Approaches for Improving Seasonal Storage Systems Based on Hydrogen Technologies. *International Journal of Hydrogen Energy* **1995**, *20* (7), 575–585. [https://doi.org/10.1016/0360-3199\(94\)00110-L](https://doi.org/10.1016/0360-3199(94)00110-L).
- (228) Taube, M.; Rippin, D.; Knecht, W.; Hakimifard, D.; Milisavljevic, B.; Gruenenfelder, N. A Prototype Truck Powered by Hydrogen from Organic Liquid Hydrides. *International Journal of Hydrogen Energy* **1985**, *10* (9), 595–599. [https://doi.org/10.1016/0360-3199\(85\)90035-7](https://doi.org/10.1016/0360-3199(85)90035-7).
- (229) Kerleau, P.; Swesi, Y.; Meille, V.; Pitault, I.; Heurtaux, F. Total Catalytic Oxidation of a Side-Product for an Autothermal Restoring Hydrogen Process. *Catalysis Today* **2010**, *157* (1), 321–326. <https://doi.org/10.1016/j.cattod.2010.02.011>.
- (230) Touzani, A.; Klvana, D.; Bélanger, G. Dehydrogenation Reactor for a Vehicle Equipped with a Hydrogen Engine: A Simulation Study. *International Journal of Hydrogen Energy* **1984**, *9* (11), 929–936. [https://doi.org/10.1016/0360-3199\(84\)90158-7](https://doi.org/10.1016/0360-3199(84)90158-7).
- (231) Niimi, T.; Nagasawa, H.; Kanezashi, M.; Yoshioka, T.; Ito, K.; Tsuru, T. Preparation of BTESE-Derived Organosilica Membranes for Catalytic Membrane Reactors of Methylcyclohexane Dehydrogenation. *Journal of Membrane Science* **2014**, *455*, 375–383. <https://doi.org/10.1016/j.memsci.2014.01.003>.

- (232) Ali, J. K.; Newson, E. J.; Rippin, D. W. T. Exceeding Equilibrium Conversion with a Catalytic Membrane Reactor for the Dehydrogenation of Methylcyclohexane. *Chemical Engineering Science* **1994**, *49* (13), 2129–2134. [https://doi.org/10.1016/0009-2509\(94\)E0035-O](https://doi.org/10.1016/0009-2509(94)E0035-O).
- (233) Pal, N.; Agarwal, M.; Maheshwari, K.; Solanki, Y. S. A Review on Types, Fabrication and Support Material of Hydrogen Separation Membrane. *Materials Today: Proceedings* **2020**, *28*, 1386–1391. <https://doi.org/10.1016/j.matpr.2020.04.806>.
- (234) Chytil, S.; Glomm, W. R.; Vollebek, E.; Bergem, H.; Walmsley, J.; Sjöblom, J.; Blekkan, E. A. Platinum Nanoparticles Encapsulated in Mesoporous Silica: Preparation, Characterisation and Catalytic Activity in Toluene Hydrogenation. *Microporous and Mesoporous Materials* **2005**, *86* (1), 198–206. <https://doi.org/10.1016/j.micromeso.2005.06.037>.
- (235) Alexeev, O.; Gates, B. C. Iridium Clusters Supported on γ -Al₂O₃: Structural Characterization and Catalysis of Toluene Hydrogenation. *Journal of Catalysis* **1998**, *176* (2), 310–320. <https://doi.org/10.1006/jcat.1998.2053>.
- (236) Weber, W. A.; Gates, B. C. Rhodium Supported on Faujasites: Effects of Cluster Size and CO Ligands on Catalytic Activity for Toluene Hydrogenation. *Journal of Catalysis* **1998**, *180* (2), 207–217. <https://doi.org/10.1006/jcat.1998.2264>.
- (237) Suppino, R. S.; Landers, R.; Cobo, A. J. G. Influence of Noble Metals (Pd, Pt) on the Performance of Ru/Al₂O₃ Based Catalysts for Toluene Hydrogenation in Liquid Phase. *Applied Catalysis A: General* **2016**, *525*, 41–49. <https://doi.org/10.1016/j.apcata.2016.06.038>.
- (238) Rousset, J. L.; Stievano, L.; Aires, F. J. C. S.; Geantet, C.; Renouprez, A. J.; Pellarin, M. Hydrogenation of Toluene over γ -Al₂O₃-Supported Pt, Pd, and Pd–Pt Model Catalysts Obtained by Laser Vaporization of Bulk Metals. *Journal of Catalysis* **2001**, *197* (2), 335–343. <https://doi.org/10.1006/jcat.2000.3083>.
- (239) Thomas, K.; Binet, C.; Chevreau, T.; Cornet, D.; Gilson, J.-P. Hydrogenation of Toluene over Supported Pt and Pd Catalysts: Influence of Structural Factors on the Sulfur Tolerance. *Journal of Catalysis* **2002**, *212* (1), 63–75. <https://doi.org/10.1006/jcat.2002.3780>.
- (240) Lindfors, L. P.; Salmi, T.; Smeds, S. Kinetics of Toluene Hydrogenation on Ni/Al₂O₃ Catalyst. *Chemical Engineering Science* **1993**, *48* (22), 3813–3828. [https://doi.org/10.1016/0009-2509\(93\)80224-E](https://doi.org/10.1016/0009-2509(93)80224-E).
- (241) Shuwa, S. M.; Jibril, B. Y.; Al-Hajri, R. S. Hydrogenation of Toluene on Ni-Co-Mo Supported Zeolite Catalysts. *Nigerian Journal of Technology* **2017**, *36* (4), 1114–1123. <https://doi.org/10.4314/njt.v36i4.17>.
- (242) Wang, J.; Huang, L.; Li, Q. Influence of Different Diluents in Pt/Al₂O₃ Catalyst on the Hydrogenation of Benzene, Toluene and o-Xylene. *Applied Catalysis A: General* **1998**, *175* (1), 191–199. [https://doi.org/10.1016/S0926-860X\(98\)00216-6](https://doi.org/10.1016/S0926-860X(98)00216-6).
- (243) Zhu, L.; Zhang, H.; Hu, W.; Zheng, J.; Zhang, N.; Yu, C.; Ye, H.; Yang, Z.; Chen, B. H. Nickel Hydroxide–Cobalt Hydroxide Nanoparticle Supported Ruthenium–Nickel–Cobalt Islands as an Efficient Nanocatalyst for the Hydrogenation Reaction. *ChemCatChem* **2018**, *10* (9), 1998–2002. <https://doi.org/10.1002/cctc.201701847>.
- (244) Okada, Y.; Sasaki, E.; Watanabe, E.; Hyodo, S.; Nishijima, H. Development of Dehydrogenation Catalyst for Hydrogen Generation in Organic Chemical Hydride Method. *International Journal of Hydrogen Energy* **2006**, *31* (10), 1348–1356. <https://doi.org/10.1016/j.ijhydene.2005.11.014>.
- (245) Wang, J.; Liu, H.; Fan, S.; Wang, S.; Xu, G.; Guo, A.; Wang, Z. Dehydrogenation of Cycloalkanes over N-Doped Carbon-Supported Catalysts: The Effects of Active Component and Molecular Structure of the Substrate. *Nanomaterials* **2021**, *11* (11), 2846. <https://doi.org/10.3390/nano11112846>.
- (246) Shukla, A. A.; Gosavi, P. V.; Pande, J. V.; Kumar, V. P.; Chary, K. V. R.; Biniwale, R. B. Efficient Hydrogen Supply through Catalytic Dehydrogenation of Methylcyclohexane over Pt/Metal Oxide Catalysts. *International Journal of Hydrogen Energy* **2010**, *35* (9), 4020–4026. <https://doi.org/10.1016/j.ijhydene.2010.02.014>.
- (247) Wu, X.; Lu, H.; Xiao, Y.; Guo, H.; Jia, L.; Li, D. Acid Site Introduced by Al³⁺-penta and Boron in Pt/Al₂O₃ Catalyst for Dehydrogenation of Methylcyclohexane. *International Journal of Hydrogen Energy* **2022**. <https://doi.org/10.1016/j.ijhydene.2022.08.085>.
- (248) Parra, C. F.; Goldwasser, M. R.; Fajula, F.; Figueras, F. A Study of the Hydrogen Transfer Reaction between Isobutene and Cyclohexane over Zeolites Using Carbon-13 Labelled Molecules. *Applied Catalysis* **1985**, *17* (2), 217–222. [https://doi.org/10.1016/S0166-9834\(00\)83206-6](https://doi.org/10.1016/S0166-9834(00)83206-6).
- (249) de la Banda, J. F. G.; Melo, A. C. y F. V. Dehydrogenation of Methylcyclohexene on a PtNaY Catalyst. Study of Kinetics and Deactivation. *Applied Catalysis* **1986**, *26*, 103–121. [https://doi.org/10.1016/S0166-9834\(00\)82545-2](https://doi.org/10.1016/S0166-9834(00)82545-2).
- (250) Van Trimpont, P. A.; Marin, G. B.; Froment, G. F. Kinetics of Methylcyclohexane Dehydrogenation on Sulfided Commercial Platinum/Alumina and Platinum-Rhenium/Alumina Catalysts. *Ind. Eng. Chem. Fund.* **1986**, *25* (4), 544–553. <https://doi.org/10.1021/i100024a014>.
- (251) Chen, L.; Verma, P.; Hou, K.; Qi, Z.; Zhang, S.; Liu, Y.-S.; Guo, J.; Stavila, V.; Allendorf, M. D.; Zheng, L.; Salmeron, M.; Prendergast, D.; Somorjai, G. A.; Su, J. Reversible Dehydrogenation and

- Rehydrogenation of Cyclohexane and Methylcyclohexane by Single-Site Platinum Catalyst. *Nat Commun* **2022**, *13* (1), 1092. <https://doi.org/10.1038/s41467-022-28607-y>.
- (252) Sebastian, O.; Nair, S.; Taccardi, N.; Wolf, M.; Søgaaard, A.; Haumann, M.; Wasserscheid, P. Stable and Selective Dehydrogenation of Methylcyclohexane Using Supported Catalytically Active Liquid Metal Solutions – Ga₅Pt/SiO₂ SCALMS. *ChemCatChem* **2020**, *12* (18), 4533–4537. <https://doi.org/10.1002/cctc.202000671>.
- (253) Manabe, R.; Okada, S.; Inagaki, R.; Oshima, K.; Ogo, S.; Sekine, Y. Surface Protonics Promotes Catalysis. *Sci Rep* **2016**, *6* (1), 38007. <https://doi.org/10.1038/srep38007>.
- (254) Kosaka, M.; Higo, T.; Ogo, S.; Seo, J. G.; Kado, S.; Imagawa, K.; Sekine, Y. Low-Temperature Selective Dehydrogenation of Methylcyclohexane by Surface Protonics over Pt/Anatase-TiO₂ Catalyst. *International Journal of Hydrogen Energy* **2020**, *45* (1), 738–743. <https://doi.org/10.1016/j.ijhydene.2019.10.133>.
- (255) Yolcular, S.; Olgun, Ö. Ni/Al₂O₃ Catalysts and Their Activity in Dehydrogenation of Methylcyclohexane for Hydrogen Production. *Catalysis Today* **2008**, *138* (3), 198–202. <https://doi.org/10.1016/j.cattod.2008.07.020>.
- (256) H. Al-ShaikhAli, A.; Jedidi, A.; Cavallo, L.; Takanabe, K. Non-Precious Bimetallic Catalysts for Selective Dehydrogenation of an Organic Chemical Hydride System. *Chemical Communications* **2015**, *51* (65), 12931–12934. <https://doi.org/10.1039/C5CC04016G>.
- (257) Al-ShaikhAli, A. H.; Jedidi, A.; Anjum, D. H.; Cavallo, L.; Takanabe, K. Kinetics on NiZn Bimetallic Catalysts for Hydrogen Evolution via Selective Dehydrogenation of Methylcyclohexane to Toluene. *ACS Catal.* **2017**, *7* (3), 1592–1600. <https://doi.org/10.1021/acscatal.6b03299>.
- (258) Zhao, W.; Chizallet, C.; Sautet, P.; Raybaud, P. Dehydrogenation Mechanisms of Methyl-Cyclohexane on γ -Al₂O₃ Supported Pt₁₃: Impact of Cluster Ductility. *Journal of Catalysis* **2019**, *370*, 118–129. <https://doi.org/10.1016/j.jcat.2018.12.004>.
- (259) Zhao, W. *Dehydrogenation mechanisms of methyl-cyclohexane on γ -alumina supported platinum subnanometric-clusters: DFT coupled with experimental kinetics and kinetic modelling*. [document.pdf](https://tel.archives-ouvertes.fr/tel-01827240/document). HAL archives-ouvertes.fr. <https://tel.archives-ouvertes.fr/tel-01827240/document> (accessed 2020-06-29).
- (260) Obodo, K. O.; Ouma, C. N. M.; Bessarabov, D. Low-Pt-Based Sn Alloy for the Dehydrogenation of Methylcyclohexane to Toluene: A Density Functional Theory Study. *Catalysts* **2022**, *12* (10), 1221. <https://doi.org/10.3390/catal12101221>.
- (261) Auer, F.; Blaumeiser, D.; Bauer, T.; Bösmann, A.; Szesni, N.; Libuda, J.; Wasserscheid, P. Boosting the Activity of Hydrogen Release from Liquid Organic Hydrogen Carrier Systems by Sulfur-Additives to Pt on Alumina Catalysts. *Catal. Sci. Technol.* **2019**, *9* (13), 3537–3547. <https://doi.org/10.1039/C9CY00817A>.
- (262) Ouma, C. N. M.; Obodo, K. O.; Modisha, P. M.; Bessarabov, D. Si, P, S and Se Surface Additives as Catalytic Activity Boosters for Dehydrogenation of Methylcyclohexane to Toluene - A Liquid Organic Hydrogen Carrier System: Density Functional Theory Insights. *Materials Chemistry and Physics* **2022**, 125728. <https://doi.org/10.1016/j.matchemphys.2022.125728>.
- (263) Zhang, C.; Song, P.; Zhang, Y.; Xiao, L.; Hou, J.; Wang, X. Technical and Cost Analysis of Imported Hydrogen Based on MCH-TOL Hydrogen Storage Technology. *International Journal of Hydrogen Energy* **2022**. <https://doi.org/10.1016/j.ijhydene.2022.06.113>.
- (264) Informatics, N. O. of D. and. *WebBook de Chimie NIST*. <https://doi.org/10.18434/T4D303>.
- (265) Popescu, A. I.; Bombos, M.; Doukeh, R.; Bombos, D.; Bolocan, I. Acidity Influence of Ru Catalysts on the Hydrogenation of Naphtalene. 5.
- (266) Popescu (Stanica), A. I.; Bombos, M.; Popovici, R. D.; Bombos, D.; Bolocan, I. Hydrogenation of Naphtalene on Pt-Pd Catalyst. *Rev. Chim.* **2017**, *68* (2), 210–214. <https://doi.org/10.37358/RC.17.2.5421>.
- (267) Park, K.-C.; Yim, D.-J.; Ihm, S.-K. Characteristics of Al-MCM-41 Supported Pt Catalysts: Effect of Al Distribution in Al-MCM-41 on Its Catalytic Activity in Naphthalene Hydrogenation. *Catalysis Today* **2002**, *74* (3), 281–290. [https://doi.org/10.1016/S0920-5861\(02\)00024-X](https://doi.org/10.1016/S0920-5861(02)00024-X).
- (268) Manríquez, M. E.; Hernández-Pichardo, M. L.; Barrera, M. C.; Ramírez-López, R.; Castro, L. V. ENHANCED CATALYTIC ACTIVITY ON THE NAPHTALENE HYDROGENATION REACTION OVER Pt-Pd/Al₂O₃-CeO₂ CATALYSTS. *Revista Mexicana de Ingeniería Química* **2018**, *17* (3), 913–925. <https://doi.org/10.24275/uam/izt/dcbi/revmexingquim/2018v17n3/Manriquez>.
- (269) Montesinos-Castellanos, A.; Zepeda, T. A. High Hydrogenation Performance of the Mesoporous NiMo/Al(Ti, Zr)-HMS Catalysts. *Microporous and Mesoporous Materials* **2008**, *113* (1), 146–162. <https://doi.org/10.1016/j.micromeso.2007.11.012>.
- (270) Kariya, N.; Fukuoka, A.; Ichikawa, M. Efficient Evolution of Hydrogen from Liquid Cycloalkanes over Pt-Containing Catalysts Supported on Active Carbons under “Wet–Dry Multiphase Conditions.” *Applied Catalysis A: General* **2002**, *233* (1), 91–102. [https://doi.org/10.1016/S0926-860X\(02\)00139-4](https://doi.org/10.1016/S0926-860X(02)00139-4).

- (271) Shinohara, C.; Kawakami, S.; Moriga, T.; Hayashi, H.; Hodoshima, S.; Saito, Y.; Sugiyama, S. Local Structure around Platinum in Pt/C Catalysts Employed for Liquid-Phase Dehydrogenation of Decalin in the Liquid-Film State under Reactive Distillation Conditions. *Applied Catalysis A: General* **2004**, *266* (2), 251–255. <https://doi.org/10.1016/j.apcata.2004.02.014>.
- (272) Kariya, N.; Fukuoka, A.; Utagawa, T.; Sakuramoto, M.; Goto, Y.; Ichikawa, M. Efficient Hydrogen Production Using Cyclohexane and Decalin by Pulse-Spray Mode Reactor with Pt Catalysts. *Applied Catalysis A: General* **2003**, *247* (2), 247–259. [https://doi.org/10.1016/S0926-860X\(03\)00104-2](https://doi.org/10.1016/S0926-860X(03)00104-2).
- (273) Ninomiya, W.; Tanabe, Y.; Sotowa, K.-I.; Yasukawa, T.; Sugiyama, S. Dehydrogenation of Cycloalkanes over Noble Metal Catalysts Supported on Active Carbon. *Res. Chem. Intermed.* **2008**, *34* (8), 663–668. <https://doi.org/10.1007/BF03036923>.
- (274) Kim, K.; Oh, J.; Kim, T. W.; Park, J. H.; Han, J. W.; Suh, Y.-W. Different Catalytic Behaviors of Pd and Pt Metals in Decalin Dehydrogenation to Naphthalene. *Catal. Sci. Technol.* **2017**, *7* (17), 3728–3735. <https://doi.org/10.1039/C7CY00569E>.
- (275) Wang, B.; Goodman, D. W.; Froment, G. F. Kinetic Modeling of Pure Hydrogen Production from Decalin. *Journal of Catalysis* **2008**, *253* (2), 229–238. <https://doi.org/10.1016/j.jcat.2007.11.012>.
- (276) Martynenko, E. A.; Pimerzin, A. A.; Savinov, A. A.; Verevkin, S. P.; Pimerzin, A. A. Hydrogen Release from Decalin by Catalytic Dehydrogenation over Supported Platinum Catalysts. *Top Catal* **2020**, *63* (1), 178–186. <https://doi.org/10.1007/s11244-020-01228-9>.
- (277) Lee, G.; Jeong, Y.; Kim, B.-G.; Han, J. S.; Jeong, H.; Na, H. B.; Jung, J. C. Hydrogen Production by Catalytic Decalin Dehydrogenation over Carbon-Supported Platinum Catalyst: Effect of Catalyst Preparation Method. *Catalysis Communications* **2015**, *67*, 40–44. <https://doi.org/10.1016/j.catcom.2015.04.002>.
- (278) Wang, Z.; Liu, G.; Zhang, X. Efficient and Stable Pt/CaO-TiO₂-Al₂O₃ for the Catalytic Dehydrogenation of Cycloalkanes as an Endothermic Hydrocarbon Fuel. *Fuel* **2023**, *331*, 125732. <https://doi.org/10.1016/j.fuel.2022.125732>.
- (279) Jiang, N.; Rao, K. S. R.; Jin, M.-J.; Park, S.-E. Effect of Hydrogen Spillover in Decalin Dehydrogenation over Supported Pt Catalysts. *Applied Catalysis A: General* **2012**, *425–426*, 62–67. <https://doi.org/10.1016/j.apcata.2012.03.001>.
- (280) Li, P.; Huang, Y.-L.; Chen, D.; Zhu, J.; Zhao, T.-J.; Zhou, X.-G. CNFs-Supported Pt Catalyst for Hydrogen Evolution from Decalin. *Catalysis Communications* **2009**, *10* (6), 815–818. <https://doi.org/10.1016/j.catcom.2008.12.004>.
- (281) Tuo, Y.-X.; Shi, L.-J.; Cheng, H.-Y.; Zhu, Y.-A.; Yang, M.-L.; Xu, J.; Han, Y.-F.; Li, P.; Yuan, W.-K. Insight into the Support Effect on the Particle Size Effect of Pt/C Catalysts in Dehydrogenation. *Journal of Catalysis* **2018**, *360*, 175–186. <https://doi.org/10.1016/j.jcat.2018.02.001>.
- (282) Tuo, Y.; Yang, L.; Ma, X.; Ma, Z.; Gong, S.; Li, P. Carbon Nanotubes-Supported Pt Catalysts for Decalin Dehydrogenation to Release Hydrogen: A Comparison between Nitrogen- and Oxygen-Surface Modification. *International Journal of Hydrogen Energy* **2021**, *46* (1), 930–942. <https://doi.org/10.1016/j.ijhydene.2020.09.225>.
- (283) Tuo, Y.; Meng, Y.; Chen, C.; Lin, D.; Feng, X.; Pan, Y.; Li, P.; Chen, D.; Liu, Z.; Zhou, Y.; Zhang, J. Partial Positively Charged Pt in Pt/MgAl₂O₄ for Enhanced Dehydrogenation Activity. *Applied Catalysis B: Environmental* **2021**, *288*, 119996. <https://doi.org/10.1016/j.apcatb.2021.119996>.
- (284) Tuo, Y.; Yang, L.; Cheng, H.; Yang, M.; Zhu, Y.-A.; Li, P. Density Functional Theory Study of Decalin Dehydrogenation for Hydrogen Release on Pt(111) and Pt(211). *International Journal of Hydrogen Energy* **2018**, *43* (42), 19575–19588. <https://doi.org/10.1016/j.ijhydene.2018.09.002>.
- (285) Wang, Y.; Shah, N.; Huggins, F. E.; Huffman, G. P. Hydrogen Production by Catalytic Dehydrogenation of Tetralin and Decalin Over Stacked Cone Carbon Nanotube-Supported Pt Catalysts. *Energy Fuels* **2006**, *20* (6), 2612–2615. <https://doi.org/10.1021/ef060228t>.
- (286) Kalenchuk, A. N.; Smetneva, D. N.; Bogdan, V. I.; Kustov, L. M. Kinetics of Decalin Dehydrogenation on Pt/C Catalyst. *Russ Chem Bull* **2015**, *64* (11), 2642–2645. <https://doi.org/10.1007/s11172-015-1202-1>.
- (287) Martynenko, E. A.; Vostrikov, S. V.; Pimerzin, A. A. Hydrogen Production from Decalin over Silica-Supported Platinum Catalysts: A Kinetic and Thermodynamic Study. *Reac Kinet Mech Cat* **2021**, *133* (2), 713–728. <https://doi.org/10.1007/s11144-021-02037-1>.
- (288) Dziewiecki, Z.; Ihnatowicz, M.; Makowski, A. Activity of Ni-Moly Catalysts in Tetralin or Decalin Dehydrogenation and in Hydrogenation of Coal-Extract Solution. *Fuel* **1979**, *58* (10), 737–740. [https://doi.org/10.1016/0016-2361\(79\)90072-3](https://doi.org/10.1016/0016-2361(79)90072-3).
- (289) Qi, S.; Li, Y.; Yue, J.; Chen, H.; Yi, C.; Yang, B. Hydrogen Production from Decalin Dehydrogenation over Pt-Ni/C Bimetallic Catalysts. *Chinese Journal of Catalysis* **2014**, *35* (11), 1833–1839. [https://doi.org/10.1016/S1872-2067\(14\)60178-9](https://doi.org/10.1016/S1872-2067(14)60178-9).

- (290) Patil, S. P.; Pande, J. V.; Biniwale, R. B. Non-Noble Ni–Cu/ACC Bimetallic Catalyst for Dehydrogenation of Liquid Organic Hydrides for Hydrogen Storage. *International Journal of Hydrogen Energy* **2013**, *38* (35), 15233–15241. <https://doi.org/10.1016/j.ijhydene.2013.09.115>.
- (291) Qi, S.; Yue, J.; Li, Y.; Huang, J.; Yi, C.; Yang, B. Replacing Platinum with Tungsten Carbide for Decalin Dehydrogenation. *Catal Lett* **2014**, *144* (8), 1443–1449. <https://doi.org/10.1007/s10562-014-1284-7>.
- (292) Brückner, N.; Obesser, K.; Bösmann, A.; Teichmann, D.; Arlt, W.; Dungs, J.; Wasserscheid, P. Evaluation of Industrially Applied Heat-Transfer Fluids as Liquid Organic Hydrogen Carrier Systems. *ChemSusChem* **2014**, *7* (1), 229–235. <https://doi.org/10.1002/cssc.201300426>.
- (293) Asif, F.; Hamayun, M. H.; Hussain, M.; Hussain, A.; Maafa, I. M.; Park, Y.-K. Performance Analysis of the Perhydro-Dibenzyl-Toluene Dehydrogenation System—A Simulation Study. *Sustainability* **2021**, *13* (11), 6490. <https://doi.org/10.3390/su13116490>.
- (294) Müller, K.; Stark, K.; Emel'yanenko, V. N.; Varfolomeev, M. A.; Zaitsau, D. H.; Shoifet, E.; Schick, C.; Verevkin, S. P.; Arlt, W. Liquid Organic Hydrogen Carriers: Thermophysical and Thermochemical Studies of Benzyl- and Dibenzyl-Toluene Derivatives. *Ind. Eng. Chem. Res.* **2015**, *54* (32), 7967–7976. <https://doi.org/10.1021/acs.iecr.5b01840>.
- (295) Marlotherm-SH-SDS.Pdf. <https://chem-group.com/wp-content/uploads/2020/07/Marlotherm-SH-SDS.pdf> (accessed 2022-11-10).
- (296) 0_HydrogeniousTechnologies.Pdf. https://www.energiewende-erlangen.de/wp-content/uploads/2018/02/0_HydrogeniousTechnologies.pdf (accessed 2022-11-09).
- (297) Kim, T. W.; Jeong, H.; Jo, Y.; Kim, D.; Park, J. H.; Kim, S. K.; Suh, Y.-W. Advanced Heterolytic H₂ Adsorption of K-Added Ru/MgO Catalysts for Accelerating Hydrogen Storage into Aromatic Benzyltoluenes. *Journal of Energy Chemistry* **2022**. <https://doi.org/10.1016/j.jechem.2022.03.047>.
- (298) Do, G.; Preuster, P.; Aslam, R.; Bösmann, A.; Müller, K.; Arlt, W.; Wasserscheid, P. Hydrogenation of the Liquid Organic Hydrogen Carrier Compound Dibenzyltoluene – Reaction Pathway Determination by ¹H NMR Spectroscopy. *Reaction Chemistry & Engineering* **2016**, *1* (3), 313–320. <https://doi.org/10.1039/C5RE00080G>.
- (299) Jorschick, H.; Preuster, P.; Dürr, S.; Seidel, A.; Müller, K.; Bösmann, A.; Wasserscheid, P. Hydrogen Storage Using a Hot Pressure Swing Reactor. *Energy & Environmental Science* **2017**, *10* (7), 1652–1659. <https://doi.org/10.1039/C7EE00476A>.
- (300) Shi, L.; Qi, S.; Qu, J.; Che, T.; Yi, C.; Yang, B. Integration of Hydrogenation and Dehydrogenation Based on Dibenzyltoluene as Liquid Organic Hydrogen Energy Carrier. *International Journal of Hydrogen Energy* **2019**, *44* (11), 5345–5354. <https://doi.org/10.1016/j.ijhydene.2018.09.083>.
- (301) Ali, A.; Rohini, A. K.; Noh, Y. S.; Moon, D. J.; Lee, H. J. Hydrogenation of Dibenzyltoluene and the Catalytic Performance of Pt/Al₂O₃ with Various Pt Loadings for Hydrogen Production from Perhydro-Dibenzyltoluene. *International Journal of Energy Research n/a* (n/a). <https://doi.org/10.1002/er.7604>.
- (302) Modisha, P.; Bessarabov, D. Stress Tolerance Assessment of Dibenzyltoluene-Based Liquid Organic Hydrogen Carriers. *Sustainable Energy & Fuels* **2020**. <https://doi.org/10.1039/D0SE00625D>.
- (303) Feng, X.; Jiang, L.; Li, Z.; Wang, S.; Ye, J.; Wu, Y.; Yuan, B. Boosting the Hydrogenation Activity of Dibenzyltoluene Catalyzed by Mg-Based Metal Hydrides. *International Journal of Hydrogen Energy* **2022**. <https://doi.org/10.1016/j.ijhydene.2022.04.234>.
- (304) T. Aakko-Saksa, P.; Vehkamäki, M.; Kemell, M.; Keskiäli, L.; Simell, P.; Reinikainen, M.; Tapper, U.; Repo, T. Hydrogen Release from Liquid Organic Hydrogen Carriers Catalysed by Platinum on Rutile-Anatase Structured Titania. *Chemical Communications* **2020**, *56* (11), 1657–1660. <https://doi.org/10.1039/C9CC09715E>.
- (305) Modisha, P.; Gqogqa, P.; Garidzirai, R.; Ouma, C. N. M.; Bessarabov, D. Evaluation of Catalyst Activity for Release of Hydrogen from Liquid Organic Hydrogen Carriers. *International Journal of Hydrogen Energy* **2019**, *44* (39), 21926–21935. <https://doi.org/10.1016/j.ijhydene.2019.06.212>.
- (306) Modisha, P.; Garidzirai, R.; Güneş, H.; Bozbag, S. E.; Rommel, S.; Uzunlar, E.; Aindow, M.; Erkey, C.; Bessarabov, D. A Promising Catalyst for the Dehydrogenation of Perhydro-Dibenzyltoluene: Pt/Al₂O₃ Prepared by Supercritical CO₂ Deposition. *Catalysts* **2022**, *12* (5), 489. <https://doi.org/10.3390/catal12050489>.
- (307) Jo, Y.; Wan Kim, T.; Oh, J.; Kim, D.; Suh, Y.-W. Mesoporous Sulfur-Decorated Pt–Al₂O₃ for Dehydrogenation of Perhydro Benzyltoluenes: Activity-Favorable Adsorption of Reaction Species onto Electron-Deficient Pt Atoms. *Journal of Catalysis* **2022**, *413*, 127–137. <https://doi.org/10.1016/j.jcat.2022.06.025>.
- (308) Lee, S.; Lee, J.; Kim, T.; Han, G.; Lee, J.; Lee, K.; Bae, J. Pt/CeO₂ Catalyst Synthesized by Combustion Method for Dehydrogenation of Perhydro-Dibenzyltoluene as Liquid Organic Hydrogen Carrier: Effect of Pore Size and Metal Dispersion. *International Journal of Hydrogen Energy* **2021**, *46* (7), 5520–5529. <https://doi.org/10.1016/j.ijhydene.2020.11.038>.

- (309) Solymosi, T.; Geißelbrecht, M.; Mayer, S.; Auer, M.; Leicht, P.; Terlinden, M.; Malgaretti, P.; Bösmann, A.; Preuster, P.; Harting, J.; Thommes, M.; Vogel, N.; Wasserscheid, P. Nucleation as a Rate-Determining Step in Catalytic Gas Generation Reactions from Liquid Phase Systems. *Science Advances* **2022**, *8* (46), eade3262. <https://doi.org/10.1126/sciadv.ade3262>.
- (310) Shi, L.; Zhou, Y.; Qi, S.; Smith, K. J.; Tan, X.; Yan, J.; Yi, C. Pt Catalysts Supported on H₂ and O₂ Plasma-Treated Al₂O₃ for Hydrogenation and Dehydrogenation of the Liquid Organic Hydrogen Carrier Pair Dibenzyltoluene and Perhydrodibenzyltoluene. *ACS Catal.* **2020**, *10* (18), 10661–10671. <https://doi.org/10.1021/acscatal.0c03091>.
- (311) Ouma, C. N. M.; Modisha, P. M.; Bessarabov, D. Catalytic Dehydrogenation Onset of Liquid Organic Hydrogen Carrier, Perhydro-Dibenzyltoluene: The Effect of Pd and Pt Subsurface Configurations. *Computational Materials Science* **2020**, *172*, 109332. <https://doi.org/10.1016/j.commatsci.2019.109332>.
- (312) Ouma, C. N. M.; Modisha, P.; Bessarabov, D. Insight into the Adsorption of a Liquid Organic Hydrogen Carrier, Perhydro-*i*-Dibenzyltoluene (*i* = m, o, p), on Pt, Pd and PtPd Planar Surfaces. *RSC Advances* **2018**, *8* (56), 31895–31904. <https://doi.org/10.1039/C8RA05800H>.
- (313) Kim, C. H.; Lee, M.-W.; Jang, J. S.; Lee, S. H.; Lee, K.-Y. Enhanced Activity of a WO_x-Incorporated Pt/Al₂O₃ Catalyst for the Dehydrogenation of Homocyclic LOHCs: Effects of Impregnation Sequence on Pt–WO_x Interactions. *Fuel* **2021**, 122654. <https://doi.org/10.1016/j.fuel.2021.122654>.
- (314) Zhou, J.; Chung, J. S.; Kang, S. G. Designing Pt-Based Subsurface Alloy Catalysts for the Dehydrogenation of Perhydro-Dibenzyltoluene: A First-Principles Study. *Applied Surface Science* **2022**, *579*, 152142. <https://doi.org/10.1016/j.apsusc.2021.152142>.
- (315) Dürr, S.; Zilm, S.; Geißelbrecht, M.; Müller, K.; Preuster, P.; Bösmann, A.; Wasserscheid, P. Experimental Determination of the Hydrogenation/Dehydrogenation - Equilibrium of the LOHC System H₀/H₁₈-Dibenzyltoluene. *International Journal of Hydrogen Energy* **2021**. <https://doi.org/10.1016/j.ijhydene.2021.07.119>.
- (316) Ali, A.; Khan, M. A.; Abbas, N.; Choi, H. Prediction of Hydrogen Storage in Dibenzyltoluene Empowered with Machine Learning. *Journal of Energy Storage* **2022**, *55*, 105844. <https://doi.org/10.1016/j.est.2022.105844>.
- (317) Müller, K.; Aslam, R.; Fischer, A.; Stark, K.; Wasserscheid, P.; Arlt, W. Experimental Assessment of the Degree of Hydrogen Loading for the Dibenzyl Toluene Based LOHC System. *International Journal of Hydrogen Energy* **2016**, *41* (47), 22097–22103. <https://doi.org/10.1016/j.ijhydene.2016.09.196>.
- (318) Ali, A.; Rohini, A. K.; Lee, H. J. Dehydrogenation of Perhydro-Dibenzyltoluene for Hydrogen Production in a Microchannel Reactor. *International Journal of Hydrogen Energy* **2022**. <https://doi.org/10.1016/j.ijhydene.2022.04.212>.
- (319) Rüde, T.; Bösmann, A.; Preuster, P.; Wasserscheid, P.; Arlt, W.; Müller, K. Resilience of Liquid Organic Hydrogen Carrier Based Energy-Storage Systems. *Energy Technology* **2018**, *6* (3), 529–539. <https://doi.org/10.1002/ente.201700446>.
- (320) Bulgarin, A.; Jorschick, H.; Preuster, P.; Bösmann, A.; Wasserscheid, P. Purity of Hydrogen Released from the Liquid Organic Hydrogen Carrier Compound Perhydro Dibenzyltoluene by Catalytic Dehydrogenation. *International Journal of Hydrogen Energy* **2020**, *45* (1), 712–720. <https://doi.org/10.1016/j.ijhydene.2019.10.067>.
- (321) Wunsch, A.; Berg, T.; Pfeifer, P. Hydrogen Production from the LOHC Perhydro-Dibenzyl-Toluene and Purification Using a 5 Mm PdAg-Membrane in a Coupled Microstructured System. *Materials* **2020**, *13* (2), 277. <https://doi.org/10.3390/ma13020277>.
- (322) Geiling, J.; Steinberger, M.; Ortner, F.; Seyfried, R.; Nuß, A.; Uhrig, F.; Lange, C.; Öchsner, R.; Wasserscheid, P.; März, M.; Preuster, P. Combined Dynamic Operation of PEM Fuel Cell and Continuous Dehydrogenation of Perhydro-Dibenzyltoluene. *International Journal of Hydrogen Energy* **2021**. <https://doi.org/10.1016/j.ijhydene.2021.08.034>.
- (323) Jorschick, H.; Geißelbrecht, M.; Eßl, M.; Preuster, P.; Bösmann, A.; Wasserscheid, P. Benzyltoluene/Dibenzyltoluene-Based Mixtures as Suitable Liquid Organic Hydrogen Carrier Systems for Low Temperature Applications. *International Journal of Hydrogen Energy* **2020**, *45* (29), 14897–14906. <https://doi.org/10.1016/j.ijhydene.2020.03.210>.
- (324) Zakgeym, D.; Engl, T.; Mahayni, Y.; Müller, K.; Wolf, M.; Wasserscheid, P. Development of an Efficient Pt/SiO₂ Catalyst for the Transfer Hydrogenation from Perhydro-Dibenzyltoluene to Acetone. *Applied Catalysis A: General* **2022**, *639*, 118644. <https://doi.org/10.1016/j.apcata.2022.118644>.
- (325) Braun, K.; Wolf, M.; De Oliveira, A.; Preuster, P.; Wasserscheid, P.; Thiele, S.; Weiß, L.; Wensing, M. Energetics of Technical Integration of 2-Propanol Fuel Cells: Thermodynamic and Current and Future Technical Feasibility. *Energy Technology* **2022**, *10* (8), 2200343. <https://doi.org/10.1002/ente.202200343>.
- (326) Clot, E.; Eisenstein, O.; H. Crabtree, R. Computational Structure–Activity Relationships in H₂ Storage: How Placement of N Atoms Affects Release Temperatures in Organic Liquid Storage Materials. *Chemical Communications* **2007**, *0* (22), 2231–2233. <https://doi.org/10.1039/B705037B>.

Literature review

- (327) Cui, Y.; Kwok, S.; Bucholtz, A.; Davis, B.; A. Whitney, R.; G. Jessop, P. The Effect of Substitution on the Utility of Piperidines and Octahydroindoles for Reversible Hydrogen Storage. *New Journal of Chemistry* **2008**, *32* (6), 1027–1037. <https://doi.org/10.1039/B718209K>.
- (328) Sotoodeh, F.; Huber, B. J. M.; Smith, K. J. The Effect of the N Atom on the Dehydrogenation of Heterocycles Used for Hydrogen Storage. *Applied Catalysis A: General* **2012**, *419–420*, 67–72. <https://doi.org/10.1016/j.apcata.2012.01.013>.
- (329) Pez, G. P.; Scott, A. R.; Cooper, A. C.; Cheng, H.; Wilhelm, F. C.; Abdourazak, A. H. Hydrogen Storage by Reversible Hydrogenation of Pi-Conjugated Substrates. US7351395B1, April 1, 2008. <https://patents.google.com/patent/US7351395B1/en> (accessed 2022-11-11).
- (330) Sotoodeh, F.; Smith, K. J. Analysis of H₂ Release from Organic Polycyclics over Pd Catalysts Using DFT. *J. Phys. Chem. C* **2013**, *117* (1), 194–204. <https://doi.org/10.1021/jp307325s>.
- (331) Sotoodeh, F.; Zhao, L.; Smith, K. J. Kinetics of H₂ Recovery from Dodecahydro-N-Ethylcarbazole over a Supported Pd Catalyst. *Applied Catalysis A: General* **2009**, *362* (1), 155–162. <https://doi.org/10.1016/j.apcata.2009.04.039>.
- (332) Hansong Cheng. Fuel Cell Division, International Association for Hydrogen Energy. <https://www.iahe-fcd.org/hansong-cheng> (accessed 2022-11-16).
- (333) 武汉氢能源有限公司. <https://www.hynertech.com/col.jsp?id=112> (accessed 2022-11-16).
- (334) Ye, X.; An, Y.; Xu, G. Kinetics of 9-Ethylcarbazole Hydrogenation over Raney-Ni Catalyst for Hydrogen Storage. *Journal of Alloys and Compounds* **2011**, *509* (1), 152–156. <https://doi.org/10.1016/j.jallcom.2010.09.012>.
- (335) Wan, C.; An, Y.; Xu, G.; Kong, W. Study of Catalytic Hydrogenation of N-Ethylcarbazole over Ruthenium Catalyst. *International Journal of Hydrogen Energy* **2012**, *37* (17), 13092–13096. <https://doi.org/10.1016/j.ijhydene.2012.04.123>.
- (336) Morawa Eblagon, K.; Tam, K.; Yu, K. M. K.; Zhao, S.-L.; Gong, X.-Q.; He, H.; Ye, L.; Wang, L.-C.; Ramirez-Cuesta, A. J.; Tsang, S. C. Study of Catalytic Sites on Ruthenium For Hydrogenation of N-Ethylcarbazole: Implications of Hydrogen Storage via Reversible Catalytic Hydrogenation. *J. Phys. Chem. C* **2010**, *114* (21), 9720–9730. <https://doi.org/10.1021/jp908640k>.
- (337) Eblagon, K. M.; Tam, K.; Yu, K. M. K.; Tsang, S. C. E. Comparative Study of Catalytic Hydrogenation of 9-Ethylcarbazole for Hydrogen Storage over Noble Metal Surfaces. *J. Phys. Chem. C* **2012**, *116* (13), 7421–7429. <https://doi.org/10.1021/jp212249g>.
- (338) Mehranfar, A.; Izadyar, M.; Esmaeili, A. A. Hydrogen Storage by N-Ethylcarbazole as a New Liquid Organic Hydrogen Carrier: A DFT Study on the Mechanism. *International Journal of Hydrogen Energy* **2015**, *40* (17), 5797–5806. <https://doi.org/10.1016/j.ijhydene.2015.03.011>.
- (339) Liu, H.; Xue, J.; Yu, P.; Zhang, Y.; Wang, J.; Che, D. Hydrogenation of N-Ethylcarbazole with Hydrogen-Methane Mixtures for Hydrogen Storage. *Fuel* **2023**, *331*, 125920. <https://doi.org/10.1016/j.fuel.2022.125920>.
- (340) Morawa Eblagon, K.; Tam, K.; Edman Tsang, S. C. Comparison of Catalytic Performance of Supported Ruthenium and Rhodium for Hydrogenation of 9-Ethylcarbazole for Hydrogen Storage Applications. *Energy & Environmental Science* **2012**, *5* (9), 8621–8630. <https://doi.org/10.1039/C2EE22066K>.
- (341) Eblagon, K. M.; Rentsch, D.; Friedrichs, O.; Remhof, A.; Zuttel, A.; Ramirez-Cuesta, A. J.; Tsang, S. C. Hydrogenation of 9-Ethylcarbazole as a Prototype of a Liquid Hydrogen Carrier. *International Journal of Hydrogen Energy* **2010**, *35* (20), 11609–11621. <https://doi.org/10.1016/j.ijhydene.2010.03.068>.
- (342) Shin, B. S.; Yoon, C. W.; Kwak, S. K.; Kang, J. W. Thermodynamic Assessment of Carbazole-Based Organic Polycyclic Compounds for Hydrogen Storage Applications via a Computational Approach. *International Journal of Hydrogen Energy* **2018**, *43* (27), 12158–12167. <https://doi.org/10.1016/j.ijhydene.2018.04.182>.
- (343) Forberg, D.; Schwob, T.; Zaheer, M.; Friedrich, M.; Miyajima, N.; Kempe, R. Single-Catalyst High-Weight% Hydrogen Storage in an N-Heterocycle Synthesized from Lignin Hydrogenolysis Products and Ammonia. *Nature Communications* **2016**, *7* (1), 1–6. <https://doi.org/10.1038/ncomms13201>.
- (344) Yu, H.; Yang, X.; Wu, Y.; Guo, Y.; Li, S.; Lin, W.; Li, X.; Zheng, J. Bimetallic Ru-Ni/TiO₂ Catalysts for Hydrogenation of N-Ethylcarbazole: Role of TiO₂ Crystal Structure. *Journal of Energy Chemistry* **2020**, *40*, 188–195. <https://doi.org/10.1016/j.jechem.2019.04.009>.
- (345) Qin, Y.; Bai, X. Hydrogenation of N-Ethylcarbazole over Ni-Ru Alloy Nanoparticles Loaded on Graphitized Carbon Prepared by Carbothermal Reduction. *Fuel* **2022**, *307*, 121921. <https://doi.org/c>.
- (346) Wang, Y.; Bai, X. Efficient Catalytic Hydrogen Storage of N-Ethylcarbazole over RuNi Alloy Nanoparticles Loaded on SBA-15 Prepared by Electrostatic Adsorption. *Fuel* **2023**, *331*, 125709. <https://doi.org/10.1016/j.fuel.2022.125709>.
- (347) Liu, X.; Bai, X.; Wu, W. Ultrasound-Assisted Green Synthesis of Ru Supported on LDH-CNT Composites as an Efficient Catalyst for N-Ethylcarbazole Hydrogenation. *Ultrasonics Sonochemistry* **2022**, 106227. <https://doi.org/10.1016/j.ultsonch.2022.106227>.

- (348) Wu, Y.; Yu, H.; Guo, Y.; Jiang, X.; Qi, Y.; Sun, B.; Li, H.; Zheng, J.; Li, X. A Rare Earth Hydride Supported Ruthenium Catalyst for the Hydrogenation of N-Heterocycles: Boosting the Activity via a New Hydrogen Transfer Path and Controlling the Stereoselectivity. *Chemical Science* **2019**, *10* (45), 10459–10465. <https://doi.org/10.1039/C9SC04365A>.
- (349) Wu, Y.; Yu, H.; Guo, Y.; Zhang, Y.; Jiang, X.; Sun, B.; Fu, K.; Chen, J.; Qi, Y.; Zheng, J.; Li, X. Promoting Hydrogen Absorption of Liquid Organic Hydrogen Carriers by Solid Metal Hydrides. *J. Mater. Chem. A* **2019**, *7* (28), 16677–16684. <https://doi.org/10.1039/C9TA05966K>.
- (350) Wu Yong; Guo Yanru; Yu Hongen; Jiang Xiaojing; Zhang Yuxuan; Qi Yue; Fu Kai; Xie Lei; Li Guoling; Zheng Jie; Li Xingguo. Nonstoichiometric Yttrium Hydride–Promoted Reversible Hydrogen Storage in a Liquid Organic Hydrogen Carrier. *CCS Chemistry* **0** (0). <https://doi.org/10.31635/ccschem.020.202000255>.
- (351) Yu, H.; Yang, X.; Jiang, X.; Wu, Y.; Chen, S.; Lin, W.; Wu, Y.; Xie, L.; Li, X.; Zheng, J. LaNi_{5.5} Particles for Reversible Hydrogen Storage in N-Ethylcarbazole. *Nano Energy* **2021**, *80*, 105476. <https://doi.org/10.1016/j.nanoen.2020.105476>.
- (352) Yang, M.; Dong, Y.; Fei, S.; Ke, H.; Cheng, H. A Comparative Study of Catalytic Dehydrogenation of Perhydro-N-Ethylcarbazole over Noble Metal Catalysts. *International Journal of Hydrogen Energy* **2014**, *39* (33), 18976–18983. <https://doi.org/10.1016/j.ijhydene.2014.09.123>.
- (353) Yang, M.; Han, C.; Ni, G.; Wu, J.; Cheng, H. Temperature Controlled Three-Stage Catalytic Dehydrogenation and Cycle Performance of Perhydro-9-Ethylcarbazole. *International Journal of Hydrogen Energy* **2012**, *37* (17), 12839–12845. <https://doi.org/10.1016/j.ijhydene.2012.05.092>.
- (354) Sobota, M.; Nikiforidis, I.; Amende, M.; Zanón, B. S.; Staudt, T.; Höfert, O.; Lykhach, Y.; Papp, C.; Hieringer, W.; Laurin, M.; Assenbaum, D.; Wasserscheid, P.; Steinrück, H.-P.; Görling, A.; Libuda, J. Dehydrogenation of Dodecahydro-N-Ethylcarbazole on Pd/Al₂O₃ Model Catalysts. *Chemistry – A European Journal* **2011**, *17* (41), 11542–11552. <https://doi.org/10.1002/chem.201101311>.
- (355) Amende, M.; Schernich, S.; Sobota, M.; Nikiforidis, I.; Hieringer, W.; Assenbaum, D.; Gleichweit, C.; Drescher, H.-J.; Papp, C.; Steinrück, H.-P.; Görling, A.; Wasserscheid, P.; Laurin, M.; Libuda, J. Dehydrogenation Mechanism of Liquid Organic Hydrogen Carriers: Dodecahydro-N-Ethylcarbazole on Pd(111). *Chemistry – A European Journal* **2013**, *19* (33), 10854–10865. <https://doi.org/10.1002/chem.201301323>.
- (356) Gleichweit, C.; Amende, M.; Schernich, S.; Zhao, W.; Lorenz, M. P. A.; Höfert, O.; Brückner, N.; Wasserscheid, P.; Libuda, J.; Steinrück, H.-P.; Papp, C. Dehydrogenation of Dodecahydro-N-Ethylcarbazole on Pt(111). *ChemSusChem* **2013**, *6* (6), 974–977. <https://doi.org/10.1002/cssc.201300263>.
- (357) Amende, M.; Gleichweit, C.; Werner, K.; Schernich, S.; Zhao, W.; Lorenz, M. P. A.; Höfert, O.; Papp, C.; Koch, M.; Wasserscheid, P.; Laurin, M.; Steinrück, H.-P.; Libuda, J. Model Catalytic Studies of Liquid Organic Hydrogen Carriers: Dehydrogenation and Decomposition Mechanisms of Dodecahydro-N-Ethylcarbazole on Pt(111). *ACS Catal.* **2014**, *4* (2), 657–665. <https://doi.org/10.1021/cs400946x>.
- (358) Amende, M.; Gleichweit, C.; Schernich, S.; Höfert, O.; Lorenz, M. P. A.; Zhao, W.; Koch, M.; Obesser, K.; Papp, C.; Wasserscheid, P.; Steinrück, H.-P.; Libuda, J. Size and Structure Effects Controlling the Stability of the Liquid Organic Hydrogen Carrier Dodecahydro-N-Ethylcarbazole during Dehydrogenation over Pt Model Catalysts. *J. Phys. Chem. Lett.* **2014**, *5* (8), 1498–1504. <https://doi.org/10.1021/jz500157r>.
- (359) Kustov, L. M.; Tarasov, A. L.; Kirichenko, O. A. Microwave-Activated Dehydrogenation of Perhydro-N-Ethylcarbazole over Bimetallic Pd-M/TiO₂ Catalysts as the Second Stage of Hydrogen Storage in Liquid Substrates. *International Journal of Hydrogen Energy* **2017**, *42* (43), 26723–26729. <https://doi.org/10.1016/j.ijhydene.2017.09.009>.
- (360) Jiang, Z.; Gong, X.; Wang, B.; Wu, Z.; Fang, T. A Experimental Study on the Dehydrogenation Performance of Dodecahydro-N-Ethylcarbazole on M/TiO₂ Catalysts. *International Journal of Hydrogen Energy* **2019**, *44* (5), 2951–2959. <https://doi.org/10.1016/j.ijhydene.2018.11.236>.
- (361) Wang, B.; Chang, T.; Jiang, Z.; Wei, J.; Zhang, Y.; Yang, S.; Fang, T. Catalytic Dehydrogenation Study of Dodecahydro-N-Ethylcarbazole by Noble Metal Supported on Reduced Graphene Oxide. *International Journal of Hydrogen Energy* **2018**, *43* (15), 7317–7325. <https://doi.org/10.1016/j.ijhydene.2018.02.156>.
- (362) Jiang, Z.; Guo, S.; Fang, T. Enhancing the Catalytic Activity and Selectivity of PdAu/SiO₂ Bimetallic Catalysts for Dodecahydro-N-Ethylcarbazole Dehydrogenation by Controlling the Particle Size and Dispersion. *ACS Appl. Energy Mater.* **2019**, *2* (10), 7233–7243. <https://doi.org/10.1021/acsam.9b01202>.
- (363) Qiao, X.; She, T.; Zhang, H.; Wen, X.; Niu, L.; Ricardez-Sandoval, L.; Li, J.; Bai, G. One-Pot Synthesis of Porous Silica-Supported Ultrafine Ni Nanoparticles as Efficient and Stable Catalyst for Selective Hydrogenation of Benzophenone. *Applied Catalysis B: Environmental* **2019**, *259*, 118111. <https://doi.org/10.1016/j.apcatb.2019.118111>.
- (364) Ding, C.; Zhu, T.; Wang, F.; Zhang, Z.; Dong, Y.; Yang, M.; Cheng, G.; Ke, H.; Cheng, H. High Active Pd@mil-101 Catalyst for Dehydrogenation of Liquid Organic Hydrogen Carrier. *International Journal of Hydrogen Energy* **2020**, *45* (32), 16144–16152. <https://doi.org/10.1016/j.ijhydene.2020.04.081>.

- (365) Gong, X.; Jiang, Z.; Fang, T. Enhancing Selectivity and Reducing Cost for Dehydrogenation of Dodecahydro-N-Ethylcarbazole by Supporting Platinum on Titanium Dioxide. *International Journal of Hydrogen Energy* **2020**, *45* (11), 6838–6847. <https://doi.org/10.1016/j.ijhydene.2019.12.203>.
- (366) Wang, B.; Chen, Y.-T.; Chang, T.-Y.; Jiang, Z.; Huang, Z.-Q.; Wang, S.-Y.; Chang, C.-R.; Chen, Y.-S.; Wei, J.-J.; Yang, S.; Fang, T. Facet-Dependent Catalytic Activities of Pd/RGO: Exploring Dehydrogenation Mechanism of Dodecahydro-N-Ethylcarbazole. *Applied Catalysis B: Environmental* **2020**, *266*, 118658. <https://doi.org/10.1016/j.apcatb.2020.118658>.
- (367) Feng, Z.; Chen, X.; Bai, X. Catalytic Dehydrogenation of Liquid Organic Hydrogen Carrier Dodecahydro-N-Ethylcarbazole over Palladium Catalysts Supported on Different Supports. *Environ Sci Pollut Res* **2020**. <https://doi.org/10.1007/s11356-020-09698-w>.
- (368) Wang, Y.; Feng, Z.; Bai, X. Ultrafine Palladium Nanoparticles Supported on Mesoporous Silica: An Outstanding Catalytic Activity for Hydrogen Production from Dodecahydro-N-Ethylcarbazole. *Fuel* **2022**, *315*, 123236. <https://doi.org/10.1016/j.fuel.2022.123236>.
- (369) Wu, Y.; Liu, X.; Bai, X.; Wu, W. Ultrasonic-Assisted Preparation of Ultrafine Pd Nanocatalysts Loaded on Cl⁻-Intercalated MgAl Layered Double Hydroxides for the Catalytic Dehydrogenation of Dodecahydro-N-Ethylcarbazole. *Ultrasonics Sonochemistry* **2022**, *88*, 106097. <https://doi.org/10.1016/j.ultsonch.2022.106097>.
- (370) Wang, B.; Chang, T.; Gong, X.; Jiang, Z.; Yang, S.; Chen, Y.; Fang, T. One-Pot Synthesis of Au/Pd Core/Shell Nanoparticles Supported on Reduced Graphene Oxide with Enhanced Dehydrogenation Performance for Dodecahydro-N-Ethylcarbazole. *ACS Sustainable Chem. Eng.* **2019**, *7* (1), 1760–1768. <https://doi.org/10.1021/acssuschemeng.8b05671>.
- (371) Wang, B.; Chang, T.; Jiang, Z.; Wei, J.; Fang, T. Component Controlled Synthesis of Bimetallic PdCu Nanoparticles Supported on Reduced Graphene Oxide for Dehydrogenation of Dodecahydro-N-Ethylcarbazole. *Applied Catalysis B: Environmental* **2019**, *251*, 261–272. <https://doi.org/10.1016/j.apcatb.2019.03.071>.
- (372) Feng, Z.; Bai, X. Enhanced Activity of Bimetallic Pd-Ni Nanoparticles on KIT-6 for Production of Hydrogen from Dodecahydro-N-Ethylcarbazole. *Fuel* **2022**, *329*, 125473. <https://doi.org/10.1016/j.fuel.2022.125473>.
- (373) Eblagon, K. M.; Tsang, S. C. E. Structure-Reactivity Relationship in Catalytic Hydrogenation of Heterocyclic Compounds over Ruthenium Black; Part B: Effect of Carbon Substitution by Heteroatom. *Applied Catalysis B: Environmental* **2015**, *163*, 599–610. <https://doi.org/10.1016/j.apcatb.2014.08.040>.
- (374) Krishnamurthy, S.; Panvelker, S.; Shah, Y. T. Hydrodeoxygenation of Dibenzofuran and Related Compounds. *AIChE Journal* **1981**, *27* (6), 994–1001. <https://doi.org/10.1002/aic.690270616>.
- (375) Wang, L.; Zhang, M.; Zhang, M.; Sha, G.; Liang, C. Hydrodeoxygenation of Dibenzofuran over Mesoporous Silica COK-12 Supported Palladium Catalysts. *Energy Fuels* **2013**, *27* (4), 2209–2217. <https://doi.org/10.1021/ef302166q>.
- (376) Wang, L.; Li, C.; Jin, S.; Li, W.; Liang, C. Hydrodeoxygenation of Dibenzofuran Over SBA-15 Supported Pt, Pd, and Ru Catalysts. *Catal Lett* **2014**, *144* (5), 809–816. <https://doi.org/10.1007/s10562-014-1236-2>.
- (377) Jang, M.; Shin, B. S.; Jo, Y. S.; Kang, J. W.; Kwak, S. K.; Yoon, C. W.; Jeong, H. A Study on Hydrogen Uptake and Release of a Eutectic Mixture of Biphenyl and Diphenyl Ether. *Journal of Energy Chemistry* **2020**, *42*, 11–16. <https://doi.org/10.1016/j.jechem.2019.05.024>.
- (378) Morton, D.; Cole-Hamilton, D. J. Rapid Thermal Hydrogen Production from Alcohols Catalysed by [Rh(2,2'-Bipyridyl)2]Cl. *J. Chem. Soc., Chem. Commun.*, **1987**, 248-249. <https://doi.org/10.1039/C39870000248>.
- (379) Nystrom, R. F.; Brown, W. G. Reduction of Organic Compounds by Lithium Aluminum Hydride. I. Aldehydes, Ketones, Esters, Acid Chlorides and Acid Anhydrides. *J. Am. Chem. Soc.* **1947**, *69* (5), 1197–1199. <https://doi.org/10.1021/ja01197a060>.
- (380) Taniguchi, T.; Curran, D. P. Silica Gel Promotes Reductions of Aldehydes and Ketones by N-Heterocyclic Carbene Boranes. *Org. Lett.* **2012**, *14* (17), 4540–4543. <https://doi.org/10.1021/ol302010f>.
- (381) Sabatier, P.; Senderens, J.-B. *Décomposition catalytique de l'alcool éthylique par les métaux divisés; formation régulière d'aldéhyde*. Gallica. <https://gallica.bnf.fr/ark:/12148/bpt6k3091c> (accessed 2022-11-21).
- (382) Redina, E. A.; Vikanova, K. V.; Kapustin, G. I.; Mishin, I. V.; Tkachenko, O. P.; Kustov, L. M. Selective Room-Temperature Hydrogenation of Carbonyl Compounds under Atmospheric Pressure over Platinum Nanoparticles Supported on Ceria-Zirconia Mixed Oxide. *European Journal of Organic Chemistry* **2019**, *2019* (26), 4159–4170. <https://doi.org/10.1002/ejoc.201900215>.
- (383) Rachmady, W.; Vannice, M. A. Acetic Acid Hydrogenation over Supported Platinum Catalysts. *Journal of Catalysis* **2000**, *192* (2), 322–334. <https://doi.org/10.1006/jcat.2000.2863>.
- (384) Pan, M.; Flaherty, D. W.; Mullins, C. B. Low-Temperature Hydrogenation of Acetaldehyde to Ethanol on H-Precovered Au(111). *J. Phys. Chem. Lett.* **2011**, *2* (12), 1363–1367. <https://doi.org/10.1021/jz200577n>.

- (385) Chen, C.-C.; Lin, L.; Ye, R.-P.; Huang, L.; Zhu, L.-B.; Huang, Y.-Y.; Qin, Y.-Y.; Yao, Y.-G. Construction of Cu-Ce Composite Oxides by Simultaneous Ammonia Evaporation Method to Enhance Catalytic Performance of Ce-Cu/SiO₂ Catalysts for Dimethyl Oxalate Hydrogenation. *Fuel* **2021**, *290*, 120083. <https://doi.org/10.1016/j.fuel.2020.120083>.
- (386) Ni, J.; Leng, W.; Mao, J.; Wang, J.; Lin, J.; Jiang, D.; Li, X. Tuning Electron Density of Metal Nickel by Support Defects in Ni/ZrO₂ for Selective Hydrogenation of Fatty Acids to Alkanes and Alcohols. *Applied Catalysis B: Environmental* **2019**, *253*, 170–178. <https://doi.org/10.1016/j.apcatb.2019.04.043>.
- (387) Kong, X.; Chen, L. Chemoselective Hydrogenation of Aromatic Aldehydes over SiO₂ Modified Co/ γ -Al₂O₃. *Applied Catalysis A: General* **2014**, *476*, 34–38. <https://doi.org/10.1016/j.apcata.2014.02.011>.
- (388) He, Z.; Lin, H.; He, P.; Yuan, Y. Effect of Boric Oxide Doping on the Stability and Activity of a Cu–SiO₂ Catalyst for Vapor-Phase Hydrogenation of Dimethyl Oxalate to Ethylene Glycol. *Journal of Catalysis* **2011**, *277* (1), 54–63. <https://doi.org/10.1016/j.jcat.2010.10.010>.
- (389) Zheng, X.; Lin, H.; Zheng, J.; Duan, X.; Yuan, Y. Lanthanum Oxide-Modified Cu/SiO₂ as a High-Performance Catalyst for Chemoselective Hydrogenation of Dimethyl Oxalate to Ethylene Glycol. *ACS Catal.* **2013**, *3* (12), 2738–2749. <https://doi.org/10.1021/cs400574v>.
- (390) Manikandan, M.; Venugopal, A. K.; Nagpure, A. S.; Chilukuri, S.; Raja, T. Promotional Effect of Fe on the Performance of Supported Cu Catalyst for Ambient Pressure Hydrogenation of Furfural. *RSC Adv.* **2016**, *6* (5), 3888–3898. <https://doi.org/10.1039/C5RA24742J>.
- (391) Yu, X.; Vest, T. A.; Gleason-Boure, N.; Karakalos, S. G.; Tate, G. L.; Burkholder, M.; Monnier, J. R.; Williams, C. T. Enhanced Hydrogenation of Dimethyl Oxalate to Ethylene Glycol over Indium Promoted Cu/SiO₂. *Journal of Catalysis* **2019**, *380*, 289–296. <https://doi.org/10.1016/j.jcat.2019.10.001>.
- (392) Zhu, Y.; Shi, L. Zn Promoted Cu–Al Catalyst for Hydrogenation of Ethyl Acetate to Alcohol. *Journal of Industrial and Engineering Chemistry* **2014**, *20* (4), 2341–2347. <https://doi.org/10.1016/j.jiec.2013.10.010>.
- (393) Huang, C.; Zhang, H.; Zhao, Y.; Chen, S.; Liu, Z. Diatomite-Supported Pd–M (M=Cu, Co, Ni) Bimetal Nanocatalysts for Selective Hydrogenation of Long-Chain Aliphatic Esters. *Journal of Colloid and Interface Science* **2012**, *386* (1), 60–65. <https://doi.org/10.1016/j.jcis.2012.07.032>.
- (394) Liu, Y.; Ding, J.; Yang, J.; Bi, J.; Liu, K.; Chen, J. Stabilization of Copper Catalysts for Hydrogenation of Dimethyl Oxalate by Deposition of Ag Clusters on Cu Nanoparticles. *Catalysis Communications* **2017**, *98*, 43–46. <https://doi.org/10.1016/j.catcom.2017.05.007>.
- (395) Wang, Y.; Duan, X.; Zheng, J.; Lin, H.; Yuan, Y.; Ariga, H.; Takakusagi, S.; Asakura, K. Remarkable Enhancement of Cu Catalyst Activity in Hydrogenation of Dimethyl Oxalate to Ethylene Glycol Using Gold. *Catal. Sci. Technol.* **2012**, *2* (8), 1637–1639. <https://doi.org/10.1039/C2CY20154B>.
- (396) Haffad, D.; Kameswari, U.; Bettahar, M. M.; Chambellan, A.; Lavalley, J. C. Reduction of Benzaldehyde on Metal Oxides. *Journal of Catalysis* **1997**, *172* (1), 85–92. <https://doi.org/10.1006/jcat.1997.1854>.
- (397) Cox, J. D.; Pilcher, G. *Thermochemistry of Organic and Organometallic Compounds*; Academic Press, 1970. https://scholar.google.com/scholar_lookup?title=Thermochemistry+of+organic+and+organometallic+compounds&author=Cox%2C+J.+D.&publication_year=1970 (accessed 2022-11-23).
- (398) Wiberg, K. B.; Crocker, L. S.; Morgan, K. M. Thermochemical Studies of Carbonyl Compounds. 5. Enthalpies of Reduction of Carbonyl Groups. *J. Am. Chem. Soc.* **1991**, *113* (9), 3447–3450. <https://doi.org/10.1021/ja00009a033>.
- (399) Church, J. M.; Joshi, H. K. Acetaldehyde by Dehydrogenation of Ethyl Alcohol. *Ind. Eng. Chem.* **1951**, *43* (8), 1804–1811. <https://doi.org/10.1021/ie50500a035>.
- (400) Zhang, P.; Wang, Q.-N.; Yang, X.; Wang, D.; Li, W.-C.; Zheng, Y.; Chen, M.; Lu, A.-H. A Highly Porous Carbon Support Rich in Graphitic-N Stabilizes Copper Nanocatalysts for Efficient Ethanol Dehydrogenation. *ChemCatChem* **2017**, *9* (3), 505–510. <https://doi.org/10.1002/cctc.201601373>.
- (401) Wang, Q.-N.; Shi, L.; Li, W.; Li, W.-C.; Si, R.; Schüth, F.; Lu, A.-H. Cu Supported on Thin Carbon Layer-Coated Porous SiO₂ for Efficient Ethanol Dehydrogenation. *Catal. Sci. Technol.* **2018**, *8* (2), 472–479. <https://doi.org/10.1039/C7CY02057K>.
- (402) Li, M.-Y.; Lu, W.-D.; He, L.; Schüth, F.; Lu, A.-H. Tailoring the Surface Structure of Silicon Carbide Support for Copper Catalyzed Ethanol Dehydrogenation. *ChemCatChem* **2019**, *11* (1), 481–487. <https://doi.org/10.1002/cctc.201801742>.
- (403) Hanukovich, S.; Dang, A.; Christopher, P. Influence of Metal Oxide Support Acid Sites on Cu-Catalyzed Nonoxidative Dehydrogenation of Ethanol to Acetaldehyde. *ACS Catal.* **2019**, *9* (4), 3537–3550. <https://doi.org/10.1021/acscatal.8b05075>.
- (404) Pampararo, G.; Garbarino, G.; Riani, P.; Villa García, M.; Sánchez Escribano, V.; Busca, G. A Study of Ethanol Dehydrogenation to Acetaldehyde over Supported Copper Catalysts: Catalytic Activity, Deactivation and Regeneration. *Applied Catalysis A: General* **2020**, *602*, 117710. <https://doi.org/10.1016/j.apcata.2020.117710>.

- (405) Hao, Y.; Zhao, D.; Liu, W.; Zhang, M.; Lou, Y.; Wang, Z.; Tang, Q.; Yang, J. Uniformly Dispersed Cu Nanoparticles over Mesoporous Silica as a Highly Selective and Recyclable Ethanol Dehydrogenation Catalyst. *Catalysts* **2022**, *12* (9), 1049. <https://doi.org/10.3390/catal12091049>.
- (406) Idriss, H. Ethanol Reactions over the Surfaces of Noble Metal/Cerium Oxide Catalysts. *Platinum Metals Review* **2004**, *48* (3), 105–115. <https://doi.org/10.1595/147106704X1603>.
- (407) Pacheco, H. P.; de Souza, E. F.; Landi, S. M.; David, M. V.; Tyler Prillaman, J.; Davis, R. J.; Toniolo, F. S. Ru Promoted MgO and Al-Modified MgO for Ethanol Upgrading. *Top Catal* **2019**, *62* (12), 894–907. <https://doi.org/10.1007/s11244-019-01177-y>.
- (408) Mitsudome, T.; Mikami, Y.; Funai, H.; Mizugaki, T.; Jitsukawa, K.; Kaneda, K. Oxidant-Free Alcohol Dehydrogenation Using a Reusable Hydrotalcite-Supported Silver Nanoparticle Catalyst. *Angewandte Chemie International Edition* **2008**, *47* (1), 138–141. <https://doi.org/10.1002/anie.200703161>.
- (409) Cornejo-Romero, J.; Solis-Garcia, A.; Vega-Diaz, S. M.; Fierro-Gonzalez, J. C. Reverse Hydrogen Spillover during Ethanol Dehydrogenation on TiO₂-Supported Gold Catalysts. *Molecular Catalysis* **2017**, *433*, 391–402. <https://doi.org/10.1016/j.mcat.2017.02.041>.
- (410) Chernov, A. N.; Astrakova, T. V.; Koltunov, K. Y.; Sobolev, V. I. Ethanol Dehydrogenation to Acetaldehyde over Co@N-Doped Carbon. *Catalysts* **2021**, *11* (11), 1411. <https://doi.org/10.3390/catal11111411>.
- (411) Mamontov, G. V.; Grabchenko, M. V.; Sobolev, V. I.; Zaikovskii, V. I.; Vodyankina, O. V. Ethanol Dehydrogenation over Ag-CeO₂/SiO₂ Catalyst: Role of Ag-CeO₂ Interface. *Applied Catalysis A: General* **2016**, *528*, 161–167. <https://doi.org/10.1016/j.apcata.2016.10.005>.
- (412) Sushkevich, V. L.; Ivanova, I. I.; Taarning, E. Mechanistic Study of Ethanol Dehydrogenation over Silica-Supported Silver. *ChemCatChem* **2013**, *5* (8), 2367–2373. <https://doi.org/10.1002/cctc.201300033>.
- (413) Wang, C.; Garbarino, G.; Allard, L. F.; Wilson, F.; Busca, G.; Flytzani-Stephanopoulos, M. Low-Temperature Dehydrogenation of Ethanol on Atomically Dispersed Gold Supported on ZnZrOx. *ACS Catal.* **2016**, *6* (1), 210–218. <https://doi.org/10.1021/acscatal.5b01593>.
- (414) Rodriguez-Gomez, A.; Holgado, J. P.; Caballero, A. Cobalt Carbide Identified as Catalytic Site for the Dehydrogenation of Ethanol to Acetaldehyde. *ACS Catal.* **2017**, *7* (8), 5243–5247. <https://doi.org/10.1021/acscatal.7b01348>.
- (415) Wadsö, I.; Bjerrum, J.; Trätteberg, M.; Grönvall, A.; Zaar, B.; Diczfalussy, E. The Heats of Hydrolysis of Some Alkyl Acetates. *Acta Chem. Scand.* **1958**, *12*, 630–634. <https://doi.org/10.3891/acta.chem.scand.12-0630>.
- (416) Christensen, C. H.; Jørgensen, B.; Rass-Hansen, J.; Egeblad, K.; Madsen, R.; Klitgaard, S. K.; Hansen, S. M.; Hansen, M. R.; Andersen, H. C.; Riisager, A. Formation of Acetic Acid by Aqueous-Phase Oxidation of Ethanol with Air in the Presence of a Heterogeneous Gold Catalyst. *Angewandte Chemie International Edition* **2006**, *45* (28), 4648–4651. <https://doi.org/10.1002/anie.200601180>.
- (417) Balaraman, E.; Khaskin, E.; Leitus, G.; Milstein, D. Catalytic Transformation of Alcohols to Carboxylic Acid Salts and H₂ Using Water as the Oxygen Atom Source. *Nature Chemistry* **2013**, *5* (2), 122–125. <https://doi.org/10.1038/nchem.1536>.
- (418) Li, J. J. Cannizzaro Reaction. In *Name Reactions*; Springer International Publishing: Cham, 2014; pp 106–107. https://doi.org/10.1007/978-3-319-03979-4_51.
- (419) Hattori, H. Solid Base Catalysts: Generation of Basic Sites and Application to Organic Synthesis. *Applied Catalysis A: General* **2001**, *222* (1), 247–259. [https://doi.org/10.1016/S0926-860X\(01\)00839-0](https://doi.org/10.1016/S0926-860X(01)00839-0).
- (420) Sawama, Y.; Morita, K.; Yamada, T.; Nagata, S.; Yabe, Y.; Monguchi, Y.; Sajiki, H. Rhodium-on-Carbon Catalyzed Hydrogen Scavenger- and Oxidant-Free Dehydrogenation of Alcohols in Aqueous Media. *Green Chemistry* **2014**, *16* (7), 3439–3443. <https://doi.org/10.1039/C4GC00434E>.
- (421) Sawama, Y.; Morita, K.; Asai, S.; Kozawa, M.; Tadokoro, S.; Nakajima, J.; Monguchi, Y.; Sajiki, H. Palladium on Carbon-Catalyzed Aqueous Transformation of Primary Alcohols to Carboxylic Acids Based on Dehydrogenation under Mildly Reduced Pressure. *Advanced Synthesis & Catalysis* **2015**, *357* (6), 1205–1210. <https://doi.org/10.1002/adsc.201401123>.
- (422) Bordoloi, K.; Kalita, G. D.; Das, P. Acceptorless Dehydrogenation of Alcohols to Carboxylic Acids by Palladium Nanoparticles Supported on NiO: Delving into Metal–Support Cooperation in Catalysis. *Dalton Trans.* **2022**, *51* (25), 9922–9934. <https://doi.org/10.1039/D2DT01311H>.
- (423) Yin, S.; Zheng, Q.; Chen, J.; Tu, T. Acceptorless Dehydrogenation of Primary Alcohols to Carboxylic Acids by Self-Supported NHC-Ru Single-Site Catalysts. *Journal of Catalysis* **2022**, *408*, 165–172. <https://doi.org/10.1016/j.jcat.2022.02.018>.
- (424) Monda, F.; Madsen, R. Zinc Oxide-Catalyzed Dehydrogenation of Primary Alcohols into Carboxylic Acids. *Chemistry – A European Journal* **2018**, *24* (67), 17832–17837. <https://doi.org/10.1002/chem.201804402>.
- (425) Li, B.; Fang, J.; Xu, D.; Zhao, H.; Zhu, H.; Zhang, F.; Dong, Z. Atomically Dispersed Co Clusters Anchored on N-Doped Carbon Nanotubes for Efficient Dehydrogenation of Alcohols and Subsequent

- Conversion to Carboxylic Acids. *ChemSusChem* **2021**, *14* (20), 4536–4545. <https://doi.org/10.1002/cssc.202101330>.
- (426) Chen, C.; Wang, Z.-Q.; Gong, Y.-Y.; Wang, J.-C.; Yuan, Y.; Cheng, H.; Sang, W.; Chaemchuen, S.; Verpoort, F. Cobalt Embedded in Nitrogen-Doped Porous Carbon as a Robust Heterogeneous Catalyst for the Atom-Economic Alcohol Dehydrogenation to Carboxylic Acids. *Carbon* **2021**, *174*, 284–294. <https://doi.org/10.1016/j.carbon.2020.12.040>.
- (427) Mittal, R.; Awasthi, S. K. Bimetallic Oxide Catalyst for the Dehydrogenative Oxidation Reaction of Alcohols: Practical Application in the Synthesis of Value-Added Chemicals. *ACS Sustainable Chem. Eng.* **2022**, *10* (4), 1702–1713. <https://doi.org/10.1021/acssuschemeng.1c07799>.
- (428) Gao, D.; Feng, Y.; Yin, H.; Wang, A.; Jiang, T. Coupling Reaction between Ethanol Dehydrogenation and Maleic Anhydride Hydrogenation Catalyzed by Cu/Al₂O₃, Cu/ZrO₂, and Cu/ZnO Catalysts. *Chemical Engineering Journal* **2013**, *233*, 349–359. <https://doi.org/10.1016/j.cej.2013.08.058>.
- (429) Franckaerts, J.; Froment, G. F. Kinetic Study of the Dehydrogenation of Ethanol. *Chemical Engineering Science* **1964**, *19* (10), 807–818. [https://doi.org/10.1016/0009-2509\(64\)85092-2](https://doi.org/10.1016/0009-2509(64)85092-2).
- (430) Iwasa, N.; Takezawa, N. Reforming of Ethanol –Dehydrogenation to Ethyl Acetate and Steam Reforming to Acetic Acid over Copper-Based Catalysts–. *BCSJ* **1991**, *64* (9), 2619–2623. <https://doi.org/10.1246/bcsj.64.2619>.
- (431) Wang, L.; Zhu, W.; Zheng, D.; Yu, X.; Cui, J.; Jia, M.; Zhang, W.; Wang, Z. Direct Transformation of Ethanol to Ethyl Acetate on Cu/ZrO₂ Catalyst. *Reac Kinet Mech Cat* **2010**, *101* (2), 365–375. <https://doi.org/10.1007/s11444-010-0216-9>.
- (432) Mitsudome, T.; Mikami, Y.; Ebata, K.; Mizugaki, T.; Jitsukawa, K.; Kaneda, K. Copper Nanoparticles on Hydrotalcite as a Heterogeneous Catalyst for Oxidant-Free Dehydrogenation of Alcohols. *Chemical Communications* **2008**, *0* (39), 4804–4806. <https://doi.org/10.1039/B809012B>.
- (433) Miura, H.; Nakahara, K.; Kitajima, T.; Shishido, T. Concerted Functions of Surface Acid–Base Pairs and Supported Copper Catalysts for Dehydrogenative Synthesis of Esters from Primary Alcohols. *ACS Omega* **2017**, *2* (9), 6167–6173. <https://doi.org/10.1021/acsomega.7b01142>.
- (434) Inui, K.; Kurabayashi, T.; Sato, S.; Ichikawa, N. Effective Formation of Ethyl Acetate from Ethanol over Cu–Zn–Zr–Al–O Catalyst. *Journal of Molecular Catalysis A: Chemical* **2004**, *216* (1), 147–156. <https://doi.org/10.1016/j.molcata.2004.02.017>.
- (435) Inui, K.; Kurabayashi, T.; Sato, S. Direct Synthesis of Ethyl Acetate from Ethanol Carried Out under Pressure. *Journal of Catalysis* **2002**, *212* (2), 207–215. <https://doi.org/10.1006/jcat.2002.3769>.
- (436) Colley, S. W.; Tabatabaei, J.; Waugh, K. C.; Wood, M. A. The Detailed Kinetics and Mechanism of Ethyl Ethanoate Synthesis over a Cu/Cr₂O₃ Catalyst. *Journal of Catalysis* **2005**, *236* (1), 21–33. <https://doi.org/10.1016/j.jcat.2005.09.012>.
- (437) Carotenuto, G.; Tesser, R.; Di Serio, M.; Santacesaria, E. Kinetic Study of Ethanol Dehydrogenation to Ethyl Acetate Promoted by a Copper/Copper-Chromite Based Catalyst. *Catalysis Today* **2013**, *203*, 202–210. <https://doi.org/10.1016/j.cattod.2012.02.054>.
- (438) Li, R.; Zhang, M.; Yu, Y. A DFT Study on the Cu (111) Surface for Ethyl Acetate Synthesis from Ethanol Dehydrogenation. *Applied Surface Science* **2012**, *258* (18), 6777–6784. <https://doi.org/10.1016/j.apsusc.2012.01.171>.
- (439) Finger, P. H.; Osmari, T. A.; Costa, M. S.; Bueno, J. M. C.; Gallo, J. M. R. The Role of the Interface between Cu and Metal Oxides in the Ethanol Dehydrogenation. *Applied Catalysis A: General* **2020**, *589*, 117236. <https://doi.org/10.1016/j.apcata.2019.117236>.
- (440) Freitas, I. C.; Gallo, J. M. R.; Bueno, J. M. C.; Marques, C. M. P. The Effect of Ag in the Cu/ZrO₂ Performance for the Ethanol Conversion. *Top Catal* **2016**, *59* (2), 357–365. <https://doi.org/10.1007/s11244-015-0439-0>.
- (441) Sato, A. G.; Volanti, D. P.; de Freitas, I. C.; Longo, E.; Bueno, J. M. C. Site-Selective Ethanol Conversion over Supported Copper Catalysts. *Catalysis Communications* **2012**, *26*, 122–126. <https://doi.org/10.1016/j.catcom.2012.05.008>.
- (442) Sato, A. G.; Volanti, D. P.; Meira, D. M.; Damyanova, S.; Longo, E.; Bueno, J. M. C. Effect of the ZrO₂ Phase on the Structure and Behavior of Supported Cu Catalysts for Ethanol Conversion. *Journal of Catalysis* **2013**, *307*, 1–17. <https://doi.org/10.1016/j.jcat.2013.06.022>.
- (443) Moromi, S. K.; Siddiki, S. M. A. H.; Ali, M. A.; Kon, K.; Shimizu, K. Acceptorless Dehydrogenative Coupling of Primary Alcohols to Esters by Heterogeneous Pt Catalysts. *Catal. Sci. Technol.* **2014**, *4* (10), 3631–3635. <https://doi.org/10.1039/C4CY00979G>.
- (444) Ouyang, M.; Cao, S.; Yang, S.; Li, M.; Flytzani-Stephanopoulos, M. Atomically Dispersed Pd Supported on Zinc Oxide for Selective Nonoxidative Ethanol Dehydrogenation. *Ind. Eng. Chem. Res.* **2020**, *59* (6), 2648–2656. <https://doi.org/10.1021/acs.iecr.9b05202>.
- (445) McCullough, L. R.; Childers, D. J.; Watson, R. A.; Kilos, B. A.; Barton, D. G.; Weitz, E.; Kung, H. H.; Notestein, J. M. Acceptorless Dehydrogenative Coupling of Neat Alcohols Using Group VI Sulfide

- Catalysts. *ACS Sustainable Chem. Eng.* **2017**, *5* (6), 4890–4896. <https://doi.org/10.1021/acssuschemeng.7b00303>.
- (446) Gnanaprakasam, B.; Ben-David, Y.; Milstein, D. Ruthenium Pincer-Catalyzed Acylation of Alcohols Using Esters with Liberation of Hydrogen under Neutral Conditions. *Advanced Synthesis & Catalysis* **2010**, *352* (18), 3169–3173. <https://doi.org/10.1002/adsc.201000663>.
- (447) Cheng, J.; Zhu, M.; Wang, C.; Li, J.; Jiang, X.; Wei, Y.; Tang, W.; Xue, D.; Xiao, J. Chemoselective Dehydrogenative Esterification of Aldehydes and Alcohols with a Dimeric Rhodium(II) Catalyst. *Chem. Sci.* **2016**, *7* (7), 4428–4434. <https://doi.org/10.1039/C6SC00145A>.
- (448) Das, U. K.; Ben-David, Y.; Leitus, G.; Diskin-Posner, Y.; Milstein, D. Dehydrogenative Cross-Coupling of Primary Alcohols To Form Cross-Esters Catalyzed by a Manganese Pincer Complex. *ACS Catal.* **2019**, *9* (1), 479–484. <https://doi.org/10.1021/acscatal.8b04585>.
- (449) Zhou, Q.-Q.; Zou, Y. Q.; Ben David, Y.; Milstein, D. A Reversible Liquid to Liquid Organic Hydrogen Carrier System Based on Ethylene Glycol and Ethanol. *Chem. Eur. J.* **2020**, chem.202002749. <https://doi.org/10.1002/chem.202002749>.
- (450) Bechthold, I.; Bretz, K.; Kabasci, S.; Kopitzky, R.; Springer, A. Succinic Acid: A New Platform Chemical for Biobased Polymers from Renewable Resources. *Chemical Engineering & Technology* **2008**, *31* (5), 647–654. <https://doi.org/10.1002/ceat.200800063>.
- (451) Javaid, A.; Bildea, C. S. Design and Control of an Integrated 1,4-Butanediol Dehydrogenation and Furfural Hydrogenation Plant. *Chemical Engineering & Technology* **2014**, *37* (9), 1515–1524. <https://doi.org/10.1002/ceat.201400210>.
- (452) Zhu, Y.-L.; Xiang, H.-W.; Wu, G.-S.; Bai, L.; Li, Y.-W. A Novel Route for Synthesis of γ -Butyrolactone through the Coupling of Hydrogenation and Dehydrogenation. *Chemical Communications* **2002**, *0* (3), 254–255. <https://doi.org/10.1039/B109658N>.
- (453) Knauth, P.; Sabbah, R. Energetics of Intra- and Intermolecular Bonds in ω -Alkanediols: (II) Thermochemical Study of 1,2-Ethanediol, 1,3-Propanediol, 1,4-Butanediol, and 1,5-Pentanediol at 298.15 K. *Struct Chem* **1990**, *1* (1), 43–46. <https://doi.org/10.1007/BF00675783>.
- (454) Koyama, H. Production of Lactone Compound. JPH02255668A, October 16, 1990. [https://patents.google.com/patent/JPH02255668A/en?q=H.+Koyama%2c+Daicel+Kagaku+Kougyou+K.+K.+Jpn.+Kokai+Tokkyo+Koho.+JP02-255668+\(1990\)](https://patents.google.com/patent/JPH02255668A/en?q=H.+Koyama%2c+Daicel+Kagaku+Kougyou+K.+K.+Jpn.+Kokai+Tokkyo+Koho.+JP02-255668+(1990).). (accessed 2022-11-28).
- (455) Ichiki, T.; Mori, K.; Suzuki, S.; Ueno, H.; Kobayashi, K. Process for the Preparation of Gamma-Butyrolactone. US5210229A, May 11, 1993. <https://patents.google.com/patent/US5210229A/en> (accessed 2022-11-28).
- (456) Mercker, H. J.; Pape, F.-F.; Simon, J.; Henne, A.; Hesse, M.; Kohler, U.; Dostalek, R.; Erdbrugger, C. F.; Kratz, D. Catalyst for Dehydrogenating 1,4-Butanediol to γ -Butyrolactone. US6093677A, July 25, 2000. [https://patents.google.com/patent/US6093677A/en?q=H.J.+Mercker%2c+F.-F.+Pape%2c+J.+Simon%2c+A.+Henne%2c+M.+Hesse%2c+U.+Koebler%2c+R.+Dostalek%2c+C.F.+Erdbrugger%2c+D.+Kratz%2c+BASF+Aktiengesellschaft%2c+US+Patent+US6093677+\(2000](https://patents.google.com/patent/US6093677A/en?q=H.J.+Mercker%2c+F.-F.+Pape%2c+J.+Simon%2c+A.+Henne%2c+M.+Hesse%2c+U.+Koebler%2c+R.+Dostalek%2c+C.F.+Erdbrugger%2c+D.+Kratz%2c+BASF+Aktiengesellschaft%2c+US+Patent+US6093677+(2000) (accessed 2022-11-28).
- (457) Mimura H.; 三村英之; Watanabe M.; 渡辺真人. Method for producing γ -butyrolactone. JPH05286959A, November 2, 1993. [https://patents.google.com/patent/JPH05286959A/en?q=H.+Mimura%2c+M.+Watanabe%2c+Tosoh+K.+K.+Jpn.+Kokai+Tokkyo+Koho.+JP05-286959+\(1993\)](https://patents.google.com/patent/JPH05286959A/en?q=H.+Mimura%2c+M.+Watanabe%2c+Tosoh+K.+K.+Jpn.+Kokai+Tokkyo+Koho.+JP05-286959+(1993).). (accessed 2022-11-28).
- (458) Ichikawa, N.; Sato, S.; Takahashi, R.; Sodesawa, T.; Inui, K. Dehydrogenative Cyclization of 1,4-Butanediol over Copper-Based Catalyst. *Journal of Molecular Catalysis A: Chemical* **2004**, *212* (1), 197–203. <https://doi.org/10.1016/j.molcata.2003.10.028>.
- (459) Bhanushali, J. T.; Prasad, D.; Patil, K. N.; Reddy, K. S.; Kainthla, I.; Rao, K. S. R.; Jadhav, A. H.; Nagaraja, B. M. Tailoring the Catalytic Activity of Basic Mesoporous Cu/CeO₂ Catalyst by Al₂O₃ for Selective Lactonization and Dehydrogenation of 1,4-Butanediol to γ -Butyrolactone. *Catalysis Communications* **2020**, *143*, 106049. <https://doi.org/10.1016/j.catcom.2020.106049>.
- (460) Zhang, B.; Zhu, Y.; Ding, G.; Zheng, H.; Li, Y. Modification of the Supported Cu/SiO₂ Catalyst by Alkaline Earth Metals in the Selective Conversion of 1,4-Butanediol to γ -Butyrolactone. *Applied Catalysis A: General* **2012**, *443–444*, 191–201. <https://doi.org/10.1016/j.apcata.2012.07.042>.
- (461) Bhanushali, J. T.; Prasad, D.; Patil, K. N.; Babu, G. V. R.; Kainthla, I.; Rao, K. S. R.; Jadhav, A. H.; Nagaraja, B. M. The Selectively Regulated Vapour Phase Dehydrogenation of 1,4-Butanediol to γ -Butyrolactone Employing a Copper-Based Ceria Catalyst. *New J. Chem.* **2019**, *43* (30), 11968–11983. <https://doi.org/10.1039/C9NJ03067K>.
- (462) Patil, K. N.; Prasad, D.; Manoorkar, V. K.; Bhanushali, J. T.; Jadhav, A. H.; Nagaraja, B. M. Selective Vapour-Phase Dehydrocyclization of Biomass-Derived 1,4-Butanediol to γ -Butyrolactone over Cu/ZnAl₂O₄-CeO₂ Catalyst. *Journal of Industrial and Engineering Chemistry* **2022**, *106*, 142–151. <https://doi.org/10.1016/j.jiec.2021.10.018>.

- (463) Reddy, K. H. P.; Suh, Y.-W.; Anand, N.; Raju, B. D.; Rao, K. S. R. Coupling of Ortho-Chloronitrobenzene Hydrogenation with 1,4-Butanediol Dehydrogenation over CuMgO Catalysts: A Hydrogen Free Process. *Catalysis Communications* **2017**, *95*, 21–25. <https://doi.org/10.1016/j.catcom.2017.02.029>.
- (464) Nagaiah, P.; Venkat Rao, M.; Thirupathiah, K.; Venkateswarlu, V.; David Raju, B.; Rama Rao, K. S. Selective Vapour Phase Dehydrogenation of Biomass-Derived 1,4-Butanediol to Gamma Butyrolactone over Cu/ZrO₂ Catalysts: Influence of La₂O₃ Promotor. *Res Chem Intermed* **2018**, *44* (10), 5817–5831. <https://doi.org/10.1007/s11164-018-3457-2>.
- (465) Hwang, D. W.; Kashinathan, P.; Lee, J. M.; Lee, J. H.; Lee, U. -hwang; Hwang, J.-S.; Hwang, Y. K.; Chang, J.-S. Production of γ -Butyrolactone from Biomass-Derived 1,4-Butanediol over Novel Copper-Silica Nanocomposite. *Green Chem.* **2011**, *13* (7), 1672–1675. <https://doi.org/10.1039/C1GC15261K>.
- (466) Raju, M. A.; Gidyonu, P.; Nagaiah, P.; Rao, M. V.; Raju, B. D.; Rao, K. S. R. Mesoporous Silica-Supported Copper Catalysts for Dehydrogenation of Biomass-Derived 1,4-Butanediol to Gamma Butyrolactone in a Continuous Process at Atmospheric Pressure. *Biomass Conv. Bioref.* **2019**, *9* (4), 719–726. <https://doi.org/10.1007/s13399-019-00406-4>.
- (467) Kim, W.-H.; Park, I. S.; Park, J. Acceptor-Free Alcohol Dehydrogenation by Recyclable Ruthenium Catalyst. *Org. Lett.* **2006**, *8* (12), 2543–2545. <https://doi.org/10.1021/ol060750z>.
- (468) Touchy, A. S.; Shimizu, K. Acceptorless Dehydrogenative Lactonization of Diols by Pt-Loaded SnO₂ Catalysts. *RSC Adv.* **2015**, *5* (37), 29072–29075. <https://doi.org/10.1039/C5RA03337C>.
- (469) Wada, E.; Tyagi, A.; Yamamoto, A.; Yoshida, H. Dehydrogenative Lactonization of Diols with a Platinum-Loaded Titanium Oxide Photocatalyst. *Photochem. Photobiol. Sci.* **2017**, *16* (12), 1744–1748. <https://doi.org/10.1039/C7PP00258K>.
- (470) Jones, D. T.; Woods, D. R. Acetone-Butanol Fermentation Revisited. *Microbiological Reviews* **1986**, *50* (4), 484–524. <https://doi.org/10.1128/mr.50.4.484-524.1986>.
- (471) Weber, M.; Pompetzki, W.; Bonmann, R.; Weber, M. Acetone. In *Ullmann's Encyclopedia of Industrial Chemistry*; John Wiley & Sons, Ltd, 2014; pp 1–19. https://doi.org/10.1002/14356007.a01_079.pub4.
- (472) Snelson, A.; Skinner, H. A. Heats of Combustion: Sec-Propanol, 1,4-Dioxan, 1,3-Dioxan and Tetrahydropyran. *Trans. Faraday Soc.* **1961**, *57*, 2125. <https://doi.org/10.1039/tf9615702125>.
- (473) Kim, T. G.; Yeo, Y. K.; Song, H. K. Chemical Heat Pump Based on Dehydrogenation and Hydrogenation of I-Propanol and Acetone. *International Journal of Energy Research* **1992**, *16* (9), 897–916. <https://doi.org/10.1002/er.4440160910>.
- (474) Thonon, C. I.; Jungers, J. C. La déshydrogénation des alcools secondaires en phase liquide sur le nickel. *Bulletin des Sociétés Chimiques Belges* **1949**, *58* (7–9), 331–349. <https://doi.org/10.1002/bscb.19490580706>.
- (475) Noda, M.; Shinoda, S.; Saito, Y. Liquid-Phase Dehydrogenation of 2-Propanol by Suspended Nickel Fine-Particle Catalyst. *BCSJ* **1988**, *61* (3), 961–965. <https://doi.org/10.1246/bcsj.61.961>.
- (476) Gastauer, P.; Prévost, M. Dehydrogenation of Isopropanol at Low Temperatures in the Vapor Phase as a Reaction for a Chemical Heat Pump. *Journal of Chemical Engineering of Japan* **1993**, *26* (5), 580–583. <https://doi.org/10.1252/jcej.26.580>.
- (477) Meng, N.; Shinoda, S.; Saito, Y. Improvements on Thermal Efficiency of Chemical Heat Pump Involving the Reaction Couple of 2-Propanol Dehydrogenation and Acetone Hydrogenation. *International Journal of Hydrogen Energy* **1997**, *22* (4), 361–367. [https://doi.org/10.1016/S0360-3199\(96\)00084-5](https://doi.org/10.1016/S0360-3199(96)00084-5).
- (478) Xin, F.; Xu, M.; Huai, X.; Li, X. Study on Isopropanol–Acetone–Hydrogen Chemical Heat Pump: Liquid Phase Dehydrogenation of Isopropanol Using a Reactive Distillation Column. *Applied Thermal Engineering* **2013**, *58* (1), 369–373. <https://doi.org/10.1016/j.applthermaleng.2013.04.033>.
- (479) Rioux, R. M.; Vannice, M. A. Hydrogenation/Dehydrogenation Reactions: Isopropanol Dehydrogenation over Copper Catalysts. *Journal of Catalysis* **2003**, *216* (1), 362–376. [https://doi.org/10.1016/S0021-9517\(02\)00035-0](https://doi.org/10.1016/S0021-9517(02)00035-0).
- (480) Rioux, R. M.; Vannice, M. A. Dehydrogenation of Isopropyl Alcohol on Carbon-Supported Pt and Cu–Pt Catalysts. *Journal of Catalysis* **2005**, *233* (1), 147–165. <https://doi.org/10.1016/j.jcat.2005.04.020>.
- (481) Kvande, I.; Chen, D.; Rønning, M.; Venvik, H. J.; Holmen, A. Highly Active Cu-Based Catalysts on Carbon Nanofibers for Isopropanol Dehydrogenation. *Catalysis Today* **2005**, *100* (3), 391–395. <https://doi.org/10.1016/j.cattod.2004.10.027>.
- (482) Said, A. E.-A. A.; Abd El-Wahab, M. M. M.; Goda, M. N. Selective Synthesis of Acetone from Isopropyl Alcohol over Active and Stable CuO–NiO Nanocomposites at Relatively Low-Temperature. *Egyptian Journal of Basic and Applied Sciences* **2016**, *3* (4), 357–365. <https://doi.org/10.1016/j.ejbas.2016.08.004>.
- (483) Morales-Anzures, F.; Salinas-Hernández, P.; Ornelas-Gutiérrez, C.; Tzompantzi-Morales, F. J.; Pérez-Hernández, R. Synthesis by the Sol-Gel Method and Characterization of Pt-Promoted CuO/TiO₂-ZrO₂ Catalysts for Decomposition of 2-Propanol. *Catalysis Today* **2020**, *349*, 228–234. <https://doi.org/10.1016/j.cattod.2018.03.017>.

- (484) Abdelhamid, H. N.; Goda, M. N.; Said, A. E.-A. A. Selective Dehydrogenation of Isopropanol on Carbonized Metal–Organic Frameworks. *Nano-Structures & Nano-Objects* **2020**, *24*, 100605. <https://doi.org/10.1016/j.nanoso.2020.100605>.
- (485) Malineni, J.; Keul, H.; Möller, M. An Efficient N-Heterocyclic Carbene–Ruthenium Complex: Application Towards the Synthesis of Polyesters and Polyamides. *Macromolecular Rapid Communications* **2015**, *36* (6), 547–552. <https://doi.org/10.1002/marc.201400699>.
- (486) Gnanaprakasam, B.; Balaraman, E.; Ben-David, Y.; Milstein, D. Synthesis of Peptides and Pyrazines from β -Amino Alcohols through Extrusion of H₂ Catalyzed by Ruthenium Pincer Complexes: Ligand-Controlled Selectivity. *Angewandte Chemie International Edition* **2011**, *50* (51), 12240–12244. <https://doi.org/10.1002/anie.201105876>.
- (487) Gunanathan, C.; Ben-David, Y.; Milstein, D. Direct Synthesis of Amides from Alcohols and Amines with Liberation of H₂. *Science* **2007**, *317* (5839), 790–792. <https://doi.org/10.1126/science.1145295>.
- (488) Ghosh, S. C.; Hong, S. H. Simple RuCl₃-Catalyzed Amide Synthesis from Alcohols and Amines. *European Journal of Organic Chemistry* **2010**, *2010* (22), 4266–4270. <https://doi.org/10.1002/ejoc.201000362>.
- (489) Saha, B.; Sengupta, G.; Sarbajna, A.; Dutta, I.; Bera, J. K. Amide Synthesis from Alcohols and Amines Catalyzed by a RuII–N-Heterocyclic Carbene (NHC)–Carbonyl Complex. *Journal of Organometallic Chemistry* **2014**, *771*, 124–130. <https://doi.org/10.1016/j.jorganchem.2013.12.051>.
- (490) Kar, S.; Xie, Y.; Zhou, Q. Q.; Diskin-Posner, Y.; Ben-David, Y.; Milstein, D. Near-Ambient-Temperature Dehydrogenative Synthesis of the Amide Bond: Mechanistic Insight and Applications. *ACS Catal.* **2021**, *11* (12), 7383–7393. <https://doi.org/10.1021/acscatal.1c00728>.
- (491) Hu, P.; Fogler, E.; Diskin-Posner, Y.; Iron, M. A.; Milstein, D. A Novel Liquid Organic Hydrogen Carrier System Based on Catalytic Peptide Formation and Hydrogenation. *Nat Commun* **2015**, *6* (1), 1–7. <https://doi.org/10.1038/ncomms7859>.
- (492) Kothandaraman, J.; Kar, S.; Sen, R.; Goepfert, A.; Olah, G. A.; Prakash, G. K. S. Efficient Reversible Hydrogen Carrier System Based on Amine Reforming of Methanol. *J. Am. Chem. Soc.* **2017**, *139* (7), 2549–2552. <https://doi.org/10.1021/jacs.6b11637>.
- (493) Nova, A.; Balcells, D.; Schley, N. D.; Dobereiner, G. E.; Crabtree, R. H.; Eisenstein, O. An Experimental–Theoretical Study of the Factors That Affect the Switch between Ruthenium-Catalyzed Dehydrogenative Amide Formation versus Amine Alkylation. *Organometallics* **2010**, *29* (23), 6548–6558. <https://doi.org/10.1021/om101015u>.
- (494) Kumar, A.; Espinosa-Jalapa, N. A.; Leitus, G.; Diskin-Posner, Y.; Avram, L.; Milstein, D. Direct Synthesis of Amides by Dehydrogenative Coupling of Amines with Either Alcohols or Esters: Manganese Pincer Complex as Catalyst. *Angewandte Chemie International Edition* **2017**, *56* (47), 14992–14996. <https://doi.org/10.1002/anie.201709180>.
- (495) Shao, Z.; Li, Y.; Liu, C.; Ai, W.; Luo, S.-P.; Liu, Q. Reversible Interconversion between Methanol-Diamine and Diamide for Hydrogen Storage Based on Manganese Catalyzed (de)Hydrogenation. *Nat Commun* **2020**, *11* (1), 591. <https://doi.org/10.1038/s41467-020-14380-3>.
- (496) Xie, Y.; Hu, P.; Ben-David, Y.; Milstein, D. A Reversible Liquid Organic Hydrogen Carrier System Based on Methanol-Ethylenediamine and Ethylene Urea. *Angew. Chem. Int. Ed.* **2019**, *58* (15), 5105–5109. <https://doi.org/10.1002/anie.201901695>.
- (497) Bryant, R. G. Polyimides. In *Ullmann's Encyclopedia of Industrial Chemistry*; John Wiley & Sons, Ltd, 2014; pp 1–27. https://doi.org/10.1002/14356007.a21_253.pub2.
- (498) Espinosa-Jalapa, N. A.; Kumar, A.; Leitus, G.; Diskin-Posner, Y.; Milstein, D. Synthesis of Cyclic Imides by Acceptorless Dehydrogenative Coupling of Diols and Amines Catalyzed by a Manganese Pincer Complex. *J. Am. Chem. Soc.* **2017**, *139* (34), 11722–11725. <https://doi.org/10.1021/jacs.7b08341>.
- (499) Kumar, A.; Janes, T.; Espinosa-Jalapa, N. A.; Milstein, D. Selective Hydrogenation of Cyclic Imides to Diols and Amines and Its Application in the Development of a Liquid Organic Hydrogen Carrier. *J. Am. Chem. Soc.* **2018**, *140* (24), 7453–7457. <https://doi.org/10.1021/jacs.8b04581>.
- (500) Grellier, M.; Sabo-Etienne, S. New Perspectives in Hydrogen Storage Based on RCH₂NH₂/RCN Couples. *Dalton Transactions* **2014**, *43* (17), 6283–6286. <https://doi.org/10.1039/C3DT53583E>.
- (501) Naeemi, E.; O'Connor, D. G. Release and Recovery from Aliphatic Primary Amines or Di-Amines. US20100210878A1, August 19, 2010. <https://patents.google.com/patent/US20100210878A1/en> (accessed 2021-03-16).
- (502) Naeemi, E.; O'Connor, D. G.; Naeemi, M. Hydrogen Storage System by Catalytic Dehydrogenation of Amines. US20140134100A1, May 15, 2014. <https://patents.google.com/patent/US20140134100A1/en> (accessed 2021-02-24).
- (503) *Advantages | Asemblon Inc.* Michael D Ramage. <https://www.asemblon.com/advantages> (accessed 2022-11-18).

Literature review

- (504) texte, A. des sciences (France) A. du. *Comptes rendus hebdomadaires des séances de l'Académie des sciences / publiés... par MM. les secrétaires perpétuels.* Gallica. <https://gallica.bnf.fr/ark:/12148/bpt6k30949> (accessed 2022-11-18).
- (505) Paal, C.; Gerum, J. Über Katalytische Wirkungen Kolloidaler Metalle Der Platingruppe. VI. Reduktionskatalysen Mit Kolloidalem Palladium. *Berichte der deutschen chemischen Gesellschaft* **1909**, *42* (2), 1553–1560. <https://doi.org/10.1002/cber.19090420222>.
- (506) Braun, J. V.; Blessing, G.; Zobel, F. Katalytische Hydrierungen Unter Druck Bei Gegenwart von Nickelsalzen, VI.: Nitrile. *Berichte der deutschen chemischen Gesellschaft (A and B Series)* **1923**, *56* (8), 1988–2001. <https://doi.org/10.1002/cber.19230560845>.
- (507) Carothers, W. H.; Jones, G. A. THE PREPARATION OF SOME PRIMARY AMINES BY THE CATALYTIC REDUCTION OF NITRILES. *J. Am. Chem. Soc.* **1925**, *47* (12), 3051–3057. <https://doi.org/10.1021/ja01689a034>.
- (508) Aller, B. V. Raney Cobalt Hydrogenation Catalysts. I. the Preparation of the Catalyst. *Journal of Applied Chemistry* **1957**, *7* (3), 130–134. <https://doi.org/10.1002/jctb.5010070307>.
- (509) Adkins, H.; 1892-1949. *Reactions of Hydrogen with Organic Compounds over Copper-Chromium Oxide and Nickel Catalysts*; University of Wisconsin Press, 1937. https://scholar.google.com/scholar_lookup?title=Reactions+of+hydrogen+with+organic+compounds+over+copper-chromium+oxide+and+nickel+catalysts&author=Adkins%2C+Homer&publication_year=1937 (accessed 2022-11-18).
- (510) Huang, Y.; Sachtler, W. M. H. On the Mechanism of Catalytic Hydrogenation of Nitriles to Amines over Supported Metal Catalysts. *Applied Catalysis A: General* **1999**, *182* (2), 365–378. [https://doi.org/10.1016/S0926-860X\(99\)00035-6](https://doi.org/10.1016/S0926-860X(99)00035-6).
- (511) Barnett, C. Hydrogenation of Aliphatic Nitriles over Transition Metal Borides. *Product R&D* **1969**, *8* (2), 145–149. <https://doi.org/10.1021/i360030a009>.
- (512) López-De Jesús, Y. M.; Johnson, C. E.; Monnier, J. R.; Williams, C. T. Selective Hydrogenation of Benzonitrile by Alumina-Supported Ir–Pd Catalysts. *Top Catal* **2010**, *53* (15), 1132–1137. <https://doi.org/10.1007/s11244-010-9546-0>.
- (513) Ryabchuk, P.; Agostini, G.; Pohl, M.-M.; Lund, H.; Agapova, A.; Junge, H.; Junge, K.; Beller, M. Intermetallic Nickel Silicide Nanocatalyst—A Non-Noble Metal–Based General Hydrogenation Catalyst. *Science Advances* **2018**, *4* (6), eaat0761. <https://doi.org/10.1126/sciadv.aat0761>.
- (514) Murugesan, K.; Senthamarai, T.; Sohail, M.; S. Alshammari, A.; Pohl, M.-M.; Beller, M.; V. Jagadeesh, R. Cobalt-Based Nanoparticles Prepared from MOF–Carbon Templates as Efficient Hydrogenation Catalysts. *Chemical Science* **2018**, *9* (45), 8553–8560. <https://doi.org/10.1039/C8SC02807A>.
- (515) Segobia, D. J.; Trasarti, A. F.; Apesteguía, C. R. Chemoselective Hydrogenation of Unsaturated Nitriles to Unsaturated Primary Amines: Conversion of Cinnamionitrile on Metal-Supported Catalysts. *Applied Catalysis A: General* **2015**, *494*, 41–47. <https://doi.org/10.1016/j.apcata.2015.01.028>.
- (516) Chandrashekar, V. G.; Senthamarai, T.; Kadam, R. G.; Malina, O.; Kašlík, J.; Zbořil, R.; Gawande, M. B.; Jagadeesh, R. V.; Beller, M. Silica-Supported Fe/Fe–O Nanoparticles for the Catalytic Hydrogenation of Nitriles to Amines in the Presence of Aluminium Additives. *Nat Catal* **2022**, *5* (1), 20–29. <https://doi.org/10.1038/s41929-021-00722-x>.
- (517) Segobia, D. J.; Trasarti, A. F.; Apesteguía, C. R. Hydrogenation of Nitriles to Primary Amines on Metal-Supported Catalysts: Highly Selective Conversion of Butyronitrile to n-Butylamine. *Applied Catalysis A: General* **2012**, *445–446*, 69–75. <https://doi.org/10.1016/j.apcata.2012.08.006>.
- (518) Liu, C.; Wang, T. Isophthalonitrile (IPN) Hydrogenation over K Modified Ni–Co Supported Catalysts: Catalyst Characterization and Performance Evaluation. *RSC Advances* **2014**, *4* (109), 63725–63733. <https://doi.org/10.1039/C4RA09607J>.
- (519) Lévay, K.; Hegedűs, L. Recent Achievements in the Hydrogenation of Nitriles Catalyzed by Transitional Metals. *Current Organic Chemistry* **2019**, *23* (18), 1881–1900. <https://doi.org/10.2174/1385272823666191007160341>.
- (520) Lévay, K.; Hegedűs, L. Selective Heterogeneous Catalytic Hydrogenation of Nitriles to Primary Amines. *Periodica Polytechnica Chemical Engineering* **2018**, *62* (4), 476–488. <https://doi.org/10.3311/PPch.12787>.
- (521) Kamiguchi, S.; Nakamura, A.; Suzuki, A.; Kodomari, M.; Nomura, M.; Iwasawa, Y.; Chihara, T. Catalytic Dehydrogenation of Aliphatic Amines to Nitriles, Imines, or Vinylamines and Dealkylation of Tertiary Aliphatic Amines over Halide Cluster Catalysts of Group 5 and 6 Transition Metals. *Journal of Catalysis* **2005**, *230* (1), 204–213. <https://doi.org/10.1016/j.jcat.2004.11.034>.
- (522) Tseng, K.-N. T.; Rizzi, A. M.; Szymczak, N. K. Oxidant-Free Conversion of Primary Amines to Nitriles. *J. Am. Chem. Soc.* **2013**, *135* (44), 16352–16355. <https://doi.org/10.1021/ja409223a>.

- (523) Wang, Z.; Belli, J.; M. Jensen, C. Homogeneous Dehydrogenation of Liquid Organic Hydrogen Carriers Catalyzed by an Iridium PCP Complex. *Faraday Discussions* **2011**, *151* (0), 297–305. <https://doi.org/10.1039/C1FD00002K>.
- (524) Dutta, I.; Yadav, S.; Sarbajna, A.; De, S.; Hölscher, M.; Leitner, W.; Bera, J. K. Double Dehydrogenation of Primary Amines to Nitriles by a Ruthenium Complex Featuring Pyrazole Functionality. *J. Am. Chem. Soc.* **2018**, *140* (28), 8662–8666. <https://doi.org/10.1021/jacs.8b05009>.
- (525) Hale, L. V. A.; Malakar, T.; Tseng, K.-N. T.; Zimmerman, P. M.; Paul, A.; Szymczak, N. K. The Mechanism of Acceptorless Amine Double Dehydrogenation by N,N,N-Amide Ruthenium(II) Hydrides: A Combined Experimental and Computational Study. *ACS Catal.* **2016**, *6* (8), 4799–4813. <https://doi.org/10.1021/acscatal.6b01465>.
- (526) Kannan, M.; Muthaiah, S. Extending the Chemistry of Hexamethylenetetramine in Ruthenium-Catalyzed Amine Oxidation. *Organometallics* **2019**, *38* (19), 3560–3567. <https://doi.org/10.1021/acs.organomet.9b00399>.
- (527) Kannan, M.; Barteja, P.; Devi, P.; Muthaiah, S. Acceptorless Dehydrogenation of Amines and Alcohols Using Simple Ruthenium Chloride. *Journal of Catalysis* **2020**, *386*, 1–11. <https://doi.org/10.1016/j.jcat.2020.03.025>.
- (528) Kannan, M.; Muthaiah, S. Ruthenium(II)-Complex-Catalyzed Acceptorless Double Dehydrogenation of Primary Amines to Nitriles. *Synlett* **2020**, *31* (11), 1073–1076. <https://doi.org/10.1055/s-0040-1708016>.
- (529) Nie, X.; Zheng, Y.; Ji, L.; Fu, H.; Chen, H.; Li, R. Acceptorless Dehydrogenation of Amines to Nitriles Catalyzed by N-Heterocyclic Carbene-Nitrogen-Phosphine Chelated Bimetallic Ruthenium (II) Complex. *Journal of Catalysis* **2020**, *391*, 378–385. <https://doi.org/10.1016/j.jcat.2020.09.005>.
- (530) Lu, G.-P.; Li, X.; Zhong, L.; Li, S.; Chen, F. Ru@UiO-66(Ce) Catalyzed Acceptorless Dehydrogenation of Primary Amines to Nitriles: The Roles of Lewis Acid-Base Pairs in the Reaction. *Green Chemistry* **2019**, *21* (19), 5386–5393. <https://doi.org/10.1039/C9GC02181G>.
- (531) Feldhues, U.; Schäfer, H. J. Oxidation of Primary Aliphatic Amines to Nitriles at the Nickel Hydroxide Electrode. *Synthesis* **1982**, *1982* (02), 145–146. <https://doi.org/10.1055/s-1982-29721>.
- (532) Huang, Y.; Chong, X.; Liu, C.; Liang, Y.; Zhang, B. Boosting Hydrogen Production by Anodic Oxidation of Primary Amines over a NiSe Nanorod Electrode. *Angewandte Chemie International Edition* **2018**, *57* (40), 13163–13166. <https://doi.org/10.1002/anie.201807717>.
- (533) Mondal, I.; Hausmann, J. N.; Vijaykumar, G.; Mebs, S.; Dau, H.; Driess, M.; Menezes, P. W. Nanostructured Intermetallic Nickel Silicide (Pre)Catalyst for Anodic Oxygen Evolution Reaction and Selective Dehydrogenation of Primary Amines. *Advanced Energy Materials* **2022**, *12* (25), 2200269. <https://doi.org/10.1002/aenm.202200269>.
- (534) Qian, W.; Yoda, Y.; Hirai, Y.; Ishihara, A.; Kabe, T. Hydrodesulfurization of Dibenzothiophene and Hydrogenation of Phenanthrene on Alumina-Supported Pt and Pd Catalysts. *Applied Catalysis A: General* **1999**, *184* (1), 81–88. [https://doi.org/10.1016/S0926-860X\(99\)00083-6](https://doi.org/10.1016/S0926-860X(99)00083-6).
- (535) Navarro, R. M.; Pawelec, B.; Trejo, J. M.; Mariscal, R.; Fierro, J. L. G. Hydrogenation of Aromatics on Sulfur-Resistant PtPd Bimetallic Catalysts. *Journal of Catalysis* **2000**, *189* (1), 184–194. <https://doi.org/10.1006/jcat.1999.2693>.
- (536) Ratner, B. D.; Naeemi, E. Method for Hydrogen Storage and Delivery. US7186396B2, March 6, 2007. <https://patents.google.com/patent/US7186396/en> (accessed 2022-11-30).
- (537) Zhao, H. Y.; Oyama, S. T.; Naeemi, E. D. Hydrogen Storage Using Heterocyclic Compounds: The Hydrogenation of 2-Methylthiophene. *Catalysis Today* **2010**, *149* (1), 172–184. <https://doi.org/10.1016/j.cattod.2009.02.039>.
- (538) Luo, J.; Rauch, M.; Avram, L.; Ben-David, Y.; Milstein, D. Catalytic Hydrogenation of Thioesters, Thiocarbamates, and Thioamides. *J. Am. Chem. Soc.* **2020**, *142* (52), 21628–21633. <https://doi.org/10.1021/jacs.0c10884>.
- (539) Luo, J.; Rauch, M.; Avram, L.; Diskin-Posner, Y.; Shmul, G.; Ben-David, Y.; Milstein, D. Formation of Thioesters by Dehydrogenative Coupling of Thiols and Alcohols with H₂ Evolution. *Nature Catalysis* **2020**, *3* (11), 887–892.
- (540) Rauch, M.; Luo, J.; Avram, L.; Ben-David, Y.; Milstein, D. Mechanistic Investigations of Ruthenium Catalyzed Dehydrogenative Thioester Synthesis and Thioester Hydrogenation. *ACS Catal.* **2021**, *11* (5), 2795–2807. <https://doi.org/10.1021/acscatal.1c00418>.
- (541) Luo, W.; Zakharov, L. N.; Liu, S.-Y. 1,2-BN Cyclohexane: Synthesis, Structure, Dynamics, and Reactivity. *J. Am. Chem. Soc.* **2011**, *133* (33), 13006–13009. <https://doi.org/10.1021/ja206497x>.
- (542) Müller, K.; Stark, K.; Müller, B.; Arlt, W. Amine Borane Based Hydrogen Carriers: An Evaluation. *Energy Fuels* **2012**, *26* (6), 3691–3696. <https://doi.org/10.1021/ef300516m>.
- (543) Campbell, P. G.; Zakharov, L. N.; Grant, D. J.; Dixon, D. A.; Liu, S.-Y. Hydrogen Storage by Boron-Nitrogen Heterocycles: A Simple Route for Spent Fuel Regeneration. *J. Am. Chem. Soc.* **2010**, *132* (10), 3289–3291. <https://doi.org/10.1021/ja9106622>.

Literature review

- (544) Liu, S.-Y. *Hydrogen Storage by Novel CBN Heterocycle Materials*; DE-FG36-08GO18143; Univ. of Oregon, Eugene, OR (United States), 2015. <https://doi.org/10.2172/1221989>.
- (545) Dai, Y.; Zhang, X.; Liu, Y.; Yu, H.; Su, W.; Zhou, J.; Ye, Q.; Huang, Z. 1,6;2,3-Bis-BN Cyclohexane: Synthesis, Structure, and Hydrogen Release. *J. Am. Chem. Soc.* **2022**, *144* (19), 8434–8438. <https://doi.org/10.1021/jacs.1c13581>.
- (546) Finholt, A. E.; Bond, A. C. Jr.; Wilzbach, K. E.; Schlesinger, H. I. The Preparation and Some Properties of Hydrides of Elements of the Fourth Group of the Periodic System and of Their Organic Derivatives. *J. Am. Chem. Soc.* **1947**, *69* (11), 2692–2696. <https://doi.org/10.1021/ja01203a041>.
- (547) Aoyagi, K.; Ohmori, Y.; Inomata, K.; Matsumoto, K.; Shimada, S.; Sato, K.; Nakajima, Y. Synthesis of Hydrosilanes via Lewis-Base-Catalysed Reduction of Alkoxy Silanes with NaBH₄. *Chem. Commun.* **2019**, *55* (42), 5859–5862. <https://doi.org/10.1039/C9CC01961H>.
- (548) Durin, G.; Berthet, J.-C.; Nicolas, E.; Thuéry, P.; Cantat, T. The Role of (TBuPOCOP)Ir(I) and Iridium(III) Pincer Complexes in the Catalytic Hydrogenolysis of Silyl Triflates into Hydrosilanes. *Organometallics* **2022**, *41* (14), 1786–1796. <https://doi.org/10.1021/acs.organomet.1c00576>.
- (549) Mitsudome, T.; Arita, S.; Mori, H.; Mizugaki, T.; Jitsukawa, K.; Kaneda, K. Supported Silver-Nanoparticle-Catalyzed Highly Efficient Aqueous Oxidation of Phenylsilanes to Silanols. *Angewandte Chemie International Edition* **2008**, *47* (41), 7938–7940. <https://doi.org/10.1002/anie.200802761>.
- (550) Han, W.-S.; Kim, T.-J.; Kim, S.-K.; Kim, Y.; Kim, Y.; Nam, S.-W.; Kang, S. O. Silane-Based Hydrogen Storage Materials for Fuel Cell Application: Hydrogen Release via Methanolysis and Regeneration by Hydride Reduction from Organosilanes. *International Journal of Hydrogen Energy* **2011**, *36* (19), 12305–12312. <https://doi.org/10.1016/j.ijhydene.2011.06.118>.
- (551) Brunel, J. M. New Efficient Hydrogen Process Production from Organosilane Hydrogen Carriers Derivatives. *International Journal of Hydrogen Energy* **2010**, *35* (8), 3401–3405. <https://doi.org/10.1016/j.ijhydene.2010.01.116>.
- (552) Mukherjee, D.; Thompson, R. R.; Ellern, A.; Sadow, A. D. Coordinatively Saturated Tris(Oxazolonyl)Borato Zinc Hydride-Catalyzed Cross Dehydrocoupling of Silanes and Alcohols. *ACS Catal.* **2011**, *1* (7), 698–702. <https://doi.org/10.1021/cs2001016>.
- (553) Ventura-Espinosa, D.; Carretero-Cerdán, A.; Baya, M.; García, H.; Mata, J. A. Catalytic Dehydrogenative Coupling of Hydrosilanes with Alcohols for the Production of Hydrogen On-Demand: Application of a Silane/Alcohol Pair as a Liquid Organic Hydrogen Carrier. *Chemistry – A European Journal* **2017**, *23* (45), 10815–10821. <https://doi.org/10.1002/chem.201700243>.
- (554) Ventura-Espinosa, D.; Sabater, S.; Carretero-Cerdán, A.; Baya, M.; Mata, J. A. High Production of Hydrogen on Demand from Silanes Catalyzed by Iridium Complexes as a Versatile Hydrogen Storage System. *ACS Catal.* **2018**, *8* (3), 2558–2566. <https://doi.org/10.1021/acscatal.7b04479>.
- (555) Porcar, R.; Mollar-Cuni, A.; Ventura-Espinosa, D.; V. Luis, S.; García-Verdugo, E.; A. Mata, J. A Simple, Safe and Robust System for Hydrogenation “without High-Pressure Gases” under Batch and Flow Conditions Using a Liquid Organic Hydrogen Carrier. *Green Chemistry* **2022**, *24* (5), 2036–2043. <https://doi.org/10.1039/D1GC03850H>.
- (556) Dai, Y.; Xing, P.; Cui, X.; Li, Z.; Zhang, X. Coexistence of Cu(II) and Cu(I) in Cu Ion-Doped Zeolitic Imidazolate Frameworks (ZIF-8) for the Dehydrogenative Coupling of Silanes with Alcohols. *Dalton Trans.* **2019**, *48* (44), 16562–16568. <https://doi.org/10.1039/C9DT03181B>.
- (557) Deyko, G. S.; Glukhov, L. M.; Kustov, L. M. Hydrogen Storage in Organosilicon Ionic Liquids. *International Journal of Hydrogen Energy* **2020**, *45* (58), 33807–33817. <https://doi.org/10.1016/j.ijhydene.2020.09.107>.
- (558) E. Schwarz, D.; M. Cameron, T.; Jeffrey Hay, P.; L. Scott, B.; Tumas, W.; L. Thorn, D. Hydrogen Evolution from Organic “Hydrides.” *Chemical Communications* **2005**, *0* (47), 5919–5921. <https://doi.org/10.1039/B511884K>.
- (559) Proceedings of the 2000 U.S. DOE Hydrogen Program Review. 995.

Table of Contents “Materials and Methods”

III. Materials and methods.....	101
III.1 Materials.....	101
III.1.1 Chemicals.....	101
III.1.2 Commercial catalysts.....	101
III.2 Experimental setups.....	102
III.2.1 Hydrogenation.....	102
III.2.2 Dehydrogenation.....	102
III.2.3 Kinetics	103
III.2.4 Activation energy.....	103
III.2.5 Computational details: DFT	103
III.3 Catalysts preparation methods	104
III.3.1 Treatment of the Ruthenium supported on alumina (Ru/Al ₂ O ₃) catalyst.....	104
III.3.2 Treatment of the Platinum supported on carbon (Pt/C) catalyst	104
III.3.3 Synthesis procedure of metal oxide supported Pt catalysts	105
III.3.4 Synthesis method of metal oxide supported Ru catalysts	105
III.4 Analysis of the LOHC	106
III.4.1 GC-MS Analysis.....	106
III.4.2 NMR spectroscopy.....	108
III.4.3 Fourier-Transfer InfraRed-Attenuated Total Reflectance (FTIR-ATR) spectroscopy ...	109
III.5 Analysis of the catalyst	110
III.5.1 X-ray Photoelectron Spectrometry (XPS)	110
III.5.2 FTIR-ATR	110
III.5.3 Raman spectroscopy	110
III.5.4 X-Ray Diffraction (XRD).....	111
III.5.5 ICP-OES	111
III.5.6 TGA and TGA-MS.....	111
III.5.7 TEM-EDX.....	112
III.5.8 Specific surface measurement by the Brunauer, Emmett and Teller (BET) method ..	114
III.5.9 Matrix Assisted Laser Desorption Ionization-Time of Flight (MALDI-TOF).....	116
III.5.10 Atmospheric Pressure Chemical Ionization (APCI-MS)	116
III.6 Definitions	117
III.6.1 Conversion.....	117
III.6.2 Selectivity	117
III.6.3 LOHC stability	117

Materials and Methods

III.6.4	Degree of Hydrogenation (DoH).....	117
III.6.5	Degree of Dehydrogenation (DoDH)	118
III.6.6	Calculation of the partial DoH during the cycling.....	119
	Bibliography.....	123

III. Materials and methods

This chapter is devoted to the materials, experimental setups and analytical equipment and procedures used during this thesis.

III.1 Materials

III.1.1 Chemicals

1-Cyclohexylethanol (98%) and Manganese acetate (>94%) was purchased from Alfa-Aesar.

Acetophenone (99%), $\text{H}_2\text{PtCl}_6 \cdot 6 \text{H}_2\text{O}$ (37.5% min. Pt basis), activated acidic, neutral and basic Brockmann I Al_2O_3 , Ethylbenzene (GC standard), 1-Phenylethanol (98%), Cyclohexylphenylketone (98%), Benzophenone (99%), Diphenylmethanol (99%), Diphenylmethane (99%), Fluoren-9-one (99%), 1,3,5-benzenetricarboxylic acid (>98%), Benzyl benzoate (99%), N-Bromosuccinimide (99%), Glacial acetic acid (99%+), Ruthenium trichloride, $x \text{H}_2\text{O}$ (45-55% Ru), Ruthenium acetylacetonate (97%), Sodium bisulfite (ACS reagent grade), Sodium thiosulfate (99%), Lithium hydroxide (98%), Sodium hydroxide (97%), Calcium hydroxide (95%), Potassium hydroxide (85%), Potassium carbonate (>99%), Sodium hydrogen phosphate (98.5%), Nickel hydroxide (60-70% Ni), Cobalt nitrate (>99%), Cerium nitrate, $6 \text{H}_2\text{O}$ (>99%), Iron chloride (97%), Iron sulfate hydrate (97%), Iron nitrate heptahydrate (97%), Potassium permanganate (99%), Manganese sulfate monohydrate (99.99%), Aluminum nitride (99.8%), 1,4-Dioxane (99.5%), Diethylether (>97.5%), Chloroform (99.8%), deuterated chloroform (99.8% D atom), Dichloromethane (>99%), Cyclohexane (>99%), N-Methylacetamide (99%) and various metal oxides (>99%) were purchased from Sigma-Aldrich.

Sulfuric acid (96%), Nitric acid (69.5%), Hydrogen chloride (37% Aq. Sol.) and Hydrogen peroxide (30% Aq. Sol.) were purchased from Carlos-Erba Reagents.

Ethylcyclohexane (99%+), Acetylcyclohexane (95%), Acetyl-1-cyclohex-1-ene (97%), 1,3-Diphenyl-1-butanone (97%), Fluorene (98%), Petroleum ether (solvent grade), Cyclohexylmethanol (99%), Melamine (99%), Tert-butyl hydroxyperoxide solution (70% AQ), Trichloroacetic acid (99%), Cesium hydroxide (96%), Aluminum hydroxide (98%), Sodium bromide (99%+), Sodium bromate (99.7%) and Gallium Nitride (99.99%) were purchased from Fisher-Bioblock.

Sodium iodide (99.5%) was bought from VWR.

All chemicals were used as received without any purification.

III.1.2 Commercial catalysts

5%Pt/ Al_2O_3 , 5%Pt/C, 5%Pt/C Evonik Noblyst P2061, 5%Ru/C, 5%Pd/ Al_2O_3 , 5%Pd/ CaCO_3 Evonik Noblyst P1151, 5%Cu/C, 5%Rh/ Al_2O_3 , 5%Rh/C and 20%Pt-10%Ru/C were supplied by Sigma-Aldrich (SA).

66%Cu/ZnO/MgO/ Al_2O_3 , 5%Ru/ Al_2O_3 , 5%Pd/C, 5%Pt/C sulfided and 5%Pt/graphite type 286 were supplied by Alfa-Aesar (AA).

Nickel/ SiO_2 - Al_2O_3 (66% Ni) was supplied by Fisher-Bioblock.

All catalysts were used as received, except when stated otherwise.

III.2 Experimental setups

III.2.1 Hydrogenation

Typically, Acetophenone (12.5 mL) and the heterogeneous catalyst (0.1 wt.% active metal to the substrate) were mixed together in a 50 mL Parr hydrogenation batch reactor (Figure III-1). The reactor was purged by three cycles of 10 bar N₂/atmospheric pressure, then one cycle 50 bar H₂/atmospheric pressure. The reactor was then pressurized with 50 bar H₂ and heated up at reaction temperature under strong stirring (1000 rpm). The flow of the H₂ inlet was controlled by a mass flow meter. The reaction started when a non-zero flow was detected by the mass flow and was used at the reaction start time. At the end of the reaction (4 h), the reaction mixture is filtered on a syringe filter (0.2 μm) before being analyzed by gas chromatography coupled with mass spectrometry (GC-MS). These conditions were chosen as they allow for advanced conversions and selectivities in 4 h.

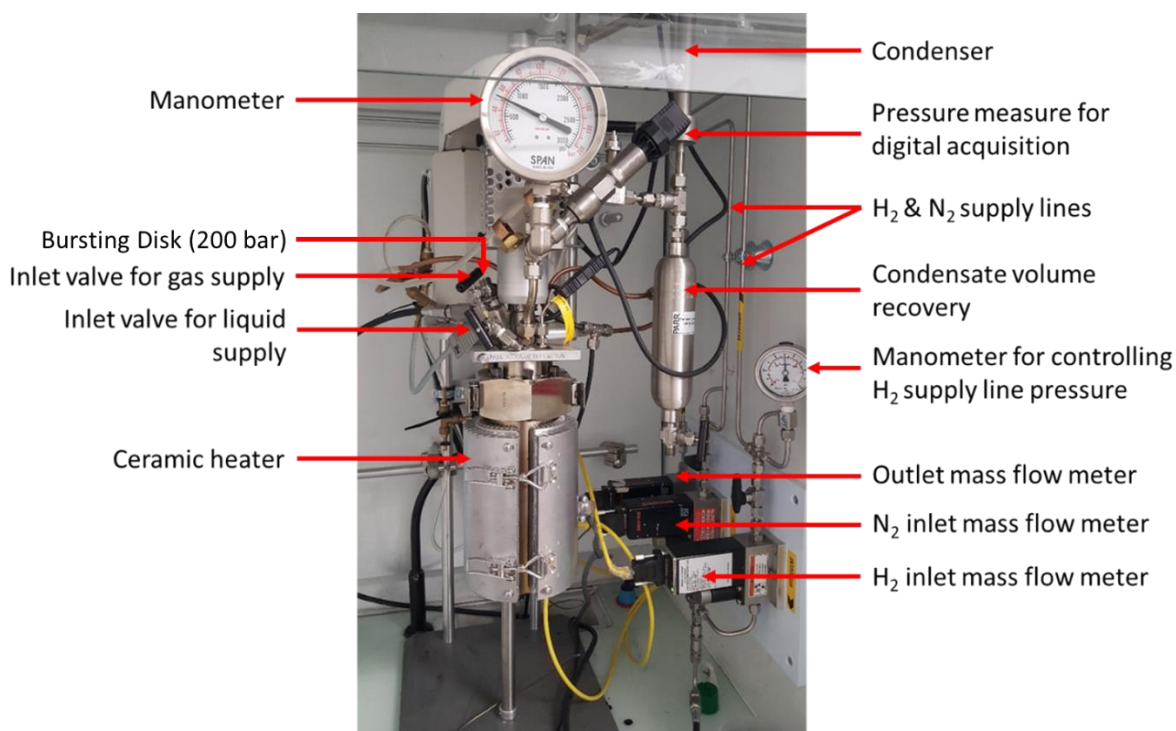


Figure III-1 - Hydrogenation setup.

III.2.2 Dehydrogenation

In a typical procedure, 2.5 mL of 1-Cyclohexylethanol (CHEA) and 5% Pt/C (1 wt% active metal to the substrate) were mixed together without a solvent in a 50 mL round-bottom flask connected to a condenser (Figure III-2) and stirred by a magnetic stirrer. The setup was purged by three cycles of vacuum/Argon before being heated under reflux of the LOHC (205 °C) and stirred at 1500 rpm for 18 h. The reaction start time was the time at which the temperature reached the reaction temperature. At the end of the reaction, the reaction mixture is filtered on a syringe filter (0.2 μm pore diameter) before being analyzed by GC-MS. These conditions were chosen as they allowed for advanced conversion and selectivity in 18 h.

Materials and Methods

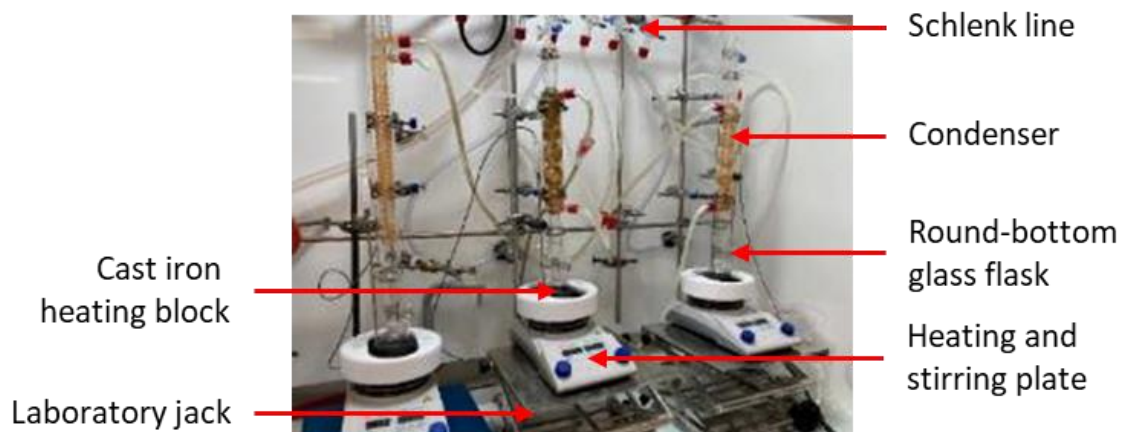


Figure III-2 - Dehydrogenation setups.

III.2.3 Kinetics

10 mL of CHEA were dehydrogenated with 0.25 wt% of the optimized Pt/C catalyst at 205 °C in argon atmosphere. Aliquots of the reaction mixture were sampled at regular time intervals: every 5 min before 15 min, then every 15 min until 1 h, then every hour until 8 h and finally every 2 h each day until the end of the reaction. These aliquots were analyzed by GC-MS, being beforehand diluted in the GC-MS solvent and filtered with a syringe filter (0.45 μm) to remove the catalyst.

III.2.4 Activation energy

The activation energy for each function of the LOHC system (cycloalkane/aromatic and alcohol/ketone) was measured during the dehydrogenation. Chemical kinetics were performed at different temperatures close to the boiling point of the LOHC (190, 205 and 210 °C) over a week, so that the equilibrium state could be achieved for each function at the desired temperature. The reactions were performed under a 10 mL/min flux of 5% H_2 in Argon in order to remove the concentration of H_2 as a parameter in the kinetics laws. As the kinetics laws of the reaction are highly complex for sequential and branched reversible reactions, a lumped kinetics approach was proposed to simplify the reaction mechanism. This approach is pertinent for complex kinetics systems and yields kinetic parameters with good accuracy.¹ Aliquots of the reaction mixture were sampled at regular time intervals and were analysed by GC-MS, being beforehand diluted in the GC-MS solvent and filtered with a syringe filter (0.45 μm) to remove the catalyst.

III.2.5 Computational details: DFT

All computations have been performed with the Gaussian 16 Rev C.01 suite, using the hybrid meta-GGA functional M06-2X and the basis set 6-311+G(2d,p) for all elements.²⁻⁵ Such parameters are known to predict accurately the thermochemistry of main-group compounds in the ground-state as well as polyenes systems.³ Each structure is solvated in Acetophenone using the SMD model which is recommended to compute thermochemical parameters. Frequency calculations were performed on the optimized structures using the same parameters; all structures were verified to possess no imaginary frequencies.

III.3 Catalysts preparation methods

III.3.1 Treatment of the Ruthenium supported on alumina (Ru/Al₂O₃) catalyst

The catalyst was calcined at 400 °C for 4 h in dry air (5 °C/min, 100 mL/min) and then reduced at 250 °C for 4 h in 2.5% H₂/Ar (2 °C/min, 100 mL/min). The reduced catalyst was stored in a storage box flushed with Argon. Further treatments for the preparation of the Ru/Al₂O₃ catalyst as supplied, activated and after hydrogenation are shown in the Figure III-3.

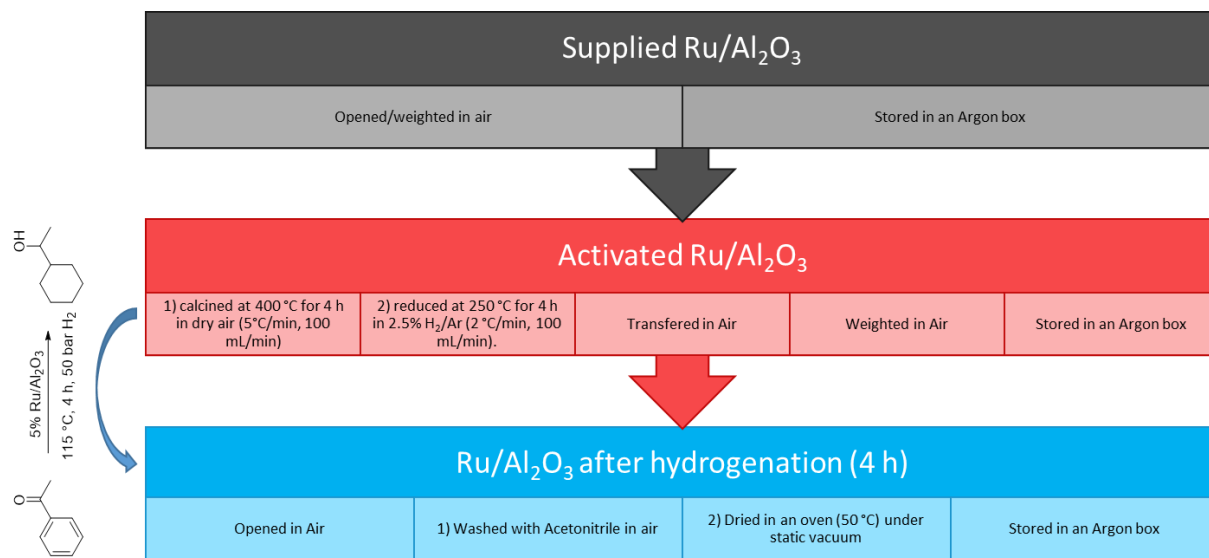


Figure III-3 - Treatments of the Ru/Al₂O₃ catalyst as supplied, activated and after hydrogenation

III.3.2 Treatment of the Platinum supported on carbon (Pt/C) catalyst

The catalyst was reduced at 280 °C for 4 h in 2.5% H₂/Ar (3 °C/min, 100 mL/min). The reduced catalyst was stored in a storage box flushed with Argon. Further treatments for the preparation of the Pt/C catalyst as supplied, activated and after hydrogenation are shown in the Figure III-4.

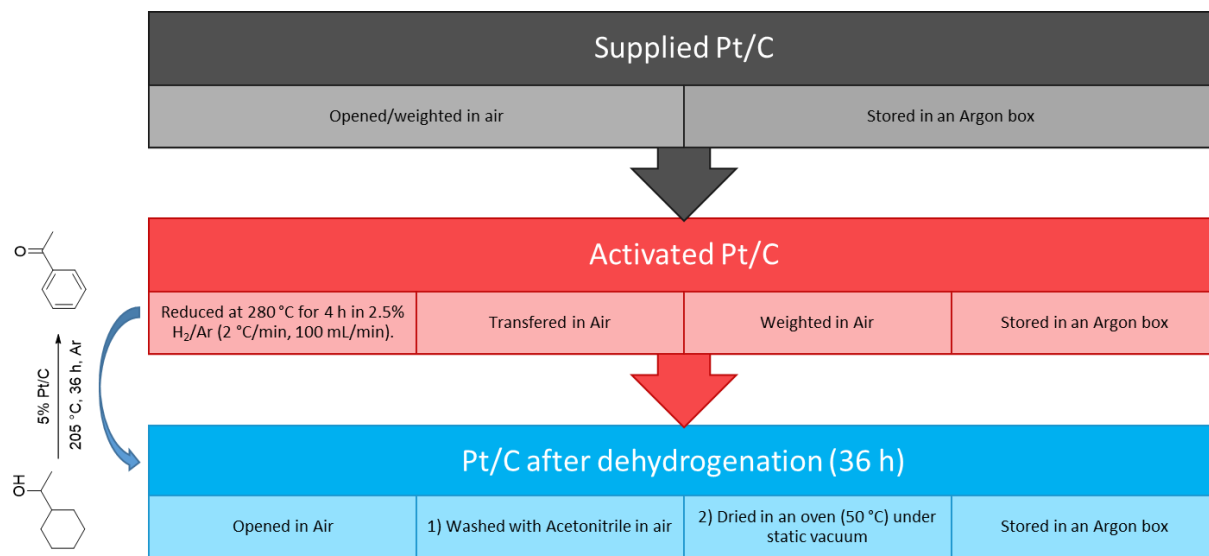


Figure III-4 - Treatments of the Pt/C catalyst as supplied, activated and after hydrogenation

Materials and Methods

III.3.3 Synthesis procedure of metal oxide supported Pt catalysts

A wet-impregnation method was used for the preparation of al catalysts. Typically, for a Pt/Al₂O₃ catalyst, acidic Al₂O₃ (2.0 g) was mixed with an aqueous solution of H₂PtCl₆ (4.5 g Pt per L), with the volume of the latter being tuned to the target loading of Pt, and the slurry was stirred at room temperature until the water was evaporated. The solid mixture was then dried at 100 °C in air overnight in an oven. The resulting solid was milled into a fine powder and then calcined in air (550 °C, heating rate: 3 °C/min). The calcined catalysts were reduced in a tubular oven under Ar/H₂ flow (2.5%; 100 mL/min) at a selected temperature (250 °C, heating rate 2 °C/min) for 2 h (Table III-1).

	Step	Gas	Gas flux	Time	Temperature (°C)
Calcination	Ramp	Dry air	100 mL/min	3 h	550 °C (3 °C/min)
	Hold	Dry air	100 mL/min	4 h	550 °C
	Ramp	Dry air	100 mL/min	As fast as possible (0)	0 °C
Reduction	Ramp	2.5%H ₂ /Ar	100 mL/min	1 h 40	250 °C (2 °C/min)
	Hold	2.5%H ₂ /Ar	100 mL/min	2 h	250 °C
	Ramp	2.5%H ₂ /Ar	100 mL/min	As fast as possible (0)	0 °C

Table III-1 – Heating program used for the preparation of Pt catalysts supported on metal oxides.

III.3.4 Synthesis method of metal oxide supported Ru catalysts

The catalysts are synthesised by wet-impregnation with 5 mL of a RuCl₃ solution (15 mg/mL) to produce a series of 3 wt.% Ru catalysts supported on metal oxides and hydrotalcites catalysts. The slurry was stirred at room temperature until the water was evaporated. After impregnation, the samples were maintained at room temperature for 12 h and then dried at 100 °C for 24 h. Following that, it was calcined at 400 °C for 4 h and then reduced at 250 °C for 2 h (Table III-2).

	Step	Gas	Gas flux	Time	Temperature (°C)
Calcination	Ramp	Dry air	100 mL/min	6 h 40	400 °C (1 °C/min)
	Hold	Dry air	100 mL/min	4 h	400 °C
	Ramp	Dry air	100 mL/min	As fast as possible (0)	0 °C
Reduction	Ramp	2.5%H ₂ /Ar	100 mL/min	1 h 40	250 °C (2 °C/min)
	Hold	2.5%H ₂ /Ar	100 mL/min	2 h	250 °C
	Ramp	2.5%H ₂ /Ar	100 mL/min	As fast as possible (0)	0 °C

Table III-2 – Heating program used for the preparation of Ru catalysts supported on metal oxides.

III.4 Analysis of the LOHC

III.4.1 GC-MS Analysis

Gas-Chromatography-Mass Spectrometry is a destructive analytical technique. It cumulates the advantages of the Gas-Chromatography that consists in the gas phase separation of the different compounds present in a sample and Mass Spectrometry that detects and identifies the compounds depending on their mass over charge ratio (m/z). Briefly, the liquid sample is first vaporized in the injector and the gases are pushed by a flux of carrier gas (mobile phase) in a capillary chromatography column (stationary phase) built in an oven. The interactions by adsorption between the mobile and stationary phases induce a separation of the chemicals. This effect is improved by a temperature program that modifies the relative affinity of the species and reduces the analysis time. At the end of the column, the separated chemicals enter the mass spectrometry part of the equipment at different times, namely retention times, where they are ionized under an electron beam before being detected depending on their mass-charge ratio. The spectrometer then separates the charged species from the uncharged species and counts the number of each m/z ion, yielding a total ion count at each retention time. The collected ions can then be compared to a database for identification.

The principal advantage of GC-MS analysis is the analysis sensitivity that is able to detect traces of compounds in complex mixtures (mg/L range). Moreover, quantification of these species can be easily performed, providing that calibration curves have been previously recorded.

Nevertheless, GC-MS has numerous limitations. During the injection, unstable compounds can be degraded by the high temperature. Moreover, heavier species that cannot be vaporized will not be observed which would limit the quantification of condensation products in the further experiments. The column temperature is limited by the column type, especially the stationary phase stability. Also, different temperature programs must be tested to ensure that all chemical compounds have peaks that are well defined. Concerning the separation, diastereoisomers can be separated while enantiomers cannot. Finally, the identification can be difficult and/or imprecise at times due to the limited molecules present in the database.

During this thesis, the identification and composition of the reaction crude mixtures were performed by a 7820A Agilent GC-MS (5977E MSD) with a 7693A Autosampler. The column was a 30 m, 0.25 mm diameter, 0.5 μm film HP-INNOWAX. Helium was used as the carrier gas (1 mL/min). To perform the analysis, the crude reaction mixtures were diluted (1:250 wt%/wt%) with an acetonitrile solution containing 0.25%vol. 3-octanone as internal standard. A split ratio of 1:20 was applied to the 1 μL injection. The heat program was: initial oven temperature 50 $^{\circ}\text{C}$, final oven temperature 260 $^{\circ}\text{C}$ for 6 min, program rate 25 $^{\circ}\text{C}/\text{min}$. The relative response factors (RFF) of each commercially available compound were obtained by dividing the compound peak area by the peak area of the internal standard. Calibration curves were then plotted to verify the linearity range of the RFF. An example is presented in Figure III-5.

Materials and Methods

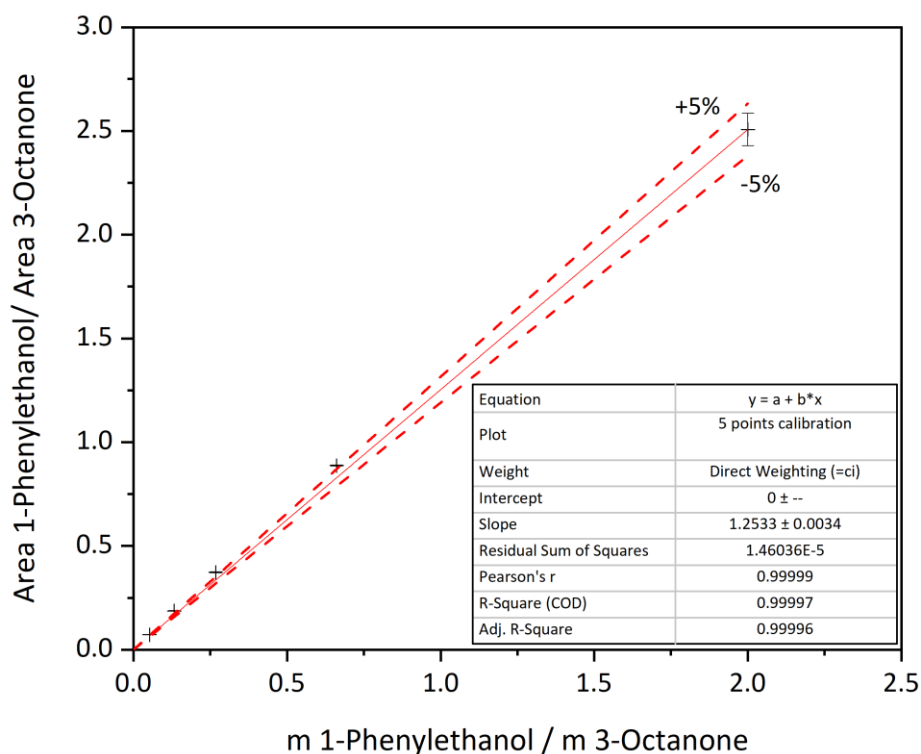


Figure III-5 - Calibration curve of the 1-Phenylethanol with 3-octanone as the internal standard. The calibration points fit between the +/-5% curves.

All calibrated compounds have error bars below 5% of the measured value. Therefore, a relative error of 5% will be accounted for each GC-MS analysis. Commercially unavailable chemicals (e.g. Bis(phenylethyl) ether) were supposed to have a response factor similar to that of already calibrated akin or related products (e.g. 1-Phenylethanol), but the error on these measure should be increased to 20% to reflect the absence of proper calibration curve (Table III-3).

Molecule	Abbreviation	Chapter	Relative response factor	GCMS error
Ethylcyclohexane	EC	1 and 2	0.59	±5%
Ethylbenzene	EB	1 and 2	0.84	±10%
Acetylcyclohexane	ACH	1 and 2	0.74	±5%
Acetyl-1-cyclohex-1-ene	ACHN	1 and 2	0.76	±5%
1-Cyclohexylethanol	CHEA	1 and 2	0.75	±5%
Acetophenone	APO	1 and 2	0.69	±5%
1-Phenylethanol	PEO	1 and 2	0.64	±5%
Hydrogenated ether	12H-ROR	1 and 2	Supposed equal to CHEA	±20%
Dehydrogenated ether	0H-ROR	1 and 2	Supposed equal to PEO	±20%
Hydrogenated coupling product	12H-Coupling	1 and 2	Supposed equal to 0H-Coupling	±20%
Partially dehydrogenated coupling product	6H-Coupling	1 and 2	Supposed equal to 0H-Coupling	±20%
Dehydrogenated coupling product	0H-Coupling	1 and 2	1.71	±5%
Dicyclohexylmethanol	DCMA	2 and 3	2.09	±5%
Dicyclohexylmethylketone	DCMK	2 and 3	Supposed equal to CPMK	±20%
Cyclohexylphenylketone	CPMK	2 and 3	2.15	±5%

Materials and Methods

Benzophenone	BPO	2 and 3	2.12	±5%
Diphenylmethanol	DPMA	2 and 3	2.08	±5%
Diphenylmethane	DPM	2 and 3	2.92	±5%
Hydrogenated forms of Diphenylmethane	-	2 and 3	Supposed equal to DPM	±20%
Fluoren-9-one	FLUK	3	2.36	±5%
Fluorene	FLU	3	2.80	±5%

Table III-3 – Relative response factors and associated GC-MS error.

Moreover, the RFF variation between samples of similar molecular weight (Ethylcyclohexane, Ethylbenzene, Acetylcyclohexane, Acetyl-1-cyclohex-1-ene, 1-Cyclohexylethanol, Acetophenone and 1-Phenylethanol) is less than 12%. Thus, the RFF of the same LOHC at different hydrogenation/dehydrogenation states are similar and can be assimilated to the same RFF value in a first approximation.⁶

A typical GC spectrum of the 1-Cyclohexylethanol/Acetophenone couple is presented in Figure III-6.

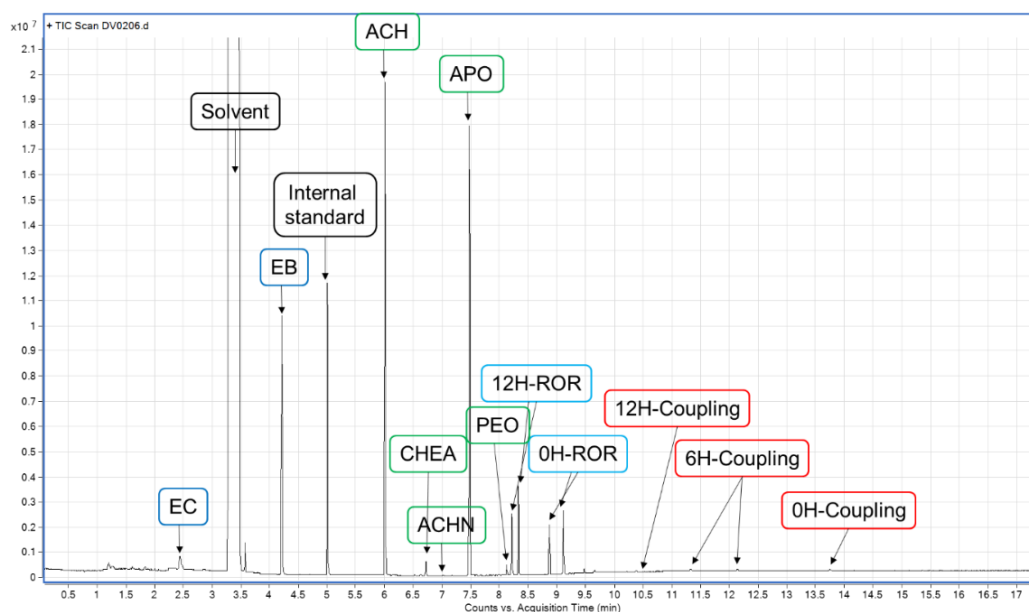


Figure III-6 - Typical GC spectrum after reaction with different molecules in Acetonitrile with 3-Octanone as the internal standard. Acetophenone (APO), Acetylcyclohexane (ACH), 1-Cyclohexylethanol (CHEA), 1-Phenylethanol (PEO), Ethylbenzene (EB), Ethylcyclohexane (EC), Hydrogenated and dehydrogenated ethers (12H-ROR and OH-ROR resp.) and aldolisation-crotonisation products (12H-Coupling, 6H-Coupling and OH-Coupling).

III.4.2 NMR spectroscopy

Nuclear Magnetic Resonance (NMR) spectroscopy is a non-destructive analysis technique based on the magnetic properties of the atomic nuclei. When the atomic spin is different from zero, the application of a uniform magnetic field and their excitation by a calibrated radio frequency allows for the detection of the desired atom (H, C, ...). The resolution of the spectra is dependent on the strength of the applied magnetic field B_0 . The resonance frequency ν_0 of each atom is approximated by the equation (III-1):

$$\nu_0 = \frac{\gamma}{2\pi} B_0 \quad (\text{III-1})$$

Materials and Methods

With γ the gyromagnetic ratio of the particle. However, due to the presence of electrons, the magnetic field around the atoms is slightly modified through a shielding effect σ . Therefore, each nuclei has its own frequency ν_L calculated by the equation (III-2):

$$\nu_L = \nu_0(1 - \sigma) \quad (\text{III-2})$$

The frequency difference between ν_0 and ν_L is called chemical displacement and is often characteristic of the chemical composition/binding of the atom. NMR spectroscopy is particularly useful as it can analyze different isotopes of the same element and their interaction with the neighboring atoms. NMR spectra can be interpreted to uncover the number of neighbor atoms, the chemical bond type (e.g. alkane, alkene, alkyne), the molecular conformation/configuration of chiral centers, interatomic distances, and so on.

In organic chemistry, ^1H and ^{13}C are particularly used to identify purified substances and measure the substances concentration in non-complex mixtures. The purified compounds are often diluted in a deuterium-enriched solvent. Indeed, due to the spin difference between H and D (1/2 and 1 resp.), only traces of the matrix is visible and can be used by the machine as a calibration point for the chemical displacement.

However, limitations of this technique can be observed for complex mixtures of similar products as the signals of similar nuclei will often superimpose. Moreover, trace quantification (below 1%) is often difficult to estimate reliably due the background noise. Finally, chemical binding to paramagnetic nuclei diminishes the sensitivity of the NMR signal.

During this thesis, NMR analysis was used to analyze the purity of synthesized molecules. All NMR analysis were performed on a 400 MHz BRUKER NMR spectrometer with deuterated chloroform CDCl_3 as the solvent.

III.4.3 Fourier-Transfer InfraRed-Attenuated Total Reflectance (FTIR-ATR) spectroscopy

FTIR is based on the non-destructive adsorption of infrared light by a sample. The advantage of a FTIR spectrometer is the simultaneous collection of a wide range of frequencies comparatively to dispersion spectrometer that are limited in their analytical range. However, FTIR requires a processing of the obtained signal by Fourier transform to obtain the spectral result. Its combination with the Attenuate Total Reflectance (ATR) method allows determining the chemical bonds nature of a sample by simply depositing the substance to be analyzed on a high density ATR crystal. The measurement method uses the optical principle of reflectance at high incidence angle θ . This specific position allows for a beam of defined wavelength to penetrate only slightly the sample (evanescent wave). The beam induces vibrations of chemical bonds and as the resonance frequency is characteristic to each bond nature, the dedicated wavelength intensity is attenuated by passing through the sample (attenuated reflected beam) (Figure III-7).

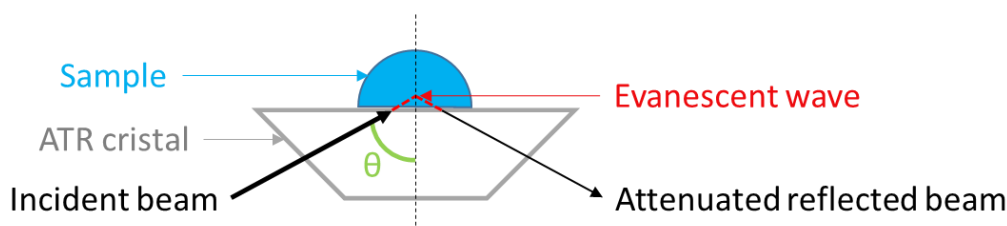


Figure III-7 - Principle of the ATR.

While this technique is particularly useful to assess which chemical functions are present in a sample, rigorous identification of an unknown structure can be complicated. In addition, a compound mixture is much more difficult to analyze with the high detection limits (5-20%) in the case of unknown compounds. FTIR analysis is also dependent on the vibration mode, thus not all structures, especially inorganic, are active in FTIR-ATR.

In this thesis, FTIR-ATR was used to assess the chemical functions present in the purified molecule as well as on the catalysts surface. All FTIR-ATR spectra of the catalysts were acquired on a Vertex 70 Bruker spectrometer.

III.5 Analysis of the catalyst

III.5.1 X-ray Photoelectron Spectrometry (XPS)

XPS is a non-destructive photoelectronic technique that uses a monochromatic X-ray beam to bombard the sample. The X-rays remove core electrons from the atom that are then detected. The emitted photoelectron energy is linked to the core electrons ionization energy, which is characteristic of the element. Small variations around the main peak are attributed to different oxidation states of the elements, with higher oxidation states being displaced to higher energies. By comparison with calibrated peak values, the sample composition can be uncovered. Elemental traces (>0.1%) can be observed, but quantification is pertinent only if the element is present in more than 5% concentrations. The quantification and comparison between samples can be performed by normalization and peak area deconvolution. XPS is versatile as it can be used on all solid materials and has a detection depth of roughly 10 nm.⁷ However, quantification is highly dependent on the material homogeneity. Finally, only elements with core electrons can be detected, therefore Hydrogen and Helium cannot be analyzed by XPS.

In this thesis, the catalysts were analyzed by XPS after three different steps: as received, after activation and after reaction (hydrogenation or dehydrogenation) in order to assess the oxidation state of the active metal as well as the support. A monochromatic beam (X-ray source Al K α 1486.6 eV) of 100 μ m in diameter and 24.9 W of power was focused on the surface of the samples. High resolution core level analyses were performed using a pass energy of 23.9 eV, which corresponds to an energy resolution of 0.6 eV. All XPS measurements were carried out under ultrahigh vacuum conditions (7×10^{-8} Pa). Each core level peak was recorded within ten scans with a scan rate of 0.1 eV/s. The binding energy calibration was performed using the C 1s peak shifted at 285 eV. The core level binding energies were recorded within an error of ± 0.1 eV. Curve fitting and background subtraction were accomplished using Casa XPS software.

III.5.2 FTIR-ATR

See III.4.3

III.5.3 Raman spectroscopy

Much like FTIR-ATR, Raman spectroscopy uses vibrational modes of molecules. A beam of light emits non-destructive photons that interacts by inelastic scattering with the molecular bonds. The molecular vibrations modify the energy of the laser photons, indicating which vibrational modes are present in the structure. However, much like FTIR-ATR, not all vibrational modes are observable by Raman spectroscopy, and both techniques are usually complementary.

Materials and Methods

In this thesis, the catalysts, in particular the presence of surface metal oxides, were analyzed by Raman spectroscopy with a Renishaw In Via Raman spectrometer, with a LWD 50 objective micro-Raman backscattering configuration and a 532 nm excitation laser.

III.5.4 X-Ray Diffraction (XRD)

XRD uses the non-destructive diffraction of X-ray on crystalline structures. Indeed, the crystalline planes create constructive and destructive interferences with the X-ray beam. Constructive interferences can be determined by the Bragg law (III-3):

$$2d \sin \theta = n\lambda \quad (\text{III-3})$$

With d the distance between two crystallographic planes, θ the half-angle of deviation corresponding to the half-angle between in incident beam and the detector direction, n the order of reflexion (n being a natural number) and λ the wavelength of the X-ray beam. Comparison of the detected interferences in function of the angle with the PDF4+ database allows for the phase identification.⁸ While this technique is particularly useful to analyze crystalline structures, amorphous structures cannot be analyzed. However, XRD allows for phase segregation of same composition, crystallite size estimation and phase structure estimation.

In this thesis, XRD spectra of the catalysts were acquired on a BRÜKER D8 ADVANCE A25 spectrometer. The X-rays source was a Copper tube, radiation $\text{Cu K}\alpha = 1.5406 \text{ \AA}$ at 40 kV and 40 mA. The analysis was performed in a rotating mode with an automated anti-diffusion blade to avoid diffusion at lower angles. The diffusion gap was automatically adapted during the analysis.

III.5.5 ICP-OES

Inductive Coupled Plasma optical emission spectroscopy (ICP-OES) is a destructive technique used to quantify simultaneously the amount of elements in a sample. After digestion of all solid products by a strong acid, the sample is ionized in an argon plasma. The ionization creates excited electrons that emit photons when they go back to their fundamental state. As the emitted wavelength is characteristic of the element, analysis of the emitted light allows for elemental identification and its intensity can be compared to a calibration curve to estimate the element quantity. Its advantages are the rapid analysis of almost all elements of the periodic table (except the hydrogen, rare gases, carbon, oxygen, nitrogen and unstable or volatile elements such as mercury) with a low detection limit as well as isotopic ratio analysis. However, this technique is quite expensive and the preparation can be complicated if the sample is not easily mineralized.

In this thesis, ICP analysis was conducted to quantify the amount of active metal on the catalyst. The results were obtained by an ICP-OES 725 Agilent equipment. Prior to analysis, 100 mg of each sample was digested in aqua regia during 24 h, then digested samples were diluted to appropriate concentrations to be analyzed by ICP-OES.

III.5.6 TGA and TGA-MS

ThermoGravimetric Analysis (TGA) is a destructive technique that consists in measuring the weight variation of a sample in function of the time and the temperature. By quantifying the weight gains or losses, sample modification (weight loss, oxidation, reduction, decomposition, ...) can then be interpreted. This analysis can be conducted under different gases in order to estimate the effect of the gas on the process.

Materials and Methods

Nevertheless, the weighting system is extremely sensible to variations and then must be isolated. In addition, rigorous sample composition analysis (e.g. XRD) must be conducted prior and after the thermal treatment to identify the phase modification.

In this thesis, TGA and its derivative TGA coupled with mass spectroscopy (TGA-MS) was used to estimate the calcination and reduction temperatures as well as observe the volatile species formed during these processes.

For the TGA analysis, all samples were analyzed under dry air with a 10 °C/min ramp up to 700 °C on a Labsys Evo Setaram equipment.

For the TGA-MS analysis, analysis were carried out by TGA-MS (STA 449 F1 - QMS AEOLOS) in dry air (10 °C/min, 500 °C) to simulate the calcination of the catalyst during the activation and in 2% H_2/Ar (5 °C/min, 500 °C) to simulate the reduction of the catalyst during the activation. Mass identification of the volatile compounds was by screening the m/z ratio related to H_2O , CO_2 , O_2 and the corresponding metal oxides.

III.5.7 TEM-EDX

Transmission electron microscopy (TEM) is a non-destructive technique that uses an electron gun under vacuum to create an image of a sample by transmission of electrons, obtaining resolution in the order of the angström. This higher resolution compared to classic optical microscopes originates from the smaller wavelength of the electrons. Moreover, electron lenses are required to afford a good focalization and contrast of the electron beam for the imaging. Optical aberrations such as astigmatism must also be corrected. Finally, by using different apertures of the intermediate lenses, two analysis modes are available (Figure III-8).

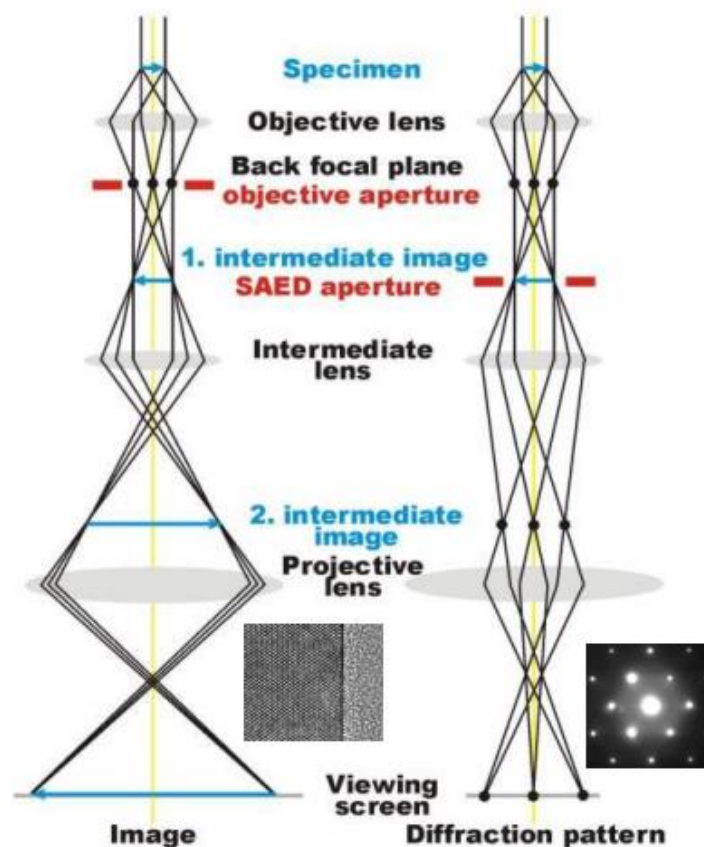


Figure III-8 - Imaging and diffraction modes of a TEM.⁹

Materials and Methods

The imaging mode allows for the formation of an intermediate image that is then projected to form an image on the viewing screen. Conversely, diffraction patterns equivalent to X-ray patterns can also be produced by using a Selected Area Electron Diffraction (SAED) aperture. The electrons are scattered by the atomic planes, in particular the nucleus and electronic cloud of the atoms composing the crystalline planes. However, in the case of electron diffraction, the incident beam must be almost parallel to the crystalline planes in order to occur. Bright spots induced by the electron scattering corresponds a reflection at the lattice planes and the Miller indices of the planes (h, k, l) can be deduced by measuring the distance between the bright spots in the reciprocal space.⁹

Nonetheless, numerous technical limitations must be taken into account. First, only no volatile materials can be observed by TEM due to the extreme vacuum present in the analysis chamber. Moreover, the sample preparation can be complicated as it must be thin enough so that electrons can pass through it. Thus, the analysis is time-intensive and requires specific training. In addition, the analysis field is reduced, which might induce interpretation errors in the case of inhomogeneous samples. Lastly, the electron beam can damage the material, in particular for unstable or biological systems.

The principle of Energy-Dispersive X-ray spectroscopy (EDX) revolves around the interaction between the sample atoms and X-rays that acts as an excitation source. The removal of an electron shell by the X-ray beam allows for the transition from an electron of the outer shell to the inner shell, emitting X-ray, also called secondary emission, in the process. This secondary emission is collected in a specific energy dispersive detector located close to the sample area. As each atomic structure has its own characteristic properties, the X-ray emissions can be related to the relative elemental composition. However, the quantification is dependent on nature of the sample as some X-ray emission peaks might overlap. Finally, the X-ray emissions are isotropic and can be attenuated by the sample it has to go through (density). Therefore, corrections have to be implemented on each sample to ensure that the quantification is pertinent.

The combination between TEM and EDX analysis allows for the correlation between elemental composition and their localization on the imaged sample, which favors phase differentiation.

In this thesis, TEM-EDX was used to evaluate the size and distribution of the supported nanoparticles. The size distribution of each catalyst was obtained by manually measuring the diameter of 200 particles with the Fiji software¹⁰ and following analytical treatment of the data by the Origin software.¹¹ The catalysts were observed with a TEM/STEM apparatus (Tecnai Osiris, FEI) equipped with a High Angle Annular Dark Field (HAADF) detector and an Energy Dispersive Spectroscopy (EDS) microanalysis system (Esprit, Bruker Nano GmbH) connected to four quadrant silicon drift detectors (ChemiStem technology, FEI). The acceleration voltage was 200 kV.

III.5.8 Specific surface measurement by the Brunauer, Emmett and Teller (BET) method

BET analysis is based on the physical adsorption theory of gas molecule (adsorbate) on a solid surface (adsorbent) hypothesizing that the adsorption forms a gas monolayer on the surface. At constant temperature, an equilibrium between the gas phase adsorbate and the adsorbed phase is only dependent on the gas pressure. This mechanism is analogous to the liquid/gas phase equilibrium with the saturated vapor pressure noted P^0 . The variation of the gas pressure P modifies the P/P^0 ratio also known as the relative equilibrium pressure. The adsorption isotherms can be classified depending on their shape (Figure III-9).

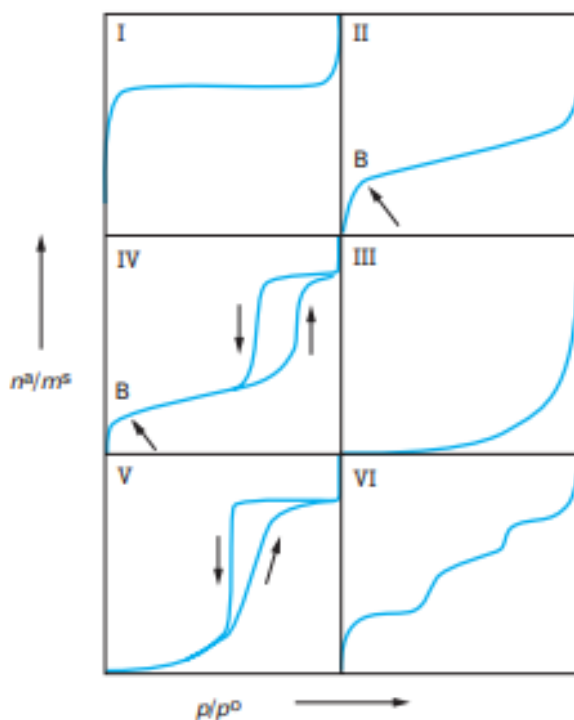


Figure III-9 – IUPAC classification of physical adsorption isotherms.¹²

Here, the isotherm I corresponds to a structure composed only of micropores. Conversely, the isotherm II corresponds to a macroporous structure where multimolecular adsorption occurs. The isotherm IV occurs on mesoporous materials with capillary condensation. The hysteresis comes from the irreversibility of the capillary condensation. The isotherms II, IV and VI are more rare and observed in the case of limited adsorbate/adsorbent interactions (III and V) and multilayer adsorption on energetically homogeneous surfaces (VI). The interpretation of the different phases of the adsorption is presented in Figure III-10.

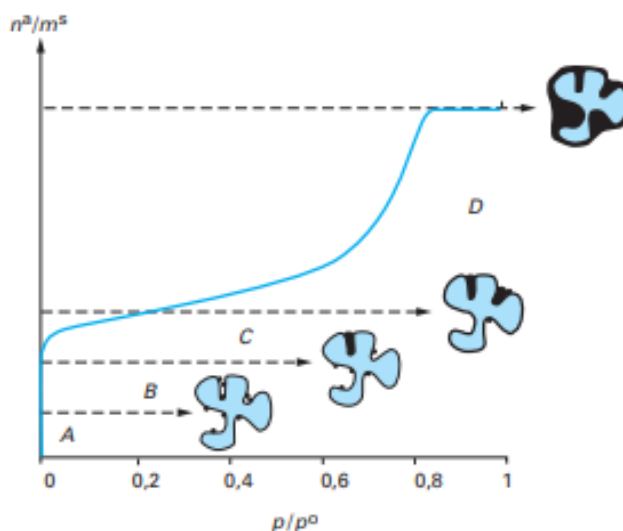


Figure III-10 – Interpretation of the physical adsorption isotherm of a type I + type IV composite material.¹²

In the phase A, the adsorbate adsorbs on the defects of the structure in an incomplete monolayer. In the phase B, micropores are filled due to their lower relative equilibrium pressure. Phase C sees the formation of a monolayer of adsorbate. At the end of this phase, the entire surface can be considered to be covered by an adsorbate monolayer. Finally, the adsorbent is covered by multilayer of adsorbate in the phase D.

The interpretation of these isotherms allows for the determination of the specific surface a by the equation (III-4):

$$a = \frac{A}{m^s} = \left(\frac{n_m^a}{m^s} \right) N_A \sigma_m \quad (\text{III-4})$$

With n_m^a the adsorbate quantity to cover the whole surface of the solid by a monolayer, m^s the weight of the adsorbate, N_A the Avogadro constant and σ_m the area covered by one molecule on the surface. The later value is obtained by the equation (III-5):

$$\sigma_m = f \left(\frac{M}{\rho_L N_A} \right)^{2/3} \quad (\text{III-5})$$

With f the compacity of the monolayer (equal to 1.091 for a hexagonal compact packing), M the molecular weight of the adsorbate and ρ_L the volumic density of the liquid adsorbate. In the case of N_2 , $\sigma_m = 0.16527 \text{ nm}^2$ at 77.4 K.¹²

Mesoporous materials can have their pore diameter estimated by the equation (III-6):

$$d_p = \frac{4V_p}{a} \quad (\text{III-6})$$

With V_p the specific mesoporous volume evaluated from the saturation plateau and considering that all N_2 is liquid inside the pores.

The catalysts were analyzed by BET adsorption on a BELSORP-MAX with N_2 as the sorption/desorption gas to obtain the specific surface and the pore size.

Materials and Methods

III.5.9 Matrix Assisted Laser Desorption Ionization-Time of Flight (MALDI-TOF)

MALDI-TOF is a mass spectroscopy analysis that couples an ionization source assisted by a matrix and a time of flight analyzer. The ionization source assisted by a matrix favors the desorption and ionization of heavy chemical compounds while the time of flight analyzer facilitates the identification of the m/z ratio by kinetically accelerating the produced ions by an electric field. As the ions speed is dependent of their m/z ratio with bigger ions being slower, time measurement to reach the detector simplifies the identification of the compounds. Moreover, the use of a reflectron (ion mirror) focalizes and increases the time of flight, which improves the resolution. (Figure III-11)

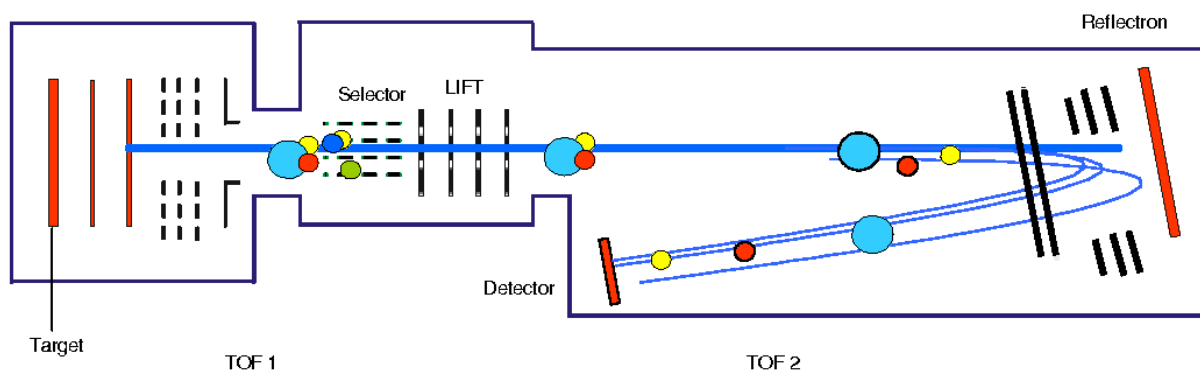


Figure III-11 – Principle of MALDI-TOF.¹³

However, while this technique is pertinent for high molecular weight ($m/z > 500$), low molecular weight molecules cannot be analyzed. In addition, the matrix favoring the ionization will also be apparent on the spectrum and might prove problematic at m/z values inferior to 500. Finally, this analysis is not quantitative.

In this thesis, MALDI-TOF analysis was performed on an AutoFlex Speed from Bruker Daltonics in positive reflectron mode to assess the presence of oligomers in the reaction mixture after cycling of the LOHC. The m/z range was 120 to 8600. The acceleration voltage of "source ion 1" (IS1) is set to 19 kV and that of "source ion 2" (IS2) is 16.65 kV. The pulse ion extraction delay (PIE) is 120 ns. An external calibration was performed using the Bruker Daltonics "Peptide Calibration Standard II" mixture. The samples were prepared with the following procedure. The matrix used was a 2 mg/ml Dithranol solution in THF. The samples were solubilized in acetonitrile and rediluted in THF if necessary. 2 μl of the sample solution was mixed with 4 μl of the matrix solution. 1 μl of this mixture was deposited on the MALDI plate, dried at room temperature, then analyzed.

III.5.10 Atmospheric Pressure Chemical Ionization (APCI-MS)

APCI-MS is a gas-phase ionization technique where radical ions like $\text{N}_2^{\bullet+}$ are transferred to a molecule to be analyzed. APCI-MS is usually more energetic than electrospray ionization (ESI) MS but less fragmenting than electron ionization (EI), thus allows for the analysis of less ionizable molecules without fragmentation.

In this thesis, APCI-MS analysis was performed on an Amazon Speed from Bruker, APCI source, in positive and negative mode. The scan range was 50-1000 m/z with an accumulation time of roughly 500 μs . The capillary voltage was 6000 V and the corona was 5000 nA. A targeted mass of 300 m/z was used to assess the presence of oligomers in the reaction mixture after cycling of the LOHC and confirm the results in MALDI-TOF.

III.6 Definitions

III.6.1 Conversion

The conversion is calculated by either using the substance amount ratio of the starting material at the starting time $n_{SM;0}$ and after reaction $n_{SM;f}$ or the molar fraction of the starting material after reaction $mol\%_{SM;f}$ using the equation (III-7):

$$Conversion = n_{SM;0} - n_{SM;f} = 1 - mol\%_{SM;f} \quad (III-7)$$

III.6.2 Selectivity

The selectivity to the product i is calculated by the ratio between the molar fraction of i after the reaction $mol\%_{i,f}$ and the conversion using the equation (III-8):

$$Selectivity_i = \frac{mol\%_{i,f}}{Conversion} \quad (III-8)$$

III.6.3 LOHC stability

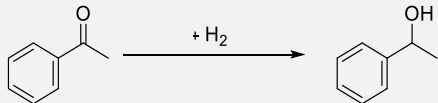
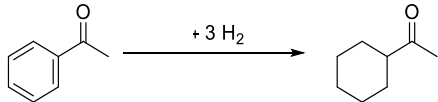
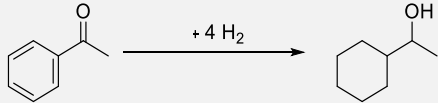
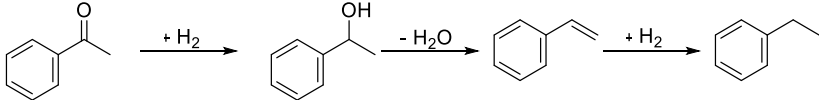
The LOHC stability represents an evaluation of the LOHC degradation through the formation of unwanted side-products. Similar to a carbon balance calculation, it consists of the sum of the molar percent of the starting material (SM), desired product (DP) and key-intermediates (KI), as shown in equation (III-9).

$$LOHC\ stability = mol\%_{SM} + mol\%_{DP} + mol\%_{KI} \quad (III-9)$$

III.6.4 Degree of Hydrogenation (DoH)

The degree of hydrogenation (DoH) is used during the hydrogenation to quantify the amount of H_2 stored by the system. Hydrogenation coefficients $C_{H,i}$ are used to qualify the amount of hydrogen stored by the system. The DoH is calculated by the equation (III-10) and examples of $C_{H,i}$ for the 1-Cyclohexylethanol/Acetophenone couple are presented in Table III-4.

$$DoH = \frac{Quantity\ of\ H_2\ stored}{Maximum\ theoretical\ H_2\ amount} = \frac{\sum_i (C_{H,i} \times mol\%_i)}{4} \quad (III-10)$$

Reaction (Hydrogenation)	Hydrogenation coefficients $C_{H,i}$
	+1
	+3
	+4
	+2

Materials and Methods

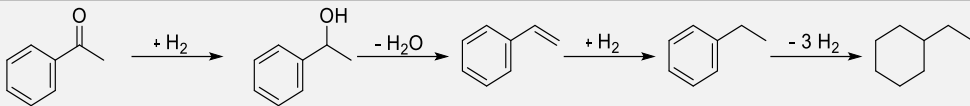
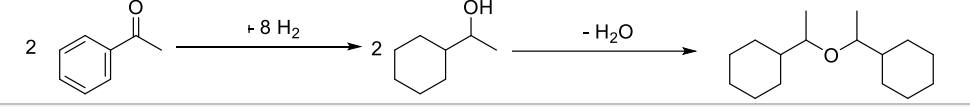
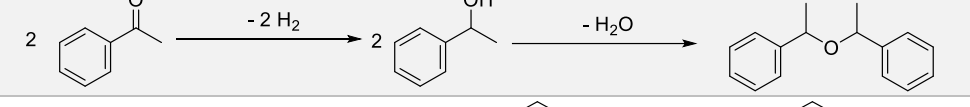
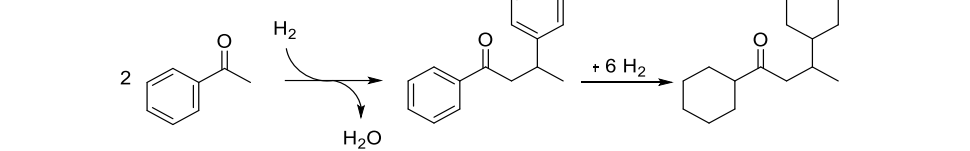
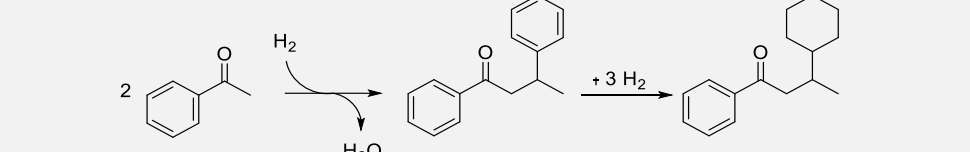
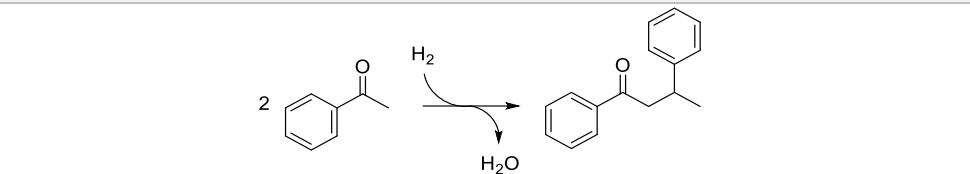
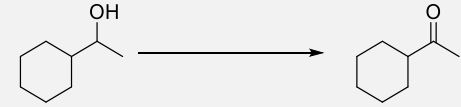

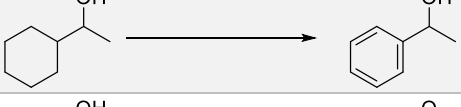
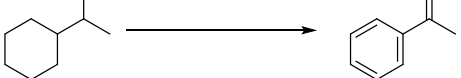
	+5
	8/2=+4
	2/2=+1
	7/2=+3.5
	4/2=+2
	1/2=+0.5

Table III-4 – Hydrogenation coefficients used for the DoH calculation of the 1-Cyclohexylethanol/Acetophenone couple.

III.6.5 Degree of Dehydrogenation (DoDH)

For the dehydrogenation, the catalyst performance is calculated in a similar fashion, by swapping DoH with DoDH and its associated coefficients (Table III-5) in the equation (III-11):

$$DoDH = \frac{\text{Quantity of } H_2 \text{ released}}{\text{Maximum theoretical } H_2 \text{ amount}} = \frac{\sum_i (C_{DH,i} \times mol\%_i)}{4} \quad (III-11)$$

Reaction (Dehydrogenation)	Dehydrogenation coefficients $C_{DH,i}$
	+1
	+2
	+3
	+4

Materials and Methods

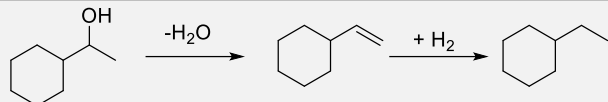
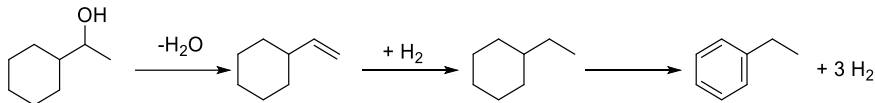
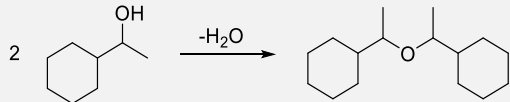
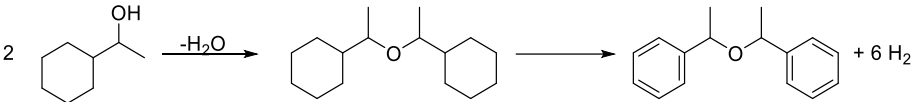
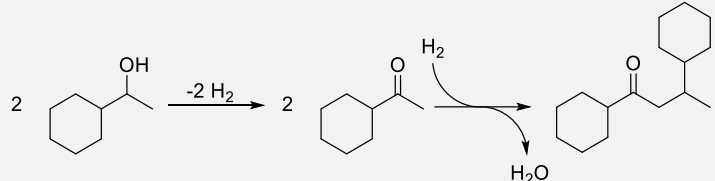
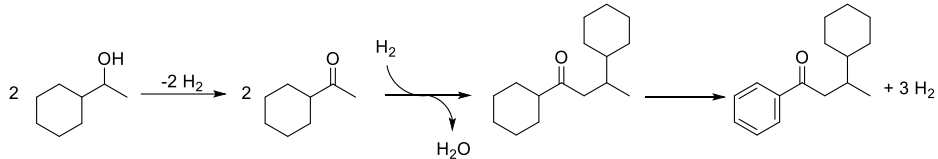
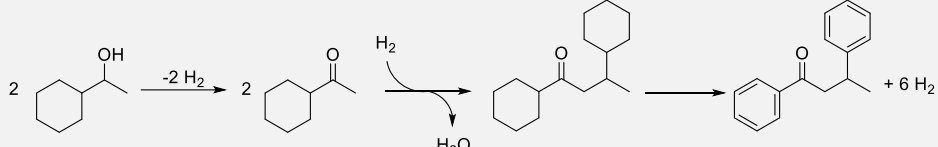
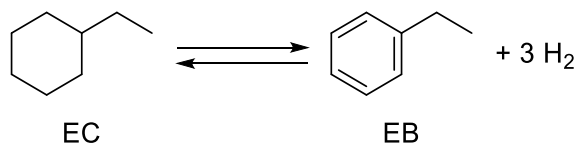
	-1
	+2
	0/2=+0
	6/2=+3
	1/2=+0.5
	4/2=2
	7/2=+3.5

Table III-5 - Dehydrogenation coefficients used for the DoDH calculation of the 1-Cyclohexylethanol/Acetophenone couple.

III.6.6 Calculation of the partial DoH during the cycling

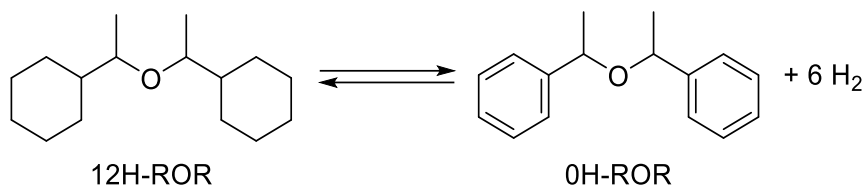
Upon multiple cycles, impurities form in the system, which change the maximum theoretical hydrogen storage capacity. Indeed, if the degradation molecules can absorb and release H₂, they must be taken into account in the calculations. In the case of the 1-Cyclohexylethanol/Acetophenone (CHEA/APO) couple, most of these impurities are already studied LOHC couples such as Ethylcyclohexane/Ethylbenzene (EC/EB) for example (Scheme III-1).



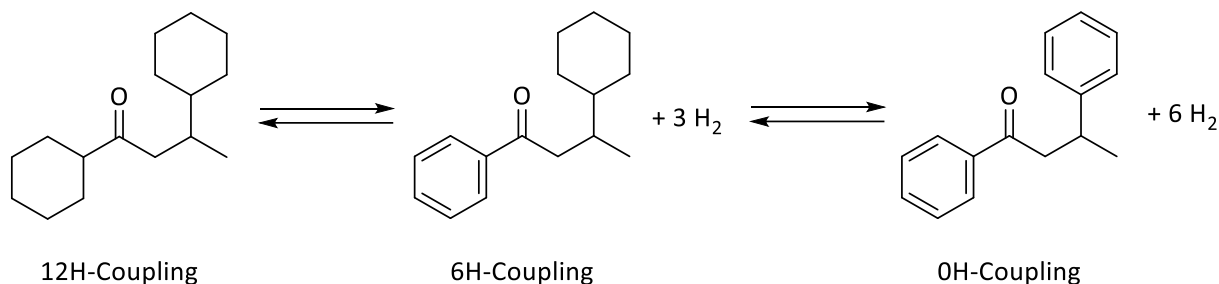
Scheme III-1 – Hydrogenation/Dehydrogenation of the degraded LOHC couple EC/EB.

Materials and Methods

The other degraded LOHC couples are the ether couple 12H-ROR/OH-ROR (Scheme III-2) and the 12H-Coupling/OH-Coupling couple with the intermediate 6H-Coupling (Scheme III-3).



Scheme III-2 – Hydrogenation/Dehydrogenation of the degraded LOHC couple 12H-ROR/OH-ROR.



Scheme III-3 - Hydrogenation/Dehydrogenation of the degraded LOHC couple 12H-Coupling/OH-Coupling with the intermediate 6H-Coupling.

Hence, the DoH is modified in order to account for the cycling of the impurities. At the step S, a partial DoH noted $DoH_{C,S}$ is calculated for each of the LOHC couples C. The complete DoH at the step S, noted DoH_S , is calculated by multiplying each $DoH_{C,S}$ with the molar fraction of the LOHC couples C noted $mol\%_{C,S}$ in the reactional mixture at the beginning of the step S, using the equation (III-12).

$$DoH_S = \sum_i (mol\%_{C,S} \times DoH_{C,S}) \quad (III-12)$$

An example is shown below. The raw data of the cycling for the LOHC couple CHEA/APO over 3 cycles is presented in Table III-6.

Step	CHEA/APO couple				EC/EB couple		ROR couple		Couplings couple		
	APO	ACH	CHEA	PEO	EB	EC	H+ROR	H-ROR	12H-Coupling	6H-Coupling	OH-Coupling
H 1	0.0%	14.7%	84.4%	0.0%	0.9%	0.0%	0.0%	0.0%	0.0%	0.0%	0.0%
D 1	23.4%	70.7%	3.1%	0.8%	0.6%	0.6%	0.4%	0.1%	0.1%	0.2%	0.1%
H 2	0.0%	0.1%	97.6%	0.0%	1.4%	0.0%	0.5%	0.0%	0.4%	0.0%	0.0%
D 2	34.6%	59.9%	1.5%	0.9%	0.4%	0.9%	0.8%	0.0%	0.2%	0.6%	0.2%
H 3	0.0%	0.5%	94.9%	0.0%	2.1%	0.0%	1.2%	0.0%	1.2%	0.0%	0.0%
D 3	34.3%	56.8%	1.4%	0.9%	2.2%	1.3%	1.2%	0.0%	0.5%	1.2%	0.2%

Table III-6 - Raw data of the cycling of the 1-Cyclohexylethanol/Acetophenone couple. Acetophenone (APO), Acetylcyclohexane (ACH), 1-Cyclohexylethanol (CHEA), 1-Phenylethanol (PEO), Ethylbenzene (EB), Ethylcyclohexane (EC), Hydrogenated and dehydrogenated ethers (12H-ROR and OH-ROR resp.) and aldolisation-crotonisation products (12H-Coupling, 6H-Coupling and OH-Coupling). H: Hydrogenation; D: Dehydrogenation.

Materials and Methods

Then, the $DoH_{C,S}$ can be calculated for each couple. The $DoH_{CHEA/APO,S}$ is obtained by multiplying the molar fraction of each product by its attributed coefficient $C_{H,i}$ (Table III-7).

Step	APO	ACH	CHEA	PEO	new EB	new EC	new 12H-ROR	new OH-ROR	new 12H Coupling	new 6H Coupling	new OH Coupling	mol% ^{CHE} _{A/APO,S}	DoH ^{CHEA} _{APO,S}
H 1	0.0%	14.7%	84.4%	0.0%	0.9%	0.0%	0.0%	0.0%	0.0%	0.0%	0.0%	100.0%	95.9%
D 1	23.4%	70.7%	3.1%	0.8%	0.2%	0.0%	0.4%	0.1%	0.1%	0.2%	0.1%	99.0%	57.6%
H 2	0.0%	0.1%	97.6%	0.0%	0.3%	0.0%	0.0%	0.0%	0.0%	0.0%	0.0%	98.0%	99.8%
D 2	34.6%	59.9%	1.5%	0.9%	0.0%	0.0%	0.3%	0.0%	0.0%	0.3%	0.2%	97.7%	48.2%
H 3	0.0%	0.5%	94.9%	0.0%	0.6%	0.0%	0.4%	0.0%	0.5%	0.0%	0.0%	96.9%	99.5%
D 3	34.3%	56.8%	1.4%	0.9%	0.1%	1.3%	0.0%	0.0%	0.5%	0.0%	0.0%	95.3%	48.6%
C_{H,i}	0	3	4	2	1	2	5	4	1	3.5	2		

Table III-7 - Example of calculations of the mol%^{CHEA}_{APO,S} and the DoH^{CHEA}_{APO,S} during the cycling.

Similarly, the $DoH_{EC/EB,S}$ can then be calculated as follows. First, the amount of the cycling EB and EC species is calculated by the difference between the data in the Table III-6 and Table III-7. Then, the obtained values are used to calculate the mol%^{EC/EB,S} and DoH^{EC/EB,S} as presented in Table III-8.

Step	Table III-6		Table III-7		Difference Table III-6 - Table III-7		mol% ^{EC/EB,S}	DoH ^{EC/EB,S}
	EB	EC	new EB	new EC	EB	EC		
H 1	0.9%	0.0%	0.9%	0.0%	0.0%	0.0%	0.0%	0.0%
D 1	0.6%	0.6%	0.2%	0.0%	0.4%	0.6%	1.0%	63.8%
H 2	1.4%	0.0%	0.3%	0.0%	1.1%	0.0%	1.1%	1.5%
D 2	0.4%	0.9%	0.0%	0.0%	0.4%	0.9%	1.2%	70.3%
H 3	2.1%	0.0%	0.6%	0.0%	1.5%	0.0%	1.5%	0.0%
D 3	2.2%	1.3%	0.1%	1.3%	2.1%	0.0%	2.1%	0.0%
C_{H,i}					0	3		

Table III-8 - Example of calculations of the mol%^{EC/EB,S} and the DoH^{EC/EB,S} during the cycling.

The same process was applied for the H+ROR/H-ROR (Table III-9) and 12H-Coupling/6H-Coupling/OH-Coupling (Table III-10).

Step	Table III-6		Table III-7		Difference Table III-6 - Table III-7		mol% ^{ROR,S}	DoH ^{ROR,S}
	H+ROR	H-ROR	new H+ROR	new H-ROR	H+ROR	H-ROR		
H 1	0.0%	0.0%	0.0%	0.0%	0.0%	0.0%	0.0%	0.0%
D 1	0.4%	0.1%	0.4%	0.1%	0.0%	0.0%	0.0%	0.0%
H 2	0.5%	0.0%	0.0%	0.0%	0.5%	0.0%	0.5%	100.0%
D 2	0.8%	0.0%	0.3%	0.0%	0.5%	0.0%	0.5%	92.4%
H 3	1.2%	0.0%	0.4%	0.0%	0.8%	0.0%	0.8%	100.0%
D 3	1.2%	0.0%	0.0%	0.0%	1.2%	0.0%	1.2%	100.0%
C_{H,i}					6	0		

Table III-9 - Example of calculations of the mol%^{ROR,S} and the DoH^{ROR,S} during the cycling.

Materials and Methods

Step	Table III-6			Table III-7			Difference Table III-6 - Table III-7			mol% _{Couplings,S}	DoH _{Couplings,S}
	12H	6H	0H	new 12H	new 6H	new 0H	12H	6H	0H		
H 1	0.0 %	0.0 %	0.0 %	0.0%	0.0%	0.0%	0.0%	0.0%	0.0%	0.0 %	0.0%
D 1	0.1 %	0.2 %	0.1 %	0.1%	0.2%	0.1%	0.0%	0.0%	0.0%	0.0 %	0.0%
H 2	0.4 %	0.0 %	0.0 %	0.0%	0.0%	0.0%	0.4%	0.0%	0.0%	0.4 %	100.0 %
D 2	0.2 %	0.6 %	0.2 %	0.0%	0.3%	0.2%	0.2%	0.3%	0.0%	0.5 %	75.1%
H 3	1.2 %	0.0 %	0.0 %	0.5%	0.0%	0.0%	0.7%	0.0%	0.0%	0.7 %	100.0 %
D 3	0.5 %	1.2 %	0.2 %	0.5%	0.0%	0.0%	0.0%	1.2%	0.2%	1.4 %	44.4%
							C_{H,i}	6	3	0	

Table III-10 - Example of calculations of the mol%_{Couplings,S} and the DoH_{Couplings,S} during the cycling.

The exploited H₂ capacity for the cycle n is noted EHC_n and calculated by subtracting the DoH obtained for the hydrogenation at the step n, DoH_{Hn}, by the DoH obtained for the dehydrogenation at the step n as presented in the equation (III-13) and Table III-11:

$$EHC_n = DoH_{Hn} - DoH_{Dn} \quad (III-13)$$

Cycle	Step	CHEA/APO,S		EB/EC		ROR		Couplings		DoH _s	EHC _n
		mol% _{CHEA/APO,S}	DoH _{CHEA/APO,S}	mol% _{EC/EB,S}	DoH _{EC/EB,S}	mol% _{ROR,S}	DoH _{ROR,S}	mol% _{Couplings,S}	DoH _{Couplings,S}		
1	H 1	100.0%	95.9%	0.0%	0.0%	0.0%	0.0%	0.0%	0.0%	95.9%	38.2%
	D 1	99.0%	57.6%	1.0%	63.8%	0.0%	0.0%	0.0%	0.0%	57.6%	
2	H 2	98.0%	99.8%	1.1%	1.5%	0.5%	100.0%	0.4%	100.0%	98.7%	49.8%
	D 2	97.7%	48.2%	1.2%	70.3%	0.5%	92.4%	0.5%	75.1%	48.9%	
3	H 3	96.9%	99.5%	1.5%	0.0%	0.8%	100.0%	0.7%	100.0%	97.9%	49.7%
	D 3	95.3%	48.6%	2.1%	0.0%	1.2%	100.0%	1.4%	44.4%	48.2%	

Table III-11 – Example of calculations of the DoH_s and EHC_n.

Bibliography

- (1) Pico, M. P.; Romero, A.; Rodríguez, S.; Santos, A. Etherification of Glycerol by Tert-Butyl Alcohol: Kinetic Model. *Ind. Eng. Chem. Res.* **2012**, *51* (28), 9500–9509. <https://doi.org/10.1021/ie300481d>.
- (2) Gaussian 16, Revision C.01, M. J. Frisch, G. W. Trucks, H. B. Schlegel, G. E. Scuseria, M. A. Robb, J. R. Cheeseman, G. Scalmani, V. Barone, G. A. Petersson, H. Nakatsuji, X. Li, M. Caricato, A. V. Marenich, J. Bloino, B. G. Janesko, R. Gomperts, B. Mennucci, H. P. Hratchian, J. V. Ortiz, A. F. Izmaylov, J. L. Sonnenberg, D. Williams-Young, F. Ding, F. Lipparini, F. Egidi, J. Goings, B. Peng, A. Petrone, T. Henderson, D. Ranasinghe, V. G. Zakrzewski, J. Gao, N. Rega, G. Zheng, W. Liang, M. Hada, M. Ehara, K. Toyota, R. Fukuda, J. Hasegawa, M. Ishida, T. Nakajima, Y. Honda, O. Kitao, H. Nakai, T. Vreven, K. Throssell, J. A. Montgomery, Jr., J. E. Peralta, F. Ogliaro, M. J. Bearpark, J. J. Heyd, E. N. Brothers, K. N. Kudin, V. N. Staroverov, T. A. Keith, R. Kobayashi, J. Normand, K. Raghavachari, A. P. Rendell, J. C. Burant, S. S. Iyengar, J. Tomasi, M. Cossi, J. M. Millam, M. Klene, C. Adamo, R. Cammi, J. W. Ochterski, R. L. Martin, K. Morokuma, O. Farkas, J. B. Foresman, and D. J. Fox, Gaussian, Inc., Wallingford CT, 2016. <https://gaussian.com/citation/>.
- (3) Zhao, Y.; Truhlar, D. G. The M06 Suite of Density Functionals for Main Group Thermochemistry, Thermochemical Kinetics, Noncovalent Interactions, Excited States, and Transition Elements: Two New Functionals and Systematic Testing of Four M06-Class Functionals and 12 Other Functionals. *Theor Chem Account* **2008**, *120* (1), 215–241. <https://doi.org/10.1007/s00214-007-0310-x>.
- (4) Krishnan, R.; Binkley, J. S.; Seeger, R.; Pople, J. A. Self-consistent Molecular Orbital Methods. XX. A Basis Set for Correlated Wave Functions. *J. Chem. Phys.* **1980**, *72* (1), 650–654. <https://doi.org/10.1063/1.438955>.
- (5) Clark, T.; Chandrasekhar, J.; Spitznagel, G. W.; Schleyer, P. V. R. Efficient Diffuse Function-Augmented Basis Sets for Anion Calculations. III. The 3-21+G Basis Set for First-Row Elements, Li–F. *Journal of Computational Chemistry* **1983**, *4* (3), 294–301. <https://doi.org/10.1002/jcc.540040303>.
- (6) Rüde, T.; Dürr, S.; Preuster, P.; Wolf, M.; Wasserscheid, P. Benzyltoluene/Perhydro Benzyltoluene – Pushing the Performance Limits of Pure Hydrocarbon Liquid Organic Hydrogen Carrier (LOHC) Systems. *Sustainable Energy & Fuels* **2022**, *6* (6), 1541–1553. <https://doi.org/10.1039/D1SE01767E>.
- (7) Watts, J. F.; Wolstenholme, J. *An Introduction to Surface Analysis by XPS and AES*; John Wiley & Sons, 2019.
- (8) PDF-4+ – ICDD. <https://www.icdd.com/pdf-4/> (accessed 2023-02-03).
- (9) Yu, K. M. AP 5301/8301; *Instrumental Methods of Analysis and Laboratory; Lecture 4; Microscopy (III): Transmission Electron Microscopy (TEM)*. http://www.cityu.edu.hk/phy/appkchu/ap5301/AP5301_lecture4_TEM.pdf (accessed 2023-02-01).
- (10) Schindelin, J.; Arganda-Carreras, I.; Frise, E.; Kaynig, V.; Longair, M.; Pietzsch, T.; Preibisch, S.; Rueden, C.; Saalfeld, S.; Schmid, B.; Tinevez, J.-Y.; White, D. J.; Hartenstein, V.; Eliceiri, K.; Tomancak, P.; Cardona, A. Fiji: An Open-Source Platform for Biological-Image Analysis. *Nat Methods* **2012**, *9* (7), 676–682. <https://doi.org/10.1038/nmeth.2019>.
- (11) *Origin: Data Analysis and Graphing Software*. <https://www.originlab.com/index.aspx?go=PRODUCTS/Origin> (accessed 2023-02-01).
- (12) *Texture des matériaux pulvérulents ou poreux*. Techniques de l'Ingénieur. <https://www.techniques-ingenieur.fr/base-documentaire/archives-th12/archives-materiaux-fonctionnels-materiaux-biosources-tian0/archive-3/texture-des-materiaux-pulverulents-ou-poreux-p1050/> (accessed 2023-02-01).
- (13) Pusch, W.; Flocco, M. T.; Leung, S.-M.; Thiele, H.; Kostrzewa, M. Mass Spectrometry-Based Clinical Proteomics. *Pharmacogenomics* **2003**, *4* (4), 463–476. <https://doi.org/10.1517/phgs.4.4.463.22753>.



Table of Contents “Chapter 1: Evaluation of new LOHC structures”

IV. Chapter 1: Evaluation of new LOHC structures	126
IV.1 Choice of the target molecules	126
IV.1.1 Preliminary criteria: Physical properties	126
IV.1.2 LOHC criteria.....	126
IV.1.3 Toxicity.....	129
IV.1.4 Estimation of the dehydrogenation enthalpy and other thermodynamic properties	131
IV.2 Study of the 1-Cyclohexylethanol/Acetophenone (CHEA/APO) LOHC couple.....	135
IV.2.1 Hydrogenation.....	137
IV.2.2 Analysis of the selected Ru/Al ₂ O ₃ hydrogenation catalyst.....	140
IV.2.3 Dehydrogenation.....	146
IV.2.4 Analysis of the selected Pt/C dehydrogenation catalyst.....	147
IV.2.5 Chemical kinetics of dehydrogenation	150
IV.2.6 Cycling.....	153
IV.2.7 Reaction mechanism	155
IV.3 Conclusion	156
Bibliography.....	157
Appendix.....	164
Appendix IV-1 - Submitted full text to the Internation Journal of Hydrogen Energy.....	164
Appendix IV-2 - Hydrogenation GCMS results	182
Appendix IV-3 - Conversion of Acetophenone with Pt/Al ₂ O ₃ , Ru/Al ₂ O ₃ and Ru/C.....	182
Appendix IV-4 - XPS analysis of the Ru 3p core level	183
Appendix IV-5 - TEM-EDX images of the Ru/Al ₂ O ₃ catalyst.....	183
Appendix IV-6 - TEM-EDX images of the Pt/C catalyst.....	184
Appendix IV-7 - Apparent specific rates and adjusted correlation factors	184
Appendix IV-8 - Estimation of the internal diffusion effects.....	185
Appendix IV-9 - Extended DFT mechanism	186

IV. Chapter 1: Evaluation of new LOHC structures

The main results presented in this chapter have been summarized in a publication recently published in the *International Journal of Hydrogen Energy* (<https://doi.org/10.1016/j.ijhydene.2023.05.024>). The full text is presented in Appendix IV-1.

The current limitations faced by numerous LOHC couples are their low gravimetric density, their high dehydrogenation enthalpy, the use of PGM-based heterogeneous or homogeneous catalysts, gas-phase reaction due to the low boiling points of the LOHC or the use of solvent and additives to perform both hydrogenation and dehydrogenation. Moreover, long term stability upon cycling needs also to be addressed. In this chapter, the methodology developed to assess potential LOHC structures will be presented. In particular, some criteria will be proposed as selection tools to afford pertinent structures from a chemically and technological standpoint.

IV.1 Choice of the target molecules

In principle, any pair of liquid molecules over an industrially accessible temperature range capable of selectively interconverting with only H₂ as co-product can be considered as a LOHC couple. Nevertheless, this definition is not strict enough to obtain technologically relevant LOHC couples. Depending on the application, many other criteria can be added such as the hydrogen capacity of the rich LOHC, the dehydrogenation enthalpy value, the toxicity, the synthetic accessibility and cost of the molecules, etc.¹ Thus, this section focuses on some relevant criteria mandatory to facilitate the industrialization of the LOHC technology.

IV.1.1 Preliminary criteria: Physical properties

The physical properties of a LOHC couple are key to ensure that it answers to the chosen application. A classic property of the LOHC technology is the liquid phase of the carrier that eases the transportation, we used the ChemNetBase database that gather the physicochemical properties of many common organic compounds, which facilitates risk assessment.² Molecules were associated in pairs following preferentially heterogeneously catalyzed reactivities presented in the literature review. Then, when reported, the melting temperature and boiling point of both structures were reviewed. A requirement on the preliminary LOHC couples was that at least one molecule possessed both a melting point below 0 °C and boiling point above 60 °C. These parameters were chosen so that the LOHC couple was in liquid or near-liquid form in ambient conditions. In addition, a high synthetic accessibility is required to favor the industrialization of the process. Hence, at least one of the molecules of the couple must be already easily synthesized and/or commercial. The best-case scenario would be that one part of the LOHC couples is a commodity chemical or their direct derivatives to ensure a low molecule cost. For example, Toluene is a commodity chemical that can be used as a LOHC. The synthetic accessibility was verified by using the SciFinder-n website.

IV.1.2 LOHC criteria

The primary criteria of the LOHC technology relates to the H₂ compression level. The main descriptors are the gravimetric (wt.%H₂) and volumetric (gH₂/L) densities. Both densities are linked by the density ρ (g/mL) of the hydrogenated organic carrier following the equation (IV-1).

$$\text{Volumetric density (gH}_2\text{/L)} = \text{Gravimetric density (wt. \%H}_2\text{)} \times \frac{1000}{100 \times \rho} \quad (\text{IV-1})$$

Here, as organic liquids have volumetric densities between 0.7 and 1.1³, the volumetric density is roughly proportional to the gravimetric density independently of the organic liquid. Thus, only the

Chapter 1: Evaluation of new LOHC structures

gravimetric density will be used as a criterion. Here, we propose to use an arbitrary minimal gravimetric density at 5 wt.% H₂ in order to have equivalent to compressed H₂ gas at 700 bar.⁴

When conceiving new LOHC systems, an often-undiscussed criteria is the elementary constitution of the molecules. Indeed, the molecules containing heavy atoms will have drastically reduced gravimetric densities (see literature review, metal hydrides). In addition, the elemental composition of a LOHC might be primordial due to the incompatibility between the limited extractible resources and the demand if the LOHC technology is to be fully implemented.⁵ Here, we will limit the molecular composition to the first three periods of the periodic table. The alkaline elements were excluded from the selection, as they would only replace a portion of the protons.

Moreover, as the dehydrogenation enthalpy is primordial for the LOHC technology (energy efficiency), the influence of the heteroatom on the LOHC structures (ring distortion, aromaticity, electronegativity and electro donation/acceptance to the adjacent ring) must be assessed. To do so, we used the carbon skeleton of indene where a carbon atom of the 5-membered ring adjacent to the 6-membered ring is replaced by a variety of elements. The dehydrogenation enthalpy of these structures was estimated by Density Functional Theory (DFT) whose principle is presented later in this chapter (IV.1.4). The results are presented in the Figure IV-1.

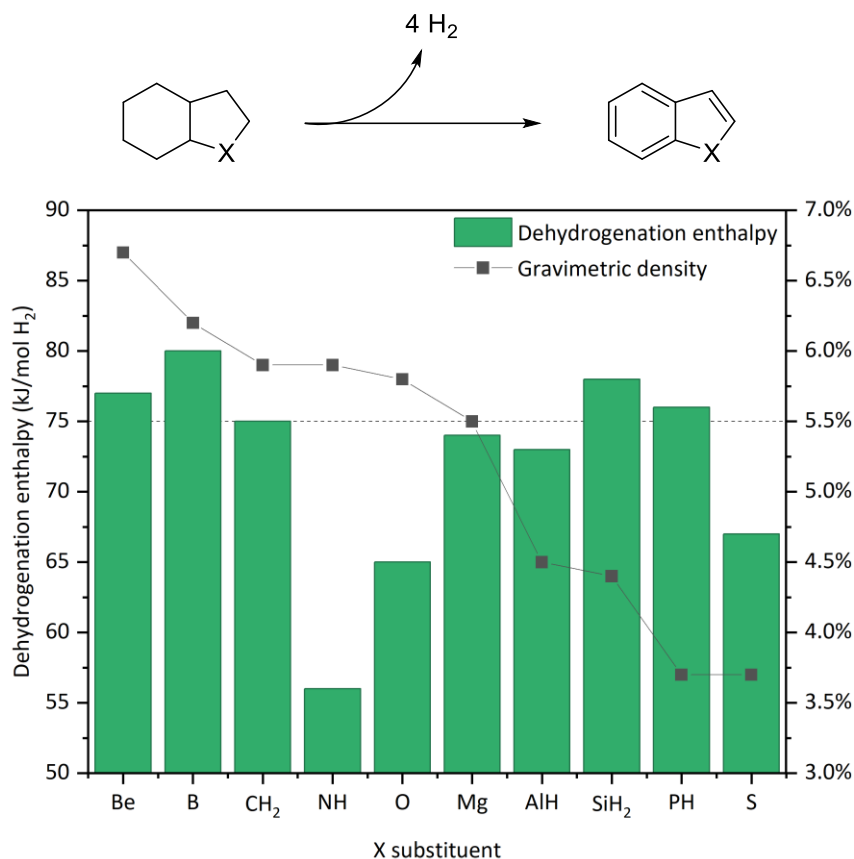


Figure IV-1 – Replacement of a carbon atom with a heteroatom on the dehydrogenation enthalpy and storage capacity of indene analogues. The dotted line represents the enthalpy of Indene. (Gaussian9, M062X/6-311G+(2d, p))

N and O based heterocycles appear as the best comprise when taking into account both the dehydration energy and the storage capacity. These results confirmed that the beneficial effect of N and O atoms on the dehydrogenation enthalpy of heterocycles compared to homocycles.^{6,7} The other elements providing a lowered dehydrogenation enthalpy were Mg, Al and S. It is worth noting that

Chapter 1: Evaluation of new LOHC structures

only acceptorless dehydrogenation mechanisms were supposed (i.e. the hydrogenated molecule releases pure H₂ in presence of a catalyst). However, as presented in the literature review, some elements like Si or Al can undergo hydrolysis or alcoholysis to release H₂ in exothermic reaction pathways. While adding such dehydrogenation mechanism to the Figure IV-1 would probably increase the gravimetric density and diminish the dehydrogenation enthalpy, the regeneration/hydrogenation of these materials is yet to be addressed without using strong reductants like LiAlH₄. Therefore, only Be, B, N, O and Mg can be substituted to provide a gravimetric density superior than 5 wt.%H₂.

When looking at the enthalpy criteria, only LOHC containing N, O, Mg Al or S could improve the dehydrogenation enthalpy compared to C. However, the development of organomagnesium compounds would be hindered due to their limited extractability and their extreme basicity that induce their sensitivity to water and violent reaction upon contact.⁸ Al addition on the cycle strongly diminishes the gravimetric density (<4.5wt.%H₂) due to its weight and sulfur-containing compounds show the same tendency with an additional sensitivity to hydrogenolysis, by-production of dangerous compounds (H₂S), catalyst poisoning and reported unreactivity as heterocycles.^{9,10} This additional criterion reduced the search for LOHC compounds to molecules containing only C, H, N or O atoms.

Finally, the succession of heteroatoms like in the diazo or triazo groups are sources of structural instability, hence molecules with successive heteroatoms were therefore removed from the selection. Lastly, already extensively studied molecules such as Toluene (Tol), Dibenzyltoluene (DBT), N-Ethylcarbazole (NEC) and their derivatives were not included in the selection. The molecule couples answering the above-addressed criteria are grouped in the Table IV-1.

ENTRY	H ₂ -RICH MOLECULE(S) H ₂ -LEAN MOLECULE	wt.%H ₂	MELTING POINT/BOILING POINT (°C)
1	Methoxycyclohexane Anisole	5.3%	-74/133 -37/155
2	Tetrahydro-2,5-furanmethanol Furfural	5.9%	57/178 -36/162
3	1-(Cyclohexylmethyl)pyrrolidine 1-Benzylpyrrole	6.0%	-/- 15/247
4	4-Piperidine methanol and Ethanol Ethyl 4-pyridinecarboxylate	6.2%	57/119 and -114/78 -/220
5	1,3-propanediamine and 4 Ethanol N,N'-1,3-Propanediylbis[N-acetylacetamide]	6.2%	-12/140 and -98/65 -/-
6	1-Cyclohexylethanol Acetophenone	6.3%	-40*/190 20/200
7	2-Cyclohexylethanol Phenylacetaldehyde	6.3%	-20/206 -10/190
8	Cyclohexylmethanol and Ethanol Ethyl benzoate	6.3%	-43/180 and -114/78 -34/212
9	Glycerol and 2 Methanol Dimethyl mesoxalate	6.4%	18/171 (dec.) and -98/65 -30/209
10	3-Cyclohexylpropanol and Ethanol Ethyl cinnamate	6.4%	-/218 and -114/78 7/271
11	Aminocyclohexane Aniline	6.5%	-18/134 -6/184
12	Decahydro-1-naphthalenamine Naphthylamine	6.5%	-/- 50/301
13	5-(methylamino)-1-Pentanol N-Methyl-2-pyridone	6.8%	-/- 30/250
14	N-Methylcyclohexylamine and Methanol N-methyl-N-phenylformamide	6.9%	-8/149 and -98/65 8/243
15	Cyclohexylmethanol Benzylaldehyde	7.0%	-43/180 -26/178
16	2 Cyclohexylmethanol Benzylbenzoate	7.0%	-43/180 21/324

Chapter 1: Evaluation of new LOHC structures

17	Cyclohexylmethanol and Cyclohexanol Phenylbenzoate	7.5%	-43/180 and 23/161 71/298
18	1,5-Pentanediol 2H-Pyran-2-one	7.7%	-18/241 8/207
19	1-Cyclohexylmethanamine Benzonitrile	8.9%	-8/161 -13/191
20	1,3-propanediamine Malononitrile	10.8%	-12/140 32/220

Table IV-1 - List of the 20 best LOHC couples with their gravimetric density and melting and ebullition temperatures standpoint. H₂-rich molecules and their melting and ebullition temperatures are written in bold. Missing data in the literature was noted by a “-“ sign. The “*” sign shows predicted temperature values by the Joback method.¹¹

Firstly, the LOHC couples **2**, **4-10** and **13-19** propose the combination of two different “chemical functions” from where H₂ can be released or stored. This approach is rarely proposed in the search of new LOHC systems as combining the simultaneous dehydrogenation of different atoms with the same catalyst is challenging. Nevertheless, it could prove useful to develop more complex LOHC couples. Here, the highest gravimetric densities were obtained for nitrile based compounds (**19**) and (**20**) that reached 8.9 wt.% H₂ and 10.8 wt.% H₂ respectively, while the lowest was 5.3 wt.% H₂ for Methoxycyclohexane (**1**). Aromatics were used as a H₂-dense foundation to add different heteroatoms to support non-participating external inductive or mesomeric functions (**1**, **3**, **11** and **12**) or enable the formation of aldehydes (**2**, **7** and **15**), ketones (**6**), homo-coupled esters (**16**), hetero-coupled esters (**4**, **8**, **9**, **10** and **17**), amides (**14**) and carbamides (**5**). Finally, the further dehydrogenation of lactones (**18**) and lactams (**13**) could also prove useful to increase their gravimetric density.

IV.1.3 Toxicity

Toxicity limitation is important to facilitate the insertion of new LOHC on the market, therefore, a toxicity level equal or inferior to the current fuels was fixed. However, assessing the risk of a substance can be arduous. The combination of different kinds of risks as a unique indicator, the Toxicity Potential Indicator (TPI), was proposed by the Fraunhofer institute. By inputting the maximum admissible concentration, the EU carcinogenicity, the technical guidance concentration, the R-phrases and the (german) water hazard classes, a number ranging on a scale from 0 to 100 (TPI/mg) was obtained, with “0” being a substance without reported hazard and 100 an extremely toxic substance. This number is a powerful tool to compare the overall toxicity of chemicals and was used in various studies.^{12,13} Sadly, this online tool is not available anymore.¹⁴ A less indicator-dependent approach required the inventory of the hazard statements and the related chemical risk levels. The Table IV-2 regroups the hazard statements of gasoline that are currently used as a transportation fuel in the automotive industry.


SUBSTANCE	CAS NUMBER	HAZARD STATEMENTS AND ASSOCIATED CHEMICAL RISKS	GHS
GASOLINE (SP95/98)	86290-81-5	H224: Flam. Liq. 1 H304: Asp. Tox. 1 H315: Skin Irrit. 2 H336: STOT SE 3 H340: Muta. 1B H350: Carc. 1B H361fd: Repr. 2 H411: Aquatic Chronic 2	

Table IV-2 - Current transportation fuels in the automotive industry and their associated risks

Chapter 1: Evaluation of new LOHC structures

Hence, only new LOHC couples with an estimated toxicity inferior to that of gasoline should be selected. Therefore, filters were applied on its toxicity (no GHS08 sign), ecotoxicity (Aquatic Chronic>2), flammability (Flam. Liq.>=2) and corrosive properties (no Skin Corr., Met. Corr. or Eye Dam.). The application of these new filters on the previously selected LOHC couples is presented in the Table IV-3.

ENTRY	H ₂ -RICH MOLECULE(S) H ₂ -LEAN MOLECULE	REASON	PASS/FAIL
1	Methoxycyclohexane Anisole	- -	Pass
2	Tetrahydro-2,5-furanmethanol Furfural	GHS08 GHS08	Fail
3	1-(Cyclohexylmethyl)pyrrolidine 1-Benzylpyrrole	- -	Pass
4	Piconol and Ethanol Ethyl 2-pyridinecarboxylate	- and - -	Pass
5	1,3-propanediamine and 4 Ethanol N,N'-1,3-Propanediylbis[N-acetylacetamide]	GHS08 and - N/A	Fail
6	1-Cyclohexylethanol Acetophenone	- -	Pass
7	2-Cyclohexylethanol Phenylacetaldehyde	- Skin Corr.1B; Eye Dam. 1; Skin Sens. 1A;	Fail
8	Cyclohexylmethanol and Ethanol Ethyl benzoate	- and - -	Pass
9	Glycerol and 2 Methanol Dimethyl mesoxalate	- and GHS08 -	Fail
10	3-Cyclohexylpropanol and Ethanol Ethyl cinnamate	- and - -	Pass
11	Aminocyclohexane Aniline	GHS08 GHS08	Fail
12	Decahydro-1-naphthalenamine Naphtylamine	N/A GHS08	Fail
13	5-(methylamino)-1-Pentanol N-Methyl-2-pyridone	- -	Pass
14	N-Methylcyclohexylamine and Methanol N-methyl-N-phenylformamide	Met. Corr. 1; Acute Tox. 3; Skin Corr. 1A; Eye Dam. 1 and GHS08 -	Fail
15	Cyclohexylmethanol Benzaldehyde	- -	Pass
16	2 Cyclohexylmethanol Benzylbenzoate	- -	Pass
17	Cyclohexylmethanol and Cyclohexanol Phenylbenzoate	- and - -	Pass
18	1,5-Pentanediol 2H-Pyran-2-one	- -	Pass
19	Cyclohexanemethylamine Benzonitrile	- -	Pass
20	1,3-propanediamine Malononitrile	GHS08 -	Fail

Table IV-3 –LOHC couples and the associated risks of each molecule.

Out of the 20 potential couples, only 12 couples complied with the filters. Methanol presents an intrinsic toxicity but it could theoretically be replaced with Ethanol at the cost of a reduced gravimetric density. Amine compounds also usually present a high toxicity and/or corrosive properties that are unsuitable for a LOHC.

IV.1.4 Estimation of the dehydrogenation enthalpy and other thermodynamic properties

The dehydrogenation enthalpy is a make-or-break criterion used to describe the energy efficiency of a LOHC system during the dehydrogenation. Indeed, the dehydrogenation is endothermic, thus it can be inferred that a portion of the produced H₂ will be used as fuel to keep the reaction running at the desired temperature. The recommended values in the literature lie between 40-70 kJ/mol H₂, 42-54 kJ/mol H₂ or 30-44 kJ/mol H₂ depending on the source in order to avoid difficulties during the hydrogenation of the hydrogen depleted compound and/or to have an equilibrium hydrogen pressure of 1 bar over a wide temperature range (-40 to +60 °C).¹⁵⁻¹⁸ As it was presented, this criterion is not unified. Therefore, we can use the H₂ average calorific value (286 kJ/molH₂) to estimate which proportion of the released H₂ would need to be consumed to compensate the heat transfers under the assumption that no additional heat source is provided to the system. For example, Tol, DBT and NEC require respectively 24%, 25% and 18% of the H₂ average calorific value. Moreover, lower dehydrogenation enthalpy would facilitate the reaction in theory. Therefore, strategies to diminish the dehydrogenation enthalpy would be highly beneficial.

Dehydrogenation enthalpy reduction can be achieved by the stabilization of the dehydrogenated state or the destabilization of the hydrogenated state. Most examples in the literature rely on the stabilization of the dehydrogenated structure by using conjugated systems like polyaromatic structures.¹⁹ Conversely, the saturated forms were usually destabilized by incorporating N-substituents that are known to induce easier cleavage of the adjacent C-H bonds and to enable bonds-lone pair interactions.^{6,20} Designing new systems requires then to find molecule couples with comparable or lower enthalpy values than state-of-the-art LOHC (50-70 kJ/mol H₂) before testing them as potential LOHC. The dehydrogenation enthalpy was calculated by the equation (IV-2) while the dehydrogenation free energy and dehydrogenation entropy were given by the equations (IV-3) and (IV-4) respectively.

$$\Delta_r H^\circ(T, P) = \sum_{Products} \Delta_f H^\circ(T, P)_{Products} - \sum_{Reactants} \Delta_f H^\circ(T, P)_{Reactants} \quad (IV-2)$$

$$\Delta_r G^\circ(T, P) = \sum_{Products} \Delta_f G^\circ(T, P)_{Products} - \sum_{Reactants} \Delta_f G^\circ(T, P)_{Reactants} \quad (IV-3)$$

$$\Delta_r G^\circ(T, P) = \Delta_r H^\circ(T, P) - T\Delta_r S^\circ(T, P) \quad (IV-4)$$

However, the enthalpies of formation and free energy of formation of organic compounds are not readily accessible except for some common compounds on public databases like NIST.²¹ Hence using a method able to quickly approximate these thermodynamic values is primordial. Numerous energetic models exist, ranging from small scale methods like Quantum Monte-Carlo in the Ångström range (to model phenomena like neutron scattering, electron-solid interactions, electron beams, ...) to empirical models that are best suited for systems containing hundreds of atoms (proteins).^{22,23} Density Functional Theory (DFT) is a nm-ranged quantum physics computer modelling technic adapted to describe atoms, molecules and crystalline structures and thus is compatible with the LOHC systems. This method relies on the iterative resolution of Schrödinger-type equations (IV-5).

$$i\hbar \frac{\partial}{\partial t} \Psi(r, t) = -\frac{\hbar^2}{2m} \nabla^2 \Psi(r, t) + V(r)\Psi(r, t) \quad (IV-5)$$

With $\Psi(r, t)$ the wave function dependent of a three-dimensional vector r and time t , m the mass of the particle and $V(r)$ an external potential. Historically, DFT was developed following several theorems and approximations. First, the Born-Oppenheimer approximation states that a time-independent solution of equation (IV-5) is the sum of independent terms (IV-6).

Chapter 1: Evaluation of new LOHC structures

$$E_{total} = E_{electronic} + E_{vibrational} + E_{rotational} + E_{nuclear\ spin} \quad (IV-6)$$

Moreover, as the electrons motion is far superior to that of atoms due to their mass difference, the Schrödinger's equation can be simplified by supposing the position of the nuclei as fixed.²⁴ Secondly, in the Born-Oppenheimer approximation, the Hohenberg-Kohn theorem describes the total energy of an interacting electron gas $\{R_I\}$ as a unique functional of the electronic density ρ with its ground-state energy calculated by the equations (IV-7) and (IV-8).²⁵

$$E_0(\{R_I\}) = \min_{\rho} E^{KS}[\rho] \quad (IV-7)$$

where

$$E^{KS}[\rho] = \int dr V_{ext}(r, \{R_I\})\rho(r) + U_0(\{R_I\}) + F[\rho] \quad (IV-8)$$

With V_{ext} the external potential applies to the system, $U_0(\{R_I\})$ to the electronic potential in the ground state and $F[\rho]$ to an unknown term. Thirdly, the Kohn-Sham formulation allows for a better formal description of the system by stipulating that the energy functional of N interacting electrons is equal to N non-interacting electrons subjected to a potential (IV-9).

$$E^{KS}[\rho] = T[\{\phi_i\}] + \int dr V_{ext}(r, \{R_I\})\rho(r) + \frac{1}{2} \int dr V_H(r)\rho(r) + E_{xc}[\rho] \quad (IV-9)$$

With $\langle \phi_i | \phi_j \rangle = \delta_{ij}$, $T[\{\phi_i\}]$ the kinetic energy of the non-interacting system, $V_{ext}(r, \{R_I\})$ the external potential, $V_H(r)$ the electrostatic interaction of the electrons and $E_{xc}[\rho]$ the exchange correlation that corresponds to the difference between the exact energy of the system and the energy calculated by the other terms of the Kohn-Sham equation.²⁶ In this advantageous formulation, only the exchange correlation has to be approximated by various approaches such as the local density approximation (LDA), generalized gradient approximations (GGA), hybrids (mix of exact exchange and GGA) and so on. Such approximations are called functionals and, in practice, several need to be tested on each studied system to assess which one describe it better.

Moreover, due to the non-interacting electrons, the many-body wave function Ψ_0 can be swapped for a set of one-particle orthonormal functions ϕ_i also known as the Kohn-Sham orbitals. Consequently, the electronic density can be written as the equation (IV-10).

$$\rho(r) = \sum_i^{occ} f_i |\phi_i(r)|^2 \quad (IV-10)$$

With f_i occupational numbers related to the quantum states occupied by electrons. The Kohn-Sham orbitals yield a qualitative description of molecular orbitals. Minimal basis approach (i.e. one basis function F_k per atom) is often not sufficient as energy levels are sometimes misattributed and a classic technique is to extend the basis functions with polarization functions for better accuracy (IV-11).²⁷

$$\phi_i(r) = \sum_k C_{ik} F_k(r) \quad (IV-11)$$

With C_{ik} the coefficient related to F_k . For molecular systems, localized basis sets can efficiently describe isolated systems (i.e. molecules in the gas phase) with only a few basis functions that are calculated following the equation (IV-12).

$$F_k(r) = A_k e^{-\alpha_k r^2} \quad (IV-12)$$

With A_k and α_k coefficients.

Chapter 1: Evaluation of new LOHC structures

In this thesis, the computations were performed with the Gaussian 16 Rev C.01 suite, using at 298 K the hybrid meta-GGA functional M06-2X and the basis set 6-311+G(2d,p) for all elements as they are known to accurately predict the thermochemical parameters of main-group compounds and efficiently describe polyenes systems.^{28–31} In order to ensure the validity of the M06-2X method, other functionals such as the GGA B3LYP, GGA B3LYP-GD3, range separated GGA WB97XD, meta-GGA M02HF as well as ab initio methods such as Hartree-Fock (HF) and post-HF MP2 were tested with the same basis set.^{32–43} The accuracy of these methods was benchmarked against the experimental dehydrogenation enthalpy of classic LOHC structures whose energy levels are well described in the literature: Methylcyclohexane/Toluene (MCH/Tol), Perhydrodibenzyltoluene/Dibenzyltoluene (18H-DBT/DBT), Cyclohexanol/Phenol (CHXOL/PhOH), Tetrahydropyrrole/pyrrole (4H-Pyrrole/Pyrrrole), perhydro-N-Ethylcarbazole/N-Ethylcarbazole (12H-NEC/NEC) and 1,4-butanediol/ γ -butyrolactone (BDO/GBL). Each dehydrogenation enthalpy was calculated following the equation (IV-2). Frequency calculations were performed on the optimized structures using the same parameters and all structures were verified to possess no imaginary frequencies. The results are presented in Figure IV-2.

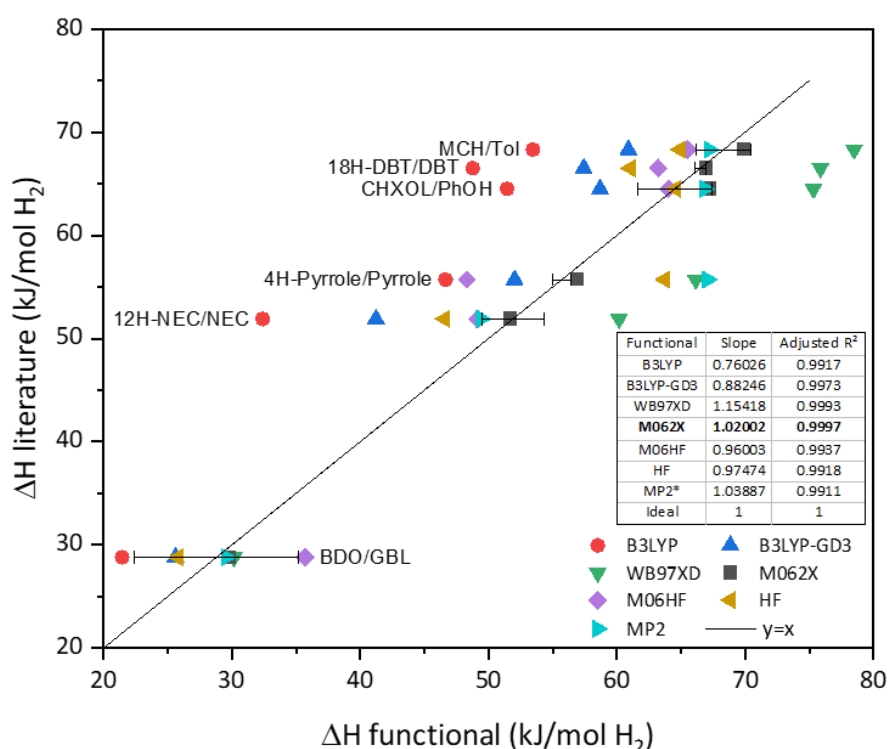


Figure IV-2 – Comparison of the gas-phase dehydrogenation enthalpy values from the literature with the DFT-calculated dehydrogenation enthalpies.

Interestingly, B3LYP produced some widely underestimated values that were partially corrected by including a dispersion term (B3LYP-GD3) but the results were not satisfactory. On the other hand, WB97XD tended to strongly overestimate the dehydrogenation enthalpy of aromatic structures and is hence not adapted for our study. Ab initio HF method was also inaccurate while MP2 presented some interesting results except for the 4H-pyrrole/pyrrole couple. Moreover, this method was computationally expensive and larger LOHC structures like 18H-DBT/DBT could not be optimized and its frequencies calculated after 24 h cluster time. Finally, both M06HF and M062X were accurate, but M062X showed the lower deviation and its slope was the closest to the ideal value. As a conclusion, M062X combined with 6-311G+(2d, p) yielded the most accurate dehydrogenation enthalpy values compared to the literature, with satisfactory errors inferior to 3 kJ/mol H₂ (Table IV-4).

Chapter 1: Evaluation of new LOHC structures

LOHC Couple	ΔH M062X (kJ/mol H ₂)	ΔH literature gas phase (kJ/mol H ₂)	Absolute error ΔH literature (kJ/mol H ₂)	References
MCH/Tol	69.9	68.3	2.1	21
18H-DBT/DBT	66.9	66.5	0.4	44-46
CHXOL/PhOH	67.2	64.5	2.9	21
12H-NEC/NEC	51.7	51.9	2.4	19,47-49
4H-Pyrrole/Pyrrole	56.9	55.7	0.7	19,21
BDO/GBL	29.8	28.8	1.0	21,50-52

Table IV-4 – Comparison of the calculated enthalpies by M062X 6-311G+(2d, p) with the averaged gas-phase dehydrogenation enthalpies and their absolute error.

The gas-phase dehydrogenation enthalpy, Gibbs free energy and entropy of the 12 potential LOHC couples were calculated and are presented in Table IV-5.

ENTRY	H ₂ -RICH MOLECULE(S) H ₂ -LEAN MOLECULE	CALCULATED DEHYDROGENATION ENTHALPY Δ_{RH} (kJ/mol H ₂)	CALCULATED DEHYDROGENATION FREE ENERGY Δ_{RG} (kJ/mol H ₂)	CALCULATED DEHYDROGENATION ENTROPY Δ_{RS} (J/K/mol H ₂)
1	Methoxycyclohexane Anisole	68	31	121
2	1-(Cyclohexylmethyl)pyrrolidine 1-Benzylpyrrole	66	29	123
3	Piconol and Ethanol Ethyl 2-pyridinecarboxylate	46	20	87
4	1-Cyclohexylethanol Acetophenone	66	29	124
5	Cyclohexylmethanol and Ethanol Ethyl benzoate	46	21	86
6	3-Cyclohexylpropanol and Ethanol Ethyl cinnamate	57	29	95
7	5-(methylamino)-1-Pentanol N-Methyl-2-pyridone	45	12	109
8	Cyclohexylmethanol Benzaldehyde	69	32	122
9	2 Cyclohexylmethanol Benzylbenzoate	56	26	101
10	Cyclohexylmethanol and Cyclohexanol Phenyl benzoate	58	28	101
11	1,5-Pentandiol 2H-Pyran-2-one	63	30	110
12	Cyclohexanemethylamine Benzonitrile	70	33	122

Table IV-5 – Dehydrogenation enthalpy, Gibbs free energy and entropy of the 12 potential LOHC.

Interestingly, most normalized dehydrogenation entropies are close to the standard entropy of hydrogen at 1 bar in gas phase: 130.68 J/K/mol.^{53,54} This value was reported in earlier modeling attempts and has been experimentally observed for many chemical hydrogen storage systems.^{19,55} Pez et al. also reported that lower entropy values in the 80-90 J/K/mol range would correspond to adsorbed H₂.¹⁹ However, as protons are covalently bound in organic molecules, it is highly probable that lower entropy values are simply derived from modeling inadequacy or that lower binding strength of mobile protons shifted the global entropy to lower values. N and O-containing structures supporting this claim can be found in Table IV-6.

Chapter 1: Evaluation of new LOHC structures

Reaction	Dehydrogenation entropy (J/K/mol H ₂)	References
$2 \text{ NH}_3 \rightarrow \text{N}_2 + 3 \text{ H}_2$	66	21,56
Methanol \rightarrow Formaldehyde + H₂	110	21,56
Ethanol \rightarrow Acetaldehyde + H₂	87	21,56
2 Ethanol \rightarrow Ethyl acetate + 2 H₂	99	21,56

Table IV-6 – Dehydrogenation entropy of small molecules.

Similarly, the introduction of external O heteroatoms (**1**, **4** and **8**) and N atoms in heterocyclic structures (**2** and **3**) diminish the dehydrogenation enthalpy. In addition, ester formation (**3**, **5**, **6**, **8**, **9** and **10**) presents a reduced dehydrogenation enthalpy (<60 kJ/mol H₂), but these couplings might be difficult to implement. Indeed, the classic dehydrogenation temperatures are above the boiling point of Ethanol or Cyclohexanol, which implies either thermodynamics limitations in closed systems due to H₂ accumulation or difficult H₂/Ethanol gas separation in open batch systems. Moreover, the selective dehydrogenation of lactams (**7**) and lactones (**11**) and the selective dehydrogenation of nitriles (**12**) with heterogeneous catalysts have yet to be reported. Aromatic aldehydes are prone to over-oxidation and are hence less desirable than ketones. Thus, the 1-Cyclohexylethanol/Acetophenone couple (CHEA/APO) was chosen as a potential bifunctional LOHC carrier.

IV.2 Study of the 1-Cyclohexylethanol/Acetophenone (CHEA/APO) LOHC couple

The CHEA/APO couple has already been partially studied, especially the hydrogenation and dehydrogenation of its alcohol/ketone function (Table IV-7). A handful of reports have described the homogeneous and heterogeneous hydrogenation of APO to CHEA. While homogeneous and heterogeneous hydrogenation in dilute conditions yielded up to 100% of conversion, solvent-free heterogeneous hydrogenation was only completed in yield inferior to 10%.^{57,58}

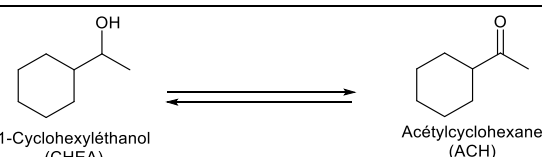
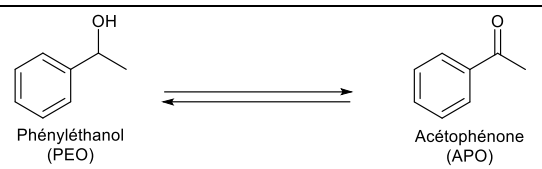
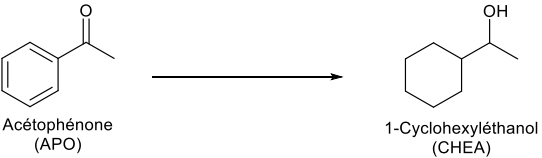
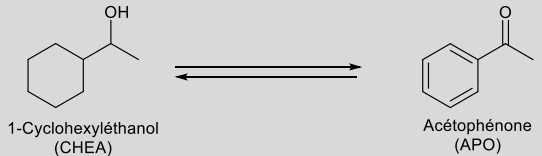
Considered reaction	Catalytic metal
 <p>1-Cyclohexylethanol (CHEA) \rightleftharpoons Acetylcyclohexane (ACH)</p>	Ru ⁵⁹
 <p>Phenylethanol (PEO) \rightleftharpoons Acetophenone (APO)</p>	Cu ^{60,61} , Cu-Fe ⁶² , Pd ⁶³⁻⁶⁶ , Ru ^{59,67,68} , Ni (MOF) ⁶⁹ , Ag ⁷⁰⁻⁷² , Au ⁷³ , Ir ⁷⁴
 <p>Acetophenone (APO) \rightarrow 1-Cyclohexylethanol (CHEA)</p>	Hydrogenation only: Rh ⁷⁵⁻⁸¹ , Ru ^{76,77,82-84} , Pt ^{57,58,85-87} , Pd ^{57,88} , Ni ⁸⁹⁻⁹¹
 <p>1-Cyclohexylethanol (CHEA) \rightleftharpoons Acetophenone (APO)</p>	This work: Hydrogenation: Ru Dehydrogenation: Pt

Table IV-7 - Literature review of the hydrogenation and dehydrogenation of the couple CHEA/APO.

Chapter 1: Evaluation of new LOHC structures

To the best of our knowledge, no work has been performed on the complete acceptorless dehydrogenation of CHEA to APO. Our aim is to determine a set of catalytic conditions that enable the full dehydrogenation and full hydrogenation, as well as evaluating the capacities of such a system to behave as a LOHC, performing several hydrogenation/dehydrogenation cycles under solvent-free conditions.

Over the reactions of hydrogenation and dehydrogenation, numerous compounds have been observed and identified by GC-MS. They are displayed with the acronyms that are used further in the text, in Figure IV-3, and sorted in 5 different classes according to their role in the reaction of interest. The classes taken into account for the LOHC stability are the "LOHC couple" and "intermediates of interest". "Intramolecular dehydration", "Intermolecular dehydration" and "Condensation" are classes regrouping the degradation products.

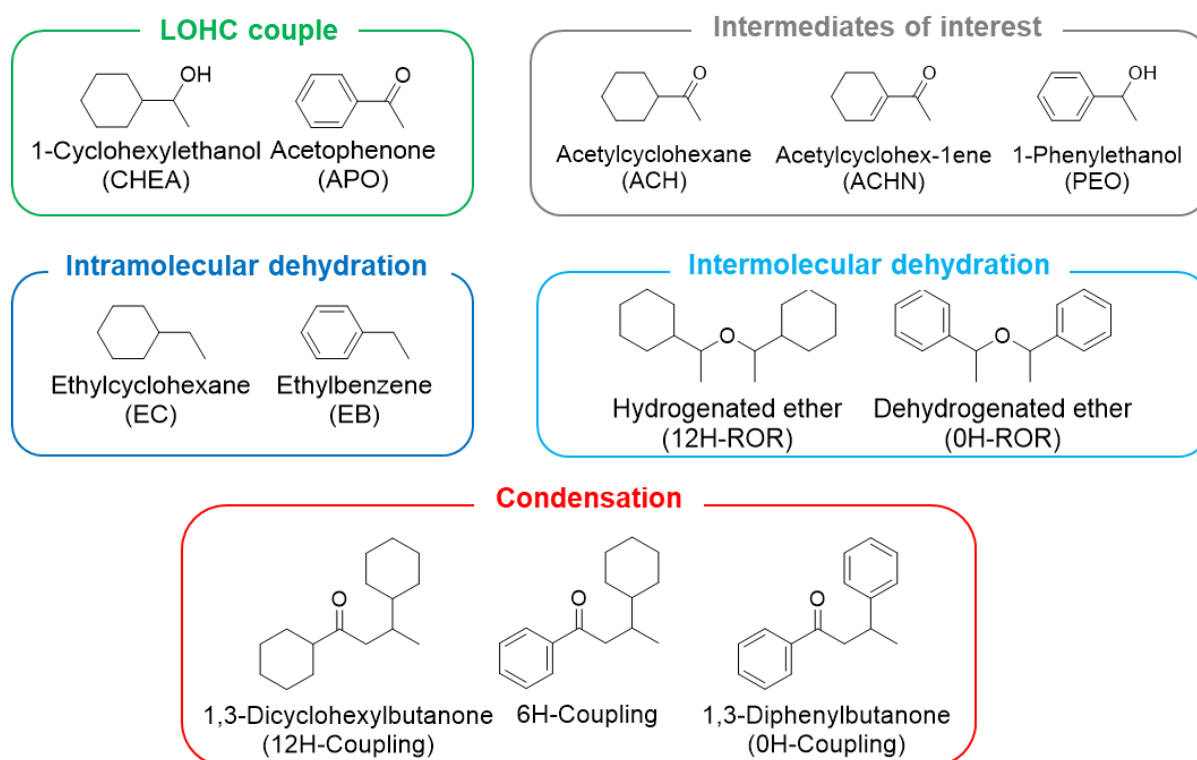
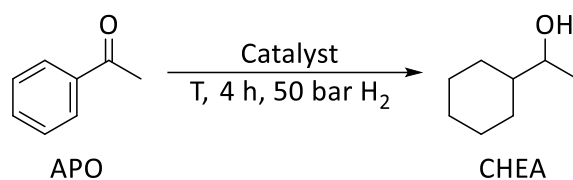


Figure IV-3 – Compounds observed during the cycling of the LOHC and their classification

Chapter 1: Evaluation of new LOHC structures

IV.2.1 Hydrogenation

The hydrogenation of APO to CHEA was first studied as the exothermic hydrogenation is the easiest reaction of the cycle. Various supported noble metal commercial catalysts were tested for the hydrogenation of Acetophenone and the results are presented in Table IV-8. The complete GC-MS results can be found in Appendix IV-2.



Conditions	Conversion	LOHC stability	DoH
5%Pt/Al ₂ O ₃ , 80 °C	98%	>99%	42%
5%Pt/C, 80 °C	99%	97%	51%
5%Pd/Al ₂ O ₃ , 80 °C	>99%	88%	23%
5%Pd/C, 80 °C	>99%	61%	15%
5%Ru/Al ₂ O ₃ , 105 °C	>99%	91%	92%
5%Ru/C, 105 °C	>99%	73%	93%

Table IV-8 – Conversion, LOHC stability and degree of hydrogenation (DOH) of the crude reaction mixture after 4 h hydrogenation of Acetophenone under 50 bar H₂. Acetophenone (12.5 mL), heterogeneous catalyst (0.1 wt% active metal with regard to the Acetophenone)

First of all, all catalysts achieve similar APO conversion levels in 4 h (> 98 %). However, the Pd catalysts produce mainly 1-Phenylethanol (PEO), showing their poor activity for the hydrogenation of the aromatic cycle as a standalone meta.⁹² An observed strong tendency for dehydration is also linked to the surface acidity for Pd heterogeneous catalysts.⁹³ Conversely, Pt and especially Ru exhibit high conversions and selectivities, as expected from the literature.^{94,95} General reactivity follows the order Ru > Pt > Pd, in agreement with the literature.⁹⁶ The support, Alumina or carbon, displays in general little to no influence on the conversion, however the LOHC stability is generally improved when alumina is used. Finally, only the Ru based catalysts showed DoH superior to 90%. After this first screening, we thus selected Ru/Al₂O₃ as the best catalytic system as it had the highest selectivity and a DoH equivalent to Ru/C. We then tried to improve it further by modifying the reaction temperature. Ru/C and Pt/Al₂O₃ were used as comparison due to the former presenting the highest DoH and the latter the highest LOHC stability.

While a modification of the temperature has almost no effect for the conversion of APO depending on the catalyst (Appendix IV-3), a strong influence on the hydrogenation selectivity to CHEA was observed. In particular, higher reaction temperatures promote dehydration on the Ru catalysts, probably due to the presence of acidic sites on the support. Conversely, the DoH rapidly reaches >99% values from 105 °C for Ru/C and from 115 °C for Ru/Al₂O₃. At 115 °C, Ru/Al₂O₃ achieves the maximal selectivity and DoH of all studied systems (93% selectivity, >99% DoH) (Figure IV-4)

Chapter 1: Evaluation of new LOHC structures

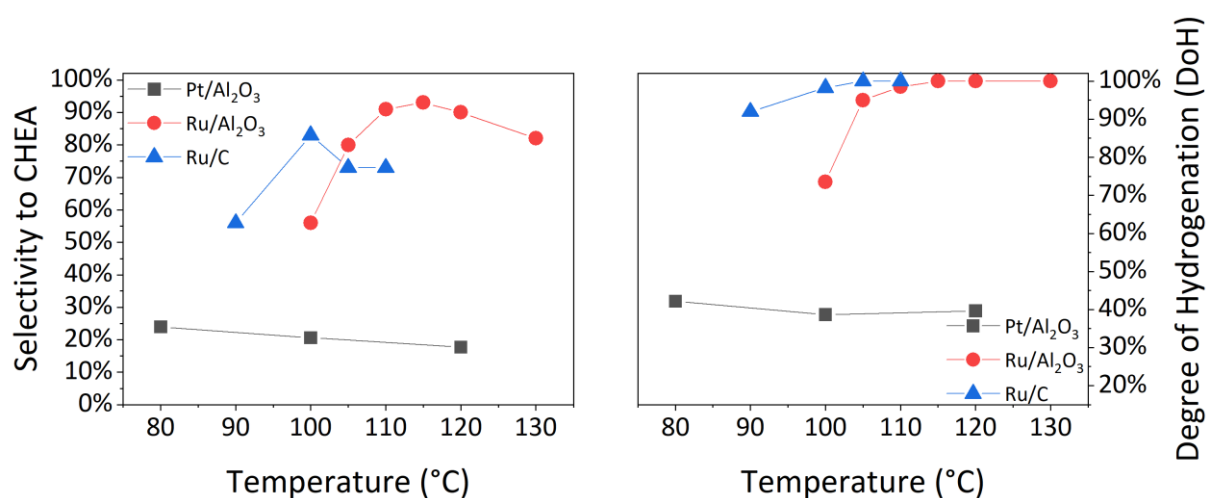


Figure IV-4 - Left: Selectivity to CHEA for Pt/Al₂O₃ (black), Ru/Al₂O₃ (red) and Ru/C (blue); right: DoH for Pt/Al₂O₃ (black), Ru/Al₂O₃ (red) and Ru/C (blue)

The effect of the pressure was also monitored in the optimized catalytic and temperature conditions and the reaction mixture composition was reported in the Figure IV-5.

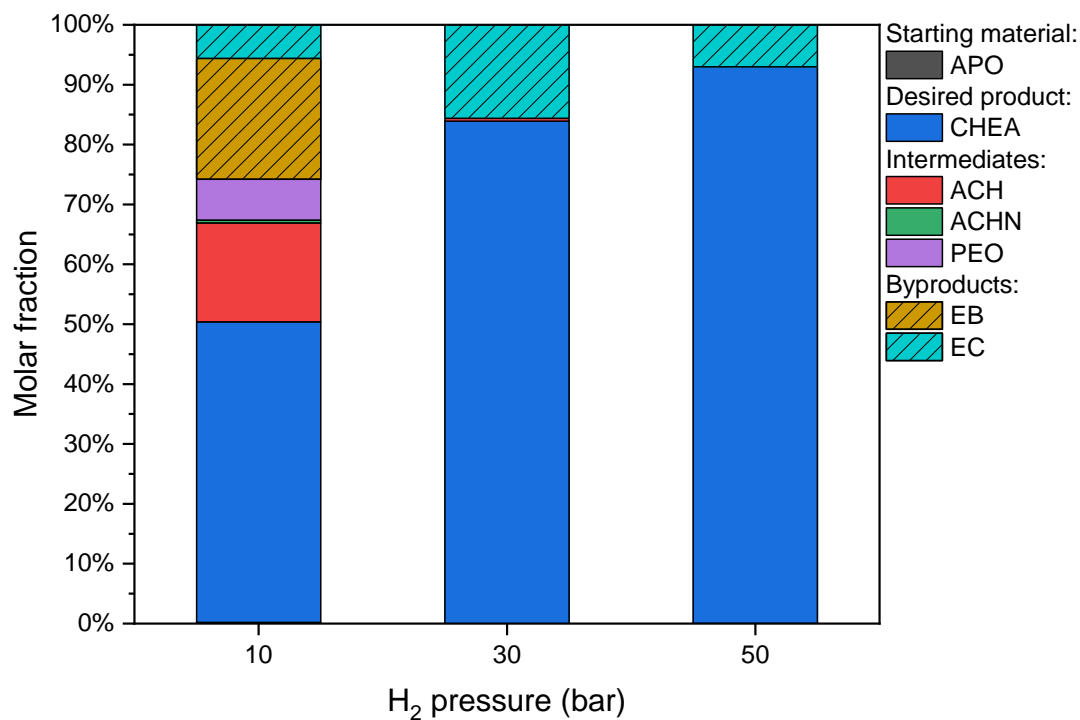
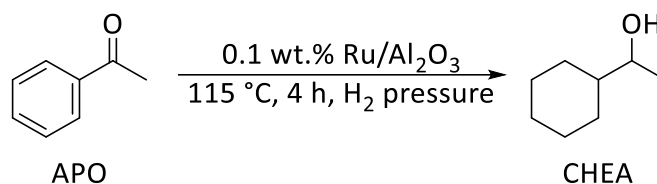


Figure IV-5 – Effect of the pressure on the hydrogenation of APO. APO (15 mL) and 5 wt.% Ru/Al₂O₃ (0.1 wt.% Ru with regard to APO), 115 °C, 4 h.

Chapter 1: Evaluation of new LOHC structures

These results can be interpreted as the influence of the H₂ pressure on the hydrogenation kinetics. Indeed, if the H₂ pressure decreases, the hydrogenation kinetics will also decrease. However, as the dehydration reaction is not related to H₂, its kinetics stays relatively the same. Moreover, a hypothesis could also have been that H₂O at lower pressure can be vaporized in the reaction conditions, displacing the equilibrium of the reaction towards the dehydration products. However, as the boiling point of H₂O at 10 bar is 181 °C, this mechanism seems unlikely.⁹⁷ Therefore, dehydration products formation is prevalently observed when the H₂ pressure is reduced.

The calcination and subsequent activation of Ru/Al₂O₃ under hydrogen increases the selectivity and reduces the reaction time (Figure IV-6).

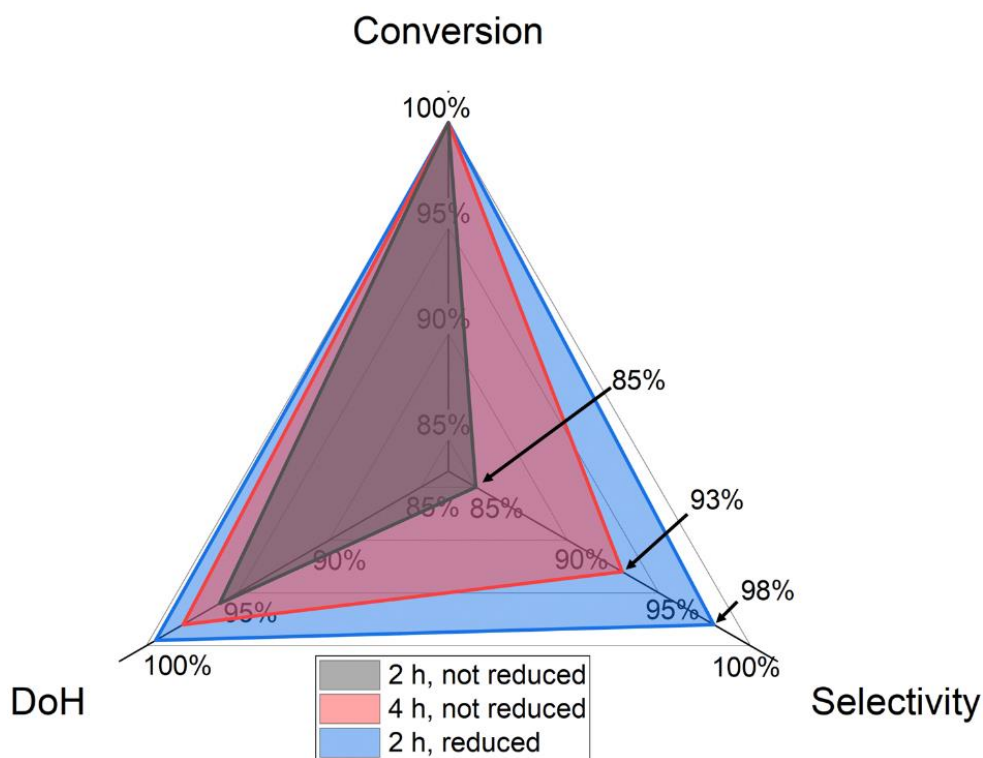


Figure IV-6 – Influence on the reductive activation of Ru/Al₂O₃ on the conversion, Selectivity to CHEA and Degree of Hydrogenation. APO (12.5 mL), Ru/Al₂O₃ (0.1 wt% Ru to APO), 115 °C, 2 h, 50 bar H₂.

After optimization, we thus selected the activated Ru/Al₂O₃ as a hydrogenation catalyst (0.1 wt% active metal to Acetophenone), used at 115 °C for 2 h, under 50 bar of H₂.

Chapter 1: Evaluation of new LOHC structures

IV.2.2 Analysis of the selected Ru/Al₂O₃ hydrogenation catalyst

The Ru/Al₂O₃ catalyst was analyzed by XPS at three different steps: as supplied, after activation and after hydrogenation. The Ru 3d and Ru 3p core levels were recorded (Figure IV-7a and Appendix IV-4) to estimate the oxidation state of the catalyst. For data treatment, a Shirley background was applied for both spectra and fitting of the Ru 3d core level spectra was achieved by using three pairs of pseudo-voigt function, a linear combination of a Gaussian and Laurentzian. The ratio between the 3d doublet area and the distance between the doublet peaks were fixed at 2 and 4.2 respectively.

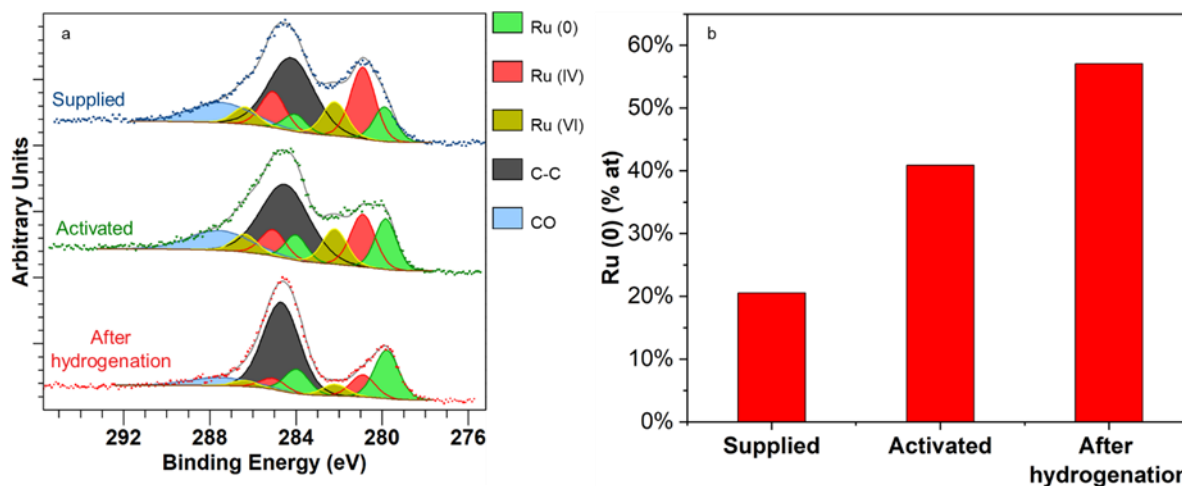


Figure IV-7 (a) Ru 3d spectra of the ruthenium of the supplied catalyst, the activated catalyst and the catalyst after hydrogenation. b) Atomic percentage of reduced Ru(0) for the supplied catalyst, the activated catalyst and the catalyst after hydrogenation.

Ru species	Binding energy (experimental) (eV)	Binding energy (reference) (eV)
Ru (0) 3d _{5/2}	279.9	280.0 ⁹⁸
		279.9 ⁹⁹
Ru (IV) 3d _{5/2}	280.9	280.7 ^{98,99}
Ru (VI) 3d _{5/2}	282.2	282.5 ⁹⁸
		282.4 ⁹⁹

Table IV-9 - Comparison of the experimental binding energies of the 3d_{5/2} peaks with references from the literature.

In Figure IV-7a, the Ru3d_{5/2} peaks at 279.9, 280.9 and 282.2 eV correspond to Ru(0), Ru (IV) and Ru(VI) oxidation states respectively (the peaks are assigned in green, red and yellow in the Figure IV-7a respectively).⁹⁹ The RuO₃ species was described as a defect structure on the surface of RuO₂.⁹⁸ As the C 1s core energy level is superimposed on the Ru 3d core level, a peak corresponding to organic surface contamination is added (C-C peak). The spectra also show the presence of oxidized carbon species (CO peak) that disappear after the catalyst is activated. All of the Ru peaks binding energies in the 279 to 283 eV range are reported in the Table IV-9. Ru (IV) and Ru (VI) were grouped as “oxidized Ru” and the percentage of reduced Ru(0) was compared to the former (Figure IV-7b). An increase of almost 20% of the reduced Ru(0) is obtained after the activation of the catalyst and a further increase of 20% is observed after the hydrogenation, leaving 40% of oxidized Ru species that are ascribed to surface oxidation in air and covalent bonds between the Ru nanoparticles and the alumina substrate.¹⁰⁰

Chapter 1: Evaluation of new LOHC structures

These results are in agreement with the removal of surface contaminants as well as reduction of oxidized Ru and modification of the support that were observed by FTIR-ATR, Raman spectroscopy, XRD and ICP-OES (Figure IV-8a, b, c and d resp.).

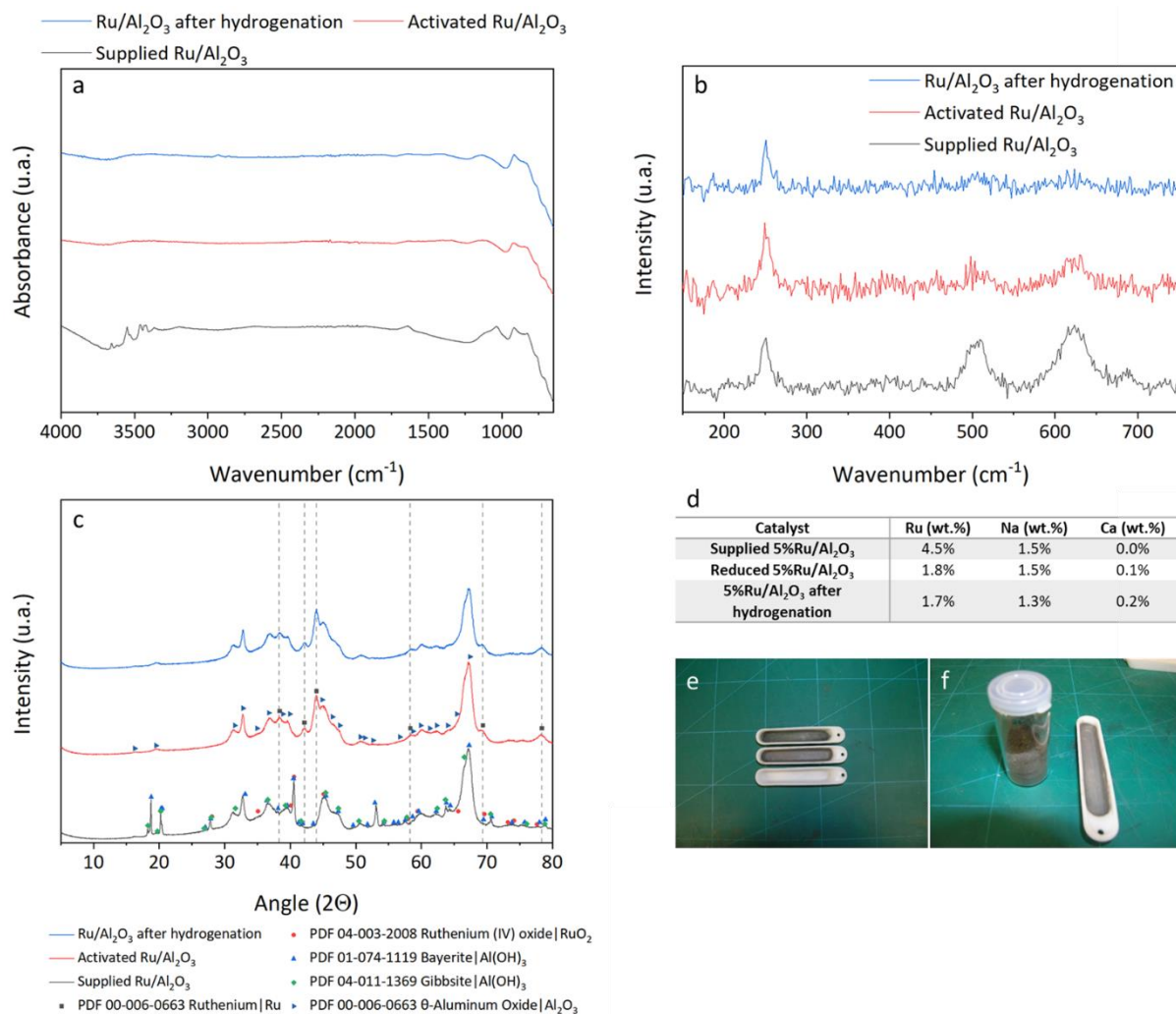


Figure IV-8 – (a) FTIR-ATR spectroscopy, (b) Raman spectroscopy, (c) XRD and (d) ICP-OES of the Ru/Al₂O₃ catalyst, as supplied (black), reduced (red) and after hydrogenation (blue). (e) Corundum boats, before activation (bottom); after activation of the Ru/Al₂O₃ catalyst (middle) and aqua regia + pyrolysis of a contaminated boat under air at 700 °C (top). (f) Color comparison between the activated catalyst (left) and the contamination of the corundum boat (right).

In the Figure IV-8a, the 3800-3670 cm⁻¹ broad band and the shoulder around 3305 cm⁻¹ are indicative of adsorbed molecular H₂O on the surface, while the distinctive peaks at 3444 and 3427 are characteristic of bayerite-type species and the peaks at 3535 and 3404 of gibbsite-type species.¹⁰¹ After the activation, the O-H vibrations disappear, which is in agreement with the XRD analysis (Figure IV-8c). Surface contaminants (1640-1040 cm⁻¹) are removed during the activation. No carbon contamination is visible post reaction. Raman spectroscopy (Figure IV-8b) reveals the 500, 620 and 685 cm⁻¹ vibration modes that corresponds to RuO₂ in the rutile phase, respectively the Eg, A1g and B2g vibrations. The position and width of the peaks confirm the nanometric size of the particles. The 248 cm⁻¹ vibration modes probably corresponds to an unknown oxide impurity in the Al₂O₃ support, as it is observed for all samples with a comparable absolute intensity. This peak is used to normalize the signal and compare the rest of the peak intensities. Traces of RuO₂ are found after reduction and reaction, potentially due to an incomplete reduction or oxidization in air. No formation of coke was

detected after reaction. XRD (Figure IV-8c) shows the reduction of RuO_2 to Ru and $\text{Al}(\text{OH})_3$ to Al_2O_3 during the activation. The reduction of the Al species diminishes the available surface acidic protons, which might in turn explain the increased selectivity due to the limitation of the dehydration reaction. Ru reduction is also beneficial for the hydrogenation kinetics and might be another pertinent hypothesis.¹⁰² ICP-OES analysis shows no lixiviation for the $\text{Ru}/\text{Al}_2\text{O}_3$ catalyst. The activation process diminishes the Ru amount, potentially due to the slow formation of gaseous RuO_3 or RuO_4 in Air.¹⁰³⁻¹⁰⁵ However, TGA-MS (Figure IV-10) did not show any presence of those compounds. It is possible that the technique was not sensitive enough. Another option is a transfer of Ru from Al_2O_3 to the corundum alumina boat: coloration of the corundum boat is similar to that of the reduced catalyst (Figure IV-8e and f). Pyrolysis in air (700 °C, 10 °C/min, 2 h) was performed, proving that the coloration was not due to an organic residue as no weight loss was observed during the process. Cleaning of the residue with aqua regia did not result in any change of coloration (Figure IV-8e). Its study of the activation mechanism was performed by TGA (Figure IV-9).

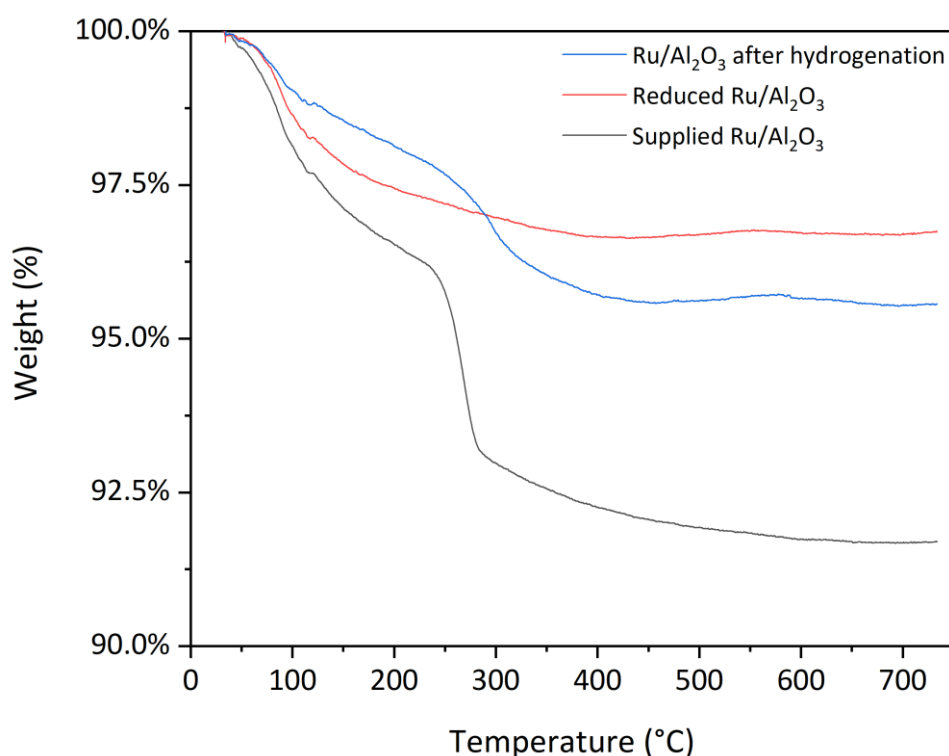


Figure IV-9 - Thermal Gravimetric Analysis (TGA) of the $\text{Ru}/\text{Al}_2\text{O}_3$ catalyst, as supplied (black), reduced (red) and after hydrogenation (blue) in dry air.

First, TGA analysis in dry air shows a weight loss (about 3 wt.%) between 50 to 200 °C, probably due to the removal after adsorbed water on the surface (Figure IV-9). The second weight loss (about 4 wt.%) observed between 250 to 300 °C could be linked to the removal of water from the hydroxyl groups on the alumina surface as characterized by XRD, forming Al_2O_3 .

A step-by-step analysis of the activation process of $\text{Ru}/\text{Al}_2\text{O}_3$ was then performed by TGA-MS (Figure IV-10).

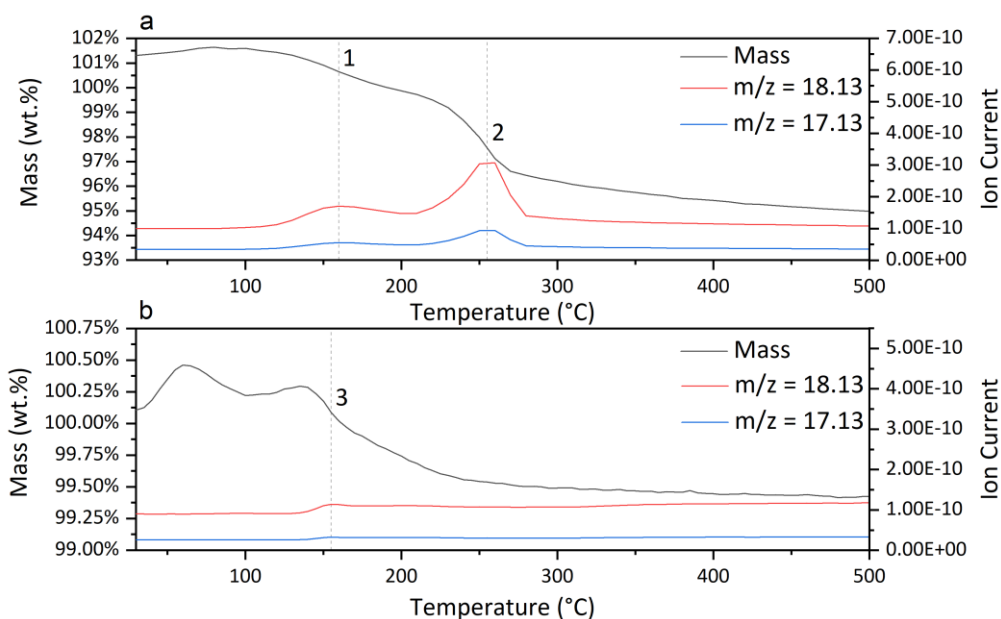


Figure IV-10 – (a) TGA-MS of the supplied Ru/Al₂O₃ catalyst in dry air; (b) TGA-MS of the oxidized Ru/Al₂O₃ catalyst under 2% H₂/Ar.

TGA-MS analysis in dry air (Figure IV-10a) presents water removal at 160 °C and 255 °C (dashed lines 1 and 2 resp.). No other signal was visible in mass spectrometry. This observation is in agreement with FTIR-ATR (Figure IV-8a) and XRD (Figure IV-8c) analysis that shows the removal of surface water and hydroxyl groups during the calcination. The calcined catalyst was submitted to TGA-MS under a 2% H₂/Ar flux (Figure IV-10b). From 155 °C onward (dashed line 3), continuous water losses are observed by mass spectroscopy in a slow process. No other species was visible by mass spectrometry. Reduction of RuO₂ into Ru is judicious as the weight loss is inferior to 1 wt.% hence not related to the bulk support. TEM-EDX analysis was performed to assess the size and distribution of the Ru nanoparticles (NP). An example of imaging and EDX analysis is presented in the Figure IV-11 and the other imaging can be found in Appendix IV-5.

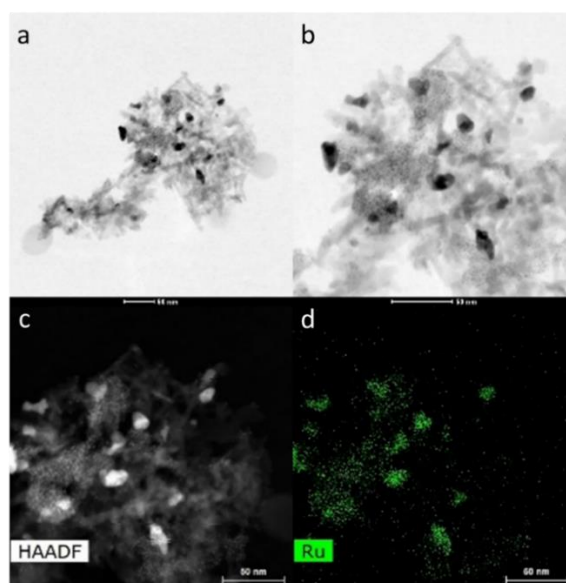


Figure IV-11 - TEM-EDX imaging of the Ru/Al₂O₃ catalyst after dehydrogenation. (a) low magnification; (b) high magnification; (c) High-angle annular dark-field imaging (HAADF); (d) Ru EDX mapping.

Chapter 1: Evaluation of new LOHC structures

The size density of the Ru NP for each catalyst was obtained by measuring the diameter of 200 particles, showing that sintering of the NP occurs after the activation and reaction (Figure IV-12).

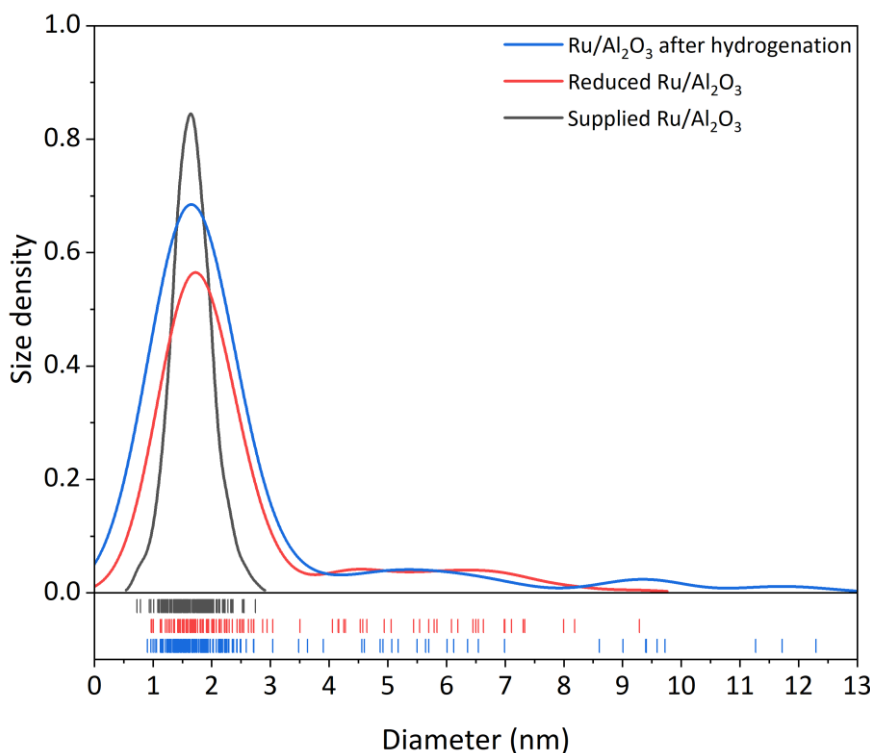


Figure IV-12 - Size density of the Ru NP in function of the diameter for the Ru/Al₂O₃ catalyst, as supplied (black), reduced (red) and after hydrogenation (blue). Each stick below the abscissa axis corresponds to a measured diameter.

The results were confirmed by the size distribution presented in Table IV-10. BET analysis of the catalyst was also conducted.

Ru/Al ₂ O ₃ catalyst state	Ru average size and dispersion (nm)	Specific surface (m ² /g)	Average pore diameter (nm)
Supplied	1.7±0.3	135	19.1
Activated	2.4±1.6	138	19.7
After hydrogenation	2.4±2.1	137	20.2

Table IV-10 – Average size and dispersion of the Ru NP and the associated specific surface and average pore diameter of the Al₂O₃ support.

A limited agglomeration of the Ru nanoparticles was observed by TEM-EDX but should have no measurable incidence on catalytic activity at these high conversions. Indeed, activity variation is usually observable only for sizes exceeding 5-10 nm.¹⁰⁶ However, the Ru reduction state matters as Ru(0) species have also been shown to increase the activity for hydrogenation reactions comparatively to Ru(IV) species.¹⁰² The structure of the support (specific surface and pore diameter) was not modified by the activation process and reaction as showed by BET adsorption. The XPS Al 2p core level spectra (Figure IV-13) shows no notable differences after activation and after hydrogenation.

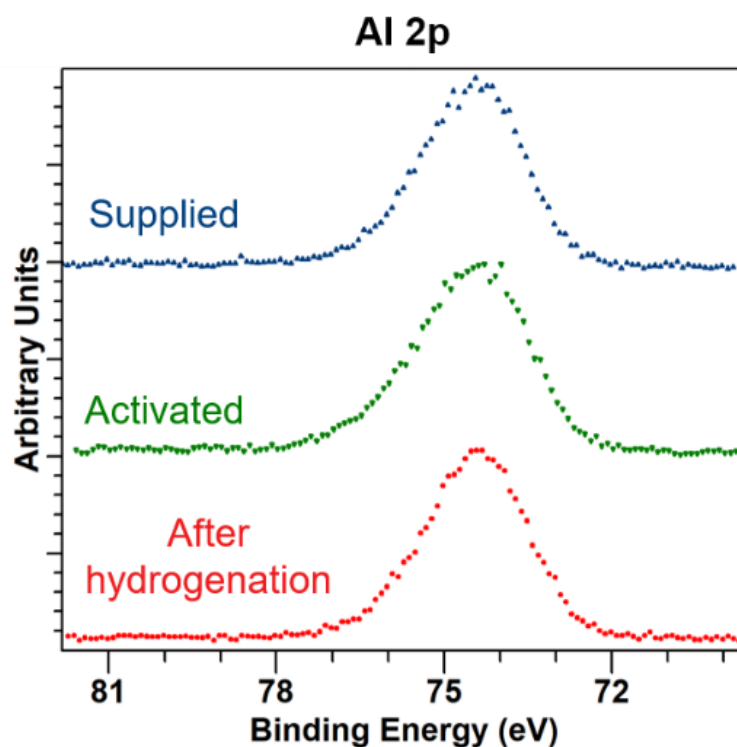


Figure IV-13 - Al 2p spectra of the ruthenium of the supplied catalyst, the activated catalyst and the catalyst after hydrogenation.

The position of the peaks around 74.5 eV corresponds to the Al³⁺ oxidation state and not to a metallic Al which is reported around 72.5 eV (Table IV-11).^{107–109}

	Binding energy (eV)
Supplied	74.5
Activated	74.8
After hydrogenation	74.6

Table IV-11 – Peak energy positions of the Al 2p peaks of the supplied catalyst, the activated catalyst and the catalyst after hydrogenation.

The presence of Al₂O₃ or Al(OH)₃ could not be determined by XPS analysis but XRD analysis (Figure IV-8c) showed Al(OH)₃ turning into Al₂O₃ during the activation of the catalyst.

IV.2.3 Dehydrogenation

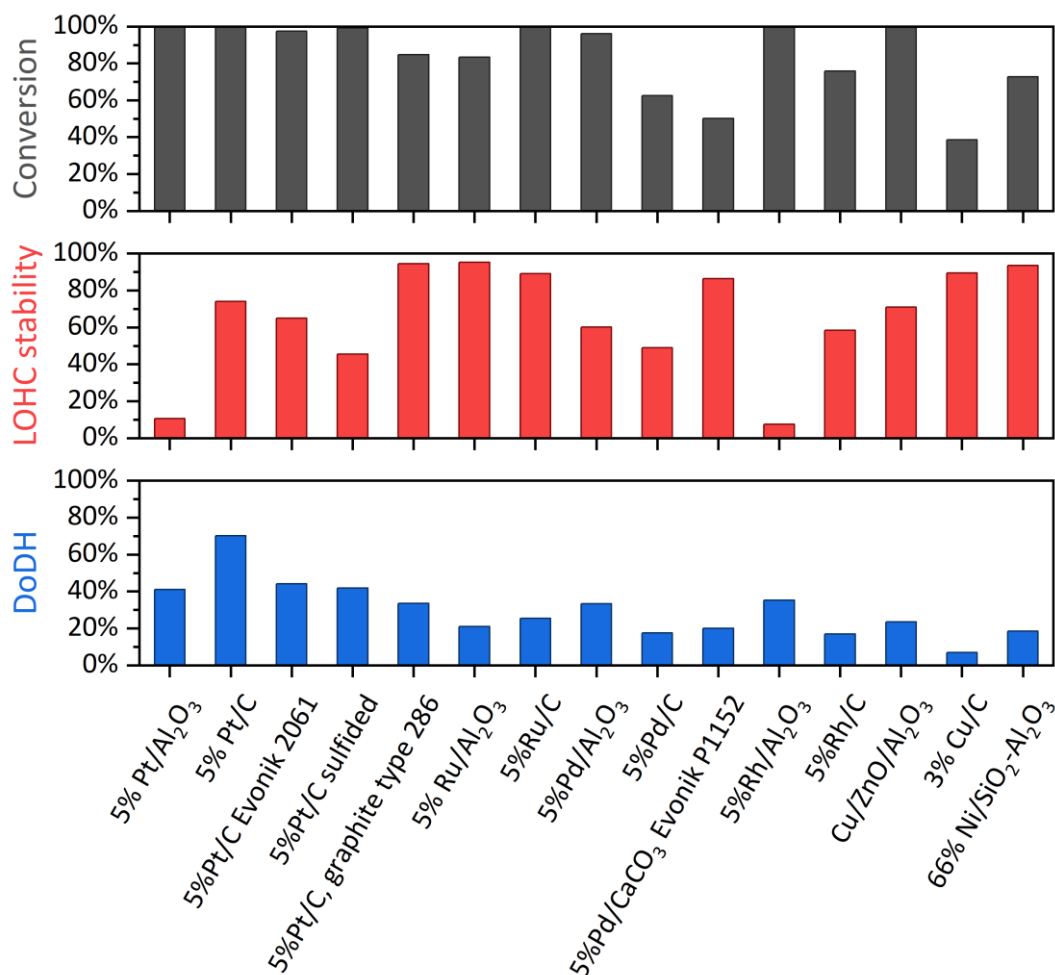
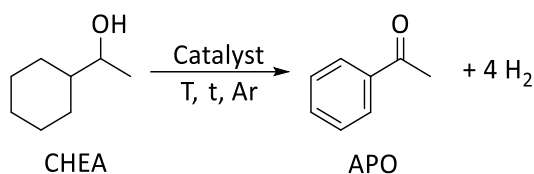


Figure IV-14 - Degree of dehydrogenation (DoDH) of the catalysts tested for the dehydrogenation of CHEA to APO. 1.5 mL CHEA, 1 wt.% active metal catalyst (with regard to APO), 18 h, 205 °C, Ar.

The dehydrogenation is endothermic, and is often the barrier to get an efficient LOHC system.¹⁷ Here we tested various noble and non-noble metal commercial catalysts for the dehydrogenation of CHEA to produce APO (Figure IV-14). The Ru, Cu and Ni catalysts showed good conversion and selectivity for the dehydrogenation of the alcohol to the ketone but a limited reactivity for the aromatization, in agreement with the literature.¹¹⁰⁻¹¹² The Pd catalysts achieved the dehydrogenation of both the cycle and the alcohol but also exhibited a strong tendency for dehydration products (Figure IV-3).^{65,113} Similarly to Pd, the Rh catalysts managed both dehydrogenation steps but favoured the formation of the coupling products instead.^{113,114} Pt catalysts displayed the best conversion of all catalysts, but intramolecular dehydration products could always be found. Various side-reactions were favoured depending on the support but no correlation with the support was found. Out of all the tested catalysts, the 5%Pt/C catalyst supplied by Sigma-Aldrich yielded the best compromise between conversion, LOHC stability and degree of dehydrogenation. Further experiments on the catalytic

Chapter 1: Evaluation of new LOHC structures

loading and time of reaction after activation were used to refine the conditions to yield the most efficient dehydrogenation parameters: 0.25 wt.% catalyst loading, 36 h. (Table IV-12).

Catalyst loading (wt.%)	Time (h)	Conversion	Degree of Dehydrogenation	LOHC stability
0.1	24	95%	50%	88%
0.1	36	98%	59%	87%
0.25	24	>99%	66%	80%
0.25	36	100%	72%	80%
1	24	100%	72%	68%

Table IV-12 - Effect of the catalyst loading and time of reaction after activation on the conversion, degree of dehydrogenation, LOHC stability and geometrical average of the three parameters for the reaction of dehydrogenation of 1.5 mL of 1-Cyclohexylethanol at 205 °C under Ar.

While this result is promising, CHEA dehydrogenation kinetics are still a hundred to a thousand times slower than the benchmark system: Dibenzyltoluene at 1 gH₂/gPt/min.¹¹⁵

IV.2.4 Analysis of the selected Pt/C dehydrogenation catalyst

The catalyst was analyzed by XPS after three different steps: as supplied, after activation and after dehydrogenation (Figure IV-15a).

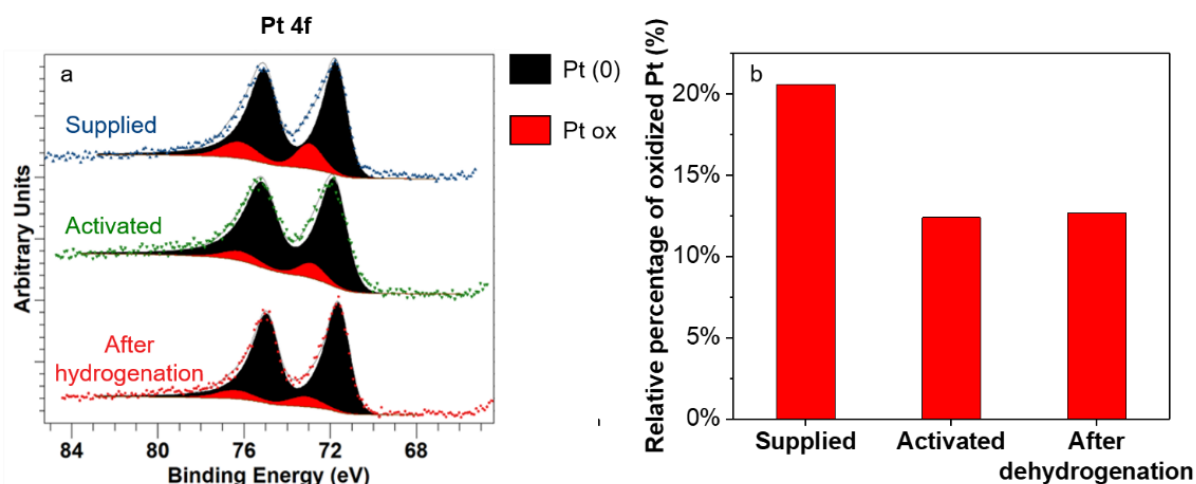


Figure IV-15 - (a) Pt 4f spectra of the supplied catalyst, the activated catalyst and the catalyst after dehydrogenation. (b) Percentage of the oxidized Pt relative to the reduced Pt for the supplied catalyst, the activated catalyst and the catalyst after dehydrogenation.

The Pt 4f core level was fitted with an asymmetric doublet corresponding to the reduced state of platinum.¹¹⁶ Another pair of pseudo-Voigt distribution (Gaussian-laurentzian peaks) corresponding to an oxidized Pt state was added, contributing for 20% of the Pt species in the supplied catalyst. The activation of the catalyst leads to the decrease of the oxidized Pt species as O₂-reactive low coordination sites are removed (Figure IV-15b).^{117,118} The proportion of the oxidized Pt species is reduced to roughly 13% after the activation of the catalyst. These oxidized species can be attributed to the links of surface Pt atoms with surface oxygen-rich functions such as CO, COO and COH groups.^{119,120} No significant variation of oxidized Pt is observed between the activated catalyst and the catalyst after dehydrogenation.

Chapter 1: Evaluation of new LOHC structures

FTIR-ATR analysis was conducted to verify the presence of such functional groups at the surface (Figure IV-16a).

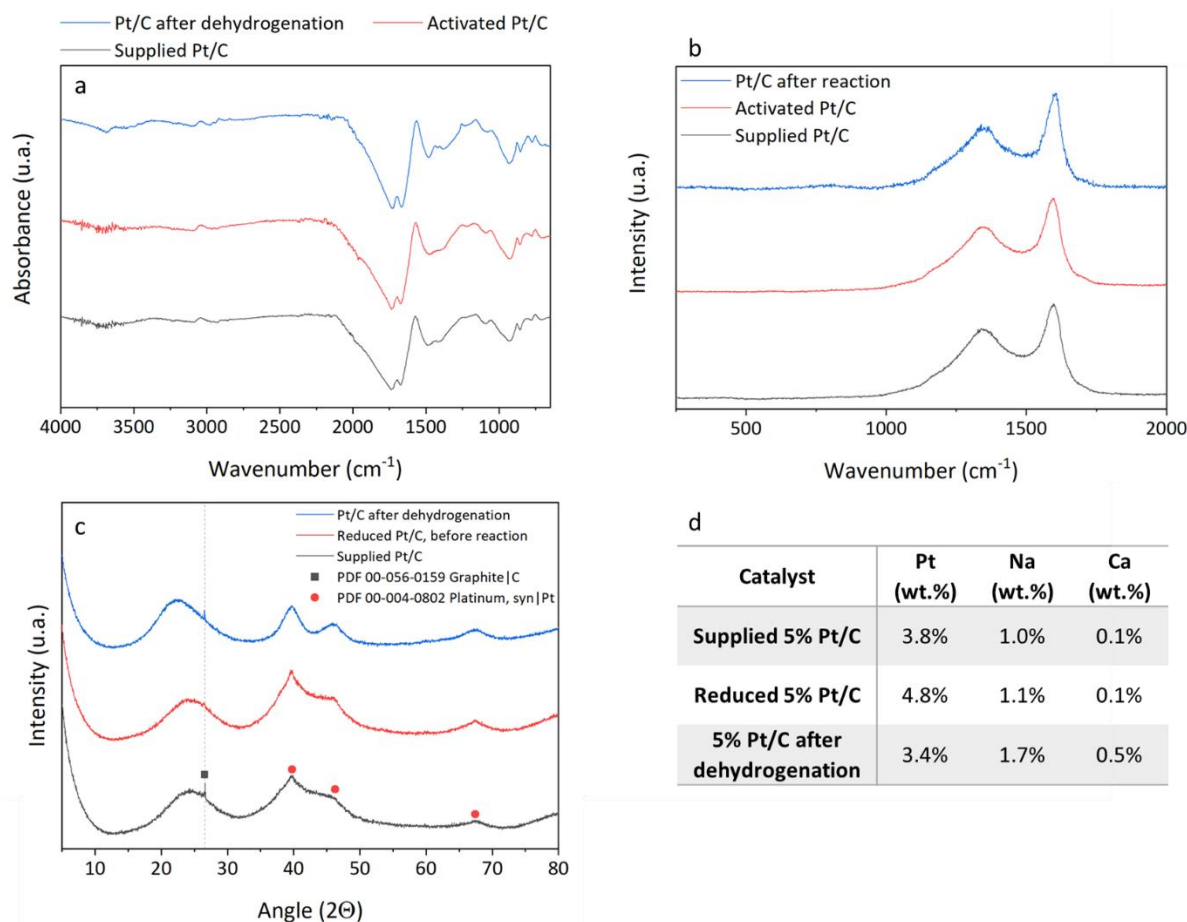


Figure IV-16 - (a) FTIR-ATR spectroscopy, (b) Raman spectroscopy, (c) XRD and (d) ICP-OES of the Pt/C catalyst, as supplied (black), reduced (red) and after hydrogenation (blue).

The presence of an intense peak at 1735 cm^{-1} , attributed to conjugated esters or lactones and another intense peak at 1670 cm^{-1} attributed to conjugated ketones, seems to confirm this hypothesis.¹²¹ Moreover, no formal PtO_2 or Pt(OH)_4 were not observed by Raman (Figure IV-16b) and XRD (Figure IV-16c). Both analysis observe the carbon support, while XRD detected nanometer-sized Pt structures. ICP-OES shows little to no variation between the samples (Figure IV-16d). TGA analysis (Figure IV-17) in dry air revealed that up to 8.3% of inorganic components were present in the catalyst, similarly to what was obtained by ICP-OES.

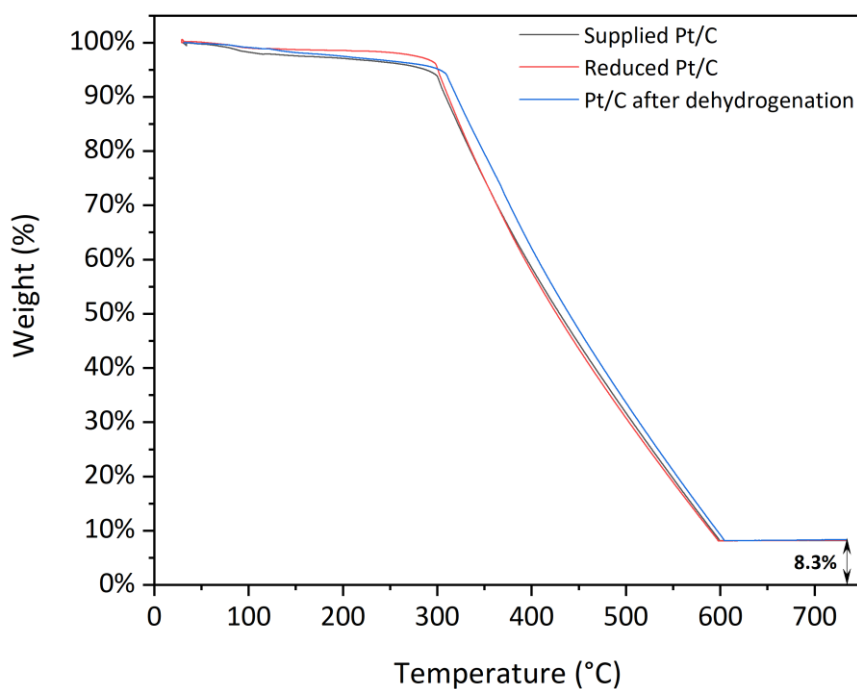


Figure IV-17 - TGA of the Pt/C catalyst as supplied (black), reduced (red) and after dehydrogenation (blue) in dry air.

A limited sintering of the Pt nanoparticles is visible by TEM-EDX (Figure IV-18 and Appendix IV-6) and XRD (Figure IV-16c) after dehydrogenation.

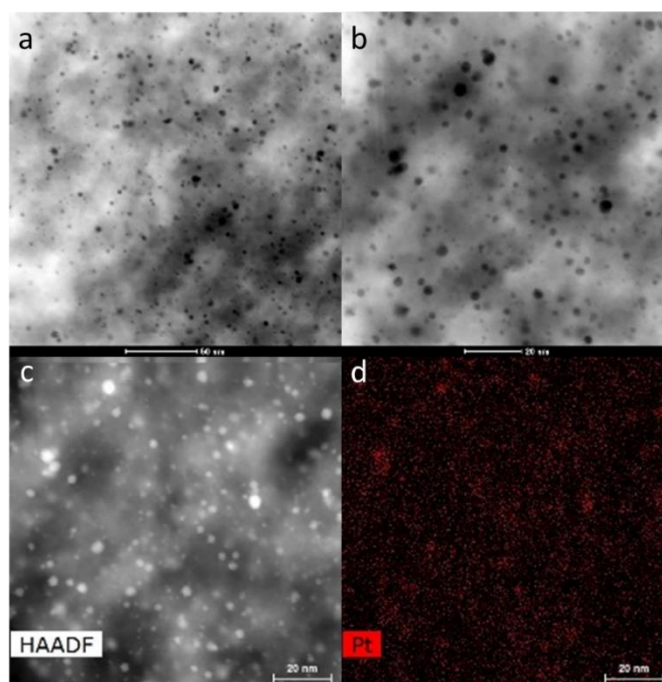


Figure IV-18 - TEM-EDX imaging of the Pt/C catalyst after dehydrogenation. (a) low magnification; (b) high magnification; (c) High-angle annular dark-field imaging (HAADF); (d) Pt EDX mapping.

The size density of each catalyst was obtained by measuring the diameter of 200 particles, showing that only limited sintering of the NP occurs during the dehydrogenation (Figure IV-19). Although the sintering is limited, it is not absent as observed by the apparition of two size modes. Therefore, catalytic development would still be required to avoid further sintering.

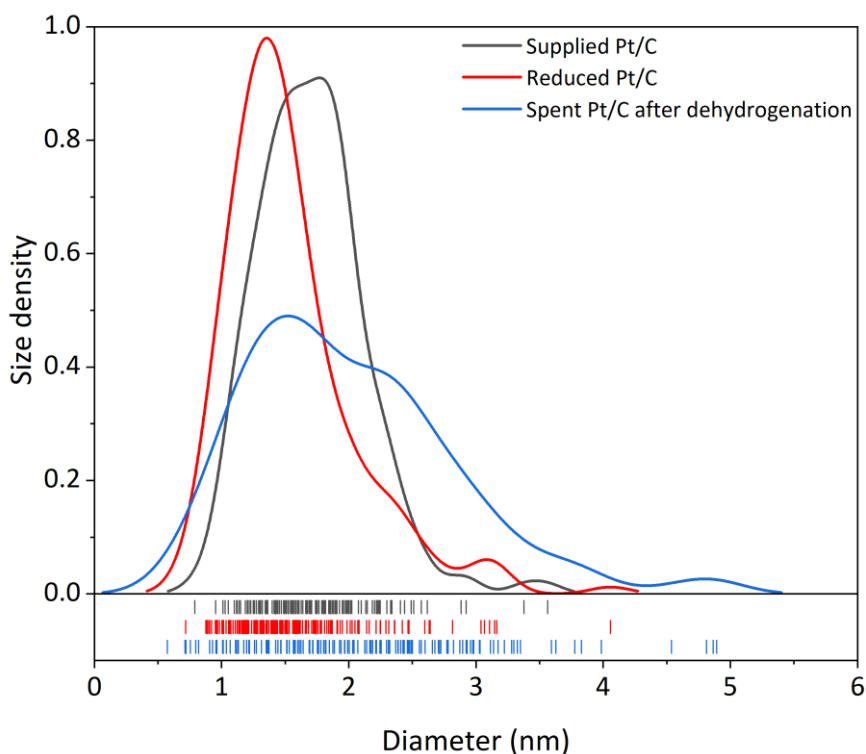


Figure IV-19 - Size density of the Pt NP in function of the diameter for the Ru/Al₂O₃ catalyst, as supplied (black), reduced (red) and after hydrogenation (blue). Each stick below the abscissa axis corresponds to a measured diameter.

The results were confirmed by the size distribution presented in Table IV-13. BET analysis of the catalyst was also conducted.

Pt/C catalyst state	Pt average size and dispersion (nm)	Specific surface (m ² /g)	Pore diameter (nm)
Supplied	1.7±0.4	1577	3.4
Activated	1.5±0.5	1598	3.4
After hydrogenation	2.0±0.8	1460	3.4

Table IV-13 - Average size and dispersion of the Pt NP and the associated specific surface and average pore diameter of the carbon support

No significant agglomeration of the Pt nanoparticles was observed by TEM-EDX. Similarly, No significant variation of specific surface and pore diameter was detected after reduction and utilization.

IV.2.5 Chemical kinetics of dehydrogenation

To better characterize the dehydrogenation pathway, chemical kinetics experiments were performed. Chemical kinetics show a near total conversion of the reactant in less than 24 h (Figure IV-20). The LOHC stability decreases linearly over time. The DoDH rapidly increases to 30% in 10 h. At that time, more than 85% of the alcohol is already converted into the ketone. Over the 10 following hours, the DoH increases only by 10%, pointing to a change in the dehydrogenation step controlling the rates. This observation is consistent with a two-step system kinetics with a fast first step and a slow second step.¹²² In addition, the formation of the dehydrogenated condensation product, OH-Coupling, as the main impurity stays below 5% during the reaction.

Chapter 1: Evaluation of new LOHC structures

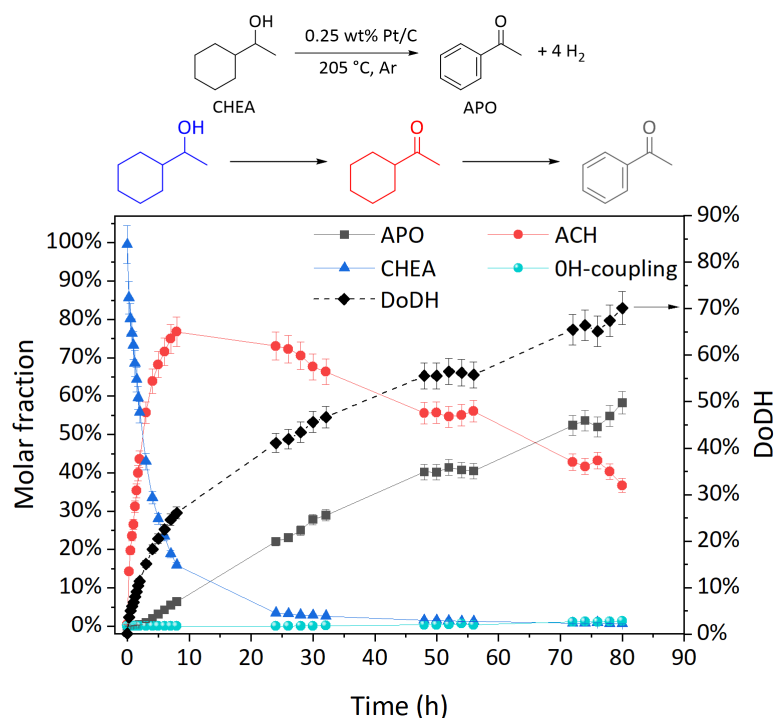


Figure IV-20 – Scheme of the reaction (top); Conversion, LOHC stability and DoDH of the dehydrogenation of CHEA over time (left); Products distribution during the dehydrogenation (right). All other products were found in quantities below 5% during the reaction. 0.25 wt.% catalyst loading, 205 °C, Ar.

Moreover, other kinetic experiments showed that each step of the dehydrogenation is reversible due to the residual H₂ pressure. Indeed, during the dehydrogenation of 1-Phenylethanol (PEO) intermediate to APO, spontaneous hydrogenation of the aromatic cycle is observed either *via* direct hydrogenation or transfer hydrogenation (Figure IV-21).

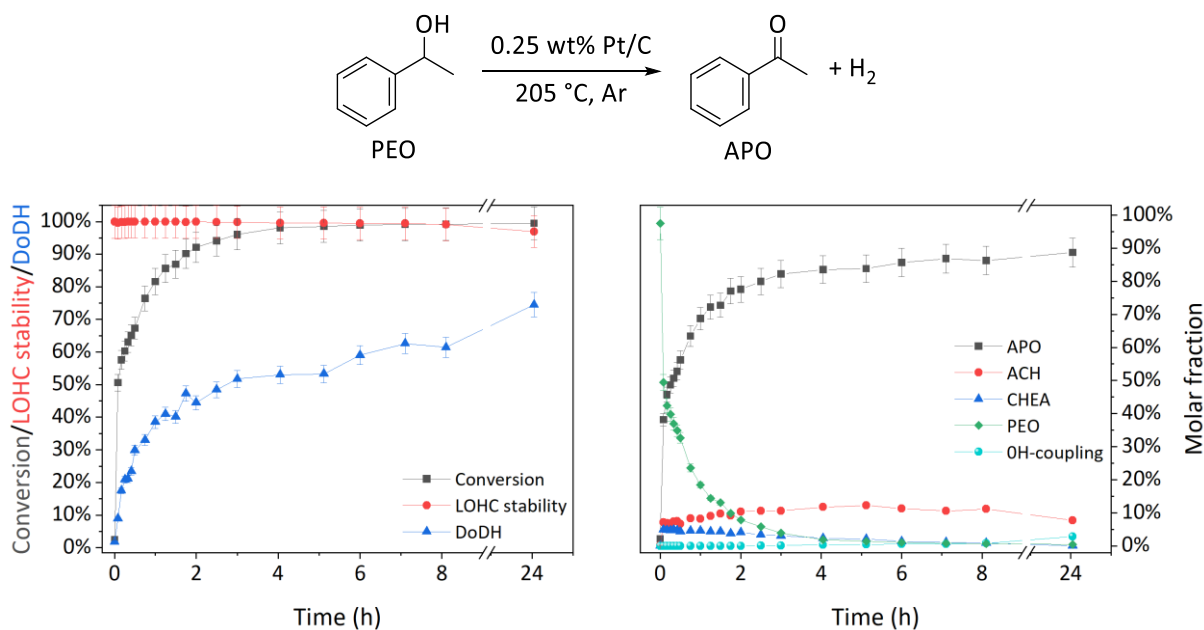


Figure IV-21 - Conversion, LOHC stability and DoDH of the dehydrogenation of PEO over time (left); Products distribution during the dehydrogenation of PEO. All other products were found in quantities below 5% during the reaction. (right). 0.25 wt.% catalyst loading, 205 °C, Ar.

Chapter 1: Evaluation of new LOHC structures

It is however difficult to conclude on which mechanism directs the reaction as the laws of the kinetics for each step are complex and the C-O bond can easily be hydrogenated or dehydrogenated and hence act as a platform for transfer-dehydrogenation.

Further kinetics experiments were carried out under a flux of 2.5%wt.%H₂ in order to calculate the activation energy of each function. Here, each molecule is characterized by 2 factors: the dehydrogenation state of the alcohol function and the one of the cycle (Figure IV-22 top left). The 6H-Coupling product contributes for half its molar fraction to both CH and Ar classes (as defined in Figure 6). No dehydration products were observed during the experiment.

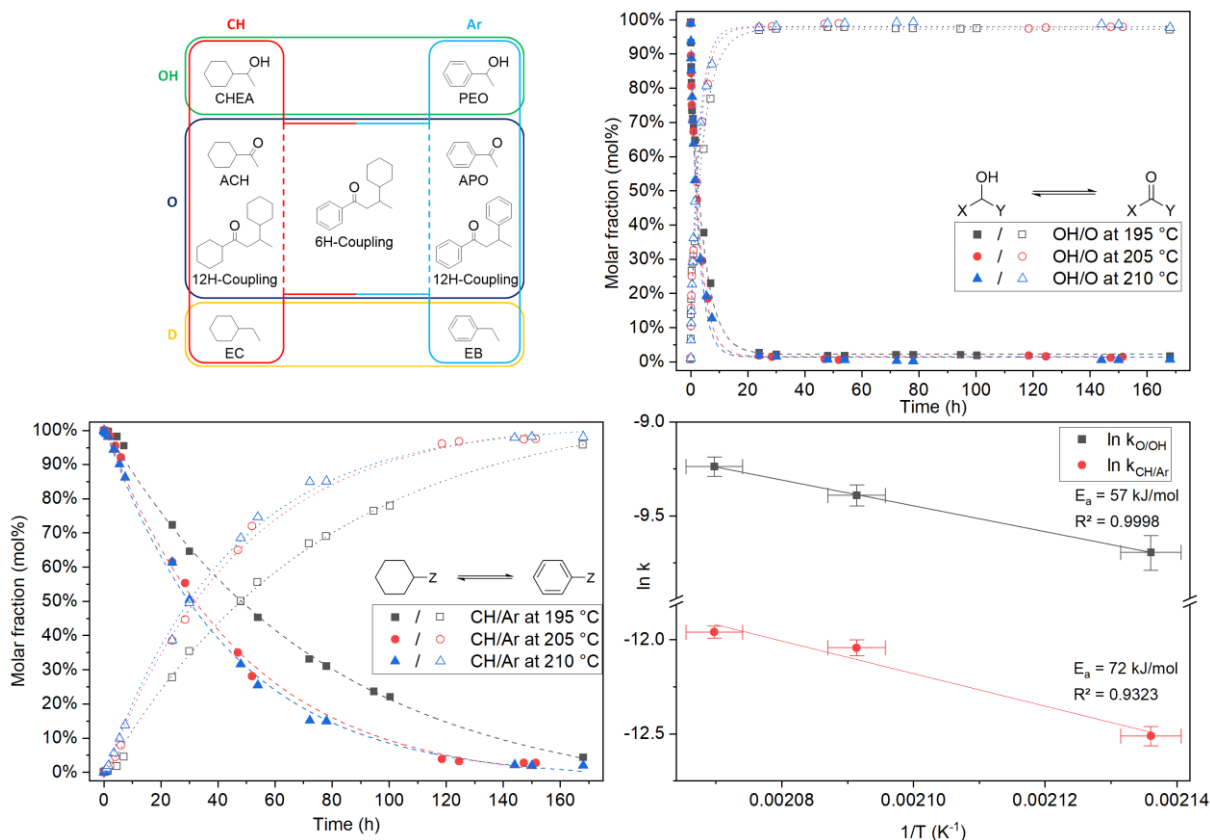


Figure IV-22 –Classification by functions of the products for the lumped kinetics: CH=Cyclohexane, Ar=Aromatic, OH=Alcohol, O=Ketone, D=Dehydration (top left); Lumped kinetics for the O and OH compounds (top right); Lumped kinetics for the CH and Ar compounds (bottom left); Activation energies for the OH/O and CH/Ar functions (bottom right).

For both the OH/O and CH/Ar functions, the increase in the temperature of reaction increases the kinetics as expected. Moreover, the equilibrium state for the OH/O function is reached after 24 h (Figure IV-22 top right), whereas the CH/Ar function reaches equilibrium between 140 and 168 h depending on the temperature of reaction (Figure IV-22 bottom left). The apparent specific rate constants were calculated for each reaction and function by performing an exponential fit on the function curves assuming 1st order kinetics in a batch stirred reactor. All adjusted R² are above 0.989 for first-order kinetics (Appendix IV-7). External diffusion effects are supposedly non limiting due to the high stirring speed (1500 rpm). Indeed, classic LOHC setups have showed external diffusion effects below 500 rpm during the dehydrogenation.¹⁹ Internal diffusion effects are also negligible as shown by internal effectiveness factors being close to 1 for each function (Appendix IV-8). The activation energy for each function was obtained by using the Arrhenius law (Figure IV-22 bottom right). As no kinetics study on the dehydrogenation of CHEA to APO was reported in the literature, the comparison of the

Chapter 1: Evaluation of new LOHC structures

activation energy was performed by assimilating the OH-O function to the dehydrogenation of isopropanol to acetone and the CH-Ar function to the dehydrogenation of cyclohexane to benzene. The OH-O activation energy was calculated to be 57 kJ/mol compared to 28 kJ/mol in the literature.¹²³ The increase in activation energy could be due to the steric hindrance of the cycle compared to the methyl group, as it was observed in the case of the S_N2 and alkaline hydrolysis of esters reactions.^{124,125} Conversely, the calculated CH-Ar activation energy is in good agreement with the literature (72 kJ/mol vs. 70 kJ/mol), which suggests that the O-group does not strongly influence the dehydrogenation of the aromatic ring.¹²⁶ The lower activation energy for OH-O is consistent with the dehydrogenation of this bond before the dehydrogenation of the cycle.

IV.2.6 Cycling

The system was cycled thrice using the optimized conditions (Figure IV-23, top left). A slight degradation occurred, mainly due to the self-coupling and the dehydration of the LOHC (Figure IV-23, top right). However, as the degradation products still possess a 6-membered cycle like EB/EC, cycling of the whole mixture is still possible without a dramatic loss of hydrogen storage.^{127,128} By pondering the theoretical capacity of each degradation product in the mixture, close to 99% of the maximum theoretical hydrogen capacity (i.e. the theoretical capacity of the CHEA/APO couple) is retained even after the third cycle (Figure IV-23, bottom left).

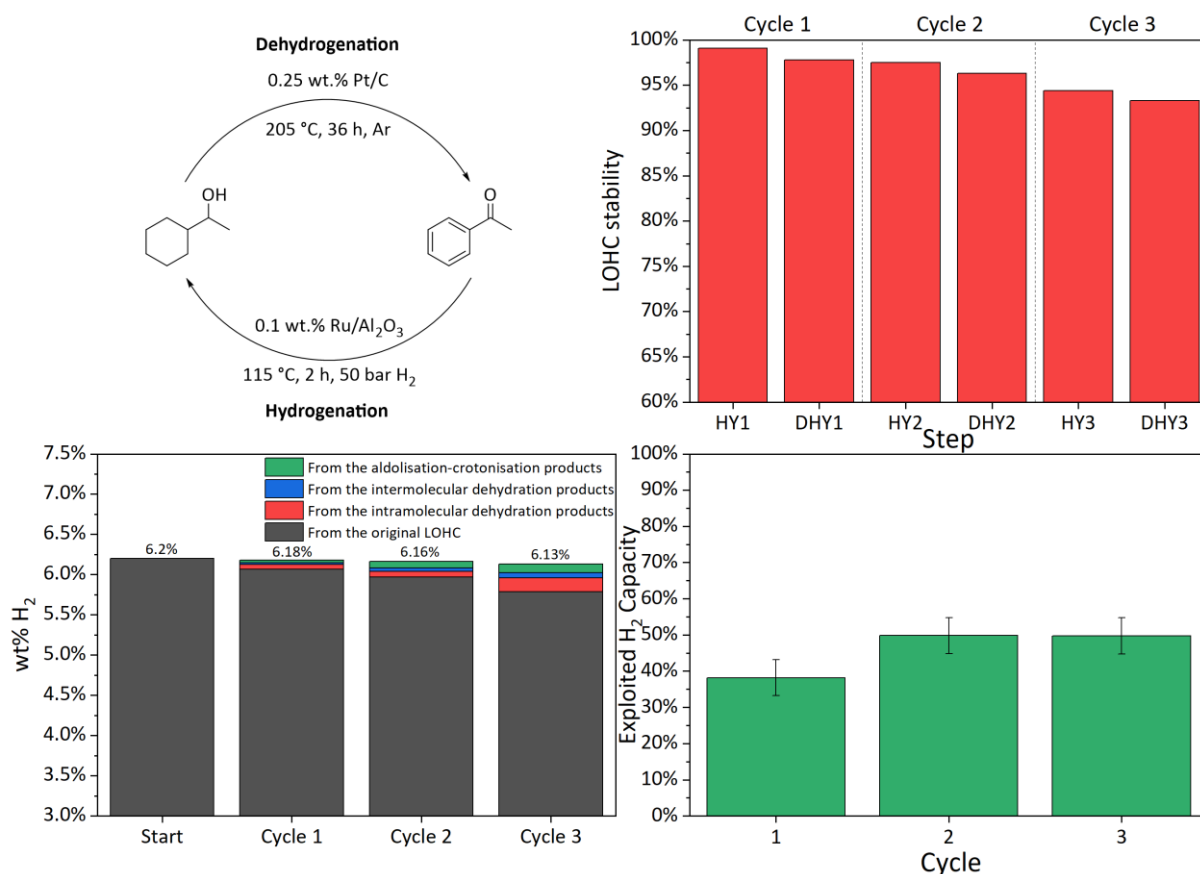


Figure IV-23 –Optimized conditions of cycling (top left); LOHC stability at the end of each step of the cycling (top right); Maximum H₂ theoretical capacity at the end of each cycle (bottom left); Exploited H₂ capacity over the cycling (bottom right).

As new LOHC couples are produced through the degradation of the CHEA/APO, their capacity to store and release H₂ must be taken into account when calculating the exploited H₂ capacity that describes

Chapter 1: Evaluation of new LOHC structures

the amount of hydrogen unloaded during a cycle by the LOHC system. During the cycling, up to 50% of the hydrogen capacity was exploited (Figure IV-23, bottom right). Further catalyst design is hence required to access the rest of the H₂ capacity and decrease the reaction time while avoiding the degradation of the LOHC. Material losses of 10 to 20% per step were visible and attributed to reactor transfers, filtrations and sampling for GC-MS analysis (Table IV-14).

Step	Weight solution (g)	Weight loss (g)	Weight loss in %
Hydrogenation 1	20.085	-4.062	20%
Dehydrogenation 1	16.023	-3.5592	22%
Hydrogenation 2	12.4638	-1.4845	12%
Dehydrogenation 2	10.9793	-2.5416	23%
Hydrogenation 3	8.4377	-1.6337	19%
Dehydrogenation 3	6.804	X	X

Table IV-14 - Weight losses during the cycling.

Moreover, APCI-MS analysis evidenced the presence of the aldolisation-crotonisation product OH-Coupling under the form [OH-Coupling+H] adduct ($m/Z=225$) as the main peak (Figure IV-24). Moreover, numerous other species of lower intensity are present in the reaction mixture. As they are all separated by a m/Z ratio of roughly 12-16, this difference indicates methyl or oxygen addition. Nonetheless, it is uncertain where these species come from. Indeed, they could originate from catalyst contamination, transfer of methyl and oxygen from the catalyst support to the LOHC substrate or unfiltered fragmentation of the carbon support. Therefore, more experimental work would be required.

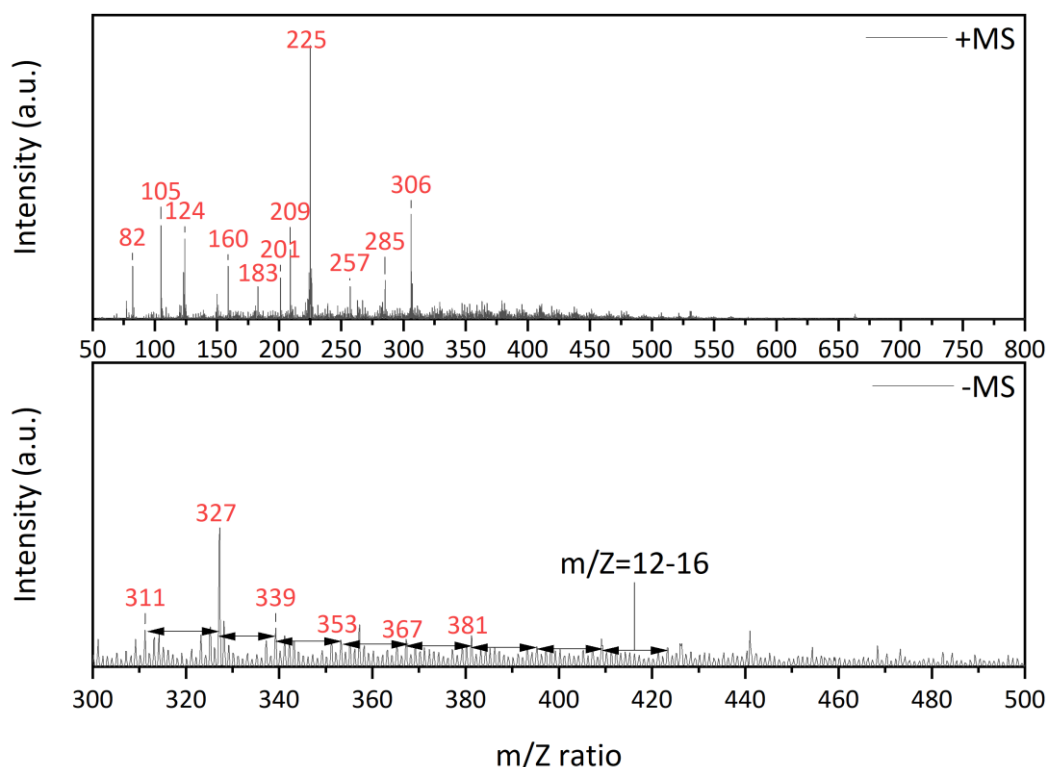


Figure IV-24 - APCI-MS analysis of the LOHC mixture after the cycling.

A dehydrogenation mass balance experiment was also conducted on 10 mL of LOHC, with a weight loss of 13%. However, the result was inconclusive due to the condensation of a portion of the LOHC on the walls of the condenser. Therefore, it is difficult to conclude on the presence and quantity of heavy products.

Chapter 1: Evaluation of new LOHC structures

IV.2.7 Reaction mechanism

We then computed a number of plausible intermediates, some of which are presented in the Figure IV-25. The enthalpy change for each potential intermediate is presented in the Appendix IV-9. Among those, some have been identified by GC-MS (highlighted by green rectangles). The other intermediates are not observed, probably due to their lack of stability or high reactivity. The structures VEC and VEB are proposed as intermediates for the intramolecular dehydration of the alcohols, which are hydrogenated to yield EC and EB as the corresponding cycloalkanes.¹²⁹ Intermolecular dehydration between two alcohol bearing molecules (CHEA and APO) is most thermodynamically favored degradation pathway and 12H-ROR ($\Delta H=-9$ kJ/mol, $\Delta G=1$ kJ/mol) and 0H-ROR ($\Delta H=-2$ kJ/mol, $\Delta G=9$ kJ/mol) should be produced as the main impurities based on the enthalpy change. The probable limitations to the ether formation are the steric hindrance and the lack of strong acidic sites on the catalyst. The coupling products, whilst the less thermodynamically favorable of the impurities ($\Delta H=25$ kJ/mol, $\Delta G=34$ kJ/mol) are formed as the main by-products through an aldol addition of two ketones bearing molecules (ACH and APO), followed by an internal dehydration (12H-AI and 0H-AI) and subsequent hydrogenation of the formed α,β -unsaturated ketones to yield 12H-Coupling, 6H-Coupling and 0H-Coupling.¹³⁰ The aldol addition is reversible with a strong base,¹³¹ however the high temperature of reaction in combination with the hydrogen in solution favors the crotonisation/hydrogenation pathway. The hydrogenation of the 12H-AI and 0H-AI intermediates is highly favorable in the presence of hydrogen (resp. $\Delta H=-110/-120$ kJ/mol, $\Delta G=-74/-85$ kJ/mol), explaining the absence of these structures in the reactional mixture. These conditions render the reaction irreversible as electrons are not stabilized anymore by resonance, which allows for the accumulation of the coupling products in solution. The aldol reaction is also possible in the presence of a metallic enolate. However, as platinum is the only metal in the reaction mixture and has not been shown to favor enol formation, this reaction pathway is less plausible.¹³²

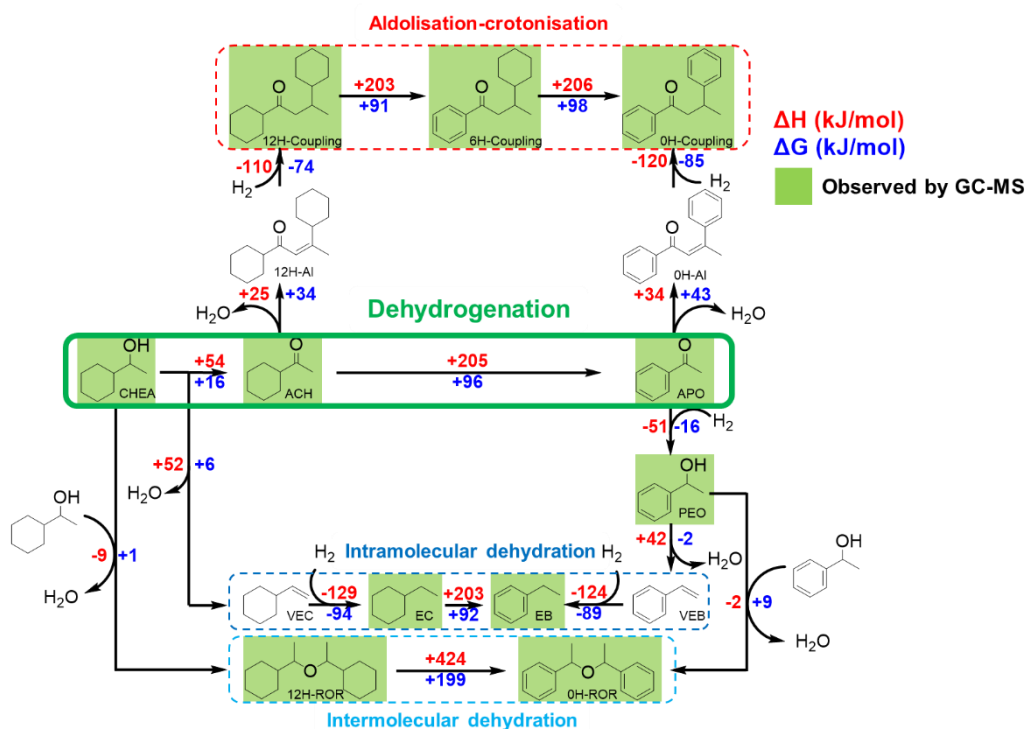


Figure IV-25 - Enthalpy (red) and free energy change (blue) between the intermediates of the system during the dehydrogenation. The products identified by GC-MS are highlighted in green.

IV.3 Conclusion

A new bifunctional LOHC couple, based on 1-Cyclohexylethanol/Acetophenone, has been evaluated by DFT and deemed a potential LOHC couple. Lab experiments showed promises on its application as a LOHC as Ru/Al₂O₃ hydrogenated the LOHC at 115 °C in 2 h with a conversion of 100% and 98% selectivity. The dehydrogenation was successfully carried out using Pt/C at 205 °C in 36 h with total conversion but with a degree of dehydrogenation (DoDH) limited to 72% and a LOHC stability of 80%. These conditions were used to cycle the system three times during which up to 50% of the total hydrogen capacity could be exploited, stable after 3 cycles. The limitations of such a system, which pairs C–O bonds and C–C bonds, have been identified: the reversible hydrogenation of the ketone group to the alcohol during the dehydrogenation facilitates the condensation and dehydration reactions, and consequently slows down the dehydrogenation of the cyclohexyl ring. Degradation of the carrier produces LOHC-like structures, some of which have already been studied in the literature such as Ethylcyclohexane/Ethylbenzene and are hence not incompatible with cycling. Further work is required on the reaction conditions to limit the side reactions, regenerate the LOHC or circumvent the reversibility of the ketone group.

Bibliography

- (1) Müller, K.; Völkl, J.; Arlt, W. Thermodynamic Evaluation of Potential Organic Hydrogen Carriers. *Energy Technol.* **2013**, *1* (1), 20–24. <https://doi.org/10.1002/ente.201200045>.
- (2) *Properties of Organic Compounds 9 Chemical Search.* <https://poc.chemnetbase.com/faces/chemical/ChemicalSearch.xhtml> (accessed 2021-06-09).
- (3) *Liquids - Densities.* https://www.engineeringtoolbox.com/liquids-densities-d_743.html (accessed 2023-01-24).
- (4) von Helmolt, R.; Eberle, U. Fuel Cell Vehicles: Status 2007. *J. Power Sources* **2007**, *165* (2), 833–843. <https://doi.org/10.1016/j.jpowsour.2006.12.073>.
- (5) H. Crabtree, R. Hydrogen Storage in Liquid Organic Heterocycles. *Energy Environ. Sci.* **2008**, *1* (1), 134–138. <https://doi.org/10.1039/B805644G>.
- (6) Clot, E.; Eisenstein, O.; H. Crabtree, R. Computational Structure–Activity Relationships in H₂ Storage: How Placement of N Atoms Affects Release Temperatures in Organic Liquid Storage Materials. *Chem. Commun.* **2007**, *0* (22), 2231–2233. <https://doi.org/10.1039/B705037B>.
- (7) Moores, A.; Poyatos, M.; Luo, Y.; H. Crabtree, R. Catalysed Low Temperature H₂ Release from Nitrogen Heterocycles. *New J. Chem.* **2006**, *30* (11), 1675–1678. <https://doi.org/10.1039/B608914C>.
- (8) Rappoport, Z.; Marek, I. *The Chemistry of Organomagnesium Compounds*; John Wiley & Sons, 2008.
- (9) Eblagon, K. M.; Tsang, S. C. E. Structure-Reactivity Relationship in Catalytic Hydrogenation of Heterocyclic Compounds over Ruthenium Black; Part B: Effect of Carbon Substitution by Heteroatom. *Appl. Catal. B Environ.* **2015**, *163*, 599–610. <https://doi.org/10.1016/j.apcatb.2014.08.040>.
- (10) Zhao, H. Y.; Oyama, S. T.; Naeemi, E. D. Hydrogen Storage Using Heterocyclic Compounds: The Hydrogenation of 2-Methylthiophene. *Catal. Today* **2010**, *149* (1), 172–184. <https://doi.org/10.1016/j.cattod.2009.02.039>.
- (11) JOBACK, K. G.; REID, R. C. Estimation of Pure-Component Properties from Group-Contributions. *Chem. Eng. Commun.* **1987**, *57* (1–6), 233–243. <https://doi.org/10.1080/00986448708960487>.
- (12) Niermann, M.; Beckendorff, A.; Kaltschmitt, M.; Bonhoff, K. Liquid Organic Hydrogen Carrier (LOHC) – Assessment Based on Chemical and Economic Properties. *Int. J. Hydrog. Energy* **2019**, *44* (13), 6631–6654. <https://doi.org/10.1016/j.ijhydene.2019.01.199>.
- (13) Zhong, H.; Chan, Y.; Wu, B. Y.; Lai, J. POTENTIAL TOXICITY OF METALS IN DISCARDED ELECTRONICS: A CASE STUDY OF MOBILE PHONES IN CHINA. **2022**.
- (14) *Fehlerseite 404 - Fraunhofer IZM.* Fraunhofer-Institut für Zuverlässigkeit und Mikrointegration IZM. <https://www.izm.fraunhofer.de/de/error404.html> (accessed 2022-12-05).
- (15) Basniev, K. S.; Omelchenko, R.; Adzynova, F. A. 18th World Hydrogen Energy Conference 2010 – WHEC 2010. June 9, 2016.
- (16) Cooper, A. C.; Campbell, K. M.; Pez, G. P. An Integrated Hydrogen Storage and Delivery Approach Using Organic Liquid-Phase Carriers.
- (17) He, T.; Pei, Q.; Chen, P. Liquid Organic Hydrogen Carriers. *J. Energy Chem.* **2015**, *24* (5), 587–594. <https://doi.org/10.1016/j.jechem.2015.08.007>.
- (18) *Target Explanation Document: Onboard Hydrogen Storage for Light-Duty Fuel Cell Vehicles.* Energy.gov. <https://www.energy.gov/eere/fuelcells/downloads/target-explanation-document-onboard-hydrogen-storage-light-duty-fuel-cell> (accessed 2021-06-04).
- (19) Alan C. Cooper. *Design and Development of New Carbon-Based Sorbent Systems for an Effective Containment of Hydrogen*; 86-377-P, 1039432; 2012; pp 86-377-P, 1039432. <https://doi.org/10.2172/1039432>.
- (20) Deslongchamps, P. Intramolecular Strategies and Stereoelectronic Effects. Glycosides Hydrolysis Revisited. *Pure Appl. Chem.* **1993**, *65* (6), 1161–1178. <https://doi.org/10.1351/pac199365061161>.
- (21) Informatics, N. O. of D. and. *WebBook de Chimie NIST.* <https://doi.org/10.18434/T4D303>.
- (22) MacKerell, A. D. Jr.; Bashford, D.; Bellott, M.; Dunbrack, R. L. Jr.; Evanseck, J. D.; Field, M. J.; Fischer, S.; Gao, J.; Guo, H.; Ha, S.; Joseph-McCarthy, D.; Kuchnir, L.; Kuczera, K.; Lau, F. T. K.; Mattos, C.; Michnick, S.; Ngo, T.; Nguyen, D. T.; Prodhom, B.; Reiher, W. E.; Roux, B.; Schlenkrich, M.; Smith, J. C.; Stote, R.; Straub, J.; Watanabe, M.; Wiórkiewicz-Kuczera, J.; Yin, D.; Karplus, M. All-Atom Empirical Potential for Molecular Modeling and Dynamics Studies of Proteins. *J. Phys. Chem. B* **1998**, *102* (18), 3586–3616. <https://doi.org/10.1021/jp973084f>.
- (23) Shimizu, R.; Ze-Jun, D. Monte Carlo Modelling of Electron-Solid Interactions. *Rep. Prog. Phys.* **1992**, *55* (4), 487. <https://doi.org/10.1088/0034-4885/55/4/002>.

Chapter 1: Evaluation of new LOHC structures

- (24) Born, M.; Oppenheimer, R. Zur Quantentheorie Der Molekeln. *Ann. Phys.* **1927**, *389* (20), 457–484. <https://doi.org/10.1002/andp.19273892002>.
- (25) Hohenberg, P.; Kohn, W. Inhomogeneous Electron Gas. *Phys. Rev.* **1964**, *136* (3B), B864–B871. <https://doi.org/10.1103/PhysRev.136.B864>.
- (26) Kohn, W.; Sham, L. J. Self-Consistent Equations Including Exchange and Correlation Effects. *Phys. Rev.* **1965**, *140* (4A), A1133–A1138. <https://doi.org/10.1103/PhysRev.140.A1133>.
- (27) Stowasser, R.; Hoffmann, R. What Do the Kohn–Sham Orbitals and Eigenvalues Mean? *J. Am. Chem. Soc.* **1999**, *121* (14), 3414–3420. <https://doi.org/10.1021/ja9826892>.
- (28) Gaussian 16, Revision C.01, M. J. Frisch, G. W. Trucks, H. B. Schlegel, G. E. Scuseria, M. A. Robb, J. R. Cheeseman, G. Scalmani, V. Barone, G. A. Petersson, H. Nakatsuji, X. Li, M. Caricato, A. V. Marenich, J. Bloino, B. G. Janesko, R. Gomperts, B. Mennucci, H. P. Hratchian, J. V. Ortiz, A. F. Izmaylov, J. L. Sonnenberg, D. Williams-Young, F. Ding, F. Lipparini, F. Egidi, J. Goings, B. Peng, A. Petrone, T. Henderson, D. Ranasinghe, V. G. Zakrzewski, J. Gao, N. Rega, G. Zheng, W. Liang, M. Hada, M. Ehara, K. Toyota, R. Fukuda, J. Hasegawa, M. Ishida, T. Nakajima, Y. Honda, O. Kitao, H. Nakai, T. Vreven, K. Throssell, J. A. Montgomery, Jr., J. E. Peralta, F. Ogliaro, M. J. Bearpark, J. J. Heyd, E. N. Brothers, K. N. Kudin, V. N. Staroverov, T. A. Keith, R. Kobayashi, J. Normand, K. Raghavachari, A. P. Rendell, J. C. Burant, S. S. Iyengar, J. Tomasi, M. Cossi, J. M. Millam, M. Klene, C. Adamo, R. Cammi, J. W. Ochterski, R. L. Martin, K. Morokuma, O. Farkas, J. B. Foresman, and D. J. Fox, Gaussian, Inc., Wallingford CT, 2016. <https://gaussian.com/citation/>.
- (29) Zhao, Y.; Truhlar, D. G. The M06 Suite of Density Functionals for Main Group Thermochemistry, Thermochemical Kinetics, Noncovalent Interactions, Excited States, and Transition Elements: Two New Functionals and Systematic Testing of Four M06-Class Functionals and 12 Other Functionals. *Theor. Chem. Acc.* **2008**, *120* (1), 215–241. <https://doi.org/10.1007/s00214-007-0310-x>.
- (30) Krishnan, R.; Binkley, J. S.; Seeger, R.; Pople, J. A. Self-consistent Molecular Orbital Methods. XX. A Basis Set for Correlated Wave Functions. *J. Chem. Phys.* **1980**, *72* (1), 650–654. <https://doi.org/10.1063/1.438955>.
- (31) Clark, T.; Chandrasekhar, J.; Spitznagel, G. W.; Schleyer, P. V. R. Efficient Diffuse Function-Augmented Basis Sets for Anion Calculations. III. The 3-21+G Basis Set for First-Row Elements, Li–F. *J. Comput. Chem.* **1983**, *4* (3), 294–301. <https://doi.org/10.1002/jcc.540040303>.
- (32) Grimme, S.; Antony, J.; Ehrlich, S.; Krieg, H. A Consistent and Accurate Ab Initio Parametrization of Density Functional Dispersion Correction (DFT-D) for the 94 Elements H–Pu. *J. Chem. Phys.* **2010**, *132* (15), 154104. <https://doi.org/10.1063/1.3382344>.
- (33) Chai, J.-D.; Head-Gordon, M. Long-Range Corrected Hybrid Density Functionals with Damped Atom–Atom Dispersion Corrections. *Phys. Chem. Chem. Phys.* **2008**, *10* (44), 6615–6620. <https://doi.org/10.1039/B810189B>.
- (34) Zhao, Y.; Truhlar, D. G. Comparative DFT Study of van Der Waals Complexes: Rare-Gas Dimers, Alkaline-Earth Dimers, Zinc Dimer, and Zinc-Rare-Gas Dimers. *J. Phys. Chem. A* **2006**, *110* (15), 5121–5129. <https://doi.org/10.1021/jp060231d>.
- (35) Zhao, Y.; Truhlar, D. G. Density Functional for Spectroscopy: No Long-Range Self-Interaction Error, Good Performance for Rydberg and Charge-Transfer States, and Better Performance on Average than B3LYP for Ground States. *J. Phys. Chem. A* **2006**, *110* (49), 13126–13130. <https://doi.org/10.1021/jp066479k>.
- (36) Becke, A. D. Density-functional Thermochemistry. III. The Role of Exact Exchange. *J. Chem. Phys.* **1993**, *98* (7), 5648–5652. <https://doi.org/10.1063/1.464913>.
- (37) Roothaan, C. C. J. New Developments in Molecular Orbital Theory. *Rev. Mod. Phys.* **1951**, *23* (2), 69–89. <https://doi.org/10.1103/RevModPhys.23.69>.
- (38) Møller, Chr.; Plesset, M. S. Note on an Approximation Treatment for Many-Electron Systems. *Phys. Rev.* **1934**, *46* (7), 618–622. <https://doi.org/10.1103/PhysRev.46.618>.
- (39) Frisch, M. J.; Head-Gordon, M.; Pople, J. A. A Direct MP2 Gradient Method. *Chem. Phys. Lett.* **1990**, *166* (3), 275–280. [https://doi.org/10.1016/0009-2614\(90\)80029-D](https://doi.org/10.1016/0009-2614(90)80029-D).
- (40) Frisch, M. J.; Head-Gordon, M.; Pople, J. A. Semi-Direct Algorithms for the MP2 Energy and Gradient. *Chem. Phys. Lett.* **1990**, *166* (3), 281–289. [https://doi.org/10.1016/0009-2614\(90\)80030-H](https://doi.org/10.1016/0009-2614(90)80030-H).
- (41) Head-Gordon, M.; Pople, J. A.; Frisch, M. J. MP2 Energy Evaluation by Direct Methods. *Chem. Phys. Lett.* **1988**, *153* (6), 503–506. [https://doi.org/10.1016/0009-2614\(88\)85250-3](https://doi.org/10.1016/0009-2614(88)85250-3).
- (42) Sæbø, S.; Almlöf, J. Avoiding the Integral Storage Bottleneck in LCAO Calculations of Electron Correlation. *Chem. Phys. Lett.* **1989**, *154* (1), 83–89. [https://doi.org/10.1016/0009-2614\(89\)87442-1](https://doi.org/10.1016/0009-2614(89)87442-1).

Chapter 1: Evaluation of new LOHC structures

- (43) Head-Gordon, M.; Head-Gordon, T. Analytic MP2 Frequencies without Fifth-Order Storage. Theory and Application to Bifurcated Hydrogen Bonds in the Water Hexamer. *Chem. Phys. Lett.* **1994**, *220* (1), 122–128. [https://doi.org/10.1016/0009-2614\(94\)00116-2](https://doi.org/10.1016/0009-2614(94)00116-2).
- (44) Brückner, N.; Obesser, K.; Bösmann, A.; Teichmann, D.; Arlt, W.; Dungs, J.; Wasserscheid, P. Evaluation of Industrially Applied Heat-Transfer Fluids as Liquid Organic Hydrogen Carrier Systems. *ChemSusChem* **2014**, *7* (1), 229–235. <https://doi.org/10.1002/cssc.201300426>.
- (45) Geburtig, D.; Preuster, P.; Bösmann, A.; Müller, K.; Wasserscheid, P. Chemical Utilization of Hydrogen from Fluctuating Energy Sources – Catalytic Transfer Hydrogenation from Charged Liquid Organic Hydrogen Carrier Systems. *Int. J. Hydrog. Energy* **2016**, *41* (2), 1010–1017. <https://doi.org/10.1016/j.ijhydene.2015.10.013>.
- (46) M.J. Schneider. *Hydrogen Storage and Distribution via Liquid Organic Carriers*. https://arpa.e.energy.gov/sites/default/files/Schneider_HydrogeniousTechnologies_TransportationFuels_Workshop_FINAL.pdf (accessed 2022-03-11).
- (47) Cui, Y.; Kwok, S.; Bucholtz, A.; Davis, B.; A. Whitney, R.; G. Jessop, P. The Effect of Substitution on the Utility of Piperidines and Octahydroindoles for Reversible Hydrogen Storage. *New J. Chem.* **2008**, *32* (6), 1027–1037. <https://doi.org/10.1039/B718209K>.
- (48) Teichmann, D.; Arlt, W.; Wasserscheid, P. Liquid Organic Hydrogen Carriers as an Efficient Vector for the Transport and Storage of Renewable Energy. *Int. J. Hydrog. Energy* **2012**, *37* (23), 18118–18132. <https://doi.org/10.1016/j.ijhydene.2012.08.066>.
- (49) Gleichweit, C.; Amende, M.; Bauer, U.; Schernich, S.; Höfert, O.; Lorenz, M. P. A.; Zhao, W.; Müller, M.; Koch, M.; Bachmann, P.; Wasserscheid, P.; Libuda, J.; Steinrück, H.-P.; Papp, C. Alkyl Chain Length-Dependent Surface Reaction of Dodecahydro-N-Alkylcarbazoles on Pt Model Catalysts. *J. Chem. Phys.* **2014**, *140* (20), 204711. <https://doi.org/10.1063/1.4875921>.
- (50) Zhu, Y.-L.; Xiang, H.-W.; Wu, G.-S.; Bai, L.; Li, Y.-W. A Novel Route for Synthesis of γ -Butyrolactone through the Coupling of Hydrogenation and Dehydrogenation. *Chem. Commun.* **2002**, *0* (3), 254–255. <https://doi.org/10.1039/B109658N>.
- (51) Bhanushali, J. T.; Prasad, D.; Patil, K. N.; Reddy, K. S.; Kainthla, I.; Rao, K. S. R.; Jadhav, A. H.; Nagaraja, B. M. Tailoring the Catalytic Activity of Basic Mesoporous Cu/CeO₂ Catalyst by Al₂O₃ for Selective Lactonization and Dehydrogenation of 1,4-Butanediol to γ -Butyrolactone. *Catal. Commun.* **2020**, *143*, 106049. <https://doi.org/10.1016/j.catcom.2020.106049>.
- (52) Javaid, A.; Bildea, C. S. Design and Control of an Integrated 1,4-Butanediol Dehydrogenation and Furfural Hydrogenation Plant. *Chem. Eng. Technol.* **2014**, *37* (9), 1515–1524. <https://doi.org/10.1002/ceat.201400210>.
- (53) Journal of Physical and Chemical Reference Data Monographs or Supplements. *NIST* **2010**.
- (54) Giauque, W. F. THE ENTROPY OF HYDROGEN AND THE THIRD LAW OF THERMODYNAMICS THE FREE ENERGY AND DISSOCIATION OF HYDROGEN. *J. Am. Chem. Soc.* **1930**, *52* (12), 4816–4831. <https://doi.org/10.1021/ja01375a023>.
- (55) Bliznakov, S.; Lefterova, E.; Bozukov, L.; Popov, A.; Andreev, P. TECHNIQUES FOR CHARACTERISATION OF HYDROGEN ABSORPTION/DESORPTION IN METAL HYDRIDE ALLOYS.
- (56) Watson, L.; Eisenstein, O. Entropy Explained: The Origin of Some Simple Trends. *J. Chem. Educ.* **2002**, *79* (10), 1269. <https://doi.org/10.1021/ed079p1269>.
- (57) Theilacker, W.; Drössler, H.-G. Die katalytische Hydrierung von Acetophenon mit Platin und Palladium. Ein Beitrag zur Selektivität der Edelmetallkatalysatoren. *Chem. Ber.* **1954**, *87* (11), 1676–1684. <https://doi.org/10.1002/cber.19540871111>.
- (58) Lin, S. D.; Sanders, D. K.; Albert Vannice, M. Influence of Metal-Support Effects on Acetophenone Hydrogenation over Platinum. *Appl. Catal. Gen.* **1994**, *113* (1), 59–73. [https://doi.org/10.1016/0926-860X\(94\)80241-6](https://doi.org/10.1016/0926-860X(94)80241-6).
- (59) Kim, W.-H.; Park, I. S.; Park, J. Acceptor-Free Alcohol Dehydrogenation by Recyclable Ruthenium Catalyst. *Org. Lett.* **2006**, *8* (12), 2543–2545. <https://doi.org/10.1021/ol060750z>.
- (60) Mitsudome, T.; Mikami, Y.; Ebata, K.; Mizugaki, T.; Jitsukawa, K.; Kaneda, K. Copper Nanoparticles on Hydrotalcite as a Heterogeneous Catalyst for Oxidant-Free Dehydrogenation of Alcohols. *Chem. Commun.* **2008**, *0* (39), 4804–4806. <https://doi.org/10.1039/B809012B>.
- (61) Damodara, D.; Arundhati, R.; Likhar, P. R. Copper Nanoparticles from Copper Aluminum Hydrotalcite: An Efficient Catalyst for Acceptor- and Oxidant-Free Dehydrogenation of Amines and Alcohols. *Adv. Synth. Catal.* **2014**, *356* (1), 189–198. <https://doi.org/10.1002/adsc.201300453>.

Chapter 1: Evaluation of new LOHC structures

- (62) Putro, W. S.; Kojima, T.; Hara, T.; Ichikuni, N.; Shimazu, S. Acceptorless Dehydrogenation of Alcohols Using Cu–Fe Catalysts Prepared from Cu–Fe Layered Double Hydroxides as Precursors. *Catal. Sci. Technol.* **2018**, *8* (12), 3010–3014. <https://doi.org/10.1039/C8CY00655E>.
- (63) Rogers, H.; Daniel, I. T.; Freakley, S. J. Acceptorless Dehydrogenation of 1-Phenylethanol Using Pd/TiO₂ Catalysts Prepared by Sol Immobilisation. *Catal. Commun.* **2021**, 106377. <https://doi.org/10.1016/j.catcom.2021.106377>.
- (64) Fu, W.; Yue, L.; Duan, X.; Li, J.; Lu, G. Acceptor-Free Dehydrogenation of 4-Hydroxy-3-Methoxybenzyl Alcohol to Vanillin over a Palladium Complex. *Green Chem.* **2016**, *18* (22), 6136–6142. <https://doi.org/10.1039/C6GC01855F>.
- (65) Nicolau, G.; Tarantino, G.; Hammond, C. Acceptorless Alcohol Dehydrogenation Catalysed by Pd/C. *ChemSusChem* **2019**, *12* (22), 4953–4961. <https://doi.org/10.1002/cssc.201901313>.
- (66) Burgener, M.; Mallat, T.; Baiker, A. Palladium-Catalysed Dehydrogenation of 1-Phenylethanol in Dense Carbon Dioxide. *J. Mol. Catal. Chem.* **2005**, *225* (1), 21–25. <https://doi.org/10.1016/j.molcata.2004.08.029>.
- (67) Karvembu, R.; Priyarega, S. Ru/g-Al₂O₃ as Reusable Catalyst for Dehydrogenation of Alcohols without Hydrogen Acceptor. *React. Kinet. Catal. Lett.* **2006**, *88* (2), 333–338. <https://doi.org/10.1007/s11144-006-0069-4>.
- (68) Feng, B.; Chen, C.; Yang, H.; Zhao, X.; Hua, L.; Yu, Y.; Cao, T.; Shi, Y.; Hou, Z. Ionic Liquid-Promoted Oxidant-Free Dehydrogenation of Alcohols with Water-Soluble Ruthenium Nanoparticles in Aqueous Phase. *Adv. Synth. Catal.* **2012**, *354* (8), 1559–1565. <https://doi.org/10.1002/adsc.201100908>.
- (69) Tilgner, D.; Klarner, M.; Hammon, S.; Friedrich, M.; Verch, A.; Jonge, N. de; Kümmel, S.; Kempe, R.; Tilgner, D.; Klarner, M.; Hammon, S.; Friedrich, M.; Verch, A.; Jonge, N. de; Kümmel, S.; Kempe, R. H₂-Generation from Alcohols by the MOF-Based Noble Metal-Free Photocatalyst Ni/CdS/TiO₂@MIL-101*. *Aust. J. Chem.* **2019**, *72* (10), 842–847. <https://doi.org/10.1071/CH19255>.
- (70) Kurhe, D. K.; Fernandes, T. A.; Deore, T. S.; Jayaram, R. V. Oxidant Free Dehydrogenation of Alcohols Using Chitosan/Polyacrylamide Entrapped Ag Nanoparticles. *RSC Adv.* **2015**, *5* (58), 46443–46447. <https://doi.org/10.1039/C5RA05046D>.
- (71) Mitsudome, T.; Mikami, Y.; Funai, H.; Mizugaki, T.; Jitsukawa, K.; Kaneda, K. Oxidant-Free Alcohol Dehydrogenation Using a Reusable Hydrotalcite-Supported Silver Nanoparticle Catalyst. *Angew. Chem. Int. Ed.* **2008**, *47* (1), 138–141. <https://doi.org/10.1002/anie.200703161>.
- (72) Bayat, A.; Shakourian-Fard, M.; Ehyaei, N.; Hashemi, M. M. Silver Nanoparticles Supported on Silica-Coated Ferrite as Magnetic and Reusable Catalysts for Oxidant-Free Alcohol Dehydrogenation. *RSC Adv.* **2015**, *5* (29), 22503–22509. <https://doi.org/10.1039/C4RA15498C>.
- (73) Fang, W.; Zhang, Q.; Chen, J.; Deng, W.; Wang, Y. Gold Nanoparticles on Hydrotalcites as Efficient Catalysts for Oxidant-Free Dehydrogenation of Alcohols. *Chem. Commun.* **2010**, *46* (9), 1547–1549. <https://doi.org/10.1039/B923047E>.
- (74) Fujita, K.; Tanino, N.; Yamaguchi, R. Ligand-Promoted Dehydrogenation of Alcohols Catalyzed by Cp*Ir Complexes. A New Catalytic System for Oxidant-Free Oxidation of Alcohols. *Org. Lett.* **2007**, *9* (1), 109–111. <https://doi.org/10.1021/ol062806v>.
- (75) Guillet, S. G.; Pisanò, G.; Chakraborty, S.; Müller, B. H.; de Vries, J. G.; Kamer, P. C. J.; Cazin, C. S. J.; Nolan, Steven. P. A Simple Synthetic Route to [Rh(Acac)(CO)(NHC)] Complexes: Ligand Property Diagnostic Tools and Precatalysts. *Eur. J. Inorg. Chem.* **2021**, *2021* (34), 3506–3511. <https://doi.org/10.1002/ejic.202100479>.
- (76) Castañón, E. B.; Kaposi, M.; Reich, R. M.; Kühn, F. E. Water-Soluble Transition Metal Complexes of Ruthenium(II), Osmium(II), Rhodium(III) and Iridium(III) with Chelating N-Heterocyclic Carbene Ligands in Hydrogenation and Transfer Hydrogenation Catalysis. *Dalton Trans.* **2018**, *47* (7), 2318–2329. <https://doi.org/10.1039/C7DT04684G>.
- (77) Llop Castelbou, J.; Bresó-Femenia, E.; Blondeau, P.; Chaudret, B.; Castellón, S.; Claver, C.; Godard, C. Tuning the Selectivity in the Hydrogenation of Aromatic Ketones Catalyzed by Similar Ruthenium and Rhodium Nanoparticles. *ChemCatChem* **2014**, *6* (11), 3160–3168. <https://doi.org/10.1002/cctc.201402524>.
- (78) Falini, G.; Gualandi, A.; Savoia, D. Rhodium/Graphite-Catalyzed Hydrogenation of Carbocyclic and Heterocyclic Aromatic Compounds. *Synthesis* **2009**, *2009* (14), 2440–2446. <https://doi.org/10.1055/s-0029-1216852>.
- (79) Jiang, H.; Cheng, H.; Bian, F. Heterogeneous Enantioselective Hydrogenation of Aromatic Ketones Catalyzed by Rh Nanoparticles Immobilized in Ionic Liquid. *Catal. Lett.* **2019**, *149* (7), 1975–1982. <https://doi.org/10.1007/s10562-019-02768-w>.

Chapter 1: Evaluation of new LOHC structures

- (80) Yoshida, H.; Onodera, Y.; Fujita, S.; Kawamori, H.; Arai, M. Solvent Effects in Heterogeneous Selective Hydrogenation of Acetophenone: Differences between Rh/C and Rh/Al₂O₃ Catalysts and the Superiority of Water as a Functional Solvent. *Green Chem.* **2015**, *17* (3), 1877–1883. <https://doi.org/10.1039/C4GC02211D>.
- (81) Moos, G.; Emondts, M.; Bordet, A.; Leitner, W. Selective Hydrogenation and Hydrodeoxygenation of Aromatic Ketones to Cyclohexane Derivatives Using a Rh@SILP Catalyst. *Angew. Chem. Int. Ed.* **2020**, *59* (29), 11977–11983. <https://doi.org/10.1002/anie.201916385>.
- (82) Srinivasan, K.; Gundekari, S. Procédé Respectueux De L'environnement D'hydrogénation Et/Ou Hydrodésoxygénation De Composé Organique À L'aide D'un Catalyseur À Oxyde De Ruthénium Hydraté. WO2017060922A1, April 13, 2017.
- (83) Nowicki, A.; Le Boulaire, V.; Roucoux, A. Nanoheterogeneous Catalytic Hydrogenation of Arenes: Evaluation of the Surfactant-Stabilized Aqueous Ruthenium(0) Colloidal Suspension. *Adv. Synth. Catal.* **2007**, *349* (14–15), 2326–2330. <https://doi.org/10.1002/adsc.200700208>.
- (84) Martínez-Prieto, L. M.; Puche, M.; Cerezo-Navarrete, C.; Chaudret, B. Uniform Ru Nanoparticles on N-Doped Graphene for Selective Hydrogenation of Fatty Acids to Alcohols. *J. Catal.* **2019**, *377*, 429–437. <https://doi.org/10.1016/j.jcat.2019.07.040>.
- (85) Chen, C.-S.; Chen, H.-W.; Cheng, W.-H. Study of Selective Hydrogenation of Acetophenone on Pt/SiO₂. *Appl. Catal. Gen.* **2003**, *248* (1), 117–128. [https://doi.org/10.1016/S0926-860X\(03\)00156-X](https://doi.org/10.1016/S0926-860X(03)00156-X).
- (86) Vetere, V.; Faraoni, M. B.; Santori, G. F.; Podestá, J.; Casella, M. L.; Ferretti, O. A. New Approach toward the Synthesis of Asymmetric Heterogeneous Catalysts for Hydrogenation Reactions. *J. Catal.* **2004**, *226* (2), 457–461. <https://doi.org/10.1016/j.jcat.2004.05.031>.
- (87) Chen, M.; Maeda, N.; Baiker, A.; Huang, J. Molecular Insight into Pt-Catalyzed Chemoselective Hydrogenation of an Aromatic Ketone by In Situ Modulation–Excitation IR Spectroscopy. *ACS Catal.* **2012**, *2* (9), 2007–2013. <https://doi.org/10.1021/cs300408x>.
- (88) Lenarda, M.; Casagrande, M.; Moretti, E.; Storaro, L.; Frattini, R.; Polizzi, S. Selective Catalytic Low Pressure Hydrogenation of Acetophenone on Pd/ZnO/ZnAl₂O₄. *Catal. Lett.* **2007**, *114* (1), 79–84. <https://doi.org/10.1007/s10562-007-9046-4>.
- (89) Bertero, N. M.; Trasarti, A. F.; Apesteguía, C. R.; Marchi, A. J. Solvent Effect in the Liquid-Phase Hydrogenation of Acetophenone over Ni/SiO₂: A Comprehensive Study of the Phenomenon. *Appl. Catal. Gen.* **2011**, *394* (1), 228–238. <https://doi.org/10.1016/j.apcata.2011.01.003>.
- (90) Masson, J.; Cividino, P.; Court, J. Selective Hydrogenation of Acetophenone on Chromium Promoted Raney Nickel Catalysts. III. The Influence of the Nature of the Solvent. *Appl. Catal. Gen.* **1997**, *161* (1), 191–197. [https://doi.org/10.1016/S0926-860X\(97\)00068-9](https://doi.org/10.1016/S0926-860X(97)00068-9).
- (91) Zhou, Y.; Klinger, G. E.; Hegg, E. L.; Saffron, C. M.; Jackson, J. E. Multiple Mechanisms Mapped in Aryl Alkyl Ether Cleavage via Aqueous Electrocatalytic Hydrogenation over Skeletal Nickel. *J. Am. Chem. Soc.* **2020**, *142* (8), 4037–4050. <https://doi.org/10.1021/jacs.0c00199>.
- (92) Rousset, J. L.; Stievano, L.; Aires, F. J. C. S.; Geantet, C.; Renouprez, A. J.; Pellarin, M. Hydrogenation of Toluene over γ -Al₂O₃-Supported Pt, Pd, and Pd–Pt Model Catalysts Obtained by Laser Vaporization of Bulk Metals. *J. Catal.* **2001**, *197* (2), 335–343. <https://doi.org/10.1006/jcat.2000.3083>.
- (93) Chen, M.; Maeda, N.; Baiker, A.; Huang, J. Hydrogenation of Acetophenone on Pd/Silica–Alumina Catalysts with Tunable Acidity: Mechanistic Insight by In Situ ATR-IR Spectroscopy. *ACS Catal.* **2018**, *8* (7), 6594–6600. <https://doi.org/10.1021/acscatal.8b00169>.
- (94) Do, G.; Preuster, P.; Aslam, R.; Bösmann, A.; Müller, K.; Arlt, W.; Wasserscheid, P. Hydrogenation of the Liquid Organic Hydrogen Carrier Compound Dibenzyltoluene – Reaction Pathway Determination by ¹H NMR Spectroscopy. *React. Chem. Eng.* **2016**, *1* (3), 313–320. <https://doi.org/10.1039/C5RE00080G>.
- (95) Jorschick, H.; Preuster, P.; Dürr, S.; Seidel, A.; Müller, K.; Bösmann, A.; Wasserscheid, P. Hydrogen Storage Using a Hot Pressure Swing Reactor. *Energy Environ. Sci.* **2017**, *10* (7), 1652–1659. <https://doi.org/10.1039/C7EE00476A>.
- (96) Suppino, R. S.; Landers, R.; Cobo, A. J. G. Influence of Noble Metals (Pd, Pt) on the Performance of Ru/Al₂O₃ Based Catalysts for Toluene Hydrogenation in Liquid Phase. *Appl. Catal. Gen.* **2016**, *525*, 41–49. <https://doi.org/10.1016/j.apcata.2016.06.038>.
- (97) *Water Boiling Points at Higher Pressures*. https://www.engineeringtoolbox.com/boiling-point-water-d_926.html?vA=10&units=B# (accessed 2023-02-02).
- (98) Kim, K. S.; Winograd, N. X-Ray Photoelectron Spectroscopic Studies of Ruthenium-Oxygen Surfaces. *J. Catal.* **1974**, *35* (1), 66–72. [https://doi.org/10.1016/0021-9517\(74\)90184-5](https://doi.org/10.1016/0021-9517(74)90184-5).
- (99) Bianchi, C. L.; Ragaini, V.; Cattania, M. G. An XPS Study on Ruthenium Compounds and Catalysts. *Mater. Chem. Phys.* **1991**, *29* (1), 297–306. [https://doi.org/10.1016/0254-0584\(91\)90025-P](https://doi.org/10.1016/0254-0584(91)90025-P).

Chapter 1: Evaluation of new LOHC structures

- (100) Chen, S.; Abdel-Mageed, A. M.; Dyballa, M.; Parlinska-Wojtan, M.; Bansmann, J.; Pollastri, S.; Olivi, L.; Aquilanti, G.; Behm, R. J. Raising the CO_x Methanation Activity of a Ru/ γ -Al₂O₃ Catalyst by Activated Modification of Metal–Support Interactions. *Angew. Chem. Int. Ed.* **2020**, *59* (50), 22763–22770. <https://doi.org/10.1002/anie.202007228>.
- (101) Lee, D. H.; Condrate, R. A. An FTIR Spectral Investigation of the Structural Species Found on Alumina Surfaces. *Mater. Lett.* **1995**, *23* (4), 241–246. [https://doi.org/10.1016/0167-577X\(95\)00039-9](https://doi.org/10.1016/0167-577X(95)00039-9).
- (102) Mazzieri, V.; Coloma-Pascual, F.; Arcoya, A.; L'Argentièrre, P. C.; Figoli, N. S. XPS, FTIR and TPR Characterization of Ru/Al₂O₃ Catalysts. *Appl. Surf. Sci.* **2003**, *210* (3), 222–230. [https://doi.org/10.1016/S0169-4332\(03\)00146-6](https://doi.org/10.1016/S0169-4332(03)00146-6).
- (103) Newkirk, A. E.; McKee, D. W. Thermal Decomposition of Rhodium, Iridium, and Ruthenium Chlorides. *J. Catal.* **1968**, *11* (4), 370–377. [https://doi.org/10.1016/0021-9517\(68\)90061-4](https://doi.org/10.1016/0021-9517(68)90061-4).
- (104) Duvigneaud, P. H.; Reinhard-Derie, D. DTA Study of RuO₂ Formation from the Thermal Decomposition of Ruthenium(III) Hydrate. *Thermochim. Acta* **1981**, *51* (2), 307–314. [https://doi.org/10.1016/0040-6031\(81\)85168-4](https://doi.org/10.1016/0040-6031(81)85168-4).
- (105) Ragaini, V.; Pirola, C.; Vitali, S.; Bonura, G.; Cannilla, C.; Frusteri, F. Stability of Metallic Ruthenium in Ru–Co Supported Silica Catalysts. *Catal. Lett.* **2012**, *142* (12), 1452–1460. <https://doi.org/10.1007/s10562-012-0903-4>.
- (106) Durndell, L. J.; Zou, G.; Shangguan, W.; Lee, A. F.; Wilson, K. Structure-Reactivity Relations in Ruthenium Catalysed Furfural Hydrogenation. *ChemCatChem* **2019**, *11* (16), 3927–3932. <https://doi.org/10.1002/cctc.201900481>.
- (107) Bou, M.; Martin, J. M.; Le Mogne, Th.; Vovelle, L. Chemistry of the Interface between Aluminium and Polyethyleneterephthalate by XPS. *Appl. Surf. Sci.* **1991**, *47* (2), 149–161. [https://doi.org/10.1016/0169-4332\(91\)90029-J](https://doi.org/10.1016/0169-4332(91)90029-J).
- (108) bvcrist. *Aluminum Spectra - Al(OH)3*. The International XPS Database 1. <https://xpsdatabase.com/aluminum-spectra-aloh3/> (accessed 2022-10-14).
- (109) bvcrist. *Aluminum Spectra - α -Al₂O₃*. The International XPS Database 1. <https://xpsdatabase.com/aluminum-spectra-al2o3/> (accessed 2022-10-14).
- (110) Karvembu, R.; Prabhakaran, R.; Senthilkumar, K.; Viswanathamurthi, P.; Natarajan, K. Ru/Al₂O₃-Catalyzed Transfer Dehydrogenation of Alcohols. *React. Kinet. Catal. Lett.* **2005**, *86* (1), 211–216. <https://doi.org/10.1007/s11144-005-0314-2>.
- (111) Yergaziyeva, G. Y.; Dossumov, K.; Mambetova, M. M.; Strizhak, P. Y.; Kurokawa, H.; Baizhomartov, B. Effect of Ni, La, and Ce Oxides on a Cu/Al₂O₃ Catalyst with Low Copper Loading for Ethanol Non-Oxidative Dehydrogenation. *Chem. Eng. Technol.* **2021**, *44* (10), 1890–1899. <https://doi.org/10.1002/ceat.202100112>.
- (112) Xia, Z.; Lu, H.; Liu, H.; Zhang, Z.; Chen, Y. Cyclohexane Dehydrogenation over Ni-Cu/SiO₂ Catalyst: Effect of Copper Addition. *Catal. Commun.* **2017**, *90*, 39–42. <https://doi.org/10.1016/j.catcom.2016.10.036>.
- (113) Wang, J.; Liu, H.; Fan, S.; Wang, S.; Xu, G.; Guo, A.; Wang, Z. Dehydrogenation of Cycloalkanes over N-Doped Carbon-Supported Catalysts: The Effects of Active Component and Molecular Structure of the Substrate. *Nanomaterials* **2021**, *11* (11), 2846. <https://doi.org/10.3390/nano11112846>.
- (114) Sawama, Y.; Morita, K.; Yamada, T.; Nagata, S.; Yabe, Y.; Monguchi, Y.; Sajiki, H. Rhodium-on-Carbon Catalyzed Hydrogen Scavenger- and Oxidant-Free Dehydrogenation of Alcohols in Aqueous Media. *Green Chem.* **2014**, *16* (7), 3439–3443. <https://doi.org/10.1039/C4GC00434E>.
- (115) Modisha, P.; Gqogqa, P.; Garidzirai, R.; Ouma, C. N. M.; Bessarabov, D. Evaluation of Catalyst Activity for Release of Hydrogen from Liquid Organic Hydrogen Carriers. *Int. J. Hydrog. Energy* **2019**, *44* (39), 21926–21935. <https://doi.org/10.1016/j.ijhydene.2019.06.212>.
- (116) Kim, H.-J.; Kim, W.-I.; Park, T.-J.; Park, H.-S.; Suh, D. J. Highly Dispersed Platinum–Carbon Aerogel Catalyst for Polymer Electrolyte Membrane Fuel Cells. *Carbon* **2008**, *46* (11), 1393–1400. <https://doi.org/10.1016/j.carbon.2008.05.022>.
- (117) Wang, L.; Roudgar, A.; Eikerling, M. Ab Initio Study of Stability and Site-Specific Oxygen Adsorption Energies of Pt Nanoparticles. *J. Phys. Chem. C* **2009**, *113* (42), 17989–17996. <https://doi.org/10.1021/jp900965q>.
- (118) Mostafa, S.; Behafarid, F.; Croy, J. R.; Ono, L. K.; Li, L.; Yang, J. C.; Frenkel, A. I.; Cuenya, B. R. Shape-Dependent Catalytic Properties of Pt Nanoparticles. *J. Am. Chem. Soc.* **2010**, *132* (44), 15714–15719. <https://doi.org/10.1021/ja106679z>.
- (119) Dablemont, C.; Lang, P.; Mangeney, C.; Piquemal, J.-Y.; Petkov, V.; Herbst, F.; Viau, G. FTIR and XPS Study of Pt Nanoparticle Functionalization and Interaction with Alumina. *Langmuir* **2008**, *24* (11), 5832–5841. <https://doi.org/10.1021/la7028643>.

Chapter 1: Evaluation of new LOHC structures

- (120) Hull, R. V.; Li, L.; Xing, Y.; Chusuei, C. C. Pt Nanoparticle Binding on Functionalized Multiwalled Carbon Nanotubes. *Chem. Mater.* **2006**, *18* (7), 1780–1788. <https://doi.org/10.1021/cm0518978>.
- (121) Lin-Vien, D.; Colthup, N. B.; Fateley, W. G.; Grasselli, J. G. *The Handbook of Infrared and Raman Characteristic Frequencies of Organic Molecules*, Academic Press.
- (122) Helfferich, F. G.; Compton, R. G.; Bamford, C. H. *Comprehensive Chemical Kinetics*; Elsevier, 2001.
- (123) Rioux, R. M.; Vannice, M. A. Dehydrogenation of Isopropyl Alcohol on Carbon-Supported Pt and Cu–Pt Catalysts. *J. Catal.* **2005**, *233* (1), 147–165. <https://doi.org/10.1016/j.jcat.2005.04.020>.
- (124) Ingold, C. K. Quantitative Study of Steric Hindrance. *Q. Rev. Chem. Soc.* **1957**, *11* (1), 1–14. <https://doi.org/10.1039/QR9571100001>.
- (125) A. Jones, R. W.; R. Thomas, J. D. Steric Influence of the Alkyl Component in the Alkaline Hydrolysis of Acetates and Propionates. *J. Chem. Soc. B Phys. Org.* **1966**, *0* (0), 661–664. <https://doi.org/10.1039/J29660000661>.
- (126) Galimova, N. A.; Pskhu, Z. V.; Naumkin, A. V.; Volkov, I. O.; Yagodovskaya, T. V.; Yagodovskii, V. D. The Influence of Plasma Chemical Treatment of a Platinum Catalyst on Its Activity in the Dehydrogenation of Cyclohexane. *Russ. J. Phys. Chem. A* **2009**, *83* (10), 1720–1726. <https://doi.org/10.1134/S0036024409100161>.
- (127) Shuikin, N. I.; Levitsky, I. I. High Temperature Catalytic Dehydrogenation of Ethylcyclohexane. *Bull. Acad. Sci. USSR Div. Chem. Sci.* **1953**, *2* (6), 895–902. <https://doi.org/10.1007/BF01167533>.
- (128) Lee, J.-Y.; Yung, T.-Y.; Liu, L.-K. The Microwave-Assisted Ionic Liquid Nanocomposite Synthesis: Platinum Nanoparticles on Graphene and the Application on Hydrogenation of Styrene. *Nanoscale Res. Lett.* **2013**, *8* (1), 414. <https://doi.org/10.1186/1556-276X-8-414>.
- (129) Knözinger, H. Dehydration of Alcohols on Aluminum Oxide. *Angew. Chem. Int. Ed. Engl.* **1968**, *7* (10), 791–805. <https://doi.org/10.1002/anie.196807911>.
- (130) Zuffanti, S.; Luder, W. F. Generalized Acids and Bases in Organic Chemistry. I. Catalytic Condensation of Aldehydes. *J. Chem. Educ.* **1944**, *21* (10), 485. <https://doi.org/10.1021/ed021p485>.
- (131) Guthrie, J. P.; Cossar, J.; Cullimore, P. A.; Kamkar, N. M.; Taylor, K. F. The Retroaldol Reaction of Chalcone. *Can. J. Chem.* **1983**, *61* (11), 2621–2626. <https://doi.org/10.1139/v83-449>.
- (132) Kurti, L.; Czako, B. *Strategic Applications of Named Reactions in Organic Synthesis*; Elsevier, 2005.

Appendix

Appendix IV-1 - Submitted full text to the International Journal of Hydrogen Energy

Evaluation of Acetophenone as a novel alcohol-cycloalkane bifunctional liquid organic hydrogen carrier (LOHC)

Introduction

The massive storage of energy is a great challenge to tackle in order to favour the implementation of renewable and intermittent energies in our energetic systems. As new energy vectors such as H₂ are expected to take over fossil fuels, appropriate means of storage need to be developed.[1–3] Of all H₂ storage technologies, the Liquid Organic Hydrogen Carrier (LOHC) technology is gaining momentum as an alternative for global transport.[4] The storage concept revolves around catalytic hydrogenation and dehydrogenation reactions using a liquid organic molecule which can respectively store (hydrogenation) and unload (dehydrogenation) H₂ molecules.[5] The chemical storage of H₂ equivalents onto an organic framework reduces the risks associated with the handling and utilization of H₂ gas and can increase at the same time the volumetric energy density of the energy vector. As a result, heavy gas tanks and other devices aiming at storing H₂ in its pure form can be circumvented while retaining high gravimetric and volumetric energy densities.[6] Current LOHC systems regroup the molecules Toluene, Dibenzyltoluene, N-Ethylcarbazole and their hydrogenated counterparts. Many other structures and their associated catalysts have been tested over the years in order to surpass the performances of these systems.[7,8]

As a technology, the enthalpy of dehydrogenation per molecule of H₂ is often regarded as a make-or-break criterion to assess the energy efficiency of a LOHC system. The secondary criteria are the gravimetric and volumetric energy densities that describe the efficiency of the energy storage. Finally, a third criteria is the stability of the system over cycling, with a target of 99.9% of stability per cycle, which corresponds to almost perfect cycling.[9] Early LOHC prototypes were mainly focused on cycloalkanes/aromatics couples to limit the endothermicity of the dehydrogenation step by harnessing the energy gain of the aromatization.[10] Two bottlenecks limit the applications of such LOHC systems: they possess a problematic toxicity and state-of-the-art LOHC catalysts are built with platinum group metals (PGM), whose price is detrimental to the development of the technology.

Targets for the LOHC system may vary depending on the application. The current target of the US Department of Energy (DOE) for the enthalpy of dehydrogenation is 30-44 kJ/molH₂ in order to reach an equilibrium pressure of 1 bar of hydrogen in the temperature range -40 °C to 60 °C (useful for on-board hydrogen storage).[11] The ultimate gravimetric and volumetric targets are 6.5 wt.%H₂ and 50 gH₂/L for a complete on-board system. Stationary systems would have more relaxed criteria as the volume of the system would be less of an issue.

New LOHC systems were proposed to meet these targets. Seminal work by Pez *et al.* opened new perspectives with N- and O-heterocyclic LOHC.[12] DFT modelling by Clot *et al.* rationalised these alternatives by linking the integration of N atoms to the diminution of the enthalpy of dehydrogenation.[13] Further modelling showed that including electrodonating substituents stabilized the aromatic cycle, decreasing the enthalpy as a function of the Hammett parameter σ (para).[14]

Recent contributions in the homogeneous and heterogeneous acceptorless dehydrogenation and hydrogenation of C–O and C–N based chemical functions, such as alcohols, ketones, esters, carbonates, amides and nitriles, are paving the way to the development of unconventional LOHC couples.[15–17] Integrating chemical functions to the LOHC technology opens a way to new

Chapter 1: Evaluation of new LOHC structures

combinations of structures, and their addition have been proven beneficial as heteroatoms can weaken the adjacent C–H bonds by inductive electron withdrawing effect and/or donating mesomeric effect.[18] Especially, O-containing LOHC are also of interest as they are usually less toxic than their carbon or nitrogen counterparts and could be sourced on renewable feedstocks.[19] In addition, from the perspective of the catalyst, noble metal-free catalysts such as copper are efficient for the hydrogenation and dehydrogenation of heteroatomic functions such as alcohol/ketone and alcohol/ester, lowering the amount of critical noble metal in the system.[20–23] Nevertheless, addition of heteroatoms has its share of downsides, and O-containing molecules (alcohols, aldehydes, ketones) can undergo a number of side reactions such as dehydration,[24] oxidation in air, and condensation reactions, leading to intermolecular esterification and to oligomerization,[25,26] or aldolisation-crotonisation reactions.[27] As a result, reaction conditions and catalytic systems must be adequately controlled in order to avoid such side reactions when hydrogenation/dehydrogenation cycles are carried out with LOHC couples involving alcohols and their derivatives.

In addition, very few contributions in the literature combine different chemical functions in a LOHC as most work specializes on optimizing/testing a single function while leaving the rest of the LOHC undisturbed.[28] While these works are fundamental to understand the reactivity of each individual function, they do not tackle an integrated system, often at the price of a reduced H₂ capacity. This approach is understandable as finding a catalyst that is efficient for multiple functions is challenging and could destabilize the system. Usually, O-containing LOHCs are either simple alcohols such as methanol or ethanol, diols or O-heterocycles such as dibenzofuran.[29,30]

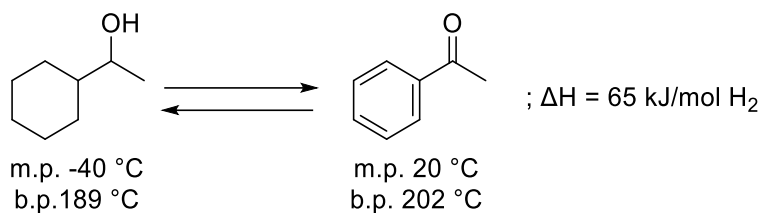
Various molecules have been suggested as bifunctional LOHCs like the couple Tetrahydro-2-furanmethanol/Furfural, whose promises have been showcased by DFT studies.[31] To the best of our knowledge, while complete hydrogenation was achieved, no article has reported so far the dehydrogenation of tetrahydro-2-furanmethanol to furfural.[32]

To date, the most similar LOHC system containing both an aromatic ring and a free O-function is the couple Cyclohexanol/Phenol. Heterogeneous hydrogenation[33] and dehydrogenation[34] were achieved in the literature. On a system level, this LOHC couple is already produced in industrial quantities which would facilitate its usage. In addition, phenol units are key building blocks in lignin and its formation from biomass molecules is actively researched.[35] However, Phenol is rather sensitive to water and its high toxicity and low explosion limit in air would be a problem for the technical implementation of a Phenol-based LOHC couple.[36]

In this work, we propose to assess the efficiency of a new bifunctional LOHC couple, 1-Cyclohexylethanol/Acetophenone (CHEA/APO). This couple is of interest as its enthalpy of dehydrogenation and H₂ storage capacity (65 kJ/molH₂, 6.3 wt.%H₂) are on-par with purely aromatic state-of-the-art systems such as Dibenzyltoluene (71 kJ/molH₂, 6.2 wt.% H₂).[37] In addition, both molecules are commercially available and present limited chemical danger. Moreover, Acetophenone is a key molecule found in the transformation of renewable feedstocks such as lignin, removing the dependency of this potential LOHC from fossil fuels in the future.[38]

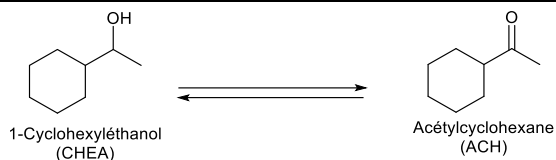
This couple has already been partially studied, especially the hydrogenation and dehydrogenation of its alcohol/ketone function (Figure 26Table IV-7). A handful of reports have described the homogeneous and heterogeneous hydrogenation of APO to CHEA. While homogeneous and heterogeneous hydrogenation in dilute conditions yielded up to 100% of conversion, solvent-free heterogeneous hydrogenation was only completed in yields inferior to 10%.[39]

Chapter 1: Evaluation of new LOHC structures

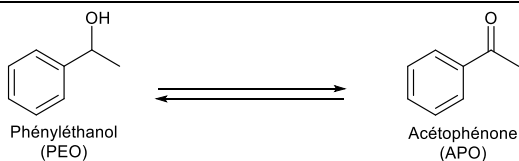


Considered reaction

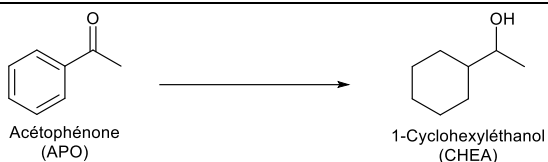
Catalytic metal



Ru[40]

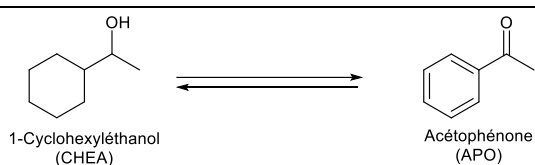


Cu[20], Cu-Fe[41], Pd[42], Ru[40], Ni [43], Ag[44], Au[45], Ir[46]



Hydrogenation only:

Rh[47], Ru[48], Pt[39], Pd[39], Ni[49]



This work:

Hydrogenation: Ru

Dehydrogenation: Pt

Figure 26 – (top) Physical data for CHEA and APO. The melting point of 1-Cyclohexylethanol was obtained by the Joback method.[50]. (bottom) Literature review of the hydrogenation and dehydrogenation of the couple CHEA/APO

To the best of our knowledge, no work has been performed on the complete acceptorless dehydrogenation of 1-Cyclohexylethanol to Acetophenone. Our aim is to determine a set of catalytic conditions that enable the full dehydrogenation and full hydrogenation, as well as evaluating the capacities of such a system to behave as a LOHC, performing several hydrogenation/dehydrogenation cycles under solvent-free conditions.

Results and discussion

Over the reactions of hydrogenation and dehydrogenation, numerous compounds have been observed by GC-MS. They are displayed with the acronyms that are used further in the text, in Figure IV-3, and sorted in 5 different classes according to their role in the reaction of interest.

Chapter 1: Evaluation of new LOHC structures

Table 15 - Conversion, LOHC stability and degree of hydrogenation (DOH) of the crude reaction mixture after 4 h hydrogenation of Acetophenone under 50 bar H₂. Acetophenone (12.5 mL), heterogeneous catalyst (0.1 wt% active metal with regard to the Acetophenone)

First of all, all catalysts achieve similar APO conversion levels in 4 h (> 98 %). However, the Pd catalysts produce mainly 1-Phenylethanol (PEO), showing their poor activity for the hydrogenation of the aromatic cycle as a standalone metal.[51] An observed strong tendency for dehydration is also linked to the surface acidity for Pd heterogeneous catalysts.[52] Conversely, Pt and especially Ru exhibit high conversions and selectivities, as expected from the literature.[53,54] General reactivity follows the order Ru > Pt > Pd, in agreement with the literature.[55] The support, Alumina or carbon, displays in general little to no influence on the conversion, however the LOHC stability is generally improved when alumina is used. Finally, only the Ru based catalysts showed DoH superior to 90%. After this first screening, we thus selected Ru/Al₂O₃ as the best catalytic system as it had the highest selectivity and a DoH equivalent to Ru/C. We then tried to improve it further by modifying the reaction temperature. Ru/C and Pt/Al₂O₃ were used as comparison due to the former presenting the highest DoH and the latter the highest LOHC stability in our preliminary study.

While a modification of the temperature has almost no effect for the conversion of APO depending on the catalyst (ESI S7), a strong influence on the hydrogenation selectivity to CHEA was observed. In particular, higher reaction temperatures promote dehydration on the Ru catalysts, probably due to the presence of acidic sites on the support. Conversely, the DoH rapidly reaches >99% values from 105 °C for Ru/C and from 115 °C for Ru/Al₂O₃. At 115 °C, Ru/Al₂O₃ achieve the maximal selectivity and DoH of all studied systems (93% selectivity, >99% DoH) (Figure IV-4)

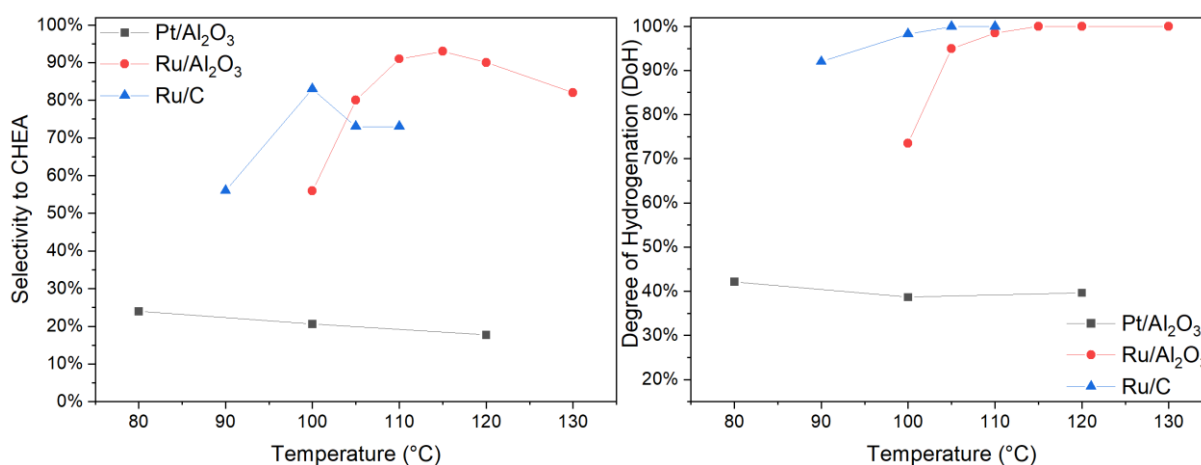


Figure 28 - Left: Selectivity to CHEA for Pt/Al₂O₃ (black), Ru/Al₂O₃ (red) and Ru/C (blue); right: DoH for Pt/Al₂O₃ (black), Ru/Al₂O₃ (red) and Ru/C (blue)

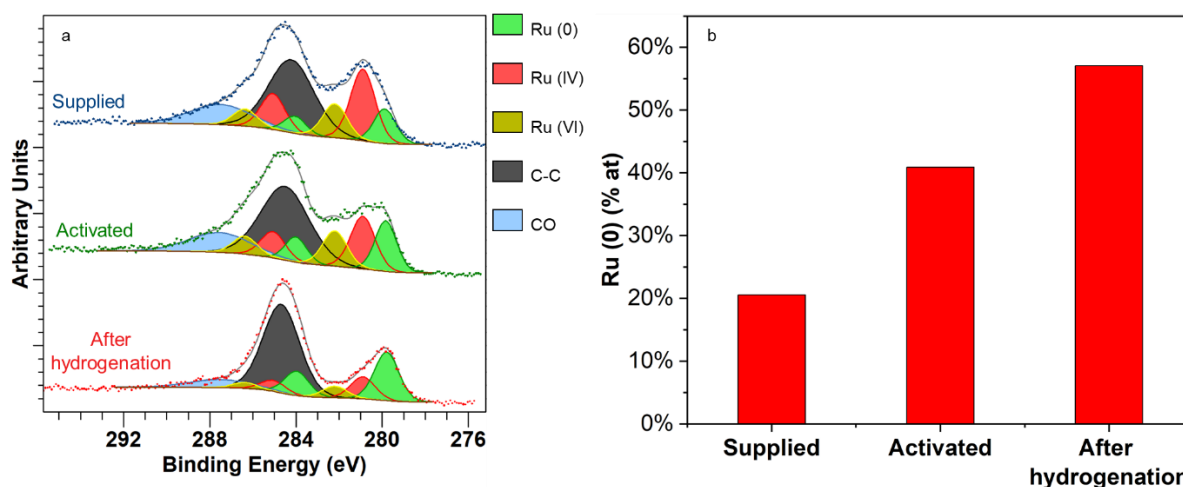
The calcination and subsequent activation of Ru/Al₂O₃ under hydrogen increases the selectivity and reduces the reaction time (ESI S8). After optimization, we thus selected the activated Ru/Al₂O₃ as a hydrogenation catalyst (0.1 wt% active metal to Acetophenone), used at 115 °C for 2 h, under 50 bar of H₂.

2. Analysis of the selected Ru/Al₂O₃ catalyst for the hydrogenation of Acetophenone

The Ru/Al₂O₃ catalyst was analyzed by XPS at three different steps: as supplied, after activation and after hydrogenation. The Ru 3d and Ru 3p core levels were recorded (Figure 29a and ESI S9) so as to estimate the oxidation state of the catalyst. For data treatment, a Shirley background was applied for

Chapter 1: Evaluation of new LOHC structures

both spectra and fitting of the Ru 3d core level spectra was achieved by using three pairs of pseudo-voigt function, a linear combination of a Gaussian and Laurentzian. The ratio between the 3d doublet area and the distance between the doublet peaks were fixed at 2 and 4.2 respectively.



Ru/Al ₂ O ₃ catalyst state	Ru average size and dispersion (nm)	Specific surface (m ² /g)	Pore diameter (nm)
Supplied	1.7±0.3	135	19.1
Activated	2.4±1.6	138	19.7
After hydrogenation	2.4±2.1	137	20.2

Figure 29 - (a) Ru 3d spectra of the ruthenium of the supplied catalyst, the activated catalyst and the catalyst after hydrogenation. (b) Atomic percentage of reduced Ru(0) for the supplied catalyst, the activated catalyst and the catalyst after hydrogenation. (bottom) Size and dispersion of the Ru nanoparticles and specific surface and pore diameter of the Al₂O₃ support.

In the Figure 29a, the Ru3d_{5/2} peaks at 279.9, 280.9 and 282.2 eV correspond to Ru(0), Ru(IV) and Ru(VI) oxidation states respectively (the peaks are assigned in green, red and yellow in the Figure 29a respectively). [56] The RuO₃ species was described as a defect structure on the surface of RuO₂. [57] As the C 1s core level is superimposed on the Ru 3d core level, a peak corresponding to organic surface contamination is added (C-C peak). The spectra also shows the presence of oxidized carbon species (CO peak) that disappear after the catalyst is activated. All of the Ru peaks binding energies in the 279 to 283 eV range are reported in the ESI S10. Ru(IV) and Ru(VI) were grouped as “oxidized Ru” and the percentage of reduced Ru(0) was compared to the former (Figure 29b). An increase of almost 20% of the reduced Ru(0) is obtained after the activation of the catalyst and a further increase of 20% is observed after the hydrogenation, leaving only 40% of oxidized Ru species that are ascribed to surface oxidation in air and covalent bonds between the Ru nanoparticles and the alumina substrate. [58]

These results are in agreement with the removal of surface contaminants as well as reduction of oxidized Ru and modification of the support that were observed by FTIR-ATR, Raman spectroscopy, XRD and ICP-OES (ESI S12, S13, S14 and S15). Its mechanism (removal of surface water and hydroxyl groups during the calcination, reduction of the oxidized Ru to Ru(0) during the activation under H₂) was studied by TGA and TGA-MS (ESI S16, S17 and S18). A limited agglomeration of the Ru nanoparticles was observed by TEM-EDX but should have no measurable incidence on catalytic activity at these high conversions (Figure 29 and ESI S19). Indeed, activity variation is usually observable only for sizes exceeding 5-10 nm. [59] However, the Ru reduction state matters as Ru(0) species have also

Chapter 1: Evaluation of new LOHC structures

been shown to increase the activity for hydrogenation reactions comparatively to Ru (IV) species.[60] Finally, the support structure (specific surface and pore diameter) is not modified by the activation process and reaction as showed by BET adsorption (Figure 29 and ESI 20).

The XPS Al 2p core level spectra (ESI S10) shows no notable differences after activation and after hydrogenation. The position of the peaks around 74.5 eV corresponds to the Al³⁺ oxidation state and not to a metallic Al which is reported around 72.5 eV.[61,62] The presence of Al₂O₃ or Al(OH)₃ can not be determined by XPS analysis but XRD analysis (ESI S14) shows Al(OH)₃ turning into Al₂O₃ during the activation of the catalyst.

3. Catalytic evaluation of supported metal catalysts for the dehydrogenation of 1-Cyclohexylethanol

The dehydrogenation is endothermic, and is often the barrier to get an efficient LOHC system.[7] Here we tested various noble and non-noble metal catalysts for the dehydrogenation of CHEA to produce APO (Figure IV-14 and ESI S21).

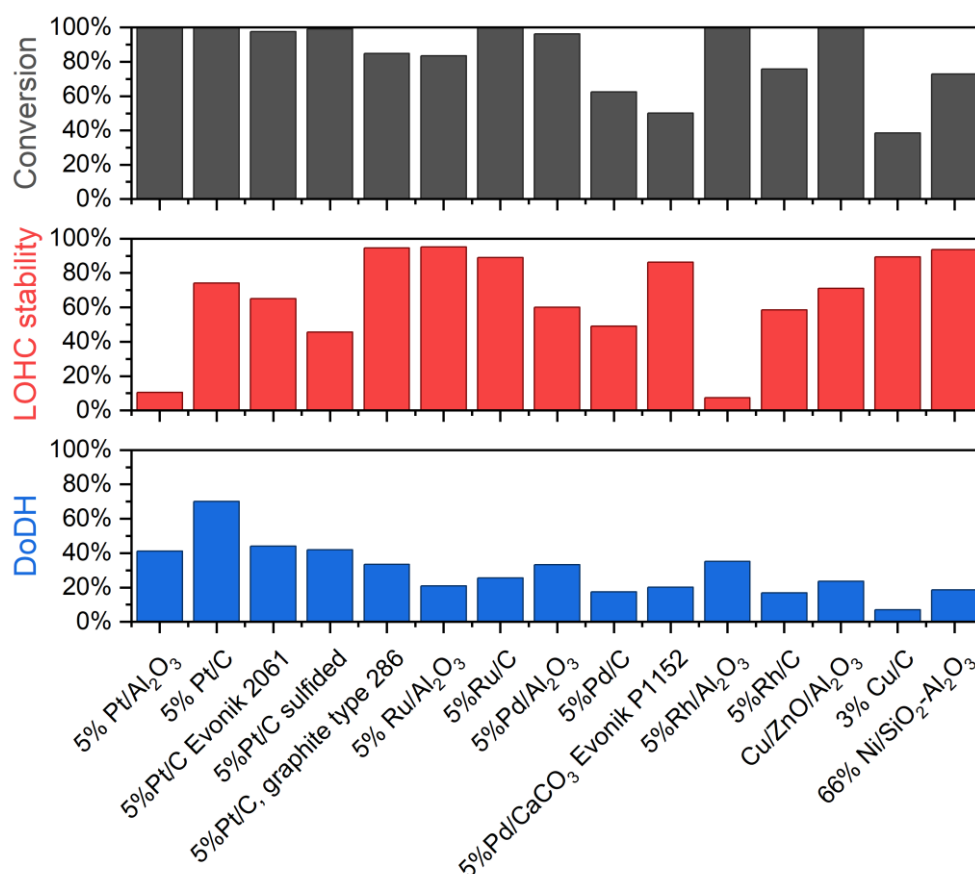
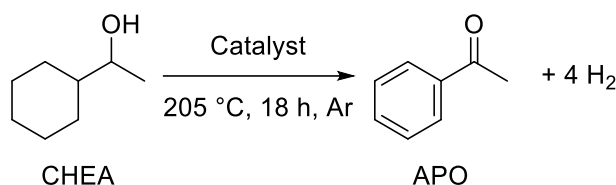


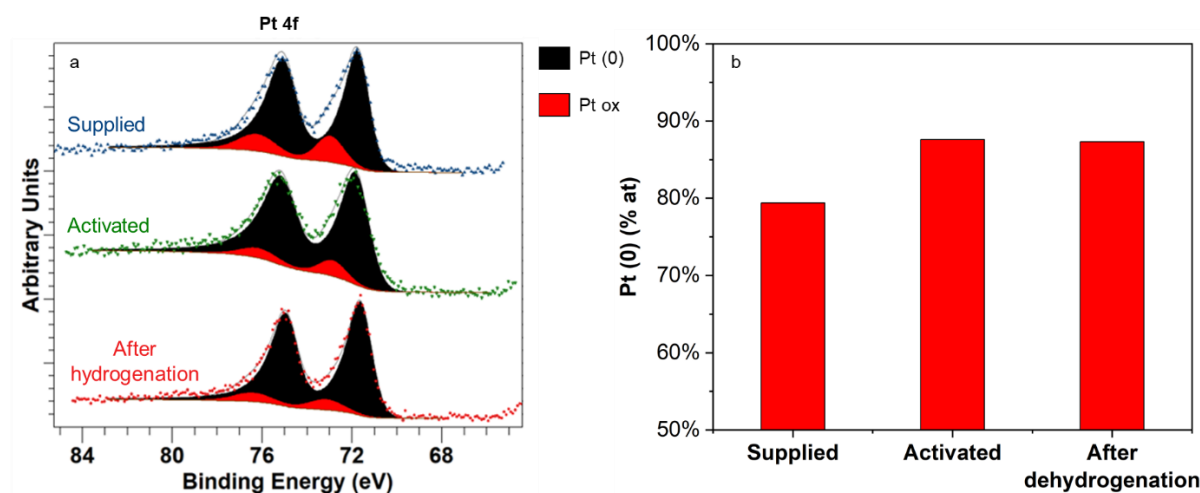
Figure 30 – CHEA conversion, LOHC stability and Degree of dehydrogenation (DoDH) of the catalysts tested for the dehydrogenation of CHEA to APO. 1.5 mL CHEA, 1 wt.% active metal catalyst (with regard to APO), 18 h, 205 °C, Ar.

Chapter 1: Evaluation of new LOHC structures

The Ru, Cu and Ni catalysts showed good conversion and selectivity for the dehydrogenation of the alcohol to the ketone but a limited reactivity for the aromatization, in agreement with the literature.[64–66] The Pd catalysts achieved the dehydrogenation of both the cycle and the alcohol but also exhibited a strong tendency for dehydration products (Figure IV-3).[67,68] Similarly to Pd, the Rh catalysts managed both dehydrogenation steps but favoured the formation of the coupling products instead.[68] Pt catalysts displayed the best conversion of all catalysts, but intramolecular dehydration products could always be found. Various side-reactions were favoured depending on the support but no correlation with the support was found. Out of all the tested catalysts, the 5%Pt/C catalyst supplied by Sigma-Aldrich yielded the best compromise between conversion, LOHC stability and degree of dehydrogenation. Further experiments on the catalytic loading and time of reaction after activation were used to refine the conditions to yield the most efficient dehydrogenation parameters. The complete CHEA conversion, a DoDH of 72% and a LOHC stability of 80% was achieved with a catalyst loading of 0.25 wt.%Pt and a reaction time of 36 h. (ESI S22). While this result is promising, CHEA dehydrogenation kinetics are still a hundred to a thousand times slower than the benchmark system: Dibenzyltoluene at 1 gH₂/gPt/min.[69]

4. Analysis of the selected Pt/C catalyst for the dehydrogenation of 1-Cyclohexylethanol

The catalyst was analyzed by XPS after three different steps: as supplied, after activation and after dehydrogenation (Figure IV-15a). The Pt 4f core level was fitted with an asymmetric doublet corresponding to the reduced state of platinum.[70] Another pair of pseudo-voigt distribution (Gaussian-laurentzian peaks) corresponding to an oxidized Pt state was added



Pt/C catalyst state	Pt average size and dispersion (nm)	Specific surface (m ² /g)	Pore diameter (nm)
Supplied	1.7±0.4	1577	3.4
Activated	1.5±0.5	1598	3.4
After hydrogenation	2.0±0.8	1460	3.4

Figure 31 - (a) Pt 4f spectra of the supplied catalyst, the activated catalyst and the catalyst after dehydrogenation. (b) Atomic percentage of Pt(0) for the supplied catalyst, the activated catalyst and the catalyst after dehydrogenation. (bottom) Size and dispersion of the Pt nanoparticles and specific surface and pores diameter of the carbon support.

Chapter 1: Evaluation of new LOHC structures

Roughly 80% of the Pt is reduced in the supplied catalyst (Figure IV-15b). The activation of the catalyst leads to the increase of the reduced Pt(0) species as O₂-reactive low coordination sites are removed (Figure IV-15b).[71] The proportion of the oxidized Pt species is reduced to roughly 12-13% after the activation of the catalyst. No significant variation of reduced Pt(0) is observed between the activated catalyst and the catalyst after dehydrogenation.

Oxidized Pt species are only visible by XPS while FTIR-ATR, Raman spectroscopy, ICP-OES, TGA and BET adsorption show little to no variation between the samples (ESI S23, 24, S25, S26 and S27). A limited sintering of the Pt nanoparticles is visible by TEM-EDX and XRD after dehydrogenation (Figure 31 - (a) Pt 4f spectra of the supplied catalyst, the activated catalyst and the catalyst after dehydrogenation. (b) Atomic percentage of Pt(0) for the supplied catalyst, the activated catalyst and the catalyst after dehydrogenation. (bottom) Size and dispersion of the Pt nanoparticles and specific surface and pores diameter of the carbon support. Figure IV-15, ESI S28 and S29). No significant variation of specific surface and pore diameter was detected after reduction and utilization.

5. Chemical kinetics of dehydrogenation

To better understand the dehydrogenation pathway, chemical kinetics experiments were performed. Chemical kinetics show a near total conversion of the reactant in less than 24 h (Figure IV-20).. The DoDH rapidly increases to 30% in 10 h. At that time, more than 85% of the alcohol is already converted into the ketone. Over the 10 following hours, the DoH increases only by 10%, pointing to a change in the dehydrogenation step controlling the rates. This observation is consistent with a two-step system kinetics with a fast first step and a slow second step.[72] In addition, the formation of the dehydrogenated condensation product, OH-Coupling, as the main impurity stays below 5% during the reaction.

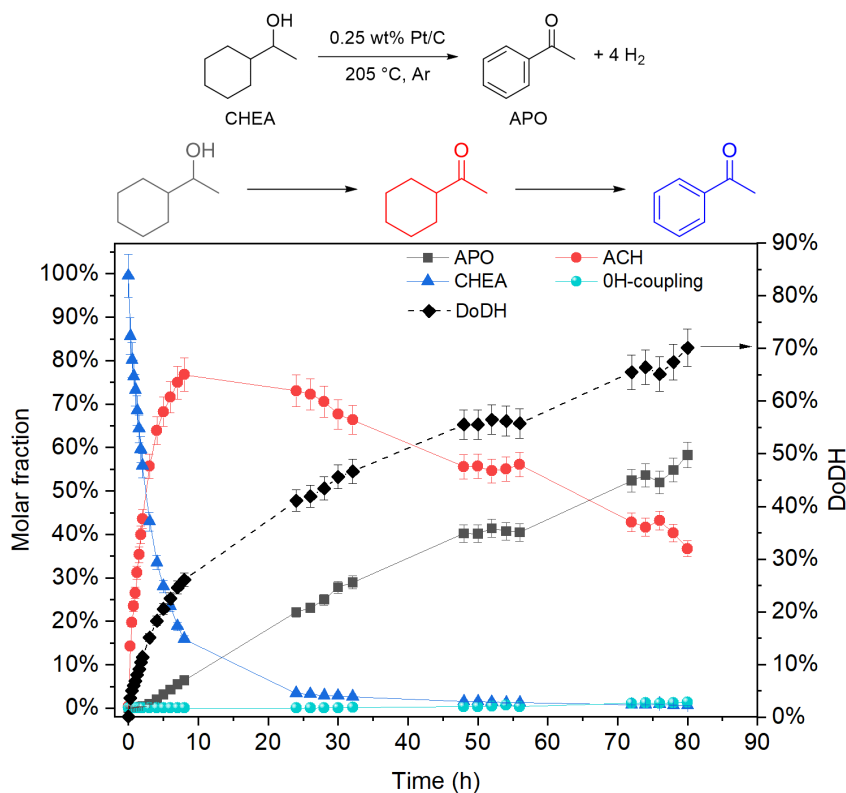


Figure 32 – Scheme of the reaction (top); Products distribution during the dehydrogenation and DoDH (bottom). All other products were found in quantities below 5% during the reaction. 0.25 wt.% catalyst loading, 205 °C, Ar.

Chapter 1: Evaluation of new LOHC structures

Moreover, other kinetic experiments showed that each step of the dehydrogenation is reversible due to the residual H₂ pressure. Indeed, during the dehydrogenation of 1-Phenylethanol (PEO) intermediate to APO, spontaneous hydrogenation of the aromatic cycle is observed either *via* direct hydrogenation or transfer hydrogenation (ESI Figure IV-20S30). It is however difficult to conclude on which mechanism directs the reaction as the laws of the kinetics for each step are complex and the C-O bond can easily be hydrogenated or dehydrogenated and hence act as a platform for transfer-dehydrogenation.

Further kinetics experiments were carried out in order to calculate the activation energy of each function. Here, each molecule is characterized by 2 factors: the dehydrogenation state of the alcohol function and the one of the cycle (Figure IV-22 top left). The 6H-Coupling product contributes for half its molar fraction to both CH and Ar classes (as defined in Figure IV-22). No dehydration products were observed during the experiment.

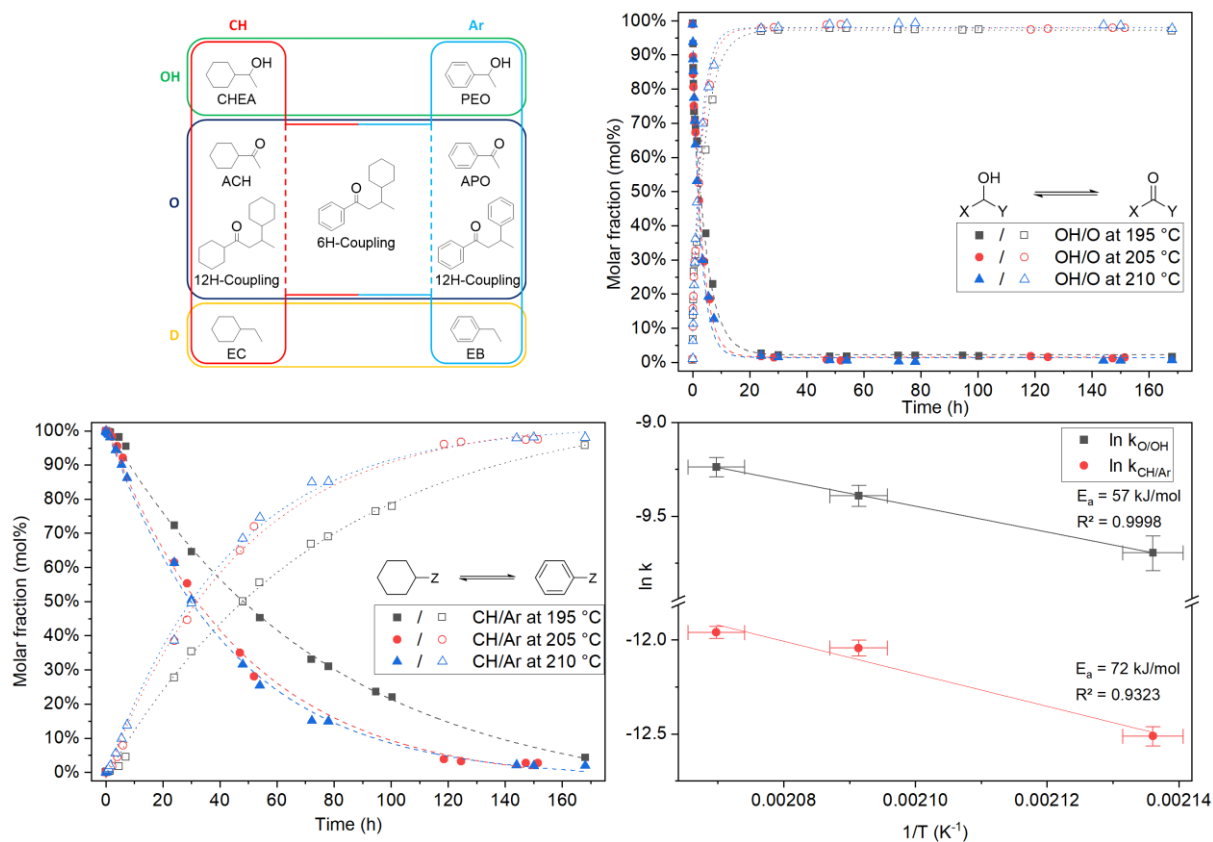


Figure 33 –Classification by functions of the products for the lumped kinetics: CH=Cyclohexane, Ar=Aromatic, OH=Alcohol, O=Ketone, D=Dehydration (top left); Lumped kinetics for the O and OH compounds (top right); Lumped kinetics for the CH and Ar compounds (bottom left); Activation energies for the OH/O and CH/Ar functions (bottom right).

For both the OH/O and CH/Ar functions, the increase of the temperature of reaction increases the kinetics as expected. Moreover, the equilibrium state for the OH/O function is reached after 24 h (Figure IV-22 top right), whereas the CH/Ar function reaches equilibrium between 140 and 168 h depending on the temperature of reaction (Figure IV-22 bottom left). The apparent specific rate constants were calculated for each reaction and function by performing an exponential fit on the function curves assuming 1st order kinetics in a batch stirred reactor. All adjusted R² are above 0.989 (ESI S31). External diffusion effects are supposedly non limiting due to the high stirring speed (1500 rpm). Indeed, classic LOHC setup have showed external diffusion effects below 500 rpm during

the dehydrogenation.[12] Internal diffusion effects are also negligible as shown by internal effectiveness factors being close to 1 for each function (ESI S32). The activation energy for each function was obtained by using the Arrhenius law (Figure IV-22 bottom right). As no kinetics study on the dehydrogenation of CHEA to APO was reported in the literature, the comparison of the activation energy was performed by assimilating the OH-O function to the dehydrogenation of isopropanol to acetone and the CH-Ar function to the dehydrogenation of cyclohexane to benzene. The OH-O activation energy was calculated to be 57 kJ/mol compared to 28 kJ/mol in the literature.[73] The difference in activation energy could be due to the steric hindrance of the cycle compared to the methyl group.[74] Conversely, the calculated CH-Ar activation energy is in good agreement with the literature (72 kJ/mol vs 70 kJ/mol), which suggests that the O-group does not strongly influence the dehydrogenation.[75] The lower activation energy for OH-O is consistent with the dehydrogenation of this bond before the dehydrogenation of the cycle.

6. Cycling

The system was cycled thrice using the optimized conditions (Figure IV-23, top left). Material losses of 10 to 20% per step were visible and attributed to reactor transfers, filtrations and sampling for GC-MS analysis (ESI S33). A slight degradation occurred, mainly due to the self-coupling and the dehydration of the LOHC (Figure IV-23, top right). However, as the degradation products still possess a 6-membered cycle like EB/EC, cycling of the whole mixture is still possible without a dramatic loss of hydrogen storage.[76,77] By pondering the theoretical capacity of each degradation product in the mixture, close to 99% of the maximum theoretical hydrogen capacity (i.e. the theoretical capacity of the CHEA/APO couple) is retained even after the third cycle (Figure IV-23, bottom left). As new LOHC couples are produced through the degradation of the CHEA/APO, the degree of hydrogenation and dehydrogenation over the cycling needs to be modified to account for the cycling of each subspecies. Indeed, each sub-LOHC couple can store various amounts of hydrogen hence the quantity of the sub-LOHC couples as well as its theoretical maximum storage capacity are taken into account to calculate the equivalent of the DoDH and DoH of the system. The exploited H₂ capacity, which describes the amount of hydrogen unloaded during a cycle by the LOHC system, is calculated by equation (IV-17). During the cycling, up to 50% of the hydrogen capacity could be used (Figure IV-23, bottom right). Further catalyst design is hence required to access the rest of the H₂ capacity and decrease the reaction time while avoiding the degradation of the LOHC.

Chapter 1: Evaluation of new LOHC structures

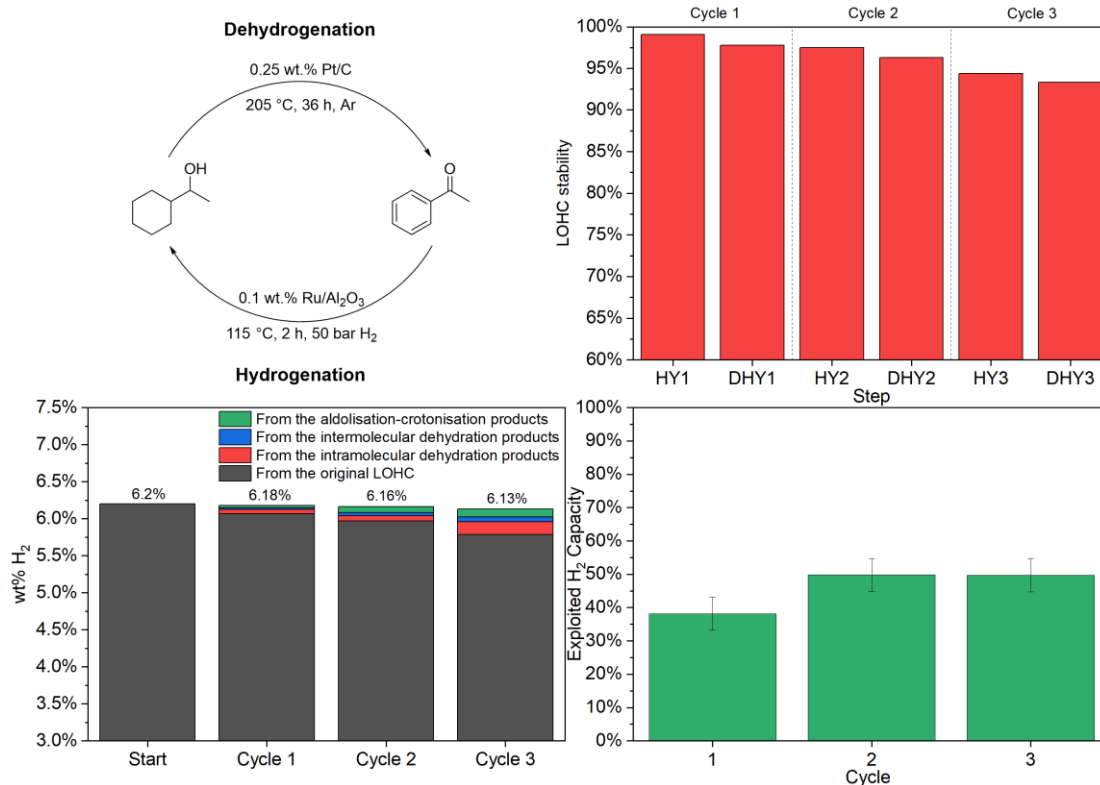


Figure 34 –Optimized conditions of cycling (top left); LOHC stability at the end of each step of the cycling (top right); Maximum H₂ theoretical capacity at the end of each cycle (bottom left); Exploited H₂ capacity over the cycling (bottom right).

Enthalpy of dehydrogenation and mechanism of reaction

The energies of the key intermediates involved in the reaction were computed by DFT. The accuracy of the method was first assessed by calculating the dehydrogenation enthalpy of known LOHC couples (Figure 35); the difference between the experimental values reported in the literature and calculated values fall below 3 kJ/molH₂ which is satisfactory (ESI S34). Based on DFT, the estimated enthalpy change for the CHEA/APO couple is 65 kJ/molH₂, which is close to that of Cyclohexanol/Phenol (64 kJ/molH₂).

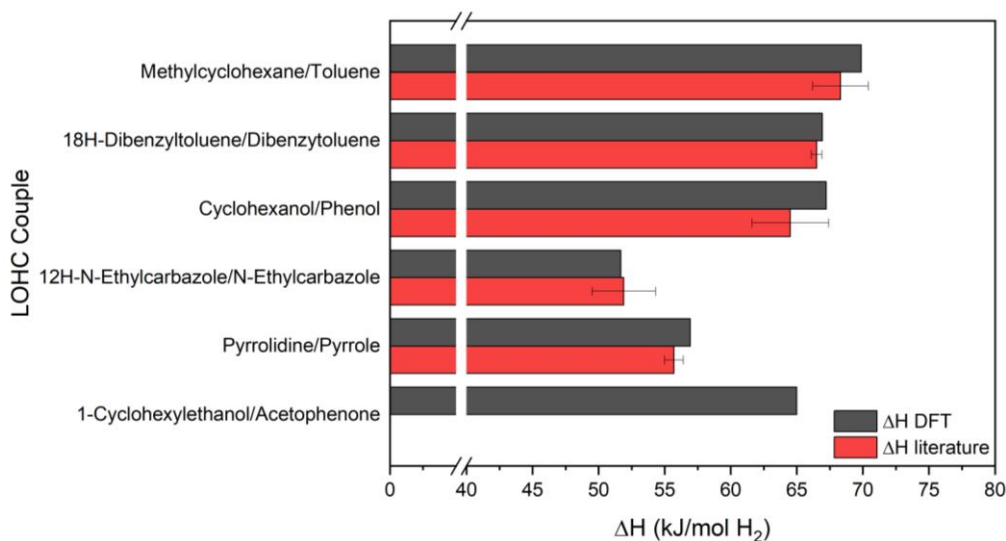


Figure 35 - Comparison of ΔH values obtained from the literature or by DFT calculations.

Chapter 1: Evaluation of new LOHC structures

We then computed a number of plausible intermediates, some of which are presented in the Figure IV-25. The enthalpy change for each potential intermediate is presented in the ESI S35. Among those, some have been identified by GC-MS (highlighted by green rectangles). The other intermediates are not observed, probably due to their lack of stability or high reactivity. VEC and VEB are proposed as intermediates for the intramolecular dehydration of the alcohols, which are hydrogenated to yield EC and EB as the corresponding cycloalkanes.[78] Intermolecular dehydration between two alcohol bearing molecules (CHEA and APO) is most thermodynamically favoured degradation pathway and 12H-ROR ($\Delta H=-9$ kJ/mol, $\Delta G=1$ kJ/mol) and OH-ROR ($\Delta H=-2$ kJ/mol, $\Delta G=9$ kJ/mol) should be produced as the main impurities based on the enthalpy change. The probable limitations to the ether formation are the steric hindrance and the lack of strong acidic sites on the catalyst. The coupling products, whilst the less thermodynamically favourable of the impurities ($\Delta H=25$ kJ/mol, $\Delta G=34$ kJ/mol) are formed as the main by-products through an aldol addition of two ketones bearing molecules (ACH and APO), followed by an internal dehydration (12H-AI and OH-AI) and subsequent hydrogenation of the formed α,β -unsaturated ketones to yield 12H-Coupling, 6H-Coupling and OH-Coupling.[79] The aldol addition is reversible with a strong base,[80] however the high temperature of reaction in combination with the hydrogen in solution favours the crotonisation/hydrogenation pathway. The hydrogenation of the 12H-AI and OH-AI intermediates is highly favourable in the presence of hydrogen (resp. $\Delta H=-110/-120$ kJ/mol, $\Delta G=-74/-84$ kJ/mol), explaining the absence of these structures in the reactional mixture. These conditions render the reaction irreversible as electrons are not stabilized anymore by resonance, which allows for the accumulation of the coupling products in solution. The aldol reaction is also possible in the presence of a metallic enolate. However, as platinum is the only metal in the reaction mixture and has not been shown to favour enol formation, this reaction pathway is less plausible.[81]

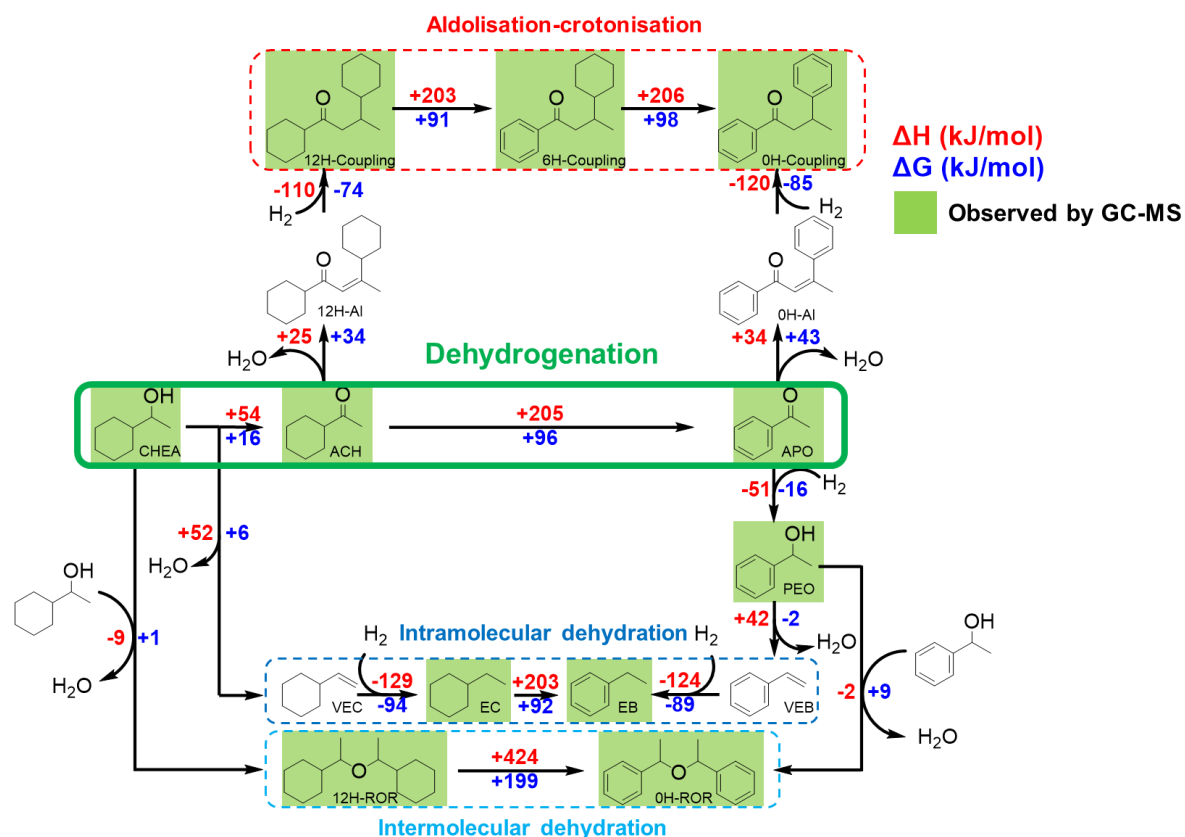


Figure 36 - Enthalpy (red) and free energy change (blue) between the intermediates of the system during the dehydrogenation. The products identified by GC-MS are highlighted in green.

Chapter 1: Evaluation of new LOHC structures

Degradation by removal of the oxygen atom or change in the carbon backbone is supposed irreversible while reactions producing hydrogen are expected to be reversible under the conditions of the system.

As unwanted dehydration and condensation reactions are catalysed by acidic or basic conditions, the effect of the acidity or basicity of the support on the reaction selectivity was investigated. Three alumina with various acidity/basicity were used to synthesize 2 wt.% Pt/Al₂O₃ catalysts. Dehydrogenation of CHEA was performed for each catalyst but no correlation between the support acidity/basicity and the composition of the impurities was found (ESI S36 and S37). Dehydration of the LOHC could not be prevented by changing the substrate to a basic alumina.

Conclusion

A new bifunctional LOHC couple, based on 1-Cyclohexylethanol/Acetophenone, has been evaluated by DFT and deemed a potential LOHC couple. Lab experiments showed promises on its application as a LOHC as Ru/Al₂O₃ hydrogenated the LOHC at 115 °C in 2 h with a conversion of 100% and 98% selectivity. The dehydrogenation was successfully carried out using Pt/C at 205 °C in 36 h with total conversion but with a degree of dehydrogenation (DoDH) limited to 72% and a LOHC stability of 80%. These conditions were used to cycle the system three times during which up to 50% of the total hydrogen capacity could be exploited, stable after 3 cycles. The limitations of such a system, which pairs C–O bonds and C–C bonds, have been identified: the reversibility of the hydrogenation of the ketone group upon dehydrogenation facilitates condensation and dehydration reactions, under the conditions required for the slower dehydrogenation of the cyclohexyl ring. Degradation of the carrier produces LOHC-like structures, some of which have already been studied in the literature such as Ethylcyclohexane/Ethylbenzene and are hence not incompatible with cycling. Further work is required on the catalysis to refine the activity to the targeted species, increase the kinetics, limit the side reactions or regenerate the LOHC mixture to further its development as a LOHC.

References

- [1] Gupta RB. Hydrogen Fuel: Production, Transport, and Storage. CRC Press; 2008.
- [2] Orecchini F. The era of energy vectors. *International Journal of Hydrogen Energy* 2006;31:1951–4. <https://doi.org/10.1016/j.ijhydene.2006.01.015>.
- [3] Kar SK, Harichandan S, Roy B. Bibliometric analysis of the research on hydrogen economy: An analysis of current findings and roadmap ahead. *International Journal of Hydrogen Energy* 2022. <https://doi.org/10.1016/j.ijhydene.2022.01.137>.
- [4] Reuß M, Grube T, Robinius M, Preuster P, Wasserscheid P, Stolten D. Seasonal storage and alternative carriers: A flexible hydrogen supply chain model. *Applied Energy* 2017;200:290–302. <https://doi.org/10.1016/j.apenergy.2017.05.050>.
- [5] Grünenfelder NF, Schucan ThH. Seasonal storage of hydrogen in liquid organic hydrides: description of the second prototype vehicle. *International Journal of Hydrogen Energy* 1989;14:579–86. [https://doi.org/10.1016/0360-3199\(89\)90117-1](https://doi.org/10.1016/0360-3199(89)90117-1).
- [6] Züttel A. Hydrogen storage methods. *Naturwissenschaften* 2004;91:157–72. <https://doi.org/10.1007/s00114-004-0516-x>.
- [7] He T, Pei Q, Chen P. Liquid organic hydrogen carriers. *Journal of Energy Chemistry* 2015;24:587–94. <https://doi.org/10.1016/j.jechem.2015.08.007>.
- [8] Cho J-Y, Kim H, Oh J-E, Park BY. Recent Advances in Homogeneous/Heterogeneous Catalytic Hydrogenation and Dehydrogenation for Potential Liquid Organic Hydrogen Carrier (LOHC) Systems. *Catalysts* 2021;11:1497. <https://doi.org/10.3390/catal11121497>.
- [9] Teichmann D, Arlt W, Wasserscheid P. Liquid Organic Hydrogen Carriers as an efficient vector for the transport and storage of renewable energy. *International Journal of Hydrogen Energy* 2012;37:18118–32. <https://doi.org/10.1016/j.ijhydene.2012.08.066>.
- [10] Taube M, Rippin D, Knecht W, Hakimifard D, Milisavljevic B, Gruenenfelder N. A prototype truck powered by hydrogen from organic liquid hydrides. *International Journal of Hydrogen Energy* 1985;10:595–9. [https://doi.org/10.1016/0360-3199\(85\)90035-7](https://doi.org/10.1016/0360-3199(85)90035-7).

Chapter 1: Evaluation of new LOHC structures

- [11] Target Explanation Document: Onboard Hydrogen Storage for Light-Duty Fuel Cell Vehicles. EnergyGov n.d. <https://www.energy.gov/eere/fuelcells/downloads/target-explanation-document-onboard-hydrogen-storage-light-duty-fuel-cell> (accessed June 4, 2021).
- [12] Alan C. Cooper. Design and Development of New Carbon-Based Sorbent Systems for an Effective Containment of Hydrogen. 2012. <https://doi.org/10.2172/1039432>.
- [13] Clot E, Eisenstein O, H. Crabtree R. Computational structure–activity relationships in H₂ storage: how placement of N atoms affects release temperatures in organic liquid storage materials. *Chemical Communications* 2007;0:2231–3. <https://doi.org/10.1039/B705037B>.
- [14] Cui Y, Kwok S, Bucholtz A, Davis B, A. Whitney R, G. Jessop P. The effect of substitution on the utility of piperidines and octahydroindoles for reversible hydrogen storage. *New Journal of Chemistry* 2008;32:1027–37. <https://doi.org/10.1039/B718209K>.
- [15] Enthaler S, Langermann J von, Schmidt T. Carbon dioxide and formic acid—the couple for environmental-friendly hydrogen storage? *Energy Environ Sci* 2010;3:1207–17. <https://doi.org/10.1039/B907569K>.
- [16] Tseng K-NT, Rizzi AM, Szymczak NK. Oxidant-Free Conversion of Primary Amines to Nitriles. *J Am Chem Soc* 2013;135:16352–5. <https://doi.org/10.1021/ja409223a>.
- [17] Siddiki SMAH, Toyao T, Shimizu K. Acceptorless dehydrogenative coupling reactions with alcohols over heterogeneous catalysts. *Green Chemistry* 2018;20:2933–52. <https://doi.org/10.1039/C8GC00451J>.
- [18] Gould ES. Mechanism and structure in organic chemistry. Holt, Rinehart and Winston; 1959.
- [19] S. Luterbacher J, Alonso DM, A. Dumesic J. Targeted chemical upgrading of lignocellulosic biomass to platform molecules. *Green Chemistry* 2014;16:4816–38. <https://doi.org/10.1039/C4GC01160K>.
- [20] Mitsudome T, Mikami Y, Ebata K, Mizugaki T, Jitsukawa K, Kaneda K. Copper nanoparticles on hydrotalcite as a heterogeneous catalyst for oxidant-free dehydrogenation of alcohols. *Chemical Communications* 2008;0:4804–6. <https://doi.org/10.1039/B809012B>.
- [21] Zhang P, Wang Q-N, Yang X, Wang D, Li W-C, Zheng Y, et al. A Highly Porous Carbon Support Rich in Graphitic-N Stabilizes Copper Nanocatalysts for Efficient Ethanol Dehydrogenation. *ChemCatChem* 2017;9:505–10. <https://doi.org/10.1002/cctc.201601373>.
- [22] Miura H, Nakahara K, Kitajima T, Shishido T. Concerted Functions of Surface Acid–Base Pairs and Supported Copper Catalysts for Dehydrogenative Synthesis of Esters from Primary Alcohols. *ACS Omega* 2017;2:6167–73. <https://doi.org/10.1021/acsomega.7b01142>.
- [23] McCullough LR, Childers DJ, Watson RA, Kilos BA, Barton DG, Weitz E, et al. Acceptorless Dehydrogenative Coupling of Neat Alcohols Using Group VI Sulfide Catalysts. *ACS Sustainable Chem Eng* 2017;5:4890–6. <https://doi.org/10.1021/acssuschemeng.7b00303>.
- [24] Falbe J, Bahrmann H, Lipps W, Mayer D, Frey GD. Alcohols, Aliphatic. *Ullmann's Encyclopedia of Industrial Chemistry*, John Wiley & Sons, Ltd; 2013. https://doi.org/10.1002/14356007.a01_279.pub2.
- [25] Kohlpaintner C, Schulte M, Falbe J, Lappe P, Weber J, Frey GD. Aldehydes, Aliphatic. *Ullmann's Encyclopedia of Industrial Chemistry*, John Wiley & Sons, Ltd; 2013. https://doi.org/10.1002/14356007.a01_321.pub3.
- [26] Kohlpaintner C, Schulte M, Falbe J, Lappe P, Weber J, Frey GD. Aldehydes, Aromatic. *Ullmann's Encyclopedia of Industrial Chemistry*, John Wiley & Sons, Ltd; 2013. https://doi.org/10.1002/14356007.m01_m03.pub2.
- [27] Siegel H, Eggersdorfer M. Ketones. *Ullmann's Encyclopedia of Industrial Chemistry*, John Wiley & Sons, Ltd; 2000. https://doi.org/10.1002/14356007.a15_077.
- [28] Kaźmierczak K, Salisu A, Pinel C, Besson M, Michel C, Perret N. Activity of heterogeneous supported Cu and Ru catalysts in acceptor-less alcohol dehydrogenation. *Catalysis Communications* 2021;148:106179. <https://doi.org/10.1016/j.catcom.2020.106179>.
- [29] Guerrero-Ruiz A, Rodriguez-Ramos I, Fierro JLG. Dehydrogenation of methanol to methyl formate over supported copper catalysts. *Applied Catalysis* 1991;72:119–37. [https://doi.org/10.1016/0166-9834\(91\)85033-R](https://doi.org/10.1016/0166-9834(91)85033-R).
- [30] Ichikawa N, Sato S, Takahashi R, Sodesawa T, Inui K. Dehydrogenative cyclization of 1,4-butanediol over copper-based catalyst. *Journal of Molecular Catalysis A: Chemical* 2004;212:197–203. <https://doi.org/10.1016/j.molcata.2003.10.028>.
- [31] Vorotnikov V, Mpourmpakis G, Vlachos DG. DFT Study of Furfural Conversion to Furan, Furfuryl Alcohol, and 2-Methylfuran on Pd(111). *ACS Catal* 2012;2:2496–504. <https://doi.org/10.1021/cs300395a>.
- [32] Merat N, Godawa C, Gaset A. High selective production of tetrahydrofurfuryl alcohol: Catalytic hydrogenation of furfural and furfuryl alcohol. *Journal of Chemical Technology & Biotechnology* 1990;48:145–59. <https://doi.org/10.1002/jctb.280480205>.

Chapter 1: Evaluation of new LOHC structures

- [33] Claus P, Berndt H, Mohr C, Radnik J, Shin E-J, Keane MA. Pd/MgO: Catalyst Characterization and Phenol Hydrogenation Activity. *Journal of Catalysis* 2000;192:88–97. <https://doi.org/10.1006/jcat.2000.2834>.
- [34] Zhang J, Jiang Q, Yang D, Zhao X, Dong Y, Liu R. Reaction-activated palladium catalyst for dehydrogenation of substituted cyclohexanones to phenols and H₂ without oxidants and hydrogen acceptors. *Chemical Science* 2015;6:4674–80. <https://doi.org/10.1039/C5SC01044F>.
- [35] Kleinert M, Barth T. Phenols from Lignin. *Chemical Engineering & Technology* 2008;31:736–45. <https://doi.org/10.1002/ceat.200800073>.
- [36] Weber M, Weber M, Kleine-Boymann M. Phenol. *Ullmann's Encyclopedia of Industrial Chemistry*, John Wiley & Sons, Ltd; 2004. https://doi.org/10.1002/14356007.a19_299.pub2.
- [37] Brückner N, Obesser K, Bösmann A, Teichmann D, Arlt W, Dungs J, et al. Evaluation of Industrially Applied Heat-Transfer Fluids as Liquid Organic Hydrogen Carrier Systems. *ChemSusChem* 2014;7:229–35. <https://doi.org/10.1002/cssc.201300426>.
- [38] Luo N, Wang M, Li H, Zhang J, Hou T, Chen H, et al. Visible-Light-Driven Self-Hydrogen Transfer Hydrogenolysis of Lignin Models and Extracts into Phenolic Products. *ACS Catal* 2017;7:4571–80. <https://doi.org/10.1021/acscatal.7b01043>.
- [39] Theilacker W, Drössler H-G. Die katalytische Hydrierung von Acetophenon mit Platin und Palladium. Ein Beitrag zur Selektivität der Edelmetallkatalysatoren. *Chemische Berichte* 1954;87:1676–84. <https://doi.org/10.1002/cber.19540871111>.
- [40] Kim W-H, Park IS, Park J. Acceptor-Free Alcohol Dehydrogenation by Recyclable Ruthenium Catalyst. *Org Lett* 2006;8:2543–5. <https://doi.org/10.1021/ol060750z>.
- [41] Putro WS, Kojima T, Hara T, Ichikuni N, Shimazu S. Acceptorless dehydrogenation of alcohols using Cu–Fe catalysts prepared from Cu–Fe layered double hydroxides as precursors. *Catal Sci Technol* 2018;8:3010–4. <https://doi.org/10.1039/C8CY00655E>.
- [42] Burgener M, Mallat T, Baiker A. Palladium-catalysed dehydrogenation of 1-phenylethanol in dense carbon dioxide. *Journal of Molecular Catalysis A: Chemical* 2005;225:21–5. <https://doi.org/10.1016/j.molcata.2004.08.029>.
- [43] Tilgner D, Klarner M, Hammon S, Friedrich M, Verch A, Jonge N de, et al. H₂-Generation from Alcohols by the MOF-Based Noble Metal-Free Photocatalyst Ni/CdS/TiO₂@MIL-101*. *Aust J Chem* 2019;72:842–7. <https://doi.org/10.1071/CH19255>.
- [44] Mitsudome T, Mikami Y, Funai H, Mizugaki T, Jitsukawa K, Kaneda K. Oxidant-Free Alcohol Dehydrogenation Using a Reusable Hydrotalcite-Supported Silver Nanoparticle Catalyst. *Angewandte Chemie International Edition* 2008;47:138–41. <https://doi.org/10.1002/anie.200703161>.
- [45] Fang W, Zhang Q, Chen J, Deng W, Wang Y. Gold nanoparticles on hydrotalcites as efficient catalysts for oxidant-free dehydrogenation of alcohols. *Chem Commun* 2010;46:1547–9. <https://doi.org/10.1039/B923047E>.
- [46] Fujita K, Tanino N, Yamaguchi R. Ligand-Promoted Dehydrogenation of Alcohols Catalyzed by Cp*Ir Complexes. A New Catalytic System for Oxidant-Free Oxidation of Alcohols. *Org Lett* 2007;9:109–11. <https://doi.org/10.1021/ol062806v>.
- [47] Falini G, Gualandi A, Savoia D. Rhodium/Graphite-Catalyzed Hydrogenation of Carbocyclic and Heterocyclic Aromatic Compounds. *Synthesis* 2009;2009:2440–6. <https://doi.org/10.1055/s-0029-1216852>.
- [48] Llop Castelbou J, Bresó-Femenia E, Blondeau P, Chaudret B, Castellón S, Claver C, et al. Tuning the Selectivity in the Hydrogenation of Aromatic Ketones Catalyzed by Similar Ruthenium and Rhodium Nanoparticles. *ChemCatChem* 2014;6:3160–8. <https://doi.org/10.1002/cctc.201402524>.
- [49] Masson J, Cividino P, Court J. Selective hydrogenation of acetophenone on chromium promoted Raney nickel catalysts. III. The influence of the nature of the solvent. *Applied Catalysis A: General* 1997;161:191–7. [https://doi.org/10.1016/S0926-860X\(97\)00068-9](https://doi.org/10.1016/S0926-860X(97)00068-9).
- [50] JOBACK KG, REID RC. Estimation of Pure-Component Properties from Group-Contributions. *Chemical Engineering Communications* 1987;57:233–43. <https://doi.org/10.1080/00986448708960487>.
- [51] Rousset JL, Stievano L, Aires FJCS, Geantet C, Renouprez AJ, Pellarin M. Hydrogenation of Toluene over γ -Al₂O₃-Supported Pt, Pd, and Pd–Pt Model Catalysts Obtained by Laser Vaporization of Bulk Metals. *Journal of Catalysis* 2001;197:335–43. <https://doi.org/10.1006/jcat.2000.3083>.
- [52] Chen M, Maeda N, Baiker A, Huang J. Hydrogenation of Acetophenone on Pd/Silica–Alumina Catalysts with Tunable Acidity: Mechanistic Insight by In Situ ATR-IR Spectroscopy. *ACS Catal* 2018;8:6594–600. <https://doi.org/10.1021/acscatal.8b00169>.

Chapter 1: Evaluation of new LOHC structures

- [53] Do G, Preuster P, Aslam R, Bösmann A, Müller K, Arlt W, et al. Hydrogenation of the liquid organic hydrogen carrier compound dibenzyltoluene – reaction pathway determination by ^1H NMR spectroscopy. *Reaction Chemistry & Engineering* 2016;1:313–20. <https://doi.org/10.1039/C5RE00080G>.
- [54] Jorschick H, Preuster P, Dürr S, Seidel A, Müller K, Bösmann A, et al. Hydrogen storage using a hot pressure swing reactor. *Energy & Environmental Science* 2017;10:1652–9. <https://doi.org/10.1039/C7EE00476A>.
- [55] Suppino RS, Landers R, Cobo AJG. Influence of noble metals (Pd, Pt) on the performance of Ru/Al₂O₃ based catalysts for toluene hydrogenation in liquid phase. *Applied Catalysis A: General* 2016;525:41–9. <https://doi.org/10.1016/j.apcata.2016.06.038>.
- [56] Bianchi CL, Ragaini V, Cattania MG. An XPS study on ruthenium compounds and catalysts. *Materials Chemistry and Physics* 1991;29:297–306. [https://doi.org/10.1016/0254-0584\(91\)90025-P](https://doi.org/10.1016/0254-0584(91)90025-P).
- [57] Kim KS, Winograd N. X-Ray photoelectron spectroscopic studies of ruthenium-oxygen surfaces. *Journal of Catalysis* 1974;35:66–72. [https://doi.org/10.1016/0021-9517\(74\)90184-5](https://doi.org/10.1016/0021-9517(74)90184-5).
- [58] Chen S, Abdel-Mageed AM, Dyballa M, Parlinska-Wojtan M, Bansmann J, Pollastri S, et al. Raising the CO_x Methanation Activity of a Ru/ γ -Al₂O₃ Catalyst by Activated Modification of Metal–Support Interactions. *Angewandte Chemie International Edition* 2020;59:22763–70. <https://doi.org/10.1002/anie.202007228>.
- [59] Durndell LJ, Zou G, Shangguan W, Lee AF, Wilson K. Structure–Reactivity Relations in Ruthenium Catalysed Furfural Hydrogenation. *ChemCatChem* 2019;11:3927–32. <https://doi.org/10.1002/cctc.201900481>.
- [60] Mazzieri V, Coloma-Pascual F, Arcoya A, L'Argentière PC, Fígoli NS. XPS, FTIR and TPR characterization of Ru/Al₂O₃ catalysts. *Applied Surface Science* 2003;210:222–30. [https://doi.org/10.1016/S0169-4332\(03\)00146-6](https://doi.org/10.1016/S0169-4332(03)00146-6).
- [61] bvcrist. Aluminum Spectra - Al(OH)₃. The International XPS Database 1 n.d. <https://xpsdatabase.com/aluminum-spectra-aloh3/> (accessed October 14, 2022).
- [62] bvcrist. Aluminum Spectra - α -Al₂O₃. The International XPS Database 1 n.d. <https://xpsdatabase.com/aluminum-spectra-al2o3/> (accessed October 14, 2022).
- [63] Karvembu R, Prabhakaran R, Senthilkumar K, Viswanathamurthi P, Natarajan K. Ru/Al₂O₃-catalyzed transfer dehydrogenation of alcohols. *React Kinet Catal Lett* 2005;86:211–6. <https://doi.org/10.1007/s11144-005-0314-2>.
- [64] Yergaziyeva GY, Dossumov K, Mambetova MM, Strizhak PY, Kurokawa H, Baizhomartov B. Effect of Ni, La, and Ce Oxides on a Cu/Al₂O₃ Catalyst with Low Copper Loading for Ethanol Non-oxidative Dehydrogenation. *Chemical Engineering & Technology* 2021;44:1890–9. <https://doi.org/10.1002/ceat.202100112>.
- [65] Xia Z, Lu H, Liu H, Zhang Z, Chen Y. Cyclohexane dehydrogenation over Ni-Cu/SiO₂ catalyst: Effect of copper addition. *Catalysis Communications* 2017;90:39–42. <https://doi.org/10.1016/j.catcom.2016.10.036>.
- [66] Nicolau G, Tarantino G, Hammond C. Acceptorless Alcohol Dehydrogenation Catalysed by Pd/C. *ChemSusChem* 2019;12:4953–61. <https://doi.org/10.1002/cssc.201901313>.
- [67] Wang J, Liu H, Fan S, Wang S, Xu G, Guo A, et al. Dehydrogenation of Cycloalkanes over N-Doped Carbon-Supported Catalysts: The Effects of Active Component and Molecular Structure of the Substrate. *Nanomaterials* 2021;11:2846. <https://doi.org/10.3390/nano11112846>.
- [68] Modisha P, Gqogqa P, Garidzirai R, Ouma CNM, Bessarabov D. Evaluation of catalyst activity for release of hydrogen from liquid organic hydrogen carriers. *International Journal of Hydrogen Energy* 2019;44:21926–35. <https://doi.org/10.1016/j.ijhydene.2019.06.212>.
- [69] Kim H-J, Kim W-I, Park T-J, Park H-S, Suh DJ. Highly dispersed platinum–carbon aerogel catalyst for polymer electrolyte membrane fuel cells. *Carbon* 2008;46:1393–400. <https://doi.org/10.1016/j.carbon.2008.05.022>.
- [70] Wang L, Roudgar A, Eikerling M. Ab Initio Study of Stability and Site-Specific Oxygen Adsorption Energies of Pt Nanoparticles. *J Phys Chem C* 2009;113:17989–96. <https://doi.org/10.1021/jp900965q>.
- [71] Helfferich FG, Compton RG, Bamford CH. *Comprehensive chemical kinetics*. Elsevier; 2001.
- [72] Rioux RM, Vannice MA. Dehydrogenation of isopropyl alcohol on carbon-supported Pt and Cu–Pt catalysts. *Journal of Catalysis* 2005;233:147–65. <https://doi.org/10.1016/j.jcat.2005.04.020>.
- [73] A. Jones RW, R. Thomas JD. Steric influence of the alkyl component in the alkaline hydrolysis of acetates and propionates. *Journal of the Chemical Society B: Physical Organic* 1966;0:661–4. <https://doi.org/10.1039/J29660000661>.
- [74] Galimova NA, Pskhu ZV, Naumkin AV, Volkov IO, Yagodovskaya TV, Yagodovskii VD. The influence of plasma chemical treatment of a platinum catalyst on its activity in the dehydrogenation of cyclohexane. *Russ J Phys Chem* 2009;83:1720–6. <https://doi.org/10.1134/S0036024409100161>.

Chapter 1: Evaluation of new LOHC structures

- [75] Shuikin NI, Levitsky II. High temperature catalytic dehydrogenation of ethylcyclohexane. *Russ Chem Bull* 1953;2:895–902. <https://doi.org/10.1007/BF01167533>.
- [76] Lee J-Y, Yung T-Y, Liu L-K. The microwave-assisted ionic liquid nanocomposite synthesis: platinum nanoparticles on graphene and the application on hydrogenation of styrene. *Nanoscale Research Letters* 2013;8:414. <https://doi.org/10.1186/1556-276X-8-414>.
- [77] Knözinger H. Dehydration of Alcohols on Aluminum Oxide. *Angewandte Chemie International Edition in English* 1968;7:791–805. <https://doi.org/10.1002/anie.196807911>.
- [78] Zuffanti S, Luder WF. Generalized acids and bases in organic chemistry. I. Catalytic condensation of aldehydes. *J Chem Educ* 1944;21:485. <https://doi.org/10.1021/ed021p485>.
- [79] Guthrie JP, Cossar J, Cullimore PA, Kamkar NM, Taylor KF. The retroaldol reaction of chalcone. *Can J Chem* 1983;61:2621–6. <https://doi.org/10.1139/v83-449>.
- [80] Kurti L, Czako B. *Strategic Applications of Named Reactions in Organic Synthesis*. Elsevier; 2005.
- [81] Pico MP, Romero A, Rodríguez S, Santos A. Etherification of Glycerol by tert-Butyl Alcohol: Kinetic Model. *Ind Eng Chem Res* 2012;51:9500–9. <https://doi.org/10.1021/ie300481d>.

Chapter 1: Evaluation of new LOHC structures

Appendix IV-2 - Hydrogenation GCMS results

Catalyst and temperature	APO	ACH	CHEA	PEO	EB	EC	Others
5%Pt/Al ₂ O ₃ , 80 °C	2%	0%	23%	75%	0%	0%	0%
5%Pt/C, 80 °C	1%	3%	34%	61%	1%	0%	2%
5%Pd/Al ₂ O ₃ , 80 °C	0%	1%	1%	86%	12%	0%	0%
5%Pd/C, 80 °C	0%	0%	0%	61%	39%	0%	0%
5%Ru/Al ₂ O ₃ , 100 °C	0%	13%	58%	25%	3%	1%	0%
5%Ru/C, 100 °C	0%	7%	83%	0%	0%	10%	0%

Table IV-16 - Composition of the crude reaction mixture after reaction at 50 bar, 4 h. Acetophenone (12.5 mL), heterogeneous catalyst (0.1 wt% active metal with regard to the Acetophenone). Acetophenone (APO), Acetylcyclohexane (ACH), 1-Cyclohexylethanol (CHEA), 1-Phenylethanol (PEO), Ethylbenzene (EB) and Ethylcyclohexane (EC).

Appendix IV-3 - Conversion of Acetophenone with Pt/Al₂O₃, Ru/Al₂O₃ and Ru/C

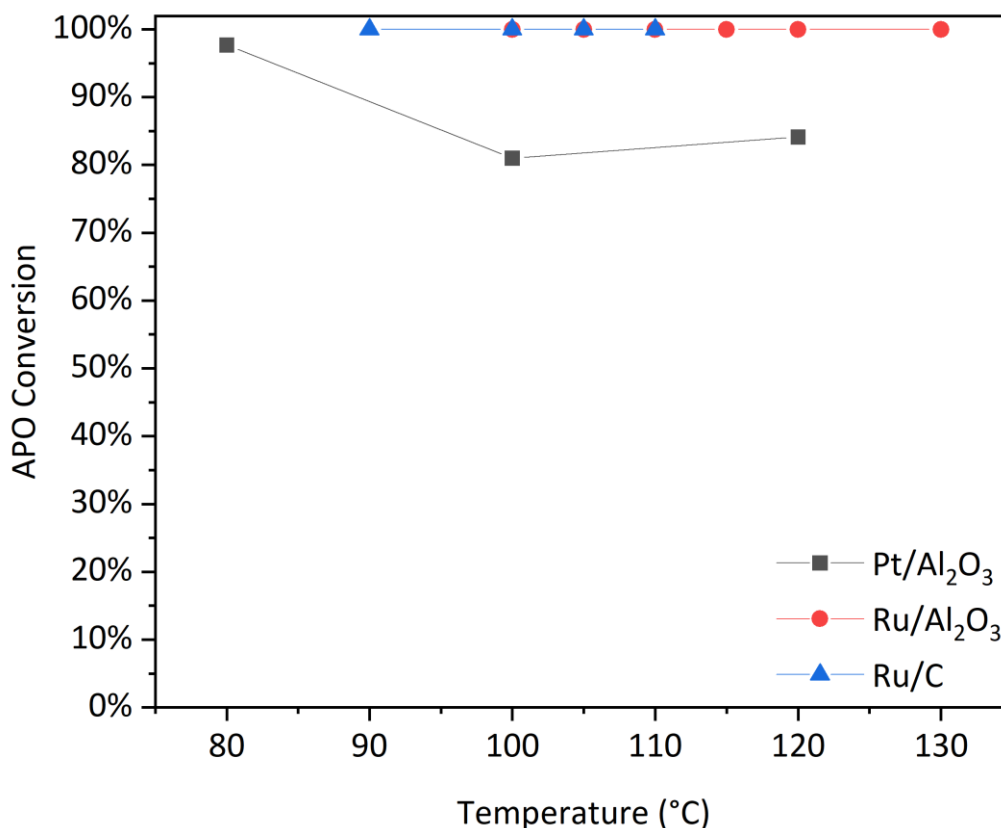


Figure IV-37 - Conversion of Acetophenone with Pt/Al₂O₃, Ru/Al₂O₃ and Ru/C at different temperatures.

Appendix IV-4 - XPS analysis of the Ru 3p core level

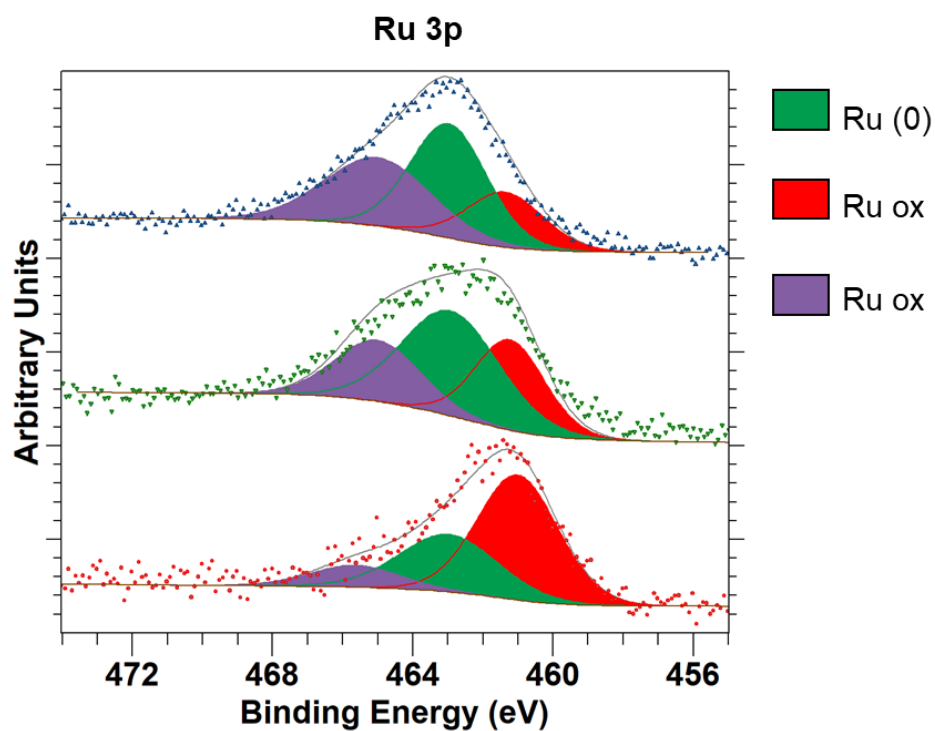


Figure IV-38 - XPS analysis of the Ru 3p core level.

Appendix IV-5 - TEM-EDX images of the Ru/Al₂O₃ catalyst

Catalyst state	Low magnification	High magnification	HAADF	Ru EDS
Supplied Ru/Al ₂ O ₃				
Activated Ru/Al ₂ O ₃				
Ru/Al ₂ O ₃ after hydrogenation				

Figure IV-39 - TEM-EDX images of the Ru/Al₂O₃ catalyst.

Chapter 1: Evaluation of new LOHC structures

Appendix IV-6 - TEM-EDX images of the Pt/C catalyst

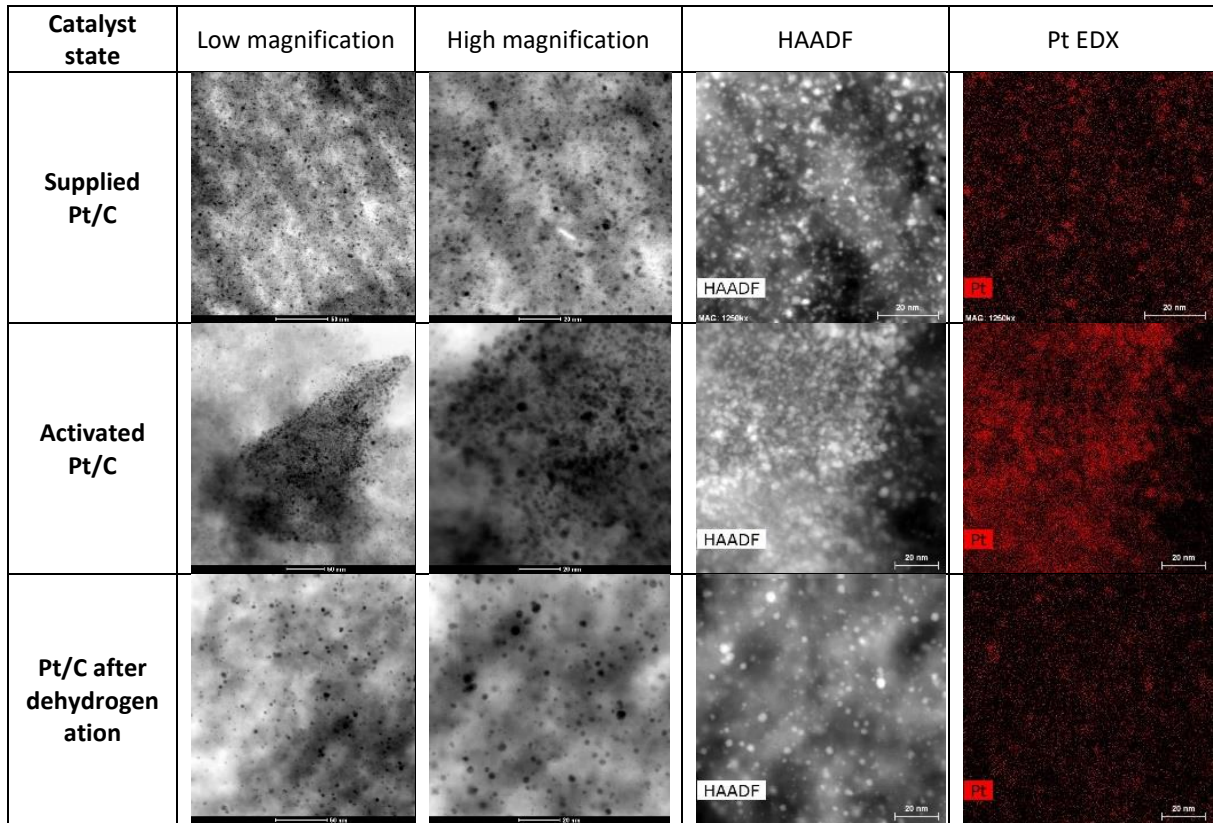


Figure IV-40 - TEM-EDX images of the Pt/C catalyst.

Appendix IV-7 - Apparent specific rates and adjusted correlation factors

The kinetics experiment were fitted assuming 1st order kinetics in a stirred batch reactor with an exponential curve of the type $y = A1 \cdot \exp(-x/t_1) + y_0$

$$y = A \times e^{\left(-\frac{t}{t_1}\right)} + y_0; \text{ with } k_{app} = \frac{1}{t_1} \quad (13)$$

Temperature reaction (°C)	of	$k_{app \text{ OH-O}}$ (s^{-1})	R^2	$k_{app \text{ CH-Ar}}$ (s^{-1})	R^2
195		6.16455E-5	0.98971	3.68224E-6	0.99786
205		8.34561E-5	0.99975	5.88066E-6	0.99792
210		9.72484E-5	0.9959	6.3957E-6	0.99851

Table IV-17 - Apparent specific rates and adjusted correlation factors.

Appendix IV-8 - Estimation of the internal diffusion effects

Internal mass-transfer limitations were estimated by calculating the Internal Effectiveness Factor η for a first-order reaction in a spherical catalyst pellet by using the Thiele modulus ϕ .

$$\eta = \frac{3}{\phi^2} (\phi \coth\phi - 1) \quad (\text{IV-14})$$

The Thiele modulus was calculated based on the expression that corresponds to spherical particles in a kinetic equation of first order, due to the complexity of the reaction system studied with d_p diameter of the catalytic particles (cm), k first order kinetics constant ($\text{cm}^3/\text{g}\cdot\text{s}$), ρ_p density of the catalytic particles (g/cm^3) and D_e the effective diffusivity (cm^2/s).

$$\phi = \frac{d_p}{6} \sqrt{\frac{k \times \rho_p}{D_e}} \quad (\text{IV-15})$$

With $d_p = 200 \mu\text{m} = 0.02 \text{ cm}$ and $\rho_p = 34.4 \text{ g}/\text{cm}^3$.¹ The effective diffusivity is given by

$$D_e = \frac{\varepsilon \times D_{AB}}{\tau} \quad (\text{IV-16})$$

With ε the porosity of the particle, τ the tortuosity of the particle and D_{AB} the infinite dilution molecular diffusivities, where the τ is 2 and ε is 0.5.² The infinite dilution molecular diffusivities D_{AB} (cm^2/s) were estimated by a modification of the Wilke-Chang equation, the Scheibel correlation, which eliminated its association factor.³

$$D_{AB} = \frac{25.2 \times 10^{-8} \times T}{\eta_B (V_A)^{1/3}} \quad (\text{IV-17})$$

With T the temperature in K, η_B the viscosity of the solution (here Acetophenone) in $\text{mPa}\cdot\text{s}$ ⁴ and V_A the molecular volume (here of Benzyl alcohol) in cm^3 as defined by Wilke.⁵ Where η_B Acetophenone = 1.681 $\text{mPa}\cdot\text{s}$ and V_A Benzyl alcohol = 121 cm^3 . Internal Effectiveness Factors being close to 1, internal mass-transfers do not limit the reactivity.

T (K)	D_{AB} (cm^2/s)	D_e (cm^2/s)	$k_{\text{CH-Ar}}$ ($\text{cm}^3/\text{g}\cdot\text{s}$)	$k_{\text{OH-O}}$ ($\text{cm}^3/\text{g}\cdot\text{s}$)	$\phi_{\text{CH-Ar}}$	$\phi_{\text{OH-O}}$	$\eta_{\text{CH-Ar}}$	$\eta_{\text{OH-O}}$
468	1.42E-05	3.55E-06	3.575E-06	5.99E-05	1.96E-02	8.03E-02	>0.9999	0.9996
478	1.45E-05	3.62E-06	5.71E-06	8.10E-05	2.45E-02	9.25E-02	>0.9999	0.9994
483	1.46E-05	3.66E-06	6.21E-06	9.44E-05	2.55E-02	9.93E-02	>0.9999	0.9993

Table IV-18 - Calculations of the internal effectiveness factor.

- (1) Carbon, Activated - Materials Handled - Flexicon Corporation. <https://www.flexicon.com/Materials-Handled/Carbon-Activated.html> (accessed 2023-01-17).
- (2) Gomes, H. T.; Serp, Ph.; Kalck, Ph.; Figueiredo, J. L.; Faria, J. L. Carbon Supported Platinum Catalysts for Catalytic Wet Air Oxidation of Refractory Carboxylic Acids. *Top Catal* **2005**, *33* (1–4), 59–68. <https://doi.org/10.1007/s11244-005-2505-5>.
- (3) Pico, M. P.; Romero, A.; Rodríguez, S.; Santos, A. Etherification of Glycerol by Tert-Butyl Alcohol: Kinetic Model. *Ind. Eng. Chem. Res.* **2012**, *51* (28), 9500–9509. <https://doi.org/10.1021/ie300481d>.
- (4) Saravanakumar, K.; Baskaran, R.; Kubendran, T. R. Densities, Viscosities, Refractive Indices and Sound Speeds of Acetophenone with Methylacetate at Different Temperatures. *Journal of Chemistry NaN/NaN/NaN*, *9*, 1711–1720. <https://doi.org/10.1155/2012/237068>.
- (5) Hayduk, W.; Laudie, H. Prediction of Diffusion Coefficients for Nonelectrolytes in Dilute Aqueous Solutions. *AIChE Journal* **1974**, *20* (3), 611–615. <https://doi.org/10.1002/aic.690200329>.

Chapter 1: Evaluation of new LOHC structures

Appendix IV-9 - Extended DFT mechanism

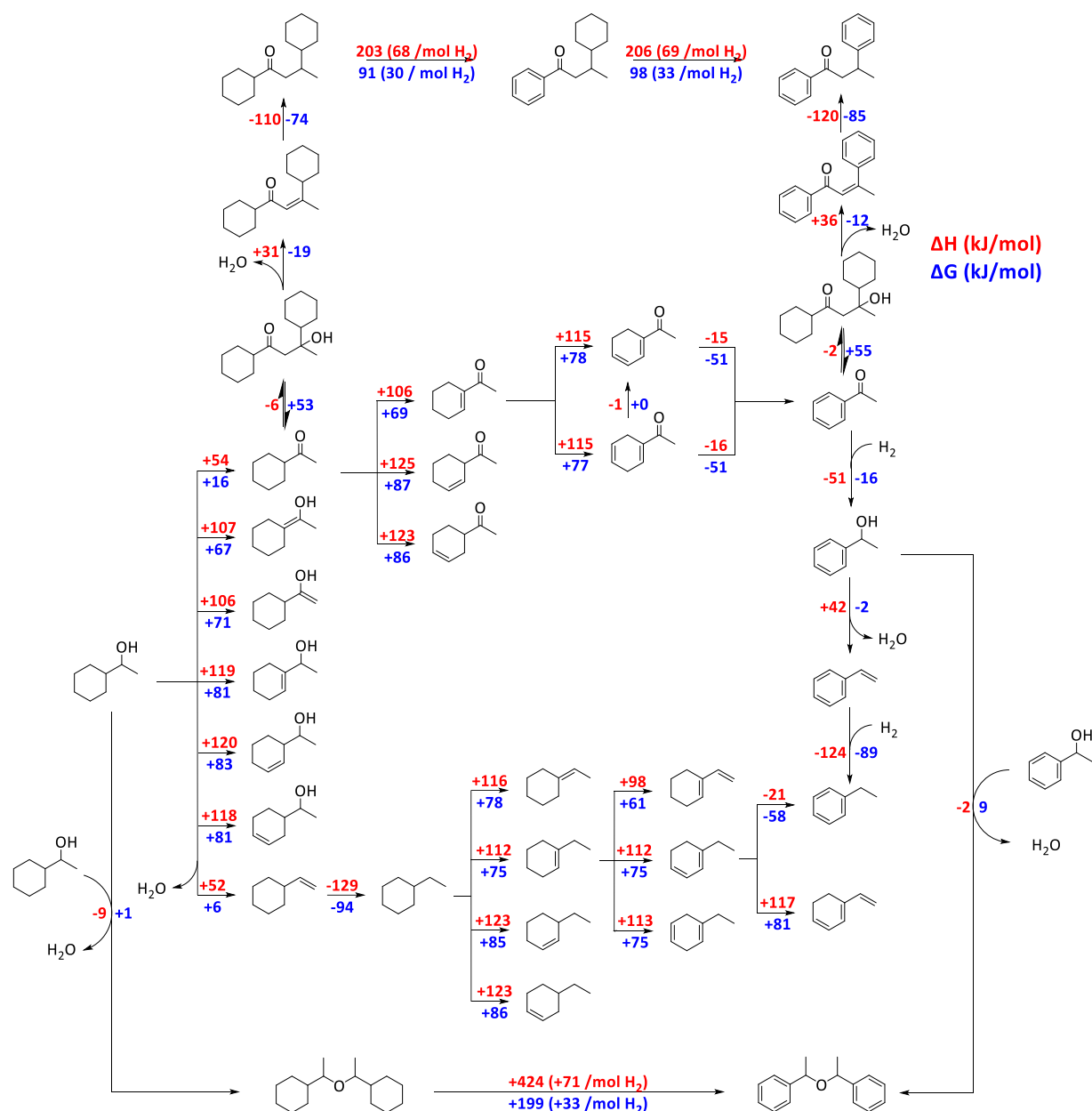


Figure IV-41 – Extended DFT mechanism of the dehydrogenation of CHEA to APO and the associated degradation pathways.

Oligomers formed by Styrene and Vinylcyclohexane units were not calculated by DFT, but their formation could potentially occur at the reaction temperature (see Chapter 2).

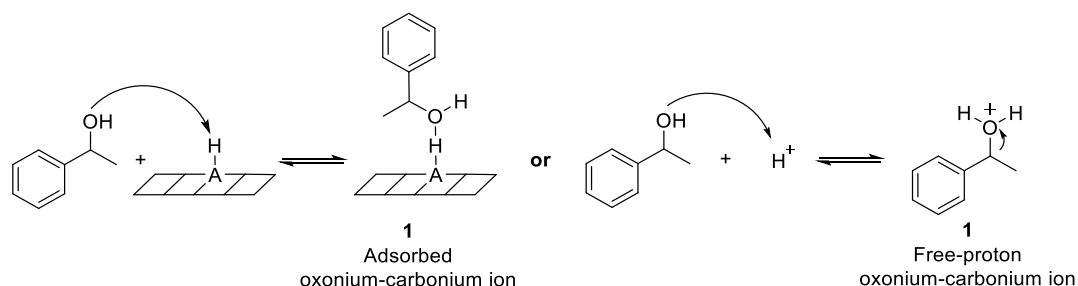
Table of Contents “Chapter 2: Degradation study and limitation”

V. Chapter 2: Degradation study and limitation	188
V.1 Degradation mechanisms.....	188
V.2 LOHC stability assessment in the reaction conditions	191
V.3 Degradation limitation by modification of the catalyst support.....	192
V.3.1 Hydrogenation.....	192
V.3.2 Dehydrogenation.....	193
V.4 Degradation limitation by additives	196
V.4.1 Hydrogenation.....	196
V.4.2 Dehydrogenation.....	197
V.5 Study of the Dicyclohexylmethanol/Benzophenone (DCMA/BPO) LOHC couple.....	203
V.5.1 Hydrogenation.....	204
V.5.2 Dehydrogenation.....	205
V.5.3 Cycling.....	206
V.6 Conclusion	208
Bibliography.....	209
Appendix.....	211
Appendix V-1 - Direct basification of the support.....	211
Appendix V-2 - XRD analysis of the 2 wt% Pt/Al ₂ O ₃ catalysts	211
Appendix V-3 - XRD basification/acidification of the hydrogenation Ru/Al ₂ O ₃ catalyst	212
Appendix V-4 - XRD basification/acidification of the dehydrogenation Pt/C catalyst	212
Appendix V-5 - NaOH quantity effect on the Pt/C dehydrogenation catalyst by XRD analysis ..	213
Appendix V-6 - Characterizations of the purified Dicyclohexylmethanol	213
Appendix V-7 - Intermediates and degradation during the dehydrogenation of DCMA to BPO	216
Appendix V-8 - DFT BPO: Dehydrogenation via stable intermediates	217

V. Chapter 2: Degradation study and limitation

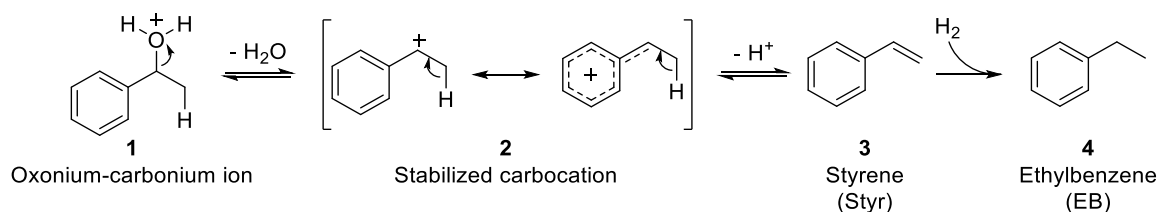
V.1 Degradation mechanisms

As a high cycling capacity is key for a LOHC couple and the main mechanism for its decrease is the degradation, the understanding of these degradation pathways is then a prerequisite to reduce their prominence and design efficient alternatives. In the previous chapter, by-products were formed during the hydrogenation and dehydrogenation and were classified by their degradation mechanism. Intramolecular and intermolecular dehydration of alcohols have been known to occur by adsorption on protonated acidic Bronsted surfaces A and by alcohol protonation in acidic medium, forming an adsorbed or free-proton oxonium-carbonium ion **1** respectively.¹ The 1-Phenylethanol (PEO) was used as a model substrate for the following examples (Scheme V-1).

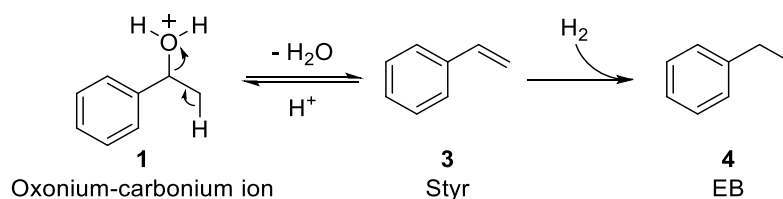


Scheme V-1 - Formation of the reactive species initiating the dehydration mechanisms. Left: adsorption of PEO on a protonated acidic Bronsted surface. Right: Direct protonation of PEO in an acidic medium.

To simplify the following reaction schemes, free-proton oxonium-carbonium-type structures will be presented for the intramolecular dehydration. The reaction pathways between intramolecular dehydration and intermolecular branch after this point. In strongly polarized H bonds, charge transfer might occur from the oxygen center to the adjacent carbon center of PEO. Further elimination of a β -proton form Styrene (Styr) **3** that can be hydrogenated to the corresponding Ethylbenzene (EB) **4**. Here, depending on the stabilization of the carbocation **2** (mesomerism, inductive donation), a two-step E1 (Scheme V-2) or E2 (Scheme V-3) mechanism can occur.



*Scheme V-2 - E1-type intramolecular dehydration mechanism of PEO to form **3** and **4**.*

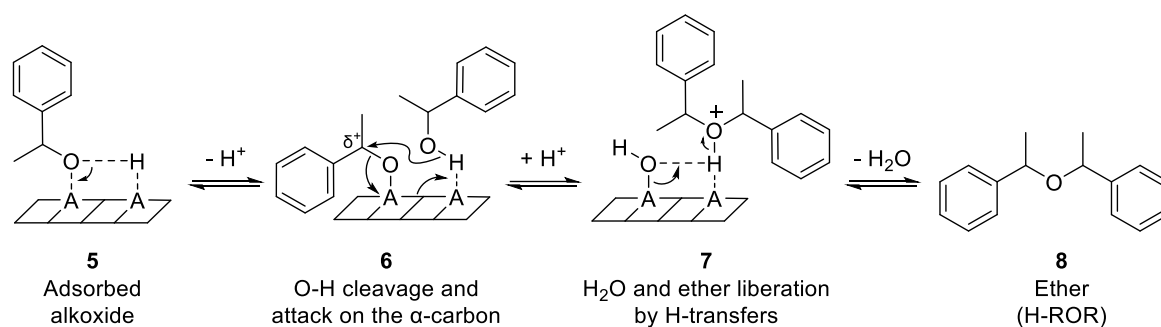


*Scheme V-3 - E2-type intramolecular dehydration mechanism of PEO to form **3** and **4**.*

Chapter 2: Degradation study and limitation

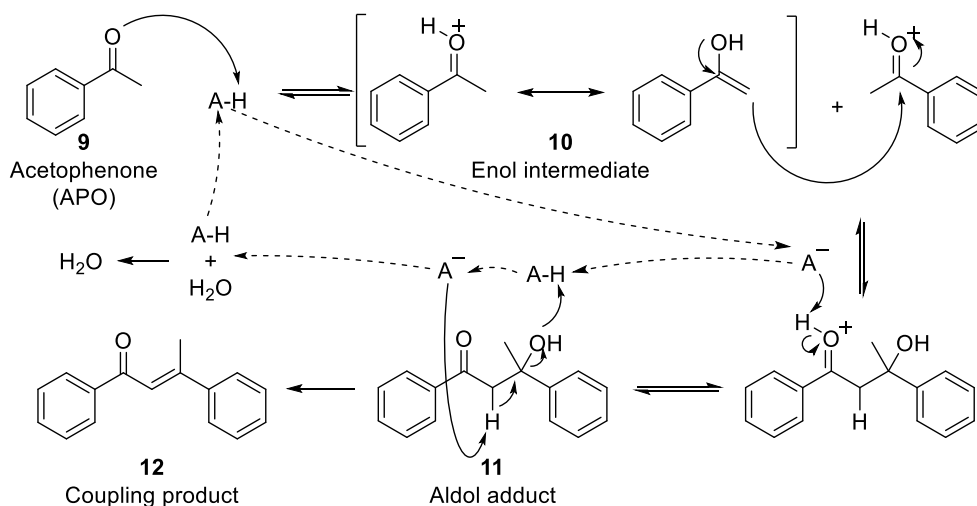
Isotopic kinetics experiments showed that the β -proton elimination of primary, secondary and tertiary alcohols was the rate-determining step on γ - Al_2O_3 below 200 °C, leading to a concerted E2-type mechanism where both C-O and C-H bond are broken following an anti-configuration.²

Ether formation as intermolecular couplings is more complicated as it requires the formation of an alkoxide species **5** on an incompletely protonated acidic surface. Then, a second PEO equivalent proceeds to a nucleophilic attack by its O-moiety on the α -carbon of the alkoxide **6**. Finally, successive H-transfers **7** allow for the formation and liberation of one equivalent of water and the corresponding ether (H-ROR) **8** (Scheme V-4).



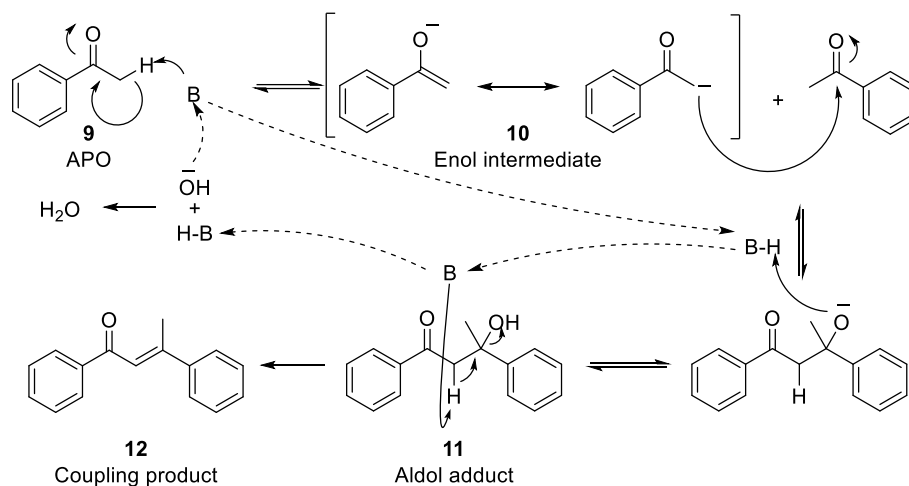
*Scheme V-4 - Intermolecular dehydration mechanism of PEO to form the ether **8** H-ROR.*

The coupling products form through an aldolisation-crotonisation pathway. First, an enol intermediate **10** is formed, enabling the formation of an aldol adduct **11** after a cascade of reversible steps. Irreversible intramolecular dehydration pushes the equilibrium to yield an α, β -unsaturated ketone **12** that can be further hydrogenated to form the 1,3-Diphenylbutanone **13** (OH-Coupling). In addition, this reaction can be catalyzed by both acidic (Scheme V-5) and basic (Scheme V-6) conditions.³ Acetophenone **9** (APO) and its hydrogenated counterpart Acetylcyclohexane (ACH) were used as model substrates for the following examples.



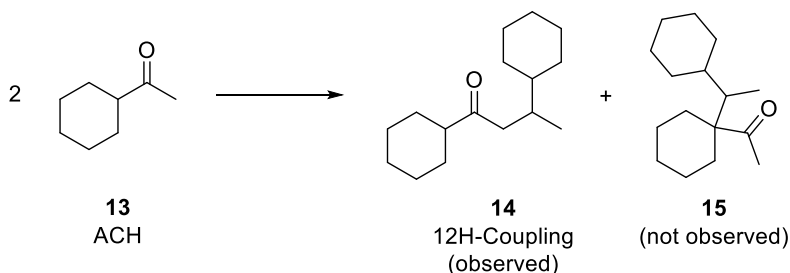
*Scheme V-5 - Aldolisation-crotonisation mechanism of APO in acidic conditions (A) to form the coupling product **12** and its hydrogenated version 1,3-Diphenylbutanone **13** (OH-Coupling).*

Chapter 2: Degradation study and limitation



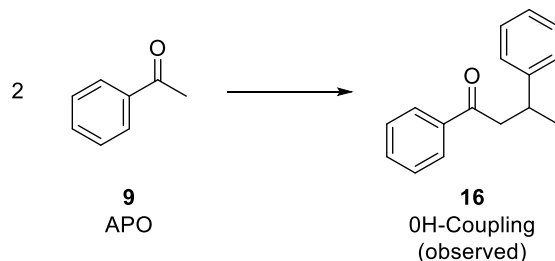
*Scheme V-6 - Aldolisation-crotonisation mechanism of APO in basic conditions (B) to form the coupling product **12** and its hydrogenated version 1,3-Diphenylbutanone **13** (OH-Coupling).*

As this reaction is favored by the keto-enol conversion and limited by the steric hindrance of the β -carbon, only the Me-aldolisation product presented as the 12H-Coupling **14** in the previous chapter was observed for the condensation of ACH **13** (Scheme V-7). The structure **15** produced by the aldolisation-crotonisation on the Cyclohexyl group was never observed experimentally. DFT calculations revealed an energy difference of +43 kJ/mol between **14** and **15**, rationalizing the absence of **15** in the reaction mixture.



*Scheme V-7 – Aldolisation-crotonisation products **14** (observed) and **15** (not observed) obtained by the reaction of 2 equivalents of ACH **13**.*

In the case of APO, the condensation can only occur on the methyl group, hence the apparition of the product (3) (Scheme V-8)

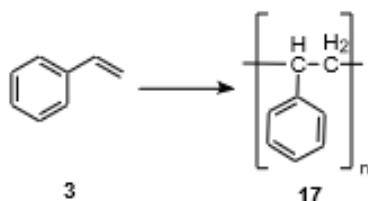


*Scheme V-8 - Aldolisation-crotonisation product OH-Coupling **16** obtained by the reaction of 2 equivalents of APO **9**.*

High molecular weight structures akin to Polystyrene **17** can also form by polymerization of the vinyl intermediate **3** and its hydrogenated counterpart (Scheme V-9). The polymerization occurs between

Chapter 2: Degradation study and limitation

95 and 120 °C in presence of radical species.⁴ Strong cationic or anionic species such as lithium alkyls can also catalyze the polymerization at room temperature or lower.^{5,6}



Scheme V-9 – Polymerization of the vinyl intermediate 3 into Polystyrene structures 17.

In this chapter, the experiments related to the rationalization of the formation of these impurities as well as the improvement of the hydrogenation and dehydrogenation reactions will be presented.

V.2 LOHC stability assessment in the reaction conditions

First of all, the stability of CHEA and APO was tested in different conditions to monitor the formation of various impurities and the results were reported in the Table V-1.

Reaction conditions	Dehydration products	Coupling products
CHEA, Al ₂ O ₃ (1 wt.%), 205 °C, 18 h, H ₂ flux	No	No
APO, Pt/Al ₂ O ₃ (1 wt.%), 205 °C, 4 h, Ar flux	No	No
APO, Pt/Al ₂ O ₃ (1 wt.%), 205 °C, 4 h, H ₂ flux	3, 4, 8	16
APO, Pt/C (0.25 wt.%), 205 °C, 24 h, Ar flux	No	16

Table V-1 – Stability of CHEA and APO and mechanism of formation of impurities.

No degradation of CHEA was observed in presence of Al₂O₃ and a H₂ flux over 18 h at 205 °C, indicating thermal stability for our reaction time, although long-term thermal stability is not assured. APO was also stable in presence of Pt/Al₂O₃ for 4 h at 205 °C under Ar flux. Nevertheless, replacement of Ar by H₂ in the same conditions promoted the formation of both intermolecular and intramolecular dehydration **3**, **4** and **8** as well as coupling product **16**. Here, it seemed that the presence of H₂ at the surface of the catalyst was sufficient to initiate the degradation pathway of all impurities. Another stability experiment of APO with the Pt/C catalyst under Ar flux during 24 h at 205 °C revealed that the aldolisation-crotonisation reaction might also proceed in H₂-free environments to form **16**. Indeed, the reaction could happen either due to acidic or basic sites on the support or through a metal-enol adduct, but as Pt was not reported as a metallic center enhancing the aldolisation reaction, this reaction pathway is less plausible.³ Most importantly, these experiments have revealed that the presence of H₂ is detrimental to the system stability. Nonetheless, as it is impossible to achieve H₂-free conditions during the hydrogenation and dehydrogenation, degradation limitation can only happen through the modification of the catalyst, the reaction conditions or by modification of the LOHC structure. No Polystyrene derivative was observed by GC-MS. Each aspect will be developed in the next parts of this chapter.

V.3 Degradation limitation by modification of the catalyst support

As unwanted dehydration and condensation reactions are catalyzed by acidic or basic conditions, the effect of the acidity or basicity of the support on the reaction selectivity was investigated in both hydrogenation and dehydrogenation.

V.3.1 Hydrogenation

As dehydration is promoted by acidic sites on the support, neutralization of said sites should increase the selectivity of the hydrogenation. The modification of the support was tested by direct basification of the support (Appendix V-1) and by synthesizing by wet-impregnation with a RuCl_3 solution a series of 3 wt.% Ru catalysts supported on metal oxides and hydrotalcites catalysts. The hydrogenation of APO to CHEA was conducted in the previously developed conditions and is presented in Figure V-1.

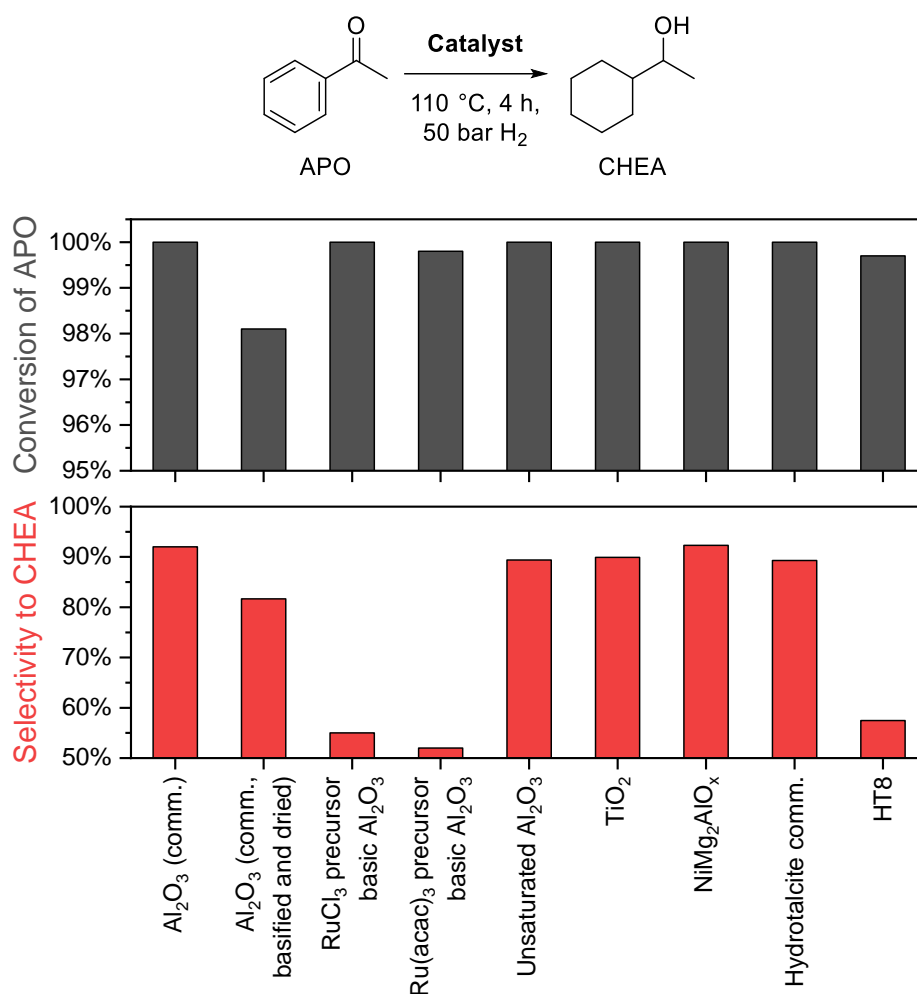


Figure V-1 – Effect of the support on the conversion and selectivity of the hydrogenation of APO to CHEA. APO (15 mL), Ru heterogeneous catalyst (0.1 wt.% Ru with regard to APO), 110 °C, 4 h, 50 bar H_2 . Hydrotalcite comm.: $\text{CH}_{16}\text{Al}_2\text{Mg}_6\text{O}_{19}$, 4 H_2O . HT8: ZnAlMg-based hydrotalcite.

The commercial $\text{Ru}/\text{Al}_2\text{O}_3$ catalyst immersed in a 0.01 M NaOH solution for 24 h had a reduced catalytic activity. Here, the potential formation of an oxide phase on the surface can modify the chemisorption properties of the active metal nanoparticles, inducing reactivity changes.^{7,8} However, XRD analysis could not conclude on the presence of an oxidized phase, possibly due to its being amorphous (Appendix V-2). Further experimental work with techniques such as Raman spectroscopy or XPS could prove the presence of such species.

Chapter 2: Degradation study and limitation

Following the assumption that the neutralization of acidic sites should limit the dehydration⁹, basic alumina was used. However, for two different Ru precursors (RuCl_3 and $\text{Ru}(\text{acac})_3$), this assumption was found untrue. On the contrary, unsaturated Al_2O_3 (i.e. acidic alumina) showed a much better performance. TiO_2 , also known to possess numerous acidic sites, showed a comparatively high selectivity.¹⁰ Here, the classic considerations seem to be reversed. Hydrotalcites supports promoted high conversions, but different selectivities were obtained based on their composition. $\text{NiMg}_2\text{AlO}_x$ was particularly efficient with comparable conversion and selectivity to the commercial $\text{Ru}/\text{Al}_2\text{O}_3$ catalyst. Nevertheless, dehydration was always observed. More analytical work like temperature program desorption experiments should be conducted to rationalize this behavior and correlate the formation of each side-product to the surface sites. Unfortunately, this equipment was not available and attempts to mimick NH_3 and CO_2 adsorption/desorption with a TGA-MS apparatus yielded no results, hence no more work was pursued in that direction and the commercial $\text{Ru}/\text{Al}_2\text{O}_3$ catalyst was used for the rest of the experiments.

V.3.2 Dehydrogenation

Three commercially available alumina with various acidity and basicity were used to synthesize 2 wt.% $\text{Pt}/\text{Al}_2\text{O}_3$ catalysts by wet-impregnation. The catalysts were analyzed by XRD to confirm the presence of native Pt on the surface of the alumina (Appendix V-3). The CHEA dehydrogenation was performed for each catalyst to assess the effect of the acidity/basicity of the support on the composition of the impurities in the reaction mixture (Figure V-2).

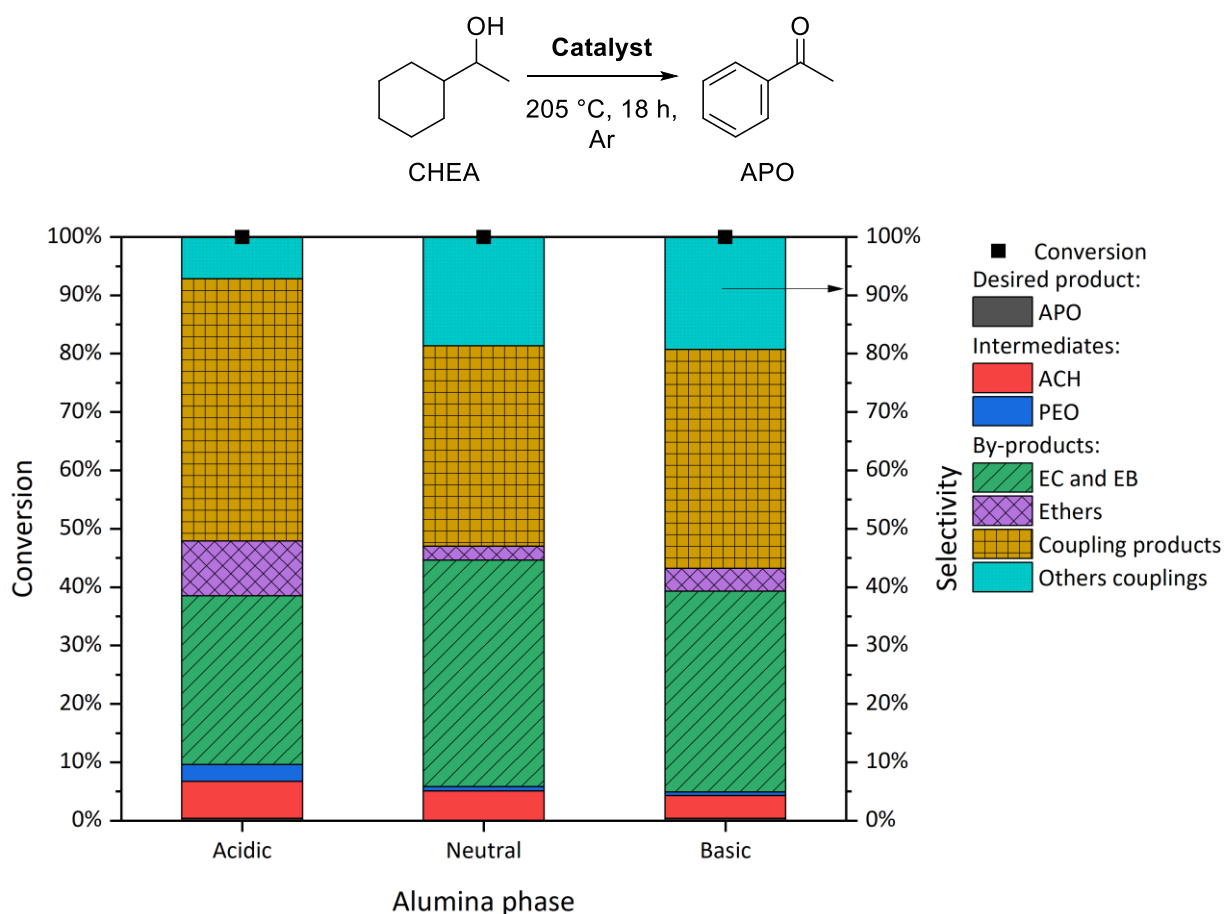


Figure V-2 - Composition of the crude reaction mixture post reaction with 2 wt.% $\text{Pt}/\text{Al}_2\text{O}_3$ catalysts on various alumina phases. CHEA (1.5 mL), 2% $\text{Pt}/\text{Al}_2\text{O}_3$ (1 wt.% Pt with regard to CHEA), 205 °C, 18 h, Ar.

Chapter 2: Degradation study and limitation

Dehydration was visible for all alumina supports and such observation is supported by mechanistic studies in the literature. The dehydration was linked to a combination of both acidic and basic sites acting in a concerted mechanism at sub-microscopic pores, crevices or channels of the alumina.¹¹ Dehydration products were more present in the neutral alumina species (i.e. alumina containing both acidic and basic sites), confirming the results of the literature. The increased formation of ethers for the acidic alumina was also in agreement with the literature. Even in a purely basic alumina support, presence of species with labile protons such as water or the hydrogenated LOHC could be adsorbed on the surface and promote dehydration.¹² In conclusion, no correlation between the support acidity/basicity and the composition of the impurities was found and dehydration of the LOHC could not be prevented by changing the substrate to basic alumina.

In addition, the dehydrogenation of the cycle is much slower than the dehydrogenation of the alcohol to ketone. In order to improve the dehydrogenation kinetics, different metal oxides, nitrides and carbon supports were bought and the corresponding Pt catalysts were synthesized by wet-impregnation. Their effect on the dehydrogenation of the intermediate ACH to APO at equivalent Pt loadings and for the same reaction time was compared with commercial Pt/Al₂O₃ and Pt/C catalysts (Figure V-3).

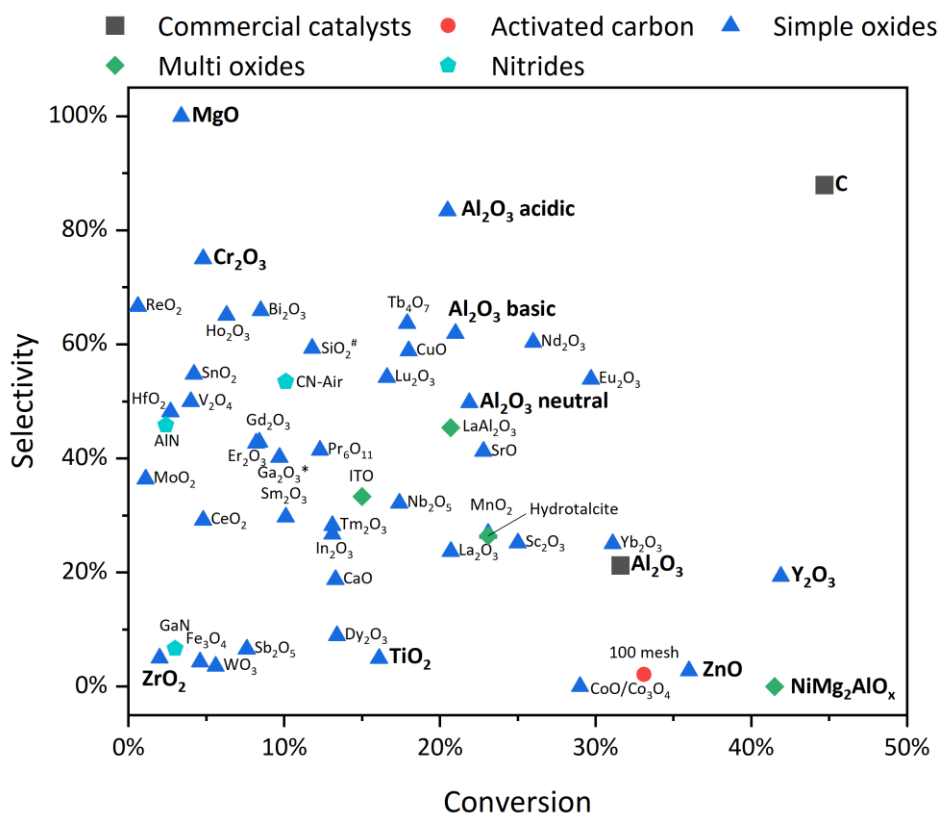
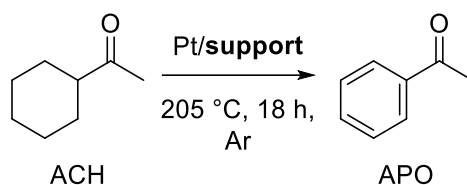


Figure V-3 - Dehydrogenation of the ACH at equivalent Pt loadings and compared with commercial Pt/Al₂O₃ and Pt/C catalysts. ACH (1 mL), Pt/X (1 wt.% with regard to ACH), 205 °C, 18 h, Ar. *: 72 h. #: 0.5 wt.% Pt loading.

Chapter 2: Degradation study and limitation

MgO was highly selective to APO, but showed only little conversion (3%). Nonetheless, it is possible that the low conversion is not sufficient to reliably estimate the selectivity. On the contrary, Y_2O_3 and hydrotalcite-type $NiMg_2AlO_x$ converted ACH in the same proportions than Pt/C, but the selectivity was shifted to the coupling products. Discussion on the selectivity is complex as reported acidic (e.g. Cr_2O_3 or TiO_2) and basic (MgO, ZnO or ZrO_2) supports have drastically different performances. The relative strength of the acidic or basic sites could be at play here, but more analytical work would be needed to rationalize these effects. Other parameters could also play a significant role such as the specific surface, defaults or reducibility of the supports as well as the NPs shape, size and agglomerates of active Pt.

The comparison of the commercial and synthesized catalysts supported on the same material is complicated for the same reason. For example, all synthesized Pt/ Al_2O_3 catalysts were more selective than the commercial Pt/ Al_2O_3 catalyst. Here, it is possible that the commercial catalyst possesses stronger acidic or basic sites that enable the formation of by-products compared to the synthesized catalysts whose support surface was buffered.¹³ The pH ranges in water for the acidic, neutral and basic alumina were 4-5, 6.5-7.5 and 9-10 respectively. However, no information is available by the supplier about the buffering method and adsorbed cations might modify the reactivity of these catalysts (see V.4.2).¹⁴ Similarly, only limited information is available on the commercial Pt/ Al_2O_3 catalyst (Color, form, %Pt and water mass on drying). Finally, the preparation method of the catalyst was not reported for the commercial catalyst, which complicates the comparison with our results.

Conversely, the synthesized Pt/C was less active and selective than its commercial counterpart. Here, we can assume that the quality of the carbon material in combination with the preparation method could introduce acidic defects such as Cl insertion in the matrix.¹⁵ Moreover, H_2PtCl_6 is an acidic compound that might modify surface oxygenated functions, thus the dehydrogenation selectivity. We can then suppose that the superior performance of the Pt/C catalyst originates from either its specific carbon support or the preparation method.

Therefore, as no synthesized catalyst was more active than the commercial Pt/C catalyst and the required characterization array was unavailable, no more work was pursued in that direction.

Future experiments should ensure that Pt is not the source of the degradation by using Pt black. In addition, more complete kinetics should be performed to better compare the evolution of the LOHC in function of the catalytic systems.

V.4 Degradation limitation by additives

V.4.1 Hydrogenation

The effect of additives on the hydrogenation was carried out by using 1 mol% acids and bases in the previously optimized conditions. (Figure V-4)

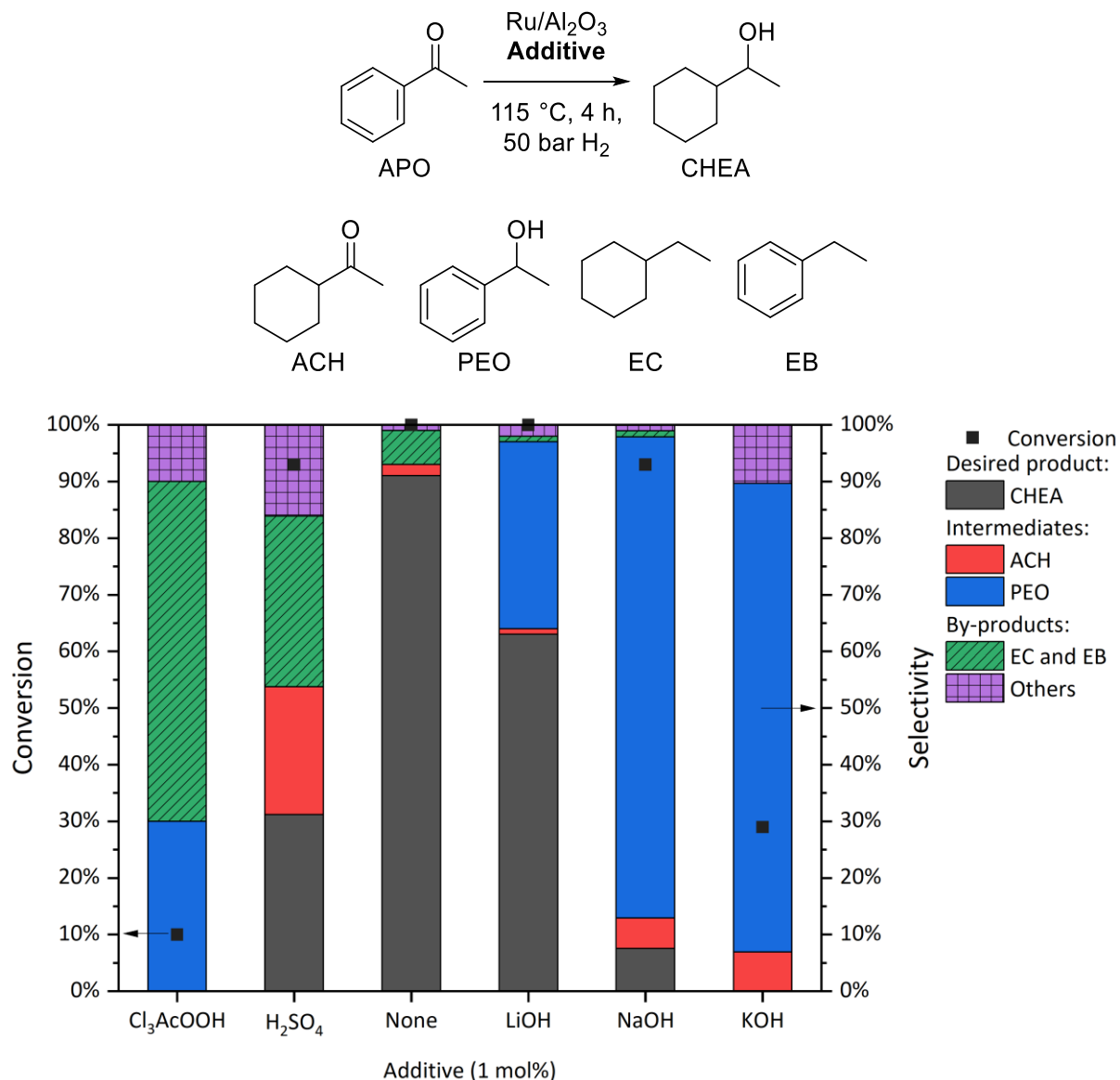


Figure V-4 - Effect of 1 mol% additive on the conversion and selectivity of the hydrogenation of APO to CHEA. APO (15 mL), 5%Pt/Al₂O₃ (0.1 wt.% Ru with regard to APO), acid/base (1 mol% with regard to APO), 115 °C, 4 h, 50 bar H₂.

Hydrogenation in the presence of acidic additives negatively affected both conversion and selectivity as intramolecular dehydration products were formed. These results are in agreement with the literature that shows that increasing the concentration of acidic species further increases the dehydration kinetics.¹⁶ On the contrary, basic additives had an adverse effect on the conversion, but a positive effect on the selectivity: the catalyst produced mainly the intermediate PEO in presence of a base. These effects could be rationalized by the covering and oxidation of the active Ru(0) sites by the basic compounds. Indeed, as the alkalinity is positively linked to the radius of the cation, larger hydroxides might more readily oxidize the Ru nanoparticles (NP).¹⁷ However, XRD measurements did

Chapter 2: Degradation study and limitation

not show any modification of the surface and more advanced characterization techniques able to measure amorphous oxide layers like Raman spectroscopy or XPS would be required to understand the exact role of the basic additives on the catalyst (Appendix V-4). Conversely, the neutralization of the acidic surface sites promoting the dehydration was beneficial on the selectivity. These findings were coherent with previous reports on Ru/C stating that ring hydrogenation in solution was slightly hindered by basic additives while the relative ketone hydrogenation rate was unchanged. Moreover, acidic additives almost completely stopped the reaction.¹⁸ From these results, no further experiments were pursued in that direction due to the pristine catalyst being more active and selective than any tested additive.

V.4.2 Dehydrogenation

Here, the Pt/Al₂O₃ catalyst was used in combination with 1 mol% of different Brønsted additives to carry out the dehydrogenation of CHEA to APO in 4 h (Figure V-5).

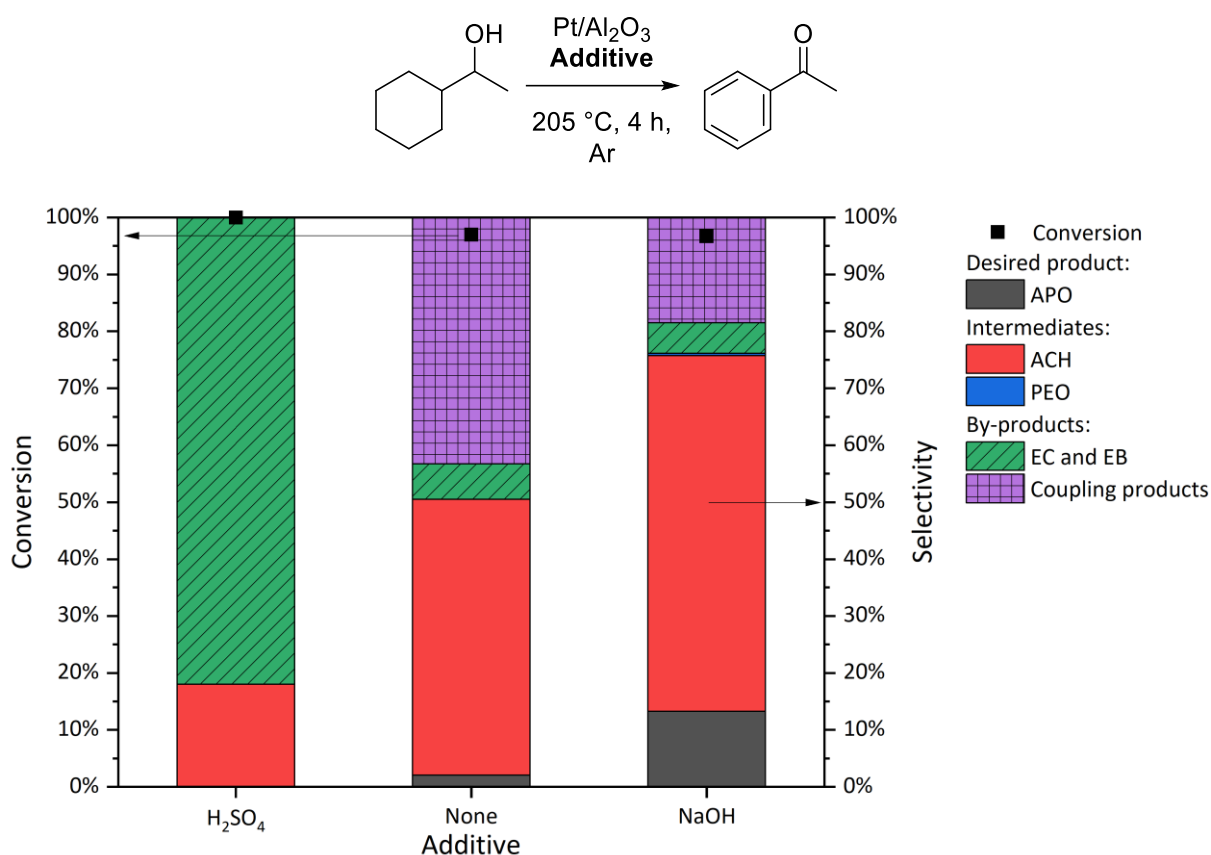


Figure V-5 - Effect of an acid or a base on the conversion and selectivity of the dehydrogenation of CHEA to APO. CHEA (5 mL), 5%Pt/Al₂O₃ (1 wt.% with regard to CHEA), additive (1 mol% with regard to CHEA) 205 °C, 4 h, Ar.

With H₂SO₄ as an additive, complete conversion was obtained with more 82% selectivity to the intramolecular dehydration products and ACH was the minor product. Here, the undesirable catalytic effect of the acidic additives on the dehydration was clear. On the contrary, the addition of NaOH had a negligible effect on the conversion (<0.3%) compared to the pristine catalyst, but increased the selectivity to APO from 2% to 13%. Moreover, the fraction of key-intermediates and APO in the reaction mixture was increased from 52% to 76%. Here, the addition of a base favored the formation of the desired product by inhibiting the acidic sites enabling side-reactions.

Chapter 2: Degradation study and limitation

As the dehydrogenation of CHEA to ACH produced mainly ACH, experiments on the dehydrogenation of ACH to APO were carried out in the presence of the same additives during 18 h to simulate their effect at higher conversion levels (Figure V-6).

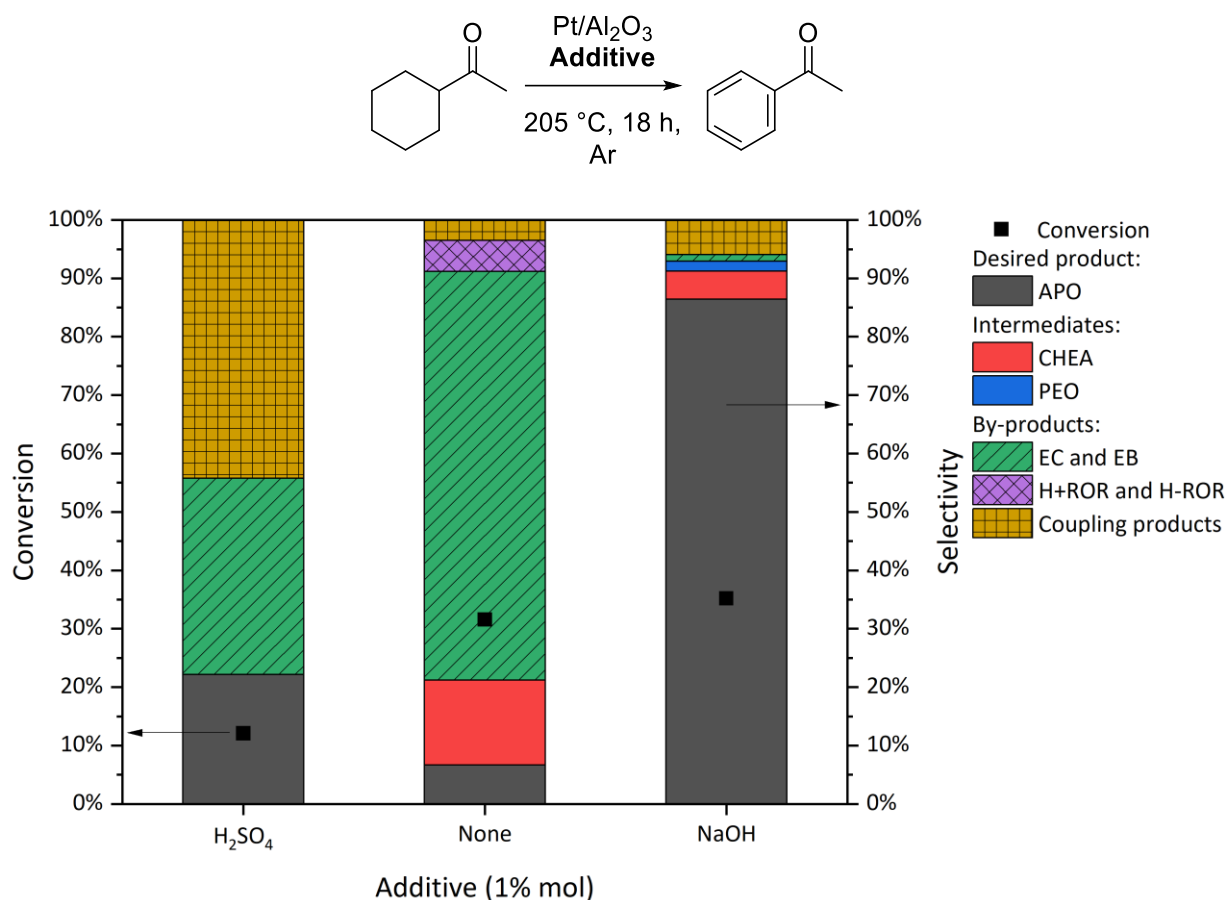


Figure V-6 - Effect of an acid or a base on the conversion and selectivity of the dehydrogenation of ACH to APO. ACH (5 mL), 5%Pt/Al₂O₃ (1 wt.% Pt with regard to ACH), 205 °C, 18 h, Ar.

Contrarily to the dehydrogenation of CHEA, ACH dehydrogenation in presence of H₂SO₄ was detrimental to the conversion and the selectivity was shifted from the intramolecular dehydration products to the coupling products compared to the pristine Pt/Al₂O₃ catalyst. As the aldolisation-crotonisation reaction can be catalyzed by acidic conditions, this selectivity shift was not surprising.³ On the contrary, addition of NaOH yielded a slightly better conversion than the pristine catalyst and an 86% selectivity to APO. Slightly more coupling products were also formed in presence of NaOH compared to the pristine catalyst (6% versus 3% respectively), which was expected due to the aldolisation-crotonisation being also catalyzed by basic conditions.³

As the addition of a hydroxide base yielded a beneficial effect for the dehydrogenation of ACH to APO, different alkaline, alkaline-earth and transition metal hydroxides were used in preliminary dehydrogenation of ACH over 4 h (Figure V-7). Moreover, weaker bases such as Na₂CO₃ (pH=10.3), Na₂HPO₄ (pH=7.2) and Na₂S₂O₃ (pH=11.3) were tested to see the effect of the 1 mol% Bronsted base strength on the conversion and selectivity of the dehydrogenation.

Chapter 2: Degradation study and limitation

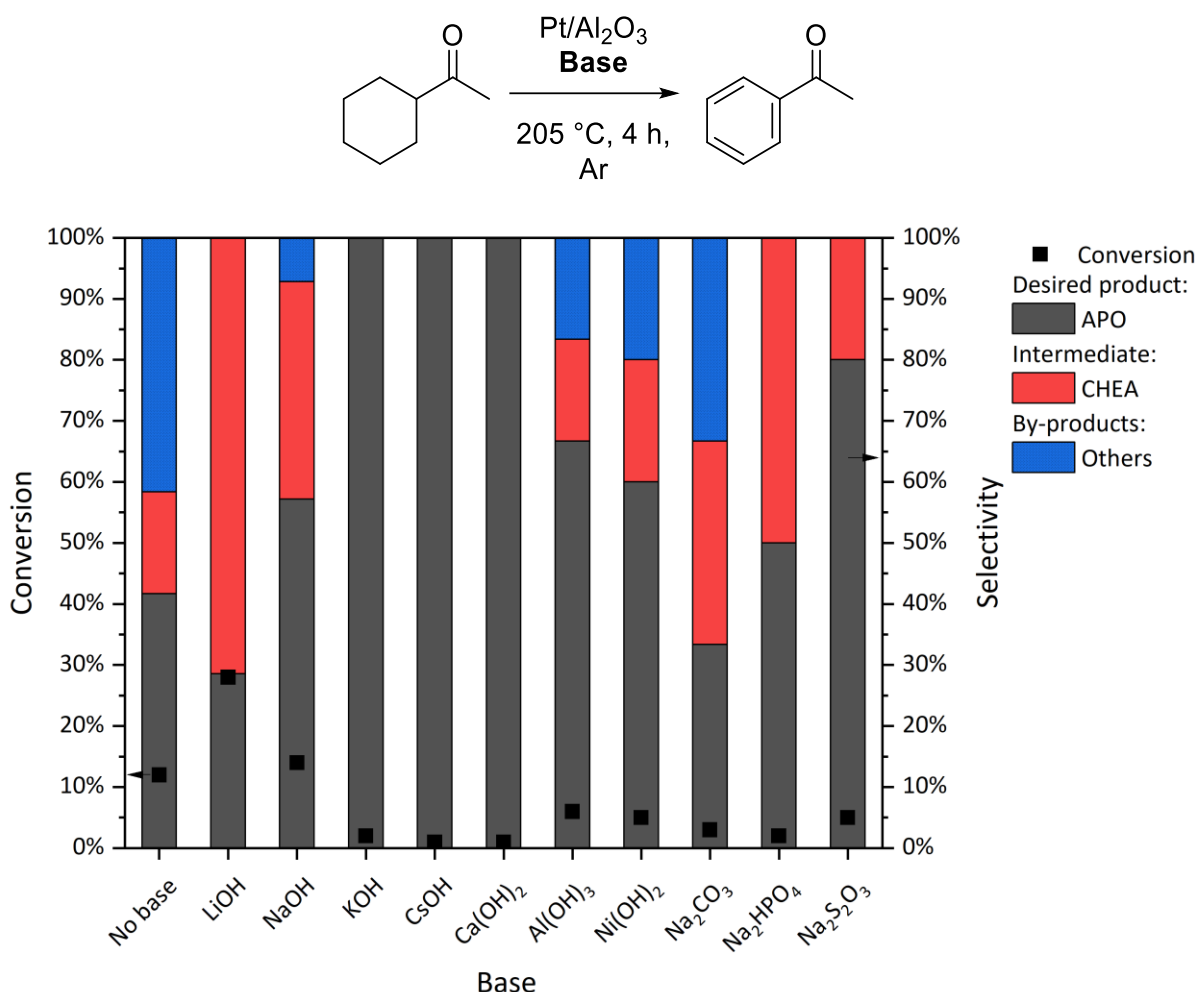


Figure V-7 –Effect of the base on the dehydrogenation of ACH to APO. ACH (5 mL), 5%Pt/Al₂O₃ (1 wt.% Pt with regard to ACH), base (1 mol% with regard to ACH), 205 °C, 4 h, Ar.

LiOH and NaOH showed an increased conversion of 28% and 14% respectively compared to the pristine catalyst (12%). All other bases had a lower conversion than the pristine catalyst. Perfect selectivity was obtained for KOH, CsOH and Ca(OH)₂, although their conversion was inferior to 2%. LiOH produced only CHEA as a by-product while NaOH produced less than 10% of by-products in the form of aldolisation-cron-tonisation products. Out of the weak bases, Na₂S₂O₃ had similar conversion to that of Ni(OH)₂ with a higher selectivity and no formation of by-products. Such result could come from the ability of Na₂S₂O₃ to neutralize free radicals.¹⁹ However, in presence of protons, the S₂O₃²⁻ ion could dismutate to form pure sulphur which would poison the catalyst.²⁰ Nevertheless, APO did not form with Na₂S₂O₃, thus no further experiments were pursued with this additive. Other weak bases such as Na₂CO₃ and Na₂HPO₄ yielded poor results potentially due to their lower solubility in the reaction mixture.

Chapter 2: Degradation study and limitation

The same dehydrogenation experiments were reproduced with the five most efficient hydroxide additives over 18 h (Figure V-8).

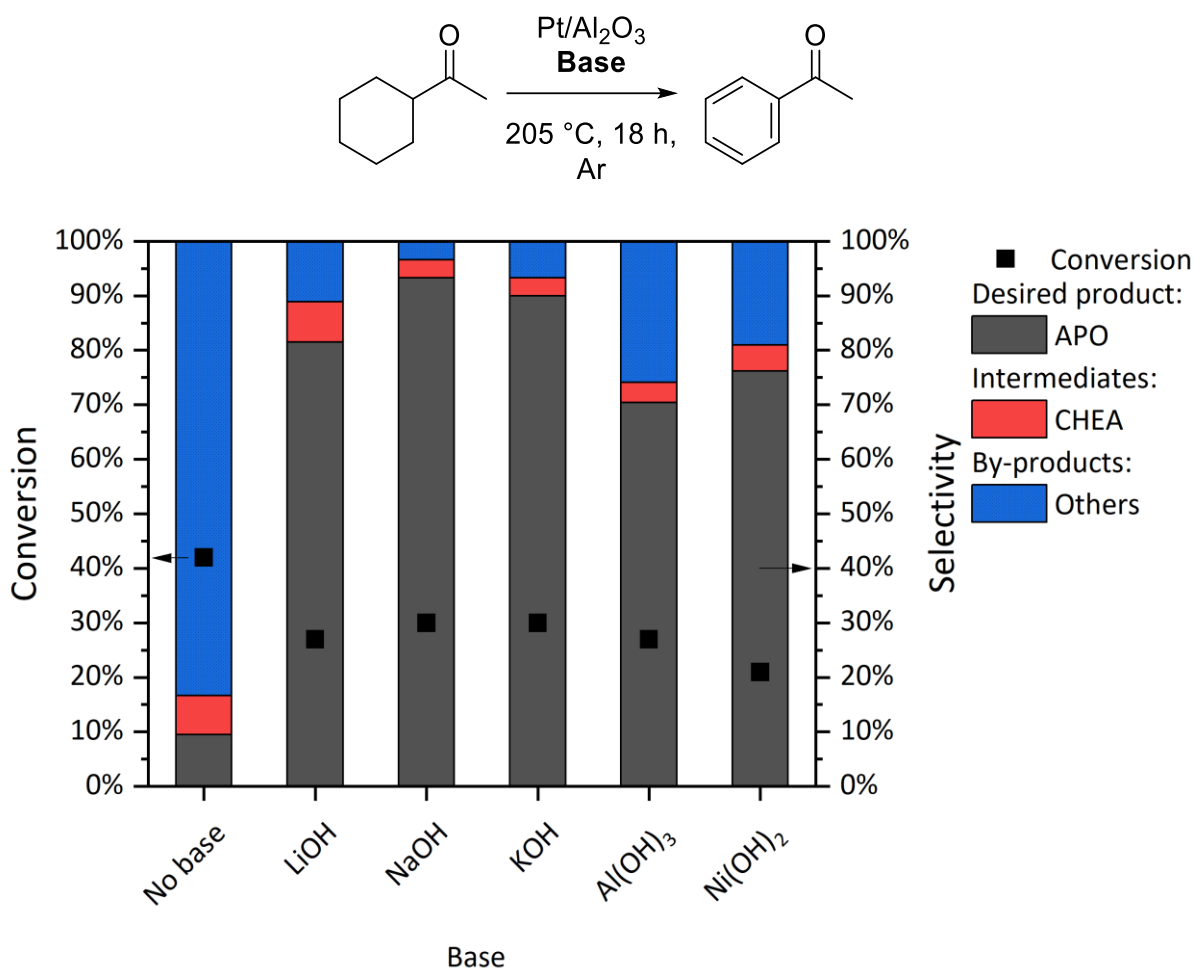
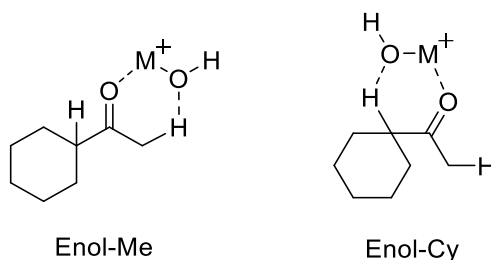


Figure V-8 - Effect of the base on the dehydrogenation of ACH to APO. ACH (5 mL), 5%Pt/Al₂O₃ (1 wt.% with regard to ACH), base (1 mol% with regard to ACH), 205 °C, 18 h, Ar.

NaOH and KOH showed a conversion of 30% but 42% conversion was achieved by the pristine catalyst. All other additives converted ACH in the 20-30% range. The beneficial effect of the base additives was observed on the selectivity to APO in presence of NaOH and KOH that drastically increased from 9.5% for the pristine catalyst to 93% and 90% respectively. This conversion reduction and selectivity change indicated that active sites responsible for the production of by-products were efficiently blocked by the basic additives.

Moreover, as similar conversions were obtained for all additives, DFT modelling was proposed to rationalize the relative fraction coupling products formed depending on the additive. An assessment of the enthalpy change required to abstract the four protons vicinal to the ketone by a base additive was performed. In particular, the four vicinal protons are not equivalent: three are positioned on the methyl group and one on the cyclohexyl group. Here, the reaction enthalpy to produce the enol-metal adduct form was calculated for the abstraction of each group of protons and the results are reported in Table V-2.

Chapter 2: Degradation study and limitation



Base	Enol-Me ΔH (kJ/mol)	Enol-Cy ΔH (kJ/mol)	Enthalpy ratio Me/Cy
LiOH	-49	-52	0.94
NaOH	-34	-44	0.77
KOH	-26	-26	1
Al(OH) ₃	-113	-104	1.09
Ni(OH) ₂	-98	-90	1.09

Table V-2 – Enthalpy of reaction for the formation of the enol-base adduct depending on the position of the abstracted proton and the enthalpy ratio Me/Cy.

Here the size of the base had a relatively strong effect on its capacity to abstract the proton linked on the cycle compared to the protons on the methyl group. Interestingly, the formation of aldolisation-crotonisation products could be correlated to both the exothermicity strength of the Enol-Me abstraction and the ratio of Me vs Cy-H abstraction. In theory, Al(OH)₃ and Ni(OH)₂ favored the enol-Me H-abstraction and the dehydrogenation in presence of these additives produced the most coupling products. KOH had a lower H-abstraction enthalpy than NaOH, but its Me/Cy ratio is higher hence the presence of more coupling products. LiOH has a similar ratio to KOH but its higher H-abstraction enthalpies promoted the formation of more coupling products. Interestingly, NaOH-Cy was the only structure inducing a formal C-H cleavage (Figure V-9). Interatomic distances between the labeled atoms in Figure V-9 were measured and reported in Table V-3.

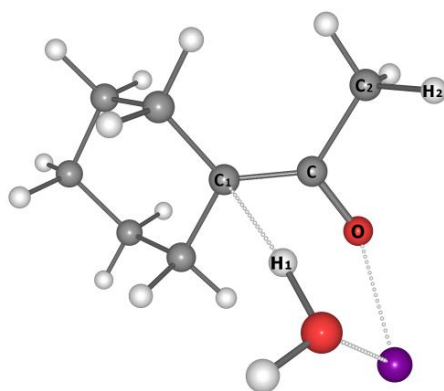


Figure V-9 - Optimized geometry of the Enol-Cy-NaOH structure. H: white, C: grey, O: red, Na: purple.

Base	Enol-Cy			Enol-Me		
	C-O (Å)	C ₁ -H ₁ (Å)	C-C ₁ (Å)	C-O (Å)	C ₂ -H ₂ (Å)	C-C ₂ (Å)
LiOH	1.22	1.09	1.51	1.22	1.09	1.5
NaOH	1.3	2.1	1.37	1.22	1.09	1.5
KOH	1.22	1.1	1.52	1.22	1.09	1.5
Al(OH) ₃	1.24	1.09	1.5	1.24	1.09	1.49
Ni(OH) ₂	1.23	1.09	1.51	1.23	1.09	1.49

Table V-3 - Bond distances of the C-O, C₁-H₁ and C-C₁ for the Enol-Cy structure (resp. C₂-H₂ and C-C₂ for the Enol-Me structure).

Chapter 2: Degradation study and limitation

Indeed, analysis of the Enol-Cy-NaOH structure revealed that the C-O (1.3 Å) and C-C₁ (1.37 Å) bond distances were consistent with an enol (1.33 Å and 1.36 Å in theory respectively). Moreover, the C1-H1 distance was increased to 2.1 Å compared to the classic Csp³-H distance (1.09 Å).²¹ This result indicates that the addition of NaOH could facilitate the dehydrogenation of the saturated cycle. Further experimental work like NMR spectroscopy coupled with mass spectroscopy in a non-fragmenting mode (ESI) would be required to verify that the enol structure does form in the calculated conditions.

From these experimental results and theoretical calculations, NaOH was chosen as the additive and the effect of its concentration on the conversion and selectivity was probed in a series of experiments presented in the Figure V-10.

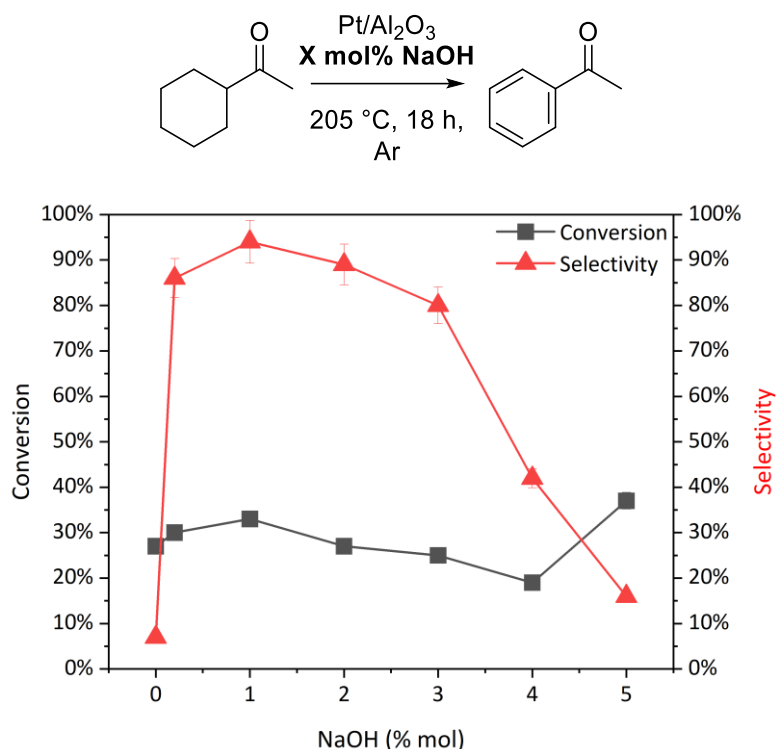


Figure V-10 - Conversion and selectivity for the dehydrogenation of ACH to APO in function of the quantity of NaOH. ACH (5 mL), 5%Pt/Al₂O₃ (1 wt.% with regard to ACH), NaOH (X mol% with regard to ACH), 205 °C, 18 h, Ar.

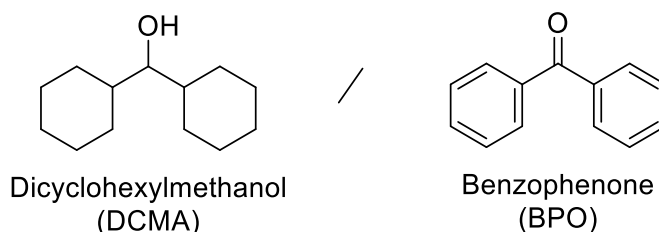
The conversion presented a local maximum at 1 mol% and decreased in a relatively constant fashion when increasing the amount of NaOH, until in solution NaOH could induce aldolisation-crotonisation in the reaction bulk (5 mol%). Conversely, a strong effect was observed on the selectivity when adding NaOH quantities as low as 0.2 mol%. A maximum of 94% selectivity was reached at 1 mol% NaOH. A volcano-shaped plot indicates that at least two competitive mechanisms are taking place. Here, the addition of a small quantity of base can cover the acidic sites of the support, leading to a selectivity improvement while an excessive addition could start to favor the aldolisation-crotonisation products. No variation of the catalyst surface was observed by XRD (Appendix V-5)

These experiments rationalized the formation of both dehydration and coupling products and correlated their apparition to the relative acidity or basicity of the reaction medium. Controlled amounts of additives increased the relative selectivity of the reaction by tuning the catalyst surface but its detrimental effect on the catalytic activity by potential surface oxidation prevented it to be a viable option to achieve high conversion.

Chapter 2: Degradation study and limitation

V.5 Study of the Dicyclohexylmethanol/Benzophenone (DCMA/BPO) LOHC couple

As shown previously, enolisable ketones can undergo an aldolisation-crotonisation pathway in both acidic and basic conditions. In addition, this reaction is favored by the keto-enol conversion and limited by the steric hindrance of the β -carbon. From the previous experiments, aldolisation-crotonisation happened by formation of an enol intermediate on the methyl group and no product from the enol intermediate on cyclohexyl group was observed. Therefore, the methyl group could be considered as a structural weakness of the CHEA/APO LOHC couple and its replacement by a phenyl group should be an efficient strategy to block the aldolisation-crotonisation pathway by steric hindrance. Moreover, the addition of a phenyl group has a beneficial effect on the gravimetric density of the LOHC system at the cost of a higher melting point. While the toxicity of the dehydrogenated form is stronger than the applied filters in the Chapter 1 (GHS08: carcinogenic, mutagenic, reprotoxic, ...), this structure was still used to assess the validity of our hypothesis. The physico-chemical properties of the Dicyclohexylmethanol/Benzophenone (DCMA/BPO) couple are presented in the Table V-4.



Molecule	Melting point (°C)	Boiling point (°C)	Chemical risk	Gravimetric density H ₂ (wt.%H ₂)	Dehydrogenation enthalpy (kJ/mol H ₂)
Dicyclohexylmethanol	63	158 (14 Torr)	OK	7.1%	67
Benzophenone	49	305	GHS08		

Table V-4 - Physico-chemical properties of the Dicyclohexylmethanol/Benzophenone LOHC couple.

Over the course of our experiments, different structures were observed by GC-MS and their classification can be found in the Figure V-11.

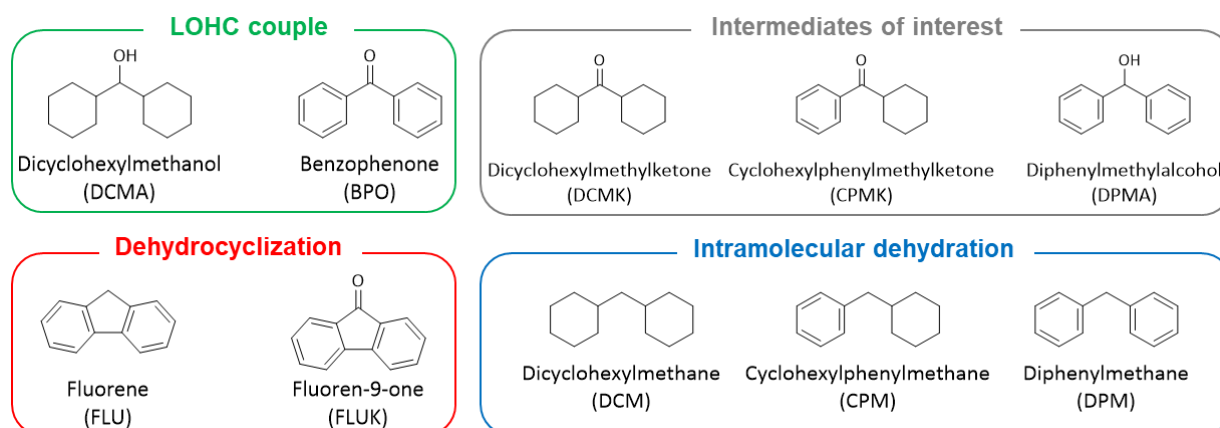


Figure V-11 - Classification of the observed products by GC-MS.

Chapter 2: Degradation study and limitation

V.5.1 Hydrogenation

As Ru/Al₂O₃ was the most efficient catalyst for the hydrogenation of APO to CHEA, the hydrogenation of BPO to DCMA was carried out with 0.066 wt.% Ru/Al₂O₃ in 4 h at different temperatures to observe any reactivity modification as well as to produce the hydrogenated form of the LOHC that was not commercially available (Figure V-12).

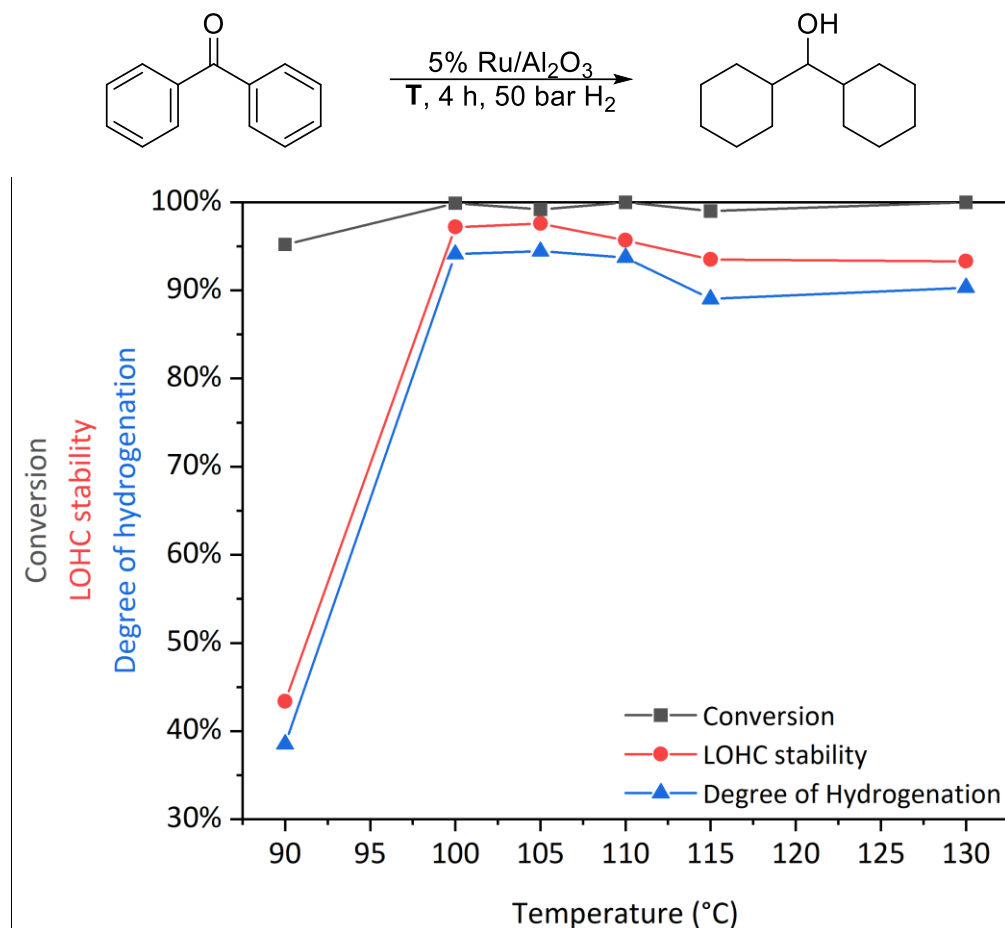


Figure V-12 - Effect of the temperature on the hydrogenation of BPO to DCMA. BPO (15 mL), 5%Ru/Al₂O₃ (0.066 wt.% Ru with regard to BPO), 4 h, 50 bar H₂.

Complete conversion was achieved from 100 to 130 °C and an optimum of selectivity was obtained around 105 °C. For the rest of this chapter, the hydrogenation conditions of BPO to DCMA were chosen as follows: BPO (15 mL), 5%Ru/Al₂O₃ (0.066 wt.% Ru with regard to BPO), 105 °C, 4 h, 50 bar H₂.

The hydrogenated products were separated by column chromatography on silica with a solvent mixture of petroleum ether and diethyl ether in a 15:2 ratio. The product was obtained in high purity (94%) with only Dimethylketone (DCMK) as an impurity as shown by ¹H and ¹³C NMR, GC-MS, FTIR-ATR and melting point analysis (see Appendix V-6).

Chapter 2: Degradation study and limitation

V.5.2 Dehydrogenation

The dehydrogenation was performed with the 5%Pt/C catalyst used for the dehydrogenation of CHEA to APO. The effect of the temperature was studied over 36 h of reaction (Figure V-13).

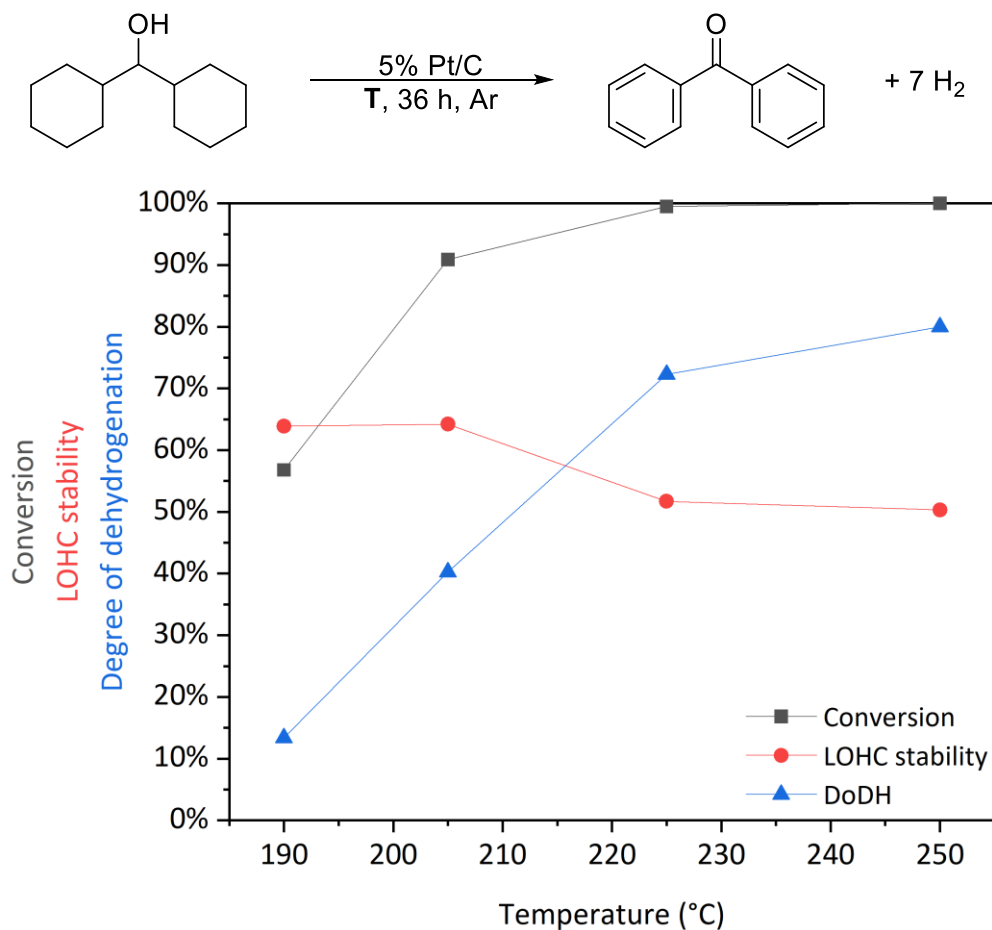


Figure V-13 - Effect of the temperature on the dehydrogenation of DCMA to BPO. DCMA (1 g), 5%Pt/C (0.25 wt.% Pt with regard to DCMA), 36 h, Ar.

Complete DCMA conversion was only achieved from 225 °C but the system stability was already below 50% from that temperature onwards with the major formation of Diphenylmethane (DPM) and its hydrogenated counterparts. In addition, fluorene derivatives were observed at 250 °C, indicating the formation of a C-C bond through dehydrocyclization. This reaction was previously reported with a Pt/C catalyst at 300 °C.²²⁻²⁴ Therefore, a reaction temperature of 225 °C was chosen to limit the formation of the dehydrocyclization by-products. Comparatively to the CHEA/APO couple, no coupling products were detected by GC-MS and dehydration was the most important degradation pathway, probably due to the higher stabilization of the secondary carbocation by the two aromatic cycles compared to one for APO. These results were confirmed by DFT calculations as the dehydration enthalpy of the DPMA intermediate is inferior to that of PEO by 6 kJ/mol and the dehydration for the respective saturated forms was also favored in the case of DCMA by 4 kJ/mol.

The complete dehydrogenation enthalpy profile was also calculated by DFT and similarly to the CHEA/APO couple, the dehydrogenation should occur first on the alcohol to form a ketone before the dehydrogenation of the cycles from a thermodynamic standpoint. The simplified energy profile is presented in Appendix V-7 and the complete energy profile of each potential intermediate is presented in Appendix V-8.

Chapter 2: Degradation study and limitation

V.5.3 Cycling

The system was cycled three times in the previously developed conditions that are reported on the Figure V-14 top-left.

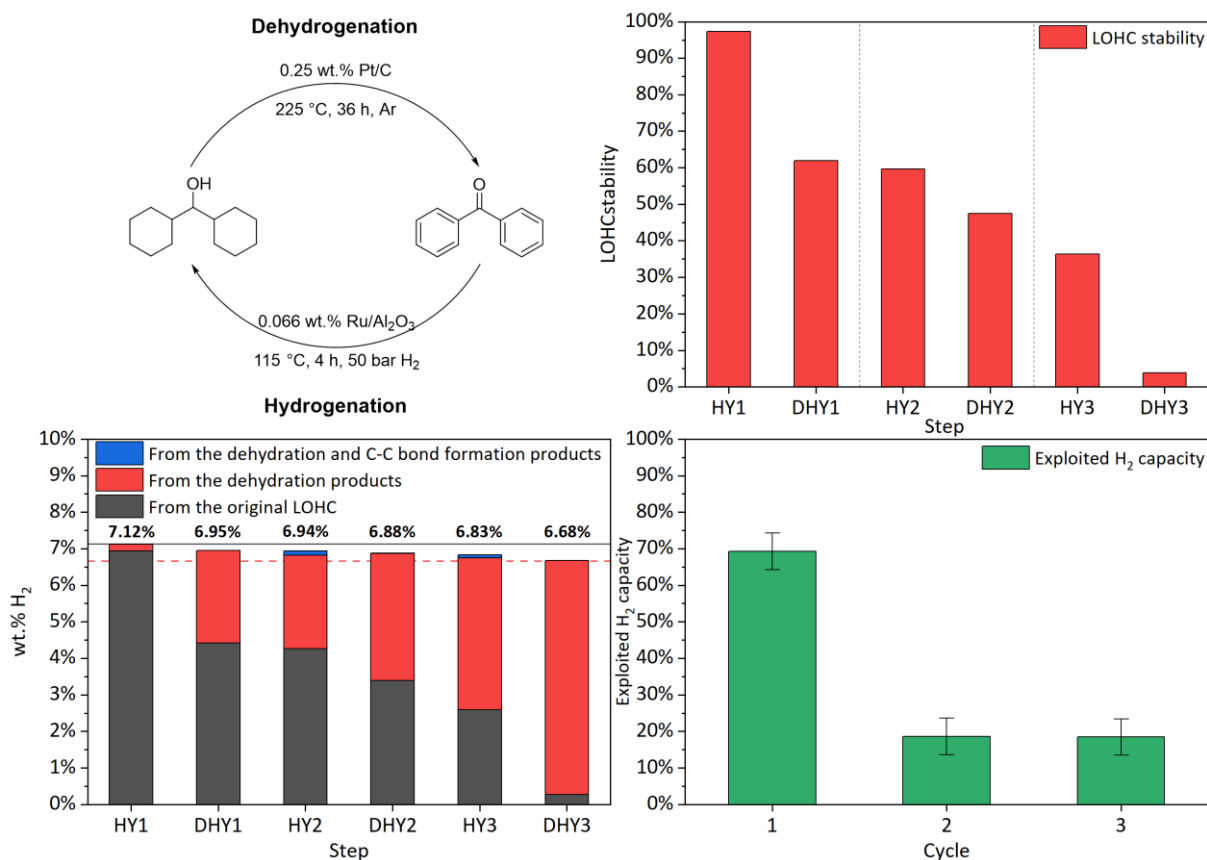


Figure V-14 – Top-left: reaction conditions for both hydrogenation and dehydrogenation. Top-right: system stability over the different steps of the cycling. HY: hydrogenation step. DHY: dehydrogenation step. Bottom-left: Theoretical maximum gravimetric capacity evolution over the different steps of the cycling. Bottom-right: exploited H₂ capacity for each cycle.

The system stability gradually decreased over the different steps of the cycling, with most degradation occurring during the dehydrogenation steps (DHY) (Figure V-14 top-right). These results were in agreement with the hydrogenation and dehydrogenation experiments as only dehydration and dehydrocyclization products were observed. In particular, dehydration products were the most present structures, overtaking the original LOHC in the reaction mixture after the DHY2 step (Figure V-14 bottom-left). At the end of the DHY3 step, almost all of the original LOHC was dehydrated and the theoretical gravimetric maximum was shifted from the gravimetric density of the original LOHC (black line) to that of the Dicyclohexylmethane/Diphenylmethane (DCM/DPM) couple (dotted red line). Regarding the exploited H₂ capacity, the first cycle allowed for a high exploited capacity of 69% (Figure V-14 bottom-right). However, this value rapidly dropped to 18% and was stable for the next two cycles. Similar to the CHEA/APO couple, these values are not sufficient to promote this structure as a LOHC. Nevertheless, the degradation pathways were reduced to simple dehydration and dehydrocyclization and no dimerization or polymerization was observed by GC-MS analysis. However, MS-APCI analyses detected DPM as the main peak ($m/z = 167$) (Figure V-15). Moreover, much like for the CHEA/APO couple, low intensity peaks separated by m/z of roughly 14-16 were observed. Therefore, the presence

Chapter 2: Degradation study and limitation

of heavy compounds due to the polymerization of the LOHC and in particular the presence of Polystyrene derivatives could not be confirmed.

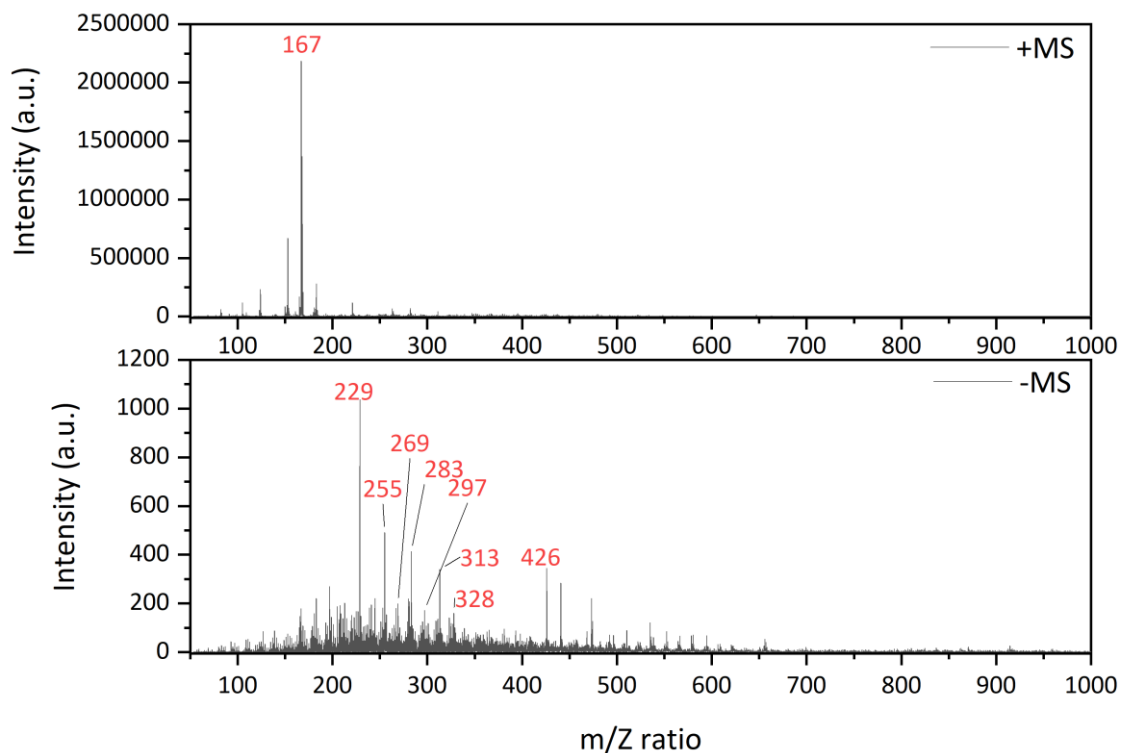


Figure V-15 – APCI-MS analysis of the reaction mixture post-cycling in positive and negative modes.

V.6 Conclusion

In conclusion, the degradation species of the CHEA/APO couple were mainly produced during the dehydrogenation due to the contact of the LOHC structure with the active metal nanoparticles in presence of H₂. In addition, it was also shown that the catalyst support could initiate the aldolisation-crotonisation in H₂-free conditions. Different strategies like support modification and additives were tested to block the degradation pathways for both the hydrogenation and dehydrogenation reaction. Unfortunately, while dehydration could sometimes be reduced to negligible proportions by neutralizing the acidic sites of the support, aldolisation-crotonisation products were observed in all instances due to their acidic and basic catalytic conditions. Aldolisation happened whenever an enol intermediate could form on the methyl group, but not the cyclohexyl group. Thus, replacement of the methyl group by a cyclohexyl group was proposed to efficiently nullify the aldolisation-crotonisation reaction. By doing so, a new LOHC couple, DCMA/BPO, was formed and studied for both hydrogenation and dehydrogenation. No more coupling products were observed, but the dehydration of the structure was enhanced by the presence of two aromatic cycles. Cycling was performed with the conditions adapted from the cycling of the CHEA/APO. After 3 cycles, almost all of the original LOHC was converted to the dehydrated DCM/DPM form. While more work could have been performed to replace the catalytic system with more basic supports in order to limit the dehydration reaction, this side-reaction would still be bound to occur even in trace amounts. Therefore, finding an efficient way to regenerate the LOHC, i.e. adding an oxygen atom on the dehydrated structure, could prove more valuable in the long term and we proposed to study the regeneration of the DCMA/BPO LOHC over the next chapter.

Bibliography

- (1) Knözinger, H. Dehydration of Alcohols on Aluminum Oxide. *Angewandte Chemie International Edition in English* **1968**, 7 (10), 791–805. <https://doi.org/10.1002/anie.196807911>.
- (2) Knözinger, H.; Scheglila, A. The Dehydration of Alcohols on Alumina: XII. Kinetic Isotope Effects in the Olefin Formation from Butanols. *Journal of Catalysis* **1970**, 17 (2), 252–263. [https://doi.org/10.1016/0021-9517\(70\)90098-9](https://doi.org/10.1016/0021-9517(70)90098-9).
- (3) Kurti, L.; Czako, B. *Strategic Applications of Named Reactions in Organic Synthesis*; Elsevier, 2005.
- (4) *Procédé de polymérisation en suspension*. Techniques de l'Ingénieur. <https://www.techniques-ingenieur.fr/base-documentaire/archives-th12/archives-operations-unitaires-genie-de-la-reaction-chimique-tiajb/archive-1/polystyrene-j6551/procede-de-polymerisation-en-suspension-j6551niv10001.html> (accessed 2023-06-27).
- (5) Wünsch, J. R. *Polystyrene: Synthesis, Production and Applications*; iSmithers Rapra Publishing, 2000.
- (6) Helary, G.; Fontanille, M. Etude de la polymérisation anionique du styrene en milieu non polaire, en présence de N,N,N',N' tetraméthyl éthylène diamine. *European Polymer Journal* **1978**, 14 (5), 345–348. [https://doi.org/10.1016/0014-3057\(78\)90118-0](https://doi.org/10.1016/0014-3057(78)90118-0).
- (7) Dowden, A. Dowden : Heterogeneous Catalysis.
- (8) McCartney, J. T.; Seligman, Bernard.; Hall, W. Keith.; Anderson, R. B. The An Electron-Microscopic Study of Metal Oxides and Metal Oxide Catalysts. *J. Phys. Chem.* **1950**, 54 (4), 505–519. <https://doi.org/10.1021/j150478a009>.
- (9) Pampararo, G.; Garbarino, G.; Riani, P.; Villa García, M.; Sánchez Escribano, V.; Busca, G. A Study of Ethanol Dehydrogenation to Acetaldehyde over Supported Copper Catalysts: Catalytic Activity, Deactivation and Regeneration. *Applied Catalysis A: General* **2020**, 602, 117710. <https://doi.org/10.1016/j.apcata.2020.117710>.
- (10) Watanabe, S.; Ma, X.; Song, C. Characterization of Structural and Surface Properties of Nanocrystalline TiO₂–CeO₂ Mixed Oxides by XRD, XPS, TPR, and TPD. *J. Phys. Chem. C* **2009**, 113 (32), 14249–14257. <https://doi.org/10.1021/jp8110309>.
- (11) Pines, H.; Manassen, J. The Mechanism of Dehydration of Alcohols over Alumina Catalysts. In *Advances in Catalysis*; Eley, D. D., Pines, H., Weisz, P. B., Eds.; Academic Press, 1966; Vol. 16, pp 49–93. [https://doi.org/10.1016/S0360-0564\(08\)60351-X](https://doi.org/10.1016/S0360-0564(08)60351-X).
- (12) Santacesaria, E.; Gelosa, D.; Giorgi, E.; Carrà, S. Role of Basic and Acid Sites in the Bimolecular Dehydration of Alcohols Catalyzed by HY Zeolite. *Journal of Catalysis* **1984**, 90 (1), 1–9. [https://doi.org/10.1016/0021-9517\(84\)90077-0](https://doi.org/10.1016/0021-9517(84)90077-0).
- (13) Shi, L.; Zhou, Y.; Qi, S.; Smith, K. J.; Tan, X.; Yan, J.; Yi, C. Pt Catalysts Supported on H₂ and O₂ Plasma-Treated Al₂O₃ for Hydrogenation and Dehydrogenation of the Liquid Organic Hydrogen Carrier Pair Dibenzyltoluene and Perhydrodibenzyltoluene. *ACS Catal.* **2020**, 10 (18), 10661–10671. <https://doi.org/10.1021/acscatal.0c03091>.
- (14) Lee, D. H.; Condrate, R. A. An FTIR Spectral Investigation of the Structural Species Found on Alumina Surfaces. *Materials Letters* **1995**, 23 (4), 241–246. [https://doi.org/10.1016/0167-577X\(95\)00039-9](https://doi.org/10.1016/0167-577X(95)00039-9).
- (15) Hernandez, J. O.; Choren, E. A. Thermal Stability of Some Platinum Complexes. *Thermochimica Acta* **1983**, 71 (3), 265–272. [https://doi.org/10.1016/0040-6031\(83\)80059-8](https://doi.org/10.1016/0040-6031(83)80059-8).
- (16) Walter Glen Cameron. *THE ACTION OF SULPHURIC ACID ON CERTAIN ARALKYL ETHERS AND ALCOHOLS*. <https://theses.gla.ac.uk/80178/1/13905554.pdf> (accessed 2022-12-22).
- (17) Zhang, C.; Wang, T.; Liu, X.; Ding, Y. Selective Oxidation of Glycerol to Lactic Acid over Activated Carbon Supported Pt Catalyst in Alkaline Solution. *Chinese Journal of Catalysis* **2016**, 37 (4), 502–509. [https://doi.org/10.1016/S1872-2067\(15\)61055-5](https://doi.org/10.1016/S1872-2067(15)61055-5).
- (18) Breitner, E.; Roginski, E.; Rylander, P. N. Low Pressure Hydrogenation of Ketones with Platinum Metal Catalysts. *J. Org. Chem.* **1959**, 24 (12), 1855–1857. <https://doi.org/10.1021/jo01094a004>.
- (19) Jones, C. W. *Applications of Hydrogen Peroxide and Derivatives*; The Royal Society of Chemistry, 1999. <https://doi.org/10.1039/9781847550132>.
- (20) Xiao, H.; Dou, C.; Shi, H.; Ge, J.; Cai, L. Influence of Sulfur-Containing Sodium Salt Poisoned V₂O₅–WO₃/TiO₂ Catalysts on SO₂–SO₃ Conversion and NO Removal. *Catalysts* **2018**, 8 (11), 541. <https://doi.org/10.3390/catal8110541>.
- (21) Haynes, W. M. *CRC Handbook of Chemistry and Physics*, 97th ed.
- (22) Graebe, C. Ueber Synthese des Phenanthrens. *Ber. Dtsch. Chem. Ges.* **1873**, 6 (1), 125–127. <https://doi.org/10.1002/cber.18730060147>.

Chapter 2: Degradation study and limitation

- (23) Zelinsky, N. D.; Titz, I. N. Über Die Bildung von Aromatischen Kohlenwasserstoffen Bei Der Dehydrogenisations-Katalyse. *Berichte der deutschen chemischen Gesellschaft (A and B Series)* **1929**, 62 (10), 2869–2873. <https://doi.org/10.1002/cber.19290621032>.
- (24) Schmidt, R.; Griesbaum, K.; Behr, A.; Biedenkapp, D.; Voges, H.-W.; Garbe, D.; Paetz, C.; Collin, G.; Mayer, D.; Höke, H. Hydrocarbons. In *Ullmann's Encyclopedia of Industrial Chemistry*; John Wiley & Sons, Ltd, 2014; pp 1–74. https://doi.org/10.1002/14356007.a13_227.pub3.
- (25) "Synthesis of the Alcohols of the Cyclohexane Series" Reference Detail | CAS SciFinder[®]. <https://scifinder-n.cas.org/searchDetail/reference/6331d086635b02638a369b19/referenceDetails> (accessed 2022-09-26).

Appendix

Appendix V-1 - Direct basification of the support

By using a commercial Ru/Al₂O₃ catalyst immersed it in 5mL of 0.01 M NaOH solution overnight (pH=12). The catalyst is dried up before reaction in an oven under vaccum at 50 °C.

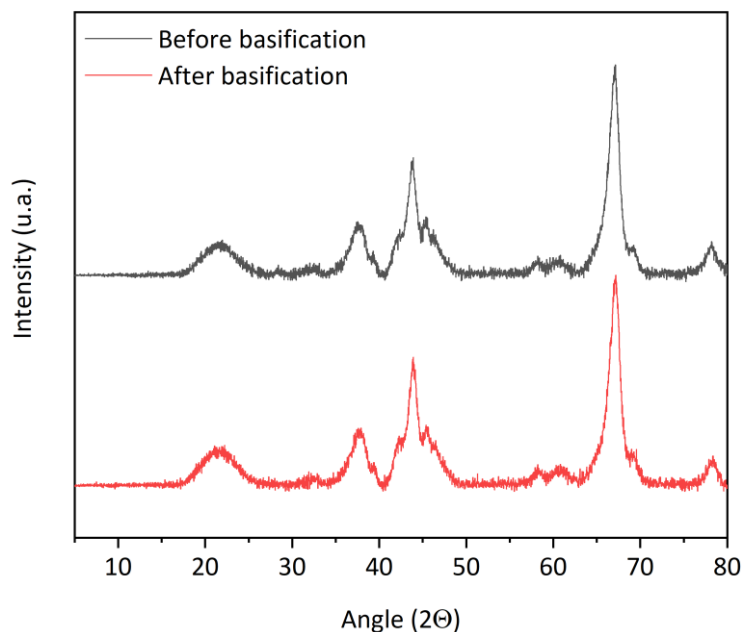


Figure V-16 - XRD analysis of the Ru/Al₂O₃ catalyst before and after basification.

Appendix V-2 - XRD analysis of the 2 wt% Pt/Al₂O₃ catalysts

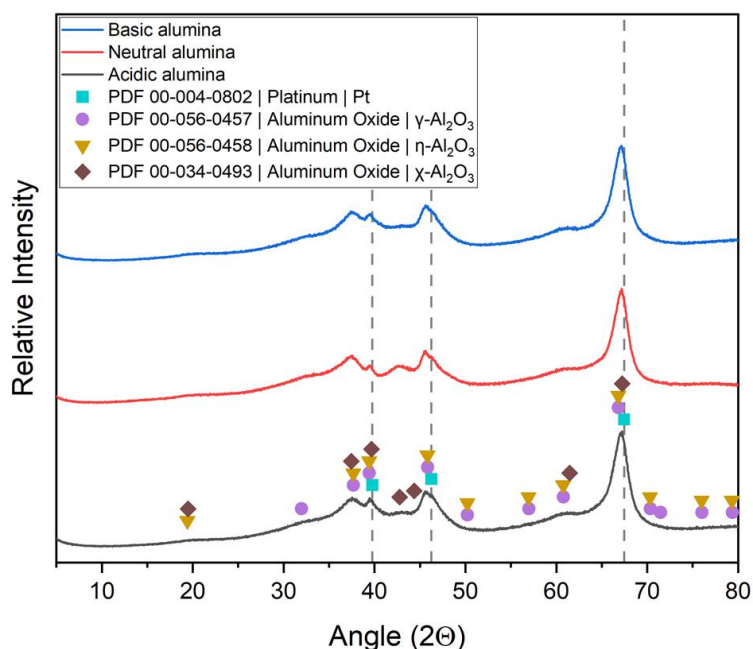


Figure V-17 - XRD analysis of the 2 wt.% Pt/Al₂O₃ catalysts.

Platinum peaks are hidden behind the Al₂O₃ patterns with only a small shoulder visible around 46°. This result is expected as Pt is present in 2 wt.% in the sample and its potential nanometer size further reduces the sharpness of the Pt signal.

Chapter 2: Degradation study and limitation

Appendix V-3 - XRD basification/acidification of the hydrogenation Ru/Al₂O₃ catalyst

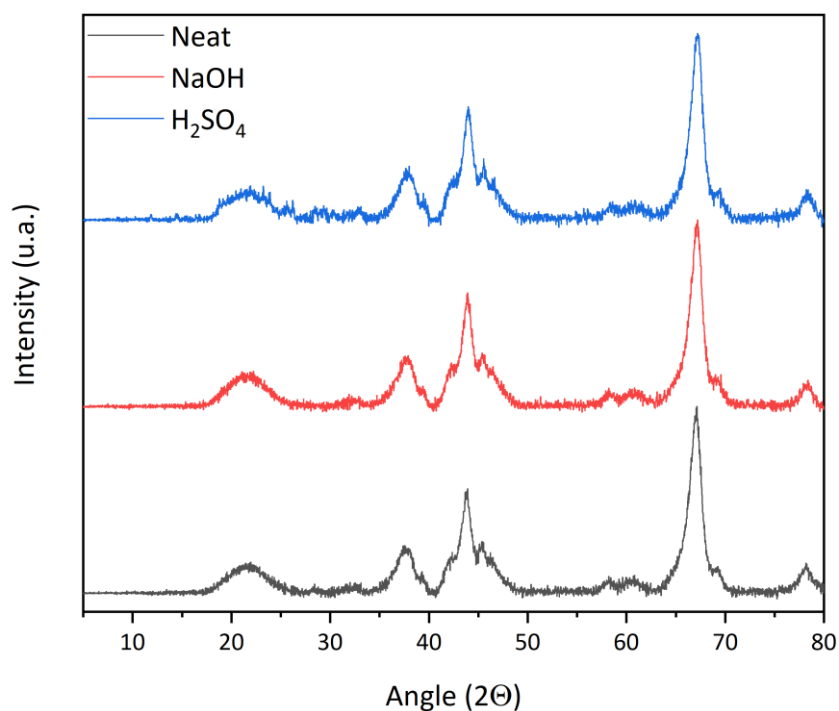


Figure V-18 - XRD basification/acidification of the hydrogenation Ru/Al₂O₃ catalyst with 1 mol% additive.

Appendix V-4 - XRD basification/acidification of the dehydrogenation Pt/C catalyst

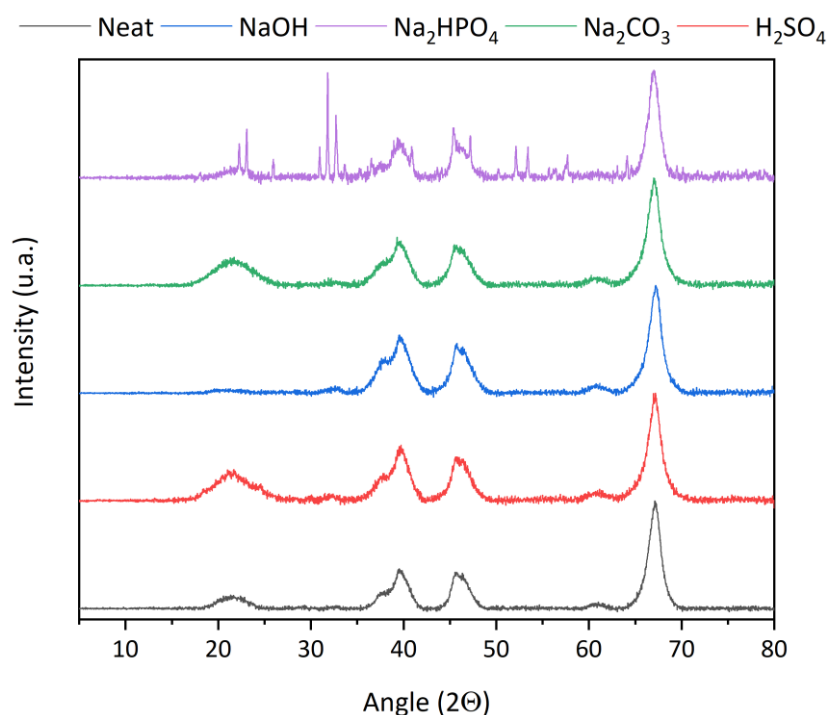


Figure V-19 - XRD basification/acidification of the dehydrogenation Pt/C catalyst with 1 mol% additive.

No difference was observed except for the catalyst brought in presence with Na₂HPO₄ where the peaks related to the base were observed (PDF 00-010-0184).

Chapter 2: Degradation study and limitation

Appendix V-5 - NaOH quantity effect on the Pt/C dehydrogenation catalyst by XRD analysis

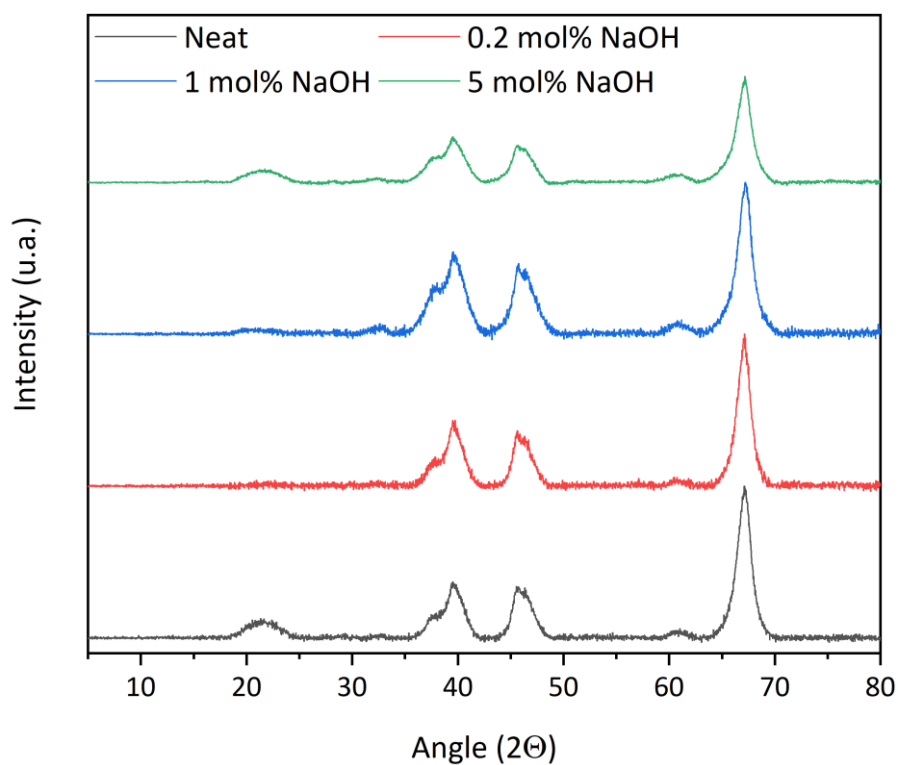


Figure V-20 – Effect of the NaOH quantity by XRD analysis of the dehydrogenation Pt/C catalyst.

Appendix V-6 - Characterizations of the purified Dicyclohexylmethanol

White solid with a melting point = 67 ± 2 °C/ 63 °C (lit.)²⁵

Purity: 94% by ¹H NMR (DCMK impurity at 2.17 ppm, 2H)

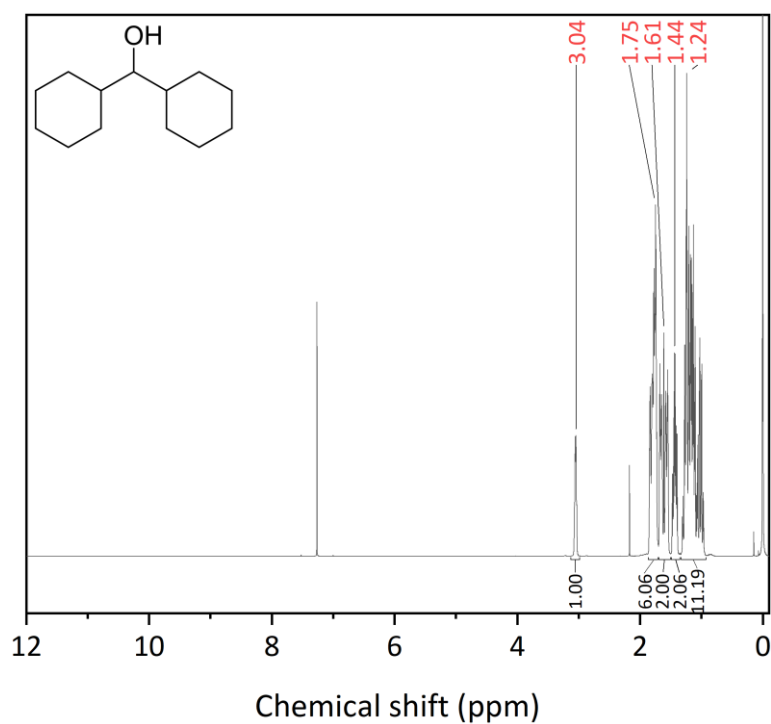


Figure V-21. - ¹H NMR analysis of the purified DCMA.

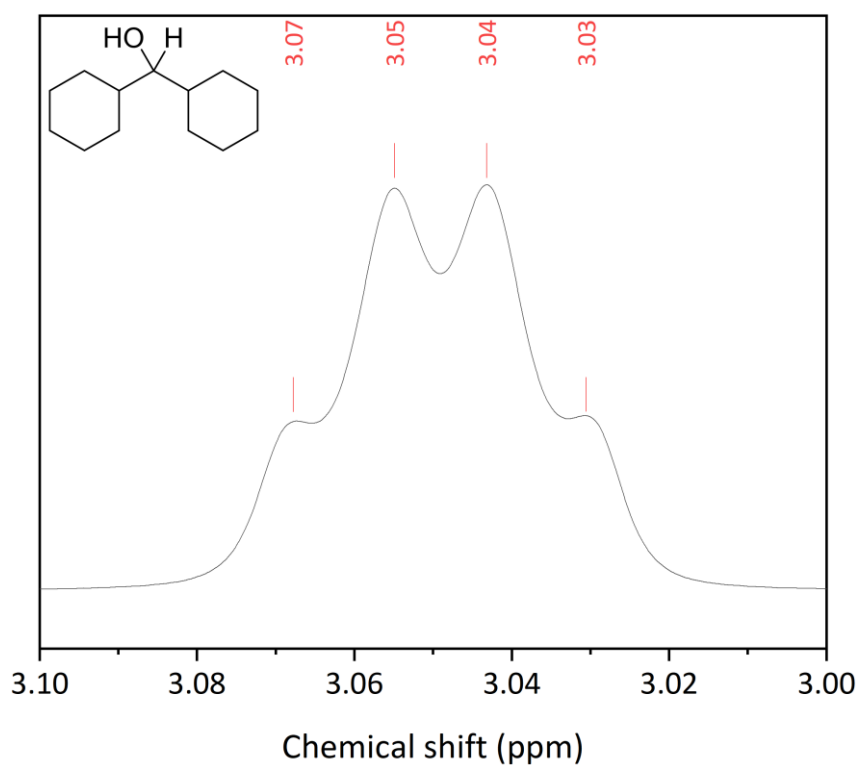


Figure V-22 - ^1H NMR analysis of the purified DCMA. Zoom on the peak at 3.05 ppm.

^1H NMR (CDCl_3) δ =0.94-1.33 (11H, m), 1.36–1.50 (2H, m), 1.52-1.60 (2H, m), 1.62–1.70 (2H, m), 1.70-1.89 (2H, m), 3.05 (1H, q, J = 4.89 Hz).

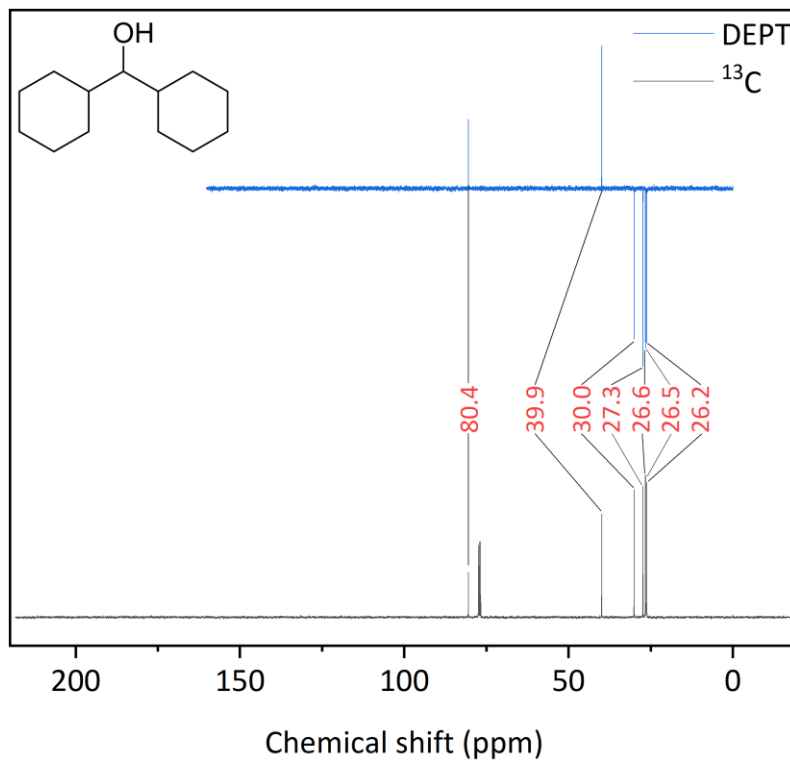


Figure V-23 – ^{13}C NMR and DEPT analysis of the purified DCMA.

^{13}C NMR (CDCl_3) δ =26.2 (s), 26.5 (s), 26.6 (s), 27.3 (s), 30.0 (s), 39.9 (t), 80.4 (t)

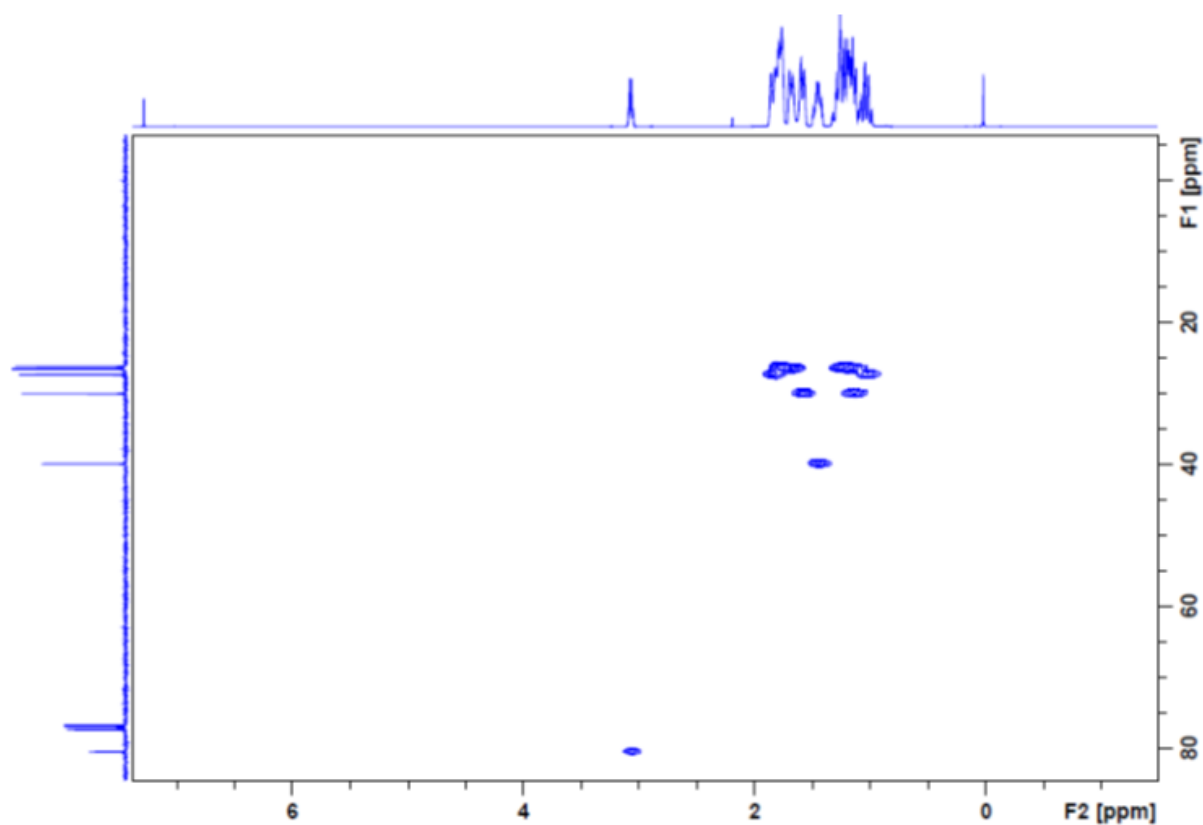


Figure V-24 - HSQC analysis of the purified DCMA.

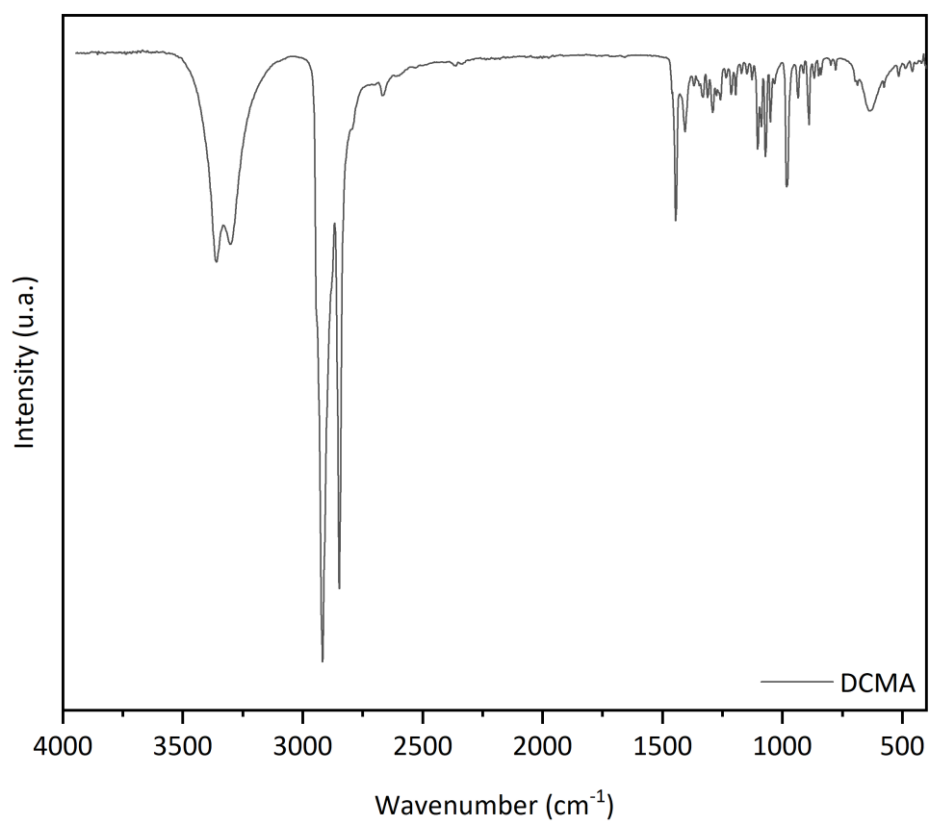


Figure V-25 - FTIR-ATR analysis of the purified DCMA.

IR (neat): alcohol: 3360, 3298 cm⁻¹; Csp³: 2916, 2847, 1444 cm⁻¹

Chapter 2: Degradation study and limitation

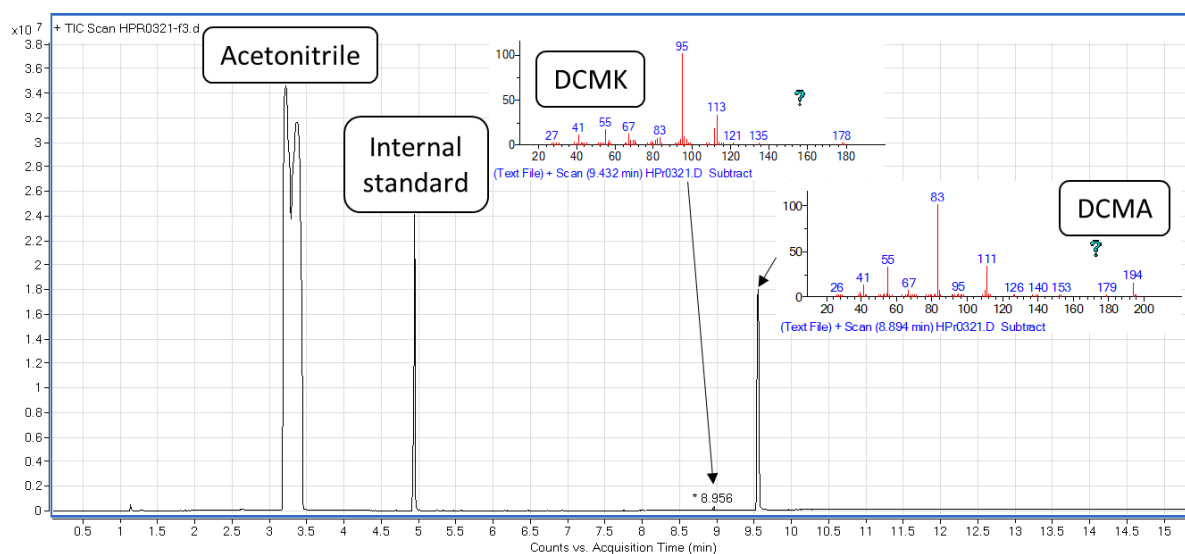


Figure V-26 - GCMS analysis of the purified DCMA.

Appendix V-7 - Intermediates and degradation during the dehydrogenation of DCMA to BPO

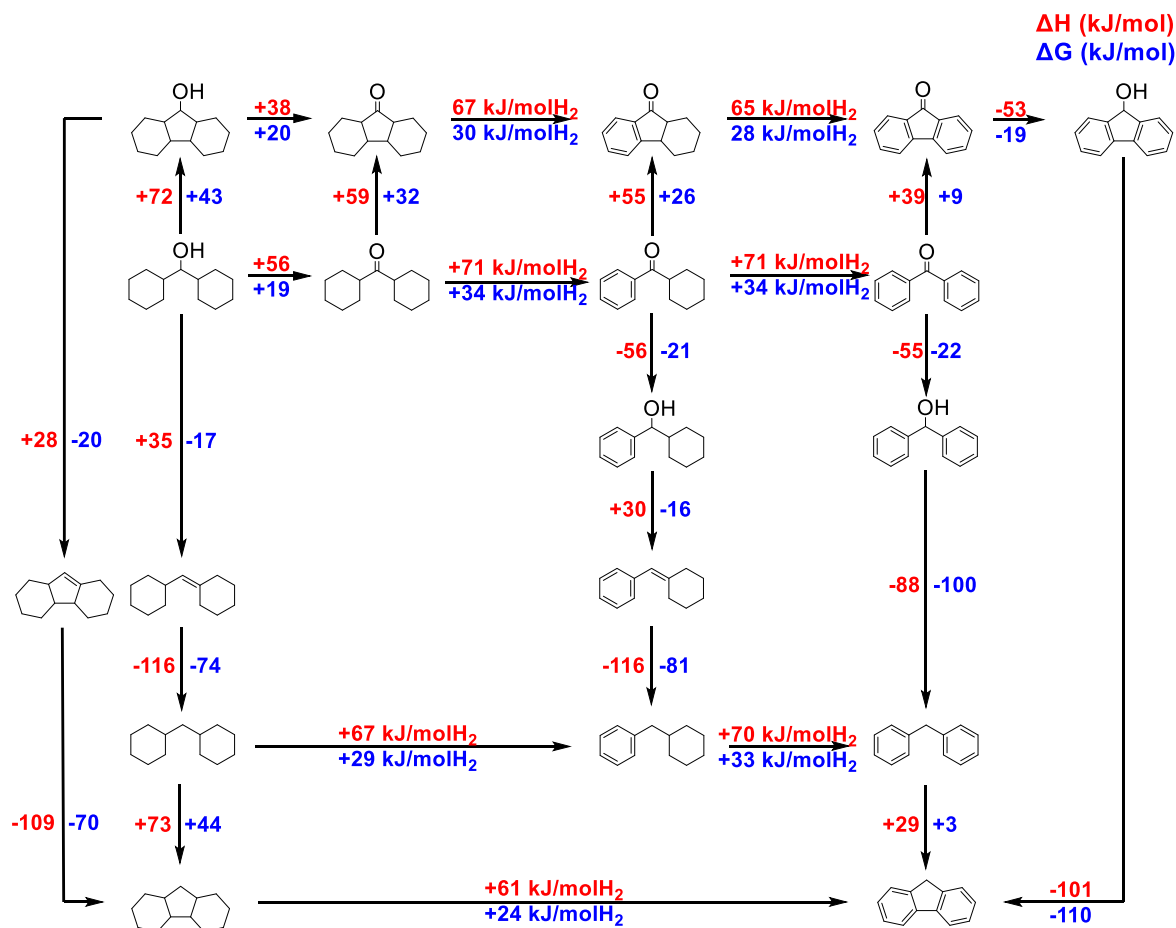


Figure V-27 – Extended DFT mechanism of the dehydrogenation of DCMA to BPO and the associated degradation pathways.

Chapter 2: Degradation study and limitation

Appendix V-8 - DFT BPO: Dehydrogenation via stable intermediates

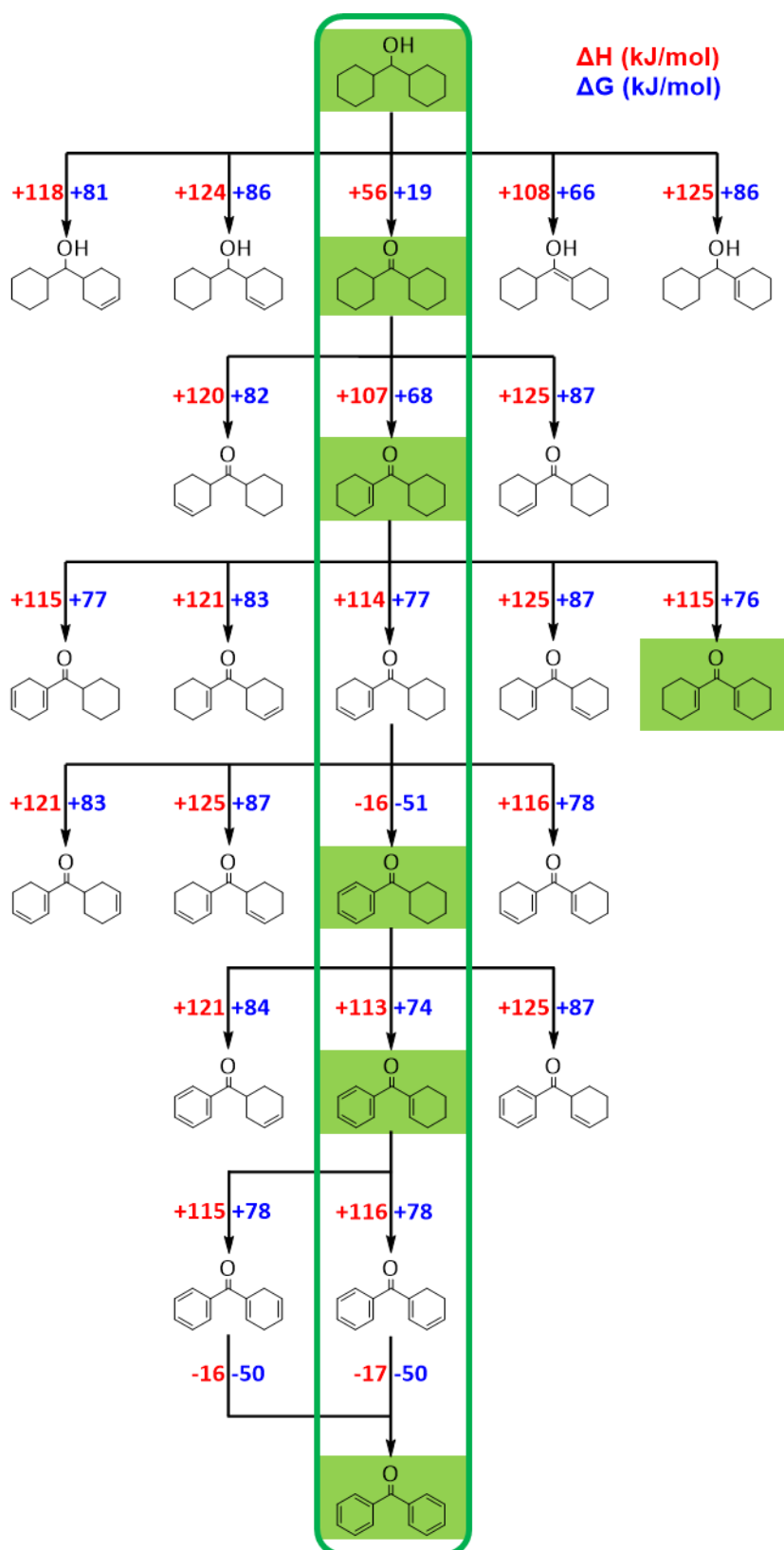


Figure V-28 – Estimation of the dehydrogenation mechanism of DCMA to BPO by DFT. The enthalpy for each step is presented in red, the Gibbs energy in blue. The products highlighted in green were observed by GC-MS.



Table of Contents “Chapter 3: Regeneration of the intramolecular dehydration products

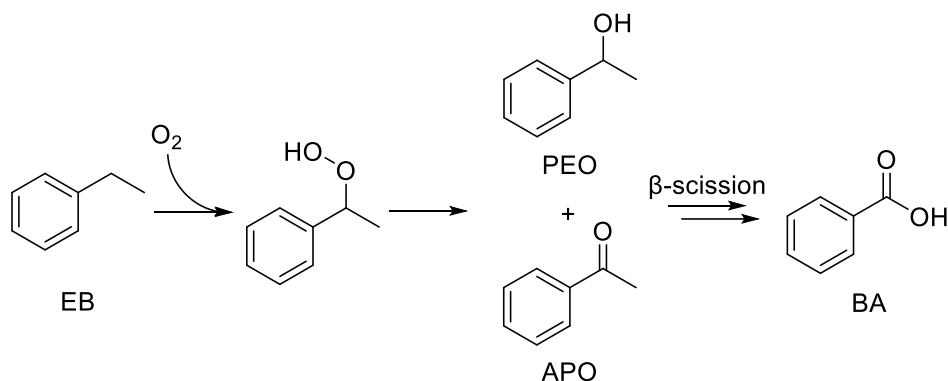
VI.	Chapter 3: Regeneration of the intramolecular dehydration products	220
VI.1	Regeneration process.....	220
VI.2	Regeneration of Diphenylmethane (DPM) to Benzophenone (BPO).....	222
VI.3	Study of the Dodecahydrofluoren-9-ol/Fluoren-9-one (12H-FLUA/FLUK) LOHC couple	230
VI.3.1	Regeneration of Fluorene to Fluoren-9-one	231
VI.3.2	Hydrogenation of FLUK.....	232
VI.3.3	Purification of 12H-FLUA	233
VI.3.4	Dehydrogenation of 12H-FLUA.....	235
VI.3.5	Cycling.....	236
VI.3.6	Analysis of the impurities	237
VI.4	Conclusion	240
	Bibliography.....	241
	Appendix.....	244
	Appendix VI-1 - 12H-FLUA analysis.....	244
	Appendix VI-2 - GC-MS analysis of the purified 12H-FLUA	246
	Appendix VI-3 - XRD of the solid products after the cyclings with regeneration, without regeneration compared to Fluorenone and Fluorene	246
	Appendix VI-4 - NMR analysis of the reaction mixture after 3 cycles without regeneration	247
	Appendix VI-5 - NMR analysis of the reaction mixture after 3 cycles with regeneration.....	248
	Appendix VI-6 - Comparison of the reaction mixtures after cyclings with regeneration, without regeneration and regeneration.....	250
	Appendix VI-7 - MALDI-TOF of the reaction mixture after the cyclings with regeneration, without regeneration and the regeneration of Fluorene to Fluorenone	251

VI. Chapter 3: Regeneration of the intramolecular dehydration products

VI.1 Regeneration process

Intramolecular dehydration is a degradation pathway that can be limited by increasing the basicity of the reaction medium (catalytic supports, additives) or diminishing the temperature of reaction.^{1,2} However, even by limiting the prevalence of this pathway by the above-mentioned approaches, the stabilization of a benzylic carbocation by the aromatic cycle could prove too high a preferential pathway to overcome, especially in the case of a twice-stabilized carbocation as it was observed during the dehydration of bicyclic ketones like Benzophenone (see V. Chapter 2). Therefore, finding an efficient strategy to add an oxygen atom on the benzylic position in order to regenerate the alcohol or the ketone could be advantageous to further the use of the keto-aromatic LOHC structures.

In the literature, alkylarene oxidation has been pursued and industrially developed since the 20th century. For example, the continuous styrene process developed by the Carbide Carbon Chemicals Company performs the air oxidation of Ethylbenzene (EB) to Acetophenone (APO) and α -Phenylethanol (PEO) in presence of a heterogeneous Mn catalyst at 115-145°C and up to 5 bar O₂.³ Another minor by-product of this reaction is the overoxidation product Benzoic acid (BA). From a reaction standpoint, a hydroxyperoxide intermediate is produced before the formation of PEO and APO while BA is formed by the cleavage of the methyl group of the APO as presented in Scheme VI-1.⁴



Scheme VI-1 - Molecules taking part in the continuous Styrene process by the Carbide Carbon Chemicals Company.³

More generally, the Carbide Carbon Chemicals Company Styrene process has a low yield per pass (<25%) in order to limit the production of PEO and BA. Therefore, product separation at the exit feed and recirculation of EB is usually employed to circumvent this issue. Here, as PEO is an intermediate of interest (see chapter 1) that can additionally be readily oxidized by the oxygen present during the reaction, the only side-product of the reaction in our case is BA.⁵ Therefore, this reactivity is particularly interesting in the case of the 1-Cyclohexylethanol/Acetophenone (CHEA/APO) couple, as it shows that the regeneration of intramolecular dehydration products is possible.

A review of the literature shows that the regeneration of the alcohol function in α of the cycle is favored for aromatic structures compared to the equivalent saturated cycles.^{6,7} In consequence, the regeneration of the dehydrated structure should be pursued when a maximum of the LOHC cycle is aromatic, hence after the dehydrogenation and before the hydrogenation. Comparatively to the classic two-step LOHC scheme, a three-step catalytic cycle could be proposed as presented in Figure VI-1.

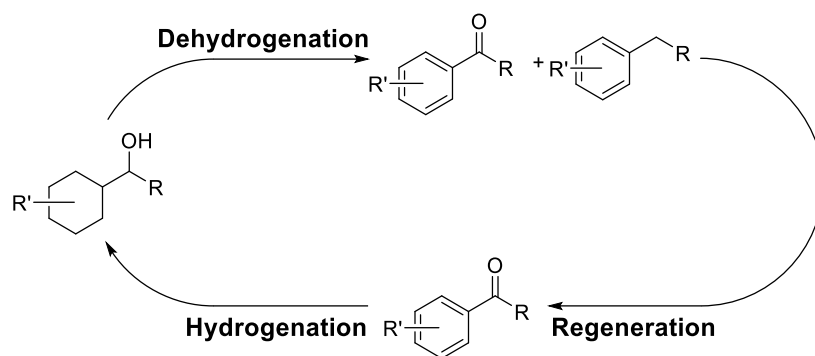


Figure VI-1 - LOHC cycle including a regeneration of the ketone function

A similar cycling process was originally proposed by Pez et al. as a way to limit the energy consumption of the dehydrogenation for onboard applications. The process revolved around the oxidation of the carrier with air onboard to produce sufficient heat to compensate the dehydrogenation enthalpy cost. A process centered around the Dodecahydrofluorene-Fluorene-Fluorenone auto-oxidative LOHC system developed by Air products is presented in Figure VI-2.

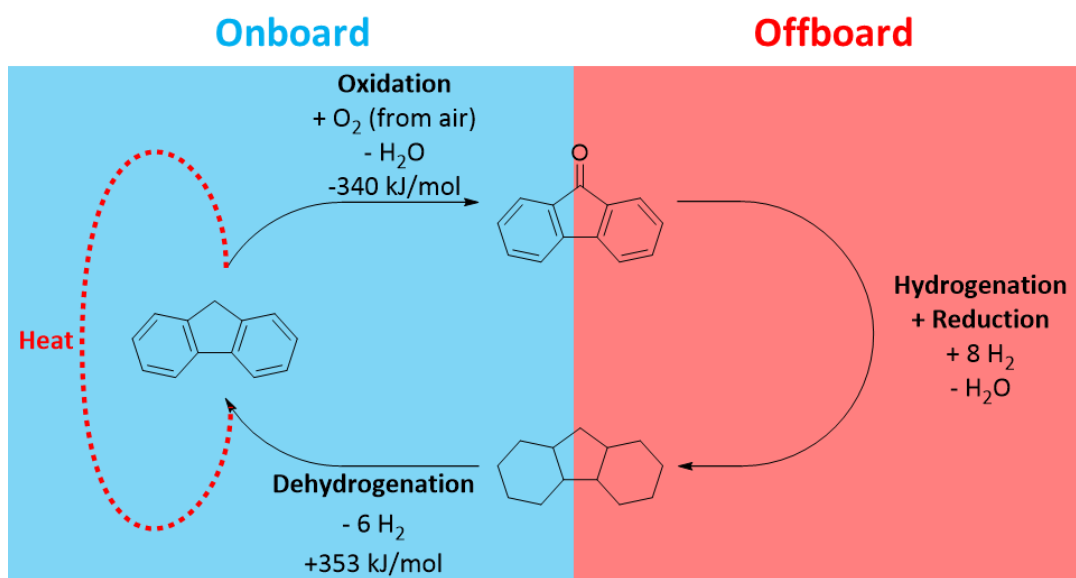


Figure VI-2 – Dodecahydrofluorene-Fluorene-Fluorenone auto-oxidative LOHC system and H₂ delivery processes.⁸

First, 2 additional equivalents of H₂ are consumed during the hydrogenation and reduction step in order to regenerate the LOHC structure. This extra H₂ consumption is the main difference between the Figure VI-1 and the Figure VI-2 that revolves respectively around the desire to keep the structure oxygenated and to remove the oxygen in order to release heat by a later oxidation of the LOHC structure.

Early regeneration attempts of EB to APO showed unsatisfying conversions (<5%). Moreover, as Diphenylmethane (DPM) is usually more simple to regenerate than EB⁹ and that the presence of the second aromatic cycle was beneficial to block the aldolisation-crotonisation pathway (see chapter 2), we will only discuss the experiments relative to the regeneration of the Dicyclohexylmethanol/Benzophenone (DCMA/BPO) LOHC couple in the rest of this chapter. Finally, we will show the influence of the regeneration on the cycling of the Dodecahydrofluorene-9-ol/Fluorene-9-one (12H-FLUA/FLUK) LOHC couple.

VI.2 Regeneration of Diphenylmethane (DPM) to Benzophenone (BPO)

Numerous procedures exist in the literature to oxidize the alkylarene position in presence of heterogeneous catalysts. However, only a few use air as the oxidant¹⁰, preferring pure oxygen (O₂)^{11,12} or peroxides such as Hydrogen peroxide (H₂O₂)¹³ or Tert-butylperoxide (TBHP)⁹. In order to limit the utilization of harmful chemicals, early attempts consisted in peroxide-free experiments. A Co catalyst supported on carbon nitride (Co/CN) was synthesized by ball-milling with a Co loading of 8 wt.% Co as analyzed by ICP analysis.¹² This catalyst was used to oxidize DPM in order to form the BPO or Diphenylmethanol (DPMA) in solvent-free conditions by using air at 8 bar in a metal reactor. Only the oxygen present in the air acted as the oxidant. The results are presented in Figure VI-3.

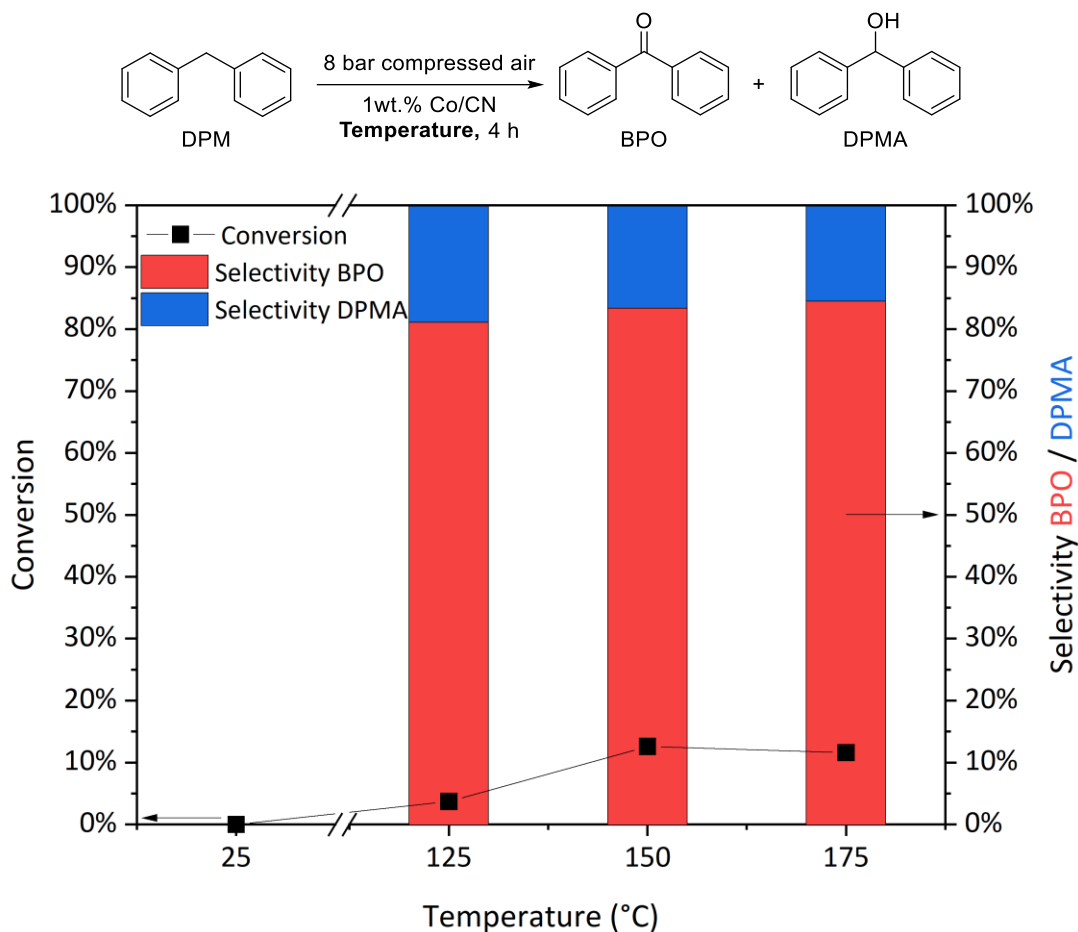


Figure VI-3 - Effect of the temperature on the conversion and selectivity of the regeneration of DPM to BPO and DPMA. DPM (2.5 g), Co/CN (1 wt.% Co with regard to DPM), 4 h, 8 bar compressed air.

In this oxidant-free reaction, only low conversion was achieved, reaching a plateau at 15% conversion. The products were the oxygenated LOHC BPO and DPMA in a 85:15 ratio and no other product was observed in these conditions.

Chapter 3: Regeneration of the intramolecular dehydration products

Following these results, the incidence of the pressure and the presence of an inorganic oxidant H_2O_2 or an organic oxidant TBHP was probed in a series of experiments with Co/CN at 125 °C over 4 h in solvent-free conditions (Figure VI-4). The choice of a temperature of 125 °C stems from previous experiments with Ethylbenzene whose lower boiling point (136 °C) forced the limitation of the reaction temperature to 125 °C. Ethylbenzene regeneration experiments are not presented in this manuscript.

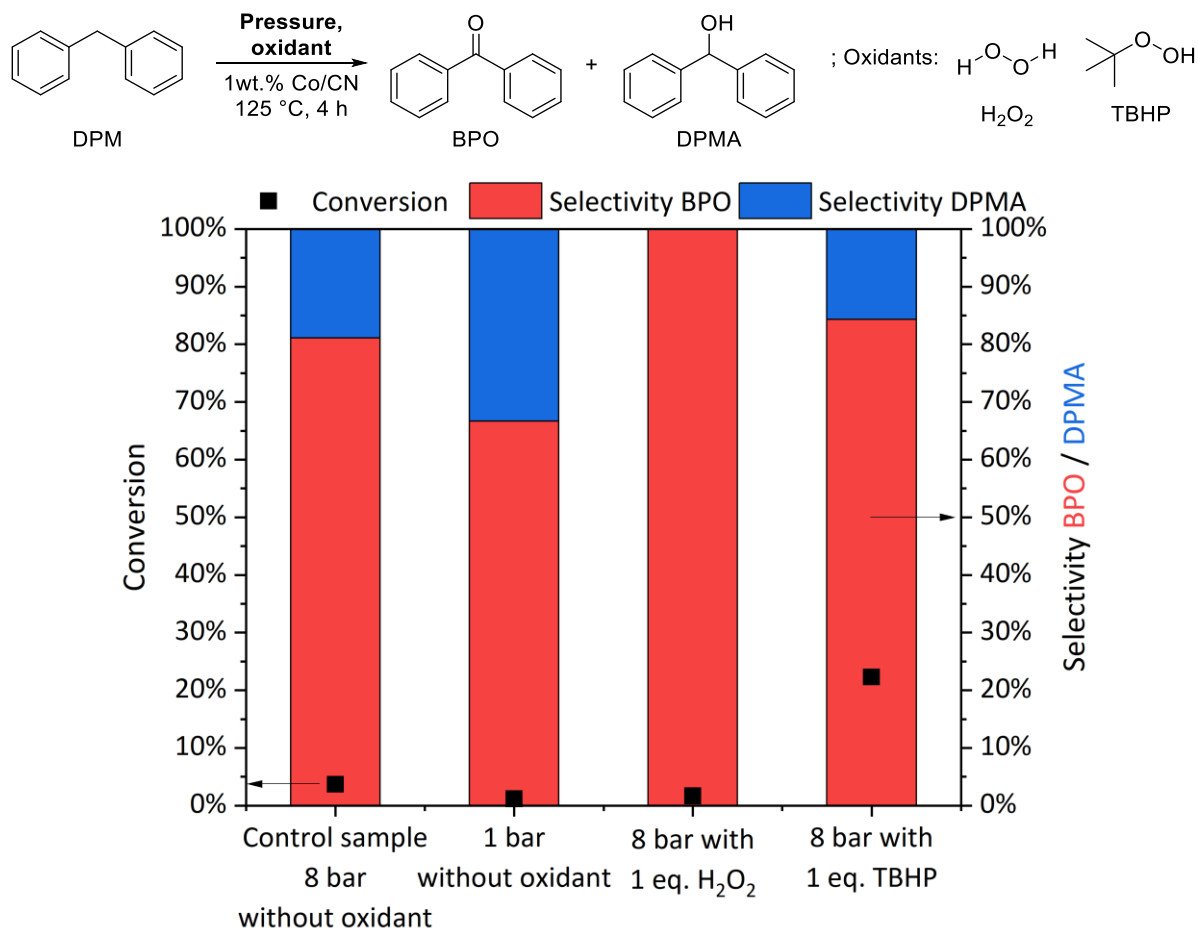


Figure VI-4 - Effect of the pressure and the oxidant on the conversion and selectivity of the regeneration of DPM to BPO and DPMA. DPM (2.5 g), C/CN (1 wt.% Co with regard to DPM), 125 °C, 4 h.

As expected, increasing the pressure displaced the equilibrium to the oxygenation of the benzylic position, indicating that higher pressures would be beneficial. The oxidant choice was primordial as its solubility with DPM strongly modified the reactivity. Indeed, the organic oxidant TBHP reached a higher conversion (22%) compared to the inorganic oxidant that achieved less than 5% conversion. Regarding the selectivity, the BPO/DPMA and the pressure were positively correlated. H_2O_2 yielded pure BPO, potentially due to a higher conversion of DPMA to BPO while the limited oxidation of DPM to DPMA was linked to the low solubility of DPM with H_2O_2 . Conversely, TBHP showed a BPO/DPMA ratio similar to that of the additive-free reaction, showing that the mechanism probably follows the same reactive pathway than the control experiment.

Chapter 3: Regeneration of the intramolecular dehydration products

Other catalysts reported in the literature such as a Mn acetate³ and Ce-MOF¹⁴ were also bought or synthesized and tested with both H₂O₂ and TBHP as oxidants with 8 bar compressed air (Figure VI-5).

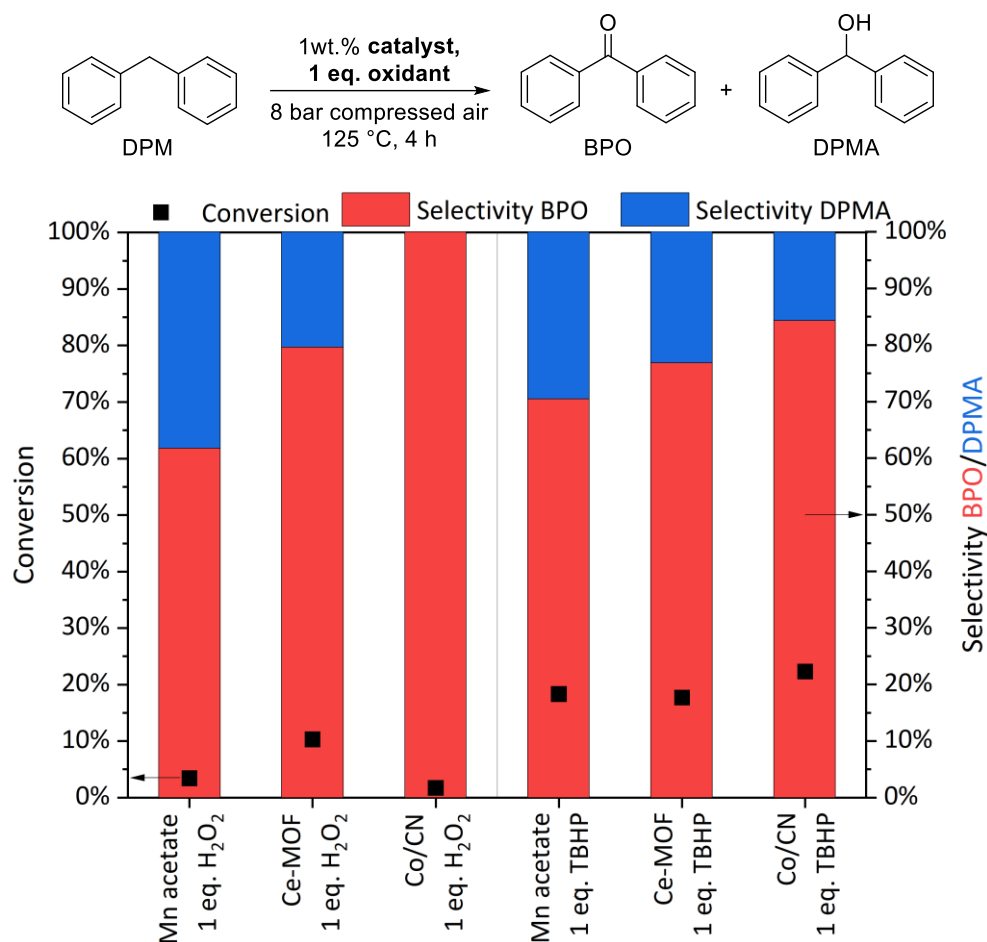


Figure VI-5 - Effect of the catalyst with H₂O₂ or TBHP as an additive. DPM (2.5 g), catalyst (1 wt.% active metal with regard to DPM), oxidant (1 equivalent), 125 °C, 4 h, 8 bar compressed air.

In presence of H₂O₂, the maximum conversion was achieved with the Ce-MOF catalyst that reached a maximum of 10%. Therefore, H₂O₂ was not used as an additive for the following experiments. With TBHP, similar conversions of roughly 20% were obtained for all three catalysts. As the conversion were still low and that the literature often reported pure oxygen atmosphere and light-driven oxidation of DPM to BPO, we hypothesized that our opaque metal reactor limited the generation of key-radical species to afford the oxygenated LOHC structure. In consequence, further tests were conducted in glass flasks at atmospheric pressure to allow for light irradiation on the reaction (Figure VI-6).

Chapter 3: Regeneration of the intramolecular dehydration products

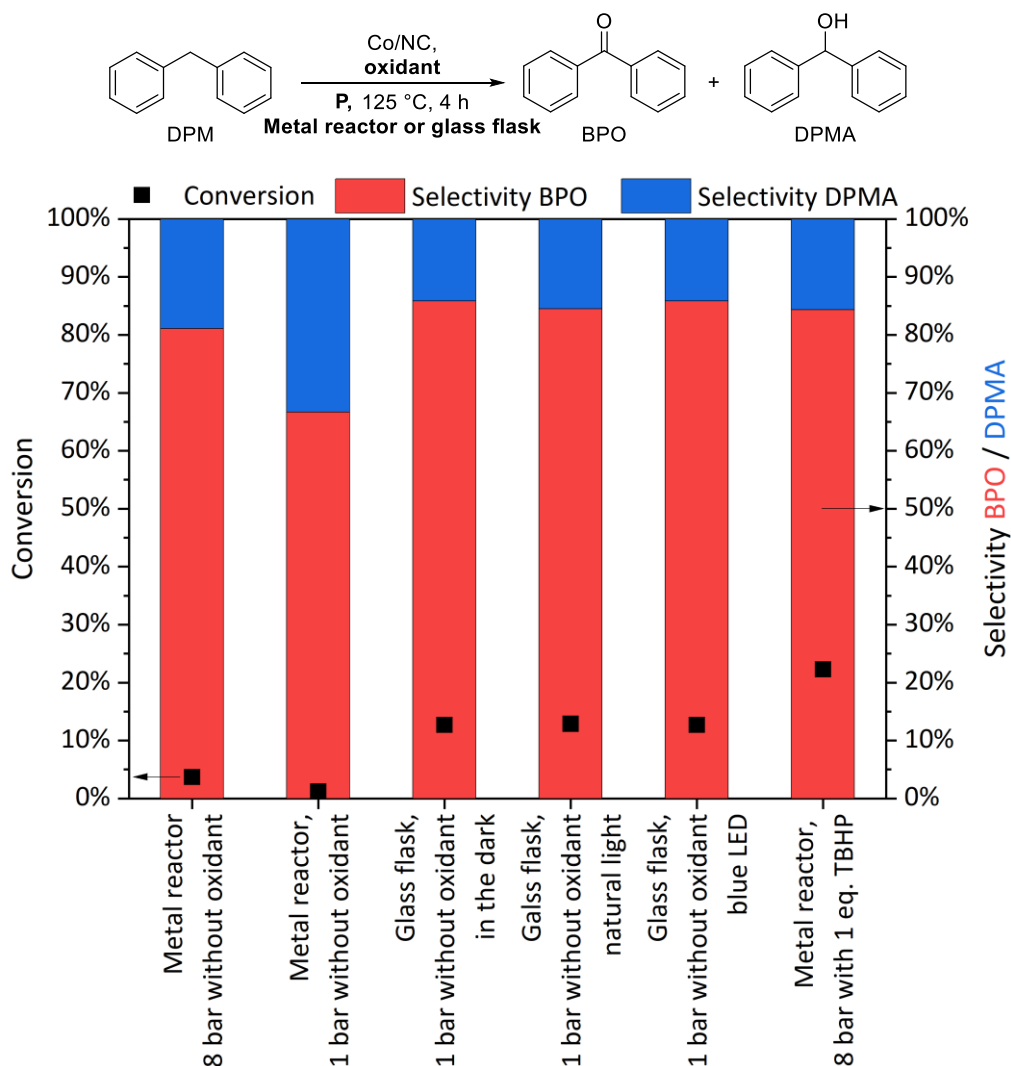


Figure VI-6 – Influence of the reaction apparatus on the conversion and selectivity of the regeneration of DPM to BPO. DPM (2.5 g), catalyst (1 wt.% active metal with regard to DPM), oxidant (1 equivalent), 125 °C, 4 h.

The replacement of the metal reactor with a glass flask increased the conversion from 1% to 13% under the same pressure conditions. In addition, the control of the light irradiation did not affect the conversion or the selectivity of the reaction, which might suggest that the mechanism does not proceed through a radical pathway with the Co/NC catalyst. The difference between the 2 apparatus might come from the better stirring in the glass flask compared to the metal reactor. Finally, the presence of TBHP at 8 bar compressed air still allowed for a higher conversion of DPM (22%) than the glass flask without oxidant. This result might indicate that the presence of the oxidant created an additional reaction pathway or activated the rate-limiting step of the reaction. Despite these mechanistic insights, the regeneration yield was still limited.

Chapter 3: Regeneration of the intramolecular dehydration products

Therefore, 9 procedures from the literature that all reported a DPM conversion superior to 50% and selectivity to BPO superior to 95% were then followed in order to increase the efficiency of the regeneration as presented in the Figure VI-7.^{12,14-20} The procedures 3 and 4 were added as comparison values.

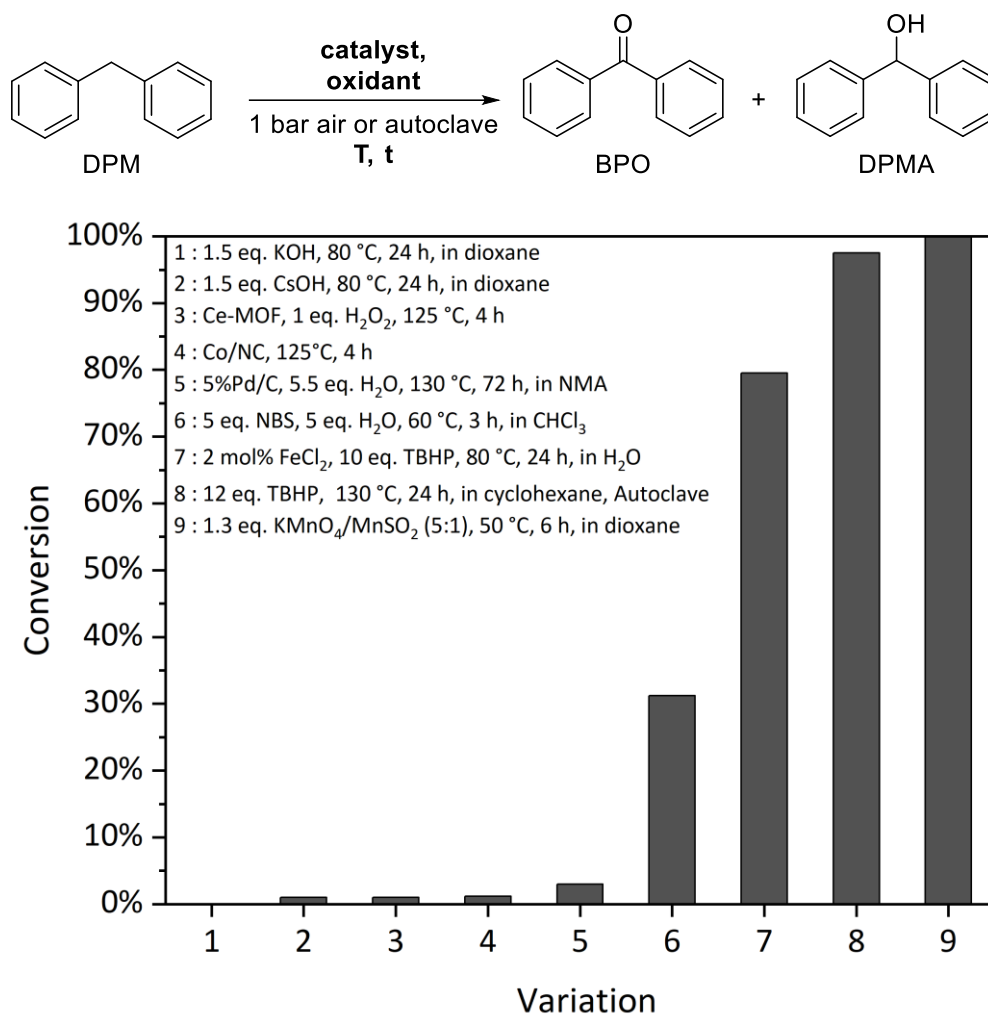


Figure VI-7 – Comparison of reaction conditions for the conversion of DPM to BPO and DPMA. All tests were performed on a 1 mmol DPM scale except for the reaction conditions 3 and 4 that were already discussed above on a 15 mmol DPM scale. NMA: N-Methylacetamide. NBS: N-Bromosuccinimide.

Only three experimental conditions sets achieved conversions superior to 50%. However, the inorganic oxidants used in the procedure (9) could not be separated by liquid/liquid extraction as the purified liquid retained a purple-dark brown coloration. In addition, limitations were also observed for the procedure (8) as a 10 mmol DPM scale-up had a conversion reduced by 51%. Conversely, the procedure (7) had a conversion only reduced by 30% when scaling-up to 50 mmol DPM. Moreover, the FeCl₂ additive was efficiently removed from the reaction mixture by the purification procedure as shown by ICP analysis (Fe not detected, inferior to 10 ppm). Thus, the procedure 7 was chosen to regenerate DPM to BPO despite using an excess of TBHP (10 equivalents). Kinetic experiments were performed to follow the composition evolution of the reaction mixture over time by GC-MS (Figure VI-8).

Chapter 3: Regeneration of the intramolecular dehydration products

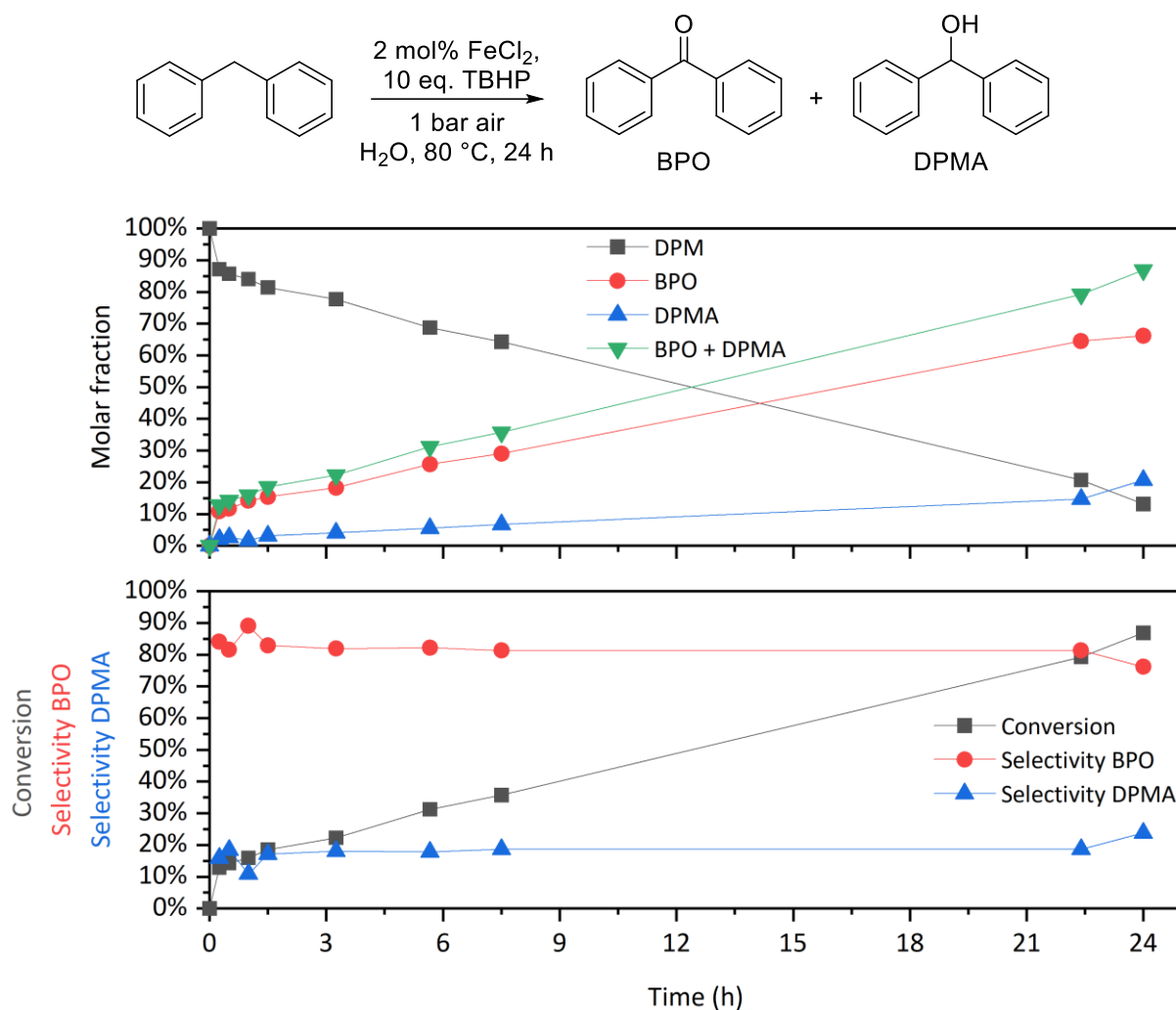


Figure VI-8 – Evolution of the reaction mixture followed by GC-MS during the regeneration of DPM to BPO and DPMA. DPM (1 mmol), FeCl₂ (0.2 mmol), TBHP (10 mmol), 80 °C, air.

The conversion increased linearly over time and the selectivity was constant with a BPO/DPMA ratio of 80/20. Up to 85% of the DPM was converted to both DPMA and BPO over 24 h and this reaction time was retained for the following experiments. Further optimization of the experimental conditions was carried out by modifying the amount of radical promoter FeCl₂, oxidant nature, irradiation conditions and stirring speed. (Figure VI-9)

Chapter 3: Regeneration of the intramolecular dehydration products

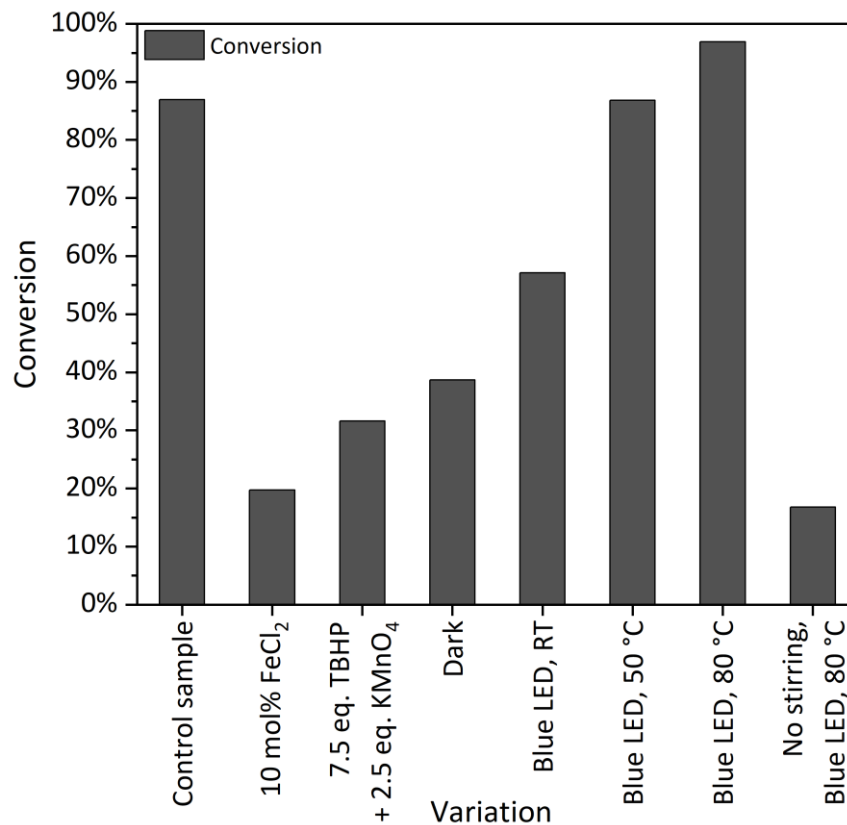
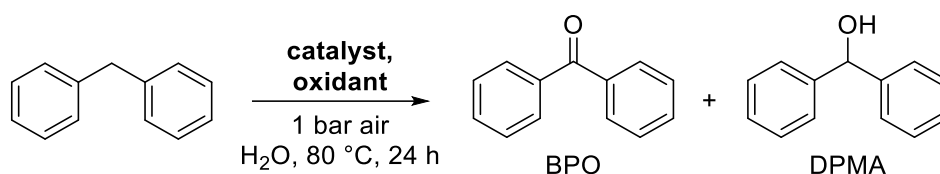


Figure VI-9 - Effect of the experimental conditions variations on the conversion and comparison with a control sample. Control sample conditions: DPM (1 mmol), FeCl₂ (2 mol%), TBHP (10 mmol), 80 °C, 24 h, air.

An increasing of the radical promoter amount was detrimental for the conversion, potentially due to the enhanced decomposition of the active species when the promoter was present in higher concentrations. The partial replacement of TBHP by KMnO₄ also yielded poorer results (32%) as rapid oxidation of the TBHP by KMnO₄ was observed through heating with a visible gaseous release when the two oxidative species were brought in contact at room temperature. A strong effect of the irradiation was also observed on the reaction. In the absence of light, the yield was drastically reduced, indicating that, for this system, a radical mechanism took place during the reaction. Conversely, direct irradiation by a strip of blue LED (<5 mW/cm²) increased the yield to 97% at 80 °C. Finally, in the optimized conditions, the absence of stirring decreased the conversion to 17% due to the biphasic nature of the system that required strong stirring to efficiently mix the two phases.

The presence of organic peroxides is mandatory to avoid chemical risks such as explosion and toxicity. Hence, different procedures were tested to neutralize TBHP in the reaction mixture after reaction (Table VI-1).

Chapter 3: Regeneration of the intramolecular dehydration products

Neutralization method	Reaction conditions	Results	Reference procedure
6 g FeSO ₄ ·7H ₂ O, 0.6 mL H ₂ SO ₄ 96% and 11 mL of water stirred with 1 L of water-insoluble solvent	5 min stirring at room temperature	Detection by KI solution	²¹
NaI (2.2 eq) in glacial acetic acid	30 min stirring at room temperature	Detection by KI solution	²¹
NaI (2.2 eq) in glacial acetic acid + 1 mL HCl 36%	30 min stirring at room temperature	Detection by KI solution	²¹
NaI (2.2 eq) in glacial acetic acid + 1 mL HCl 36%	5 h stirring at 100 °C	Detection by KI solution	²¹
10% NaHSO ₃ solution: 10 mL of solution per gram of peroxide	24 h stirring at room temperature	No detection by KI solution	²²

Table VI-1 – Neutralization procedures use to neutralize TBHP after the regeneration reaction. All procedures were performed on 0.5 mL of a reaction mixture post regeneration. The presence of peroxide was detected by a brown coloration of the reaction mixture after the addition of a few drops of 5% KI solution mixed with 1 mL acetic acid.

Only the neutralization with the 10% NaHSO₃ solution over 24 h yielded an absence of detection of peroxides. However, GC-MS analysis revealed that the organic peroxide neutralization was still incomplete after 24 h in an organic solution. It is probable that the yellow coloration of the reaction mixture due to the presence of FLUK hid the colorimetric response of the KI solution or that the indicator was not reliable enough to assess the presence of TBHP in reduced quantities. Therefore, neutralization with 10% NaHSO₃ solution was prolonged to 96 h and followed by GC-MS every 24 h (Figure VI-10).

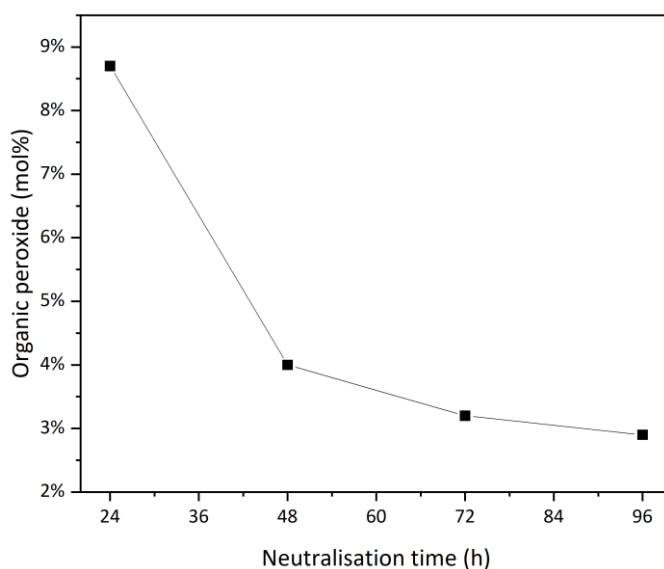
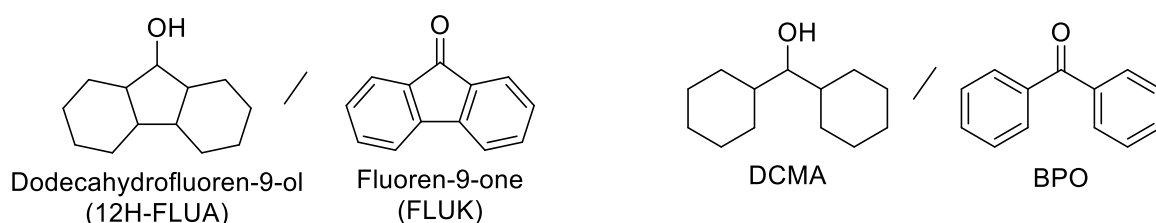


Figure VI-10 - Neutralization of the organic peroxide in the reaction mixture after regeneration. TBHP-containing reaction mixture (0.5 mL), 10% NaHSO₃ solution (10 mL/g of peroxide), room-temperature.

Unfortunately, the neutralization of TBHP was still incomplete after 96 h and reached a plateau around 3 mol% TBHP. Thus, as the neutralization of the peroxide could not be achieved and no other procedure permitted the quantitative regeneration of DPM to BPO, experiments related to the regeneration of DPM to BPO were abandoned.

VI.3 Study of the Dodecahydrofluoren-9-ol/Fluoren-9-one (12H-FLUA/FLUK) LOHC couple

As no procedure was found to efficiently regenerate the DCMA/BPO LOHC, a modification of the LOHC structure was proposed in order to test the effect of the regeneration on the cycling of a LOHC. The Dodecahydrofluoren-9-ol/Fluoren-9-one couple (12H-FLUA/FLUK) presents a structural similarity with the DCMA/BPO couple, in particular the steric hindrance of the α -carbon by an aromatic cycle. In addition, numerous reports from the literature showed that the oxidation of Fluorene (FLU) to FLUK was much more efficient than DPM to BPO, usually with a reduced reaction time and/or temperature.^{9,23-26} While FLUK is a commercially available product, 12H-FLUA and its properties are only reported in a handful instances in the literature.²⁷⁻²⁹ In addition, from a reactivity standpoint, only the hydrogenation of FLUK to 12H-FLUA was reported, but the precise conditions are not available.²⁹ The physico-chemical properties of this couple are presented in the Table VI-2.



Molecule	Melting point (°C)	Boiling point (°C)	Chemical risk	Gravimetric density H ₂ (wt.%H ₂)	Dehydrogenation enthalpy (kJ/mol H ₂)
Dodecahydrofluoren-9-ol	131	-	-	7.2	67
Fluoren-9-one	84	341	-		

Table VI-2 - Physico-chemical properties of the Perhydro-fluoren-9-ol/Fluoren-9-one LOHC couple

In the rest of this chapter, the experiments related to the hydrogenation, dehydrogenation and regeneration of the 12H-FLUA/FLUK couple will be described. Over the course of our experiments, various structures were observed that are classified in the Figure VI-11.

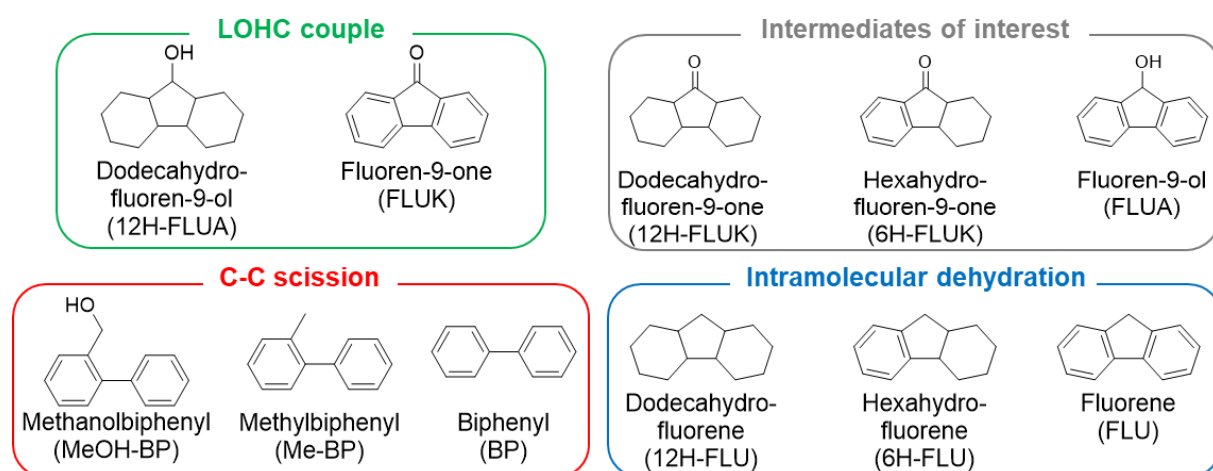


Figure VI-11 - Classification of the main products observed by GC-MS during the experiments related to 12H-FLUA/FLUK couple.

Chapter 3: Regeneration of the intramolecular dehydration products

VI.3.1 Regeneration of Fluorene to Fluoren-9-one

FLUK has a similar structure to BPO, but an increased capacity to create radicals as shown by the classically better yields obtained for the oxygenation of FLU to FLUK compared to DPM to BPO in the literature.¹⁹ Therefore, by using the procedure 2 from the Figure VI-7, FLU could be selectively oxygenated to FLUK (Figure VI-12).

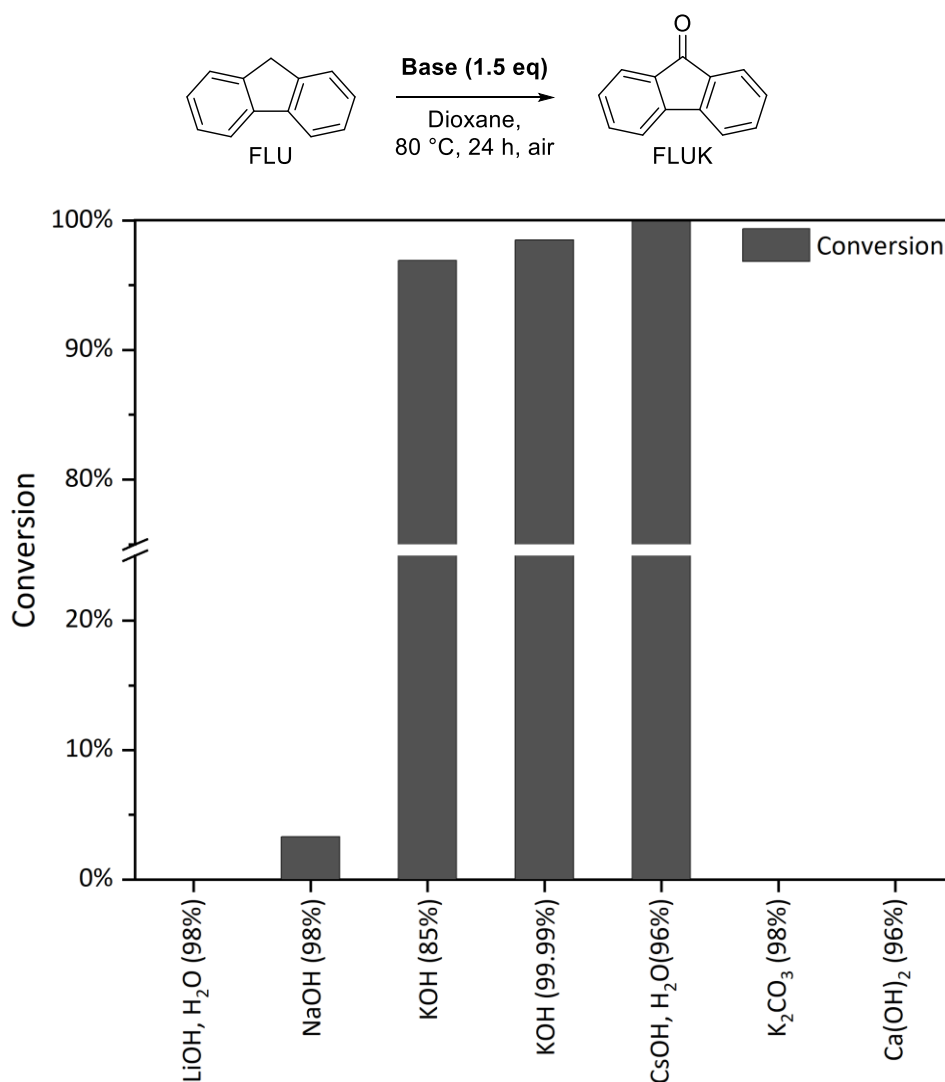


Figure VI-12 - Effect of the base on the conversion of FLU to FLUK and FLUA. Fluorene (5 mmol), base (1.5 eq), dioxane (15 mL), 24 h, 80 °C, air.

Quantitative conversion was achieved with CsOH while no conversion was observed for the weak basis K₂CO₃ despite its activity being reported in the literature.^{19,30} Aerobic oxidation of fluorene to fluorenone by hydroxyl radical was reported in numerous instances.^{31,32} Similarly to the literature, a positive correlation was observed between the increasing size of the cation and the conversion in the order Cs>K>Na>Ca=Li=0.^{19,33,34} When the reaction was scaled-up to 10 g, the conversion diminished to 47% while the selectivity was retained as analyzed by GCMS. This effect might be due to the poorer phase-transfer properties due to stirring in larger volumes. Despite the lowered regeneration efficiency, these reaction conditions were chosen as they allowed for a peroxide-free regeneration of the dehydrated LOHC structure.

Chapter 3: Regeneration of the intramolecular dehydration products

VI.3.2 Hydrogenation of FLUK

The hydrogenation of FLUK to 12H-FLUA was performed in the same conditions than developed previously and reaction optimization was carried out by modifying the temperature as presented in the Figure VI-13.

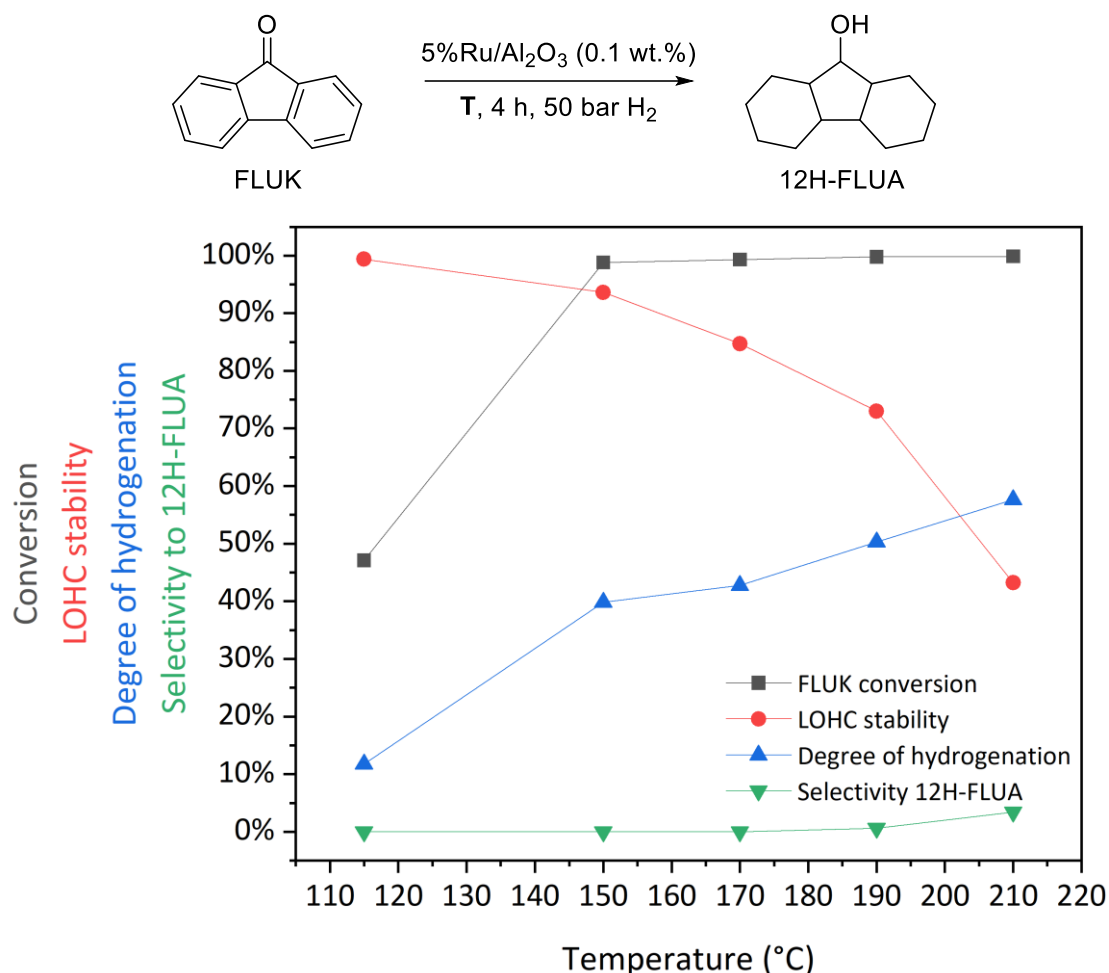


Figure VI-13 – Effect of the temperature on the hydrogenation of FLUK to 12H-FLUA. FLUK (12.5 mL), 5%Ru/Al₂O₃ (0.1 wt.% Ru with regard to FLUK), 4 h, 50 bar H₂.

The hydrogenation of FLUK was performed at temperatures ranging from 115 to 210 °C. Comparatively to the CHEA/APO and DCMA/BPO couples, a hydrogenation temperature of 110 °C was not efficient to convert selectively FLUK to 12H-FLUA. Here, the conversion rapidly increased to >95% at 150 °C but the system stability also started to decrease from that temperature onwards. Finally, the degree of hydrogenation (DoH) was below 60% at all temperatures, indicating an incomplete reaction. Indeed, the reaction was not selective to 12H-FLUA which started to appear in the reaction mixture only at 190 °C.

To improve the hydrogenation progress, the catalyst amount was increased to 0.2 wt.%. The presence of more catalyst was beneficial with regard to the selectivity to 12H-FLUA with an optimum around 200 °C as shown in Figure VI-14.

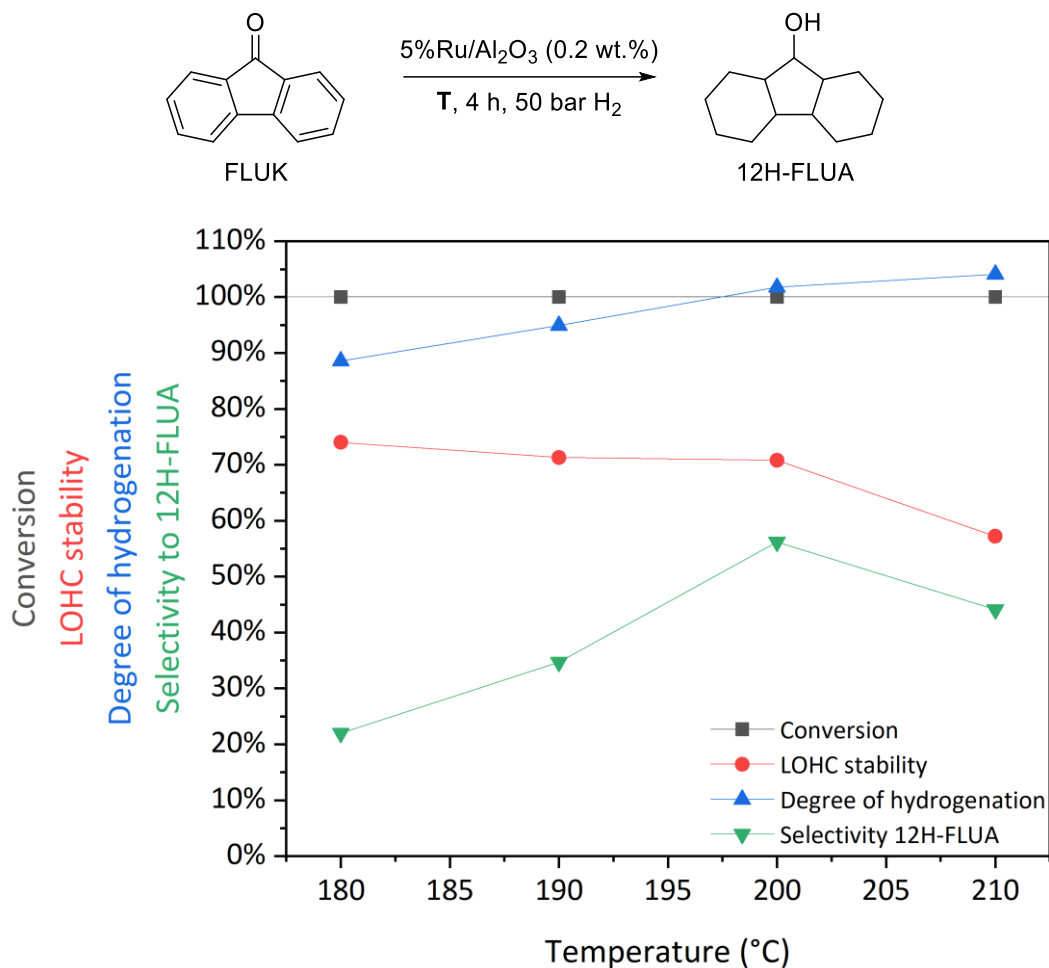


Figure VI-14 - Effect of the temperature on the hydrogenation of FLUK to 12H-FLUA. FLUK (12.5 mL), 5%Ru/Al₂O₃ (0.2 wt.% Ru with regard to FLUK), 4 h, 50 bar H₂.

Degree of hydrogenation above 100% were obtained due to the over-consumption of H₂ related to the dehydration of the LOHC structure. Over 100% values were not observed for the CHEA/APO and DCMA/BPO couples as the dehydration was much lower in these instances. Therefore, a temperature of 200 °C was chosen to carry out the hydrogenation in the following cycling.

VI.3.3 Purification of 12H-FLUA

As the hydrogenated 12H-FLUA product is not commercially available, it was purified from hydrogenation experiments by column chromatography using a petroleum ether/Diethyl ether mixture in a 15:2 ratio as the solvent system. The purity of the purified products was assessed by ¹H-NMR, ¹³C-NMR, FTIR (Appendix VI-1). Interestingly, 12H-FLUA possesses different stereoisomers as observed by GC-MS (Appendix VI-2). Such structures were probable as they were observed for the analogous perhydro-N-Ethylcarbazole, indicating isomerization of the LOHC structure on the hydrogenation catalyst by a desorption/readsorption mechanism due to either a weak 12H-FLUA-metal interaction or the hydrophilicity of the support surface as well as low temperatures yielding more kinetically favoured isomers as it was proposed for 12H-NEC in the literature (Figure VI-15).^{35,36}

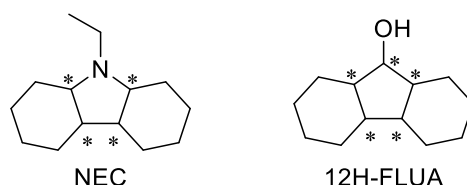


Figure VI-15 - Comparison of the 12H-NEC and the 12H-FLUA structures. The asymmetric carbons are marked by an asterisk *.

Based on the structures presented in the Figure VI-15, the 12H-FLUA structure could present 32 isomers due to the 5 asymmetric carbons (2^5). However, due to the symmetric aspect of the structure, only 12 isomers can form as presented in the Figure VI-16.

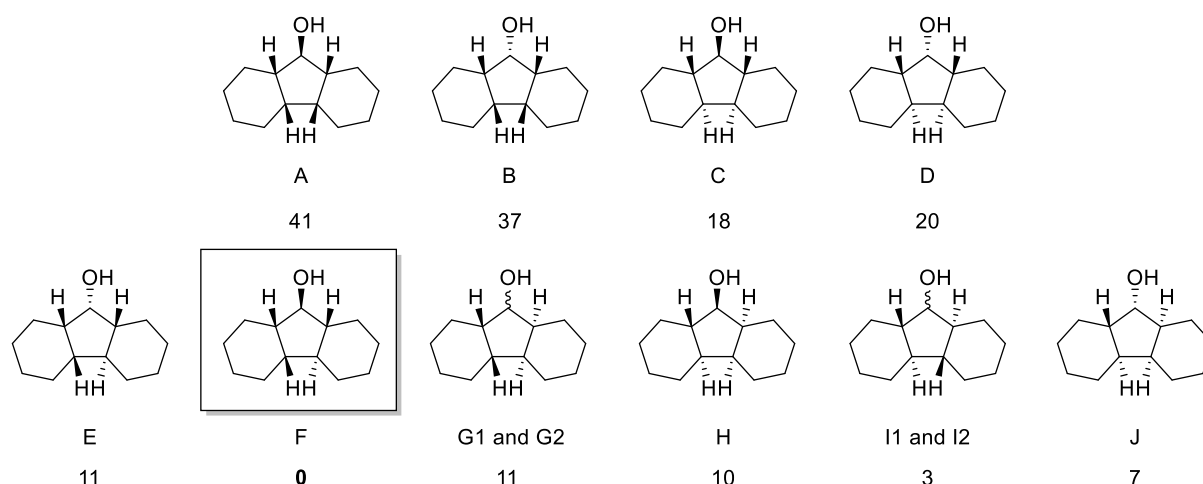


Figure VI-16 - Isomers of the 12H-FLUA compound. The first line (A-D) corresponds to the symmetric isomers, the second line (E-J) to the asymmetric isomers. The isomers G1 and G2 (reps. I1 and I2) are enantiomers. The value under each isomer corresponds to the energy difference in kJ/mol with the structure F and was calculated by DFT (Gaussian 9, M062X, 6-311g+(2d, p)).

As 12H-FLUA is similar to 12H-NEC, their ^{13}C NMR properties should also be similar. Therefore, symmetric structures should present 7 ^{13}C resonances while asymmetric structures should have 13. From our ^{13}C NMR experiments, only structures with 13 vibrations were observed, hence we could only confirm the formation of the asymmetric isomers of 12H-FLUA (Appendix VI-1). DFT calculations performed with the method previously described showed that not all isomers are of equivalent energy. In particular, symmetric isomers present much higher energies than the asymmetric isomers (Figure VI-16), thus rationalizing why symmetric structures were not observed. During the purification of the hydrogenated products, different spots were attributed to 12H-FLUA by thin layer-chromatography, indicating that such isomers could potentially be separated. However, despite our attempts, the separation of the corresponding isomers could not be achieved.

Chapter 3: Regeneration of the intramolecular dehydration products

VI.3.4 Dehydrogenation of 12H-FLUA

The dehydrogenation was performed by using the same Pt/C catalyst than the previous experiments with APO and BPO (Figure VI-17).

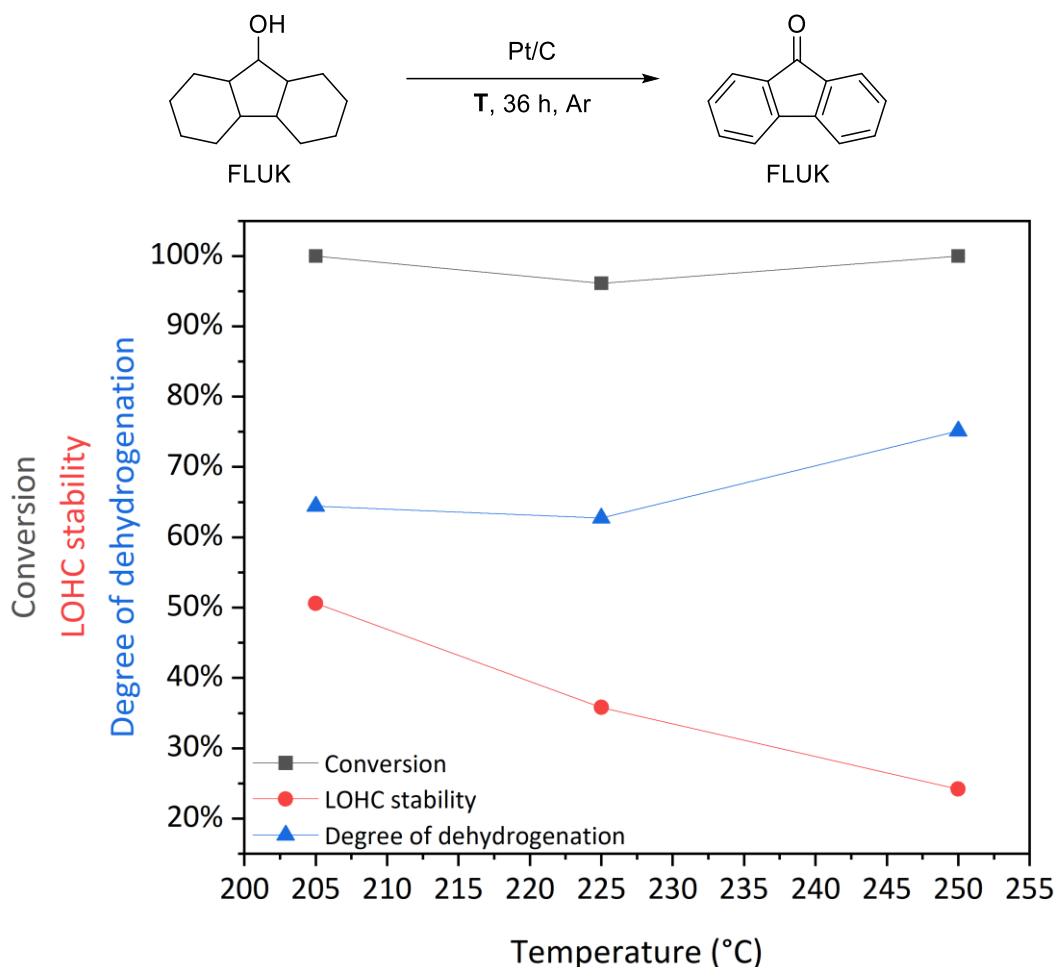


Figure VI-17 - Effect of the temperature on the dehydrogenation of 12H-FLUA to FLUK. 12H-FLUA (1 g), 5%Pt/C (0.25 wt.% with regard to 12H-FLUA), 36 h, Ar.

Temperature experiments showed a rapid LOHC stability decrease when increasing the reaction temperature. In order to compare the cycling of the DCMA/BPO couple with the 12H-FLUA/FLUK couple, a dehydrogenation temperature of 225°C was chosen.

Chapter 3: Regeneration of the intramolecular dehydration products

VI.3.5 Cycling

The cycling of the 12H-FLUA/FLUK LOHC was performed in the previously developed conditions. Here, two different cyclings were conducted in order to assess the efficiency of the regeneration of the LOHC. The cycling conditions with and without regeneration are presented in the Figure VI-18.

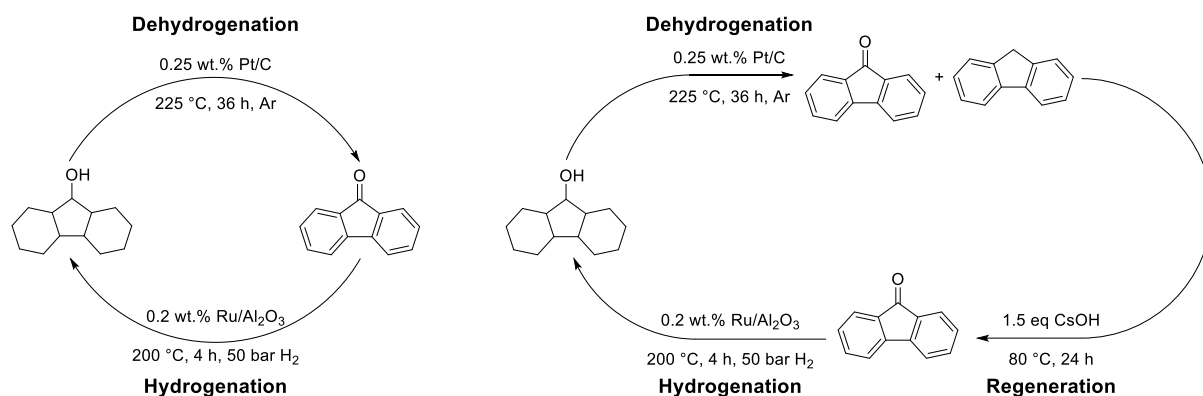


Figure VI-18 - Cycling conditions. Left: without regeneration. Right: with regeneration.

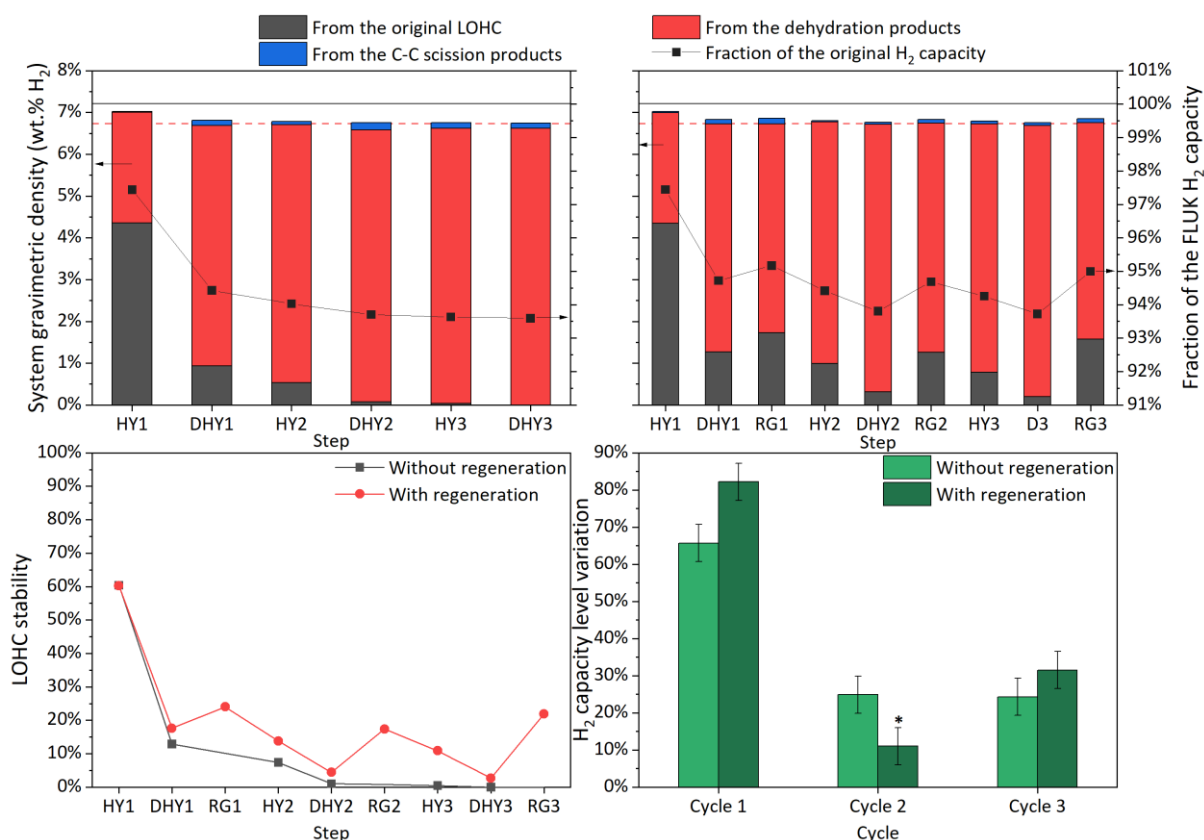


Figure VI-19 - Top-left: cycling without regeneration. Top-right: cycling with regeneration. Bottom-left: comparison of the system stability without (black) and with regeneration (red). Bottom-right: H₂ capacity level variation for the cycling without regeneration (black) and with regeneration (red). HY: hydrogenation; DHY: dehydrogenation; *: the magnetic stirrer got stuck during the regeneration, limiting its efficiency.

Complete dehydration of the LOHC structure was observed after 3 cycles without regeneration. The dehydration linked with a rapid diminution of the system gravimetric density from 7.2% to 6.7%, equivalent to a loss of roughly 6.5% of the original FLUK gravimetric density (Figure VI-19-top-left).

Chapter 3: Regeneration of the intramolecular dehydration products

Conversely, the cycling with regeneration also showed a diminution of the gravimetric density that was limited to 6.9%, equivalent to a loss of 5% of the original FLUK gravimetric density (Figure VI-19-top-right). Similarly, the LOHC stability diminished to 0% after 3 cycles without regeneration and was kept at 22% with regeneration (Figure VI-19-bottom-left). Finally, when comparing the exploited H₂ capacity, both rapidly decreased after 3 cycles, but the regeneration allowed for an overall better exploitation of the H₂ capacity of the system for the cycles 1 and 3 (Figure VI-19-bottom-right). The reduction of the exploited H₂ capacity during the cycling could be due to the reduced activity of the catalyst for the dehydrated species. Indeed, homocyclic structures usually require reactions temperatures above 250 °C to be efficiently catalyzed.³⁷

VI.3.6 Analysis of the impurities

Nevertheless, the coloration of the LOHC was different depending on the presence or the absence of the regeneration step. Indeed, for the cycling without regeneration, the LOHC was forming white-grey crystals, similar to that of Fluorene, which was confirmed by ¹H-NMR and XRD (Appendix VI-3 and VI-4). Conversely, the LOHC after regeneration was not yellow like FLUK, but orange-red. 9,9'-bifluorenylidene (Figure VI-20) is a potential impurity well known to be orange-red that was first hypothesized as the impurity.^{38,39}

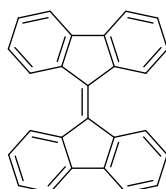


Figure VI-20 - 9,9'-Bifluorenylidene dimer formed during the regeneration.

Further ¹H NMR analysis of the reaction mixture after 3 cycles with regeneration presented a peak at 8.54 ppm that was incompatible with the 9,9'-Bifluorenylidene dimer and revealed the influence of the regeneration on the formation of this impurity (Appendix VI-5). MS-APCI analysis showed that a Polyfluorene structure formed, but the precise carbons where the monomers link are still unclear (Figure VI-21).⁴⁰

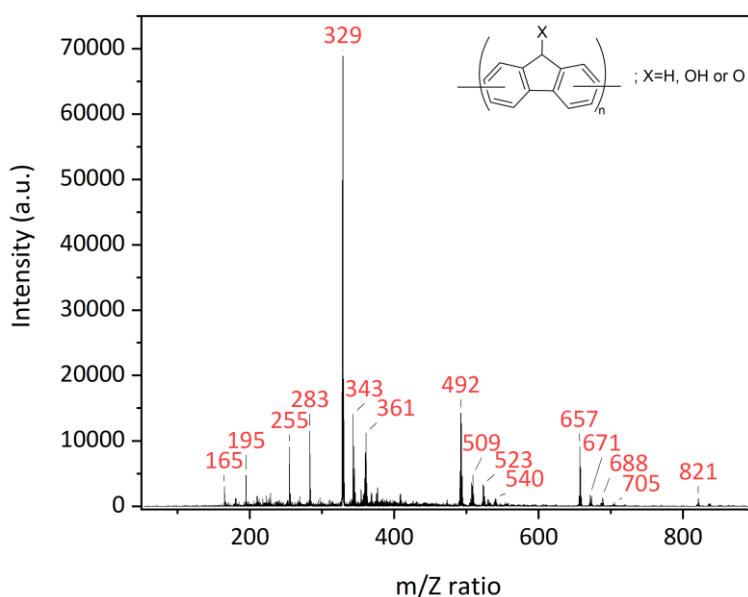


Figure VI-21 –APCI-MS negative polarization analysis of the reaction mixture after the regeneration of FLU to FLUK and the associated polymer structure.

Chapter 3: Regeneration of the intramolecular dehydration products

From a color perspective, these oligomers are also known to be orange-red, confirming the color modification of the LOHC.⁴¹ MALDI-TOF analysis confirmed these results, with a monomer unit of $m/z=162-164$ (Figure VI-22).

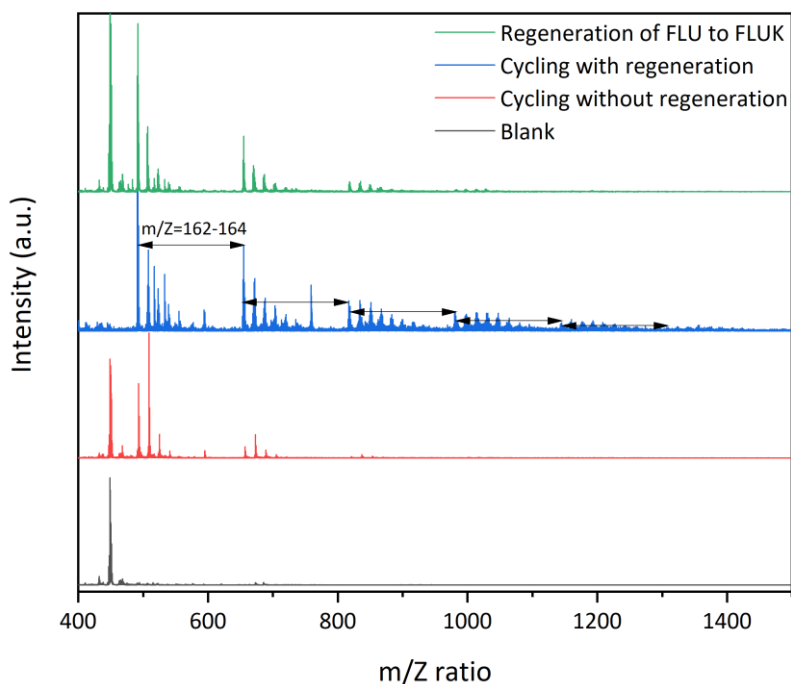


Figure VI-22 - MALDI-TOF comparison of the reaction mixture after three cycles with regeneration, without regeneration and regeneration of FLU to FLUK. Comparison with the blank of the matrix. Each group of peaks is separated by a $m/Z=162-164$.

Moreover, each peak was subdivided with peaks separated by 15-18 m/Z that were attributed to the presence or absence of oxygen atoms on the oligomer (Figure VI-23).

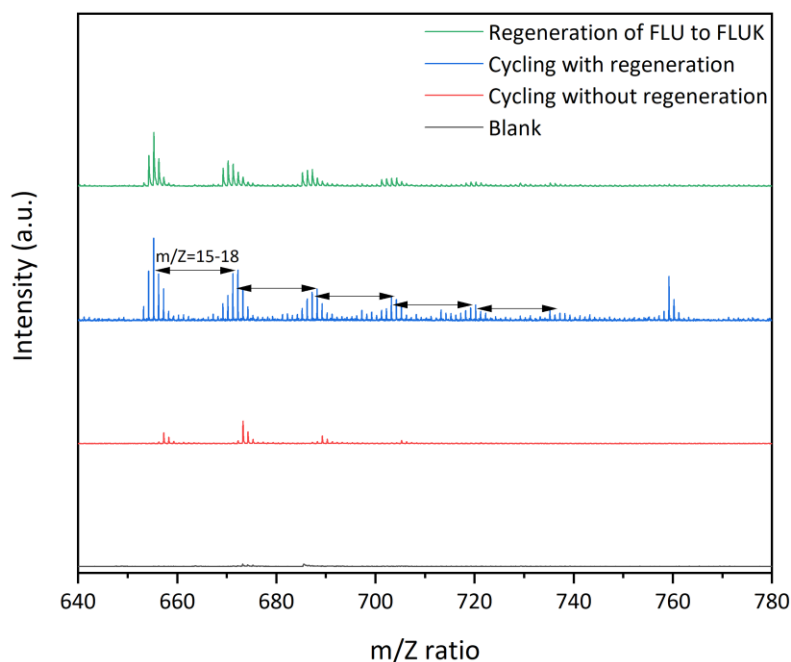


Figure VI-23 - MALDI-TOF comparison of the reaction mixture after the cyclings with regeneration, without regeneration and regeneration of FLU to FLUK. Comparison with the blank of the matrix. Each subpeak is separated by a $m/Z=15-18$.

Chapter 3: Regeneration of the intramolecular dehydration products

Here, the regeneration was confirmed to be responsible for the formation of Polyfluorene during the cycling. However, the post-cycling MALDI-TOF analysis without regeneration after 3 cycles also showed traces of similar oligomer peaks. Nonetheless, the oligomerization seemed less advanced for the latter. ¹H NMR comparison of the three reaction mixtures showed that Polyfluorene was forming in limited quantity during the cycling without regeneration as the characteristic doublet at 8.54 ppm was not observed (Figure VI-24 and Appendix VI-6).

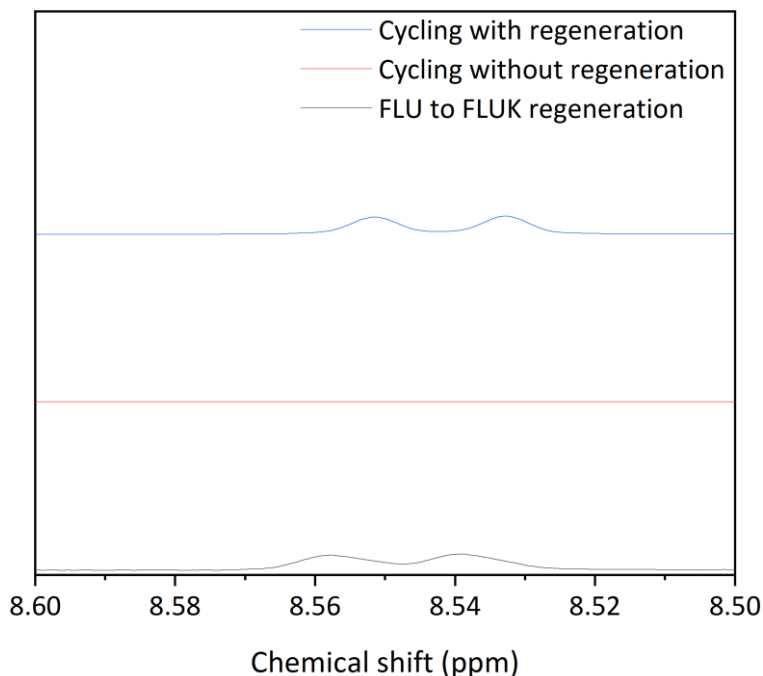
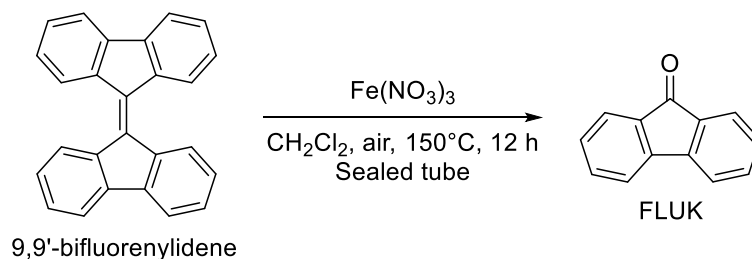


Figure VI-24 - ¹H-NMR comparison of the reaction mixture after the cyclings with regeneration, without regeneration and regeneration of FLU to FLUK.

Moreover, NMR and XRD analysis showed that the main product of the cycling without regeneration was FLU without any trace of Polyfluorene. Therefore, it is possible that either the polymer structure is completely different or in insufficient quantity to be analyzed by NMR. Also, no XRD peaks similar to the reaction mixture after the cycling with regeneration were obtained for the cycling without regeneration, inducing that, if an oligomer is formed, the structure might not be crystalline. (Appendix VI-7)

The cleavage of the oligomer bond to form back the FLU, FLUA and FLUK monomers was attempted. By following a procedure from the literature known to efficiently cleave double bonds in structures similar to 9,9'-Bifluorenylidene, only more degradation of the carrier was observed. (Scheme VI-2).⁴²



Scheme VI-2 – Conversion of the 9,9'-Bifluorenylidene to FLUK following the procedure from⁴².

Hence, this experiment confirmed that the impurity had a form similar to Polyfluorene where each monomer is linked by single bonds, thus the cleavage could not be achieved.

VI.4 Conclusion

The regeneration of the alkylarenes was limited with DPM. Numerous catalytic conditions were probed, with only the use of strong organic peroxides like TBHP favoring the production of BPO. Nevertheless, their neutralization in the reaction mixture was incomplete even after 3 days of neutralization with an excess of NaHSO_3 . In consequence, a new couple, 12H-FLUA/FLUK, was proposed due to its enhanced reactivity towards the oxygenation in order to study the effect the regeneration on the cycling of the LOHC. After 3 cycles, the cycling without regeneration afforded the completely dehydrated structure while the cycling with regeneration limited this side-reaction by introducing back the oxygen atom. The comparison of the exploited H_2 capacity showed that the oxygenated structure produced more H_2 over the cycling compared to the dehydrated one. This difference might come from the reduced reactivity of the homocyclic carrier as they usually require higher reaction temperature. Nevertheless, MALDI TOF and APCI-MS analysis revealed that oligomerization of the structure was a side-reaction. In particular, an oligomer with a unit of $m/z = 162-164$ was detected by APCI. However, attempts to form back the Fluoren-9-one was unsuccessful. Here, conversely to the previous chapters, APCI-MS and MALDI-TOF analysis revealed the presence of oligomers. Therefore, we can induce that the CHEA/APO and DCMA/BPO couples did not produce a significant amount of oligomers. Nonetheless, the negative influence of the ketone was observed over the course of the past three chapters as it induced several side-reactions as well as hindered the dehydrogenation kinetics. Thus, for the last chapter of this thesis, a new LOHC couple already assessed in our first choice of molecules (see Chapter 1), Cyclohexylmethanol/Benzylbenzoate, was suggested. By replacing the ketone by an ester, the LOHC structure could potentially be more stable and less sensitive to retro-hydrogenation during the dehydrogenation, hence increase the kinetics during the dehydrogenation.

Bibliography

- (1) Miura, H.; Nakahara, K.; Kitajima, T.; Shishido, T. Concerted Functions of Surface Acid–Base Pairs and Supported Copper Catalysts for Dehydrogenative Synthesis of Esters from Primary Alcohols. *ACS Omega* **2017**, *2* (9), 6167–6173. <https://doi.org/10.1021/acsomega.7b01142>.
- (2) Pampararo, G.; Garbarino, G.; Riani, P.; Villa García, M.; Sánchez Escribano, V.; Busca, G. A Study of Ethanol Dehydrogenation to Acetaldehyde over Supported Copper Catalysts: Catalytic Activity, Deactivation and Regeneration. *Applied Catalysis A: General* **2020**, *602*, 117710. <https://doi.org/10.1016/j.apcata.2020.117710>.
- (3) Sanders, H. J.; Keag, H. F.; McCullough, H. S. ACETOPHENONE. *Ind. Eng. Chem.* **1953**, *45* (1), 2–14. <https://doi.org/10.1021/ie50517a017>.
- (4) Hermans, I.; Peeters, J.; Jacobs, P. A. Autoxidation of Ethylbenzene: The Mechanism Elucidated. *J. Org. Chem.* **2007**, *72* (8), 3057–3064. <https://doi.org/10.1021/jo070040m>.
- (5) Romero, M. D.; Aguado, J.; Arriaga, M.; García, A.; Díaz, I. Effect of Final Products on the Kinetics of 1-Phenylethanol Oxidation with Air. *Chemical Engineering Research and Design* **2011**, *89* (11), 2442–2447. <https://doi.org/10.1016/j.cherd.2011.07.017>.
- (6) Zhang, P.; Lu, H.; Zhou, Y.; Zhang, L.; Wu, Z.; Yang, S.; Shi, H.; Zhu, Q.; Chen, Y.; Dai, S. Mesoporous MnCeOx Solid Solutions for Low Temperature and Selective Oxidation of Hydrocarbons. *Nat Commun* **2015**, *6* (1), 8446. <https://doi.org/10.1038/ncomms9446>.
- (7) Wang, A.; Zhou, W.; Sun, Z.; Zhang, Z.; Zhang, Z.; He, M.; Chen, Q. Mn(III) Active Site in Hydrotalcite Efficiently Catalyzes the Oxidation of Alkylarenes with Molecular Oxygen. *Molecular Catalysis* **2021**, *499*, 111276. <https://doi.org/10.1016/j.mcat.2020.111276>.
- (8) Alan C. Cooper. *Design and Development of New Carbon-Based Sorbent Systems for an Effective Containment of Hydrogen*; 86-377-P, 1039432; 2012; pp 86-377-P, 1039432. <https://doi.org/10.2172/1039432>.
- (9) Kanarat, J.; Bunchuay, T.; Klysubun, W.; Tantirungrotechai, J. Cu₂O–CuO/Chitosan Composites as Heterogeneous Catalysts for Benzylic C–H Oxidation at Room Temperature. *ChemCatChem* **2021**, *13* (22), 4833–4840. <https://doi.org/10.1002/cctc.202101187>.
- (10) Xiong, Y.; Sun, W.; Han, Y.; Xin, P.; Zheng, X.; Yan, W.; Dong, J.; Zhang, J.; Wang, D.; Li, Y. Cobalt Single Atom Site Catalysts with Ultrahigh Metal Loading for Enhanced Aerobic Oxidation of Ethylbenzene. *Nano Res.* **2021**, *14* (7), 2418–2423. <https://doi.org/10.1007/s12274-020-3244-4>.
- (11) Kamata, K.; Kasai, J.; Yamaguchi, K.; Mizuno, N. Efficient Heterogeneous Oxidation of Alkylarenes with Molecular Oxygen. *Org. Lett.* **2004**, *6* (20), 3577–3580. <https://doi.org/10.1021/ol0485363>.
- (12) Nie, S.; Wang, J.; Huang, X.; Niu, X.; Zhu, L.; Yao, X. Ball-Milled Co–N–C Nanocomposite for Benzylic C–H Bond Oxidation: A Facile, Practical, and Recyclable Catalyst under Neat Conditions and Atmospheric Pressure Oxygen. *ACS Appl. Nano Mater.* **2018**, *1* (12), 6567–6574. <https://doi.org/10.1021/acsanm.8b01607>.
- (13) Chang, F.; Li, W.; Xia, F.; Yan, Z.; Xiong, J.; Wang, J. Highly Selective Oxidation of Diphenylmethane to Benzophenone over Co/MCM-41. *Chem. Lett.* **2005**, *34* (11), 1540–1541. <https://doi.org/10.1246/cl.2005.1540>.
- (14) Peng, M. M.; Ganesh, M.; Vinodh, R.; Palanichamy, M.; Jang, H. T. Solvent Free Oxidation of Ethylbenzene over Ce-BTC MOF. *Arabian Journal of Chemistry* **2019**, *12* (7), 1358–1364. <https://doi.org/10.1016/j.arabjc.2014.11.024>.
- (15) Zhang, J.; Du, J.; Zhang, C.; Liu, K.; Yu, F.; Yuan, Y.; Duan, B.; Liu, R. Selective Oxidation of Alkylarenes to the Aromatic Ketones or Benzaldehydes with Water. *Org. Lett.* **2022**, *24* (5), 1152–1157. <https://doi.org/10.1021/acscorglett.1c04154>.
- (16) Wang, L.; Zhang, M.; Zhang, M.; Sha, G.; Liang, C. Hydrodeoxygenation of Dibenzofuran over Mesoporous Silica COK-12 Supported Palladium Catalysts. *Energy Fuels* **2013**, *27* (4), 2209–2217. <https://doi.org/10.1021/ef302166q>.
- (17) Shaabani, A.; Rahmati, A.; Sharifi, M.; Rad, J. M.; Aghaaliakbari, B.; Farhangi, E.; Lee, D. G. Green Oxidations. Manganese(II) Sulfate Aided Oxidations of Organic Compounds by Potassium Permanganate. *Monatsh. Chem.* **2007**, *138* (7), 649–651. <https://doi.org/10.1007/s00706-007-0667-5>.
- (18) He, C.; Zhang, X.; Huang, R.; Pan, J.; Li, J.; Ling, X.; Xiong, Y.; Zhu, X. Synthesis of Structurally Diverse Diarylketones through the Diarylmethyl Sp³ CH Oxidation. *Tetrahedron Letters* **2014**, *55* (32), 4458–4462. <https://doi.org/10.1016/j.tetlet.2014.06.047>.

Chapter 3: Regeneration of the intramolecular dehydration products

- (19) Zhang, X.; Ji, X.; Jiang, S.; Liu, L.; L. Weeks, B.; Zhang, Z. Highly Efficient Synthesis of 9-Fluorenones from 9 H -Fluorenes by Air Oxidation. *Green Chemistry* **2011**, *13* (7), 1891–1896. <https://doi.org/10.1039/C1GC15136C>.
- (20) Tan, J.; Zheng, T.; Yu, Y.; Xu, K. TBHP-Promoted Direct Oxidation Reaction of Benzylic Csp³-H Bonds to Ketones. *RSC Adv.* **2017**, *7* (25), 15176–15180. <https://doi.org/10.1039/C7RA00352H>.
- (21) Read "Prudent Practices in the Laboratory: Handling and Disposal of Chemicals" at NAP.Edu. <https://doi.org/10.17226/4911>.
- (22) Armour, M.-A. Hazardous Laboratory Chemicals Disposal Guide.
- (23) Xu, B.; Xu, Q.; Wang, Q.; Liu, Z.; Zhao, R.; Li, D.; Ma, P.; Wang, J.; Niu, J. A Copper-Containing Polyoxometalate-Based Metal–Organic Framework as an Efficient Catalyst for Selective Catalytic Oxidation of Alkylbenzenes. *Inorg. Chem.* **2021**, *60* (7), 4792–4799. <https://doi.org/10.1021/acs.inorgchem.0c03741>.
- (24) Nakai, S.; Uematsu, T.; Ogasawara, Y.; Suzuki, K.; Yamaguchi, K.; Mizuno, N. Aerobic Oxygenation of Alkylarenes over Ultrafine Transition-Metal-Containing Manganese-Based Oxides. *ChemCatChem* **2018**, *10* (5), 1096–1106. <https://doi.org/10.1002/cctc.201701587>.
- (25) Albadi, J.; Alihosseinzadeh, A.; Jalali, M.; Mansournezhad, A. Highly Selective Aerobic Oxidation of Alkylarenes Catalyzed by Cobalt-Based Nanocatalyst in Aqueous Solution. *Applied Organometallic Chemistry* **2018**, *32* (3), e4193. <https://doi.org/10.1002/aoc.4193>.
- (26) Kuwahara, Y.; Yoshimura, Y.; Yamashita, H. Liquid-Phase Oxidation of Alkylaromatics to Aromatic Ketones with Molecular Oxygen over a Mn-Based Metal–Organic Framework. *Dalton Trans.* **2017**, *46* (26), 8415–8421. <https://doi.org/10.1039/C7DT01351E>.
- (27) Rayhan, U.; Do, J.-H.; Arimura, T.; Yamato, T. Reduction of Carbonyl Compounds by Raney Ni–Al Alloy and Al Powder in the Presence of Noble Metal Catalysts in Water. *Comptes Rendus Chimie* **2015**, *18* (6), 685–692. <https://doi.org/10.1016/j.crci.2014.10.011>.
- (28) House, H. O.; Paragamian, V.; Ro, R. S.; Wluka, D. J. The Synthesis of Hexahydrofluorenone Derivatives. *J. Am. Chem. Soc.* **1960**, *82* (6), 1457–1462. <https://doi.org/10.1021/ja01491a045>.
- (29) Tsutsumi K.; 堤聖晴; Itokazu T.; 糸数輝雄. フォトリジスト用化合物およびフォトリジスト用樹脂組成物 (Photoresistive compound and photoresistive resin composition). JP2002265530A, September 18, 2002. <https://patents.google.com/patent/JP2002265530A/en?qoq=%E5%85%AC%E9%96%8B%E7%89%B9%E8%A8%B1%E5%85%AC%E5%A0%B1+JP2002-265530A> (accessed 2023-01-03).
- (30) Park, K. K.; Tsou, L. K.; Hamilton, A. D. Facile and Selective Aerobic Oxidation of Arylalkanes to Aryl Ketones Using Cesium Carbonate. *Synthesis* **2006**, *2006* (21), 3617–3620. <https://doi.org/10.1055/s-2006-950189>.
- (31) Kwok, E. S. C.; Atkinson, R.; Arey, J. Kinetics of the Gas-Phase Reactions of Indan, Indene, Fluorene, and 9,10-Dihydroanthracene with OH Radicals, NO₃ Radicals, and O₃. *International Journal of Chemical Kinetics* **1997**, *29* (4), 299–309. [https://doi.org/10.1002/\(SICI\)1097-4601\(1997\)29:4<299::AID-KIN9>3.0.CO;2-P](https://doi.org/10.1002/(SICI)1097-4601(1997)29:4<299::AID-KIN9>3.0.CO;2-P).
- (32) Ding, Z.; Yi, Y.; Zhang, Q.; Zhuang, T. Theoretical Investigation on Atmospheric Oxidation of Fluorene Initiated by OH Radical. *Science of The Total Environment* **2019**, *669*, 920–929. <https://doi.org/10.1016/j.scitotenv.2019.02.400>.
- (33) Yamashita, J.; Ishikawa, S.; Hashimoto, H. Base-Catalyzed Autoxidation of Fluorene in the Presence of Phase Transfer Catalysts. *BCSJ* **1980**, *53* (3), 736–739. <https://doi.org/10.1246/bcsj.53.736>.
- (34) Shannon, R. D. Revised Effective Ionic Radii and Systematic Studies of Interatomic Distances in Halides and Chalcogenides. *Acta Cryst A* **1976**, *32* (5), 751–767. <https://doi.org/10.1107/S0567739476001551>.
- (35) Morawa Eblagon, K.; Tam, K.; Edman Tsang, S. C. Comparison of Catalytic Performance of Supported Ruthenium and Rhodium for Hydrogenation of 9-Ethylcarbazole for Hydrogen Storage Applications. *Energy & Environmental Science* **2012**, *5* (9), 8621–8630. <https://doi.org/10.1039/C2EE22066K>.
- (36) Eblagon, K. M.; Tam, K.; Yu, K. M. K.; Tsang, S. C. E. Comparative Study of Catalytic Hydrogenation of 9-Ethylcarbazole for Hydrogen Storage over Noble Metal Surfaces. *J. Phys. Chem. C* **2012**, *116* (13), 7421–7429. <https://doi.org/10.1021/jp212249g>.
- (37) Brückner, N.; Obesser, K.; Bösmann, A.; Teichmann, D.; Arlt, W.; Dungs, J.; Wasserscheid, P. Evaluation of Industrially Applied Heat-Transfer Fluids as Liquid Organic Hydrogen Carrier Systems. *ChemSusChem* **2014**, *7* (1), 229–235. <https://doi.org/10.1002/cssc.201300426>.
- (38) Clar, E. *Polycyclic Hydrocarbons*; ACADEMIC PRESS INC (LONDON) LTD, 1964; Vol. 2. <https://doi.org/10.1007/978-3-662-01668-8>.
- (39) Eisch, J. J.; Fregene, P. O. Vanadium(I) Chloride and Lithium Vanadium(I) Dihydride as Selective Epimetallating Reagents for π - and σ -Bonded Organic Substrates. *European Journal of Organic Chemistry* **2008**, *2008* (26), 4482–4492. <https://doi.org/10.1002/ejoc.200800461>.

Chapter 3: Regeneration of the intramolecular dehydration products

- (40) Assadi, N.; Pogodin, S.; Agranat, I. Peterson Olefination: Unexpected Rearrangement in the Overcrowded Polycyclic Aromatic Ene Series. *European Journal of Organic Chemistry* **2011**, *2011* (33), 6773–6780. <https://doi.org/10.1002/ejoc.201100789>.
- (41) Liu, J.; Shao, S. Y.; Chen, L.; Xie, Z. Y.; Cheng, Y. X.; Geng, Y. H.; Wang, L. X.; Jing, X. B.; Wang, F. S. White Electroluminescence from a Single Polymer System: Improved Performance by Means of Enhanced Efficiency and Red-Shifted Luminescence of the Blue-Light-Emitting Species. *Adv. Mater.* **2007**, *19* (14), 1859–1863. <https://doi.org/10.1002/adma.200602942>.
- (42) Amaya, T.; Fujimoto, H. Iron(III) Nitrate-Induced Aerobic and Catalytic Oxidative Cleavage of Olefins. *Tetrahedron Letters* **2018**, *59* (27), 2657–2660. <https://doi.org/10.1016/j.tetlet.2018.05.070>.
- (43) Fluorene(86-73-7) ¹H NMR spectrum. https://www.chemicalbook.com/SpectrumEN_86-73-7_1HNMR.htm (accessed 2023-01-27).
- (44) Fluorene(86-73-7) ¹³C NMR spectrum. https://www.chemicalbook.com/SpectrumEN_86-73-7_13CNMR.htm (accessed 2023-01-27).
- (45) Dong, B.; Song, D.; Zheng, L.; Xu, J.; Li, N. Electrosynthesis of Polyfluorene in an Ionic Liquid and Characterization of Its Stable Electrocatalytic Activity for Formic Acid Oxidation. *Journal of Electroanalytical Chemistry* **2009**, *633* (1), 63–70. <https://doi.org/10.1016/j.jelechem.2009.04.032>.

Appendix

Appendix VI-1 - 12H-FLUA analysis

White cristal

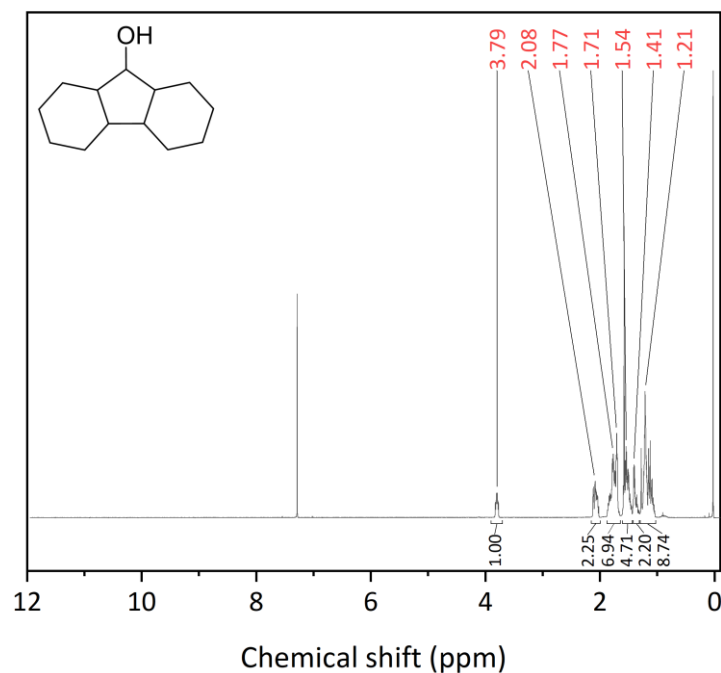


Figure VI-25 – $^1\text{H-NMR}$ analysis of the purified 12H-FLUA in CDCl_3 .

$^1\text{H NMR}$ (CDCl_3) δ =1.01-1.30 (9H, m), 1.3–1.43 (2H, m), 1.44-1.62 (5H, m), 1.66–1.89 (7H, m), 2.00-2.13 (2H, m), 3.79 (1H, m).

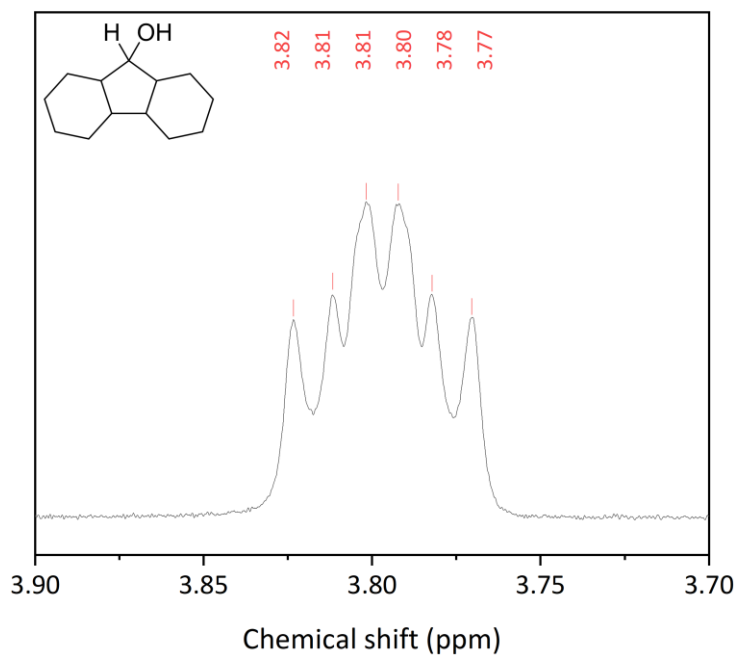


Figure VI-26 - $^1\text{H-NMR}$ analysis of the purified 12H-FLUA in CDCl_3 . Zoom on the multiple at 3.79 ppm.

Multiplet at 3.79 ppm: not a sextuplet as the 1 5 10 10 5 1 intensities are not respected. This indicates a fusion of triplets and therefore more than 1 isomer.

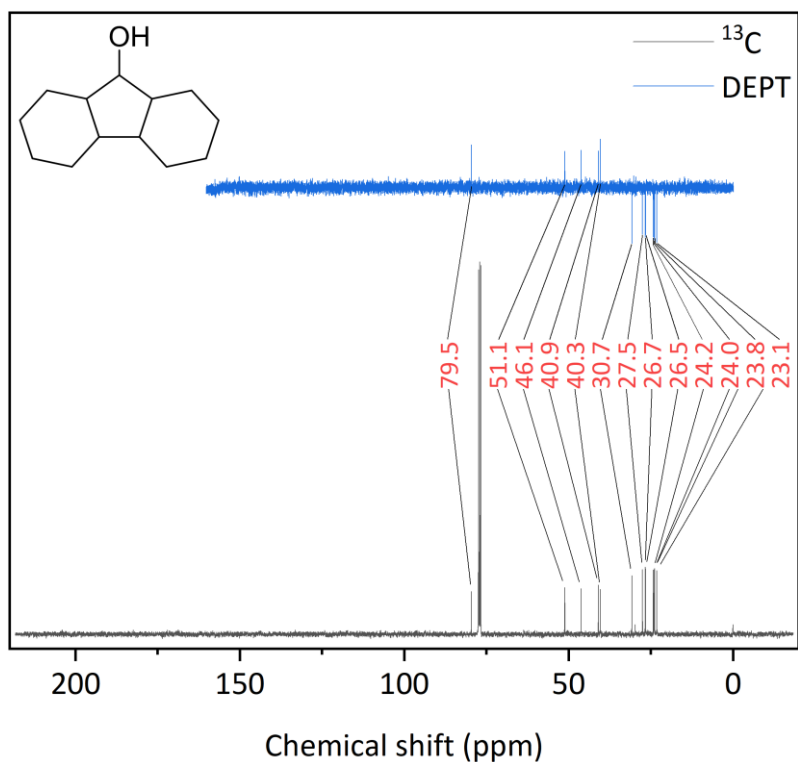


Figure 27 – ^{13}C -NMR and DEPT analysis of the purified 12H-FLUA in CDCl_3 .

^{13}C NMR (CDCl_3) δ =23.1 (s), 23.8 (s), 24.0 (s), 24.2 (s), 26.5 (s), 26.7(s), 27.5 (s), 30.7 (s), 40.3 (t), 40.9 (t), 46.1 (t), 51.1 (t), 79.5 (t)

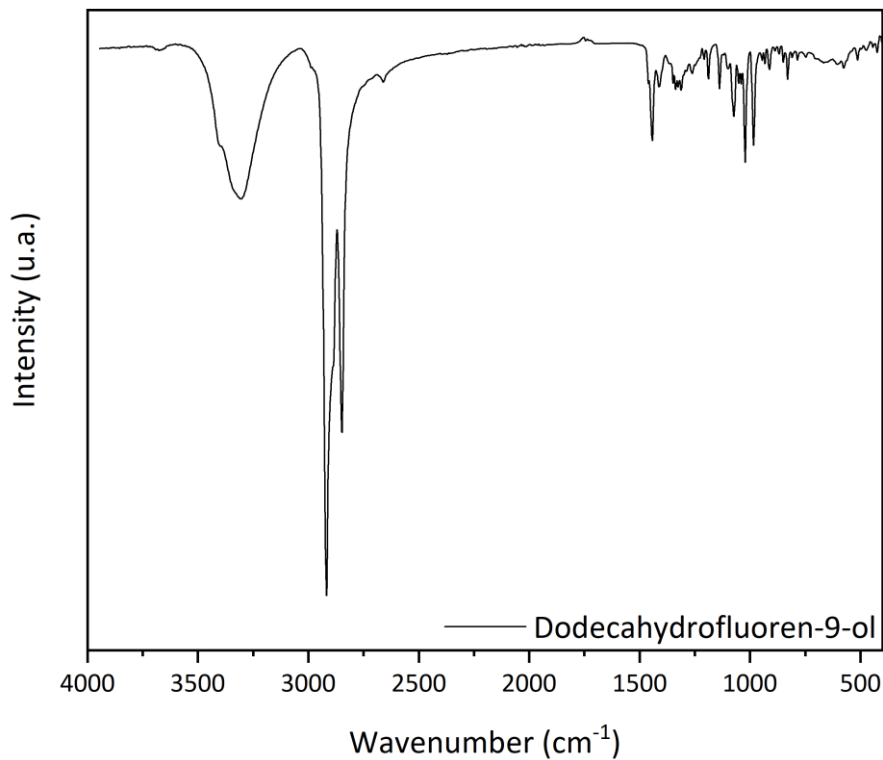


Figure VI-28 - FTIR-ATR analysis of the purified 12H-FLUA.

IR (neat): alcohol: 3300 cm^{-1} ; C sp 3 : $2918, 2848, 1444, 1022\text{ cm}^{-1}$

Chapter 3: Regeneration of the intramolecular dehydration products

Appendix VI-2 - GC-MS analysis of the purified 12H-FLUA

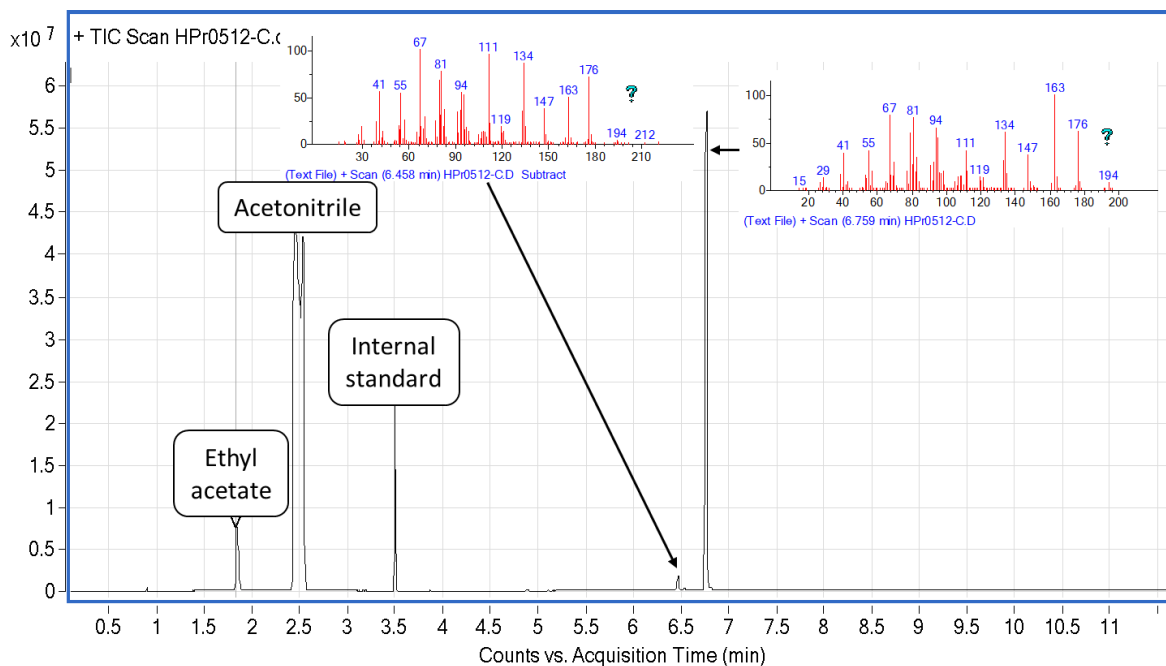


Figure VI-29 - GC-MS analysis of the purified 12H-FLUA.

As 2 peaks at m/z 12H-FLUA=194 are observed, at least 2 isomers are present in the purified product.

Appendix VI-3 - XRD of the solid products after the cyclings with regeneration, without regeneration compared to Fluorenone and Fluorene

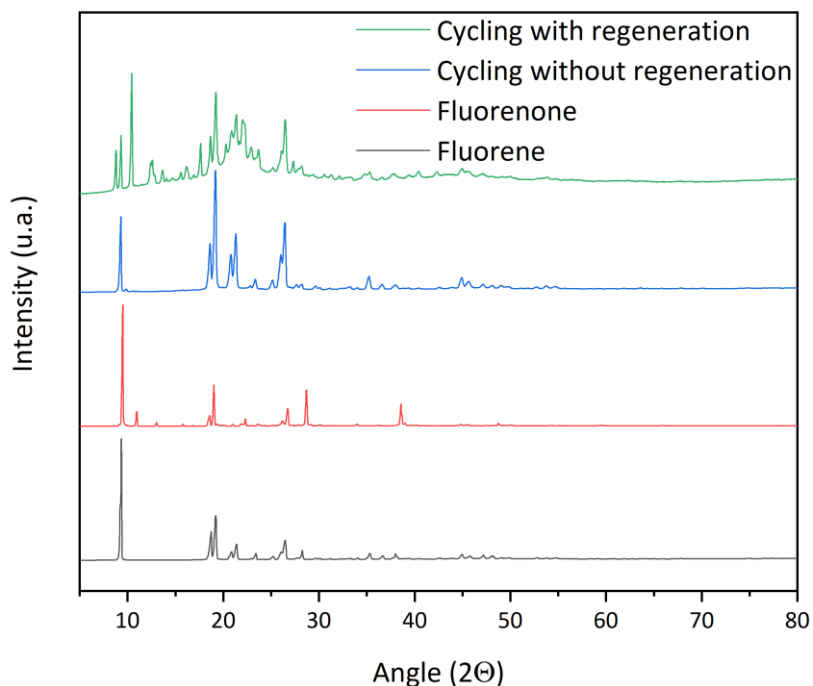


Figure VI-30 - XRD analysis of the solid products after the cyclings with regeneration, without regeneration as well as the pure compounds Fluorenone and Fluorene.

The cycling without regeneration forms mainly Fluorene. The cycling with regeneration forms Fluorenone, Fluorene and at least another crystalline impurity.

Chapter 3: Regeneration of the intramolecular dehydration products

Appendix VI-4 - NMR analysis of the reaction mixture after 3 cycles without regeneration

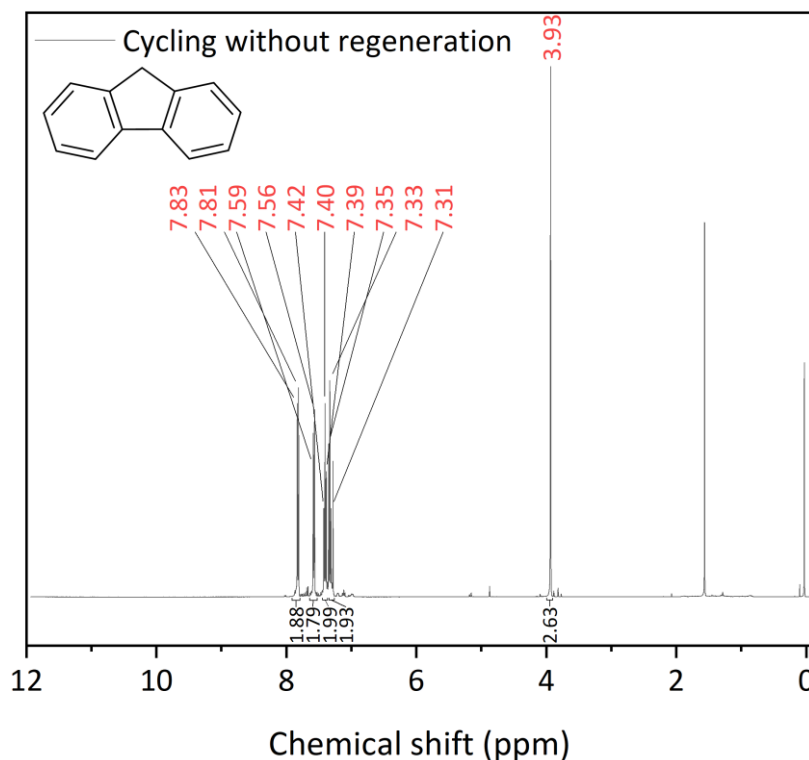


Figure VI-31 – ^1H NMR analysis of the reaction mixture after 3 cycles without regeneration in CDCl_3 .

^1H NMR (CDCl_3): $\delta = 7.82$ (d, $J = 7.4$ Hz, 2H, CH), 7.57 (d, $J = 7.4$ Hz, 2H, CH), 7.41 (t, $J = 7.4$ Hz, 2H, CH), 7.22 (dt, 2H, $J = 7.4, 1.1$, 2H, CH), 3.94 (s, 2H, CH_2). Corresponds to Fluorene.⁴³

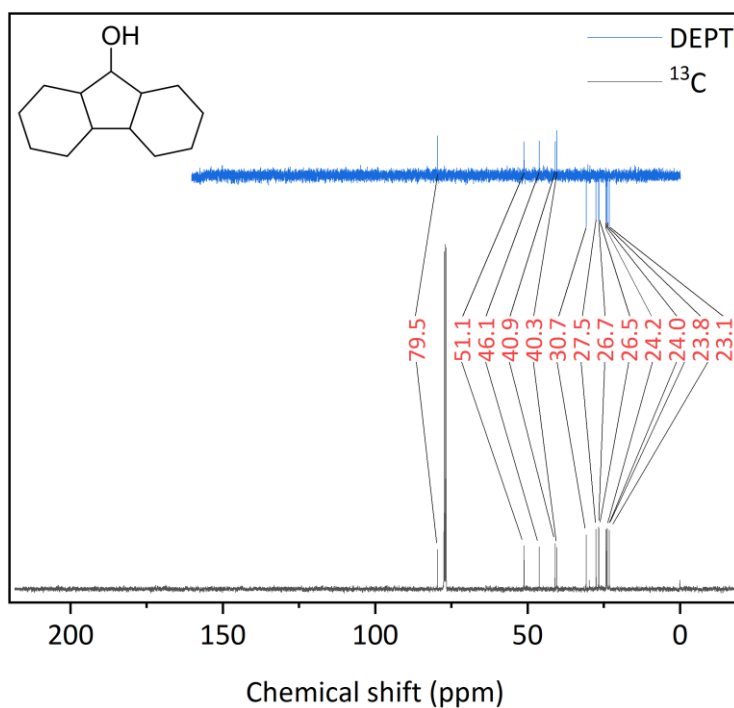


Figure VI-32 – ^{13}C and DEPT NMR analysis of the reaction mixture after 3 cycles without regeneration in CDCl_3 .

Chapter 3: Regeneration of the intramolecular dehydration products

^{13}C NMR (CDCl_3) $\delta=36.9$ (d), 119.9 (t), 125.0 (t), 126.7 (t), 126.7 (t), 141.7 (q), 143.2 (q). Confirmed the presence of Fluorene.⁴⁴

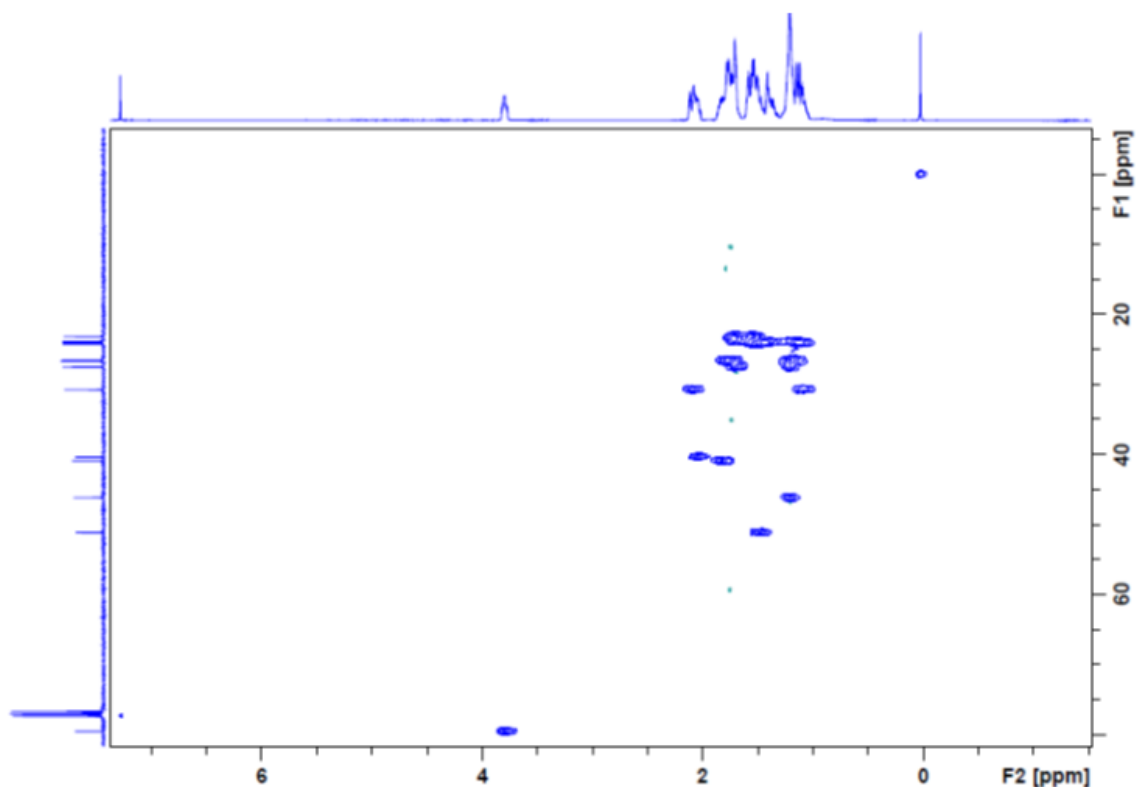


Figure VI-33 - HSQC analysis of the reaction mixture after 3 cycles without regeneration in CDCl_3 .

Appendix VI-5 - NMR analysis of the reaction mixture after 3 cycles with regeneration

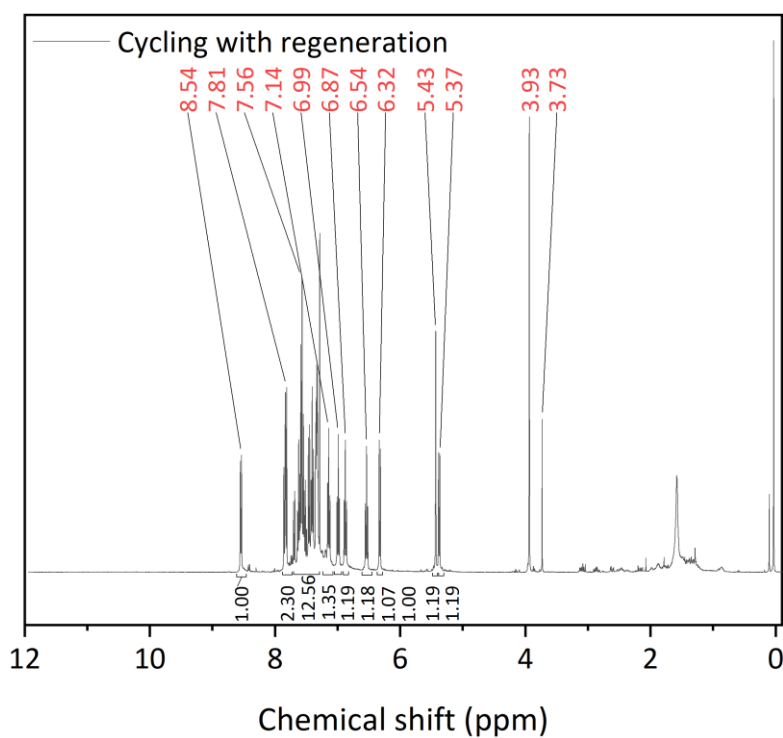


Figure VI-34 – ^1H NMR analysis of the reaction mixture after 3 cycles with regeneration in CDCl_3 .

Chapter 3: Regeneration of the intramolecular dehydration products

^1H NMR (CDCl_3): δ = 8.54 (d, $J=7.5$ Hz, 1H), 7.88-7.79 (m, 2H), 7.75-7.30 (m, 12H), 7.14 (t, 1H, $J=7.4$ Hz), 6.99 (t, 1H, $J=7.4$ Hz), 6.87 (t, 1H, $J=7.5$ Hz), 6.54 (t, 1H, $J=7.5$ Hz), 6.32 (d, 1H, $J=7.7$ Hz), 5.43 (s, 1H), 5.37 (d, 1H), 3.93 (s, 1.8H), 3.73 (s, 0.2H).

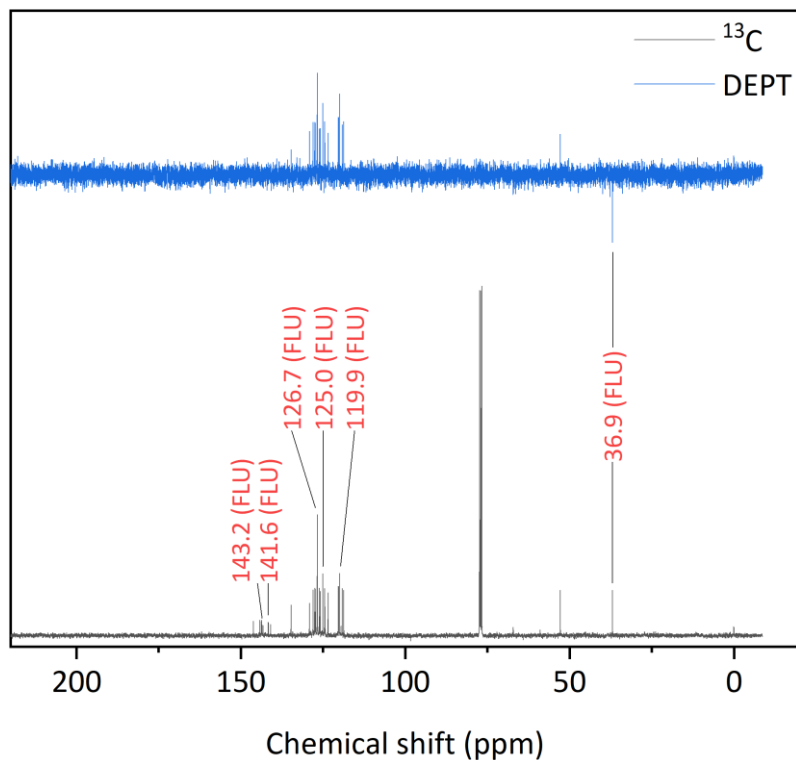


Figure VI-35 – ^{13}C and DEPT NMR analysis of the reaction mixture after 3 cycles with regeneration in CDCl_3 .

Apparition of a characteristic peak at 8.54 ppm in ^1H NMR. FLU with another aromatic product. Does not correspond to 9,9'-Bifluorenylidene.³⁹ Probably a Polyfluorene CDCl_3 ⁴¹, DMSO-d_6 .⁴⁵

Chapter 3: Regeneration of the intramolecular dehydration products

Appendix VI-6 - Comparison of the reaction mixtures after cyclings with regeneration, without regeneration and regeneration

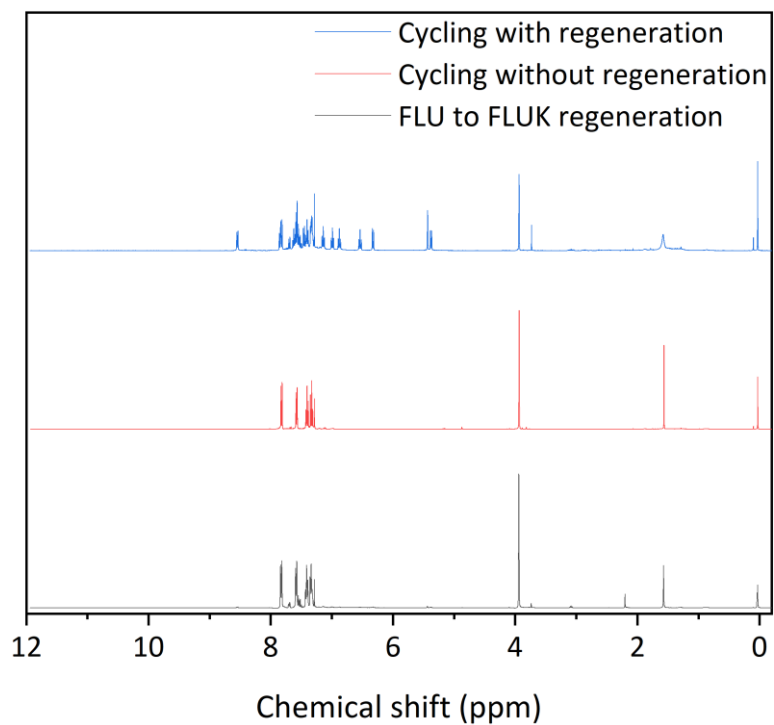


Figure VI-36 - Comparison of the reaction mixtures after cyclings with regeneration, without regeneration and regeneration by ¹H NMR analysis in CDCl₃.

Chapter 3: Regeneration of the intramolecular dehydration products

Appendix VI-7 - MALDI-TOF of the reaction mixture after the cyclings with regeneration, without regeneration and the regeneration of Fluorene to Fluorenone

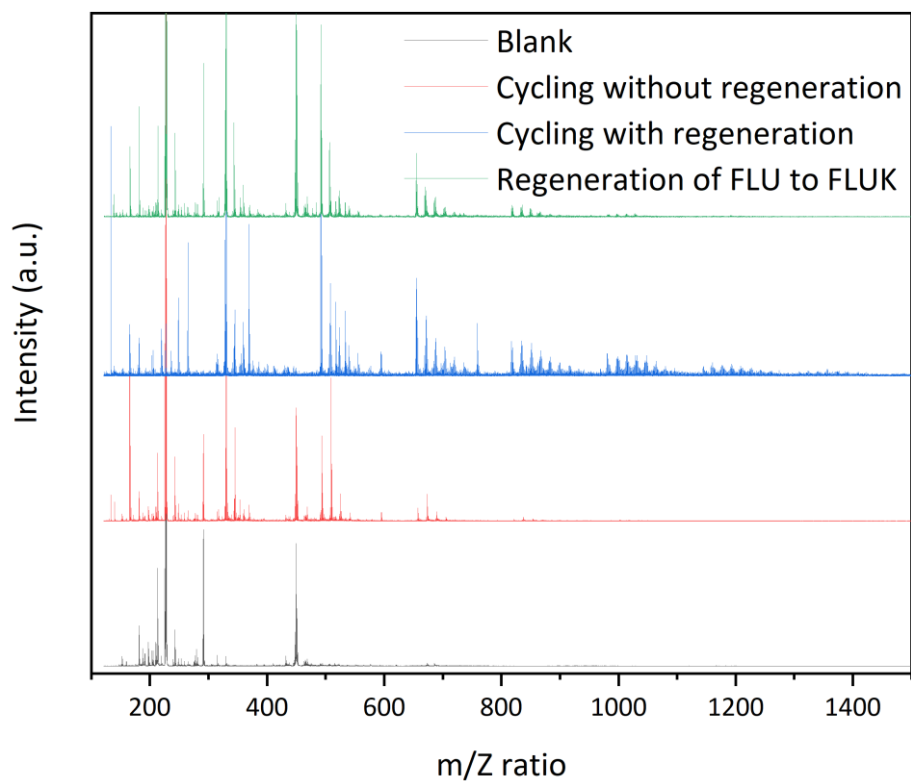


Figure VI-37 - MALDI-TOF analysis of the reaction mixture after the cyclings with regeneration, without regeneration and the regeneration of Fluorene to Fluorenone.

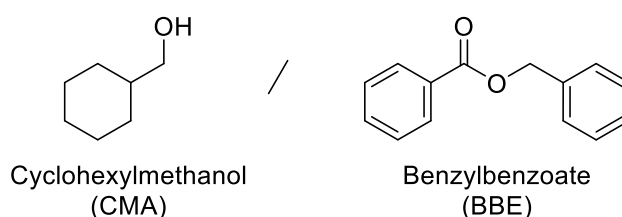


Table of Contents “Chapter 4: Substitution of the ketone by an ester”

VII. Chapter 4: Substitution of the ketone by an ester.....	254
VII.1 Hydrogenation.....	255
VII.2 Dehydrogenation.....	258
VII.3 Stability of the ester function.....	262
VII.4 Conclusion	265
Bibliography.....	266
Appendix.....	267
Appendix VII-1 - CCE purification and analysis.....	267

VII. Chapter 4: Substitution of the ketone by an ester

As observed during the previous chapters, the ketone function induced a number of side-reactions such as aldolisation crotonisation and also reversibly hydrogenated during the dehydrogenation, hindering the system dehydrogenation kinetics. These reactions are intrinsically linked to the alcohol/ketone function; therefore, it is rather difficult to completely avoid them. Solving this issue would then only be possible by replacing the ketone function by another one. Homoesters have been studied over the years and noble-free heterogeneous catalytic systems based on Cu have been developed for both hydrogenation and dehydrogenation.¹ Thus, for this last chapter, the combination aromatic-ester was tested using the couple Cyclohexylmethanol/Benzylbenzoate (CMA/BBE). The LOHC structures and physicochemical properties are presented in Table VII-1.



Molecule	Melting point (°C)	Boiling point (°C)	Chemical risk	Gravimetric density H ₂ (wt.%H ₂)	Dehydrogenation enthalpy (kJ/mol H ₂)
Cyclohexylmethanol	19	181	-	7	58
Benzylbenzoate	18	323	Ecotoxic		

Table VII-1 - Physicochemical properties of the Cyclohexylmethanol/Benzylbenzoate LOHC couple.

This couple presents high gravimetric and volumetric densities with reduced chemical risks that are in agreement with our defined strategy (see chapter 1). In addition, both hydrogenated and dehydrogenated forms are liquid at room temperature. In the rest of this chapter, the hydrogenation and dehydrogenation of both forms will be presented. The various structures encountered during our experiments are sorted in Figure VII-1.

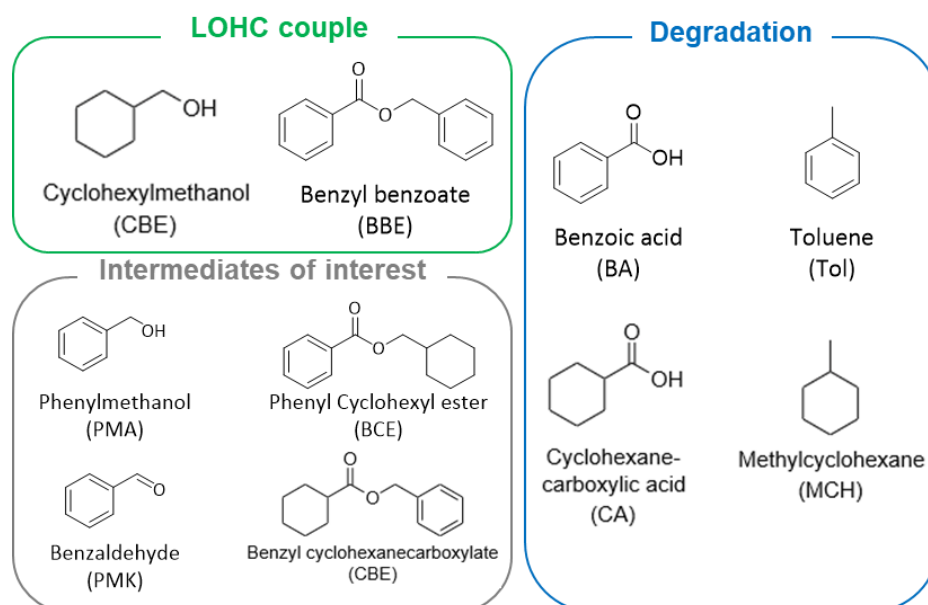


Figure VII-1 - Classification of the main products observed by GC-MS during the experiments related to CMA/BBE couple.

Chapter 4: Substitution of the ketone by an ester

Moreover, all GC-MS results in this chapter are provided without the associated calibration curves. The area of the GC-MS peaks was used as a proxy for the quantity of matter of each species of the system, i.e. all relative response factors are supposed to be equal to 1. The literature shows that ester and alcohol relative response factor vary by roughly 10% when the ester chain is small.² For the rest of this chapter, the GC-MS error will be then set at 10% for all compounds.

VII.1 Hydrogenation

The hydrogenation of BBE to CMA was first performed with noble metal catalysts in 4 h at 115 °C under 50 bar H₂ in solvent-free conditions (Figure VII-2).

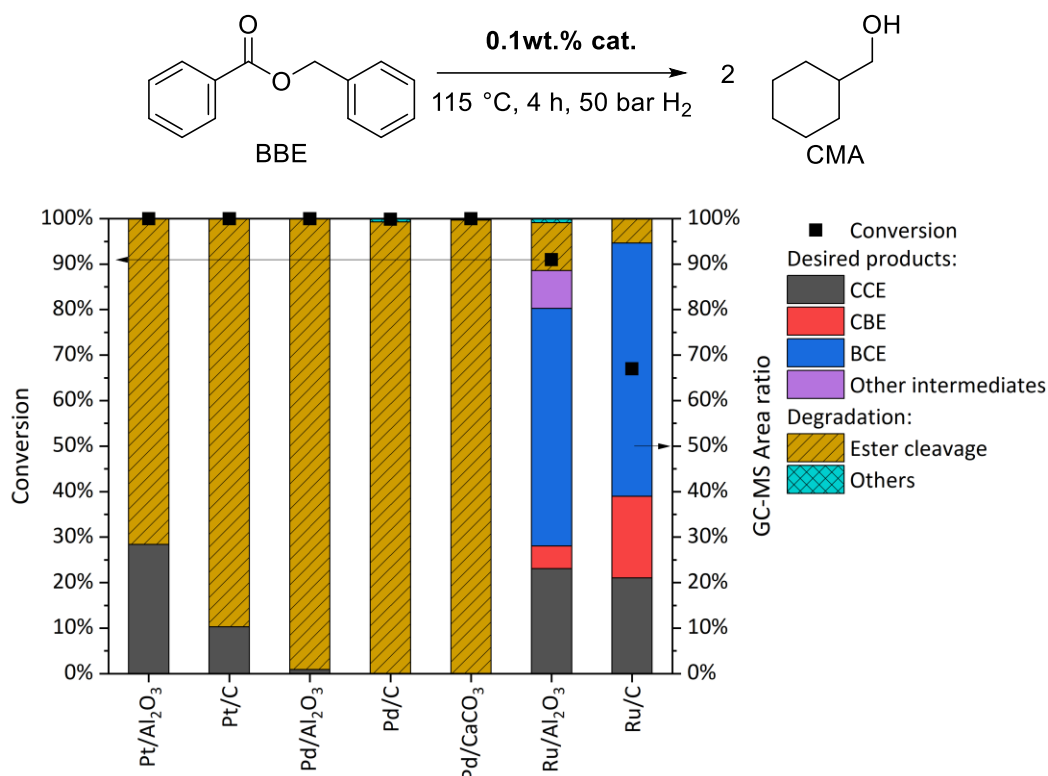
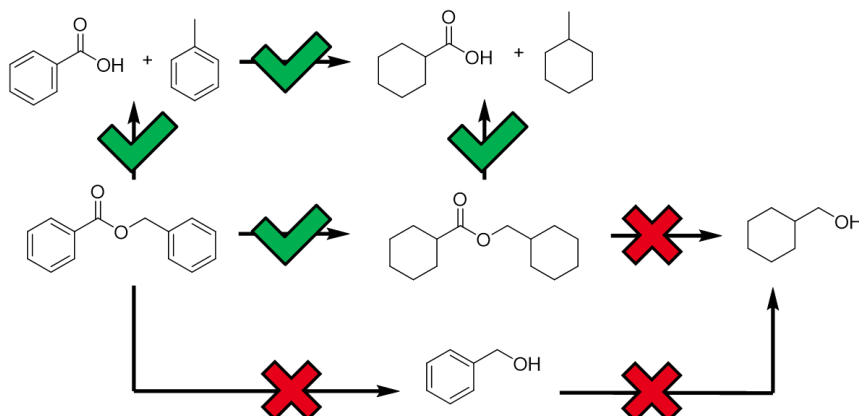


Figure VII-2 - Hydrogenation of BBE to CMA with noble metal catalysts. BBE (12.5 mL), catalyst (0.1 wt.% active metal with regard to BBE), 115 °C, 4 h, 50 bar H₂.

Pt and Pd catalysts reached complete conversion of BBE to a stable intermediate Cyclohexylmethyl cyclohexanecarboxylate (CCE). However, they also induced the alkoxy C-O ester cleavage, forming the Tol/BA and MCH/CA pairs. No acyl C-O cleavage was observed. On the contrary, Ru catalysts achieved lower conversion (65-95%) but the selectivity to intermediates of interest was higher. In particular, Ru/C produced less than 10% alkoxy C-O cleavage. Similar reactivities have been reported in the literature with the hydrogenation of Diphenylether to Dicyclohexylether in similar temperature (120 °C) and pressure (50 bar H₂) ranges.³ There, the alkoxy C-O bond cleavage was favored for the Pt catalysts with high reaction times (>65 h). Contrary to our results, the Pd catalysts did not induce the C-O cleavage but required exceedingly long reaction times (up to 189 h !). The difference in reactivity might come from ester chemical function that might induce a different reactivity compared to the ether. Finally, the Ru catalysts achieved the hydrogenation with a similar selectivity order depending on the support (C>Al₂O₃). From their study, Rh catalysts, in particular Rh/C could be good hydrogenation catalysts leaving the ester function undisturbed when lowering the reaction temperature (60 °C) and H₂ pressure (20 bar). However, these catalysts were not used in our study due to a lack of time.

Chapter 4: Substitution of the ketone by an ester

In conclusion, noble metal catalysts seem to readily hydrogenate the aromatic cycles, but not the ester. Moreover, the ester function is unstable in their presence at high pressures, forming hydrogenolysis products by cleavage of the C_{alkoxy}-O bond (Scheme VII-1).



Scheme VII-1 - Summary of the hydrogenation of BBE to CMA with noble metal catalysts. Green ticks mark effective reaction pathways (presence of products) while red crosses mark unobserved reaction pathways (absence of products).

Therefore, the prior hydrogenation of the ester to the corresponding alcohols might allow for the following clean hydrogenation of the aromatic cycles in a successive reaction scheme. The hydrogenation with noble metal-free Cu and Ni catalysts supported on metal oxides and hydrotalcites (HT) was performed at temperatures between 215 and 250 °C in 4 h and at 50 bar H₂.

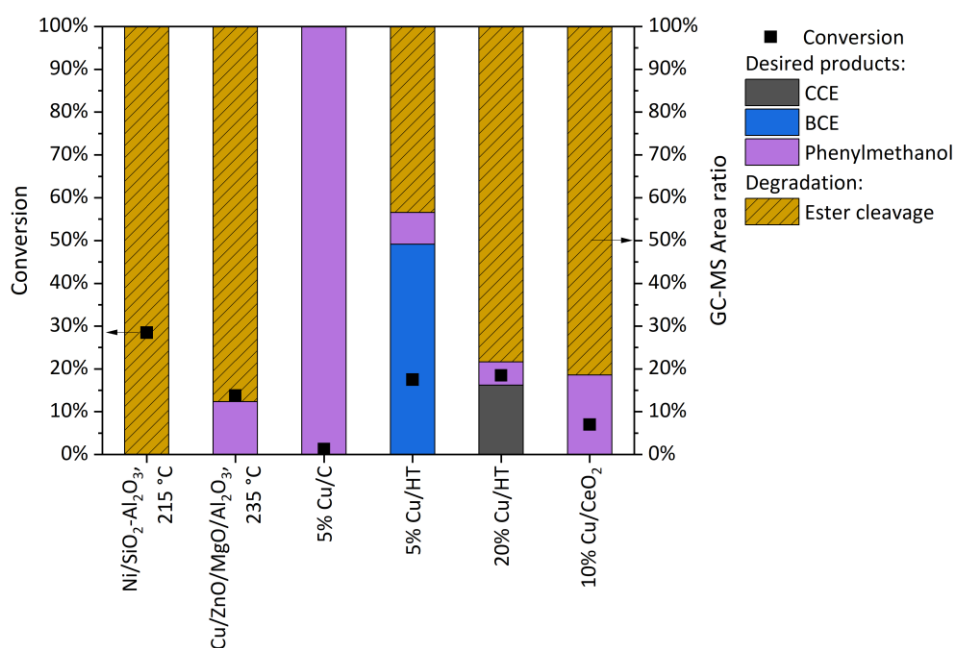
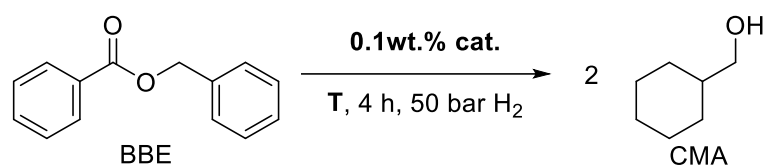
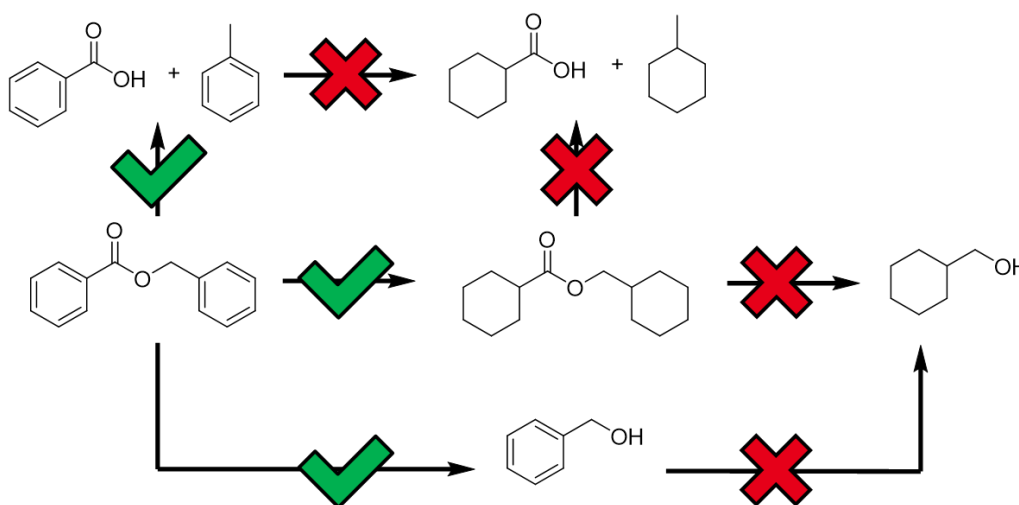


Figure VII-3 - Hydrogenation of BBE to CMA with noble metal-free catalysts. BBE (12.5 mL), catalyst (0.1 wt.% active metal with regard to BBE), 250 °C, 4 h, 50 bar H₂. Different temperatures were employed for Ni/SiO₂-Al₂O₃ (215 °C) and Cu/ZnO/MgO/Al₂O₃ (235 °C).

Chapter 4: Substitution of the ketone by an ester

The conversion was limited to less than 30% for all catalysts and alkoxy C-O cleavage was observed in all instances except the 5%Cu/HT catalyst. Nevertheless, the small conversion obtained with this catalyst might not be sufficient to assess its selectivity. Despite the reported literature, the Cu catalysts were inefficient to selectively hydrogenate the ester function (i.e. favor the Acyl C-O cleavage).⁴ Moreover, hydrogenolysis was reported to form ethers in the case of strong acidic sites close the active metal nanoparticle, but such products were not observed in our experiments.⁵ Here, it seems that more catalytic development would be required to selectively hydrogenate the ester function as literature insights show that this reaction should be theoretically possible.⁴

In conclusion, noble metal-free catalysts showed slower conversions than their noble metal counterparts. Moreover, the C_{alkoxy}-O bond cleavage still prevailed over the C_{acyl}-O bond cleavage. (Scheme VII-2).



Scheme VII-2 - Summary of the hydrogenation of BBE to CMA with noble metal-free catalysts. Green ticks mark effective reaction pathways (presence of products) while red crosses mark unobserved reaction pathways (absence of products).

No more work was pursued on the hydrogenation. More work on the hydrogenolysis of BBE and CCE is presented in later parts of this chapter. (see VII.3)

VII.2 Dehydrogenation

The dehydrogenation of CMA was performed with a variety of heterogeneous catalysts in 18 h at 205 °C (Figure VII-4).

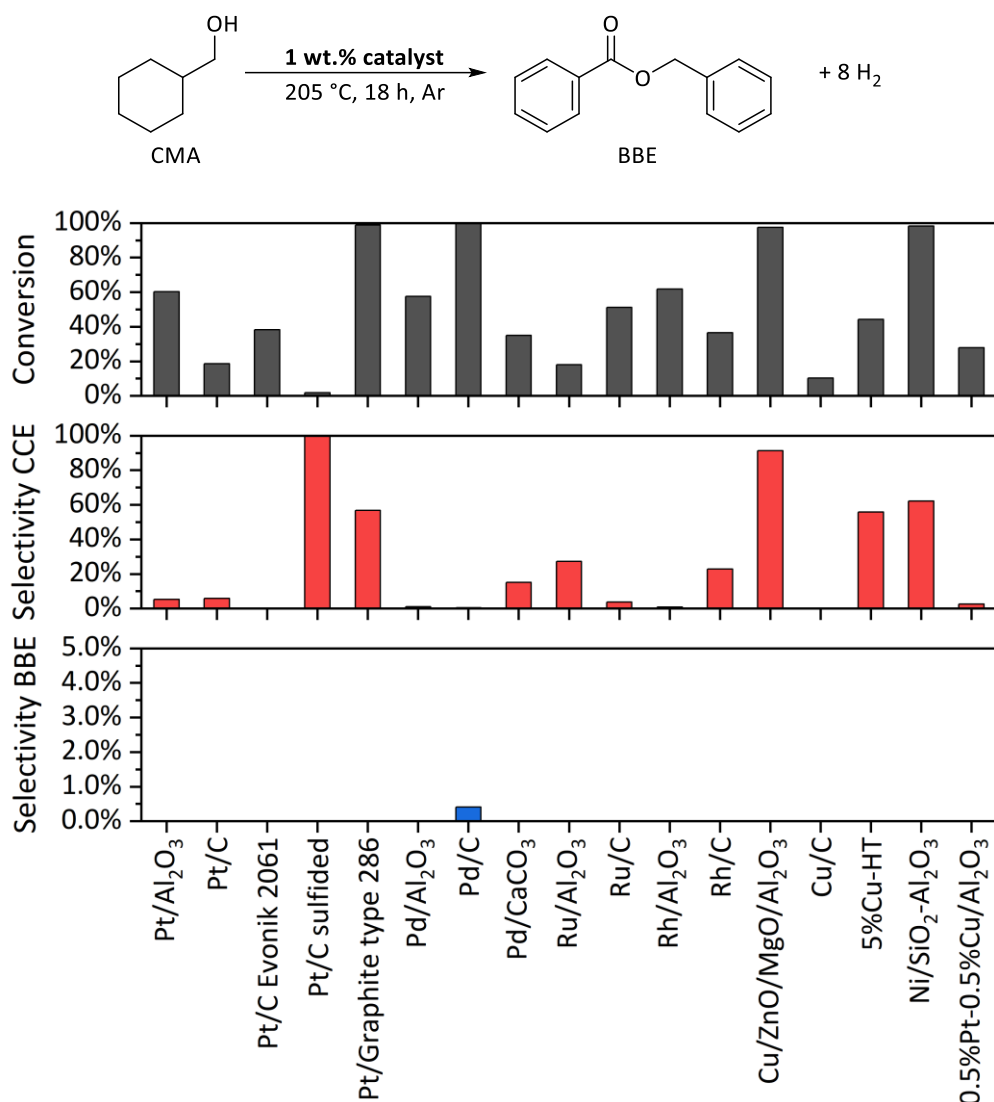
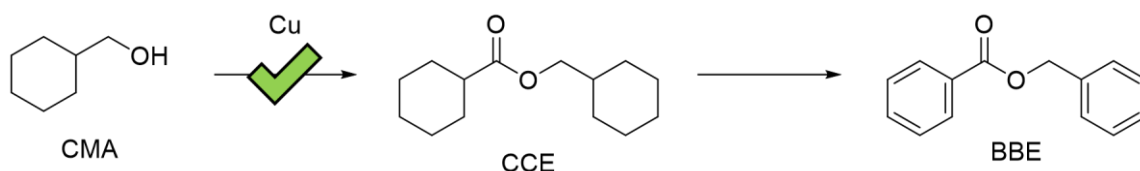


Figure VII-4 - Dehydrogenation of CMA to BBE. CMA (2 g), catalyst (0.1 wt.% active metal with regard to CMA), 205 °C, 18 h, Ar.

Only traces of BBE were observed for the Pd/C catalyst. However, >90% selectivity to the intermediate CCE was obtained for the sulfided Pt/C and Cu/ZnO/MgO/Al₂O₃ catalysts. In addition, the Cu catalyst reached complete conversion while the Pt catalyst conversion was inferior to 5%. As high conversion and selectivity of Cu catalysts doped with transition elements were often reported for the dehydrogenation of alcohols to esters in the literature, better performances could theoretically be achieved by further catalytic development.⁶

While no catalysts were able to efficiently perform the dehydrogenation of CMA to BBE in one-step, the dehydrogenation could be carried out in a two-step process with first the formation of the ester by a Cu based catalyst (CMA to CCE) then the dehydrogenation of the cycles by another catalyst (CCE to BBE). (Scheme VII-3)

Chapter 4: Substitution of the ketone by an ester



Scheme VII-3 - Summary of the dehydrogenation of CMA to BBE with noble metal-free catalysts. Green ticks mark effective reaction pathways (presence of products).

In order to study the dehydrogenation of the no commercial CCE intermediate, its synthesis was performed by following a procedure from the literature.⁷ The intermediate was obtained in large quantities (>15 g per batch) and more precision on the protocol and analysis are presented in Appendix VII-1. The dehydrogenation of CCE to BBE was performed by a range of noble and non-noble metal catalysts in 18 h at 205 °C with higher catalytic loadings (Figure VII-5).

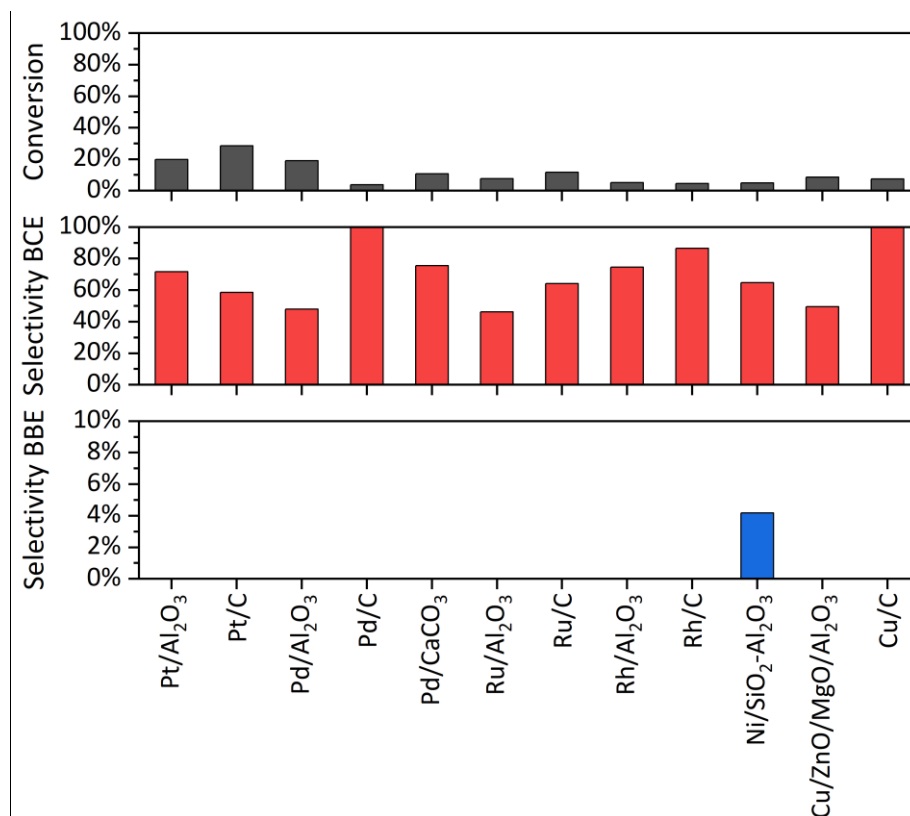
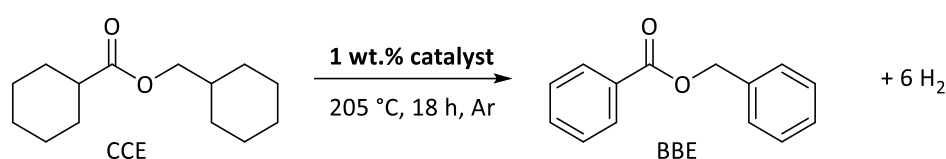


Figure VII-5 - Dehydrogenation of CCE to BBE. CCE (1.5 g), catalyst (1 wt.% active metal with regard to CMA), 205 °C, 18 h, Ar.

All catalysts presented conversions inferior to 30% and only traces of BBE were observed for a Ni/SiO₂-Al₂O₃ catalyst. Interestingly, another intermediate, BCE was formed while CBE was not observed by GC-MS. In order to increase the conversion to BBE, further experiments were performed with the Pd/C and Ni/SiO₂-Al₂O₃ catalysts that were the only catalysts that produced BBE over the course of the previous experiments. Pd/C, Rh/C and Cu/C were also tested due to their high selectivity to BCE while

Chapter 4: Substitution of the ketone by an ester

Ru/Al₂O₃ was used as a low selectivity comparison point. The reaction temperature was then increased to 250 °C (Figure VII-6).

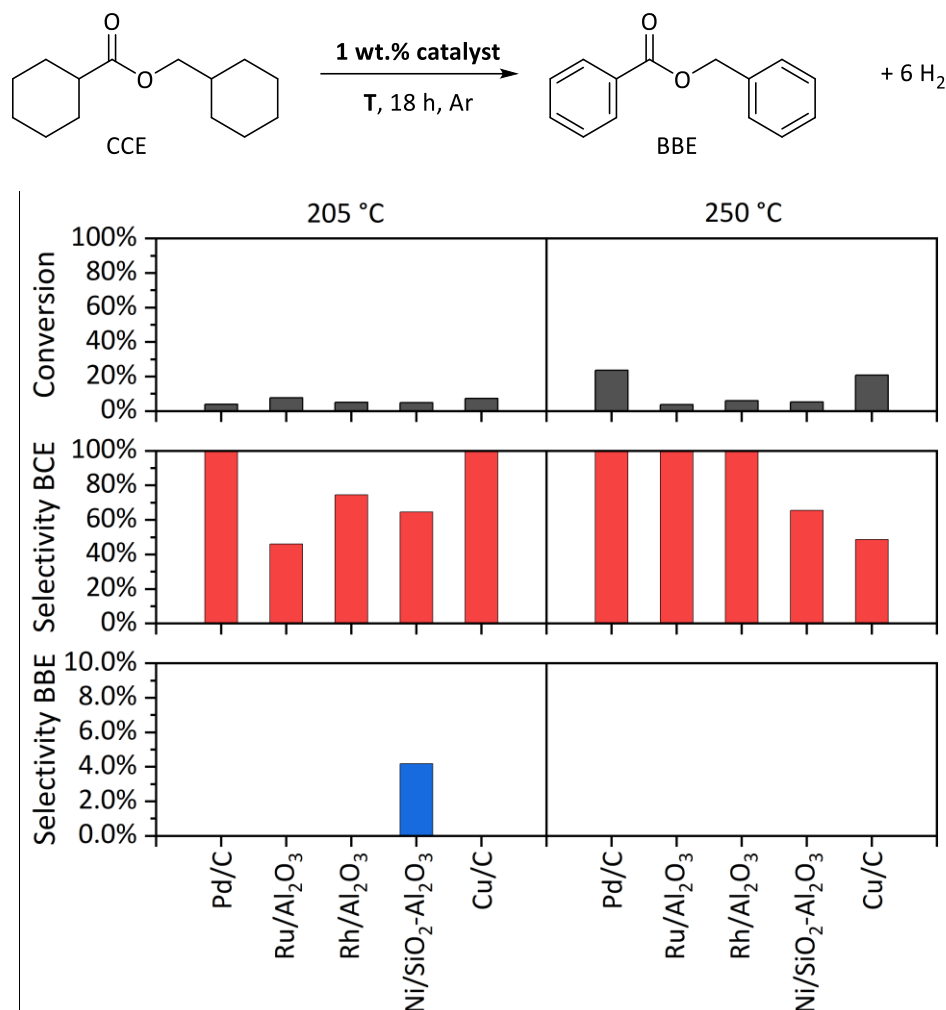


Figure VII-6 - Dehydrogenation of CCE to BBE. CCE (1.5 g), catalyst (1 wt.% active metal with regard to CMA), 250 °C, 18 h, Ar.

Here, the conversion generally increased while the selectivity to the intermediate BCE were also improved except in the case of the Cu/C catalyst. However, it is highly possible that, due to the low conversion, trace amounts of degradation products could be unaccounted for. It is also possible that some heavier compounds that cannot be analyzed by GC-MS form as well as lighter degradation products. A mass-balance should be performed to assess their proportion; however it was not done in this instance due to a lack of time. More experiments related to the degradation products are presented in VII.3.

As increasing the reaction temperature was inefficient to improve the conversion while maintaining trustworthy selectivities, an increase of the reaction time from 18 to 48 h was carried out with Pd/CaCO₃ and Ni/SiO₂-Al₂O₃ (Figure VII-7).

Chapter 4: Substitution of the ketone by an ester

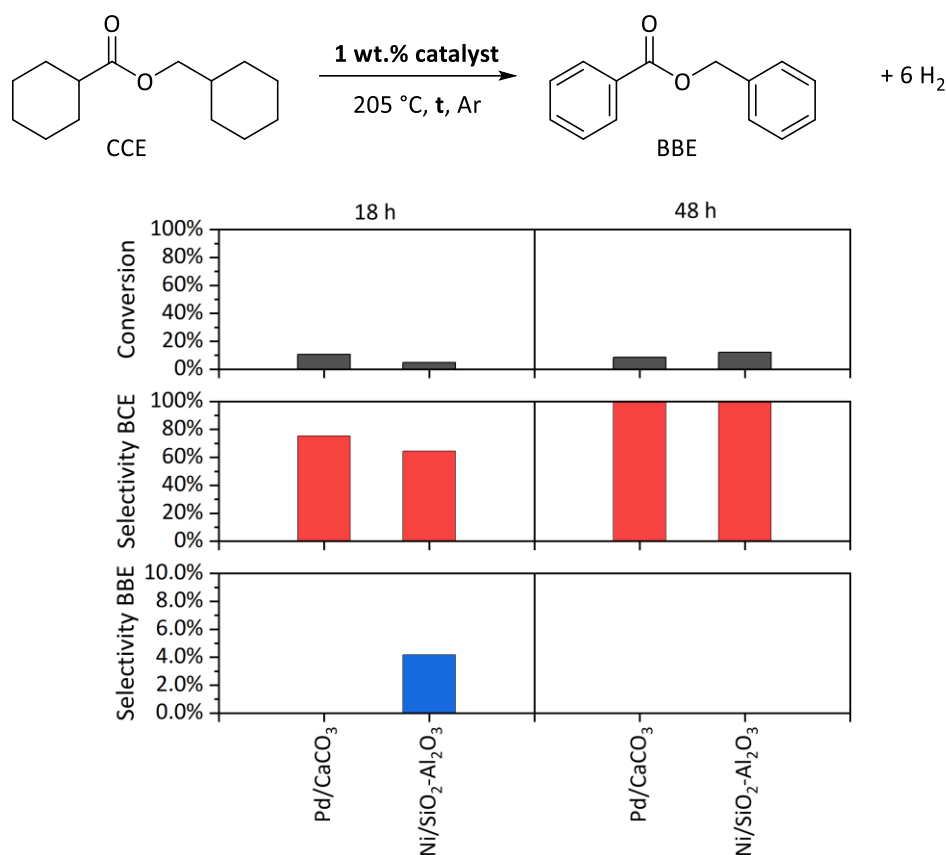
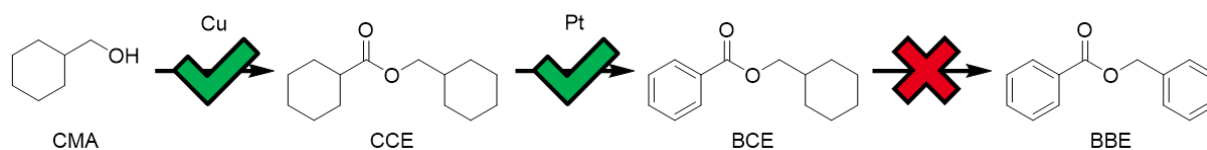


Figure VII-7 - Dehydrogenation of CCE to BBE. CCE (1.5 g), catalyst (1 wt.% active metal with regard to CMA), 205 °C, 48 h, Ar.

Here again, a 48 h reaction time was insufficient to afford better conversions. As Ni/SiO₂-Al₂O₃ produced up to 4% BBE at 18 h, an increase of this species amount in the reaction mixture was expected. Nonetheless, the 48 h experiments showed the BBE disappearance. As the boiling point of BBE is much higher than the reaction temperature (323 °C), we can postulate that BBE degraded during the reaction. Moreover, as the selectivity increased at 48 h with both catalysts, it is also possible that traces amounts of lighter degradation products could not be analyzed.

A summary of the dehydrogenation advances is presented in Scheme VII-4.



Scheme VII-4 - Summary of the dehydrogenation of CMA to BBE with noble metal-free catalysts. Green ticks mark effective reaction pathways (presence of products) while red crosses mark unobserved reaction pathways (absence of products).

The dehydrogenation was carried out in a two-step process with first the formation of the ester by a Cu based catalyst (CMA to CCE) then the dehydrogenation of the cycle by a Pt-based catalyst (CCE to BCE). Unfortunately, no catalyst was found to efficiently catalyze the dehydrogenation of BCE to BBE, limiting the interest of the CMA/BBE couple. Moreover, our experiments casted serious doubt on the stability of BBE and or CCE in the reaction conditions. Therefore, no more experiments related to the dehydrogenation of CMA to BBE were carried out. Over the last part of this chapter, experiments related to the stability tests of BBE and CCE will be briefly presented.

VII.3 Stability of the ester function

As seen over the course of our experiments in both hydrogenation and dehydrogenation, a number of side-reactions happened in the vicinity of the ester function. In order to rationalize these events, a series of tests on the stability of the BBE and CCE esters were performed over 24 h and the results are presented hereinafter. The stability of BBE was tested by performing various modification of the dehydrogenation conditions (Figure VII-8).

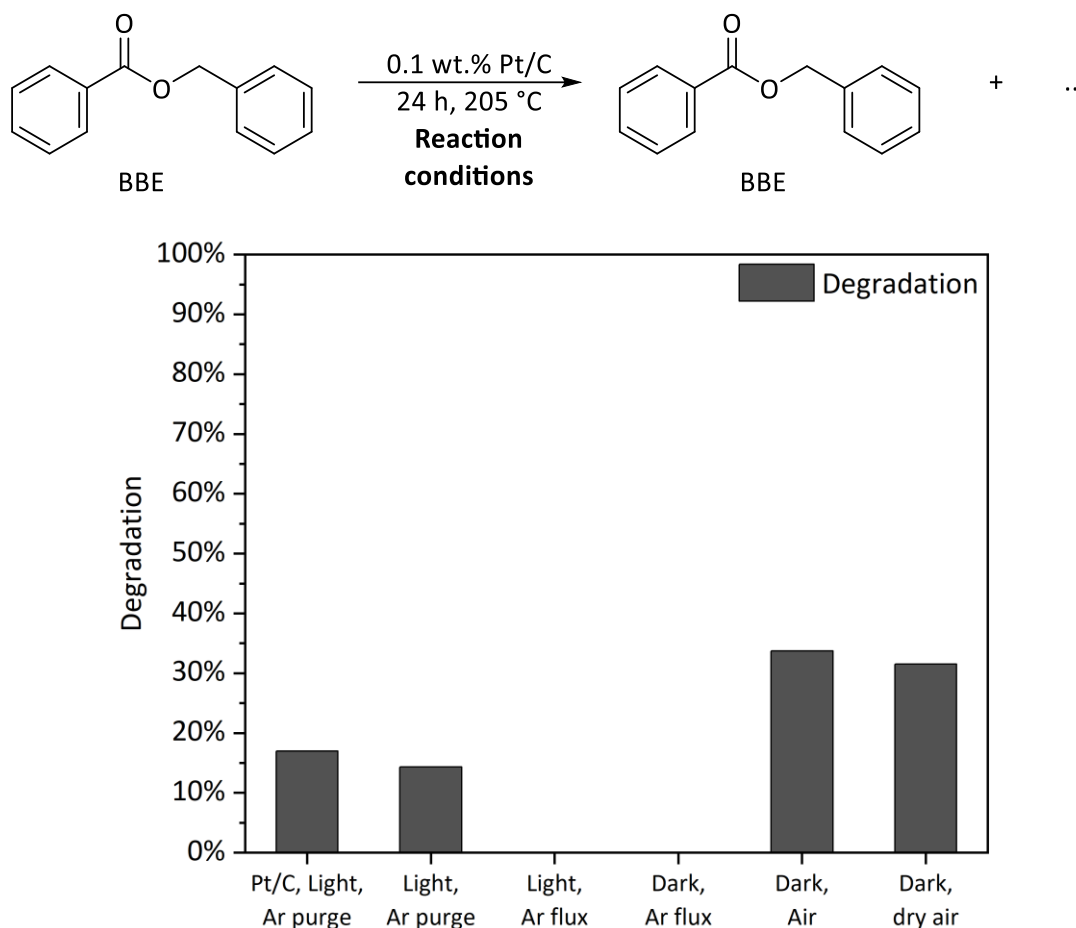


Figure VII-8 - BBE stability tests. BBE (1 mL), catalyst (0.1 wt.% Pt with regard to BBE), 24 h, 205 °C.

First, a BBE stability test in presence of Pt/C in the classic dehydrogenation conditions produced roughly 15% $C_{alkoxy}-O$ cleavage degradation products, with Benzaldehyde and Benzoic acid in roughly equivalent proportions. Removing the catalyst did not significantly improve the BBE stability, indicating that the catalyst was not primarily responsible for the degradation of the LOHC.

During the dehydrogenation, H_2 must be removed from the reaction vessel in order to avoid a pressure build-up that would lead to thermodynamic limitations. On one hand, procedures in the literature often use an Ar flux to ensure that no O_2 would come back into the reaction vessel. However, such procedure would also diminish the H_2 partial pressure by dilution, enabling near-vacuum conditions. This reaction state would then displace the reaction thermodynamics to the formation of the products, not reflecting an industrial process.⁸ On the other hand, over the course of this manuscript, we performed the dehydrogenation reaction by purging the reaction vessel with alternating three cycles of vacuum and Ar, before opening a glass tap at the top of the condenser at the reaction start to remove the forming H_2 . While this setup could allow for O_2 retro-diffusion to the reaction vessel, it is also more on-line with an industrial process.

Chapter 4: Substitution of the ketone by an ester

In order to test the influence of this parameter on the stability of the LOHC, an experiment under Ar flux was performed, showing that no degradation products were forming. By using the same Ar flux setup, the reaction in the dark (aluminum foil) revealed that light had no influence on the degradation. We then postulated that O₂ or water were responsible for the degradation of BBE. By performing the reaction in the dark without purging the reaction vessel, degradation was observed in higher proportions (roughly 35%) than the classic dehydrogenation conditions. Moreover, the BA/PMK ratio shifted from 1 to 6, indicating that an increased O₂ concentration favored the overoxidation of PMK. These results confirmed that an element present in the air, presumably O₂, was responsible for the BBE degradation. Finally, we removed water as a primary degradation initiator by drying the LOHC on molecular sieves over 24 h and removing any entering water in the reaction system by adding a MgSO₄ water gas trap at the top of the condenser. In this water-free environment, roughly 30% degradation still occurred with a similar BA/PMK ratio; inducing that air (O₂) was probably responsible for the degradation of BBE. In the literature, similar results were obtained for the pyrolysis of BBE at 250 °C in 24 h, with the formation of PMK and BA as the main byproducts. However, no Tol or Benzoic anhydride was observed in our experiments.⁹

We can conclude that, during the dehydrogenation, BBE degraded in presence of O₂ to yield BA and PMK. Conversely, as shown previously in this chapter (see VII.1), BBE degraded during the hydrogenation to yield BA and Tol. DFT calculations showed that all reactions were highly exothermic and exergonic, as presented in the Table VII-2.

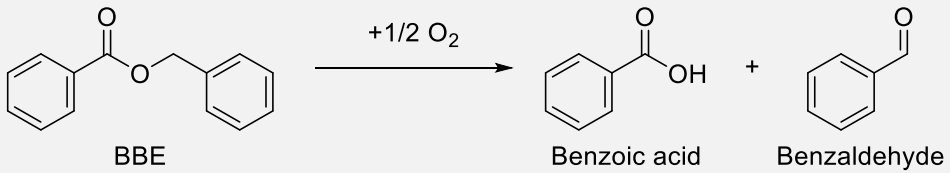
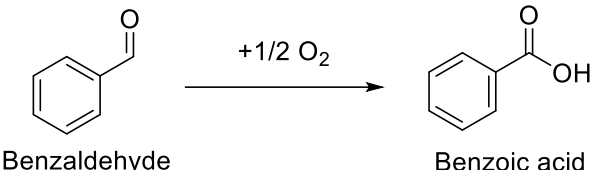
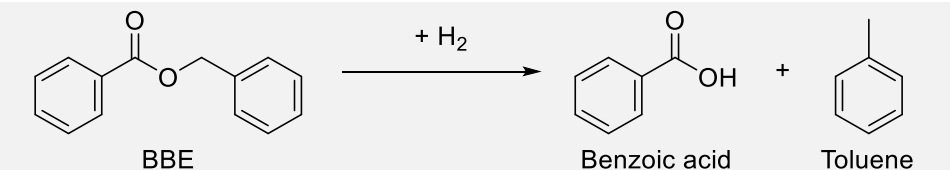
Degradation reaction		$\Delta_r H/\Delta_r G$ (kJ/mol)
 <p>BBE + 1/2 O₂ → Benzoic acid + Benzaldehyde</p>	-167/-193	
 <p>Benzaldehyde + 1/2 O₂ → Benzoic acid</p>	-254/-230	
 <p>BBE + H₂ → Benzoic acid + Toluene</p>	-85/-103	

Table VII-2 - Summary of BBE degradation reactions during the dehydrogenation and the hydrogenation.

The stability of CCE was also briefly studied and the effect of O₂ on its stability was undeniable. However, its potency was reduced, potentially due to the absence of the adjacent aromatic structures. Indeed, only roughly 15% degradation was observed in the conditions containing the most O₂ (Figure VII-9).

VII.4 Conclusion

The CMA/BBE LOHC couple could not be efficiently hydrogenated or dehydrogenated by commercially available catalysts in the imparted time. In particular, two degradations pathways, hydrogenolysis and oxygenolysis, were observed and identified. While the prevalence of the oxygenolysis could be limited by directly modifying the experimental setup (Ar flux compared to Ar purge), the hydrogenolysis would require more catalytic development and tuning of the reaction conditions. In addition, the development of efficient and selective dehydrogenation catalysts is still required to further this LOHC couple as reaction times comparable to the CHEA/APO, DCMA/BPO and 12H-FLUA/FLUK were also obtained.

Bibliography

- (1) Miura, H.; Nakahara, K.; Kitajima, T.; Shishido, T. Concerted Functions of Surface Acid–Base Pairs and Supported Copper Catalysts for Dehydrogenative Synthesis of Esters from Primary Alcohols. *ACS Omega* **2017**, *2* (9), 6167–6173. <https://doi.org/10.1021/acsomega.7b01142>.
- (2) Mangas, J. J.; González, M. P.; Rodríguez, R.; Blanco, D. Solid-Phase Extraction and Determination of Trace Aroma and Flavour Components in Cider by GC-MS. *Chromatographia* **1996**, *42* (1), 101–105. <https://doi.org/10.1007/BF02271063>.
- (3) Jang, M.; Shin, B. S.; Jo, Y. S.; Kang, J. W.; Kwak, S. K.; Yoon, C. W.; Jeong, H. A Study on Hydrogen Uptake and Release of a Eutectic Mixture of Biphenyl and Diphenyl Ether. *Journal of Energy Chemistry* **2020**, *42*, 11–16. <https://doi.org/10.1016/j.jechem.2019.05.024>.
- (4) A. Strekalova, A.; A. Shesterkina, A.; M. Kustov, L. Recent Progress in Hydrogenation of Esters on Heterogeneous Bimetallic Catalysts. *Catalysis Science & Technology* **2021**, *11* (22), 7229–7238. <https://doi.org/10.1039/D1CY01603B>.
- (5) Yun, Y. S.; Berdugo-Díaz, C. E.; Luo, J.; Barton, D. G.; Chen, I.; Lee, J.; Flaherty, D. W. The Importance of Brønsted Acid Sites on CO Bond Rupture Selectivities during Hydrogenation and Hydrogenolysis of Esters. *Journal of Catalysis* **2022**, *411*, 212–225. <https://doi.org/10.1016/j.jcat.2022.05.014>.
- (6) Inui, K.; Kurabayashi, T.; Sato, S.; Ichikawa, N. Effective Formation of Ethyl Acetate from Ethanol over Cu-Zn-Zr-Al-O Catalyst. *Journal of Molecular Catalysis A: Chemical* **2004**, *216* (1), 147–156. <https://doi.org/10.1016/j.molcata.2004.02.017>.
- (7) Reddy, N. N. K.; Ravi, C.; Adimurthy, S. Oxidative Esterification of Primary Alcohols at Room Temperature under Aqueous Medium. *Synthetic Communications* **2018**, *48* (13), 1663–1670. <https://doi.org/10.1080/00397911.2018.1458320>.
- (8) Müller, K. Acceptorless Dehydrogenation of Amines to Nitriles for Hydrogen Storage: Reality or Wishful Thinking? *Energy Technology n/a* (n/a). <https://doi.org/10.1002/ente.202200468>.
- (9) Risinger, G. E.; Mach, E. E. Thermal Decomposition of Certain Benzyl Esters. *Nature* **1963**, *199* (4892), 484–485. <https://doi.org/10.1038/199484a0>.
- (10) Mori, N.; Togo, H. Facile Oxidative Conversion of Alcohols to Esters Using Molecular Iodine. *Tetrahedron* **2005**, *61* (24), 5915–5925. <https://doi.org/10.1016/j.tet.2005.03.097>.

Appendix

Appendix VII-1 - CCE purification and analysis

Purification by liquid-liquid extraction: 3*10 mL 1M KHCO₃. The product was a colorless to slightly yellow transparent oil. NMR analysis showed that the obtained product had a similar structure to that of reference from the literature.¹⁰

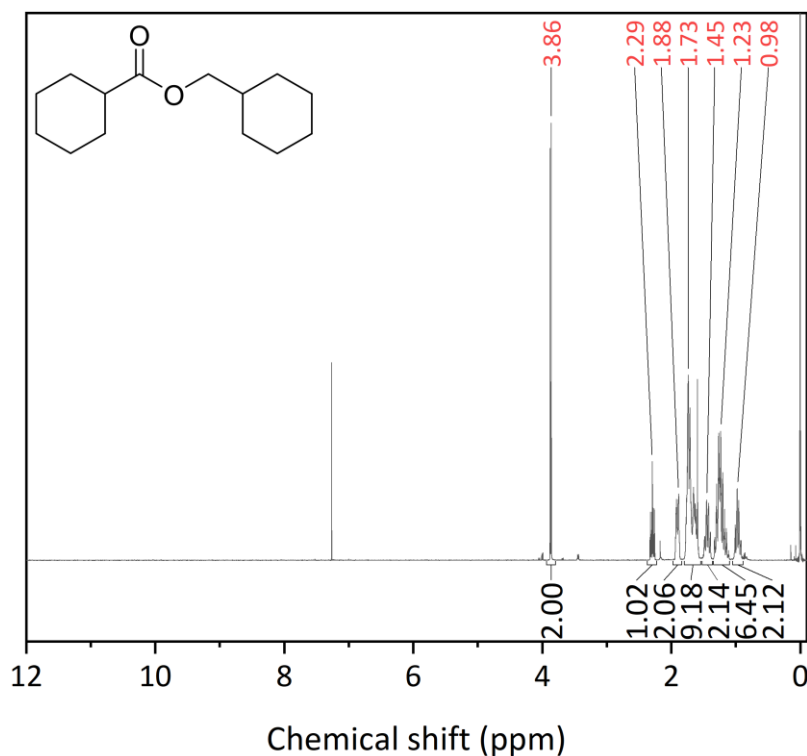


Figure VII-10 - ¹H NMR analysis of the purified CCE in CDCl₃.

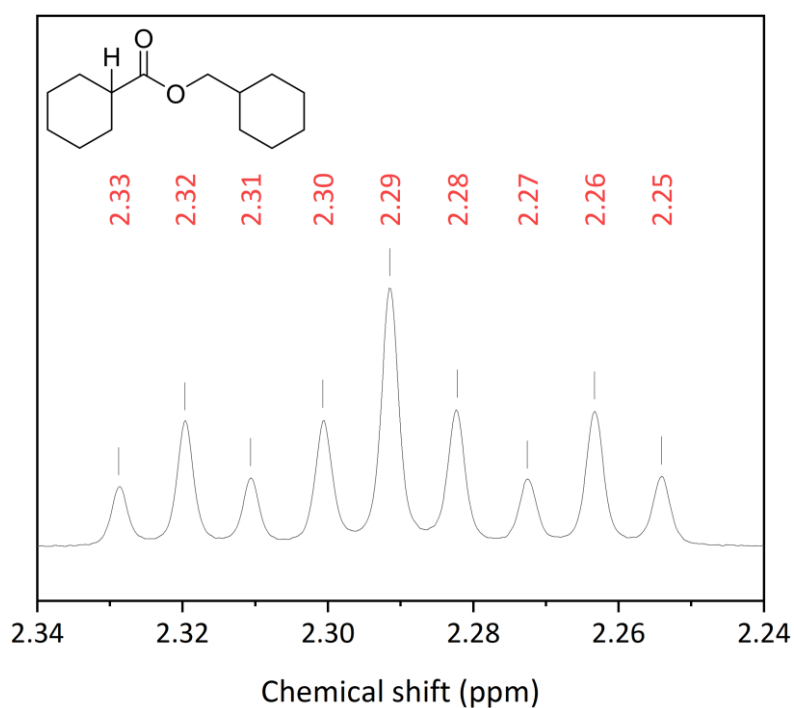


Figure VII-11 - ¹H NMR analysis of the purified CCE. Zoom on the tripled triplet at 2.29 ppm in CDCl₃.

Chapter 4: Substitution of the ketone by an ester

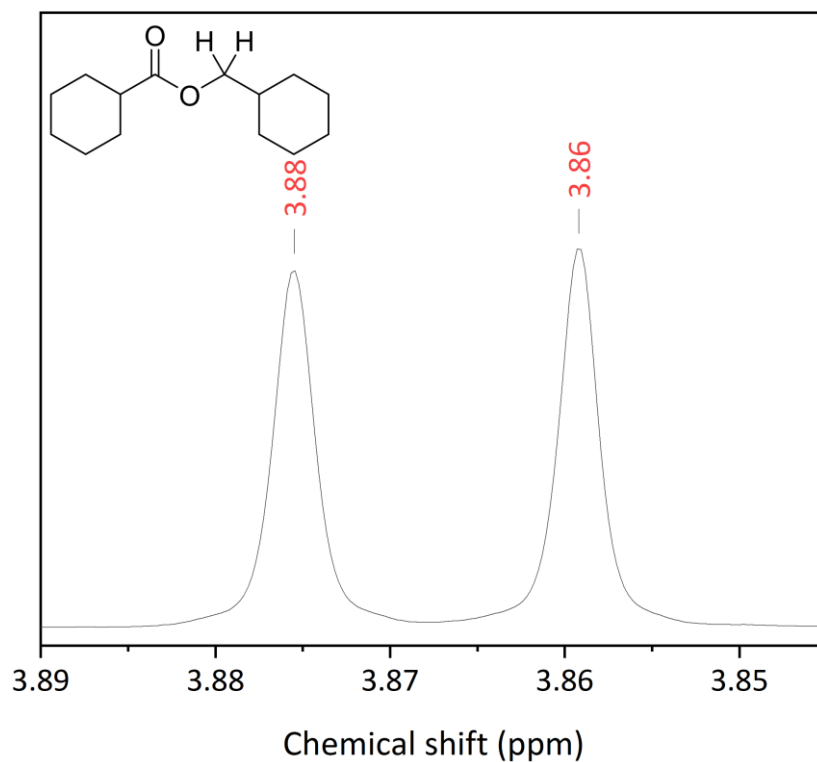


Figure VII-12 - ¹H NMR analysis of the purified CCE. Zoom on the doublet at 3.86 ppm in CDCl₃.

¹H NMR (CDCl₃) δ=0.98 (2H, m), 1.12–1.32 (6H, m), 1.44 (2H, m), 1.57–1.78 (9H, m), 1.88 (2H, m), 2.29 (1H, tt, J=11.3, 3.6 Hz), 3.86 (2H, d, J=6.5 Hz);

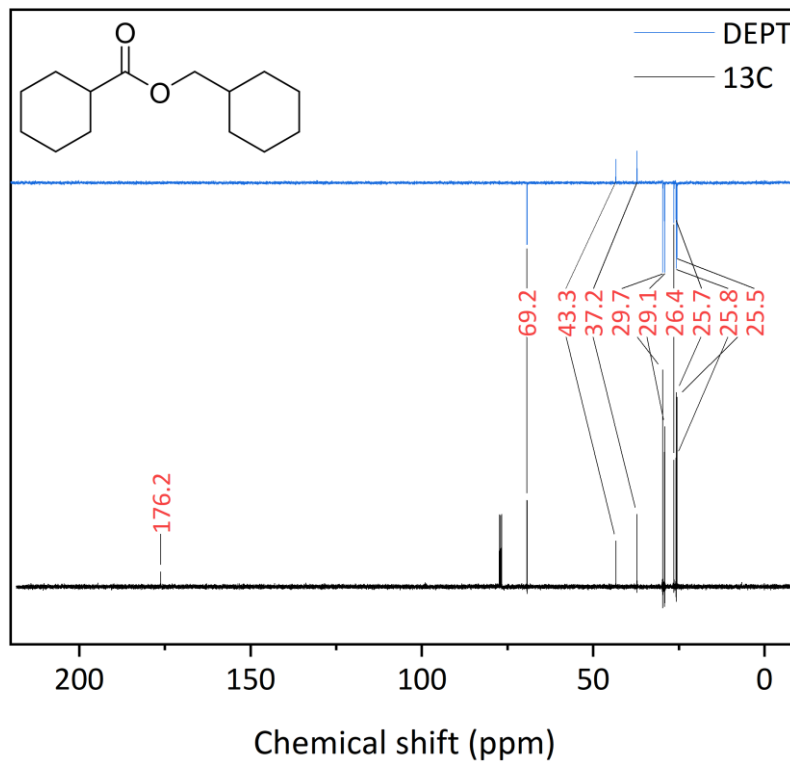


Figure VII-13 - ¹³C and DEPT NMR analysis of the purified CCE in CDCl₃.

¹³C NMR (CDCl₃) δ=25.5 (s), 25.7 (s), 25.8 (s), 26.4 (s), 29.1 (s), 29.7 (s), 37.2 (t), 43.3 (t), 69.2 (s), 176.2 (q)

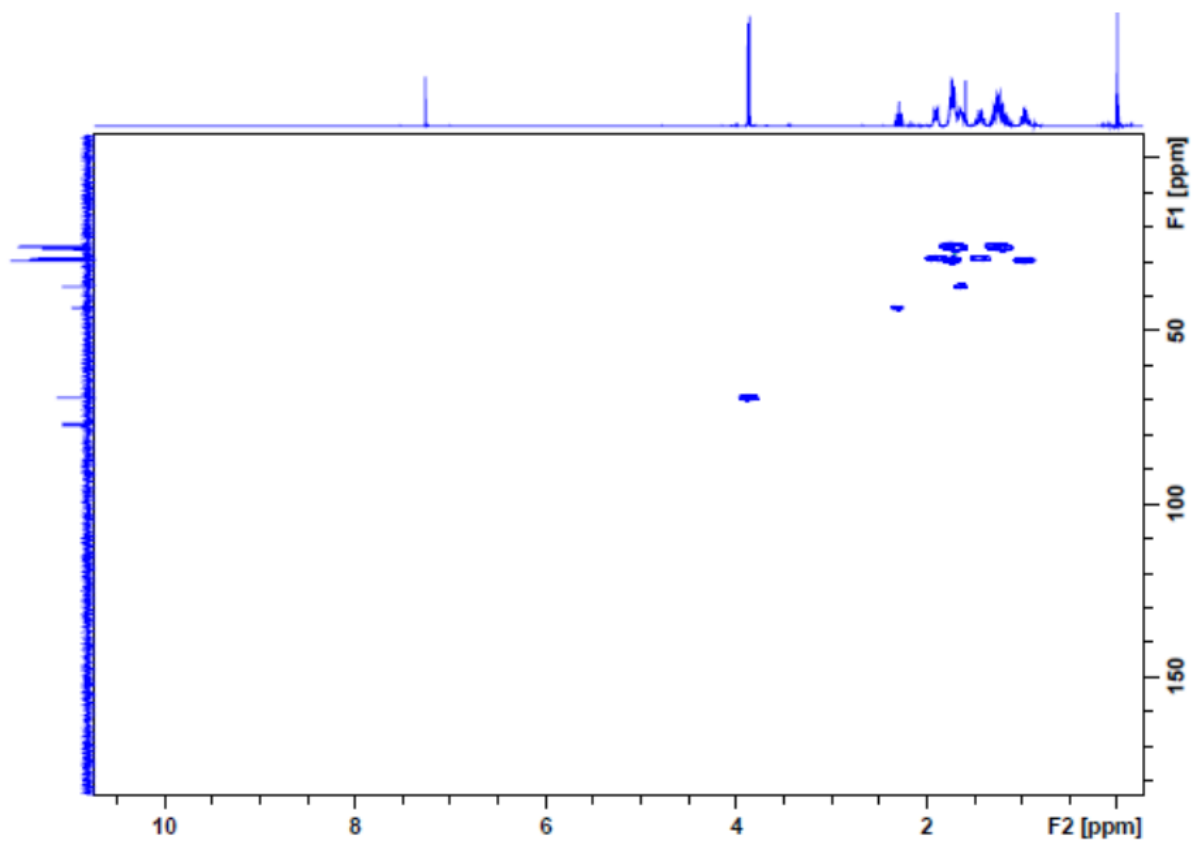


Figure VII-14 - HSQC analysis of the purified CCE in $CDCl_3$.

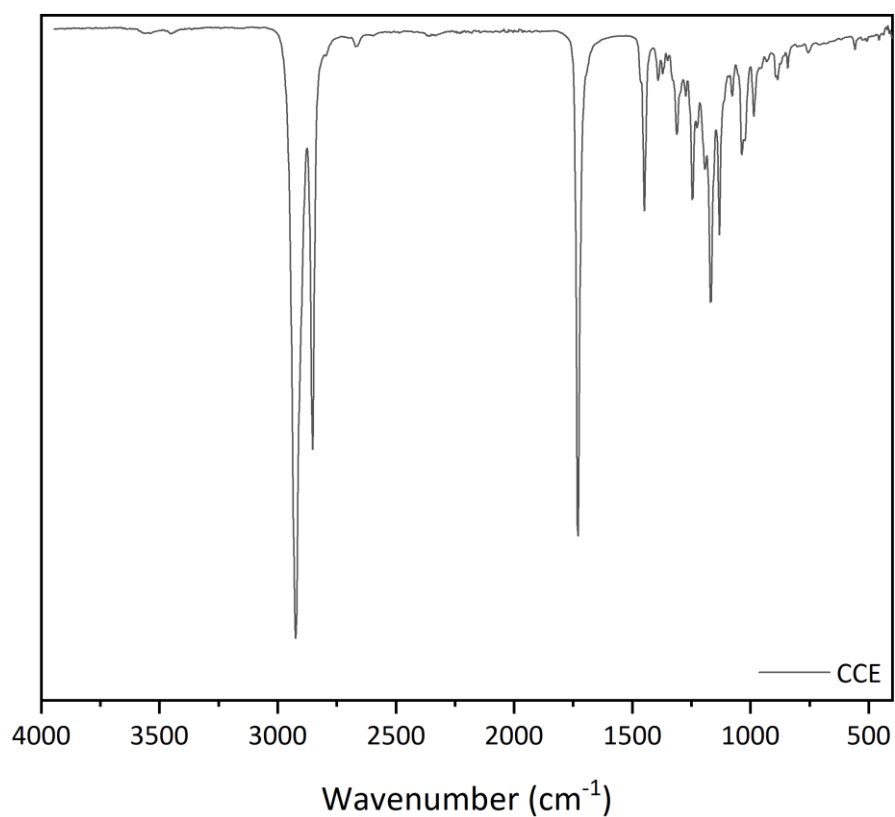


Figure VII-15 - FTIR-ATR analysis of the purified CCE in $CDCl_3$.

IR (neat): ester: 1730, 1176, 1132 cm^{-1} ; C sp³: 2922, 2852, 1448 cm^{-1}



VIII. Conclusion and perspectives

In this thesis, we assessed the viability of new potential LOHC systems. The literature review showed that the current state-of-the-art LOHC systems present barriers that still need to be addressed, in particular, their high dehydrogenation enthalpy, intrinsic toxicity, rarity and cost of the platinum group metals (PGM) used for the current hydrogenation and dehydrogenation catalysts and finally the LOHC stability after multiple hydrogenation/dehydrogenation cycles. Thus, an efficient answer to the previously highlighted barriers would be to develop organic structures with novel reactivities, in particular bifunctional LOHC that were not reported in the literature.

Many aspects must be taken into account in order to choose a pertinent LOHC system such as its H₂ gravimetric and volumetric densities, dehydrogenation enthalpy, synthetic accessibility, safety, transportability, environmental impact, produced H₂ quality and flux. These non-exhaustive secondary criteria are actually primordial and highly dependent on the targeted application and were discussed in the first chapter of this thesis.

Firstly, the physico-chemical properties (gravimetric density, elemental composition, melting point and boiling point, toxicity, reactivity, ...) of potential LOHC structures were gathered to ensure that only pertinent molecules were chosen. Conversely, industrial requirements such as the size and weight of the system, the network for the H₂ recharging (containers, distribution, competition with already-in-use systems...), economic costs and lastly the overall efficiency of the system were not included as they were premature with regard to the development of the targeted systems. While DFT studies englobing the entirety of the LOHC, catalysts and their interactions were presented in the literature review, this approach was not chosen for this thesis due to the relative novelty of the studied LOHC couples. Here, an *ab-initio* DFT methodology was developed to estimate the dehydrogenation enthalpy of these structures, aiming for dehydrogenation enthalpies inferior to 50 kJ/mol H₂ if possible (dehydrogenation enthalpy of the state-of-the-art N-Ethylcarbazole). By using these criteria as selection tools, previously unreported LOHC structures were suggested, although no structure attained dehydrogenation enthalpies lower than 50 kJ/mol H₂. As a LOHC system is described by its molecules (gravimetric and volumetric H₂ densities, dehydrogenation enthalpy) but also its catalysts (active metals, catalytic supports, additives, preparation method, performance and stability) and dedicated reaction systems, we used commercial heterogeneous catalysts in batch systems to simplify our study.

A rapid catalytic screening of the most promising structure, 1-Cyclohexylethanol/Acetophenone (CHEA/APO), was conducted afterwards for both hydrogenation and dehydrogenation reactions before performing the cycling of the LOHC. Lab experiments showed that Ru/Al₂O₃ catalyzed the hydrogenation of the LOHC at 115 °C in 2 h with a conversion of 100% and 98% selectivity. The dehydrogenation was successfully carried out using Pt/C at 205 °C in 36 h with total conversion but with a degree of dehydrogenation (DoDH) limited to 72% and a LOHC stability of 80%. These conditions were used to cycle the system three times during which up to 50% of the total hydrogen capacity was exploited. The exploited H₂ capacity was stable after 3 cycles, but more cycles would be required to verify this tendency. The limitations of such a system that pairs C–O bonds and C–C bonds were identified: the reversibility of the hydrogenation of the ketone group upon dehydrogenation facilitated the condensation and dehydration reactions, under the conditions required for the slower dehydrogenation of the cyclohexyl ring. Degradation of the carrier produced LOHC-like structures, some of which have already been studied in the literature such as Ethylcyclohexane/Ethylbenzene and are hence not incompatible with cycling due to their hydrogen storage capacity.

Secondly, the degradation pathways were identified for both hydrogenation and dehydrogenation. The degradation products formation was linked to the contact between the LOHC structure and the

Conclusion and perspectives

active metal nanoparticles in presence of H₂ that was responsible for the formation of intramolecular dehydration, intermolecular dehydration and aldolisation-crotonisation products. In addition, the catalyst support also initiated the aldolisation-crotonisation in H₂-free conditions. Different strategies like support modification and additives were tested to block the degradation pathways for both the hydrogenation and dehydrogenation reactions. Unfortunately, while dehydration was sometimes reduced to undetected proportions by neutralizing the acidic sites of the support, aldolisation-crotonisation products were observed in all instances due to their formation being catalyzed in both acidic and basic conditions. Aldolisation happened whenever an enol intermediate could form on the methyl group, but not on the cyclohexyl group. Thus, replacing the methyl group by a cyclohexyl group was proposed to efficiently nullify the aldolisation-crotonisation reaction and a new LOHC couple, Dicyclohexylmethanol/Benzophenone (DCMA/BPO), was suggested as a modification of the CHEA/APO couple. Both hydrogenation and dehydrogenation reactions showed no more coupling products by GC-MS, but the dehydration of the LOHC structure was enhanced by the presence of two aromatic cycles. Cycling was performed with the conditions adapted from the cycling of the CHEA/APO. After 3 cycles, almost all of the original LOHC was converted to the dehydrated Dicyclohexylmethane/Diphenylmethane (DCM/DPM) form. While more work could have been performed to replace the catalytic system with more basic supports in order to limit the dehydration reaction, this side-reaction would still occur even in trace amounts. Therefore, finding an efficient way to regenerate the LOHC, i.e. adding an oxygen atom on the dehydrated structure, could prove more valuable in the long term.

Thirdly, a methodology to regenerate the dehydrated LOHC was proposed. Regeneration of the alkylarene Diphenylmethane (DPM) was limited. Indeed, out of all tested catalytic conditions, only strong organic peroxides like Tert-butylperoxide favored the production of BPO. Nevertheless, their neutralization in the reaction mixture was incomplete even after 3 days of neutralization. In consequence, a new couple, Dodecahydrofluoren-9-ol/Fluoren-9-one (12H-FLUA/FLUK), was suggested due to the enhanced reactivity of Fluorene. Suitable reaction conditions were found and the effect of the regeneration on the cycling of the LOHC was tested. After 3 cycles, the cycling without regeneration afforded the completely dehydrated structure while the cycling with regeneration limited this side-reaction by introducing back the oxygen atom: 20% of the oxygenated structure was present at the end of the cycle. The comparison of the exploited H₂ capacity showed that the oxygenated structure produced more H₂ over the cycling compared to the dehydrated one. This difference might come from the reduced reactivity of the homocyclic carrier as higher dehydrogenation temperatures are usually required for homocyclic structures. Nevertheless, MALDI TOF and APCI-MS analysis revealed oligomerized structures, indicating that polymerization was a side-reaction. In particular, an oligomer with a unit of $m/z=162-164$ was detected and identified as probably Polyfluorene. However, attempts to form back Fluoren-9-one were unsuccessful. Here, the negative influence of the ketone was observed over the past three chapters. Reactivity modification (i.e. replacing the ketone by another chemical function) was then suggested.

Lastly, the hydrogenated form 1-Cyclohexylethanol was modified to Cyclohexylmethanol in order to form the Cyclohexylmethanol/Benzylbenzoate (CMA/BBE) LOHC couple. Unfortunately, the CMA/BBE LOHC couple could not be efficiently hydrogenated or dehydrogenated by commercially available catalysts. Two degradations pathways, hydrogenolysis and oxygenolysis, were observed and identified during the hydrogenation and dehydrogenation respectively. While the prevalence of oxygenolysis could be limited by directly modifying the experimental setup (Ar flux compared to Ar purge), the hydrogenolysis would require more catalytic development and tuning of the reaction conditions. In addition, the development of efficient and selective dehydrogenation catalysts is still required to further this LOHC couple.

Conclusion and perspectives

Despite our efforts to develop and improve new bifunctional LOHC structures that present undeniable reduced toxicity and alternative sourcing from renewable feedstock benefits over the state-of-the-art LOHC, their perspectives are limited on an industrial point of view. Especially, the presence of a ketone seems to drastically hinder the dehydrogenation and induce multiple incompatible side-reactions like intramolecular dehydration and aldolisation/crotonisation that are catalyzed by acidic and acidic/basic species respectively. Moreover, the prospective regeneration procedure of these dehydrated compounds promoted an oligomerization of the LOHC structure that was visible by MALDI-TOF and APCI-MS analysis. While the quantification of these heavy products is yet to be conducted, they reveal that the molecule design or the catalysts could be responsible for the generation of heavier products. Nevertheless, more experiments would be required to verify which and to design an efficient alternative. Replacement of the ketone by an ester was unsuccessful with commercial catalysts, with important degradation during both hydrogenation and dehydrogenation. In addition, the dehydrogenation could not be completed to the desired product. Nonetheless, the development of a high throughput methodology to develop and test new couples catalysts/support is required. Overall, catalytic development is a major limitation in this study as the dehydrogenation kinetics were 100 to 1000 times slower than the state-of-the-art Dibenzyltoluene or N-Ethylcarbazole LOHC. In addition, the replacement of critical platinum group metal catalysts was not achieved over this thesis and is a crucial step for the development of the LOHC technology. Moreover, experimental assessment of the DFT methodology by direct measurement of the dehydrogenation enthalpy would drastically improve the selection of low dehydrogenation enthalpy LOHC couples and enhance the understanding of the degradation of the carrier.

In addition to catalytic development, refinement of the LOHC molecular design could be beneficial. Indeed, only homocyclic structures were covered during this thesis and the integration of N atoms into the cycles might facilitate the dehydrogenation. Moreover, the development of C-O-based structures is particularly interesting as non-noble metal catalysts such as Cu can catalyze both hydrogenation and dehydrogenation reactions. As numerous C-O bonds-containing molecules able to store/release H₂ exist in Nature, it is only a matter of time before their pivotal role is recognized. Another approach would be to simplify drastically the molecular systems, as complex structures tend to induce more side-reactions. The design and comprehension of the LOHC-metal-support interfaces in heterogeneous catalytic systems is also key as the objective of complete reaction selectivity might be unachievable if these interfaces cannot be rationally constituted and analyzed. Finally, a more realistic approach would be to observe which degradation structures with H₂ storage capacity form during the cycling of the LOHC as they probably are the most stable LOHC structures with the currently available catalytic systems.

Nonetheless, massive energy storage is a major concern due to the implementation of intermittent renewable energies. Both must concentrate research efforts to achieve a successful energy transition. While early studies targeted individual mobility as a LOHC application, the dehydrogenation temperature, limited H₂ gravimetric and volumetric densities as well as a low cycling capacity of most current LOHC systems make this application unsuitable. Conversely, stationary systems for off-grid energy generation might be interesting if the system cost is low (LOHC, catalysts, H₂ production, hydrogenation, dehydrogenation and H₂-to-power setups). Moreover, the system volume might be less of an issue. Here, the degradation products could be used as either H₂ storage materials of reduced capacity or fuel to compensate the high dehydrogenation energy. The presence of degradation products in the H₂ output can be detrimental for the H₂-to-Power setups such as Proton-Exchange Membrane Fuel Cell where contamination of the membrane will drastically shorten their life expectancy. Thermal engines are unaffected by traces of contaminants, but while release greenhouse gases such as CO₂ and NO_x accordingly. Nowadays, massive energy storage and transportation is the

Conclusion and perspectives

most promising short-term application of the LOHC technology, but it would necessitate both a low system cost and high H₂ densities. Here, the LOHC technology has a real pertinence to safely transport and distribute energy worldwide if the previously raised issues are answered. Indeed, providing that H₂ has been produced, heating energy is free, all required equipment is available and the yield for the conversion from H₂ to electricity is 100%, roughly 1400000 to 2400000 m³ of hydrogenated LOHC 18H-DBT (6 to 10 M€) with 1.5 to 2.5 tons of Pt (45 to 75 M€) would be necessary to generate 3-5 GWh over 1 h. Under these assumptions, these values show the extreme cost of the catalyst on the LOHC technology. Of course, a more in-depth study might reveal that another parameter of the system is more important than anticipated (H₂ and energy costs, energy efficiency, ...). These values also show that using this technology as the only source of energy might be impossible due to its high price. Therefore, a primary concern would be the reduction of the price of the catalyst if this technology is to compete with other H₂ storage and transport technologies like Ammonia.

Summaries

L'hydrogène représente un excellent vecteur énergétique afin de pallier à l'intermittence des énergies renouvelables pour peu qu'il soit stocké et transporté en toute sécurité et à faible coût. Cependant, l'hydrogène est un gaz à très faible masse volumique. Ainsi, son transport et stockage présentent de nombreux défis, tant au niveau de la quantité transportée que de son confinement.

Une réponse potentielle à ces problématiques consiste à utiliser des molécules organiques type LOHC (Liquid Organic Hydrogen Carrier). Celles-ci sont capables de créer des liaisons covalentes avec l'hydrogène, améliorant de fait la sécurité et la manipulation de l'hydrogène tout en conservant des densités volumétriques en hydrogène comparables à celles des stockages traditionnels. En effet, les LOHC présentent des capacités massiques en hydrogène à température ambiante et pression atmosphérique pouvant être supérieures à celles du stockage à 700 bar ou cryogénique tout en limitant les risques associés. En général, les LOHC sont des molécules liquides capables de stocker et produire de l'hydrogène à un endroit et un temps désirés par le biais de réactions catalytiques d'hydrogénation exothermique et de déshydrogénation endothermique. Ainsi, l'acheminement de l'hydrogène consiste à transporter un liquide et non plus un gaz. La déshydrogénation est ensuite assurée au point d'utilisation de l'hydrogène. Le LOHC pauvre en hydrogène est le seul sous-produit de la réaction qui peut ensuite être réutilisé pour stocker à nouveau de l'hydrogène. Néanmoins, le haut coût énergétique pour déshydrogéner ces molécules constitue aujourd'hui un verrou à l'émergence de cette technologie. Les objectifs de cette thèse consistent donc à déterminer de nouvelles molécules LOHC dont l'enthalpie de déshydrogénation est inférieure à l'enthalpie de déshydrogénation de l'état de l'art N-Ethylcarbazole (50 kJ/mol H₂). Ensuite, des tests expérimentaux évalueront la pertinence de ces molécules au niveau de leurs réactions d'hydrogénation et déshydrogénation.

Dans cette thèse, la viabilité des LOHC potentiels a été évaluée au préalable en calculant leurs propriétés thermodynamiques par ab-initio Density Functional Theory. La gamme de température du liquide, les densités gravimétriques et volumétriques en hydrogène, l'accessibilité synthétique et la sécurité ont aussi été pris en compte. Bien qu'aucun potentiel LOHC ne possède une enthalpie inférieure à celles du N-Ethylcarbazole, ces critères ont mis en évidence l'intérêt des LOHC bifonctionnels jusqu'alors non étudiés, c'est-à-dire des systèmes LOHC dont les molécules peuvent stocker/libérer de l'hydrogène dans/à partir de deux fonctions chimiques différentes comme un cycle aromatique/cycle saturé et une cétone/alcool. Les performances et mécanismes de réaction du couple 1-Cyclohexylethanol/Acétophénone ont été évalués avec des catalyseurs hétérogènes commerciaux dans des systèmes batch en hydrogénation et déshydrogénation afin de développer des conditions de réaction adaptées à son cyclage.

Ensuite, les voies de dégradation du LOHC ont été identifiées pour l'hydrogénation et la déshydrogénation et la formation des produits de dégradation a été liée aux différents composants du système LOHC. La modification du support, des additifs et la modification de la structure du LOHC en Dicyclohexylméthanol/Benzophénone ont ainsi été testés pour bloquer les voies de dégradation.

Une méthodologie pour régénérer les LOHC déshydratés a également été développée. Un nouveau couple, Dodécahydrofluorène-9-ol/Fluorène-9-one a été suggéré en raison de la conversion accrue du Fluorène en Fluorène-9-one dans les conditions développées. L'effet de la régénération sur le cyclage du LOHC a ensuite été testé.

Enfin, le couple LOHC Cyclohexylméthanol/Benzylbenzoate a été étudié pour mettre en évidence l'effet du remplacement de la fonction cétone par un ester. Les effets de la modification sur la réactivité et la stabilité du couple LOHC ont été rationalisés.

Mots-clés : Hydrogène, LOHC, Stockage d'hydrogène, Catalyse, DFT, Modélisation

Summaries

Summaries

Summaries

English summary:

Hydrogen is an excellent energy vector to compensate for the intermittence of renewable energies, if it is stored and transported safely at low cost. However, hydrogen possesses a very low-density gas, thus its transport and storage present many challenges, both in terms of the quantity transported and in terms of its containment.

A potential answer to these problems consists in using LOHC (Liquid Organic Hydrogen Carrier) type organic molecules. These are capable of creating covalent bonds with hydrogen, thus improving the safety and handling of hydrogen while maintaining volumetric densities of hydrogen comparable to those of traditional storage systems. Indeed, LOHCs have hydrogen gravimetric densities at room temperature and atmospheric pressure that can be higher than those of 700 bar or cryogenic storage systems while limiting the associated risks. In general, LOHCs are liquid molecules capable of storing and producing hydrogen at a desired location and time through catalytic exothermic hydrogenation and endothermic dehydrogenation reactions. Thus, the transportation of hydrogen consists in transporting a liquid instead of a gas with the dehydrogenation carried out at the point of use of the hydrogen. The hydrogen-poor LOHC is the only by-product of the reaction that can then be reused to store hydrogen again. Nevertheless, the high energy cost to dehydrogenate these molecules is a barrier to the emergence of this technology. This thesis objectives are therefore to determine new LOHC molecules whose dehydrogenation enthalpy is lower than the dehydrogenation enthalpy of the state of the art N-Ethylcarbazole (50 kJ/mol H₂). Then, experimental tests will evaluate the suitability of these molecules for their hydrogenation and dehydrogenation reactions.

In this thesis, the viability of potential LOHCs was previously evaluated by calculating their thermodynamic properties by ab-initio Density Functional Theory. The liquid temperature range, gravimetric and volumetric hydrogen densities, synthetic accessibility, and safety were also considered. Although no LOHC potential had a lower enthalpy than N-Ethylcarbazole, these criteria highlighted the interest of previously unstudied bifunctional LOHCs, i.e. LOHC systems whose molecules can store/release hydrogen in/from two different chemical functions such as an aromatic ring/saturated ring and a ketone/alcohol. The performance and reaction mechanisms of the 1-Cyclohexylethanol/Acetophenone couple were evaluated with commercial heterogeneous catalysts in hydrogenation and dehydrogenation batch systems in order to develop suitable reaction conditions for its cycling.

Then, the LOHC degradation pathways were identified for hydrogenation and dehydrogenation and the formation of degradation products was related to the different components of the LOHC system. Modification of the carrier, additives and modification of the LOHC structure to Dicyclohexylmethanol/Benzophenone were thus tested to block the degradation pathways.

A methodology to regenerate the dehydrated LOHC was also developed. A new couple, Dodecahydrofluoren-9-ol/Fluoren-9-one was suggested due to the increased conversion of Fluorene to Fluoren-9-one under the developed conditions. The effect of regeneration on the LOHC cycling was then tested.

Finally, the LOHC Cyclohexylmethanol/Benzylbenzoate couple was studied to highlight the effect of replacing the ketone function with an ester. The effects of the modification on the reactivity and stability of the LOHC couple were rationalized.

Keywords: Hydrogen, LOHC, Hydrogen storage, Catalysis, DFT, Modeling